https://ntrs.nasa.gov/search.jsp?R=19750011054 2018-07-19T15:23:58+00:00Z

(NASA-CR-142295) PROCEEDINGS OF THE 9TH ANNUAL CONFERENCE ON MANUAL CONTROL (Massachusetts Inst. of Tech.) 414 p HC $10.50 CSCL 01C

N75-19126 THRU N75-19164 Unclas G3/01 13253

PROCEEDINGS OF THE NINTH ANNUAL CONFERENCE ON MANUAL CONTROL

May 23-25, 1973

Massachusetts Institute of Technology
Cambridge, Massachusetts
02139

Sponsored by:

National Aeronautics and Space Administration

United States Department of Transportation

MAR 1975
RECEIVED
NASA STI FACILITY
INPUT BRANCH

PROCEEDINGS OF THE

NINTH ANNUAL CONFERENCE

ON

MANUAL CONTROL

May 23-25, 1973

Massachusetts Institute
of Technology
Cambridge, Massachusetts
02139

Sponsored by:

National Aeronautics and Space Administration

United States Department of Transportation

FOREWORD

The Ninth Annual Conference on Manual Control was held May 23, 24, and 25th at Massachusetts Institute of Technology, Cambridge, Massachusetts. The Conference was attended by more than 100 scientists interested in the areas encompassed by manual control related fields. Papers were presented in the areas of displays, ride qualities and handling, driving and psychomotor skills, control, system identification and signal detection, electrophysiological systems analysis, and modelling. Over 50 papers were presented, both formal and informal, and all are included in this volume.

The Conference itself was funded by the National Aeronautics and Space Administration and the publication of the Proceedings was funded by the United States Department of Transportation.

CONTENTS

SESSION I. DISPLAYS I..... 1

Effects of Visual Flight Display Dynamics on Altitude Tracking Performance in a Flight Simulator, E.F. Weener, R.M. Howe, and R.W. Pew..... 3

A Study on Aircraft Map Display Location and Orientation, D.L. Baty, T.E. Wempe, and E.M. Huff..... 9

The Effect of Communications and Traffic Situation Displays on Pilot's Awareness of Traffic in the Terminal Area, D. Melanson, R.E. Curry, J.D. Howell and M.E. Connelly..... 25

An Investigation of Transfer of Training from Prediction to Conventional Displays, D.J. Prosin, W.B. Knowles, and J.W. Wulfeck..... 41

Dynamic Reading Analog and Digital Displays, E. Schubert..... 43

A Tactual Pilot Aid for the Approach and Landing Task - Inflight Studies, R.D. Gilson and R.E. Fenton..... 49

Evaluation of Tactual Displays for Flight Control, W.H. Levison, R.B. Tanner, and T.J. Triggs..... 55

The Design and Evaluation of an Aural Stall Warning System (ASWS), M.H. Redlin and P.E. Mullowney..... 71

SESSION II. RIDE QUALITIES AND HANDLING..... 73

Pitch Paper Pilot Revisited, J.D. Arnold, R.B. Johnson, and J.D. Dillow..... 75

Roll Paper Pilot, F.R. Naylor, J.D. Dillow, and R.A. Hannen..... 83

Ride Quality Simulation using Data Recorded from Commercial Airline Flights, H.P. Bergeron..... 93

Pilot Model Sensitivity graphs and Flying Qualities Parameters, E.D. Onstott..... 93

Paper Pilot Ponders Supersonic Transports, J.R. Stone..... 95

Handling Properties of Diverse Automobiles and Correlation with Full Scale Response Data, R.H. Hoh and D.H. Weir..... 103

SESSION III. DISPLAYS II..... 119

A display Evaluation Methodology Applied to Vertical Situation Displays, S. Baron and W.H. Levison..... 121

A Conformal Head-Up Display for the Visual Approach, J.M. Naish..... 133

Pilot Performance During a Simulated Standard Instrument Procedure Turn with and without a Predictor Display, J.G. Kreifeldt and T. Wempe..... 147

A Model Based Technique for the Design of Flight Directors, W.H. Levison..... 163

Some Effects of a Quantized Display Format on Human Operator Tracking Performance, R.A. Hess and W.M. Teichgraber..... 173

Improvements in Pilot/Aircraft-Integration by Advanced Contact Analog Displays, V. Wilckens..... 175

Visually Induced Sensations of Motion, L.R. Young, J.M. Dichgans, and C.M. Oman..... 193

Flight-Test Experience with a Snap-shoot Display, A.E. Preyss, J.L. Meiry, J.E. Potter, and R.E. Curry.. 195

Application of Describing Functions for Evaluation of Space Shuttle Landing Aid Display Concepts, W.D. Chase..... 197

SESSION IV. DRIVING AND PSYCHOMOTOR SKILLS..... 199

Sensitivity of a Critical Tracking Task to Alcohol Impairment, J.A. Tennant and R.R. Thompson.... 201

Effects of Alcohol on Continuous Driver Control Dynamics, D.T. McRuer, H.R. Jex, and R.W. Allen..... 215

Performance Assessment via the Critical Task and Dowel Balancing, R.W. Pew..... 215

Measurement of Driver/vehicle Multiloop Response Properties with a single Disturbance Input, D.T. McRuer, D.H. Weir, H.R. Jex, R.E. Magdaleno, and R. W. Allen..... 217

An Experimental Study of The Motorcycle Roll Stabilization Task, D.J. Eaton..... 233

Comparisons of Population Subgroups Performance on a Keyboard Psychomotor Task, R.L. Stapleford..... 245

SESSION V. CONTROL..... 257

Optimization of Control Gain by Operator Adjustment, W. Kruse and G. Rothbauer..... 259

The Effects of Display Variables and Secondary Loading on the Dual Axis Critical Task Performance, G.M. Swisher and S. Nataraj..... 265

Manual Control of Vehicles with Slowly-Varying Dynamics, T.E. Moriarty, R.M. Howe, and R.W. Pew..... 279

A Multi-Axis Side-Arm Controller for the Tactical Aircraft Guidance System (TAGS) Program, M. Gordon-Smith..... 279

Vibration Feedthrough to Manual Control Systems, R.W. Allen, R.E. Magdeleno, and H.R. Jex..... 281

Flight Investigation of Pilot Describing Function for Lateral Directional Control of an Airplane in Turbulent Air, G. Beppu..... 281

On the Dynamics of Human Pilots in Marginally Controllable Systems, N. Goto and F. Washizu..... 283

SESSION VI. SYSTEM IDENTIFICATION AND SIGNAL DETECTION..... 285

Identification of the Optimal Control Model for the Human Operator, A.V. Phatak, R.K. Mehra and C. Day.... 287

Parameter Estimation in Linear Models of the Human Operator in a Closed Loop with Application of Deterministic Test Signals, A.van Lunteren and H. G. Stassen..... 289

An Adaptive Approach to Nonlinear System Identification, R. Mekel..... 299

Identification of Human Operator Performance Models Utilizing Time Series Analysis, F.M. Holden and S.M. Shinners..... 301

In-Flight Measured Human Pilot Describing Function and Remnant for Pitch Attitude Control, H.A. Mooij.... 311

A Simplified Signal Analysis Technique for Obtaining Optimal Estimates of System Dynamics, R.F. Whitbeck... 319

SESSION VII. ELECTROPHYSIOLOGICAL SYSTEMS ANALYSIS... 325

A Stochastic Model of the Electromyogram, G.C. Agarwal and G.L. Gottlieb..... 327

Modelling and Measuring Limb Fine-motor Unsteadiness, R.E. Magdeleno, H.R. Jex, and R. W. Allen..... 335

Evaluation of Flight Simulation Displays using Electrophysiological Techniques, L.J. Leifer, and G.Buckland..... 351

The Muscle Spindle as a Feedback Element in Muscle Control, L.T. Andrews, A.M. Iannone, and D.J. Ewing..... 353

Continuously Varying Skin Potentials Elicited by Sinusoidally Varying Electric Shock Potentials, J.W. Senders, V.L. Senders, and B. Tursky..... 363

SESSION VIII. HUMAN MODELLING..... 365

Modelling the Behavior of the Helmsman steering a Ship, W. Veldhuyzen and H.G. Stassen..... 367

Human Operator Performance in a Simulated AAA Task, W.H. Levison and S. Baron..... 377

Further Examination of Pilot Instrument Scanning Data and Development of a New Link Value Estimator, L.G. Hofmann, W.F. Clement and R.E. Blodgett..... 379

A Direct Procedure for Partitioning Scanning Workload in Control Display System Design, W.F. Clement, L.C. Hofmann, and D. Graham..... 389

Signal Detection with Time-varying Signal to Noise Ratio, E.G. Gai and R.E. Curry..... 401

Input Signal Adaptivity of the Human Operator - A Linear and Non-Linear Analysis, K. Etschberger..... 403

A Linear Stochastic Model of the Human Operator, J.C. Durrett..... 405

Models of Man as a Suboptimal Predictor, W.B. Rouse... 413

Analysis of Response to Wind-Shears using the Optimal Control Model of the Human Operator, S. Baron..... 419

The Preview Control Problem with Application to Man-Machine System Analysis, M. Tomizuka and D.E. Whitney..... 429

On Modeling Performance of Open-Loop Mechanisms T.B. Sheridan..... 443

Prediction of Pilot Performance in STOL Landing, D.L. Kleinman and W.R. Killingsworth..... 451

Variable Structure System Model of a Man Machine Adaptive Characteristic, R.J. Niemela..... 451

I SAYTISID

I NOISSES

ORIGINAL PAGE IS
OF POOR QUALITY

EFFECTS OF VISUAL FLIGHT DISPLAY DYNAMICS ON ALTITUDE TRACKING PERFORMANCE IN A FLIGHT SIMULATOR

by

E. F. Weener, R. M. Howe, R. W. Pew
Department of Aerospace Engineering
&
Department of Psychology
The University of Michigan

ABSTRACT

A study of the effects of visual display dynamics on pilot tracking performance in a simulator has been performed. The tracking task consisted of maintaining the piloted aircraft at the same altitude as two aircraft positioned three-hundred feet ahead, as would be required in level formation flying. The two leading aircraft were represented symbolically along with the horizon on a CRT display. Vertical position of these aircraft with respect to the horizon indicated the altitude of the subject's aircraft, which was disturbed by atmospheric turbulence. Various bandwidths of second-order dynamics were interposed between the true aircraft altitude and the displayed altitude, whereas no dynamics were interposed in the attitude display. Experiments were run using two experienced pilots and two substantually different longitudinal dynamics for the piloted aircraft. Preliminary results indicate a significant decrease in altitude tracking performance for display dynamics with natural frequencies below ten radians per second.

N75 19127

Introduction

Both fixed-base and moving-base simulators are often used to simulate flight by visual reference to objects outside of the cockpit. Often, these visual displays are generated by a TV camera moving with respect to a scale model. However, in many cases, the multiple degree of freedom TV camera servo drives exhibit appreciable dynamic lags, especially in their response to translational commands. These display dynamics may have natural frequencies as low or lower than the short-period dynamics of the simulated aircraft. This paper presents some of the results of a study of the effects of vertical axis translational servo dynamics on the tracking performance of a pilot in a rudimentary fixed-based simulator.

Experimental Set-Up

The longitudinal equations of motion of an airplane were simulated on a hybrid computer. The pilot/subject controlled the simulated airplane with a side-stick controller which provided elevator commands to the airplane. The CRT display provided the visual cues to the pilot. Figure 1 shows the block diagram representation of the simulation. The tracking task consisted of a simplified formation flying task. The two lead aircraft were positioned three hundred feet ahead of the piloted aircraft and maintained a constant altitude. The pilot/subject flew in the trailing position and was instructed to simply maintain the same altitude as the lead aircraft. However, the piloted aircraft was disturbed by a simulated vertical gust spectrum. This spectrum was essentially the one-dimensional Dryden model with break frequencies at

PRECEDING PAGE BLANK NOT FILMED

1-radian/sec and 10 radians/sec , and was produced by analog filtering of a pseudo-random binary noise generator.

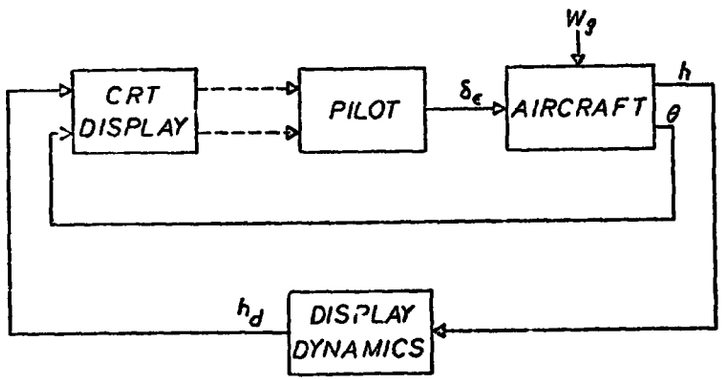

Fig. 1, simulation block diagram

The CRT display was an inside-out display and showed both pitch angle and altitude displacement. A horizon line positioned at infinity provided a reference for the pitch attitude of the piloted aircraft. This angle was displayed directly with no external dynamics. The display is illustrated in Figure 2.

The altitude deviation away from nominal was represented by the displacement between the horizon line and the aircraft symbols. The nominal flight condition of level flight at the same altitude as the lead aircraft is illustrated by Figure 2c. Level flight, but below the nominal altitude, is shown by Figure 2a. A nose up pitch angle, but still below nominal altitude situation is depicted by Figure 2b. The planform of a delta-wing appeared whenever the piloted aircraft was above or below the nominal altitude. The amount and shape of the planform observed was proportional to the amount of altitude displacement and to the direction of displacement, respectively.

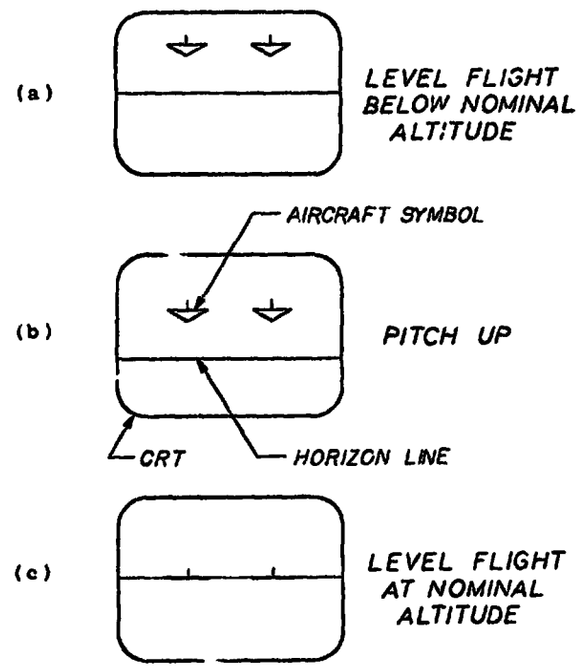

Fig. 2, typical visual display scenes

The altitude displayed on the CRT was not necessarily the true altitude of the aircraft. Various bandwidths of second order dynamics were interposed between the true altitude of the airplane and the altitude displayed to the pilot. The natural frequencies of the display dynamics were varied from infinity, (i.e., no dynamics) to 3 radians/second. The damping ratio of the display dynamics was held constant at 0.707. These dynamics are representative of TV camera servo drives which have both inertia and damping. This simulation represented vertical axis (z-axis) translational visual display dynamics only.

Two different types of aircraft longitudinal dynamics were simulated. These represented fairly different handling qualities. The dynamic characteristics are presented in Table 1. Airplane #1 has a rather high short-period natural frequency and a rather low short-period damping ratio. By comparison, airplane #2 has a lower short-period natural frequency and a larger short-period damping ratio. Airplane #1 exhibited a quicker response to elevator commands than did airplane #2. The elevator coefficients for the two airplanes were adjusted so that the elevator gains in the region of open-loop unity gain crossover frequency were approximately equal.

AIRCRAFT DYNAMICS

Aircraft	Short period		Phugoid	
	ω_{sp}	ζ_{sp}	ω_p	ζ_p
	4.8 r/s	0.38	0.07 r/s	0.09
2	2.6 r/s	0.54	0.11 r/s	0.06

Table 1

ORIGINAL PAGE IS OF POOR QUALITY

Experimental Conditions

Twelve different experimental configurations were examined for each of two subjects. These twelve conditions consisted of six different display dynamics natural frequencies for each of the two airplanes. Fifteen runs of two minute duration were made at each condition. The two subjects who participated in the experiment were both experienced pilots. Subject #1 was a military pilot with both fixed and rotary-wing experience. The second subject was a commercial airline first officer with only fixed-wing experience.

Experimental Data

Each run was recorded on-line with a digital computer. At the termination of each of these 2 minute runs, the mean square altitude deviation and the mean square vertical gust velocity (noise disturbance) were also recorded. These two quantities were employed to define a performance rating, designated as PR.

$$PR = \frac{\text{mean-square altitude deviation}}{\text{mean-square vertical gust velocity}}$$

This quantity is proportional to the mean-square altitude but normalized to remove some of the effects of the variability of the noise input from run to run. To further facilitate comparisons between the various conditions, a normalized performance rating was defined as follows:

$$\text{Normalized PR} = \frac{\text{mean PR (with display dynamics)}}{\text{mean PR (without display dynamics)}}$$

This measure was defined for each combination of pilot and aircraft. The data for these four combinations are shown in Figures 3 and 4. The data points represent the mean of fifteen runs at that particular display dynamics natural frequency. The 95% confidence levels of the mean are indicated by the bars above and below each data point. The results for both subjects' performance with airplane #1 are shown in Figure 3. For this airplane, on the basis of t-tests, all the differences are statistically significant at the $P < .001$ level with the exception of the 8.5 radian/second condition for subject #1, which was still significant at the $P < .01$ level.

Figure 4 shows the means for both subjects controlling aircraft #2. For subject #1, only the condition for display dynamics at 3 rad/sec has differences statistically significant from the no display dynamics condition. Performance differences for the remaining four display dynamics frequencies are not statistically significant. For the second subject, same airplane, the first three points, 3.0, 5.0, and 8.5 radian/second, have differences significant at $P < .001$ level, but the remaining two points are not statistically different from the no dynamics condition. These data seem to indicate a

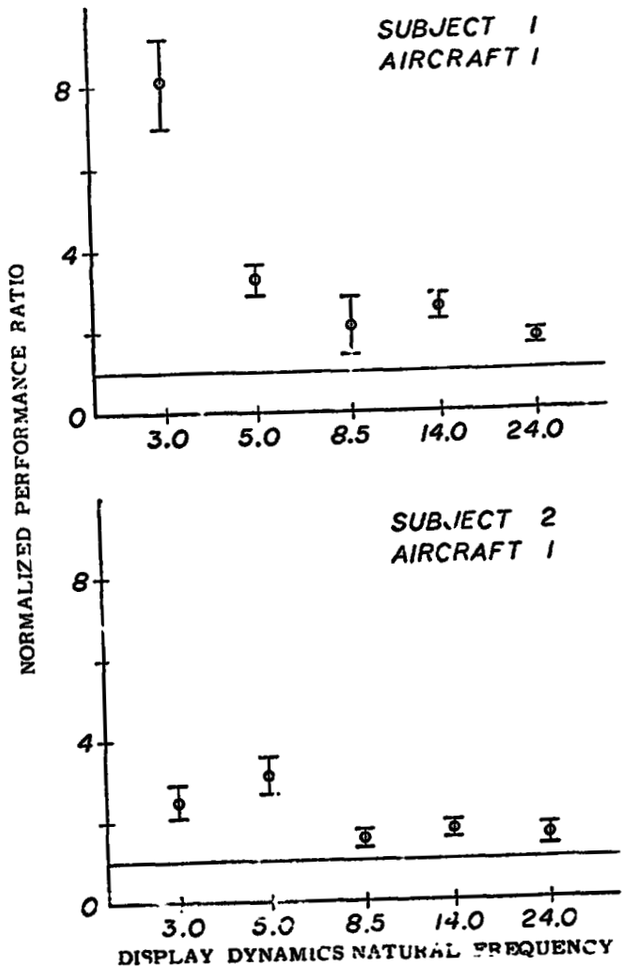

Fig. 3, effects of display dynamics natural frequencies on tracking performance for aircraft 1

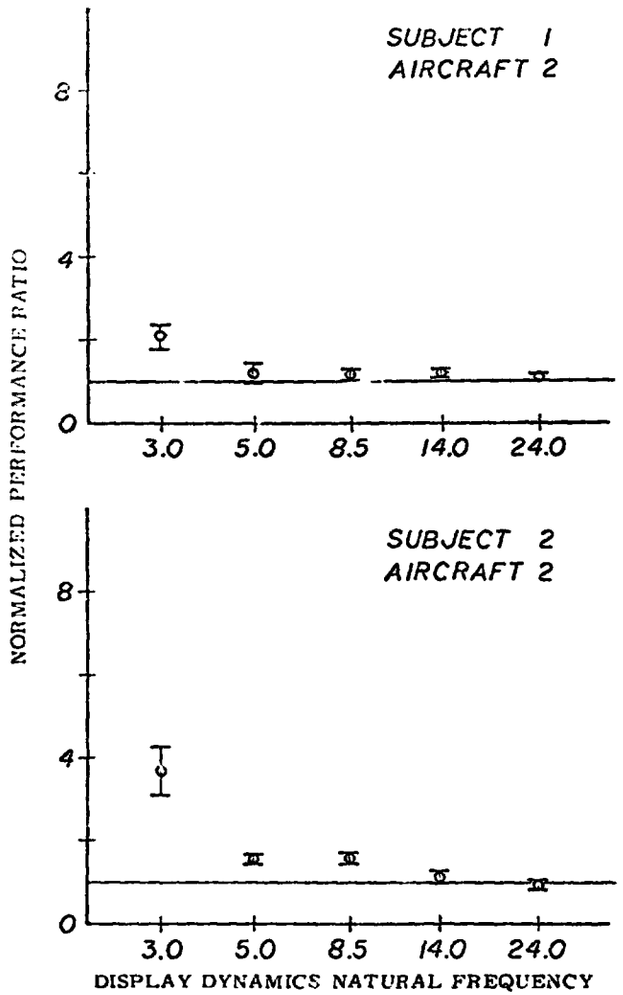

Fig. 4, effects of display dynamics natural frequencies on tracking performance for aircraft #2

relationship between display dynamics and the short-period dynamics of the simulated aircraft.

The second subject, when controlling airplane #1 with display dynamics natural frequency of 3.0 rad/sec, exhibited a level of performance which appeared to be inconsistent with his trends for other display dynamics and also inconsistent with the performance and trends of the first subject. In the frequency domain, the closed loop transfer function relating vertical gusts as the input and altitude deviation as the output shows a substantial change in characteristics for this particular experimental condition as compared to the general form exhibited for all other configurations. It is interesting to note that this second subject flies one specific type of aircraft almost exclusively, an aircraft whose pitch dynamics may be similar to airplane #1 in this study.

The two independent parameters which seem to best characterize these data are:

a) the short-period damping ratio

b) the relationship between the display dynamics and the short-period natural frequency.

Figure 5 shows the means of the Normalized PR plotted vs the ratio of display dynamics natural frequency to short-period natural frequency. The blocked points represent airplane #1 and the open points represent airplane #2. In general, the data for the same airplane flown by both subjects seems to group rather well. The means for airplane #1 are generally higher than for airplane #2. However, a single curve appears to represent the mean data fairly well.

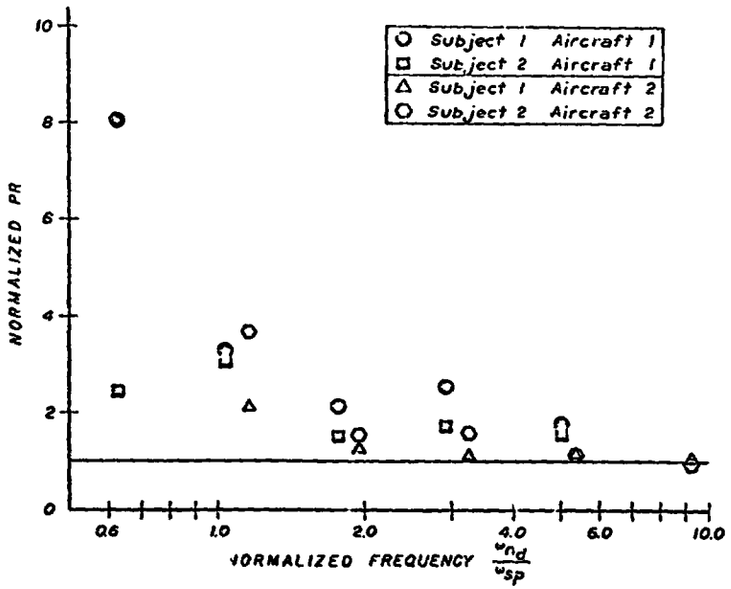

Fig. 5, normalized PR v.s. normalized frequency, two subjects-two airplanes

Conclusions

There are two conclusions which can be drawn from these data:

1) for this type of altitude tracking task, if the simulated aircraft is lightly damped the presence of display dynamics with natural frequencies as high as 5 times the short-period natural frequency causes significant degradation of altitude tracking performance.

2) when the simulated aircraft is more heavily damped, the presence of display dynamics is not significant until the ratio of display dynamics natural frequency to short-period natural frequency is approximately two or less.

In summary, whether dynamical display lags will cause degradation of altitude tracking performance depends on both the short-period damping ratio, and the ratio of the display dynamics natural frequency to the short-period natural frequency of the simulated aircraft.

N75 19128

A STUDY ON AIRCRAFT MAP DISPLAY LOCATION AND ORIENTATION

D. L. Baty, T. E. Wenn & E. M. Huff

Ames Research Center, NASA, Moffett Field, Ca. 94035

ABSTRACT

Six airline pilots participated in a fixed-base simulator study to determine the effects of two Horizontal Situation Display (HSD/map) panel locations relative to the Vertical Situation Display (VSD), and of three map orientations on manual piloting performance. Pilot comments and opinions were formally obtained. Significant performance differences were found between wind conditions and among pilots but not between map locations and orientations. The results also illustrate the potential tracking accuracy of such a display. Recommendations concerning display location and map orientation are made.

INTRODUCTION

Many advanced aircraft display designs include the use of cathode ray tubes (CRT) to present attitude information on a Vertical Situation Display (VSD) and navigation information on a Horizontal Situation Display (HSD). Due to the size of these tubes and mounting structures, there is often some restriction on their placement in the aircraft panel, which in some cases may require that they be positioned side-by-side (most pilots seem *a priori* to prefer over-under placement).

A simulator study was conducted to investigate the effect of the relative position of these two displays on manual performance and included, as the other major variable, three (3) variations in HSD map orientation to test for interactions. Although there have been studies using projected map and CRT displays, e.g., (1)-(3), no comparative studies on location or orientation have been done. The results of this experiment which deal specifically with different map display locations and orientations should be applicable not only to CRT map displays but also to two other major types of map displays, namely, film projection and rear projection CRTs.

The simulator piloting task consisted of making a series of right and left procedure turns in level flight both in the presence and absence of cross winds. Pilot performance was measured by computing both lateral and vertical RMS errors. At the end of the experiment each pilot completed a detailed questionnaire about the experiment. The results of both the pilot performance data and the questionnaire data are presented and discussed.

TASK AND PROCEDURES

Task and Displays

The task was to fly from point A to point B, as in Fig. 1, following the 360°, 315°, 135°, 180°, 225°, 045° and 360° legs in that sequence while maintaining constant altitude. The aircraft dynamics were a simplified version of the DC-8. Throttle setting remained constant with a nominal airspeed of 160 knots. All flight information was displayed on a 17 in. CRT monitor. The display was generated by an Evans & Sutherland LDS-2 graphics display computer using an SEL 840 as the main computer. Aircraft dynamics and scoring procedures were also generated by the SEL 840. Appropriate force-feel characteristics were provided by a hydraulic control loader system. Figure 2 is a photograph of the simulator interior.

Both the Vertical Situation Display (VSD) and the Horizontal Situation Display (HSD) were contained within 5 in. squares. Figure 3 is a photograph of the VSD with labels describing the display elements. The number at the top left corner of the display shows airspeed in knots. The center number is aircraft heading in degrees. The top right number is altitude in feet, and the number just below altitude is the vertical speed readout in feet per minute. The aircraft symbol remained fixed in the center of the display with pitch and roll indicated by movement of the horizon, ground plane lines and pitch lines. The altitude error bar moved across the scope in the vertical direction only. A zero altitude error was indicated when the error bar was centered over the center square of the aircraft symbol. Motion from the center position to the end of the bar in either direction indicated a 100 ft. error. The aircraft was 100 ft. too high when the top end of the bar was just touching the square, i.e., the bar below the aircraft symbol, and 100 ft. too low when the bottom end of the bar was touching the square. The rectangle of the turn rate indicator moved horizontally. Center position indicated zero turn rate and a 3°/sec. turn was indicated with the rectangle centered over the right or left bar.

Figure 4 is a photograph of the HSD with labels describing the display elements. The primary display elements were the reference ground trajectory and the aircraft symbol. The aircraft symbol gave both heading and position information. The aircraft position was the junction point of the wings and body. The other symbols were present to provide a touch of realism and to provide background display motion which was considered particularly important for the two conditions where the aircraft remained in the center of the display during the flight. For these two conditions the map translated and additional symbols, not shown here, would come into view at different points along the flight. The map scale is 1.6 n. mi./in.

One additional feature was shown on both the VSD and HSD to aid in timing the start of the turns. Approximately 5 seconds before the transition point from a straight line section of the reference ground trajectory to a circular section, the center

square of the VSD aircraft symbol and the aircraft symbol on the HSD both began to flash at a 2 Hz rate. Referring to Fig. 1 it can be seen that there are 2 turns of 180° and 4 turns of 45°. For the 45° turns the flashing began 5 seconds before the tangent point of a circle with the same radius as the 180° turns. This is illustrated on Fig. 1 at the 045° to 360° heading transition.

The VSD was always in the same scope location for either the over-under or the side-by-side condition. The VSD center-line was centered directly in front of the pilot. The map (HSD) was positioned either to the right of the VSD or below it.

Experimental Variables

Relative display location Two levels, VSD and HSD located either over-under (D_2) or side-by-side (D_1).

Map orientation: Three levels were used.

1. North up, fixed map (0_1). With this condition all elements were fixed, the only moving symbol being the aircraft which moved around the course to indicate present position and heading.

2. Aircraft heading up (0_2). The aircraft symbol always remained fixed in the center of the display, heading up. The entire map would translate and rotate to keep proper relative position with the aircraft.

3. North up, moving map (0_3). The center of the aircraft remained centered in the display and rotated about this center to indicate aircraft heading. The map always remained north-up (no rotation) and translated vertically and horizontally to maintain relative position with the aircraft. This configuration was chosen because it is a mix of inside-out and outside-in displays. The "north-up, fixed map" display is a pure outside-in display and the aircraft heading up display is a pure inside-out display. In this (3rd) display the aircraft position is inside-out, while the aircraft heading is outside-in.

Figures 5, 6 and 7 are photographs showing a combination of the display locations and map orientations.

Winds: Two levels; wind present (W_1) and wind absent (W_0). When present the wind velocity was always 32 knots. Wind direction was randomly selected from four choices, blowing from either 068°, 143°, 223° or 338°.

Pilot groups. Two groups selected on the basis of a pre-experiment questionnaire. The group of 3 pilots preferring the side-by-side placement of the display was designated Group A, and 3 pilots preferring the over-under placement was called Group B.

Pilots: Six airline pilots were chosen from a group of 19 pilots on the basis of their responses to a Display Location Preference questionnaire. Figure 8 is a reproduction of the paired-comparison part of the questionnaire. This page was preceded by explanatory material concerning CRT, VSD and map displays along with illustrations The questionnaire also included a 5 point rating scale designed to determine the strength of their preference. (See Appendix A for further discussion.) The six airline pilots represented four airlines. One was a Captain and five were copilots, of which two were currently flying as second officers due to "bumping" procedures. The average age was 39, average total flight time was 9,000 hrs., and all had military experience with an average total of 3,000 hrs.

Procedure

Instructions: The purpose of the experiment, the details of the displays, the aircraft dynamics and the experimental conditions were all explained the first day. The stated task was, "stay as close to the reference ground trajectory as possible at all times while still maintaining altitude." They were instructed to set up approximately the same turn rate for the 45° turns as for the 180° turns, using the blinking of the aircraft symbols to aid in timing the beginning of the turns. They were informed of all the conditions before each run, including wind direction. They were instructed that "once we start a run for data, I want you to complete that run unless something unplanned happens, e.g., something obviously wrong with the simulation." They had a separate printed chart on a clipboard similar to Fig. 1, with headings and wind directions for handy reference.

At the end of each flight the pilot was shown the ground track of his entire flight path relative to the reference ground trajectory as in Fig. 9. Also shown were the average mean square errors for both horizontal and vertical track (digits in upper left).

Performance measure: Average mean square errors (AMSE) for the total run were computed on-line for both horizontal and vertical errors.

Training and experiment design: The combination of two display locations, three map orientations and two wind conditions made a total of twelve experimental conditions per pilot. Each pilot flew only one display orientation per day. With six pilots all possible sequence combinations were used as shown in Table 1. These were also divided so that the three different orientations were present within preference groups for each day. Twelve recorded flights were made each day making three replications per map orientation for each of the two display locations (2) by wind conditions (2). These four conditions were randomized in blocks of four runs.

The first day was devoted entirely to training. Before collecting data on each of the following days two runs were made for warmup – one with and one without wind. The pilots were given the option of more warmup, but generally felt one run would have been sufficient. Each pilot averaged one or two sessions per week. Each run lasted approximately 6-1/2 minutes with about three minutes between runs. It was left to the individual pilot to take a longer break whenever he wished. The average break lasted about 20 minutes and was taken about halfway through the data runs.

RESULTS AND DISCUSSION

This section is divided into two major parts. The first part presents the results of the pilot performance data, including a subsection dealing with an unexpected phenomenon that has been termed "fascination." The second part presents the results of the Post Experiment Questionnaire.

Performance Data

The magnitudes of the performance scores for each experimental variable are shown in Figs. 11-14. The overall mean for each choice of a variable is designated by the diamond symbol. For Figs. 11-13, the range of individual pilot mean scores are also shown. Figure 11 shows that lateral performance was slightly better with map orientation 0_2, and vertical performance slightly better with orientation 0_1. These differences were not statistically significant. (See Tables III and IV for a statistical summary of results.) Figure 12 shows very little performance difference between the two display location choices, with an average RMS lateral error slightly less than 100 meters and an RMS vertical error slightly less than 8 meters.

The mean performance on wind conditions is shown in Fig. 13. These differences between wind conditions are statistically significant. The scores for each pilot are shown in Fig. 14. The differences shown among pilots are also statistically significant. The scores at the top of the dotted lines are the means for these runs with wind added, and those at the bottom are for runs without winds.

It is clear that there was a difference in emphasis between the lateral and vertical task among pilots. Pilot Y, for example (Fig. 14) was consistently lower than the others for the lateral task, and pilot U was consistently lower for the vertical task. To form a single score for pilot performance it was noted that for all pilots the overall RMS lateral error was roughly 12 times the overall RMS vertical error. A resultant vector score was then found for each pilot as $\sqrt{(\text{Lateral score})^2 + (12\ \text{Vertical score})^2}$. The results of these calculations are shown in Fig. 15. It can be seen that pilot Y had the lowest overall score with the smallest amount of difference between the wind and no-wind conditions. Pilot U had the second to the lowest overall mean score but the difference between his wind and no-wind scores was the largest of the group. This comparison points out the difference in technique between these two pilots. Pilot Y approached the problem as one task, while pilot U gave primary attention to altitude. An analysis of variance of these scores showed the same results as summarized in Tables III and IV and it is not included.

The differences in performance among the pilots as they fell into the preference groups were quite small and were not statistically significant. These performance data are not shown.

No particular significance can be attached to the map orientation prior interaction shown in Tables III and IV. Figure 16 shows that although the largest block of learning for this task was made during the practice day, there was still a steady indication of learning throughout the experiment. So with the balanced experimental sequence used (Table I) it would be expected that how well a pilot performed with a given orientation relative to the other two orientations would be related to where that orientation appeared in the sequence.

The presence of the significant wind-pilot interaction can be seen in Figs. 14 and 15. It is clear that there was a wide range in the ability to cope with the presence of wind in the task.

An expected interaction between orientation and wind was not shown by the data. The pilot comments did not indicate any particular advantage with any display orientation in correcting for wind. One pilot did indicate that it was slightly easier to keep track of the wind direction on 0_1 and 0_2, and two pilots indicated a wind vector on all maps would be helpful.

The significant differences in performance between the pilots and their differences in ability to handle the wind conditions is not surprising. Differences in ability are accepted as a fact in any population. What was slightly surprising was the small value of some of the errors which indicates the potential accuracy of such displays. (Of course this does not include potential operational errors due to ground and airborne equipment errors.) For example, pilot Y had an overall average lateral RMS score for all conditions without wind of 39 meters (128 ft.). This is even more impressive when this is translated to the actual error distance on the face of the display. With the 1.6 n. mi./in. scale that was used, this was a calculated .033 cm. (.013 in.) error on the display. This is close to the width of the display line elements themselves. This points out that very small differenc between the required ground track and the parallel element of the aircraft symbol can be detected. (Pilot Y made two runs where RMS errors were only about half his average value.)

Fascination: One of the pilots (Y) demonstrated atypical behavior on two different runs with the fixed, north-up map. Such events could not be planned in an experiment, but having occurred they provide valuable insight into this pilot's approach to his task and also illustrate the potential for blunder with a north-up map display. Figure 10 is a drawing showing the ground track for the two runs relative to the reference track. Track A was the fifth run of the day (not counting practice) and was flown with the over-under display location. Track B was the eighth run of the day and used a side-by-side location. Both tracks were flown with the "no-wind" condition. Track B was the next "no-wind" run after track A. This pilot normally flew ground tracks with a small error under the "no-wind" conditions. He was, in fact, the most proficient tracker of the six pilots. (The data from these two runs were not included in the overall performance data analysis.)

On track A the turn to go from the 135° leg to the 180° leg was initiated at the proper time in the wrong direction. Then there was a pause in action for a short time while the aircraft maintained a heading of about 100°. About 8 seconds after the initiation of the turn in the wrong direction he called on the intercom and asked if the run could be aborted. He was reminded of the instructions to complete all flights except in the case of equipment malfunction. Following the run he had two comments. First, the task was getting too easy and he was "fine controlling" at the expense of "thinking." Secondly, it was easy to "recover" with this presentation, i.e., easy to see where he had to go to get back on the track, once off the track. After completing track B there was no further comment other than a disgusted acknowledgement that he had "done it again." Though it is seldom as clear cut as in these examples this behavior is not unique and seems to be aptly described by the term

"fascination" as defined by Clark and Graybiel.[4] "In these situations (involving fascination) the pilot had his attention so intently on one item that he did not attend to other items of importance during the flight." Pilot Y was, in fact, always intent on "bettering his scores."

Post Experiment Questionnaire

At the end of their last day each pilot was asked a set of questions concerning the experiment. The procedure took the form of a structured interview.

They were first asked to rank order the six conditions in order of preference. There was some protest to this with comments that there "really wasn't that much difference" between some of the conditions. Table II is a tabulation of the rankings. The number one indicates a first choice, two a second choice, etc. As a coarse means of comparing subgroups these numbers were treated as being "equal interval" and simply added together. A higher total indicates a lower average preference.

The first thing to note in Table II is the wide variety of opinion. No column shows more than two selections of the same ranking. In fact, within the first, fourth and fifth columns there are an equal number of first and last place rankings. It can be seen by looking at the pilot preference group subtotals for the over-under and side-by-side placement that there is essentially no difference for either preference group. Looking at the map orientation results, the heading up orientation (0_2) seems to hold a very slight overall edge in preference.

There were specific reasons behind these differences of opinion as can be seen by their responses when asked to list a major pro and con for each display. Appendix B summarizes these responses from all pilots concerning the three different map orientations. It can be seen that there are valid strengths and weaknesses to be considered for each one. The comments of one of the pilots who had experienced mild vertigo with the heading up orientation (0_2) are especially interesting. He normally preferred the side-by-side placement because the scan "was more relaxed," but preferred the over-under placement with 0_2 because there was "less distraction" from the motion. The effect was strong enough that this pilot ranked 0_2 with over-under placement as his first choice, and 0_2 with side-by-side placement as his last choice.

The over-under/side-by-side preference can be most easily summarized as a difference of opinion regarding whether it is easier to scan sideways or vertically. Four of the six pilots, two in each preference group, answered that it was easier to scan "sideways" and expressed a slight preference for the side-by-side position. The other two pilots maintained that vertical scan was easier. One of the pilots that preferred the side-by-side position and was in the original over-under preference group, expressed mild surprise in finding he actually preferred the side-by-side condition for flying.

Five questions were intended to elicit comments about the display content and method of its presentation. The most general comment was that they liked both displays (VSD and map) better after using them for awhile than they thought they would at the beginning of the experiment. The display element most commented upon was the altitude error bar. Three pilots said to delete it and another said to change it some way or delete it. Two commented that it simply was not needed (i.e., sufficient information was available from the altimeter and vertical speed indicator (VSI) and added clutter, while two commented that they wanted the information but this presentation was "somehow confusing." The following is a listing of the other more pertinent comments.

"A wind vector arrow on map would help." (2)

"On map show heading for next leg."

"VSI should be other than digital." (2)

"For over-under displays put digital readouts at the bottom of the VSD."

"Would prefer an analog heading."

"Make (+) and (−) signs larger in front of VSI."

"The less cluttered you keep the map display, the quicker you will be able to pick up the aircraft."

They generally agreed to the "realism" of the display and were of the opinion that their preferences and comments would be the same in a flight situation. They all felt that they were doing a "reasonably good job" by the second day but were still improving some at the end of the experiment.

Five of them answered that they would find a CRT map display to be useful in their present aircraft. The "no" answer was for current ATC procedures, but changed to "yes" for more crowded airspace. They would find it most useful for terminal area use such as fixed transitions, holding patterns, etc. They felt it would cut down on cockpit workload by relieving the "mental" load of planning ahead.

CONCLUDING REMARKS

The results of a study designed to investigate the effects of two HSD/map panel locations, relative to the VSD, and of three map orientations have been presented. Both pilot performance results and Post Experimental Questionnaire results have been discussed. Based on these results the following conclusions and recommendations are indicated.

Considering both the performance data and the results of a Post Experimental Questionnaire it is concluded that either of the VSD-map display locations used in this experiment would be satisfactory as an instrument panel location. Either choice might meet some resistance at first but the adaptation time to either would be short.

The general performance data indicate that there is nothing to choose from among the three map display orientations. There were no significant differences in performance among the orientations and there was no indication that any one of the three gave either an advantage or disadvantage in keeping track of the wind directions.

The pilot comments throughout the experiment and the answers to the Post Experiment Questionnaire indicate, however, that there are further considerations to be made in the choice of a map orientation. Each orientation has at least one definite advantage and disadvantage. The emphasis on each varied widely among the pilots (Table II) Further research is needed to determine the relative importance of these advantages and disadvantages. Specifically, the use of these map display orientations needs to be evaluated in other phases of flight, such as enroute and transition from enroute to terminal areas. This evaluation should be done in the workload context of a more complete mission simulation than was used for this experiment. The following comments and recommendations concerning map orientation are based strictly on the results of this experiment.

The fixed north-up orientation with a moving aircraft (0_1) provided the pilots with a stable map which they generally liked. However, there seemed to be more of a need to plan ahead Also, there was less feeling of direct identification with the aircraft symbol than was the case with 0_2. The data show that good performance on this type of task is possible, but the possible outcome of a lapse of attention has been shown by the performance previously described in Fig. 10. This orientation is probably best suited for use where the map display is primarily used for planning purposes, i.e., outer loop as opposed to inner loop control.

The rotating map with fixed center aircraft (0_2) would at first appear to have the best combination of advantages There is always left-right control compatibility, the aircraft is readily located at the center of the display and there is always an equal amount of terrain shown around the aircraft. These features are balanced against an unexpected objection to the motion of the display background. Three pilots mentioned a tendency to vertigo, one adapted fairly quickly to where it did not bother him, while the other two continued to be disturbed by it. The conflict seems to stem from the presentation in the single frontal plane of two moving fields representing two different planes Rotation of large areas in the frontal plane is usually associated with aircraft roll and part of the conflict may be due to a lack of adaptation to this new mode of presentation. This orientation may be the one best suited to be used as an instrument for direct guidance of the aircraft. More study and experience is needed to determine the importance of the potential vertigo problem.

The third orientation, north-up with moving map and rotating aircraft (0_3), was originally included in the experiment as sort of a "worst case", with a combination of "inside-out" and "outside-in" elements as already explained. In actual use, however, with the map scaling of 1.6 n. mi./in., the background moved so slowly that it was very little different than the 0_1 orientation with basically the same pros and cons. The ratings for this orientation (Table II) generally fell between those for 0_1 and 0_2 and seemed, therefore, to be a compromise choice. This orientation is recommended primarily for planning purposes, the same use as 0_1. In an operational environment it would have the added advantage that the aircraft would never fly off the edge of the display, i.e., there would be no map frame changes with the aircraft jumping to a new spot on the screen. The aircraft is always at the center of the display.

Generally, the pilots were quite receptive to the idea of using such displays. Those with some prior reservation seemed to have changed their opinion by the end of the practice day. The consensus was that any one of these map displays would be of help for planning purposes, particularly in terminal areas.

These conclusions and recommendations are for the display elements as they were used in this experiment. Addition of other information elements such as flight directors, predictors, etc., could significantly alter these conclusions.

APPENDIX A

DISPLAY LOCATION PREFERENCE QUESTIONNAIRE

While planning this experiment it was recognized that pilot attitudes regarding relative display placement, i.e., over-under vs. side-by-side, could conceivably be a factor in their performance with the two display placements. It was decided to control for this difference, if it did exist, by selecting two groups of pilots on the basis of their responses to a questionnaire mailed to their home. It was anticipated that the larger percentage of the pilots would prefer the over-under arrangement, so in order to increase the chances of filling the side-by-side preference group the questionnaire was sent to three times as many pilots as were needed, nineteen of the pilots contacted by phone. All pilots responded, sixteen of them with complete questionnaires. Preference ranking was possible for 18 pilots. Based on the identifying letter labels shown in Fig. 8, the following preference orders were obtained. Ten pilots ordered the choices by CBA; five pilots by BCA, two pilots by ACB; and one pilot by BAC. Two pilots from BCA and one from ACB were chosen for Preference Group A, i.e., the side-by-side preference group, and three pilots from CBA were chosen for Preference Group B, the over-under preference group. Strength of preference and availability both entered into the final choice of pilots.

APPENDIX B

PILOT COMMENTS ABOUT MAP ORIENTATIONS – SUMMARY

North up with moving aircraft symbol (0_1)

Pro. Stable map – (3)*
Easier to figure wind corrections (1)
No response (2)

Con Had to think some about left-right turns (4)
Left him detached from aircraft (1)
Hard to locate aircraft quickly on scan (1)

Aircraft heading up (0_2)

Pro: Instant orientation regarding direction to turn (3)
Easier to identify with aircraft position (2)
Always know where aircraft located, i.e., at center (1)
Better turn rate information (1)

Con: Didn't like the motion and rotation - tendency to vertigo (3)
Aircraft heading not obvious (1)
No response (2)

North up with moving map (0_3)

Pro: Easy to locate aircraft, i.e., always at center (2)
Stable picture (2)
Liked to see ground move (1)
Easier to figure out wind corrections (1)

Con. Did not like map to move - lose parts (3)
Had to think some about left-right turns (2)
Neutral (1)

* = Number of Responses

REFERENCES

1. Norman S. Selsby and Michael C. Fischer, "A simulator study of a pictorial navigation display in instrument departures of the supersonic transport." NASA TN D-4029, July 1967.

2. S. N. Roscoe, "The navigation director: An area navigation system." Hughes Aircraft Company TM-898, June 1968.

3. James R. Gannett, "Flight management concept II." 1970 Human Factors Society Annual Meeting, San Francisco, California, October 13-16, 1970.

4. Brant Clark and Ashton Graybiel, "Vertigo as a cause of pilot error in jet aircraft." The Journal of Aviation Medicine, Volume 28, pp. 469-478, October 1957.

TABLE I – EXPERIMENTAL SEQUENCE SUMMARY

Preference Group	Pilot	Training Day	Experiment Day 1	Experiment Day 2	Experiment Day 3
A	S	0_1	0_2	0_3	0_1
(Side-by-side)	T	0_2	0_3	0_1	0_2
	U	0_3	0_1	0_2	0_3
B	X	0_1	0_3	0_2	0_1
(Over-under)	Y	0_2	0_1	0_3	0_2
	Z	0_3	0_2	0_1	0_3

TABLE II – POST EXPERIMENT PILOTS RATINGS* FOR DISPLAY COMBINATIONS

Preference Group	Pilot	Over-Under Placement 0_1	Over-Under Placement 0_2**	Over-Under Placement 0_3	Side-by-Side Placement 0_1	Side-by-Side Placement 0_2	Side-by-Side Placement 0_3
A Side-by-side	S	4	2	6	3	1	5
	T	1	5	3	2	6	4
	U	6	2	4	5	1	3
	Sub Total	11	9	13	10	8	12
	Group Total		33			30	
B Over-under	X	5	1	2	4	6	3
	Y	5	1	3	6	2	4
	Z	4	6	5	1	3	2
	Sub Total	14	8	10	11	11	9
	Group Total		32			31	
Conditions Total		25	17	23	21	19	21

* Most preferred was 1 and least preferred was 6.

** Map orientations

0_1 = North-up with moving aircraft symbol

0_2 = Aircraft heading up

0_3 = North-up with moving map

TABLE III – ANALYSIS OF VARIANCE – LATERAL SCORES

	SS[1]	dF[2]	MS[3]	F
Map Orientation (O)	4,610	2	2,305	< 1
Display Location (D)	37	1	37	< 1
Wind (W)	270,512	1	270,512	47.72**
Pilots (P)	64,687	5	12,937	14.39**
Groups[t]	54	1	54	< 1
O x D	214	2	107	< 1
O x W	2,392	2	1,196	1.60
D x W	33	1	33	< 1
O x P	23,523	10	2,352	2.62**
D x P	2,838	5	568	< 1
W x P	28,341	5	5,668	6.30**
O x D x W	599	2	299	< 1
O x D x P	7,788	10	779	< 1
O x W x P	7,475	10	747	< 1
D x W x P	4,573	5	914	1.02
O x D x W x P	9,370	10	937	1.04

t = Separate test
1 = Sum of squares
2 = Degrees of Freedom
3 = Mean square
** = Significant at .01 level

TABLE IV – ANALYSIS OF VARIANCE – VERTICAL SCORES

	SS[1]	dF[2]	MS[3]	F
Map Orientation (O)	97.6	2	48.8	1.25
Display Location (D)	4.2	1	4.2	1.99
Wind (W)	504.2	1	504.2	22.35**
Pilots (P)	1,113.1	5	222.6	55.59**
Groups[t]	80.7	1	80.7	< 1
O x D	4.1	2	2.0	1.33
O x W	.9	2	.4	< 1
D x W	1.2	1	1.2	< 1
O x P	390.2	10	39.0	9.74**
D x P	10.4	5	2.1	< 1
W x P	112.8	5	22.6	5.63**
O x D x W	16.0	2	8.0	1.36
O x D x P	15.3	10	1.5	< 1
O x W x P	17.9	10	1.8	< 1
D x W x P	45.6	5	9.1	2.28*
O x D x W x P	58.5	10	5.9	1.46

t = Separate test
1 = Sum of squares
2 = Degrees of Freedom
3 = Mean square
* = Significant at .05 level
** = Significant at .01 level

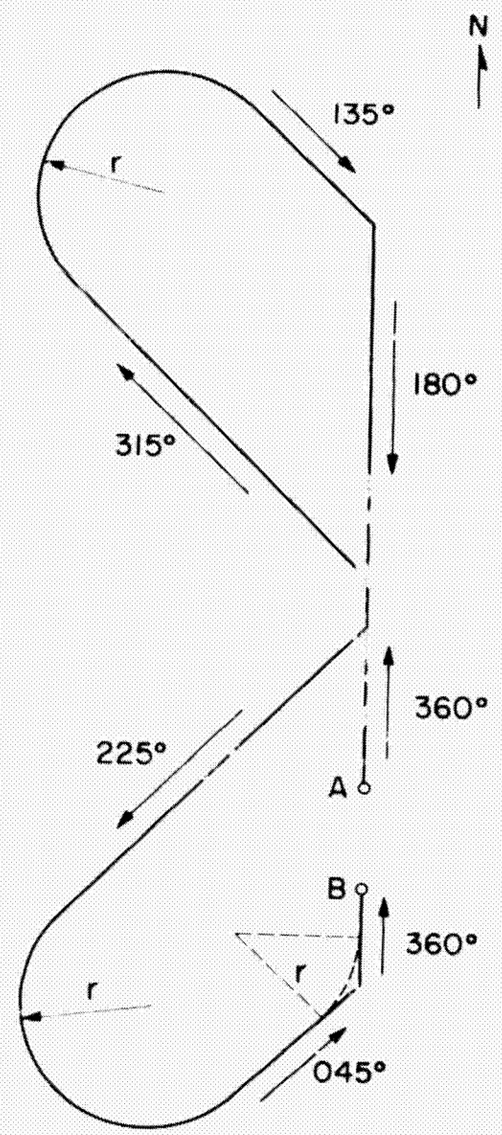

Figure 1. Reference ground trajectory.

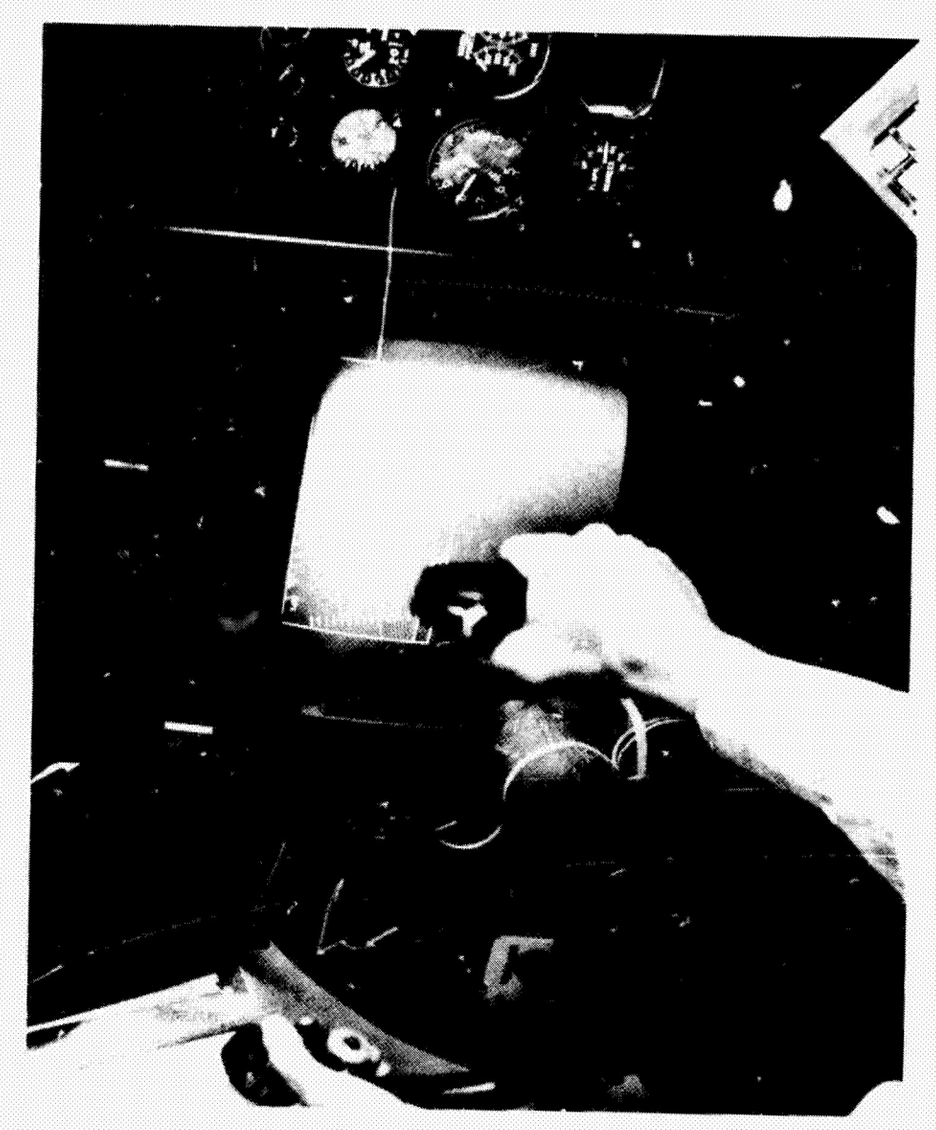

Figure 2. Simulator interior.

ORIGINAL PAGE IS
OF POOR QUALITY

ORIGINAL PAGE IS
OF POOR QUALITY

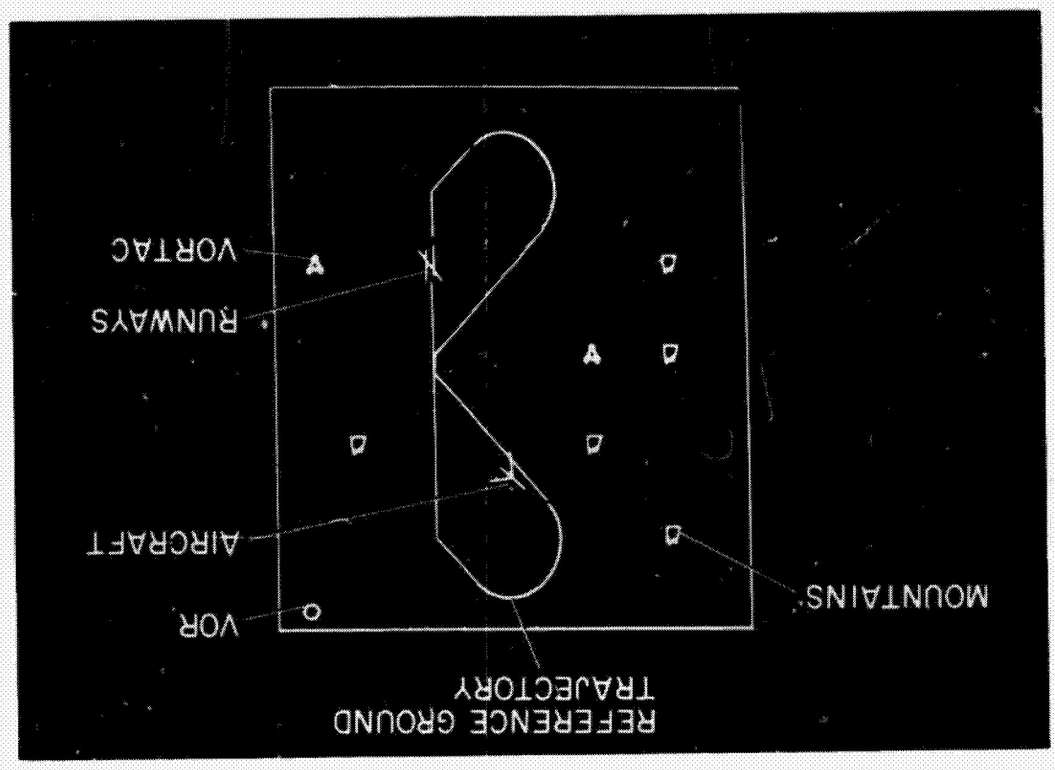

Figure 4. Elements of the horizontal situation display.

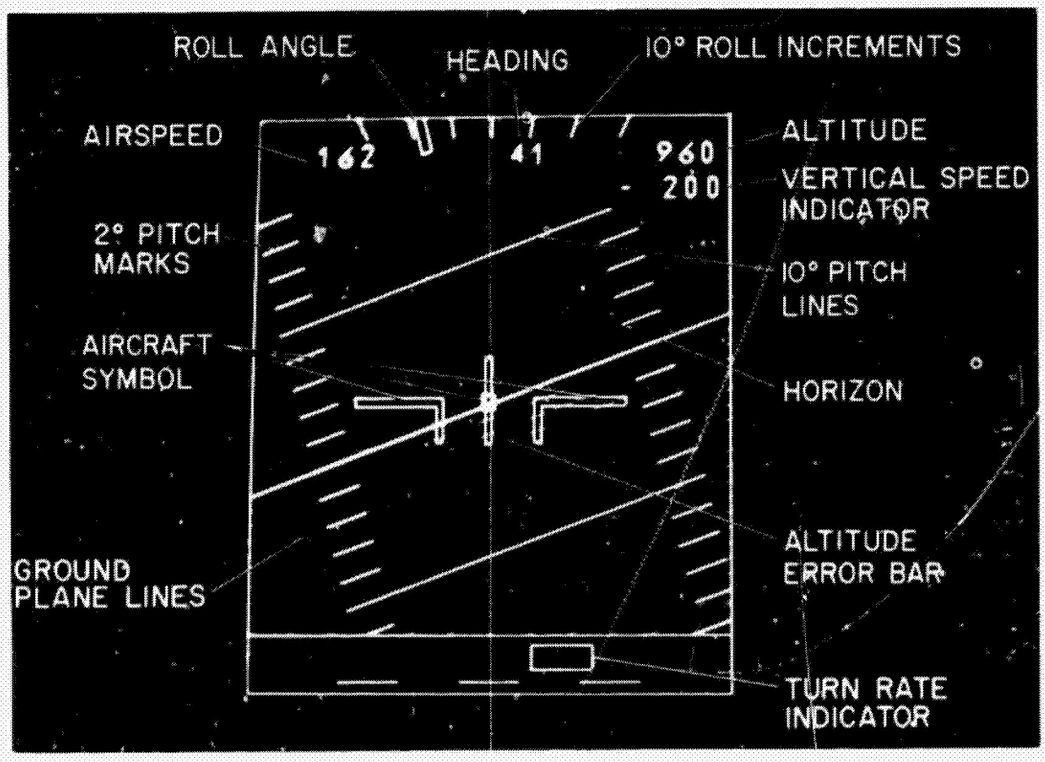

Figure 3. Elements of the vertical situation display.

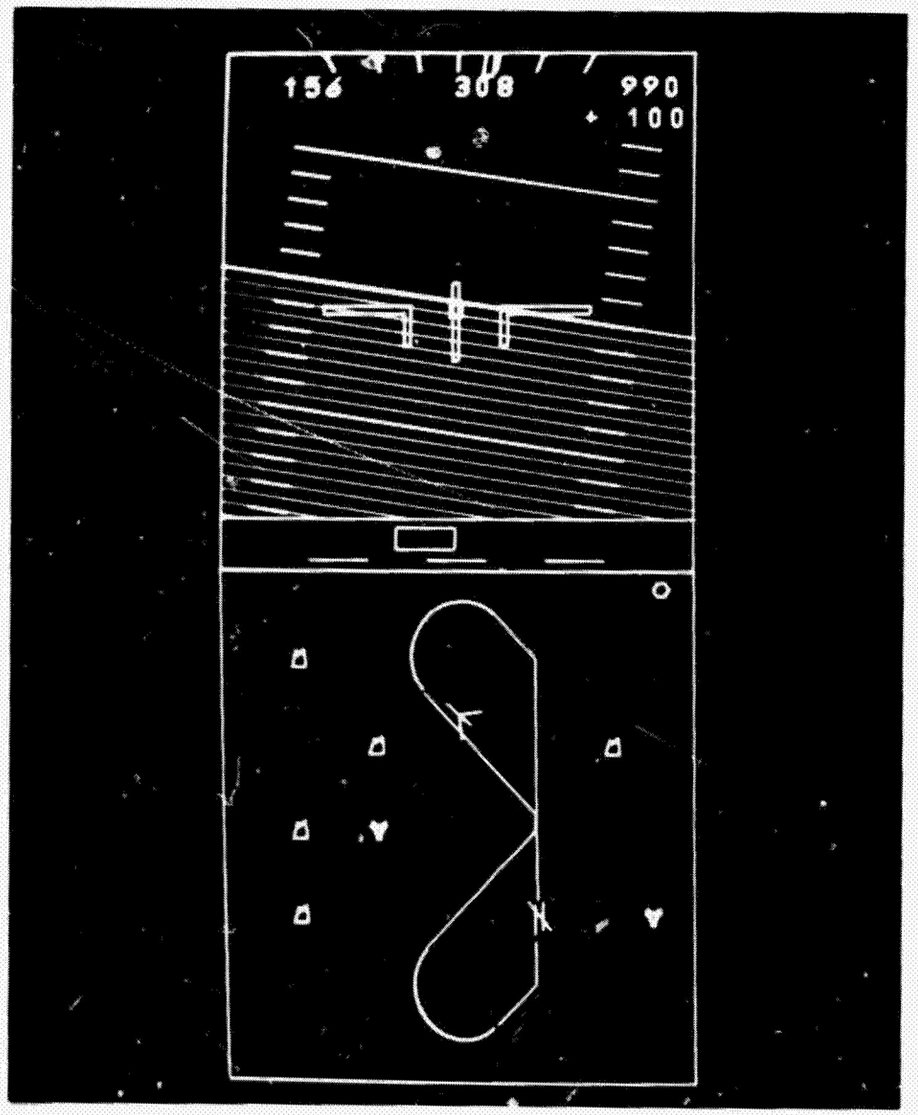

Figure 5. Over-under displays, north-up fixed-map.

ORIGINAL PAGE IS
OF POOR QUALITY

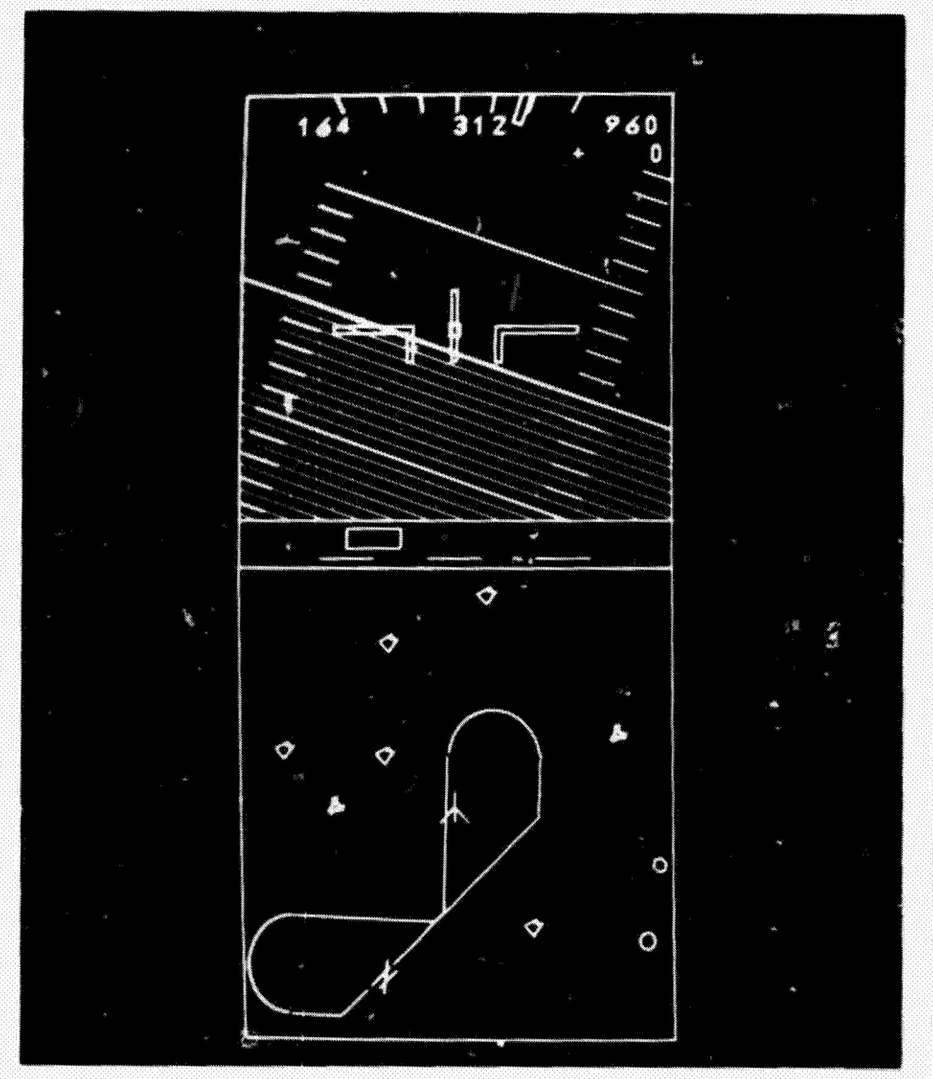

Figure 6. Over-under displays; aircraft heading up — translating and rotating map.

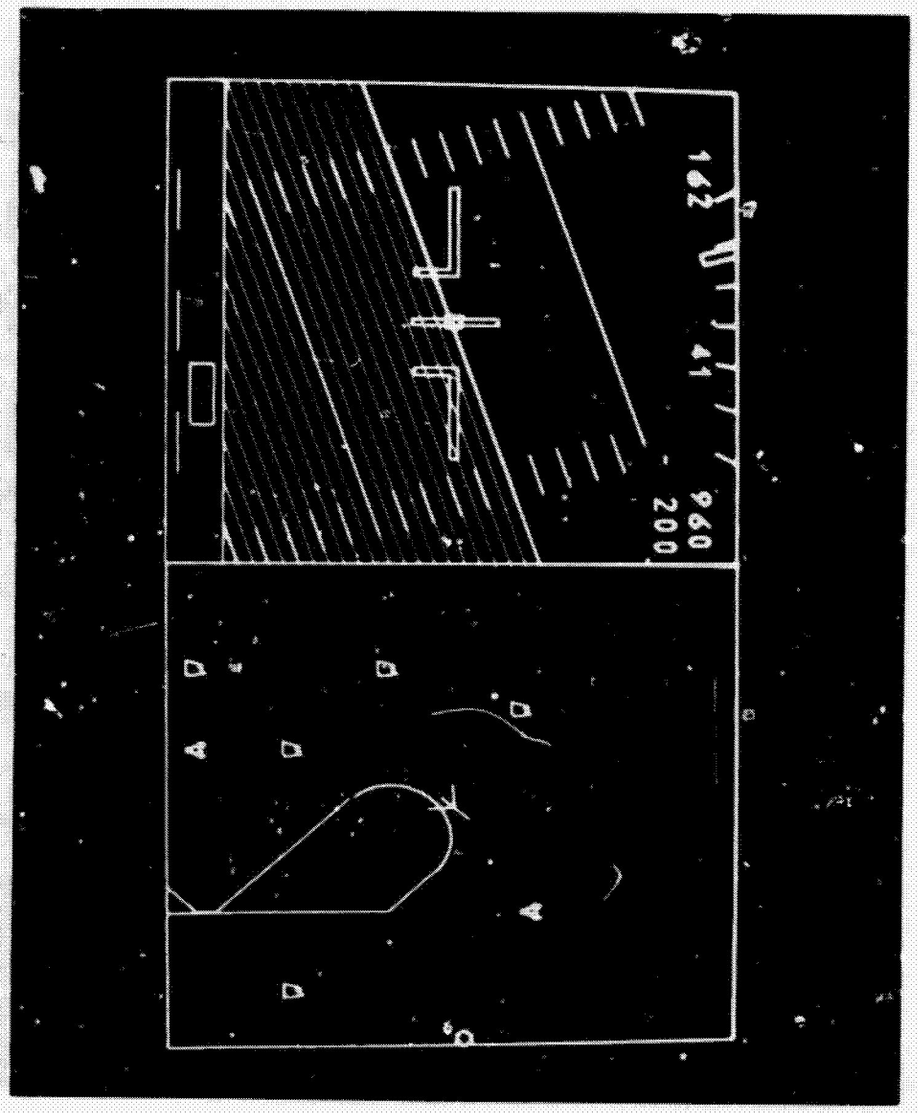

Figure 7. Side-by-side displays; northup translating map.

NAME _____ DATE _____

DISPLAY LOCATION PREFERENCE

Below are three pairs of relative display locations or orientations. For each pair choose the display orientation you prefer. If you have no reason for choosing either one then mark "No Preference." ℄ refers to the location of the pilot's center line-of-sight.)

1.

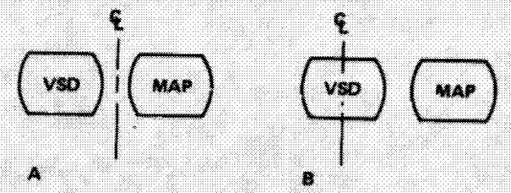

Prefer A _____
Prefer B _____
No Preference _____

2.

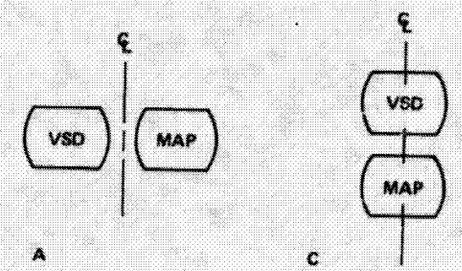

Prefer A _____
Prefer C _____
No Preference _____

3.

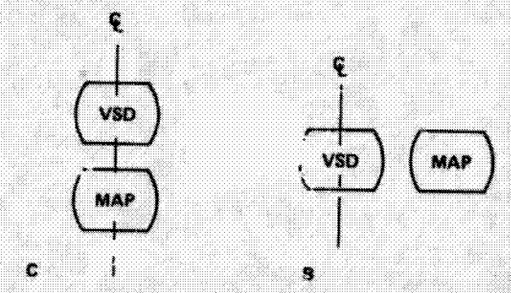

Prefer C _____
Prefer B _____
No Preference _____

Figure 8. Pre-test comparison section of pre-experiment questionnaire.

Figure 10. Two atypical runs — pilot Y.

Figure 9. End-of-flight results.

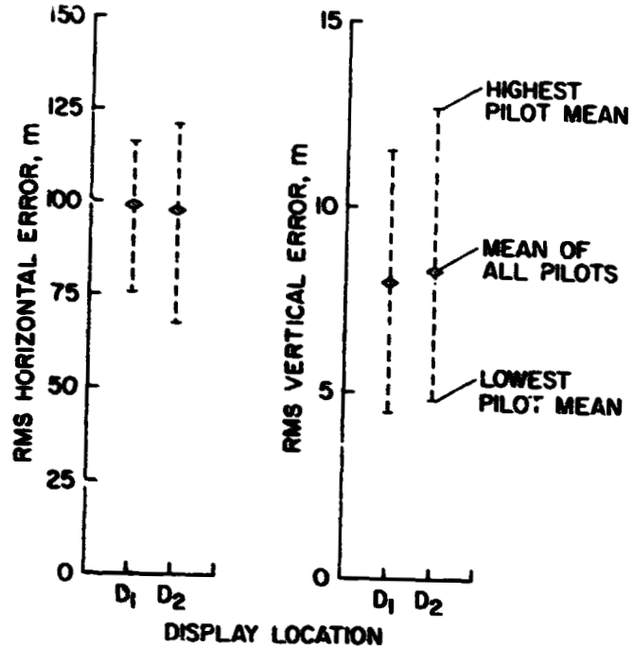

Figure 12. Pilot performance – two display locations – six pilots.

ORIGINAL PAGE IS
OF POOR QUALITY

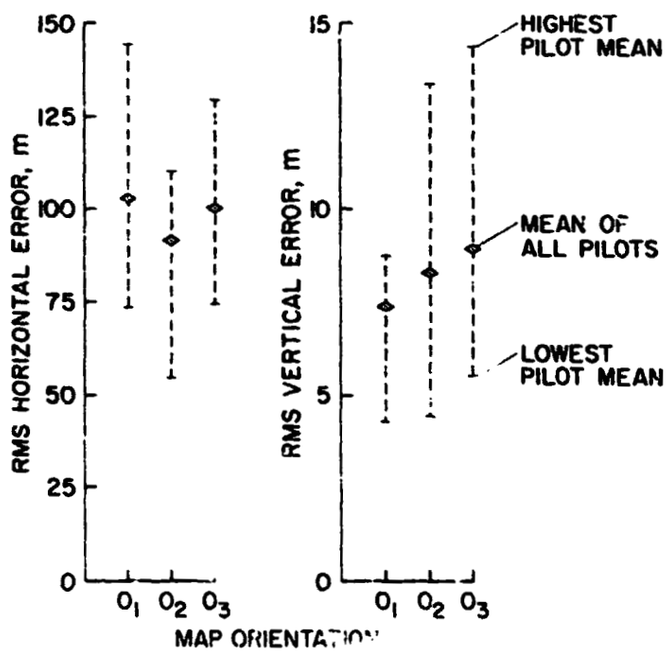

Figure 13. Pilot performance – three map orientations – six pilots.

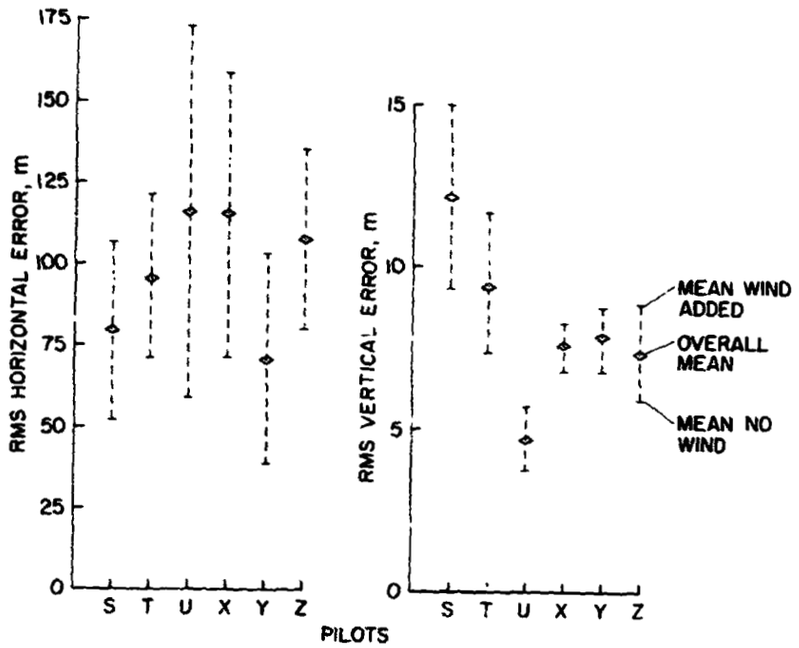

Figure 14. Individual pilot performance -- with and without wind.

ORIGINAL PAGE IS
OF POOR QUALITY

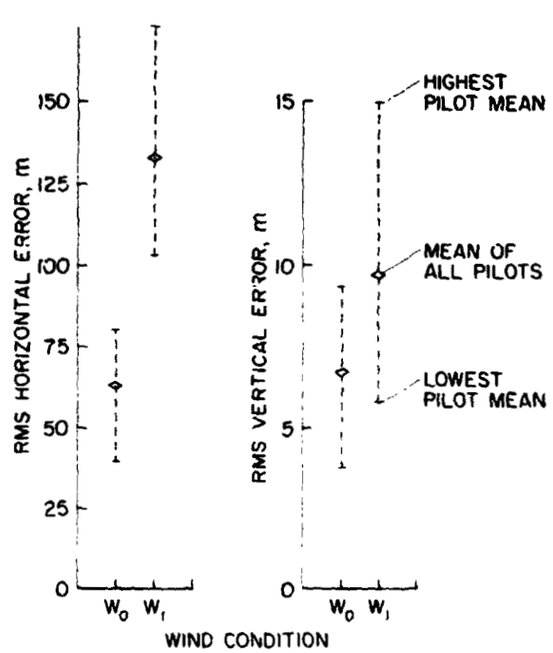

Figure 13. Pilot performance with and without wind -- six pilots

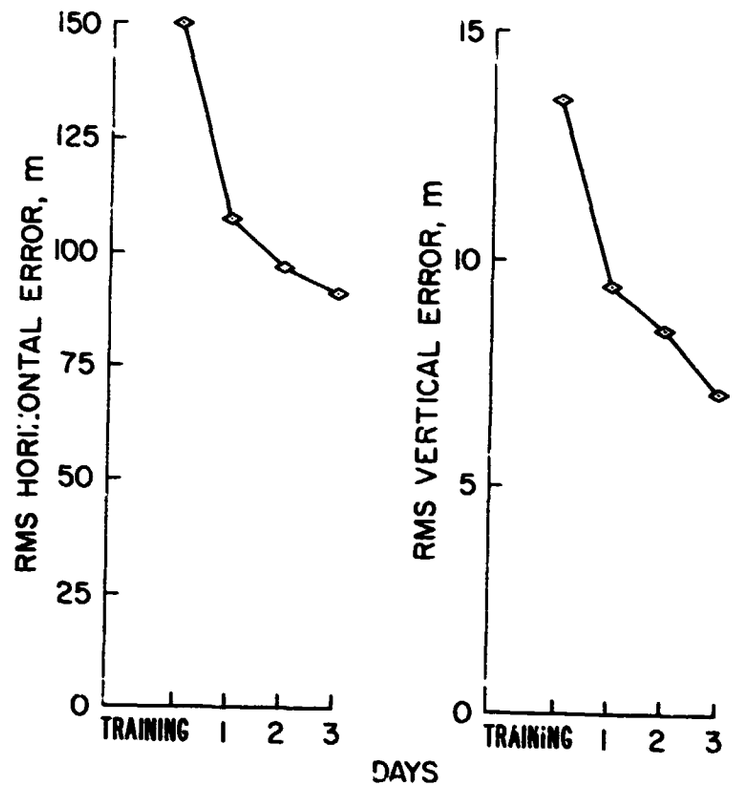

Figure 16. Overall mean performance for sequential days – six pilots.

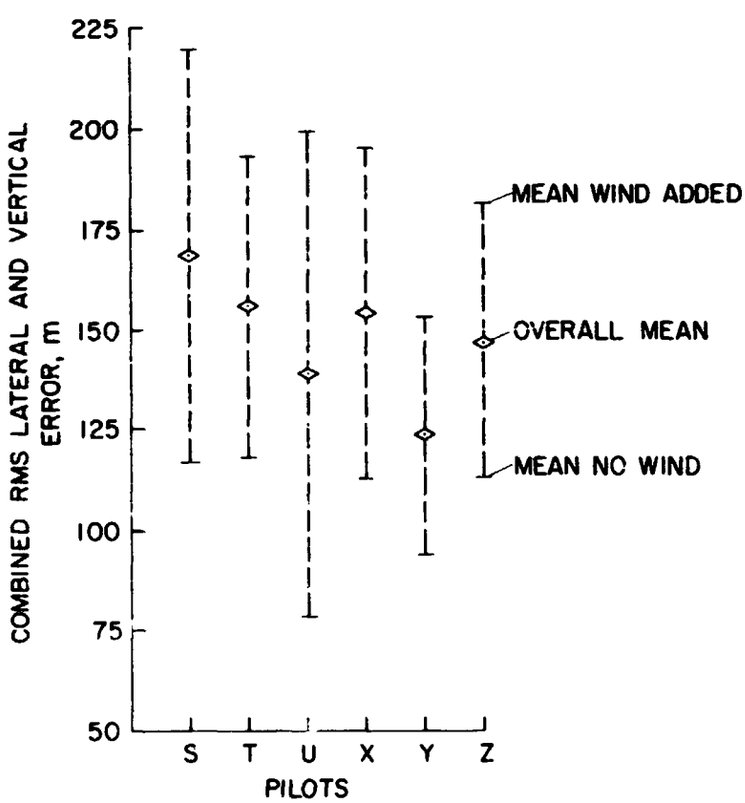

Figure 15. Weighted lateral and vertical performance

THE EFFECT OF COMMUNICATIONS AND TRAFFIC SITUATION DISPLAYS ON PILOTS AWARENESS OF TRAFFIC IN THE TERMINAL AREA

D. Melanson*, R.E. Curry*, J.D. Howell**, and M.E. Connelly***

Massachusetts Institute of Technology

ABSTRACT

The Air Traffic Control (ATC) system is evolving under a general plan specified by the Federal Aviation Administration. Among the developments being considered is the Discrete Address Beacon System (DABS). The use of this system, although relieving congestion on the communications frequencies, would eliminate informatyion about other aircraft because the "party line" communications now in use would be lost. One alternative to restore this lost information is an Airborne Traffic Situation Display (TSD). Having been requested to evaluate the "assurance" that this display gives the pilot, we defined assurance to be equivalent to awareness, which is true for the majority of pilots. Experienced airline and military pilots participated in a factorial design to evaluate two types of communication (discrete address, party line) and two types of displays (TSD, no TSD). A stop-action quiz was used to evaluate their knowledge of other aircrafts' position, altitude, speed, heading, rate of climb, identity, and landing sequence number. Significant differences between conditions were detected, primarily in the position variables. Workload, as measured by a spare capacity side-task, showed a main effect of displays and a significant interaction between displays and communications. The data are summarized by plotting each display/communication condition configuration in the plane defined by information and workload index. A limited number of blunders by other aircraft were included in the simulations with a significant, but not entirely satisfactory, improvement in blunder detection attributed to the TSD.

* Man-Vehicle Laboratory
** Flight Transportation Laboratory
*** Electronic Systems Laboratory

N75 19129

I. INTRODUCTION

Background

The basic idea of presenting an onboard pictorial display of traffic information is not new. This was introduced as early as 1946 by RCA in their TELERAN program (RCA, 1946). In 1963, the FAA conducted simulations using a cockpit display (Sluka, 1963), and more recently in 1966, an effort to provide televised radar pictures for pilots was tested in the Boston area under the direction of the FAA (FAA, 1966). A priori investigations declare that definite advantages for the air traffic control (ATC) system could be derived from such information, but that the attention span required to derive enough information from a rather poor quality of display was too high. What these initial efforts lacked was the ability to provide the essential elements of information about traffic in an easily discernable format for quick interpretation by the pilot. The advent of computerized radar tracking systems in the terminal area and computer-generated displays now overcomes this previous drawback with symbolic and alpha-numeric presentation of traffic information in an appropriate format.

One approach to the presentation of this information is presented by Bush et al (1970) where it is assumed that a Traffic Situation Display (TSD) could be devised that would make portions of the NAS/ARTS (National Airspace System/Automated Radar Terminal System) computerized data base available to the air crew by an omnidirectional broadcast of traffic information throughout the terminal area. This information would be received by all aircraft equipped with a TSD and onboard processing would be performed to present a symolic representation with either a north-up or heading-up display format.

Three academic research labs at M.I.T. participated in the design and construction of a fixed-based simulator to evaluate the concept of a Traffic Situation Display with flexible format

under pilot control. A basic evaluation of the concept with the new display techniques has been completed (Imrich, 1971) with initial indications that several aspects of air traffic control can be improved through implementation of such a cockpit display. Furthermore, it was found that these improvements can reduce radar controller workloads significantly by increasing air crew participation in ATC functions. Other studies (Anderson, 1971) examined the effect of different display formats on pilot's scan workload and ability to follow other aircraft in trail.

Because a pictorial traffic situation display has the capability of presenting both navigation information and traffic situation information at a glance it became of interest to determine whether or not such a display would increase the overall flow rate of traffic within the terminal area under Instrument Meteorological Conditions (IMC) as compared to Visual Meteorological Conditions (VMC). Aircraft separations of about 2 or 3 miles are maintained during VMC by direct sightings; during IMC, the air traffic controller is responsible for maintaining separations and these are on the order of 5 miles. Thus the TSD has the potential for giving the pilots information nearly equivalent to VMC under IMC, with the attendant potential for increasing landing rate by reducing separations.

Scope of the Present Work

Whether or not the pilots can maintain separations with a TSD depends largely on the type and quality of information that the pilots have about their position relative to the ground and other aircraft. To evaluate the information transfer, we have undertaken a set of simulation studies to determine the type of information that the pilot has with respect to his navigation and traffic situation within the terminal area. The information the pilot has about his own aircraft and those surrounding him seems to be of general interest, and to our knowledge, this is the first time that a quantitative study has been undertaken. We evaluated the information transfer under four major treatment conditions resulting from the factorial combination of with and without TSD and with shared communications channel and discrete address commands. No display, shared communications corresponds to the present day air traffic control system and provides a convenient base line for comparison purposes. No TSD, discrete address commands corresponds to the case where the pilot receives only the commands directed towards his aircraft as will be the situation under the Discrete Address Beacon System. TSD, discrete address commands corresponds to the situation where a display is added to the DABS, whereas, TSD, shared communications corresponds to the information situation that would exist if the TSD were added to the present day ATC system.

The original request og the sponsoring agency was the evaluation of the TSD as an "assurance" device. To do this, we have here equated assurance with awareness. We have defined, for the purpose of this investigation, awareness to consist of the following elements:

1. The pilot's knowledge of his current position with respect to the air route structure
2. The pilot's knowledge of the position of other aircraft around him
3. The pilot's ability to predict the evolution of the traffic situation in the short term (especially the evolution of abnormal situations)
4. The pilot's ability to choose appropriate escape routes should an emergency occur.

The simulations, then, were designed to evaluate these facets of awareness under the four display/communications conditions described above.

II. SIMULATION FACILITIES

Cockpit

The basic component of the simulation facility is a fixed-base cockpit simulator that uses three cathode ray tubes to

produce the primary flight instruments and a TSD. The basic cockpit was built from an SST prototype donated by the Boeing Company, and the interior panels, assorted switches, and instrumentation facsimiles are representative of a Boeing 707-123B aircraft. An ADAGE AGT-30 digital computer with 16K core memory and a two microsecond cycle time was used to simulate the aircraft dynamics and perform calculations for the displays.

The aircraft dynamics are representative of a Boeing 707 aircraft; the flight instrument package is patterned after a Collins FD-109 integrated flight system but does not have the flight director. The flight control system simulates control wheel steering (an attitude rate command system) as is available on the newer wide-body jets. This not only provides a uniform flying workload for either maintaining or changing altitudes, but in addition, it is felt that the attitude control task with control wheel steering in a fixed base simulator (no motion cues) is comparable to that with conventional controls in a moving base simulator.

The experiment was conducted by the simulated air traffic controller in an adjacent room. Communications between the pilot-subject and the controller were accomplished through the use of standard head sets and intercom lines. Responses from other aircraft in the traffic scenarios were stored sequentially on a tape recorder and played back in response to the controller commands. The cockpit, controller, display, computer and associated hardware are shown in block diagram form in figure 3.

Traffic Situation Display

The TSD was presented in the simulator by a cathode ray tube masked to a 7" square size. The CRT was mounted to the instrument panel where the weather radar is normally located in a Boeing 707. The display presentation was a heading-up own-ship centered format with a four second display information update rate (Figure 4). Traffic elements were shown as small circles with points at the centers. Each element was trailed by three dots that marked the past position of that aircraft (12, 24 and 36 seconds previously). Associated with each traffic element was the NAS/ARTS data block showing aircraft identification, altitude in hundreds of feet, and ground speed in knots; the own-ship data tag had only ground speed readout. Also displayed on the CRT were navigation stations, route structure, and ground features, providing the pilot with a pictorial display of his geographic position.

The display controls were mounted to the left of the CRT and allowed the pilot to select the amount of traffic and map information by adjusting the volume of displayed airspace and limiting the amount of alpha-numeric readouts for each aircraft. The major controls were an altitude layer above and below the subject aircraft within which traffic would be displayed and ranges of 4, 8, 16, 32, 64, and 128 nautical miles. A typical group of settings used during ascent and approach phase was 15 nautical miles range, and a display of other aircraft within 1000 feet above and 5000 feet below the subject aircraft.

The presence of the alpha-numeric readout was controlled by four toggle switches, which could selectively eliminate identification, ground speed, altitude, and the tracer dot feature of the other aircraft. These combinations would allow the pilot to minimize clutter and to have high resolution in the area of special interest to him.

III. METHODS

Subjects

The participants who flew the simulator for the data runs were all professional pilots. Most were licensed air carrier pilots; others were military personnel and/or general aviation pilots with instrument ratings. All subjects participated on a voluntary basis. Of the twenty subjects used in the data runs, the minimum flight time was 1800 hours, all but three had over 4000 flight hours, and eleven had over 10,000 flight hours.

All participants were given a nominal three hour training session prior to performing in the data runs. In the training run, the subject was required to fly landing approaches to Logan Airport, while establishing and maintaining proper sequencing and precise spacing intervals on the preceding aircraft. A subject was considered adequately trained when he demonstrated proficiency in maintaining a specified spacing interval of 0.1 nautical miles and when he agreed that he could at least maintain this proficiency through the subsequent evaluation series at a later date. Those candidates who felt that they needed more than one training session to gain this proficiency were given that opportunity, and three of the subjects took advantage of this opportunity.

Experimental Conditions

As was described in the introduction, there are four experimental conditions resulting from a 2 x 2 matrix of display/communications possibilities: with and without TSD and simultaneously discrete or shared communications. Henceforth, a display/communications condition will be denoted by X-Y, where X is either T or $\overline{T}$ corresponding to TSD or no TSD and Y is D or S corresponding to discrete and shared communications, respectively.

Except for a subset of experiments with four subjects which were arranged in a Latin Square configuration, the D/C conditions were not arranged in a balanced experimental design. This resulted from the fact that our interest was primarily in determining the amount and type of information that the pilots had about the other aircraft and their ability to detect and resolve blunders, and the $\overline{T}$-D congiguration resulted in no information to the pilot about other traffic. Thus we concentrated our effort on those D/C approaches in which information was available.

Seven approach simulations were developed providing different dynamic preprogrammed traffic situations at Logan Airport. Four featured merging streams of traffic to a single runway and three featured independent approaches to parallel runways spaced only 2600 feet apart. For each of the single runway simulations four different communication dialogues were prepared corresponding to the four D/C combinations. Thus any D/C combination could be used with any of these single runway simulations. For the parallel runway set of traffic situations, only two communication dialogues were prepared to represent the conditions of T-S and T-D. Simultaneous independent approaches to runways separated by less than 5000 feet are illegal under today's ATC regulations. An effort was made to evaluate the possibility that the TSD would contribute to the pilot's acceptance of closely-spaced parallel runways. Thus the dialogues without the TSD were not of primary interest for these simulations.

Scenario Development

In each of the seven basic traffic simulations, all the aircraft conformed to the Standard Terminal Arrival Route (STAR) chart constructed for this work. The transition routes appeared on the TSD along with the three fixes and the two ILS (Instrument Landing System) courses for runways 04 left and 04 right. Prior to each data run, the subject was briefed on his position, responsibilities, and tasks, and the D/C system being simulated. Responsibilities and tasks were of two general types:

> Without TSD - subject to fly from holding fix to localizer in accordance with step-by-step commands from the radar controller.
>
> With TSD - subject to fly from holding fix to localizer on designated STAR, achieving and maintaining spacing from preceding aircraft as initially specified by the radar controller.

The primary difference, and one that we feel has an influence on the results of the experiment, is that the subject must acquire and maintain a desiganted spacing from another aircraft, whereas this task is not required in those runs made without the TSD. To verify this, data from a follow-up study (Melanson, in preparation) taken under the T-D format but without the spacing task is included.

To distinguish between these two groups, the notation T-D(SP) and T-D($\overline{SP}$) is used to differentiate the T-D treatments with and without the spacing task, respectively.

Each data run began with a formal clearance which included a weather summary read by the air traffic controller. The simulation was begun once the correct response was given. The controller then, if the treatment warranted it, read a series of commands intermittently directing the pre-programmed targets and the subject in the simulator. The commands were timed to fit the pre-programmed trajectories, and were sequenced by referring to a stop-watch. Responses from the program targets were played back from a tape recorder, while the dialogue with the subject was, of course, live.

Stop-Action Quiz

One of the primary goals of this investigation was to determine the type of information that the pilot had about other traffic within the terminal area. A stop-action quiz was used to evaluate this type of information. When the situation had developed to the extent that a reasonable amount of information had been presented to the pilot and the traffic density was approaching maximum, the simulation was halted without warning. A given situation was always halted at the same point for all subjects. Presentations on the CRTs were blanked. The pilot was then required to complete the quiz on a map shown in Figure 5. The pilot was asked to supply the following information about each aircraft in the traffic situation: position, identification, landing sequence number, heading, ground speed, altitude, and 'attitude', i.e. climbing, descending, or maintaining altitude. These maps were the primary source of quantitative information in the results described below.

The stop action quiz responses were graded for accuracy and completeness. Errors in subject estimates of information components were recorded. Those components which could be graded on a right or wrong basis (i.e. identification, landing sequence number, and attitude) were scored on a point system. Correct responses received a positive point score, while incorrect responses received a negative point score. Position error was defined as the pilot's estimate of the position of aircraft including his own, with respect to the route structure. For all other information components a component error was computed by subtracting the estimated value form the true value of the particular component. Thus both positive and negative errors were possible. Those cases where it was obvious that the subject's estimate for a given aircraft had it originating from the wrong holding fix, were scored as gross errors. Missing entries were recorded as null responses.

Spacing error was measured to determine the pilot's accuracy in estimating the other aircraft positions with respect to his own craft. It was computed in the same manner as the other information components.

Blunder Detection

Four of the seven traffic situations culminated with intrusions by other aircraft in the subject's airspace. Each intrusion was due to some abnormal event, and evidence of those events was provided to the pilot through each of the D/C conditions prior to the pause for the stop-action quiz. The subjects were required to specify on the quiz whether or not the traffic situation was normal. If the blunder intrusion had not been detected before the quiz when the subject was using the TSD, the simulation was continued until either the controller was notified of an intruder, or until the point of closes approach had been reached. If the blunder had not been detected before the quiz and if the TSD was not being used, there was little likelihood that the intrusion could be detected subsequent to the quiz and the simulations were not continued. Two of the conflict scenarios occurred during single runway approach situations, while the other two occurred during independent operations on closely spaced parallel runways.

One of the single runway approach conflicts was the misinterpretation of a heading change instruction from the approach controller. This resulted in a potential collision abeam of the subject's own aircraft which at the time was flying on the ILS. This blunder could be monitored in all the treatment conditions except $\overline{T}$-D since the erring pilot read back the wrong heading.

The second single runway conflict consisted of a radio failure and subsequent failure to turn to a new heading, thus bringing the intruding aircraft into a head-on collision course with the subject's aircraft.

The parallel runway conflicts were both essentially ILS crossover blunders. The first conflict had the intruding aircraft overshooting his ILS and acquiring the subject's ILS. The second blunder had the intruding aircraft veering sharply from his ILS towards the subject aircraft after both craft had passed the outer marker.

Workload Measurements

Four of the subjects participated in a standard Latin Square counterbalanced for order effects. These subjects participated in four runs, one for each of the possible D/C combinations. A low intensity light was placed at a point which subtended equal visual angles from the center of the primary flight instruments and the TSD. An auxilliary self-paced task was presented to the subjects by having them extinguish the light whenever they noticed that it was on. The light would come on at random intervals (mean of 10 seconds after it was last extinguished) and the subwould respond by tripping a switch on the control wheel. The measure of workload was taken as the response latency in extinguishing the light when compared with the mean "unloaded" response latency obtained when the subject fixated on the center of the primary flight instruments and was performing no other tasks.

IV. RESULTS

Information Components

This section summarizes the results of the stop-action quiz (SAQ) for the various information components, thus addressing the first two points of the presented definition of pilot awareness (and consequently, pilot assurance). The data is presented in such a way as to show general trends in the pilot's ability to estimate aircraft information components as a function of relative landing sequence (RLS), which is defined as follows: All aircraft in the landing sequence are indexed with respect to the subject's aircraft which is "0". The aircraft just ahead of the subject in the sequence is designated as "+1", while the aircraft just behind is designated "-1". The aircraft two slots ahead and behind in the sequence are indexed "+2" and "-2", respectively, and so forth. Generally, there were four or five aircraft including the subject in the landing sequence ranging from -1 to +3; however only the -1 through +2 aircraft will be considered here.

The manner in which the data is summarized reflects the assumptions that were made during analysis. These assumptions were:

1) The four scenarios used during the experiment were representative of the entire ensemble of possible scenarios.
2) All subject-pilots were representative of a homogeneous group of equal abilities and motivation.

It is realized that this data summary format obscures some of the more subtle aspects of information component estimation; however it does provide a means by which the treatment conditions can be compared.

Data summary tables consisting of the mean error, standard deviation and percent null responses as a function of relative landing sequence have been prepared for the position, spacing, altitude, ground speed and heading information components

(see tables 1-9). In addition, composite graphs for the comparison of mean error responses as a function of RLS for these information components have been generated. Similar composite graphs have been developed for null responses and gross errors (Figures 7-13).

To determine statistical significance, a simple analysis of variance was performed between aircraft (RLS) for a given treatment condition and between treatment conditions for a given aircraft. The results of this analysis are summarized in Tables 6 and 7. Statistical variation was judged as either not significant (n.s.), significant at the five percent level (5%), or significant at the one percent level (1%) using standard F ratio tables. The data for the identification, landing sequence and altitude are not summarized here but are discussed later.

Blunder Detection

The blunder detection results for the single runway approach scenarios and the parallel runway approach scenarios are collected in Tables 8 and 9. Contingency tables indicating the statistical significance between treatment conditions with and without the TSD and with and without the spacing task are shown in Tables 10 and 11.

The $\overline{T}$-S, T-D(SP) and T-D($\overline{SP}$) treatment conditions were tested in the first blunder case while the T-S and T-D($\overline{SP}$) were used in the second.

For the single runway case the table indicates how many subject-pilots detected the conflict before or at the stop-action quiz (SAQ) as well as before or at the closest point of approach (CPA).

For the parallel runway case, the number of detections at or before the uncorrected CPA for each treatment condition tested (T-D(SP) and T-D($\overline{SP}$)) is recorded. The uncorrected CPA is taken to be the closest point of approach of the intruding aircraft had the subject not performed an avoidance manuever.

Workload Measurement

The statistics for the perceptual sidetask response latencies are presented in Figure 14 for each of the treatment conditions tested ($\overline{T}$-D, $\overline{T}$-S, T-S, T-D(SP)) plus the unloaded (UNL) condition. A logarithmic transformation was done on each response delay in order to normalize the reaction time distribution. The mean log response times and standard errors were then transformed back to a linear scale.

A workload index (WI) was defined as

$$WI = 1 - M_{UL}/M_L$$

where M_{UL} was defined as the mean unloaded response time for the particular treatment condition in question and M_L was defined as the mean loaded response time. A higher value of WI indicates a higher workload level.

A graph of WI versus information (INF) is plotted in Figure 15. Here information is defined as

$$INF = 1/\bar{e}^2$$

where $\bar{e}^2$ is the mean squared spacing error taken over all aircraft. The units of INF are therefore (nautical miles)$^{-2}$.

V. DISCUSSION

Information Components

The quality of information component responses is highly dependent upon the accuracy and completeness of the pilot's internal model of the air route structure and traffic environment

and the information sources available to him. The shared communications channel allows the pilot to monitor air traffic control (ATC) radio transmissions. These transmissions give the pilot specific indications of the information components of the surrounding aircraft. A communication concerning any given information component of any given aircraft occurs rather infrequently. In fact such a transmission occurs only when a change in that component is desired by the approach controller. The lack of visual presentation of information requires that the pilot use his memory for the storage of the information components. Moreover, if the pilot has no other means of monitoring traffic motion, he must assume that each aircraft is following instructions. This assumption is not always justified, especially in the case of blunders.

The TSD on the other hand, provides the pilot with a nearly continuous source of information, but by its nature requires that the pilot specifically seek out a desired information component. In addition, the display acts as an auxiliary memory, thus eliminating the necessity of memorizing information components.

The addition of the shared communication channel information source to the TSD presentation augments information transfer by providing a periodic readout of commanded information component values, i.e. changes in these values. The pilot can then compare these commanded values with the actual values and can therefore confirm that the other aircraft are behaving correctly. In addition, verbal cues such as a heading readback error or a failure to reply to a transmission, can be used to draw his attention to an abnormal situation.

Requiring the pilot to performaa spacing task with respect to the +1 aircraft has a tendency to focus most of the pilot's attention on that aircraft. This fact is most evident in the T-D (SP) treatment as indicated in the composite graph for the mean position error and the position null responses (Figures 7 and 8). When the spacing task is removed, as is the case for the T-D($\overline{SP}$) treatment, position estimation accuracy becomes a monotonically decreasing function of landing sequence. The null response curve retains the same basic form, but the number of null responses for the -1 and +2 aircraft decrease while those for the -1 aircraft increase slightly.

The mean position response plot tor the T-S treatment which also has a spacing task does not follow the same trend as the T-D(SP) treatment, however a comparable null response pattern occurs. It is believed that communication transmissions concerning the -1 and +2 aircraft which occur prior to the stop-action quiz and which place these aircraft leaving a holding fix (-1 aircraft) and acquiring the ILS (+2 aircraft) aid the pilot in estimating the positions of these craft.

As a consequence of the air route structure used in the simulations, the other information components (altitude, ground speed, and heading) change rather infrequently and in a generally predictable way (except of course for abnormalities). When these components change to their new values, however, they usually change fairly rapidly, thus requiring a high sampling rate on the part of the pilot in order to effectively monitor these changes. The increased sampling rate is clearly impossible under the $\overline{T}$-S treatment, but is possible when the TSD is employed.

It happens that at the time of the SAQ, some information parameters of some aircraft are in transition, while others are relatively stable. The errors in the responses for these components reflect this fact (see Figures 7-13). At the time of the SAQ, the -1 aircraft was always descending at a rate of about 2000 fpm, while the +1 aircraft was usually flying straight and level or descending at a slower rate of about 500 fpm. The +2 aircraft was almost always flying straight and level on the ILS but not yet on the glideslope. These facts seem to account for the trends observed in the altitude data.

In the case of ground speed at the SAQ, the -1 aircraft was generally reducing to 1.0 knots. At this point, the +2 aircraft

was usually reducing to 160 knots. At the quiz point during some scenarios, the -1 and +1 aircraft had just turned to a new heading while the +2 craft was established on the ILS (thus making its heading that of the ILS).

Responses to aircraft identification were comparable and quite good for all treatment conditions. This is not surprising since there were only a small number of aircraft in each scenario.

The munber of correct responses to the landing sequence component were comparable and quite high for those cases with the TSD, but were quite poor when the TSD was not employed. This fact strongly indicates the superiority of the visual display in allowing the pilot to extrapolate the evolution of the traffic situation and conversely, the difficulty in doing this on the basis of aural information alone.

The attitude responses showed no discernable trend and the very high number of null responses indicated hhat the pilots did not take this component into consideration or at least thought that it was implied in the other information components.

Blunder Detection

The culprit in the heading command readback error was the -1 aircraft. The $\overline{T}$-S treatment required that the pilots pick up the transmission cue (i.e. the readback error) in order to detect the blunder. If they missed this cue thay would have no other opportunity to detect the conflict. The T-D(SP) and T-D($\overline{SP}$) conditions did not have the communications cue, but they . d allow the pilot to monitor the development of the abnormal situ ion that was a consequence of the readback error.

In the radio failure-track deviation conflict simulation, the intruding aircraft was the +1 aircraft. The T-S treatment provided a communication cue as well as the TSD presentation. The T-D($\overline{SP}$) treatment group did not have the transmission cue.

To the extent that these blunder scenarios are in some way representative, some conclusions can be drawn concerning the pilots conflict detection capabilities under the different treatment conditions. At least during instrument meteorological conditions it seems evident that the TSD provides the pilot with a more effective means of detecting potential conflicts than is currently available to him (see Tables 8 and 10). The addition of the spacing task seems to focus the pilot's attention on the -1 aircraft and therefore detracts from his ability to detect abnormalities associated with the other aircraft.

The only two treatments compared during the parallel runway simulations were T-D (SP) and T-D ($\overline{SP}$). This effectively compared pilot performance both with and without the spacing task.

It would seem apparent (see Tables 9 and 11) that the inclusion of the spacing task detracts from the pilot's ability to monitor the adjacent aircraft effectively by drawing most of his attention from the conflict detection task to the spacing task.

It is recognized that conflict detection in itself is insufficient because enough lead time must be provided in order that the pilot be given an adequate opportunity to execute an avoidance manuever. This important problem is not discussed here, but is reported elsewhere (Howell 1972; Melanson, in preparation).

Workload Measurement

The perceptual workload versus information plot (Figure 15) indicates comparative values of workload and information for the four treatment conditions. Subjects in the $\overline{T}$-D condition had zero information (infinite variance) about aircraft other than their own. Since they did not have to monitor the TSD, their perceptual workload was relatively small.

In the $\overline{T}$-S condition, the subjects had an aural source of information input. As a result, their knowledge of surrounding traffic was improved over that of the subjects in the $\overline{T}$-D condition. Although the $\overline{T}$-S pilots did not have to monitor the TSD, the fact that they were receiving auditory distractions resulted in an increased workload index level.

In the T-D(SP) treatment, subjects had visual but no aural information about other aircraft. In fact, monitoring the TSD for spacing and sequencing tasks was a primary pilot responsibility in this condition. It can be seen that although the pilot's information about his surroundings was susbstantially improved, this improvement was gained at the cost of a significantly higher workload.

During simulations run under the T-S treatment conditions the pilots had both a visual and an aural information source. As a result, the measured information for this treatment was higher than all other treatments and the workload index is high (but lower than the T-D(SP) treatment). The increased information and decreased workload can be attributed, we think, to the addition of redunt aural information leading to less reliance on the visual modality, which was, of course, the same modality as the side task. In an analysis of variance of the response times, the D-C interaction was significatn ($p < .01$), i.e. going from discrete to shared communications without the TSD increases the workload index while going from discrete to shared communications with the TSD decreases the workload index.

VI. SUMMARY AND CONCLUSIONS

We have evaluated the transfer of traffic and navigation information to a pilot in a fixed-base simulation. The experimental conditions were derived from the combinations of with/without TSD and shared/discrete address communications. Dependent variables were the information components of other traffic (position, attitude,etc) scanning workload, and the detection of blunders.

Analysis of variance showed most of the information components to be sensitive to the display-communications configuration and the landing sequence number relative to the subject aircraft for the scenarios and the time of the stop action quiz.

The workload index shows a significant main effect for displays and a significant display-communication interaction (adding shared communications without a display increases workload, but decreases workload when the display is present.)

The ability to detect intruders in the subject's airspace was found to depend significantly on the display condition (with or without). The ability of a pilot to detect a blunder while performing a spacing task is significantly worse than when the spacing task is not required.

REFERENCES

Bush, R.W., Blatt, H., Brady, F.X., A Cockpit Situation Display of Selected NAS/ARTS Data, Lincoln Laboratory Technical Note 1970-39, Lexington, Massachusetts, December 1970.

Feasibility Test of Televised Radar, NAFEC Project 241-023-01X, RD-66-1, Atlantic City, New Jersey, January, 1966.

Howell, J.D., Simulator Evaluation of Pilot Assurance Derived from an Airborne Traffic Situation Display, FAA Report No. FAA-EM-72-3, Cambridge, Massachusetts, February, 1972.

Imrich, Thomas, Concept Development and Evaluation of Airborne Traffic Displays, Flight Transportation Laboratory Report R71-2, Massachusetts Institute of Technology, June 1971.

Melanson, D.W., Pilot Awareness and Conflict Detection Capability Derived from an Airborne Traffic Situation Display, Department of Aeronautics and Astronautics, Massachusetts Institute of Technology, Master of Science Thesis, June 1973.

Radio Corporation of America, TELERAN, Camden, New Jersey, September, 1946.

Sluka, A.L., Dynamic Simulation Studies of Pictorial Navigation Displays as Aids to Air Traffic Control in a Low-Density Terminal Area in an En-Route Area, NAFEC Project FAA-115-703X, AD-608 952, Atlantic City, New Jersey, February, 1963.

ORIGINAL PAGE IS
OF POOR QUALITY

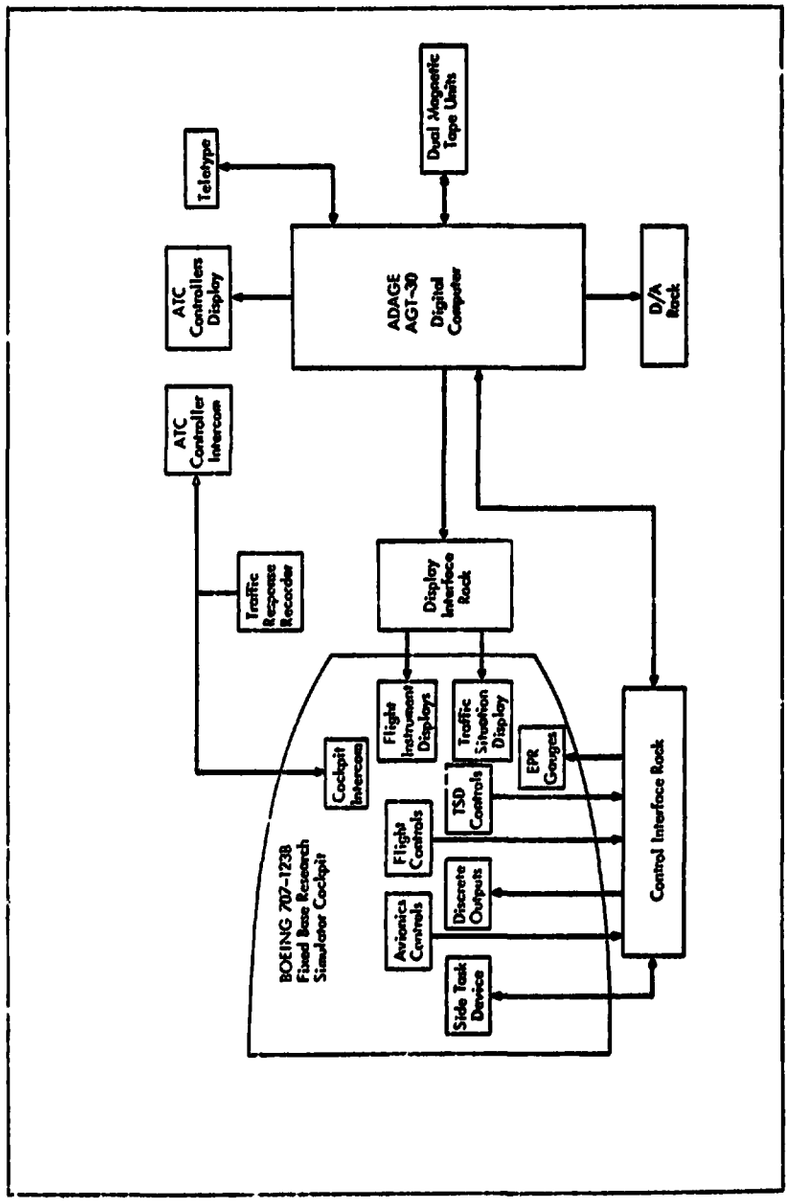

Figure 3 Simulation Facility Block Diagram

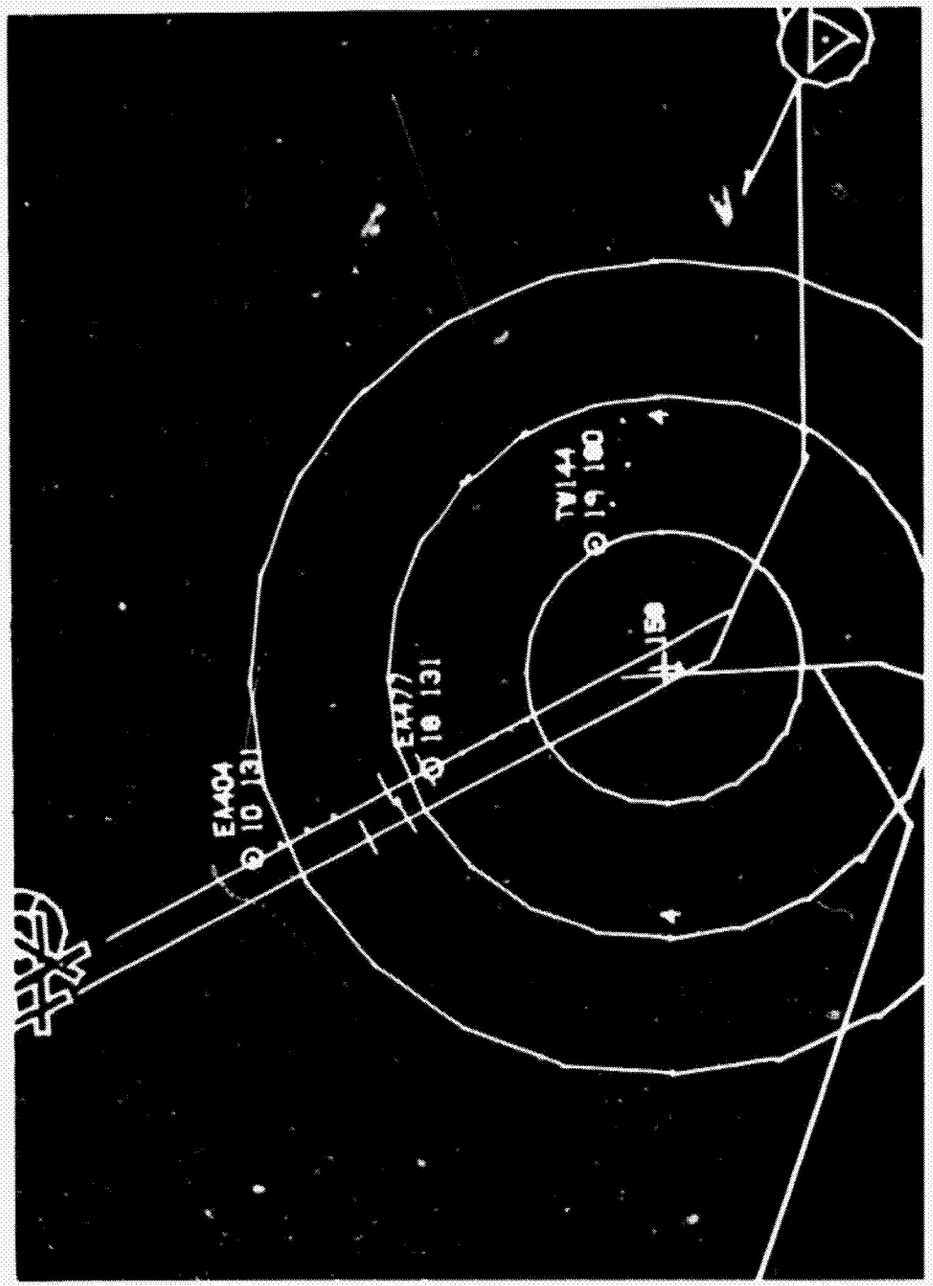

FIGURE 4. Sample Display

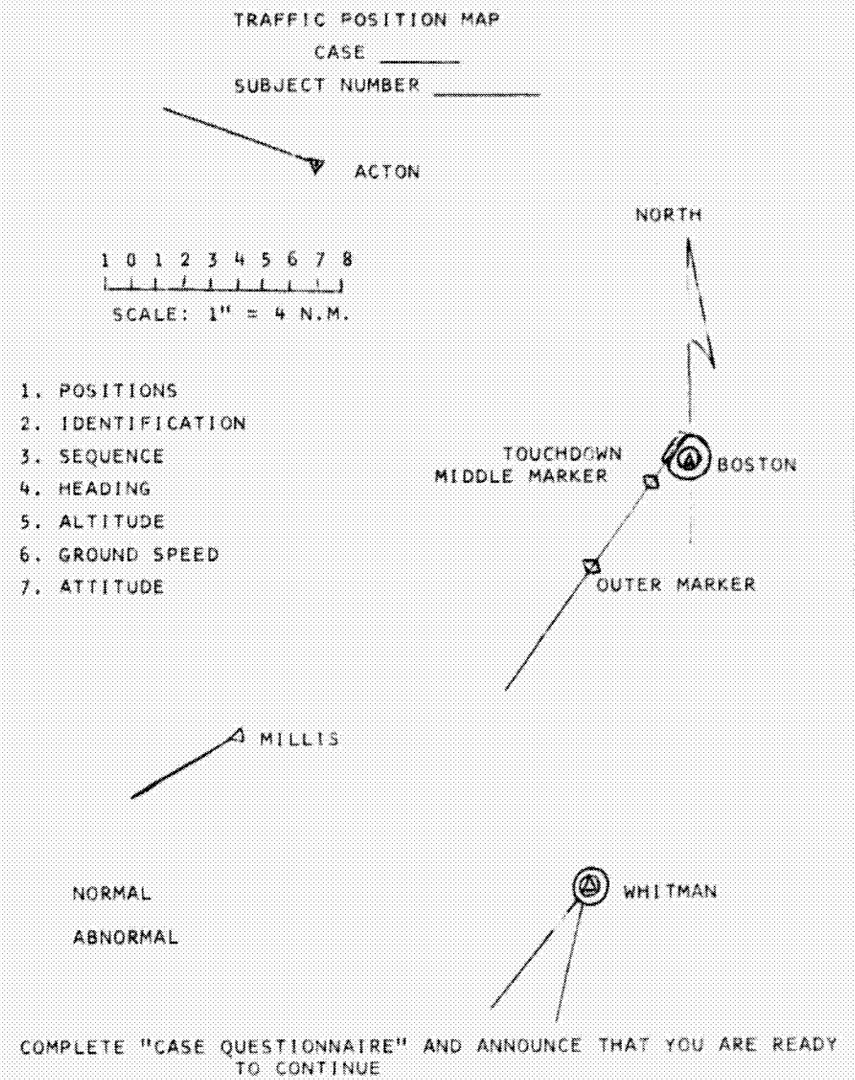

FIGURE 6. STOP-ACTION QUIZ MAP

TABLE I. POSITION ERROR (Nautical Miles)

TREATMENT CONDITIONS	RELATIVE LANDING SEQUENCE -1 M	-1 S.D.	-1 %N	0 M	0 S.D.	0 %N	+1 M	+1 S.D.	+1 %N	+2 M	+2 S.D.	+2 %N
$\bar{T}$-S	3.8	2.8	14	3.6	2.6	0	3.9	3.1	3	2.4	2.6	0
T-S	3.4	1.9	25	1.8	1.5	0	2.3	1.5	4	1.0	0.6	18
T-D (SP)	4.0	1.1	37	2.0	1.4	0	1.6	1.4	0	1.7	1.5	26
T-D ($S\bar{P}$)	3.3	2.4	13	2.6	1.6	0	2.1	1.2	5	1.7	1.0	7

TABLE 2. SPACING ERROR (Nautical Miles)

TREATMENT CONDITIONS	RELATIVE LANDING SEQUENCE -1 M	-1 S.D.	+1 M	+1 S.D.	+2 M	+2 S.D.
$\bar{T}$-S	-2.4	4.2	-5.1	5.0	-2.5	4.3
T-S	-1.2	2.9	-0.3	1.9	-0.4	1.6
T-D (SP)	1.8	3.9	-1.3	2.1	-1.2	2.1
T-D ($S\bar{P}$)	0.0	3.8	0.6	2.0	0.5	2.1

TABLE 3. HEADING ERROR (Degrees)

TREATMENT CONDITIONS	RELATIVE LANDING SEQUENCE -1 M	-1 S.D.	-1 %N	+1 M	+1 S.D.	+1 %N	+2 M	+2 S.D.	+2 %N
$\bar{T}$-S	-5	54	32	-1	25	18	14	28	14
T-S	-5	10	39	12	30	14	0	0	21
T-D (SP)	14	60	58	-2	18	10	1	7	16
T-D ($S\bar{P}$)	29	74	40	10	38	33	-1	3	35

TABLE 4. GROUNDSPEED ERROR (knots)

TREATMENT CONDITIONS	RELATIVE LANDING SEQUENCE -1 M	-1 S.D.	-1 %N	+1 M	+1 S.D.	+1 %N	+2 M	+2 S.D.	+2 %N
$\bar{T}$-S	-5	54	32	-1	25	18	14	28	14
T-S	-5	10	39	12	30	14	0	0	21
T-D (SP)	14	60	58	-2	18	10	1	7	16
T-D ($S\bar{P}$)	29	74	40	10	38	33	-1	3	35

TABLE 5. ALTITUDE ERROR (Feet)

TREATMENT CONDITIONS	RELATIVE LANDING SEQUENCE -1 M	-1 S.D.	-1 %N	+1 M	+1 S.D.	+1 %N	+2 M	+2 S.D.	+2 %N
$\bar{T}$-S	375	619	27	-1029	1550	36	8	519	41
T-S	-520	1121	64	-315	983	26	43	253	50
T-D (SP)	725	1517	79	-288	574	16	-54	238	42
T-D ($S\bar{P}$)	57	913	25	-147	564	10	-117	292	25

TABLE 6. RESULTS OF ANALYSIS OF VARIANCE BETWEEN TREATMENT CONDITIONS FOR A GIVEN AIRCRAFT

	RELATIVE LANDING SEQUENCE			
	-1	0	+1	+2
POSITION	n.s.	1%	1%	1%
ALTITUDE	1%		1%	n.s.
GROUNDSPEED	5%		1%	n.s.
HEADING	n.s.		n.s.	1%

n.s. Not Significant 1% Significant at 1% level
5% Significant at 5% level

TABLE 7. RESULTS OF ANALYSIS OF VARIANCE BETWEEN AIRCRAFT FOR A GIVEN TREATMENT CONDITION

	TREATMENT CONDITIONS			
	$\overline{TS}$	TS	TD(SP)	TD($\overline{SP}$)
POSITION	n.s.	1%	1%	1%
ALTITUDE	1%	n.s.	1%	n.s.
GROUNDSPEED	1%	1%	5%	n.s.
HEADING	n.s.	n.s	n.s	n.s.

TABLE 8. CONFLICT DETECTION DURING SINGLE RUNWAY SIMULATIONS

CONFLICT DESCRIPTION	TREATMENT CONDITIONS	DETECTION		
		NO. OF TRIALS	BEFORE OR AT SAQ	BEFORE OR AT CPA
HEADING COMMAND READBACK ERROR (COLLISION ABEAM)	$\overline{TS}$	10	1	1
	TD(SP)	8	1	5
	TD($\overline{SP}$)	6	3	6
RADIO FAILURE-TRACK DEVIATION (COLLISION HEAD-ON)	TS	10	4	10
	TD($\overline{SP}$)	6	2	6

$\overline{TS}$ = Shared communications, no display

TS = Shared communications, with display

TD(SP) = Discrete communications, display, and spacing task

TD($\overline{SP}$) = Discrete communications, display, and spacing task

SAQ = Stop Action quiz

CPA = Closest point of approach

TABLE 9. CONFLICT DETECTION DURING INDEPENDENT OPERATIONS ON CLOSELY SPACED PARALLEL RUNWAYS

CONFLICT DESCRIPTION	TREATMENT CONDITIONS	DETECTION	
		NO. OF TRIALS	BEFORE OR AT CPA
ACQUISITION OF WRONG ILS	TD(SP)	7	7
	TD($\overline{SP}$)	11	11
SUDDEN ILS CROSSOVER MANUEVER	TD(SP)	7	4
	TD($\overline{SP}$)	8	8

TABLE 10.

	WITH TSD	WITHOUT TSD
DETECTED	57	1
UNDETECTED	3	9

$\chi^2 = 42.1$ ($p < .001$)
d.f. = 1

TABLE 11.

	TSD WITH SPACING TASK	TSD WITHOUT SPACING TASK
DETECTED	16	31
UNDETECTED	6	0

$\chi^2 = 4.07$ ($p < .01$)
d.f. = 1

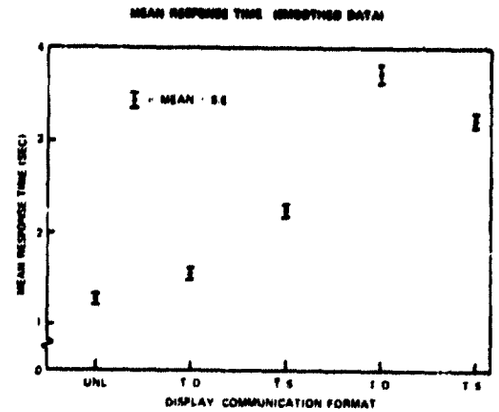

FIGURE 14

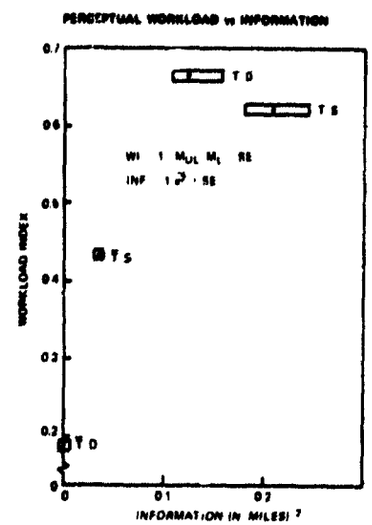

FIGURE 15

ORIGINAL PAGE IS OF POOR QUALITY

AN INVESTIGATION OF TRANSFER OF TRAINING FROM PREDICTION TO CONVENTIONAL DISPLAYS*

Daniel J. Prosin
William B. Knowles
Joseph W. Wulfeck

Dunlap and Associates, Inc.
Santa Monica, California

PRECEDING PAGE BLANK NOT FILMED

Many manual control tasks require that the human operator remain in the control loop because he has the flexibility and decision making ability that automatic controllers lack. Such tasks are initially difficult because it is hard for the human to predict what the system under his control is going to do.

If learning to perform a difficult manual control task is primarily a matter of learning to predict, then training on such tasks should be oriented around teaching an operator to predict. This study explores the usefulness of a predictor display as a training device for a task in which there is no such display available in the operational task. The function of the predictor display is to reduce training time or improve terminal skills for a complex manual control task.

An adaptive training paradigm controls the amount of predictive information supplied to the trainee as an inverse function of his level of skill. Initially the trainee has both conventional instruments and a predictor display available to him. As he learns to control the system dynamics, the predictor is adaptively taken away so that when he reaches the desired performance criterion only conventional instruments are available to him and he has learned to produce his own predictions from the information provided by them.

*The work reported in this paper is being supported by the Air Force Office of Scientific Research under Contract No. F44620-73-C-0014.

DYNAMIC READING OF ANALOG AND DIGITAL DISPLAYS: A COMPARATIVE STUDY

E. Schubert
Forschungsinstitut für Anthropotechnik, Mockenheim
Germany

N75 19130

Introduction

Analog and digital meters are used to present the actual value of a parameter to an observer. The selection of a suitable display format for a special task depends essentially on whether accurate (digital) or quick (analog) reading is demanded. To combine both properties – accurate and quick reading – within one display, analog and digital elements have to be presented simultaneously in a way, that is most suitable for human perception.

Since this problem can not be solved by theoretical means, several display-formats were compared by a comparative experimental study (see fig. 1). Beside analog (1) and digital (6) scales, some hybrid (analog-digital) formats were taken into consideration. System 4 is a moving scale meter.

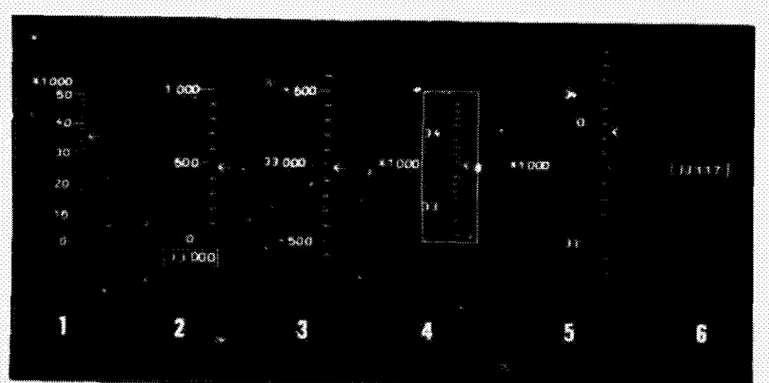

analog hybrid digital

fig. 1 : Examined display formats

Experimental procedure

The meters are presented subsequently to the subjects. During this time, the indicated value was changing with constant rate and statistically alternating direction. At the end of a presentation interval an acoustic signal was

PRECEDING PAGE BLANK NOT FILMED

ORIGINAL PAGE IS OF POOR QUALITY

3) A mixture of the two systems mentioned before represents a third possibility. A section of the total range ist indicated by an analog scale and a digital display indicates the range of the actual value. The measured variable is shown by the pointer on the scale and by the digital indication. In the following this display is called "hybrid display" (see figure 1, display No. 2-5).

In the present research various display systems had to be compared as to their readability. For that purpose, the rate of change of the displayed value is varied over a large range, in order to obtain quantitative data in the transition range between static and dynamic use.

The reading-error is selected as a measure. The introduction of the pointer-velocity as an independent variable in these experiments leads to the problem of a suitable research-method. Until now only static methods (e.g., by means of the tachistoscope) are known form literature. For this experimental study a new "dynamic procedure" was developed which I will describe later on.

2. Experimental set-up

Figure 1 shows the various displays, which were presented to the subjects. All systems had the same range of 50 000 units. Four hybrid displays (No. 2 through 5) were examined in addition to one analog (No. 1) and one digital display (No. 6). The length of the scale was the same for the displays No. 1 through 5. The scales subtended a visual angle of 8°, with the lin-of-sight perpendicular to the display surface. As a scale-form the line-scale was selected and arabic figures were chosen for numbering of the scales and the digital display. The geometric dimensions of these display characteristics correspond to the rules available in the literature.

The displays, which are presented on a CRT, are generated by means of a symbol-generator developed in our institute. The location of individual symbols, for exampel the pointers position on the scale, can be changed by an external analog voltage, and individual symbols, for example the figures of a scale, can be changed by digital information externally supplied (see figure 2).

Figure 2 : Experimental set - up

The screen observed by the subject was installed in a cockpit. The CRT is sloped such that a subject of average size looks vertically upon the projection screen.

3. Experimental procedure

In the following I'll describe the dynamic method, I used in this experiment. At the beginning of a given trial one preselected display is presented on the CRT screen and the subject has to read this display (figure 3). The pointer starts at a statistically determined position of the available range and then moves up or down with a constant velocity according to the chosen rate of change for the displayed value, as you can see here. After a few seconds an accoustic signal is given and the subject has to read the value at that moment. Simultaneously the pointer and other parts of the display, which are important for the reading, are turned off. The subject reports the detected value to the experimenter verbally. The latter writes this reported value into an electronic memory coupled to a digital display, which is situated above the CRT-screen for confirmation by the subject. This "reported-value-display" was switched

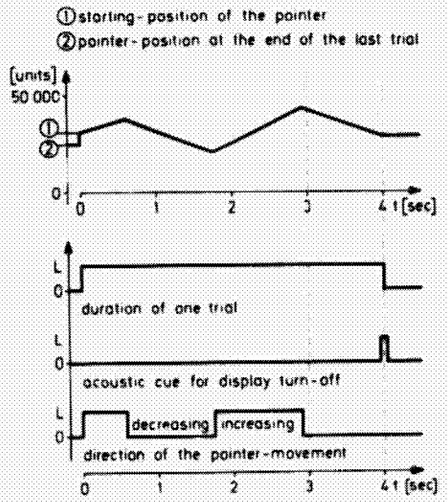

Figure 3 : Experimental procedures diagram

off during the trial run. The duration of one trial was stochastically varied among three fixed-time periods so that the subject could not predict the required moment of reading. The starting-position of the pointer, the rate of change of the displayed value, and the time of presentation are fixed for each trial. The direction in which the pointer moves is controlled by a random-generator. An electronic control prevents the pointer from changing the direction in the last second before the turn off. The rate of change of the displayed value is systematically varied for each trial. The speed values are logarithmically graduated and cover a range of 20 to 5000 units per second for the displays No.1 through 5. The rate of change can also be expressed as a pointer velocity in degrees per second. For a scale viewing angle of 8°, as mentioned before, values between 0.0032 and 40 degrees per second are obtained. In display No. 6 the numbering frequency was varied over a range from 5 to 1000 units per second. On the average the readings were made half at increasing and half at decreasing tendency of the displayed value.

The difference X between the value reported by the subject and the displayed value was chosen as the performance measure and is called the "reading error" :

$$X = V_R - V_D$$

4. Experimental results and discussion

For these experiments a readability index for a display is derived from proportional "correct readings". Contrary to the digital display an accurate reading is hardly possible in analog displays. For that reason a certain range of tolerance needs to be chosen, in my case ± 50 units, and the proportion of answers is determined, for which the reading error X is situated within this limit. This evaluation method proved to be advantageous, especially for the comparison between analog and digital forms of displays and enables a comparison among the distributions of the reading errors X.

Concerning the diagrams, which I'll show in a moment, it should be noted, that the rate of change is always shown in logarithm units, whereas the ordinate, which represents the readability index, shows a linear subdivision.

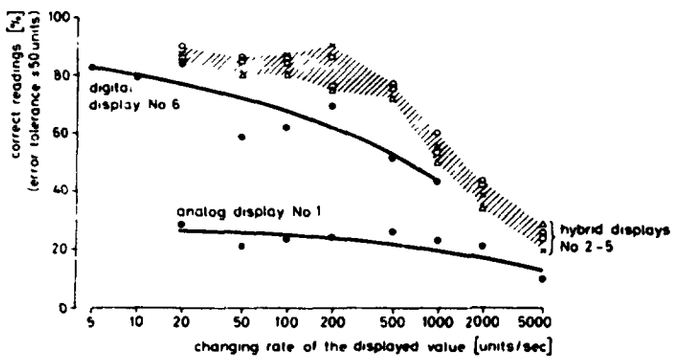

Figure 4 : Correct readings as a function of the changing rate of the displayed value

The results in terms of proportional "correct readings" are shown in figure 4. As you can see, the hybrid displays No.2 through 5 present the best readability, when the answers are interpreted as "correct" with a reading error criterion of maximal ± 50 units. As the hatched surface shows, these displays are approximately equally well read. Comparing the hybrid displays with the digital display performance was about 10 % worse than the hybrid display performance. The pure analog display (No. 1) shows the worst result as could be expected form the scale-resolution used (2 000 units per scale division with a scale spacing of 20 arc-minutes).

The load on the subject, associated with reading the individual display systems, was examined in a second experiment using an additional secondary task (see figure 2). A fixed circle and a cross, which is movable in the image field, are presented toward the right of the displays. The subject must bring the cross back into the circle by means of a control stick, which can be moved in two dimensions during the run of trial. The subject has to try to keep the cross at the null point. At the beginning of each trial the cross is displaced form the null position in the circle with a certain initial acceleration.

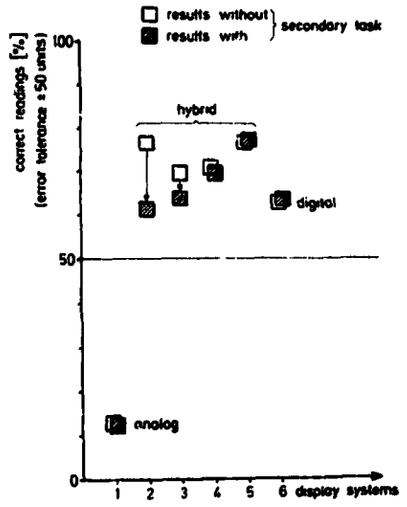

Figure 5 : The influence of the secondary task

In figure 5 the influence of the additional secondary task is shown. The open square represents the mean value of the correct readings for each system corresponding to the experiments without secondary tasks. The corresponding results with the additional secondary task are marked by the shaded squares. For the second experimental run, differences now can be noted in the reading performance of the hybrid displays. Whereas the displays No. 4 and 5 show almost no influence, the number of correct readings for display No.3 is about 5 % lower. Display No. 2 clearly shows that the subjects already were very much stressed with their main task of reading the display so that the number of correct answers became nearly 15 % less when simultaneously executing the secondary task. Altough the digital display No. 6 shows no change compared to the results of the first series, i.e. without secondary task, now it is read better than display No. 2 by about 3 %.

In the figure 6 the mean error of reading $\bar{X}$ for the six displays are represented. About 200 answers were given by the subjects for the analysis of one velocity-step in one display with increasing or decreasing tendency. The mean values $\bar{X}_{IN}$ and $\bar{X}_{DE}$ as well as the variances σ^2_{IN} and σ^2_{DE} were calculated from these data.

In the upper diagram the relationship between $\bar{X}_{IN}$ and changing displayed value rate is shown for the various display systems under the experimental condition of "increasing tendency". The lower diagram shows the simular relationships except for the "decreasing tendency". As the results show, the reading performance depends not only on the display system and on the rate of change of the displayed value, but also clearly on the direction of movement (or tendency).

It is generally true that toolarge a reading is made during an increasing tendency ($\bar{X}_{IN} > 0$), whereas during decreasing tendency the mean error $\bar{X}_{DE}$ is smaller than zero ($\bar{X}_{DE} < 0$). That means : in an increasing tendency the subjects always tend to read higher value - compared to the actual value - and they read a lower value in a decreasing tendency. Furthermore it was found that the absolute mean error $|\bar{X}|$ is somewhat smaller during the decreasing tendency ($|\bar{X}_{DE}| < |\bar{X}_{IN}|$).

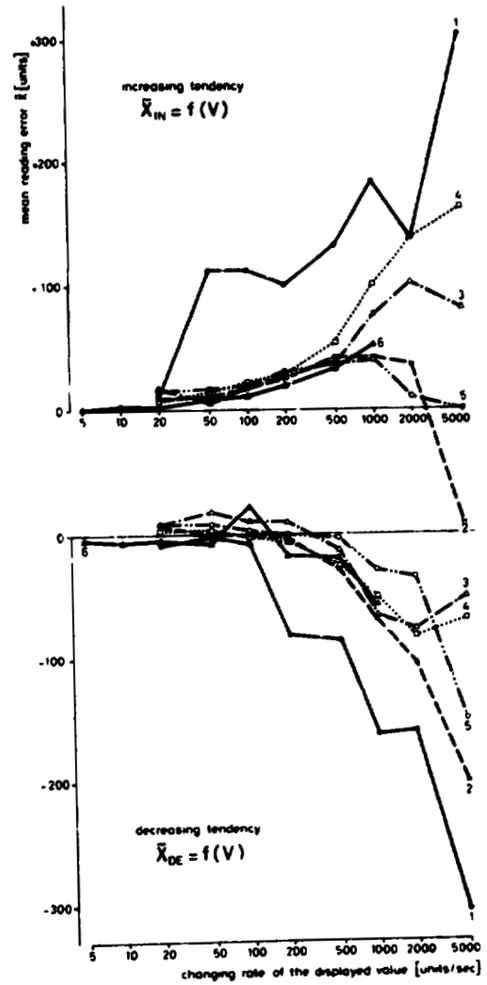

Figure 6 : Mean reading error as a function of the changing rate of the displayed value

ORIGINAL PAGE IS
OF POOR QUALITY

The same effect is observed for the corresponding values of the variance. That means : the subjects tend to read more accurately under conditions of decreasing tendency. Regarding the results for display No. 6, the digital display, *it should be noted that - contrary to statements in the literature* - subjects did perceive the change of direction of the displayed value, especially at high rates of change.

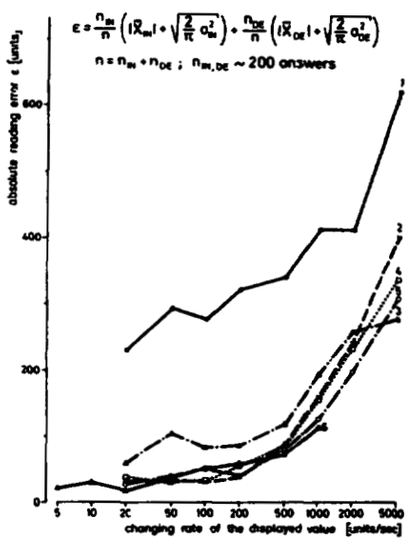

Figure 7 Absolute reading error as a function of the changing rate of the displayed value

A further possibility for defining an index of readability of a display is given by the "absolute reading error". This error was formed from the values mentioned before by the equation in the upper part of the diagram in figure 7.

The significant influence of the velocity is quanlitatively the same for all displays and grows with the increasing values for the rate of change. In the hybrid displays (No. 2 through 5) the corresponding values of the pointer-velocity vary between .08 and 40 degrees per second. Even in the analog display (No. 1) in which the pointer moves with a maximal velocity of .8 degrees per second, a clear influence can be seen. As results from literature have shown this dependence of the reading error on the pointer-velocity cannot be argued for by the "dynamic visual accuity".

5. Conclusion

To recapitulate the results of this investigation I would like to state the following :

the experimental method used has proved to be useful for showing differences in the performance of dynamically reading several display systems.

The results of this research can be summarized under three aspects :

1) The effect of the several displays on the reading performance in terms of correct reading shows, that the hybrid displays are superior to the digital and the analog displays. The analog display shows the smallest number of correct answers, as should be expected by the small scale-resolution. Whereas *in the first experiments without the secondary task nearly the same results* were obtained for the hybrid displays, differences were obtained in the experiments with an additional secondary task.

2) The influence of the tendency of the displayed value shows, that during the increasing tendency a reading error greater than zero is obtained, *during decreasing tendency the error is smaller than zero.*

3) The effect of the changing rate of the displayed value on the reading performance is qualitatively the same for all examined displays.

References

ESG Elektronik-System-GmbH. "Functional Equipment Requirement for Head-up-Displays and Camera", 1969

Grether, W F. "Instrument Dials, Instrument Arrangement and Cockpit Design", in : Mercier (ed.) "Visual Problems in Aviation Medicine", Pergamon Press, 1962

Schmidtke, H.
und Carl Graf Hoyos

"Psychologische Aspekte der Arbeitsgestaltung in Mensch-Maschine-Systemen",
Kap. II. Probleme der Informationsaufnahme,
in : A Mayer und O. Herwig (Hrsg.) Handbuch der Psychologie, Bd. 9, Betriebspsychologie, S. 94 ff. 2. Auflage, bei Dr. C.J. Hogrefe, Goettingen, 1970

Murell, K.F.H.

"Ergonomics",
Kap. 9, Design Factors III, "Design of Instrumental Displays", by : Chapmann and Hall, London 1969

Bauer, R.W. et al.

"Panel layouts for rectilinear instruments",
in : Human Factors 8, pp. 493-497, 1966

Mc Cormick, E.J.

"Human Factors Engineering, Kap. 6, Information Displays,
Mac Graw Hill Book Company, 1964

Morgan, C.T. et al.

"Human Engineering Guide to Equipment Design",
Mac Graw Hill Book Company, Inc. 1963

Scheid, E.

"Untersuchungen über die Sehschärfe für bewegte Objekte. Der Einfluß von Blickhebung und Blicksenkung",
Med. Dissertation, Heidelberg, 1967

Woodson, W.E.
and Conover, D.W.

"Human Engineering Guide for Equipment Designers",
2. Auflage University of California Press, Berkely, Californien, 1964

Grether, W F.
Williams, A.C., jr.

"Speed and Accuracy of Dial Reading as a Function of Dial Diameter and Angular Separation of Scale Divisions",
in : P.M. Fitts (ed.) "Psychological Research in Equipment Design",
Army Air Force, Aviation Psychology Program, Research Report No. 19, 1947

Miller, J.W.
Ludvigh, E.

"The Effect of Relative Motion on Visual Acuity",
in : Survey of Ophthalmology 7, pp 83-116, 1962

N75 19131

A TACTUAL PILOT AID FOR THE APPROACH-AND-LANDING TASK -- INFLIGHT STUDIES

Richard D. Gilson
Department of Aviation

Robert C. Fenton
Department of Electrical Engineering

The Ohio State University
Columbus, Ohio 43210

ORIGINAL PAGE IS OF POOR QUALITY

ABSTRACT

A pilot aid -- a kinesthetic-tactual compensatory display -- for assisting novice pilots in various inflight situations has undergone preliminary inflight testing. The efficacy of this display, as compared with two types of visual displays, was evaluated in both a highly structured approach-and-landing task and a less structured test involving tight turns about a point. In both situations, the displayed quantity was the deviation ($\alpha_0 - \alpha$) in angle at attack from a desired value α_0.

In the former, the performance with the tactual display was comparable with that obtained using a visual display of ($\alpha_0 - \alpha$), while in the later, substantial improvements (reduced tracking error (55%), decreased maximum altitude variations (67%), and decreased speed variations (43%)), were obtained using the tactual display. It appears that such a display offers considerable potential for inflight use.

INTRODUCTION

The manual control of an aircraft during approach and landing is a relatively difficult task even under the best of conditions as is vividly illustrated by accident statistics. Approximately one-half of all aircraft accidents take place during this phase of operation despite its constituting only a brief portion of total flight time.[1]

The difficulties inherent in an accurate landing are primarily caused by the heavy demands placed on the pilot. He must simultaneously control both vehicle attitude, usually from visual cues outside the aircraft, and airspeed which he obtains via a cockpit display. This results in a division of visual attention -- a division which can be especially critical for novice pilots who lack the experience to use relevant pitch, inertial and aural cues.

It was hypothesized that if this division could be eliminated for a student pilot, then the following benefits would accrue:

1) His task would be simplified;
2) His performance would be improved; and
3) The number of accidents during the learning phase should be decreased.

The first two of these were evaluated via a preliminary inflight study in which information pertaining to airspeed was presented tactually to the pilot.*

DISPLAY DESCRIPTION

A control loop which is used by a pilot in making a final approach is shown in Fig. 1. The reference input is a desired angle-of-attack (α_0) which is, of course, intimately related to the desired approach airspeed. The feedback signal is the measured angle-of-attack (α), and the display input is simply the difference $\alpha_0 - \alpha$.

The display consisted of a m... "finger" which was mounted in the head of the aircraft control stick shown in Fig. 2. A forward protrusion of the finger, such as is depicted in Fig. 3, corresponded to an unwanted increase in α, ($(\alpha_0 - \alpha) < 0$), and a pilot would respond by moving the stick forward so as to decrease α and return the finger to its neutral or flush position. An aft protrusion of the finger would require an aft corrective motion of the control stick. That is, a pilot would "follow" the displayed tactual signal to reduce the displayed error to zero. This signal was proportional to error and thus one has a continuous tactual compensatory display. It was controlled by a closed-loop servo with a natural frequency of some 32 rad/sec and a damping ratio of 0.5; thus the display dynamics were negligible in comparison with those of the pilot and aircraft.

This display was initially evaluated in a series of car-following experiments performed under both simulated and full-scale conditions.[3-5] In both these tests, and the ones to be described here, the subjects frequently referred to the compelling nature of the display and how quickly one began performing the required control actions without conscious thought.

EXPERIMENTAL DESCRIPTION

Novice pilot behavior was considered under two conditons:

1) A final approach to landing; and
2) The execution of a continuous tight turn around a point.

A) Final-Approach-To-Landing Study

A flight instructor maneuvered the test aircraft, a Cessna 172, into position for a final approach, selected an appropriate power setting, and then turned control over to a novice pilot (see Point A in Fig. 4). The latter was instructed to conduct his approach at an airspeed of 72 mph and

---

*It is of interest to note the approach taken by Hasbrook and Rasmussen[2] to a related aspect of the approach-and-landing problem. They used aural glide slope cues in an inflight simulated ILS approach study.

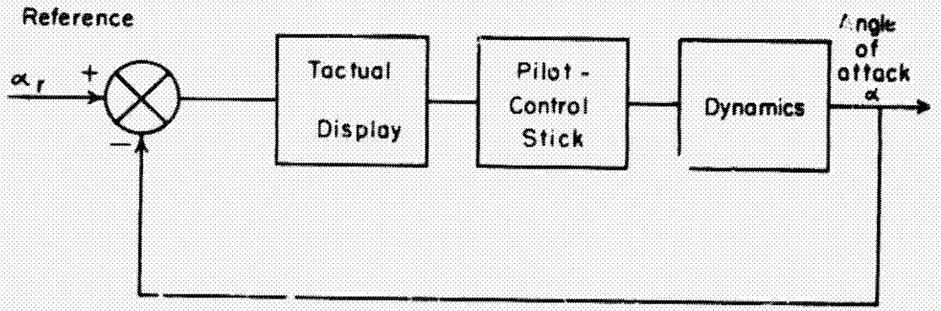

Fig. 1 Control loop for angle-of-attack

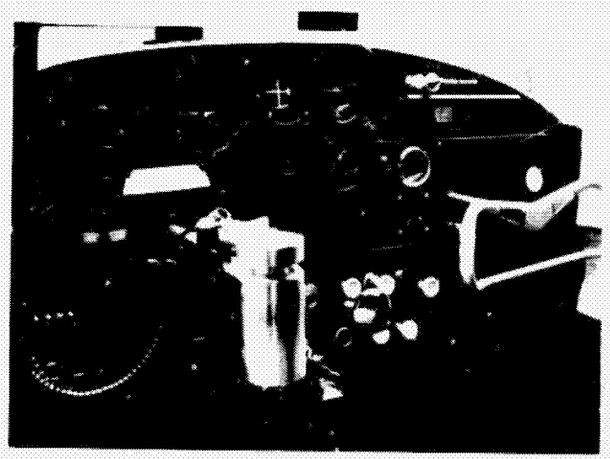

Fig. 2 Aircraft control stick with built-in tactual display

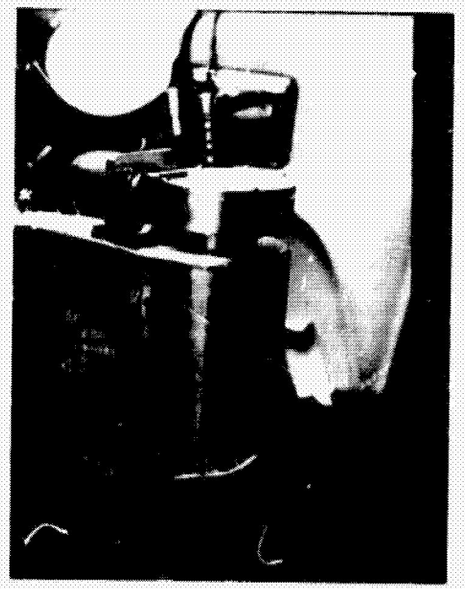

Fig. 3 Control stick with "finger" protruding forward.

to remain aligned with t. : runway center lane. He retained full control of the aircraft until his altitude decreased to some 50 ft; then the flight instructor took control and subsequently repositioned the aircraft for another approach.

These tests were conducted at the Ohio State University airport with only limited air traffic present. Thus, the testing situation was highly structured and each student could focus his full attention on the landing task.

Airspeed information, or some aspect of same, was provided in three ways with no more than one of these being used in any given approach:

i) A conventional visual display of airspeed;
ii) A visual display of α-- via a display which was mounted on top of the glareshield; and
iii) The tactual display.

Performance was assessed on the amount of time a subject exceeded a threshold of error in maintaining the desired angle-of-attack. The quantity α was recorded on a magnetic tape for the complete final approach; however the data were only evaluated for 50 sec beginning some 10 sec after a subject took control (See Fig. 5). This was done to minimize the effects, on the reduced data, of the changeover in control which occurred at both the beginning and the end of each run. It was also planned to use vehicle lateral position with respect to the desired flight path as a performance indicator; however, the prevalence of heavy traffic ruled out the use of the only locally available ILS facility for this purpose.

Six subjects, each of whom was making his first flight participated with each student making 3 approaches with each type of display. Counterbalancing was employed to evenly distribute any bias due to learning.

The results are shown in summary form in Table I where the percent time beyond threshold (the average of 3 runs on each of 6 subjects) is shown for each of the three display modes.*

TABLE I

	DISPLAY MODE		
	Airspeed	Angle of Attack (Visual)	Angle of Attack (Tactual)
% Time beyond threshold (Avg. of 18 runs)	23.9 %	13.9 %	16.7 %

* The raw data from this study are contained in Ref. 6.

Clearly, the least satisfactory performance was obtained when the airspeed indicator was used as the subjects were, on the average, beyond threshold 23.9% of the time. A dramatic improvement was obtained by using the visual angle-of-attack indicator as the subjects were beyond threshold only 12.9% of the time. Nearly as great an improvement was realized with the tactual display. Results showed a beyond threshold percentage of only 16.7%.

In evaluating the results from these highly structured tests, it appears worthwhile to consider the following factors. First, the approach task was somewhat unrealistic in that the testing proceeding in the absence of

a) Subject maneuvering into position for the final approach;
b) Other air traffic; and
c) Ground-to-air communication.

Further, in the visual display of α condition, the subjects vision was always directed along the display. Second, it also appears important to note that the subjects had never used the tactual display, until they were exposed to it in this flight situation.

B. Turns-Around-a-Point Study

In order to evaluate the efficacy of the tactual display in a relatively unstructured and more realistic flight situation, novice pilot performance for turns about a point was considered. Each of six subjects was instructed to maintain a continuous tight turn about a point while maintaining both a constant speed (85 mph) and a constant altitude (800 ft.)* In essence, a subject was now frequently required to direct his attention out of the side window, and hence he could not devote as much attention to a visual display.

Each subject made 2 complete turns about the selected point and α, altitude (h), and airspeed (v) were recorded. Performance was assessed on the basis of the amount of time a subject exceeded an α threshold, the maximum altitude deviation, and the maximum airspeed deviation.

The average results are shown in Table II, and are so striking as to require no detailed discussion.** In essence, by using the tactual display as compared to either of the visual displays, the time beyond threshold was reduced by 55%, the range in airspeed was reduced from 60-130 mph to 75-95 mph, and the estimated altitude deviations from ± 600 ft. to ± 200 ft.

* Two of these subjects have previously participated in the final-approach-to landing study. The remaining four were making their first flight.

** The raw data from this study are contained in Ref. 6.

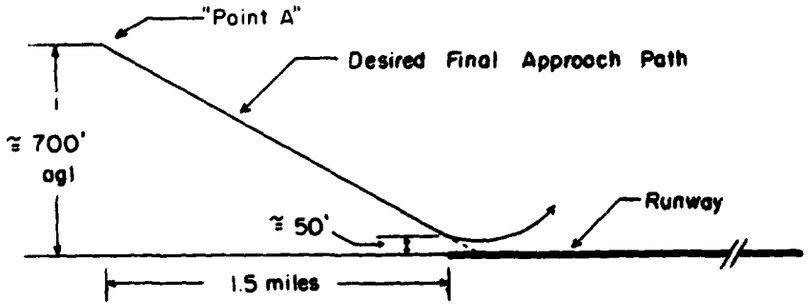

Fig. 4 Final Approach detail.

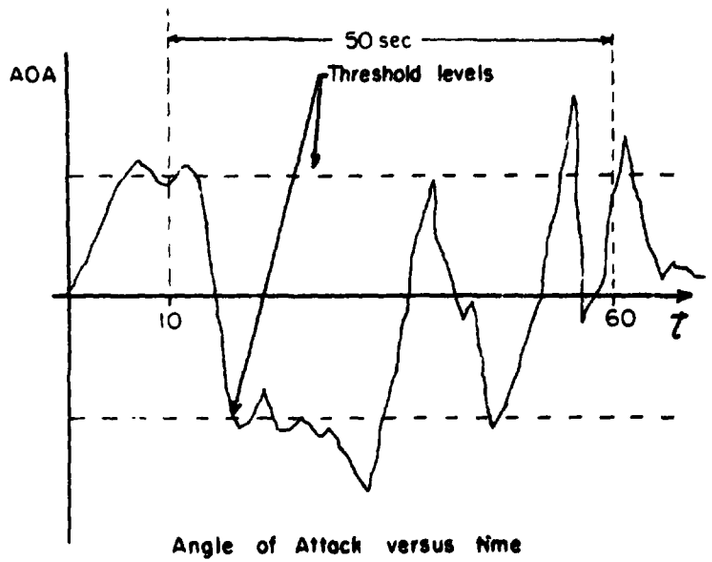

Fig. 5 Angle of attack versus time showing data evaluation interval.

TABLE II

	DISPLAY MODE		
	Airspeed	Angle of Attack (Visual)	Angle of Attack (Tactual)
% Time beyond threshold	21.5 %	25.3 %	11.4 %
Range of Airspeed (85mph desired)	50-130 mph	50 - 130 mph	75 - 95 mph
Estimated Variation in Altitude (h_d= 800 ft)	±600 ft	±600 ft.	±200 ft

CONCLUSIONS

In a highly structured approach-and-landing task, roughly comparable results were obtained by using either a visual display of angle-of-attack or a tactile one. This was despite the fact that the subjects were not trained in the use of the latter. In a more realistic, and less structured situation where the subjects' attention was required off to one side, the use of the tactual display was clearly superior.

These conclusions should not be generalized beyond this study; however, it does seem clear that a tactual display such as the one tested here, offers considerable promise for use in flight instruction, and perhaps ultimately in various operational situations.

ACKNOWLEDGMENTS

Dr. Marlin O. Thurston first suggested that the tactual display described here could be profitably used in the approach-and-landing task. Mr. Ronald Ventola was responsible for the design of the control stick-display combination and enthusiastically participated in the collection of the test data. It is a pleasure to acknowledge these contributions.

REFERENCES

1. National Transportation Safety Board, Annual Review of U.S. General Aviation Accidents Occuring in Calender Year 1969.

2. Hasbrook. A.H. and Rasmussen, P.G., "Aural Glide Slope Cues: Their Effect on Pilot Performance During In-Flight Simulated ILS Instrument Approaches," Federal Aviation Administration, Office of Aviation Medicine, Oklahoma City, Oklahoma, Report Number FAA-AM-11-24, May 1971.

3. Fenton, R.E., "An Improved Man-Machine Interface for the Driver-Vehicle System," IEEE Transactions HFE-7, No. 4, December 1966, pp. 150-157.

4. Fenton, R.E., and Montano, W.B., "An Intervehicular Spacing Display for Improved Car-Following Performance," IEEE Transactions MMS, Vol. MMS-9, No. 2, June 1968, pp. 29-35.

5. Rule, R.G., and Fenton, R.E., "On the Effects of State Information on Driver-Vehicle Performance in Car Following," IEEE Transactions SMC, Vol. SMC-2, No. 5, November 1972, pp. 630-637.

6. Gilson, R.D., and Fenton, R.E., "Improving Pilot Performance Through a Tactual Display", Engineering Experiment Station Working Paper 73-1, The Ohio State University, Columbus, Ohio, May 1973.

N75 19132

EVALUATION OF TACTUAL DISPLAYS FOR FLIGHT CONTROL*

by

William H. Levison
Robert B. Tanner
Thomas J. Triggs

Bolt Beranek and Newman Inc.
Cambridge, Massachusetts

Presented at the Ninth Annual Conference on
Manual Control, May 1973

ABSTRACT

A set of manual tracking experiments has been conducted to determine the suitability of tactual displays for presenting flight-control information in multi-task situations. Although tracking error scores are considerably greater than scores obtained with a continuous visual display, preliminary results indicate that inter-task interference effects are substantially less with the tactual display in situations that impose high visual scanning workloads. The single-task performance degradation found with the tactual display appears to be a result of the coding scheme rather than the use of the tactual sensory mode per se. Analysis with the state-variable pilot/vehicle model shows that reliable predictions of tracking errors can be obtained for wide-band tracking systems once the pilot-related model parameters have been adjusted to reflect the pilot-display interaction.

*This research was supported by the Advanced Research Projects Agency, Department of Defense, and was monitored by the Office of Naval Research under Contract No. N00014-73-C-0031 (Dr. John J. O'Hare, Scientific Officer, Engineering Psychology Programs). The authors also acknowledge the significant contributions to this program by Mr. Don Ross and Mr. Richard A. Sanneman of Sanders Associates, Inc.

PRECEDING PAGE BLANK NOT FILMED

I. INTRODUCTION

Objectives

In current aircraft, nearly all the flight parameter information available to the pilot is transmitted to him visually, whether under visual contact or instrument flying conditions. It has long been recognized that during instrument flying conditions the task of scanning just the essential instruments is a taxing, fatiguing one. It may be that displays using information from other modalities can alleviate the demands of this task. Furthermore, the importance of maintaining continuous attention to the visual scene outside the cockpit is being increasingly realized for a number of situations. Traditional panel-mounted visual displays do not permit this, whereas display of information to other modalities could free the eyes substantially from tasks inside the cockpit.

The goal of the study reported in this paper has been to develop tactual displays that can be utilized for flight control. The work has been conducted in three distinct phases: (a) review and selection of elemental tactual transducers (tactors) for operation in display arrays, (b) development of tactual display configurations for flight control, and (c) evaluation of the proposed tactual displays in a series of manual tracking experiments utilizing the tactual arrays together with suitable dynamics simulation of aircraft motions.

This paper summarizes the results of the tracking experiments. Additional details on all phases of this project may be found in [1].

Background

Both auditory and tactual displays have been applied to the area of vehicle control. Perhaps the best known study in the area of auditory displays was the program known as flying by auditory reference (FLYBAR) [2, 3]. The attempt was to supply the pilot with all the information he required to enable him to maintain a required flight path. By so doing, he would be able to devote more time to scanning the outside environment. Although initial experimental success was achieved, an operational system was never developed.

Tactual displays can offer two distinct advantages over auditory presentations. First, tactual displays should not interfere in any real way with speech communications. Second, the tactual modality is not limited in its ability to present information in a spatial pattern. Ballard and Messinger [4] report an early attempt to supply flight control information using just four vibrators mounted on one thumb. Hirsch and Kadushin [5] and Fenton [6] have both used tactual displays to supplement visual display information and have found an enhancement compared with using the visual display alone.

In addition to these studies relating specifically to vehicle control, there have been a number of studies dealing with the characteristics of tactual tracking. Most of these studies have displayed information to the more moveable parts of the body, such as the hand and arm [7-10] and the head and face [11-12]. Those investigators that have displayed information to the torso [13, 14] used just three vibrators per tracking dimension to indicate either zero error, left-right or up-down displacement. Hill et al. [7] suggested that tactile displays are correctly interpreted more frequently when located on body locations not involved with motion.

We considered that display-control compatibility would be an important variable in determining vehicle control performance. Because of this, we selected the chest and abdomen as the display area, since it is usually relatively immobile, and the display-control relationships are unlikely to be altered as the human operator performs his various functions. The torso also provides a relatively uniform display area for exploring various display sizes and geometries.

We also wished to evaluate a two-dimensional tracking display with minimal confusion between axes as well as high display-control compatibility without the use of large numbers of stimulators. Preliminary experimentation explored various configurations for possible use as flight control displays, and an X-Y display was selected with 7 stimulators on each dimension with a common stimulator shared at the point of the axis crossing. In order to enhance the pilot's ability to interpret the tactual information, X- and Y axis tracking errors were presented sequentially, rather than simultaneously.

Because of previously reported studies which indicated that simple intensity coding would not be adequate in a multi-task situation [13, 15], other coding dimensions were employed in this study. A ripple display was designed that used both number of tactors stimulated in a sequence as well as the rate of strobing to indicate the magnitude of the tracking error. Since preliminary experimentation indicated that pilots would have difficulty in distinguishing between different rates for ripple rates greater than 26 Hz, the ripple rate was varied continuously with error magnitude over a range of 2.6 to 26 Hz. (This range is lower than that found to be optimal by Hill [8] in his study with a ripple display, but we were using a different form of coding and a different type of stimulation.)

2. PROCEDURES

Description of the Task

The bulk of the experimental program was devoted to an investigation of continuous manual tracking performance with tactual and visual displays. In addition, combined tracking and visual monitoring tasks were studied in order to provide comparisons of tactual and visual tracking displays in situations imposing a high scanning workload.

Descriptions of the tracking and monitoring tasks are given below, followed by descriptions of the tracking displays and of the procedures used in analyzing the experimental data. Additional experimental details are provided in the discussion of experimental results (Section 3).

Tracking Tasks

Two very important constraints were placed on the selection of a tracking task. First, we wished to simulate the important aspects of a flight-control task. Secondly, it was important to obtain an accurate and complete characterization of the pilot-display interaction so that the results of this experiment could be extrapolated to other manual control tasks using tactual displays.

These two considerations led to the selection of a simulated attitude regulation task. A wings-level operating point was selected, thereby allowing the pitch and roll axes to be uncoupled. This task not only provided the required degree of face validity, but interpretation of the measurements was greatly facilitated by allowing each perceptual dimension of the tactual display to relate to an independent single-variable control task. In this manner we minimized the liklihood that the pilot's response to a particular tactual display variable would be confounded by his response to other tactual (or visual) display variables.

Simplified vehicle dynamics were selected to represent the response of a high-speed fighter aircraft having good handling qualities [16, 17]. Pitch dynamics were of the form

$$\frac{\theta}{\delta_e}(s) = \frac{K_\theta(s + 1/T_\theta)}{s(s^2 + 2\xi\omega_o s + \omega_o^2)} \tag{1}$$

and the roll dynamics were

$$\frac{\phi}{\delta_a}(s) = \frac{K_\phi}{s(s + 1/T_r)} \tag{2}$$

Values for the dynamic parameters were

T_θ = 0.25 sec*
ω_o = 6.0 rad/sec
ξ = 0.85
T_r = 0.3 sec

and the control gains K_θ and K_ϕ were selected during training to provide acceptable system responsiveness.

The pitch and roll axes were perturbed by independent random-appearing inputs which were applied as vehicle disturbances. The transfer function relating pitch response to pitch-axis disturbance was the same as the pitch/control relationship shown in Equation (1) except that the numerator contained no root. The roll-axis disturbance was applied in parallel with the pilot's control input.

Both disturbance inputs were constructed by summing together 13 sinusoids of random phase relationships to simulate first-order Gaussian noise processes having break frequencies of 2.0 rad/sec. Input amplitudes were adjusted during training to yield nearly equal pitch and roll mean-squared error scores for the visual display condition.

A two-axis hand control provided independent control inputs to the pitch and roll axes. The control was primarily a force-sensitive device (.12 cm of stick motion per newton of force) and could be manipulated with wrist and finger motions.

*A T_θ on the order of 1.0 second is more commonly associated with high-speed pitch dynamics. But because the hand control used in these experiments allowed a very rapid control response, it was necessary to lower the value of T_θ to provide reasonable response dynamics.

Two instrument-rated pilot served as test subjects for the entire experimental program. Subject "A" was a commercial airline pilot with over 1000 hours of instrument flight time; subject "B" was a recent Navy pilot with over 300 hours of instrument time. Subject B had accomplished approximately 150 carrier-landings with medium-attack aircraft.

Visual Monitoring Task

A visual monitoring task was used in the final evaluation experiment to provide a substantial scanning workload. The pilot was required to scan between two meter movements and to depress a hand-held response button whenever either or both of the meter indicators was outside a clearly-marked "allowable" region. Separation between the meters and between each meter and the visual tracking display was sufficient to require overt visual scanning. The display panel for the combined monitoring and visual tracking task is diagrammed in Figure 1.

Each meter was driven by an independent simulated first-order noise process filtered by an additional first-order network having a break frequency of 1.0 rad/sec. Signal amplitudes – nominally equal for the two meters – were adjusted so that the two meter indicators were jointly within their allowable regions about 50% of the time. The rate at which the subjects had to change the state of the response button was determined experimentally to be about twice every three seconds. This relatively high response rate, coupled with the separation between displays, assured a high scanning workload whenever the visual monitoring task was performed.

Tracking Displays

Three tracking displays were employed in this experimental program: (1) a continuous visual display, (2) a tactual display, and (3) a quantized visual display that was designed to be a visual analog of the tactual display.

Continuous Visual Display

The continuous visual display consisted of a CRT presentation of an artificial horizon. Display motion was compatible with that found in an aircraft attitude instrument; i.e., a clockwise roll of the aircraft was represented by a counter-clockwise rotation of the display indicator, and a nose-down attitude was designated by an upward displacement of the indicator. The display panel was located approximately 30 inches from the subject's point of regard.

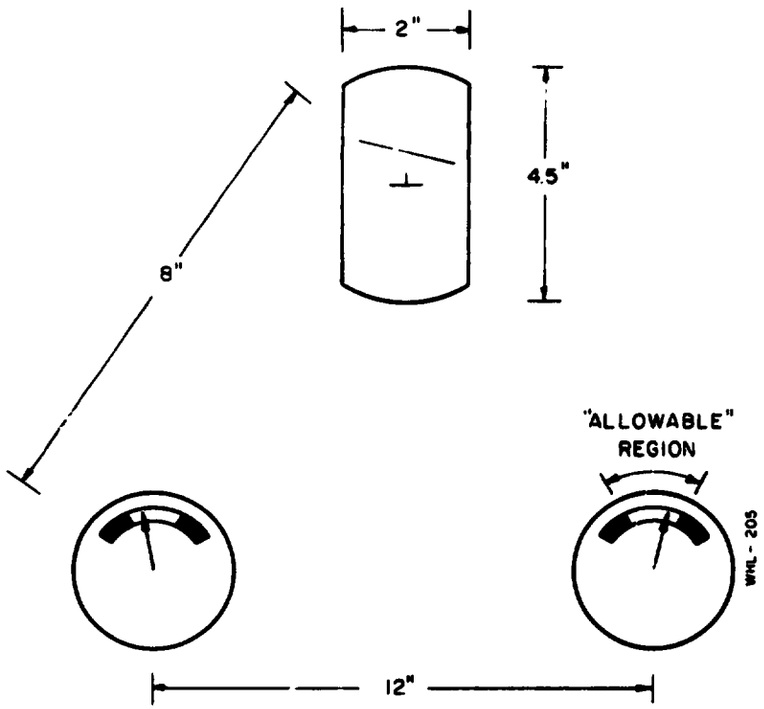

FIGURE 1. Diagram of Combined Tracking and Monitoring Display

Tactual Display

A variety of tactual display configurations were explored and evaluated during the initial training phase of this program. Only the configuration used in the formal data-taking sessions is described in this paper; details on the preliminary display designs may be found in [1].

A diagram of the tactual display is given in Figure 2. Thirteen mechanical vibrators (bimorphs) were arranged in the shape of a cross with three tactors in each of the four arms and a single tactor at the junction. Tactors were concentrated towards the outer limits of each arm to provide a clear cue as to the directionality of the tracking error. The upper and lateral arms of the display were of equal dimensions, whereas the lower arm was compressed to enhance comfort in wearing the display on the chest and abdomen.

The display was coded so that both the number of tactors excited and the rate at which successive tactors were stimulated (the "ripple rate") provided information related to the magnitude of the tracking error. When tracking error was below a certain threshold level, only the center tactor was stimulated at infrequent intervals. For larger errors, two or more tactors were stimulated in succession, with the interval between successive tactor stimulations being inversely proportional to the magnitude of the error. The ripple rate, then, gave a signal proportional (within limits) to tracking error, whereas the number of tactors stimulated in a single sweep gave a quantized indication of magnitude.

A single display sweep was always initiated at the center and proceeded outwards along one of the four display arms. Thus, an additional cue was provided in that the portion of the anatomy stimulated by the tactors indicated the directionality of the signal. In order to maximize the ability of the pilot to interpret information obtained from the tactual display in a two-axis tracking situation, signals were presented sequentially, rather than simultaneously. The penalty for this coding scheme, of course, was an increase in the effective perceptual delay time.

Operation of the tactual display is perhaps best visualized by reference to the timing diagram of Figure 3. Assume that the X-axis and Y-axis errors are large enough to excite three tactors in each axis, and assume that the X-axis error is detected first. As soon as this error is detected, a 35.3-msec pulse (6 cycles of a 170 Hz waveform) is generated on the center tactor. An inter-stimulus-interval (ITI) proportional to the error at sample time is then generated, followed by stimulation of the second tactor. Another ITI is generated, followed by stimulation of the third tactor. Presentation of X-axis information is completed, and a pre-determined quiet interval (the IAI, or inter-axis-interval) follows.

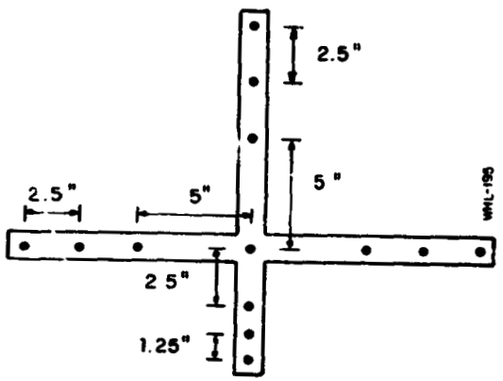

FIGURE 2. Diagram of the Tactual Display

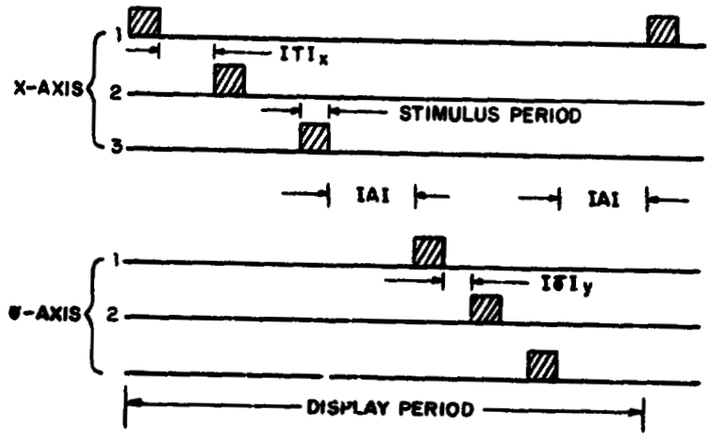

FIGURE 3. Timing Diagram for Tactual Information

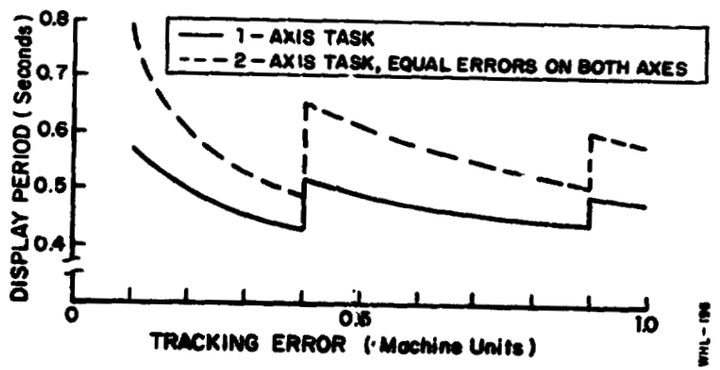

FIGURE 4. Relation Between Tactual Display Period and Tracking Error

ORIGINAL PAGE IS
OF POOR QUALITY

During the IAI, the Y-axis error is sampled, and the process repeats itself for the Y-axis information while the X-axis tactors remain quiet. If only a single axis is tracked (i.e., if the error on one axis is insufficient to stimulate two tactors), successive sweeps are generated on a single display axis. In this case, the inter-sweep dwell period is automatically extended.

Independent inputs to the display control unit allowed individual control of the number of tactors stimulated as well as of the ripple rate. Thus, some flexibility was available in determining the relationship between tracking error and the various coding dimensions. A single such relationship was used during the course of the formal experiments.

The tactual display operated in a sample-and-hold fashion; the period of the sweep along a given axis was determined by the error sample obtained prior to the initiation of the sweep. Because X- and Y-axis information was presented sequentially, the "display period" (i.e., the time between initiations of successive presentations on a given axis) was a function of the error samples obtained from both axes.

Figure 4 shows the relationship between display period and tracking error for both one-axis and two-axis tracking situations. (Equal X and Y errors are assumed for the two-axis case.) The discontinuities in the curves occur at values of tracking error where an additional tactor is stimulated. Because of the greater inter-sweep dwell time for the 1-axis situation, the two-axis display periods are less than double the one-axis periods for a given tracking error.

In order to maximize transfer of learning between visual and tactual displays, tactual stimulation corresponded as closely as possible to motions of the artificial horizon. Accordingly, a nose-down attitude produced an upward ripple of the tactors, and a roll-left attitude produced a right-directed ripple.

Quantized Visual Display

A visual analog of the tactual display was used to distinguish performance degradations associated with the tactual sensory mode from degradations associated with the particular coding scheme. This display consisted of an array of thirteen light-emitting diodes (LED) arranged in an X-Y pattern. The coding for this display was identical to that of the tactual display; thus, stimulation of a given LED corresponded to stimulation of a particular tactor.

Analysis Procedures

Data analysis was performed in order to provide quantitative descriptions of tracking efficiency with regard to specific tasks explored in this study and to allow the results to be extrapolated to other flight-control situations. Primary data reduction yielded standard measures of system performance and pilot behavior for both the tracking and monitoring tasks. The reduced data were then compared with the outputs of the state-variable pilot/vehicle model developed at BBN [18, 19]. A model-adjustment procedure allowed the pilot-display interaction to be characterized in terms of pilot-related model parameters so that predictions of system performance in other tasks could then be obtained.

Primary Data Reduction

Mean-squared tracking error and mean-squared control effort were computed both during training and during the formal data sessions. In addition, means and standard deviations for these variables were computed from the formal data. These (and all other) performance measures were computed from approximately the middle 200 seconds of each 4-minute run.

Amplitude density functions were computed from selected time histories of tracking error and control input. Each such density function was normalized with respect to its mean and standard deviation to facilitate comparison with the normalized Gaussian density function.

Fast-Fourier transform techniques facilitated computation of power spectral density functions of error and control signals. Each "spectrum" so computed was separated into two components: (a) a portion linearly correlated with the external input disturbance, and (b) a "remnant-related" component associated with stochastic pilot response behavior not linearly related to the input. The input-correlated portions of error and control spectra were used in the computation of pilot describing functions; both input-correlated and remnant-related components of control spectra were used in the model-matching procedure.

Relative levels of remnant-related and input-correlated power provided an indication of measurement reliability. If the estimated input-correlated error and control power were not both at least 4 dB greater than corresponding estimates of remnant-related power, frequency-domain measures computed at this frequency were considered insufficiently reliable for model analysis.

The frequency-domain analysis techniques described above are similar to those employed in previous studies and are described in greater detail in [20, 21].

A performance score was obtained for the monitoring task which yielded a number proportional to the fraction of time that the pilot's response button was not in the appropriate state. The combined state of the stimulus meters was continuously monitored ("in" if both meter indications were in the allowable region, "out" if not), as was the instantaneous state of the subject's response button. An integrator was charged whenever the response was inappropriate. Only a single performance measure for the total search task was obtained; no attempt was made to distinguish between the various types and sources of monitoring error.

Model analysis

In order to relate the pilot-display interaction to relevant pilot parameters, the tracking performance measures described above were compared with theoretical results from the state-variable (or "optimal-control") pilot/vehicle model. As this model has been well documented in the literature [18, 19], no detailed description is given in this paper. We shall, however, briefly review the pilot-related parameters of this model.

Three classes of model parameters characterize pilot limitations in laboratory tracking situations. First, an effective transport lag (i.e., "time delay") is associated with each perceptual variable. Current implementation of the model requires a single value for all such delays. Typical values range from 0.15 to 0.2 seconds.

Second, a "motor time constant" is associated with each control variable. Typical values range from about 0.08 to 0.10 for laboratory tasks.

Finally, one or more variables related to pilot remnant are required. Pilot remnant is accounted for in the model by a set of white-noise disturbances added to each sensory variable used by the pilot (i.e., "observation noise"). In addition, noise may also be considered to be added directly to the pilot's control (i.e., "motor noise").

In situations using idealized display and controls with optimally-selected display and control gains, each observation noise variance tends to scale with the variance of the associated display quantity [22]. The constant of proportionality is approximately the same for all inputs derived from a single display indicator (typically, indicator displacement and rate). In this case, pilot remnant can be related to an effective "observation noise/signal ratio". Experimental evidence suggests that this ratio varies inversely with the amount of attention paid to the task [20, 23]. A value of 0.01π (i.e., -20 dB) is a typical observation noise/signal ratio for single-variable laboratory tracking tasks using stable vehicle dynamics.

Display-related sources of pilot remnant can be included to account for sensory threshold and resolution limitations in non-idealized display situations [21, 24, 25]. Typical values of effective "thresholds" for continuous CRT presentations are 0.05 degrees visual arc for indicator displacement and 0.2 degrees/second visual arc for indicator velocity.*

Motor noise has usually been found to contribute relatively little to pilot remnant and system error and has been included mainly to reflect the pilot's imperfect knowledge of his control inputs. A typical value for motor noise/signal ratio is -25 dB.

ORIGINAL PAGE IS OF POOR QUALITY

3. EXPERIMENTAL RESULTS

Initial Training

Prior to the first formal data session, the subjects were given considerable practice on the simulated pitch and roll tracking tasks described in Section 2. They were trained first with the continuous visual display to facilitate rapid learning of the system dynamics. Each subject received about thirty 4-minute trials with the visual display, which was enough training to yield reasonably stable performance scores on the order of what we had expected from past levels of pilot performance. Training then commenced with the tactual display.

Each subject received over 100 training trials with the various tactual display geometries and coding schemes explored in this study. On the basis of mean-squared error scores obtained during this phase of the program, the geometry and coding described in Section 2 were adopted for the remainder of the experimental program.

Although the subjects were trained mainly on the combined pitch/roll task, they also received training on each component task individually. Subjects were instructed to minimize mean-squared tracking error when tracking a single axis and to minimize the sum of the mean-squared pitch and roll errors when tracking two axes. Performance scores were reported after each training trial. Training was continued until performance under each condition appeared to reach a reasonably stable level.

*Threshold-like effects are handled by a statistical linearization procedure. The observation noise variance associated with a given display variable is incremented whenever the predicted rms signal level fails to be large relative to the assumed threshold. The noise-adjustment procedure is described in [24].

ORIGINAL PAGE IS OF POOR QUALITY

Experiment 1: Tactual Tracking Performance

The primary objective of the first formal experiment was to quantify the interaction between the pilot and the tactual display in terms of pilot-related model parameters. A secondary objective was to provide a comparison of tactual tracking performance to performance with a continuous visual display.

Experimental Conditions

The simulated attitude-regulation task was performed alternately with the tactual and continuous visual displays. Performance measures were obtained for each axis tracked separately as well as for the combined pitch/roll task.

Two levels of input amplitude were employed for tactual tracking so that display-related threshold effects could be quantified. Because of the large performance scores obtained with the tactual display, input amplitudes used with this display were lower than the level used with the visual display.

The various conditions explored in this experiment are listed in Table 1. Input amplitudes are shown relative to the amplitude used with the visual display. To the extent possible, the various tasks were presented in a balanced order.

Table 1

Conditions Explored in Experiment 1

Display	Tasks (P=Pitch, R=Roll)	Rel. Input Amplitude	No. Replications Per Condition Per Subject
Visual	P, R, P + R	1.	2
Tactual	P, R, P + R	.5	3
Tactual	P, R, P + R	.25	3

Tracking Performance

Average standard deviation (SD) scores for tracking error are shown in Figure 5. (Mean errors were negligible, for the most part, and are not shown here.) The performance scores shown in this figure and throughout the paper are given in terms of analog machine units. One machine unit of error corresponds to 2 cm vertical deflection of the visual error presentation for pitch and about 50° rotation for roll. One unit of control effort represents approximately 7.7 newtons of force.

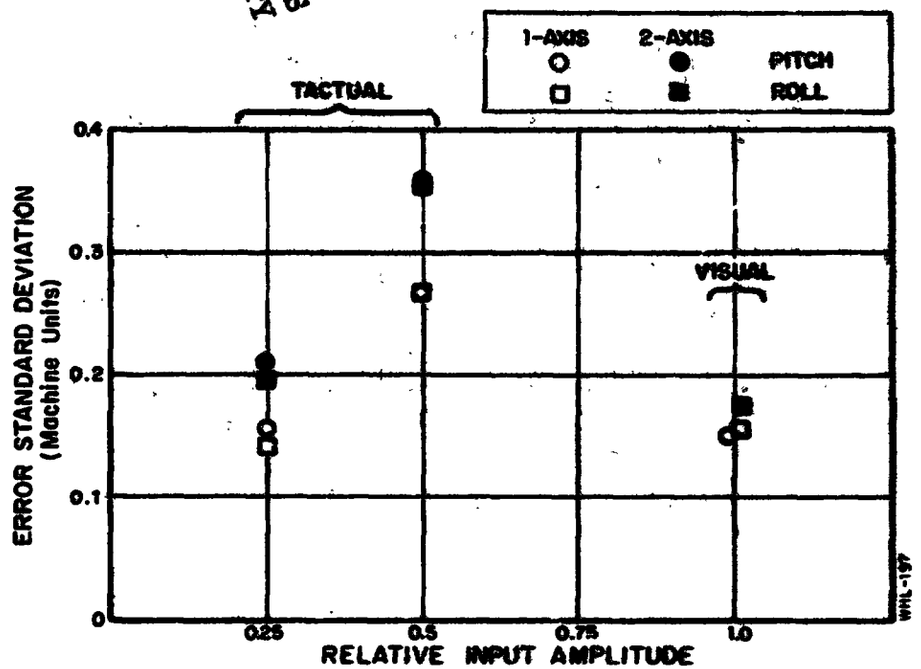

FIGURE 5. Effect of Input Amplitude on Error SD Scores (Average of Two Subjects)

As expected from considerations of the display coding scheme, tactual tracking performance was considerably less efficient than performance with the visual display. When corrected for differences in input amplitude, the single-axis tactual scores were found to be about 3.5 times as large as the visual scores. Also as expected, the scores associated with the tactual display did not vary proportionally with input amplitude. Extrapolation to zero input yields a (positive) non-zero error score, which suggests the presence of threshold-like effects.

No significant inter-axis interference effects were found with the visual display. The 1-axis and 2-axis pitch error scores were virtually identical; the small increment (about 15%) associated with the 2-axis roll score was not found to be statistically significant.*

Interference effects with the tactual display were larger, more consistent, and statistically significant. Two-axis standard deviations were about 35% greater for both pitch and roll. This relative difference was unaffected by input amplitude. As shown later in the paper, a good portion of the interference effects seen with the tactual display can be predicted from analysis of the coding scheme.

Use of the tactual display resulted in pulse-like control inputs, whereas the visual display allowed continuous-looking control activity. Both subjects commented that the pulse-like behavior reflected a "wait-and-see" strategy that was dictated by the relatively long time delay associated with the tactual presentation.

Sample time histories of error and control signals in a 2-axis training session are shown in Figure 6. Control pulses were applied singly and in bursts at irregular intervals. Pulses within a single burst were separated by about 0.4 seconds, and intervals between bursts of activity with a given control input ranged up to 5 seconds. Figure 6 shows that the pitch and roll tasks were controlled sequentially.

Since the pilot/vehicle model used in this study is predicated on Gaussian tracking variables, amplitude density distributions were obtained for selected time histories to determine the extent to which this assumption was violated. Time histories for error and control (one per subject) were analyzed for the 1-axis, larger-input, pitch tracking task with tactual display. As expected, the control amplitude-density curves were highly non-Gaussian and had large peaks associated with zero control activity. The error amplitude densities, however, were much more nearly Gaussian in appearance.

*Statistical significance was tested by analysis-of-variance.

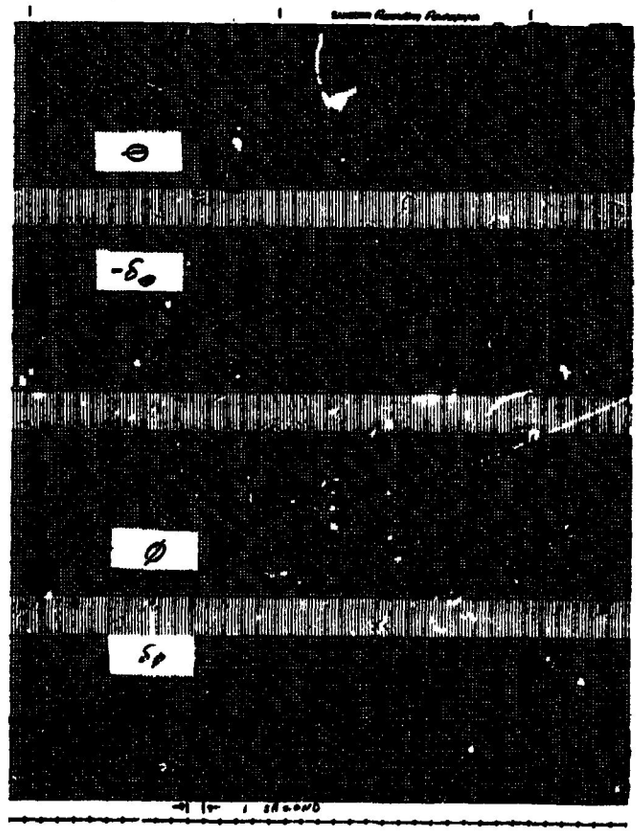

FIGURE 6. Time Histories of Error and Control Signals

Because of the non-Gaussian pilot response activity, the pilot/vehicle model must be applied with caution. Clearly, one cannot expect to obtain accurate predictions of detailed *control* behavior. It is possible, nevertheless, that reliable predictions of *tracking error* can be obtained, once the model parameters have been "calibrated" to account for the interaction between the pilot and the tactual display.

Model Analysis

Model analysis was undertaken with the following two objectives in mind: (1) obtain a representation of pilot-display interaction in terms of pilot-related model parameters, and (2) demonstrate the utility of the pilot/vehicle model in predicting system performance with the tactual display. Except for an initial calibration of display-related parameters, emphasis was on *predicting*, rather than *matching*, experimental results.

We adopted the following strategy for model analysis:

1. Match the experimental measurements obtained for the single-axis pitch task with the visual display in order to determine pilot time delay, motor time constant, and observation noise/signal ratio.

2. Match the data from the single-axis, large-input pitch task with the tactual display in order to determine the changes in pilot-related parameters required to account for the pilot's interaction with the tactual display.

3. Use the parameter values determined above to predict the effects of input amplitude, multiple-tasks, and system dynamics on system performance.

Data-fitting was performed by an informal search of the model-parameter space and was terminated when visual inspection revealed a "good" match between model outputs and experimental measurements. In general, error and control scores were matched to within 10 percent, and pilot describing functions and control spectra were matched within 2 or 3 dB. All data used for comparison with model results represents average performance of the two test subjects.

An acceptable match to single-axis pitch performance was obtained with a time delay of 0.2 seconds, a motor time constant of about 0.11 seconds, an observation noise/signal ratio of approximately -21.5 dB, and a motor noise ratio of about -25 dB. These parameter values are consistent with previous analysis of single-variable laboratory tracking tasks [18, 19].

Comparison of experimental frequency-domain measures with model results is provided in Figure 7. Note that comparisons are shown for both the input-correlated and remnant-related components of the control spectrum.

Having quantified the pilot-related parameters on the basis of visual tracking, we then attempted to predict differences between visual and tactual tracking performance from an analysis of the tactual display properties alone. Since a minimum tracking error of 0.1 units was required to generate a sequence of two or more tactors, an effective threshold of 0.1 unit was assumed for perception of error displacement. An essentially infinite threshold was specified for error rate on the assumption that the sample-and-hold type of coding scheme programmed for the tactual display would prohibit the direct perception of useful rate information.

Perceptual time delay was incremented to account for the delay imposed by the tactual coding scheme. The size of the increment had to be recomputed for each experimental condition because of the dependent relationship between display-related time delay and tracking error. The display period associated with the error SD score was taken as a rough estimate of the required increment and was determined from the appropriate timing curve of Figure 4.

An incremental time delay of approximately 0.45 seconds was derived for the single-axis, large-input pitch task. This increment was added to the 0.2 seconds determined from the visual tracking data to yield a combined pilot-display time delay of 0.65 seconds.

Values for motor time constant and noise/signal ratios derived from the visual tracking experiments, along with the revised computations of time delay and perceptual thresholds, allowed a tentative prediction of tactual tracking performance. These predictions did not provide a satisfactory match to the data, however. Only slightly over half of the difference between visual and tactual errors was accounted for. Moreover, the model predicted a substantially lower control SD score than was actually measured for the tactual display. We found, however, that an increase in motor noise/signal ratio to about -14.5 dB allowed both error and control SD scores to be matched to within 10%. As the reader can judge from Figure 8, a good match to the frequency-domain measures was also obtained. Apparently, the unexpectedly large value of motor noise was needed to account for the way in which pulse-like control behavior influenced the measurements.

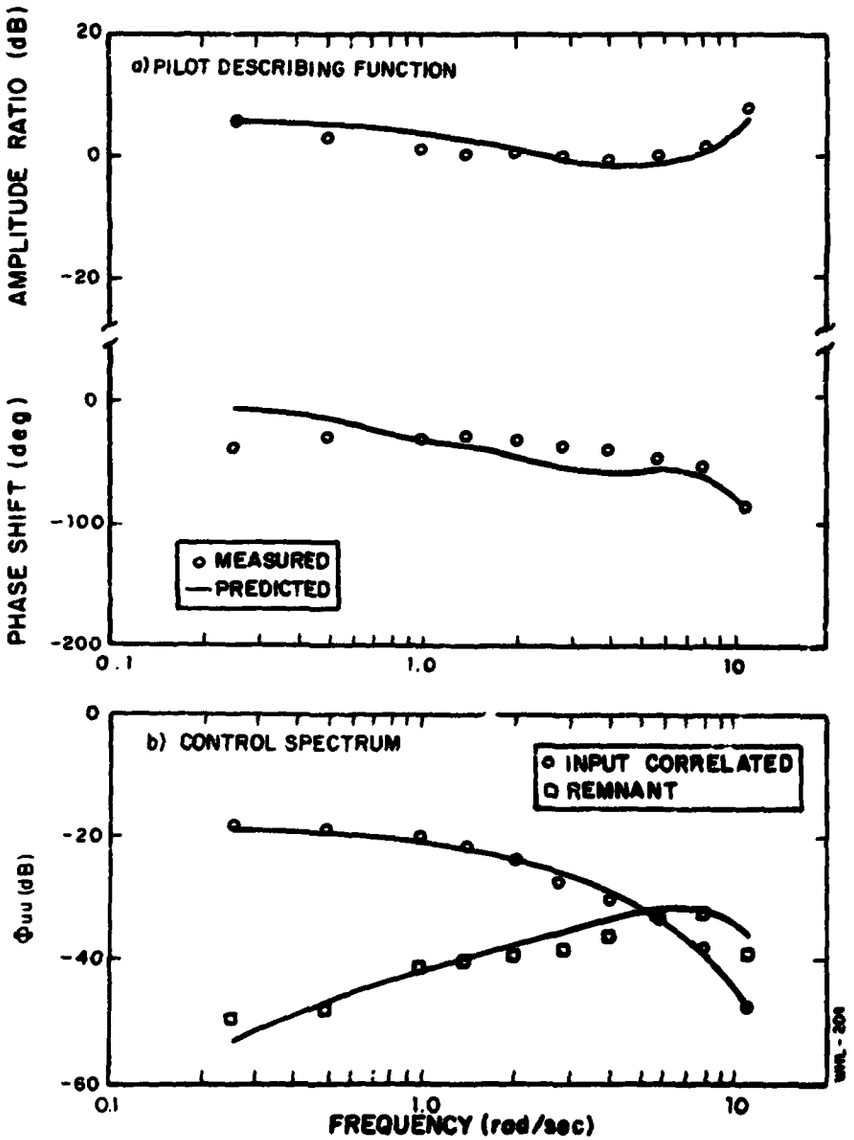

FIGURE 7. Frequency-Domain Measures for Visual Tracking, 1-axis Pitch (Average of 2 Subjects, 2 Trials/Subject)

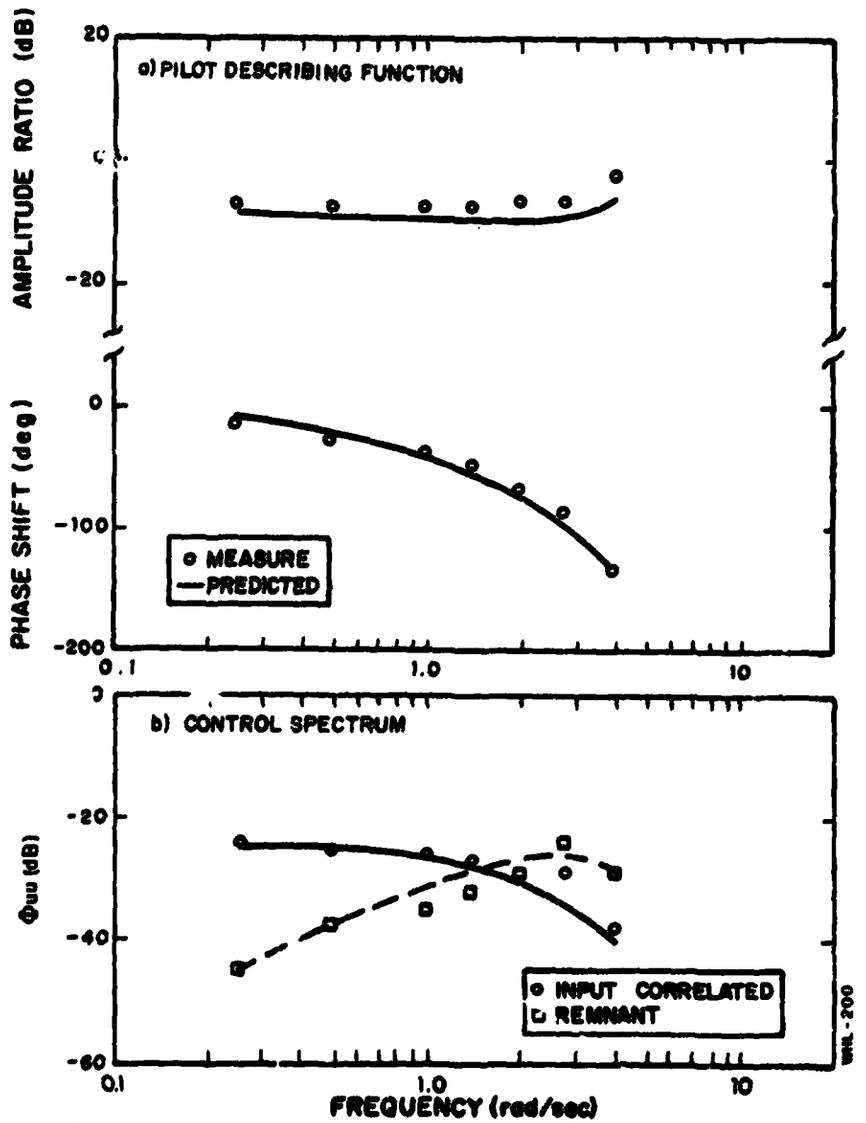

FIGURE 8. Frequency-Domain Measures for Tactual Tracking, 1-axis Pitch (Average of 2 Subjects, 3 Trials/Subject)

Except as noted below, model parameter values determined in this calibration effort were used to predict the effects on system performance of (a) a change in input amplitude, (b) the addition of a second axis of tracking, and (c) the effects of changing the vehicle dynamics from pitch to roll. Time delay was recomputed in each case, and the effects of central attention-sharing in the two-axis task were represented by a doubling of the observation noise/signal ratio (see Refs. 20, 21). Parameter values used in obtaining these predictions, as well as those used in the preceding calibration efforts, are shown in Table 2.

Table 2

Values for Pilot-Related Model Parameters

Experimental Condition	Parameter Values					
	τ	T_n	v_o	$\dot{v}_o$	P_y	P_m
1-axis pitch, visual disp.	.20	.11	0.0	0.0	-21.5	-25
1-axis pitch, tactual disp., larger input	.65	.11	0.1	10.	-21.5	-14.5
1-axis pitch, tactual disp., smaller input	.72	.11	0.1	10.	-21.5	-14.5
2-axis pitch, tactual disp., larger input	.78	.11	0.1	10.	-18.5	-14.5
1-axis roll, tactual disp., larger input	.65	.11	0.1	10.	-21.5	-14.5

τ = effective perceptual time delay, seconds.
T_n = rotor time constant, seconds.
v_o = displacement threshold, machine u.
$\dot{v}_o$ = rate threshold, machine units.
P_y = observation noise/signal ratio, dB.
P_m = rotor noise/signal ratio, dB.

ORIGINAL PAGE IS OF POOR QUALITY

A comparison of predicted and measured error and control SD scores is provided in Figure 9. Except for the 1-axis, larger-input pitch scores, all model results are true predictions; parameter values have not been readjusted to provide the best match in each case.

As expected, the SD scores for tracking error were predicted more accurately than the scores for control effort. Performance measures for the low-input, 1-axis pitch task were predicted most closely; the difference between predicted and measured SD scores for tracking error was negligible, and a good match to the frequency-domain measures (not shown here) was obtained.

The model accounted for about half of the increment in the pitch error score when the roll task was added, with a resulting matching error of about 15%. On the other hand, the model failed to account for the observed increase in control score. Comparison of the measured and predicted control spectra shown in Figure 10 suggests that the mismatch results from an under-prediction of the increase in controller remnant. The accurate prediction of the pilot describing function – particularly the phase-shift behavior – indicates that a reasonable approximation was made to the effective time delay imposed by the tactual display.

The 1-axis roll error score was predicted to within about 10% of its measured value. Inspection of the frequency-domain results (not shown here) indicates that modelling errors stemmed primarily from a too-high prediction of remnant-related control power.

Experiment 2: Comparison of Tactual and Quantized Visual Displays

The second formal experiment was designed to determine the extent to which the substantial performance decrement associated with the tactual display could be attributed to the coding scheme itself. Performance scores obtained with the tactual display were compared with those obtained with the quantized visual display described earlier. One- and two-axis pitch and roll performance was explored. Vehicle and input dynamics were identical to those used in the first experiment, and a single level of input amplitude (relative amplitude of 0.5) was used.

Average error and control SD scores are cross-plotted for the two displays in Figure 11. With one exception, performance scores obtained with the quantized visual display differed by less than 10% from corresponding measures obtained with the tactual display. Since these performance measures showed no apparent differences between displays, further analysis of the data obtained with the quantized visual display was considered to be redundant and, therefore, unnecessary.

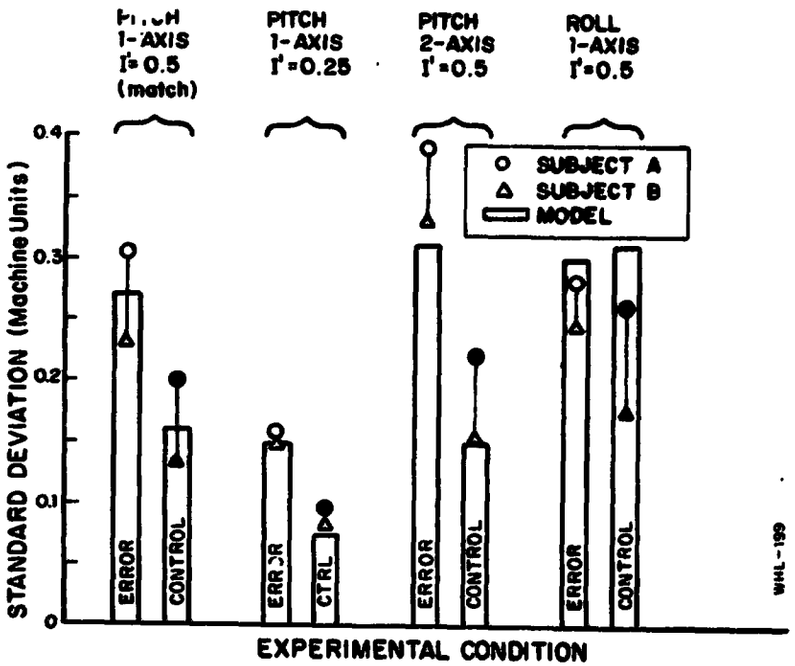

FIGURE 9. Measured and Predicted SD Scores

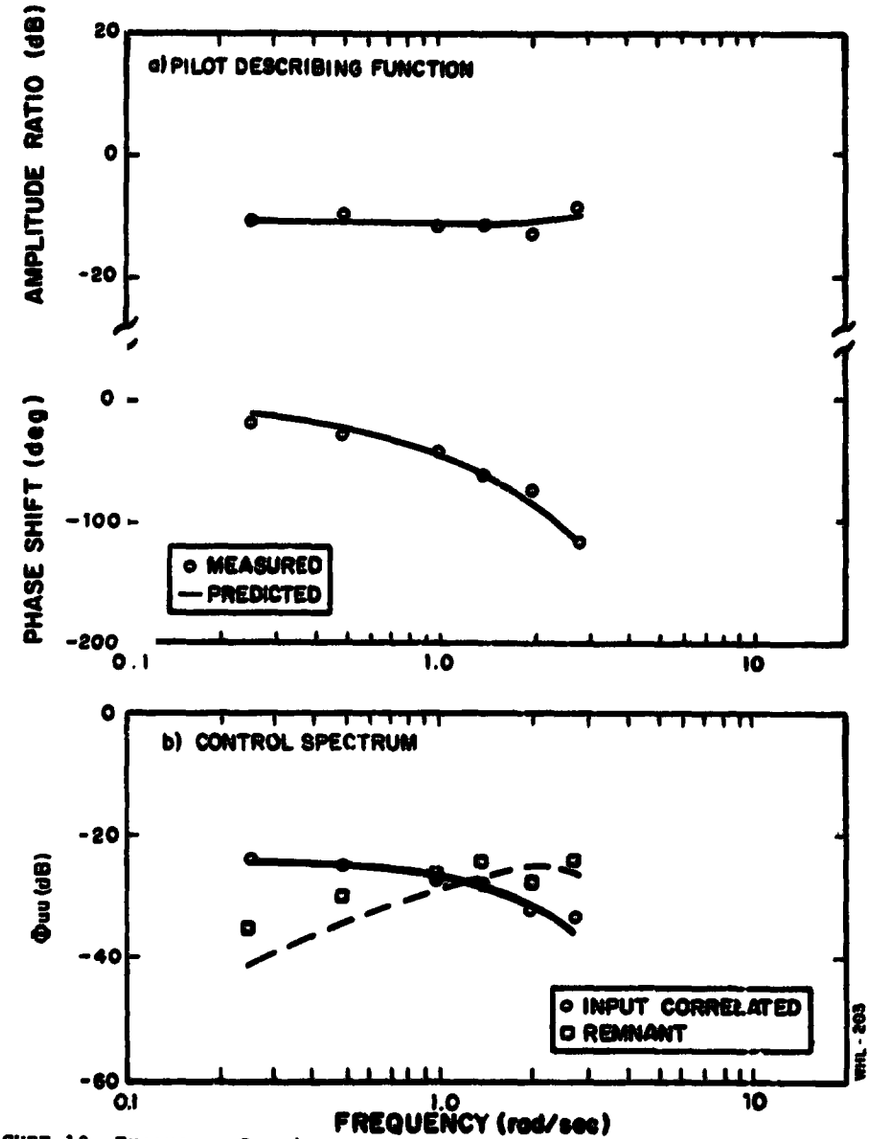

FIGURE 10. Frequency-Domain Measures for Tactual Tracking, 2-axis Pitch (Average of 2 Subjects, 3 Trials/Subject)

ORIGINAL PAGE IS OF POOR QUALITY

On the basis of the results shown in Figure 11 we conclude that the degradation in tracking performance associated with the tactual display was due primarily to the coding scheme and not to the use of the tactual sensory mode per se. We do not rule out the possibility that such effects were present – asserting only that they were small compared to the effects of the coding scheme.

Experiment 3: Combined Tracking and Visual Monitoring

The visual monitoring task described in Section 2 was combined with a tracking task in order to determine the potential effectiveness of tactual displays in multi-task situations that impose a high visual scanning workload. The tracking task was modified to provide a lower-bandwidth task of the type to which a tactual display might reasonably be applied in practice. In order that we could explore a single source of task interference – namely, interference between tracking and monitoring – a single – axis tracking task was employed.

The roll-axis task was eliminated, and the simulated pitch dynamics used in the previous experiments were modified as follows: (a) the natural frequency of the second-order filter was reduced from 6 to 1 rad/sec, and (b) the zero in vehicle transfer function was eliminated. The disturbance input was the same as used in previous experiments and was added in parallel with the pilot's control input. One of the test subjects – the former Navy pilot – commented that the revised system behavior was similar to the response of the angle-of-attack indicator to control inputs during carrier approach. In order to reduce the disparity between tactual and visual tracking error scores, the input amplitude used for tactual tracking was 1/3 of that used for visual tracking.

The subjects were trained on the following five tasks: (a) monitoring only, (b) tracking-only with the continuous visual display, (c) tracking-only with the tactual display, (d) combined monitoring and tracking with the visual display, and (e) combined monitoring and tracking with the tactual display. Each subject received a minimum of 15 trials on each task, which appeared to be sufficient training to yield near-asymptotic levels of performance in the various tasks.

Tracking and monitoring scores are shown in Figure 12 for single- and combined-task situations. Tracking scores are given in terms of mean-squared error in machine units (1 machine unit = 2 cm indicator displacement); monitoring scores are in terms of fraction-of-time of incorrect response, divided by 5 to make the monitoring score numerically comparable to the tracking score.

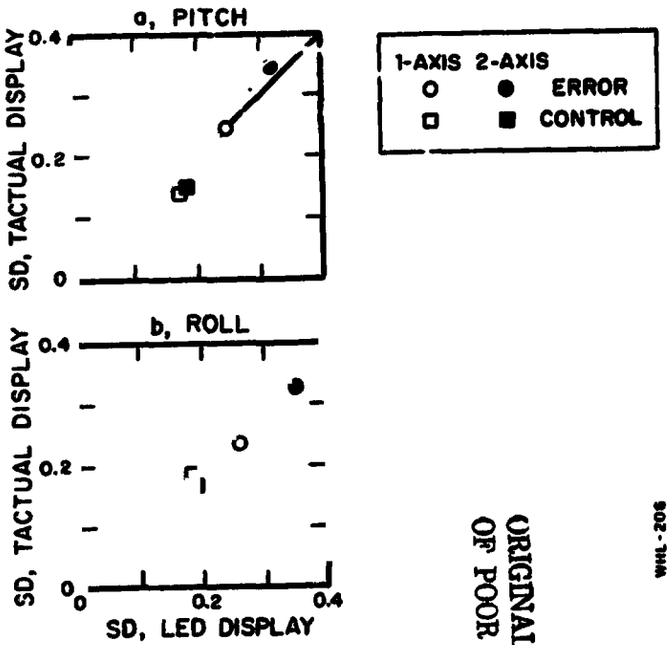

ORIGINAL PAGE IS
OF POOR QUALITY

WHL-206

FIGURE 11. Effect of Sensory Mode on SD Scores

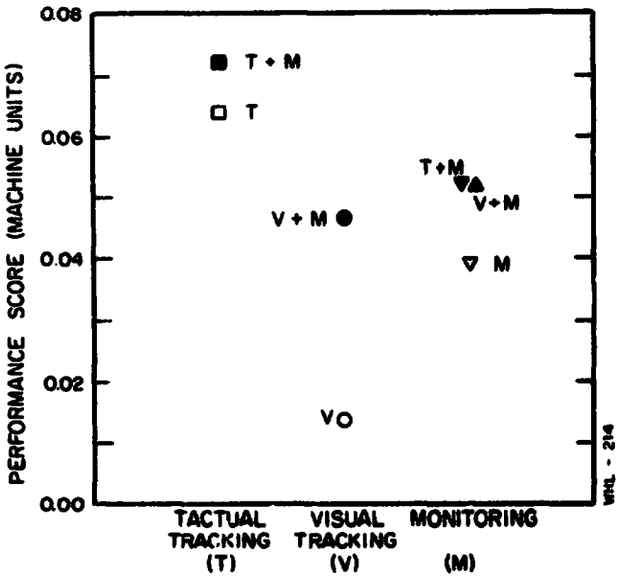

FIGURE 12. Comparison of Single- and Combined-Task Tracking and Monitoring Performance Scores

Average of 2 subjects, 3 trials/subject

Although visual tracking scores were consistently lower than corresponding tactual tracking scores, the interference of the monitoring task with tracking performance was considerably less when the tactual display was used. Single-task and combined-task tactual tracking scores differed on the average by about 12% – a difference that was not found by an analysis of variance to be statistically significant. The combined-task visual tracking score, on the other hand, was over three times as great as the single-task score. This difference was found to be statistically significant at the 0.001 level.

Interference in the reverse direction was also statistically significant; that is, the monitoring score increased significantly in the presence of the tracking task. The increase in score was about 35% (significant at the 0.01 level) and was the same whether the tactual or the visual display was used in the concurrent tracking task.

4. CONCLUSIONS

An experimental program was conducted to evaluate the suitability of a tactual display for aircraft flight control. The tactual display was configured in an X-Y format, and tracking error was indicated both by the number of vibrotactors excited in a sequence and by the rate at which successive tactors were excited. Tracking performance was observed in simulations of high-bandwidth and low-bandwidth aircraft dynamics, and combined tracking and visual-monitoring tasks were performed.

The experimental results lead to the following conclusions:

1. Interference between a tracking task and a visual monitoring task is considerably reduced when the tactual tracking display replaces a continuous visual tracking display.

2. Tracking errors obtained with the tactual display used in this study are substantially greater than errors obtained with a continuous visual display in a similar flight-control situation. Differences between 1-axis and 2-axis tracking performance are also greater for the tactual display.

3. Performance degradation of the tactual display is due primarily to the coding scheme adopted in this study – not to the use of the tactual sensory mode itself.

4. Tracking errors are corrected by intermittent pulse-like control inputs when the tactual display is used, apparently because of the large effective time lag imposed by the coding scheme.

5. The state-variable model for pilot/vehicle systems can be used to obtain reasonably accurate predictions of tracking error scores when the vehicle dynamics are wide-band, despite non-Gaussian pilot response behavior. Once the pilot-related model parameters have been adjusted to reflect the pilot-display interaction, the effect of changes in various aspects of the system configuration may be predicted.

Preliminary results suggest that the particular coding scheme used in this study has fulfilled our original expectations. At the cost of degraded single-task tracking performance, a tactual display has been designed which appears to allow relatively little interference between tracking and visual monitoring tasks. The question remains: can an alternative coding scheme be devised which provides improved single-task performance while maintaining minimum interference effects?

Tactual coding schemes that are more akin to simple intensity-coding have been found to provide superior single-task tracking efficiency. To our knowledge, however, such displays have not been shown to be effective in multi-task situations. Accordingly, we recommend that alternative coding schemes be explored in order to arrive at a tactual display design which best fulfills the twin objectives of good single-task performance and minimum task interference.

ORIGINAL PAGE IS
OF POOR QUALITY

5. REFERENCES

1. Levison, W. H., R. Tanner, and T. Triggs, "Tactile Display for Aircraft Control", Semi-Annual Technical Report, Sanders Associates, Inc., Nashua, New Hampshire, January 1973.

2. Forbes, T. W., W. R. Garner and J. C. Howard, "Flying by Auditory Reference ("Flybar"). Psycho-Acoustic Laboratory, Harvard University, OSRD Report No. 5123, 1945.

3. Flynn, J. P., S. J. Goffard, I. P. Truscott and T. W. Forbes, "Auditory Factors in the Discrimination of Radio Range Signals: Collected Informal Reports", Psycho-Acoustic Laboratory, Harvard University, OSRD Report No. 6292, 1945.

4. Ballard, J. W. and R. W. Kessinger, "Human-Engineered Electromechanical Tactual Sensory Control System", Elect. Manuf., 118-121, 1954.

5. Hirsch, J. and I. Kadushin, "Experiments in Tactile Control of Flying Vehicles", 6th Annual Conf. of Aviation and Astronautics, 64-68, 1968.

6. Fenton, R. E., "An Improved Man-Machine Interface for the Driver-Vehicle System", IEEE Trans. Human Factors in Electronics, 7, 150-157, 1966.

7. Hill, J. W., J. C. Bliss and K. W. Gardiner, "Applications of Tactile Displays for Pilot Cueing", Fifth Annual NASA-University Conference on Manual Control, NASA SP-215, 285-290, 1969.

8. Hill, J. W., "A Describing Function Analysis of Tracking Performance Using Two Tactile Displays", IEEE Transactions on Man-Machine Systems, 11, 92-101, 1970.

9. Weissenberger, S. and T. B. Sheridan, "Dynamics of Human Operator Control Systems Using Tactile Feedback", J. Basic Engr'g., 297-301, 1962.

10. Bliss, J. C., "Tactual Perception: Experiments and Models", Final Report, SRI Project 6070, Contract NAS2-3649, Stanford Research Institute, Menlo Park, California, 1967.

11. Seeley, H. F. and J. C. Bliss, "Compensatory Tracking with Visual and Tactile Displays", IEEE Transactions on Human Factors in Electronics, 7, 84-90, 1966.

12. Hoffman, M. A.,"A Comparison of Visual, Auditory, and Electrocutaneous Displays in a Compensatory Tracking Task", unpublished doctoral dissertation, University of South Dakota, 1968.

13. Durr, L. B., "Effect of Error Amplitude Information", M. A. Thesis, University of Virginia, 1961.

14. Howell, W. C. and C. F. Briggs, "An Initial Evaluation of a Vibrotactile Display in Complex Control Tasks", Ohio State University Technical Report (813)-5, AD-320472, 1959.

15. Geldard, F. A., "Cutaneous Channels of Communication", In Sensory Communication, (W. A. Rosenblith, Ed), MIT Press, Cambridge, Massachusetts, 73-88, 1959.

16. Neal, T. P. and R. E. Smith, "An In-Flight Investigation to Develop Control System Design Criteria for Fighter Airplanes", Wright-Patterson Air Force Base, Ohio, AFFDL-TR-70-74, Volume 1, 1970.

17. Boothe, E. M. and M. L. Parrag, "Evaluation of Lateral-Directional Handling Qualities and Roll-Sideslip Coupling of Fighter Class Airplanes", Wright-Patterson Air Force Base, Ohio, AFFDL-TR-72-36, Volume 1, 1972.

18. Kleinman, D. L., S. Baron and W. H. Levison, "An Optimal Control Model of Human Response Part I: Theory and Validation, Automatica, 6, 357-369, 1970.

19. Kleinman, D. L., S. Baron and W. H. Levison, "A Control Theoretic Approach to Manned-Vehicle Systems Analysis", IEEE Transactions on Automatic Control, Volume AC-16, No. 6, 1971.

20. Levison, W. H., J. I. Elkind, and J. L. Ward, "Studies of Multivariable Manual Control Systems: A Model for Task Interference", NASA CR-1746, 1971.

21. Levison, W. H., "The Effects of Display Gain and Signal Bandwidth on Human Controller Remnant", AMRL-TP-70-93, Aerospace Medical Research Laboratory, Wright-Patterson Air Force Base, Ohio, 1971.

22. Levison, W. H., S. Baron and D. L. Kleinman, " A Model for Human Controller Remnant", IEEE Trans. Man-Machine Systems, Vol. MMS-10, No. 4, 1969. Also NAS8-21136, 1968.

23. Levison, W. H., "A Model for Task Interference", International Symposium on Man-Machine Systems, September 1969, IEEE Conference Record No. 69C58-MMS.

24. Kleinman, D. L. and S. Baron, "Analytic Evaluation of Display Requirements for Approach to Landing", NASA CR-1952, 1971.

25. Baron, S. and W. H. Levison, "A Manual Control Theory Analysis of Vertical Situation Displays for STOL Aircraft", Bolt Beranek and Newman Inc., Cambridge, Mass., Rept. No. 2484, 1973.

ORIGINAL PAGE IS OF POOR QUALITY

THE DESIGN AND EVALUATION OF AN AURAL STALL WARNING SYSTEM (ASWS)

by

Professor Michael H. Redlin

Lieutenant P. E. Mullowney

The Aural Stall Warning System (ASWS) addresses itself to the prevention of stall and the resulting spin of high performance aircraft. Utilizing a distinctive yet simple aural display format, the ASWS not only warns the pilot of impending stall but also provides accurate angle of attack information in the high angle of attack region where visual presentation has heretofore proven to be inadequate. Small, lightweight ASWS prototypes have been designed, fabricated and evaluated in a laboratory environment and in the Air Combat Maneuvering (ACM) arena in the Differential Maneuvering Simulators located at the NASA Langley Research Center, Hampton, Virginia. Results obtained indicate a marked increase in pilot performance while in the ACM environment and a definite prevention of stall with the addition of the ASWS.

PRECEDING PAGE BLANK NOT FILMED

SESSION II

RIDE QUALITIES AND HANDLING

N75 19133

PRECEDING PAGE BLANK NOT FILMED

PITCH PAPER PILOT REVISITED

John D. Arnold, Robert B. Johnson, James D. Dillow

Air Force Institute of Technology

Wright-Patterson AFB, Ohio

ABSTRACT

Two methods are described for predicting the handling qualities of an aircraft in pitch. Both methods are based on minimizing a pilot rating expression with respect to free pilot parameters. In one case the pilot rating expression was developed from a set of moving base simulation data. In the other case, the pilot rating expression was developed from a set of fixed base simulation data. In both cases pilot rating is primarily a function of pitch attitude and pitch rate; however, in the moving base case, the pilot rating is more sensitive to pitch rate than in the fixed base case. For each method, predicted pilot ratings and performance measures agree well with the measured data corresponding to that case. Both methods are used to predict pilot ratings for a set of flight test configurations and the results of the two methods agree to within one half a rating unit. The predicted ratings in both cases correlate well with the actual pilot ratings from the flight tests.

INTRODUCTION

The paper pilot concept for predicting aircraft handling qualities in a specified piloted task is based on the following hypothesis.

1. For a well defined task, the pilot rating is a function of the closed loop performance and the pilot workload. This function is called the pilot rating expression.

2. The predicted pilot rating can be obtained by minimizing the pilot rating expression with respect to free pilot parameters in the closed loop pilot-vehicle model. (The lower the rating--the better the handling qualities.) The minimal value of the pilot rating expression corresponds to the pilot rating for the task.

The paper pilot concept was successfully used to develop a method of predicting the longitudinal handling qualities of a VTOL aircraft in a precision hover task (Refs 1 and 2). In this case the pilot rating expression is a function of rms pitch rate, rms longitudinal hover error and two pilot lead time constants in the pilot model. The predicted pilot ratings agree well with actual pilot ratings from a fixed base flight simulation study (Refs 3 and 4).

The paper pilot concept was next applied to a pitch tracking task (Ref 5). The pilot rating expression, for the commanded pitch tracking task was taken to be a function of the rms tracking error and the pilot lead time constant in the pilot model. In this application, the predicted pilot ratings did not compare well with actual ratings for certain cases. For those cases where the short period approximation to the aircraft dynamics has a high natural frequency and is lightly damped, the predicted rating tends to be well below the actual ratings (Ref 5).

Two new methods for predicting aircraft handling qualities in pitch have been developed to correct the deficiencies in the original pitch paper pilot (Ref 5). They were developed independently; however, both methods are based on the paper pilot concept. In one case the pilot rating expression was developed based on an existing set of data from a moving base simulation. In the other case a set of fixed based simulation data was generated and used to develop the pilot rating expression. The two methods are described and compared in this paper.

PILOT VEHICLE MODEL

The piloted task considered was that of maintaining a nominal or zero pitch attitude in the presence of a vertical gust disturbance. The closed loop system is represented by the block diagram of Fig. 1.

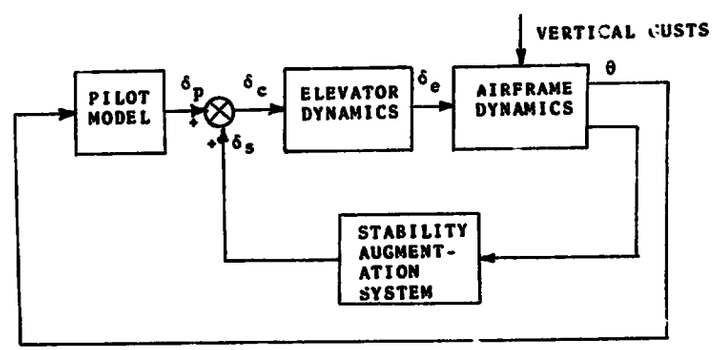

Fig. 1. Pilot-Vehicle Model.

The form of the pilot model used is based on the cross-over model of Ref 6 and is

$$\frac{\delta_p}{\theta} = \frac{K_p(T_L s+1)}{T_I s+1} e^{-\tau s}$$

where K_p is the pilot gain, T_L is the pilot lead time constant, T_I is the pilot lag time constant, and $e^{-\tau s}$ is a pure time delay.

The elevator dynamics are modeled by a first order lag with a relatively high band width.

The airframe dynamics are modeled by linearized longitudinal equations of motion (Ref 5).

The vertical gusts are modeled by shaped, Gaussian amplitude, noise. In each method, a different form for the shaping filter is used; however, in both cases the power spectral density of the gust approximates that of the Dryden model (Ref 7).

The stability augmentation system that was considered included linear feedbacks on pitch rate, pitch acceleration, and normal acceleration.

RBJ PITCH PAPER PILOT

The data used to develop the RBJ pitch paper pilot was taken from a report by Onstott, Salmon, and McCormick (Ref 8). This report includes data from a moving base simulation of the F-5 and A-7 aircraft. Eight configurations for each aircraft were simulated. The simulation studies included the task of holding the pitch attitude to zero in the presence of a vertical gust disturbance. Pilot ratings and rms pitch angles are reported for a variety of rms gust intensities for each aircraft configuration. For each of the 16 aircraft configurations, two cases were selected corresponding to low and high turbulence levels. These 32 cases of different gust/aircraft configurations were then used to determine the pilot rating expression.

The resulting pilot rating expression is

$$J = PERF + .5T_L + 1$$

where

$$PERF = \sigma_\theta + 4\sigma_q$$

and σ_θ and σ_q are the closed loop rms values of pitch attitude and pitch rate, respectively.

The pilot lag time constant is taken to be .1 sec corresponding to a typical neuromuscular lag (Ref 9). The pilot time delay is taken to be $\tau = .32$ sec. The values of K_p and T_L in the pilot model are selected to minimize the value of J.

The predicted pilot rating is then given by

$$PR = R_1(PERF) + .5T_L + 1$$

where

$$R_1(PERF) = \begin{cases} PERF, & 0 \le PERF \le 5.5 \\ 5.5, & PERF > 5.5 \end{cases}$$

The upper limit on R_1 is based on the assumption that there is some limit to the degradation of pilot rating due to poor performance. The $.5T_L$ is a measure of pilot work load. The addition of the constant 1 insures that the predicted pilot rating is greater than 1, which is the minimum (or best) rating on the Cooper pilot rating scale.

The correlation between the predicted pilot rating and the actual pilot ratings from Ref 8 is shown in the scatter diagram of Fig. 2. Good agreement was obtained between the actual and predicted ratings in those cases. In addition the predicted rms values of pitch attitude agree well with the measured values as indicated by Fig. 3.

Details of the RBJ pitch paper pilot are contained in Ref 10.

JDA PITCH PAPER PILOT

A fixed base simulation was conducted to develop the data base from which the JDA pitch paper pilot was developed. The flight tests of the USAF/CAL variable-stability T-33 aircraft (Ref 11) were used as a basis for the fixed-base simulation. These tests were chosen because a full range of aircraft dynamics and pilot ratings were presented. In particular, several configurations had a high short-period natural frequency and were lightly damped. The pilot ratings given in the report were for overall pitch handling qualities, although tracking tasks were accomplished during the flights. The fourteen base configurations described in Ref 11 were selected to simulate. A rms gust intensity (w_g) of 10 ft/sec was used in the simulation. This level of gust intensity was selected as the one which resulted in the best agreement in

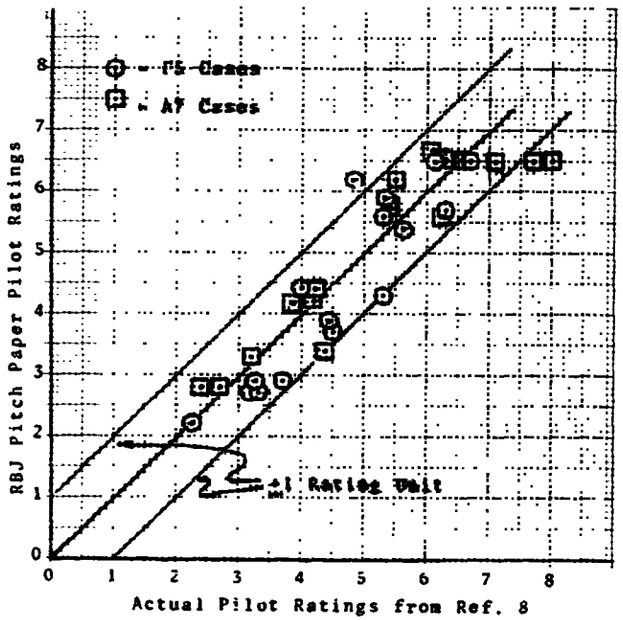

Fig. 2. Comparison of Predicted Pilot Rating and Simulation Pilot Ratings

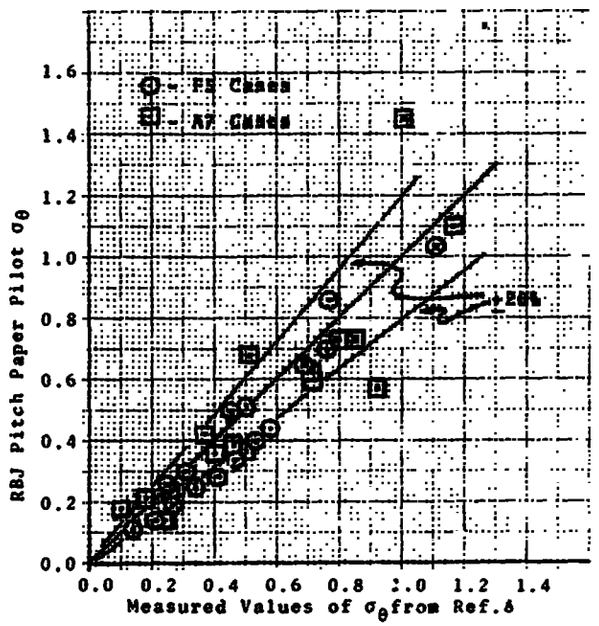

Fig. 3. Comparison of Measured and Predicted σ_θ

pilot ratings between the fixed base simulation and Ref 11. Pilot ratings were given and the rms values of pitch attitude, pitch rate, pitch acceleration, aerodynamic angle of attack, and stick output were measured for seven to twelve runs for each configuration.

The average pilot ratings given during the simulation compare fairly well with the average ratings of the flight tests (Ref 12). The differences in ratings are primarily due to the fact that the flight tests rated overall pitch handling qualities, while the simulation ratings were based only on pitch tracking ability. The results of the simulation were used to determine a pilot rating expression.

The resulting pilot rating expression is

$$J = PERF + .43T_L + 1$$

where

$$PERF = 5.8\sigma_\theta + .43\sigma_q$$

The pilot time delay, τ, was taken to be .3 sec based on an analysis of the simulation data. The values of K_p, T_L and T_I in the pilot model are selected to minimize the value of J.

The predicted pilot rating is then given by

$$PR = R_1(PERF) + .43T_L + 1$$

where

$$R_1(PERF) = \begin{cases} PERF & , 0 \le PERF \le 5.5 \\ 5.5 + .5(PERF - 5.5), & PERF > 5.5 \end{cases}$$

The definition of R_1 is based on the assumption that once the performance deteriorates beyond a certain point, a further deterioration of performance is not as consequential in the pilot rating. The $.43T_L$ is a measure of pilot work load. The addition of the constant 1 insures that the predicted pilot rating is greater than 1.

The correlation between the predicted pilot ratings and the actual pilot ratings from Ref 12 is shown in the scatter diagram of Fig. 4. Excellent agreement was obtained between the actual and predicted ratings in these cases. In addition, the predicted rms values of the system states agree well with the measured values as indicated in Figs. 5 through 8.

Details of the JDA pitch paper pilot are contained in Ref 12.

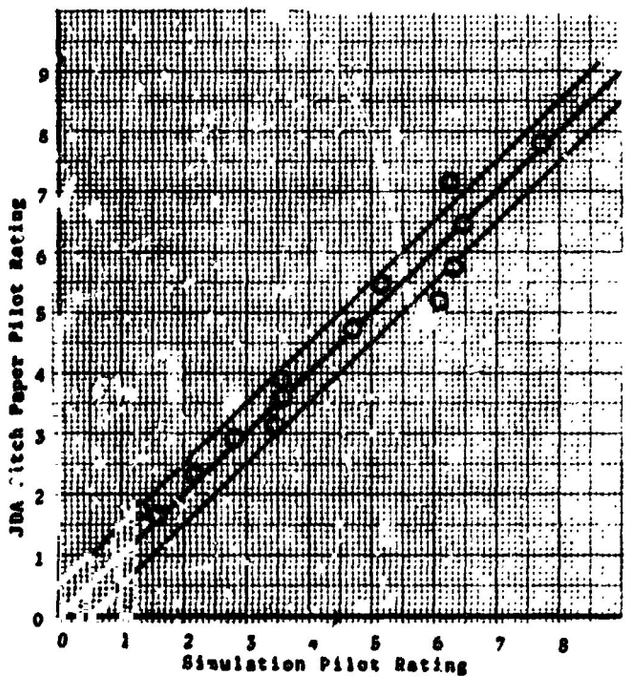

Fig. 4. Predicted Pilot Ratings vs Simulation Pilot Ratings

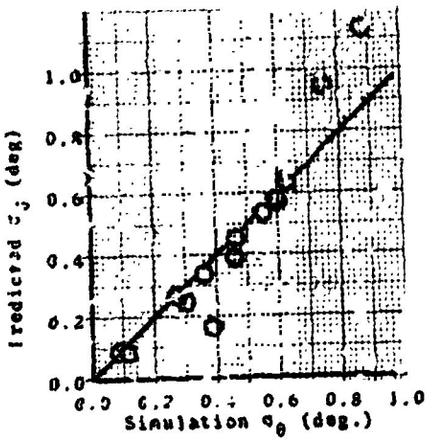

Fig. 5. Predicted vs Simulation σ_θ

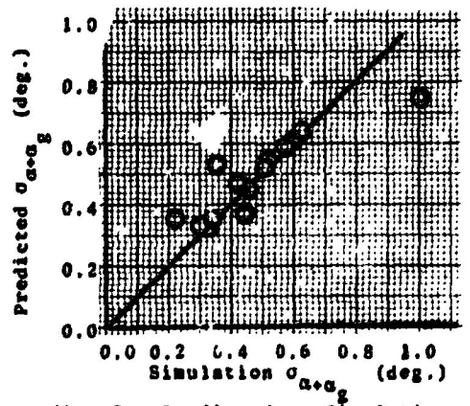

Fig. 7. Predicted vs Simulation $\sigma_{\alpha+\alpha_g}$

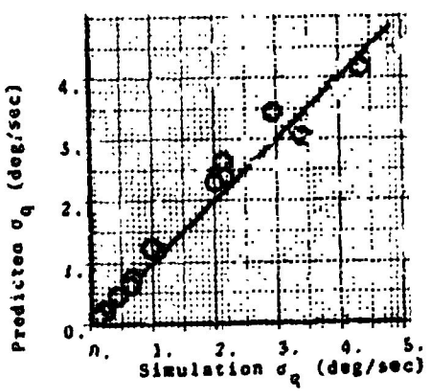

Fig. 6. Predicted vs Simulation σ_q

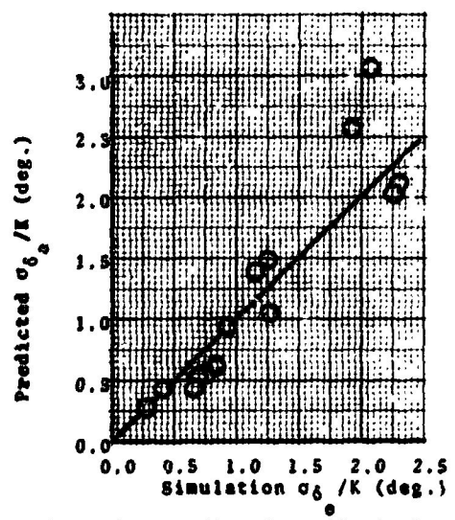

Fig. 8. Predicted vs Simulation σ_{δ_e}/K

COMPARISON OF THE TWO METHODS

Although the two methods of predicting pilot rating are very similar, there are differences in the details. The two major differences are as follows:

1. J is function of σ_θ, σ_q, and T_L in both cases. However in the RBJ method the dominate weighting is on $\sigma_q(\sigma_\theta + \sigma_q)$, where in the JDA method, the dominate weighting is on $\sigma_\theta(5.8\sigma_\theta + .43\sigma_q)$.

2. In the JDA method, pilot lag, T_I is considered as a free parameter in the pilot model and thus in the minimization procedure. There was no indication, however, that the lag term is a significant pilot opinion factor.

In order to determine which method is best, a flyoff was performed. Data from a low altitude, high speed, flight test study (Ref 13) was used in attempt to determine which method would work the best. It was this data that caused the old pitch paper pilot to crash and burn. An rms gust intensity of 10 ft/sec was used in the JDA method. This was the level used in the fixed base simulation used to develop the pilot rating expression. An rms gust intensity of 6.5 ft/sec was used in the RBJ method. This level resulted from finding the rms gust intensity that would give the best agreement between the predicted pilot ratings using the RBJ method and those given in Ref 11.

A comparison of actual pilot ratings and predicted pilot ratings are given in Table I. Predicted ratings are shown for the old pitch paper pilot (Ref 5), the RBJ method and the JDA method. This comparison is shown graphically in Fig. 9.

Table I

Comparison of Predicted and Actual Pilot Ratings

Case (Ref 13)	Pilot Rating: Actual (Ref 13)	Old Pitch Paper Pilot (Ref 5)	RBJ	JDA
LA	4.	2.18	1.94	2.25
LB	2.5	2.25	1.74	1.97
LC	2.25	2.42	1.47	1.70
LD	4.	2.17	3.50	3.80
LE	3.6	2.18	3.24	3.57
LF	2.63	2.24	2.84	3.21
LG	1.33	2.34	2.42	2.71
LH	5.33	2.83	6.05	6.64
LJ	4.	2.66	5.23	5.27
LK	4.	2.63	4.78	5.01
LL	4.1[illegible]	2.62	4.28	4.80

CONCLUSIONS

In both methods, the predicted ratings generally agree well with the rating data that was used to develop the pilot rating expression for that method. Better agreement was obtained with the JDA method, but fewer cases were considered.

In addition both methods give rms performance values that agree well with the actual data that was available for comparison. In particular, the JDA method resulted in predicted rms values that agreed well with measured values for all of the significant states in the pitch task.

When both methods were used on an independent data set (the flight test data of Ref 13), they both resulted in answers that were quite close. There is good correlation between the actual ratings and those predicted by the RBJ and JDA methods. The greatest exception is in the LA case where there is a difference in the order of two rating units. It is of course possible that the actual rating for this case is incorrect.

It is clear from Table I that a great improvement has been realized over the old pitch paper pilot and that the "low damping-high natural frequency" problem of pitch paper pilot has been fixed.

YOU DONE GOOD PAPER PILOT!

REFERENCES

1. Anderson, Ronald O. A New Approach to the Specification and Evaluation of Flying Qualities. AFFDL-TR-69-120. Wright-Patterson Air Force Base, Ohio: Air Force Flight Dynamics Laboratory, June 1970.

2. Dillow, James D. The "Paper Pilot" - A Digital Computer Program to Predict Pilot Rating for the Hover Task. AFFDL-TR-70-40. Wright-Patterson Air Force Base, Ohio: Air Force Flight Dynamics Laboratory, March 1971.

3. Miller, D. P. and E. W. Vinge. Fixed-Base Flight Simulator Studies of VTOL Aircraft Handling Qualities in Hovering and Low Speed Flight. AFFDL-TR-67-152. Wright-Patterson Air Force Base, Ohio: Air Force Flight Dynamics Laboratory, January 1968.

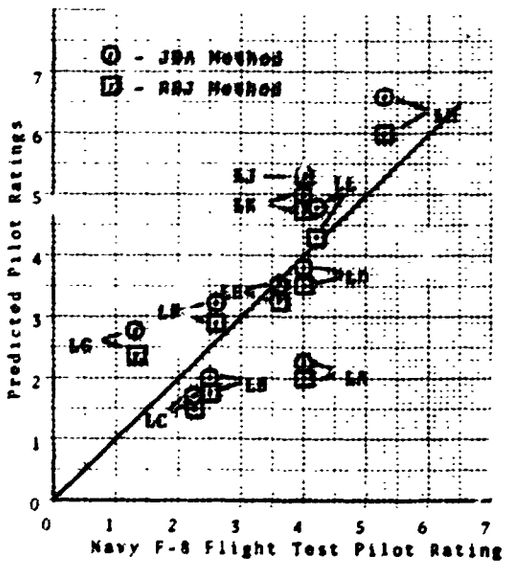

Fig. 9. Comparison of Predicted Pilot Rating and Actual Pilot Ratings from Flight Test Study

4. Vinge, E. W. and D. P. Miller. Analytical and Flight Simulator Studies to Develop Design Criteria for VTOL Aircraft Control Systems. AFFDL-TR-68-165. Wright-Patterson Air Force Base, Ohio: Air Force Flight Dynamics Laboratory, April 1969.

5. Anderson R. O., A. J. Conners, and J. D. Dillow. Paper Pilot Ponders Pitch. AFFDL-TM-70-1. Wright-Patterson Air Force Base, Ohio: Air Force Flight Dynamics Laboratory, November 1970 (Revised January 1971).

6. McRuer, D. T., et al. Human Pilot Dynamics in Compensatory Systems. AFFDL-TR-65-15. Wright-Patterson Air Force Base, Ohio: Air Force Flight Dynamics Laboratory, July 1965.

7. Chalk, C. R.,et al. Background Information and Users Guide for MIL-F-8788 (ASG), "Military Specification - Flying Qualities of Piloted Airplanes." AFFDL-TR-69-72. Wright-Patterson Air Force Base, Ohio: Air Force Flight Dynamics Laboratory, August 1969.

8. Onstott, E. D., E. P. Salmon, R. L. McCormick. Prediction and Evaluation of Flying Qualities in Turbulence. AFFDL-TR-71-162. Wright-Patterson Air Force Base, Ohio: Air Force Flight Dynamics Laboratory, February 1972.

9. Kleinman, D. L. and Baron, S. Manned Vehicle Systems An Analysis by Means of Modern Control Theory. NASA CR-1753. Washington: National Aeronautics and Space Administration, June 1971

10. Johnson, Robert B. Predicting Pitch Task Flying Qualities Using Paper Pilot. AFIT Thesis GGC/MA/73-2, Wright-Patterson Air Force Base, Ohio: Air Force Institute of Technology, June 1973.

11. Neal, T. P. and R. E. Smith. An In-Flight Investigation to Develop Control System Design Criteria for Fighter Airplanes. Vols. I and II. AFFDL-TR-70-74. Wright-Patterson Air Force Base, Ohio: Air Force Flight Dynamics Laboratory, June 1970.

12. Arnold, John D. An Improved Method of Predicting Aircraft Longitudinal Qualities Based on the Minimum Pilot Rating Concept. AFIT Thesis GGC/MA/73-1. Wright-Patterson Air Force Base, Ohio: Air Force Institute of Technology, June 1973.

13. Kastner, T. M., J. A. Evey, and J. J. McCue. Flight Evaluation of Various Short Period Dynamics in the Variable Stability F-8D. NADC-NATC Report No. FT-13R-70, 13 March 1970.

N75 19134

ROLL PAPER PILOT

Flynoy R. Naylor*, James D. Dillow, Russell A. Hannen

Air Force Institute of Technology

Wright-Patterson AFB, Ohio

ABSTRACT

A mathematical model for predicting the pilot rating of an aircraft in a roll task is described. The model includes: (1) the lateral-directional aircraft equations of motion; (2) a stochastic gust model; (3) a pilot model with two free parameters; and (4) a pilot rating expression that is a function of rms roll angle and the pilot lead time constant. The pilot gain and lead time constant are selected to minimize the pilot rating expression. The pilot parameters are then adjusted to provide a 20% stability margin and the adjusted pilot parameters are used to compute a "roll paper pilot" rating of the aircraft/gust configuration. The "roll paper pilot" rating was computed for 25 aircraft/gust configurations. A range of actual ratings from 2 to 9 were encountered and the "roll paper pilot" ratings agree quite well with the actual ratings. In addition there is good correlation between predicted and measured rms roll angle.

ORIGINAL PAGE IS
OF POOR QUALITY

PRECEDING PAGE BLANK NOT FILMED

*Currently assigned to the Air Force Flight Dynamics Laboratory, Air Force Systems Command, Wright-Patterson AFB, Ohio.

I. INTRODUCTION

The paper pilot concept for analytically evaluating the handling qualities of an aircraft is based on the following hypothesis.

1. The numerical pilot rating of an aircraft's handling qualities in a well defined piloted task is a function of the closed loop performance and the pilot work load. This function is called a pilot rating expression.
2. Given the pilot rating expression, the adaptable parameters in the appropriate pilot model are selected to minimize the numerical value of the pilot rating expression for the closed loop system (the lower the rating the better handling qualities). The resultant minimal value for the pilot rating expression provides a "good" analytic indication of the actual numerical pilot rating of the aircraft.

The first part of the hypothesis just suggests that there is some rational basis for a numerical pilot rating. The second part of the hypothesis is based on the assumption that a pilot will adapt so that the closed loop system is the best possible in the sense of what the pilot thinks is best!

The first successful application of the paper pilot concept was the hover task for a VTOL aircraft (Refs 1 and 2). In this particular case only the longitudinal handling qualities were considered.

The pilot rating expression for longitudinal handling qualities in hover developed by Crazy Anderson (Ref 1) is a function of the rms pitch rate, the rms longitudinal hover error, and the pilot work load. The pilot work load is a function of the lead time constants in the pilot model. The pilot work load increases with increasing values of the lead time constants.

The paper pilot rating (the numerical rating derived by minimizing the pilot rating expression) was computed for 79 aircraft/gust intensity combinations (Ref 2). The paper pilot ratings were compared with actual pilot ratings derived from a fixed base simulation as reported in Refs 3 and 4. The correlation is excellent. The paper pilot rating differed from the actual rating by more than 1 rating unit in only 9 of the 79 cases. The difference exceeded 1 1/2 rating units in only 1 case (a difference of 1.69). Actual pilots seldom agree that well!

The paper pilot concept was next applied to a pitch tracking task (Ref 5). The pilot rating expression was based on the limited data of Ref 6. The pilot rating expression for the commanded pitch tracking task was taken to be a function of the rms tracking error and the pilot lead time constant. This time Crazy Anderson didn't fare so well and some problems were encountered. In particular, for those cases where the short period mode is lightly damped and the short period natural frequency is high, the paper pilot ratings tend to be well below the actual rating (Ref 5) or tend to rate an aircraft as "good" when the open loop characteristics are clearly undesirable (Ref 7).

In this paper, the paper pilot concept is applied to the evaluation of aircraft handling qualities in roll. The piloted task considered is to keep wings level in the presence of side gusts. The aircraft equations, control system equations, gust model, and pilot model are described.

The pilot rating expression was developed using data from Ref 8. In Ref 8 the results of a moving base simulation for 25 aircraft/gust configurations are described. The pilot rating expression was then used to analytically determine a roll paper pilot rating and the closed loop performance for each case. The roll paper pilot ratings are compared with actual ratings and the predicted rms roll angles are compared with measured rms roll angles for these 25 cases in the Conclusion section of this paper.

II. PILOT-VEHICLE MODEL

The pilot-vehicle model used for the roll task was taken from Appendix III of Ref 8. A block diagram of the system is shown in Fig. 1. It can be noted from the block diagram, the pilot is regulating roll angle against a side gust disturbance using only aileron inputs.

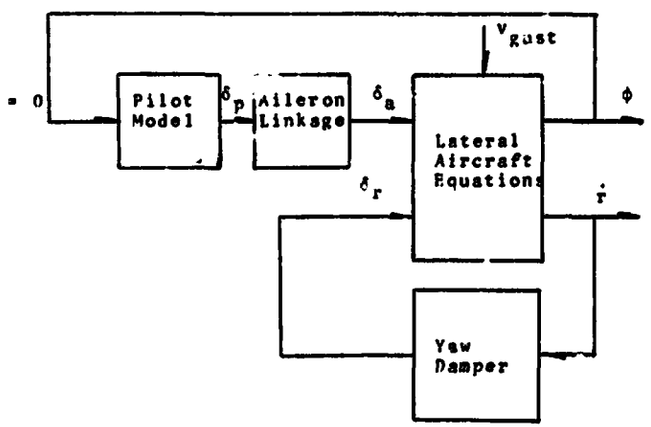

Fig. 1. Closed Loop System for the Roll Task.

1. Aircraft Equations

The linearized lateral equation of motion for the aircraft in response to control deflections and gust inputs as adopted from Ref 8 are (in primed stability axis notation)

$$\dot{\beta} = Y_\beta \beta - r + g/V_0 \phi + Y_\beta \beta_{gust} + Y_{\delta r} \delta_r$$

$$\dot{p} = L'_\beta \beta + L'_p p + L'_r r + L'_{\delta a} \delta_a + L'_\beta \beta_{gust} + L'_{\delta r} \delta_r$$

$$\dot{r} = N'_\beta \beta + N'_p p + N'_r r + N'_{\delta a} \delta_a + N'_\beta \beta_{gust} + N'_{\delta r} \delta_r$$

$$\dot{\phi} = p$$

where β is sideslip angle, p is roll rate, r is yaw rate, ϕ is roll angle, δ_a is aileron deflection, δ_r is rudder deflection, and β_{gust} is the gust input. β_{gust} is equal to v_g/V_0 where v_g is the gust intensity along the y axis and V_0 is the nominal longitudinal velocity.

2. Gust Model

The Dryden model for the lateral β_{gust} is used (Ref 9). The spectral form of β_{gust} is

$$\phi_{g_\beta}(\omega) = \sigma_v^2 \frac{L}{V_0} \frac{1 + 3\left(\frac{L\omega}{V_0}\right)^2}{\left[1 + \left(\frac{L\omega}{V_0}\right)^2\right]^2}$$

where σ_v is the rms gust level in rad/sec and L is a scale length of 1000 ft. The corresponding filter that can be used to generate the gust from white noise is

$$H(s) = \frac{\beta_g(s)}{N_g} = \sigma_v \sqrt{L/V_0} \frac{1 + \frac{\sqrt{3}L}{V_0} s}{\left[1 + \left(\frac{L}{V_0}\right)s\right]^2}$$

where N_g is white Gaussian noise.

3. Pilot Model

The pilot model is adopted from Ref 5 and is

$$Y_p = K_p(T_L s + 1)e^{-\tau s}$$

where K_p and T_L are the pilot's gain and lead, respectively, and τ is a pure time delay. A value of $\tau = .3$ seconds was used to agree with that used in Ref 8 for a pilot with acceleration cues. A first order Pade' approximation to the time delay was used. The block diagram for the pilot is shown in Fig. 2.

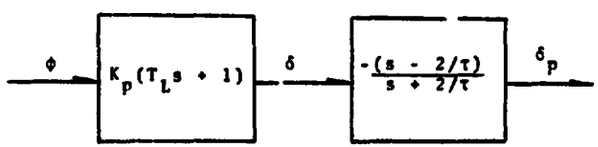

Fig. 2. Block Diagram of Pilot Model.

4. Control Systems

The control system model includes an aileron linkage time lage and a yaw damper.

(a) Aileron control

An aileron control lag was used to represent the case where a power boosted aileron system results in a time lag between the pilot input and the control surface deflection. The transfer function for the aileron control lag is

$$\frac{\delta_a}{\delta_p} = \frac{1/\tau_{con}}{s + 1/\tau_{con}}$$

(b) Rudder control

The rudder control consists only of a yaw damper. The transfer function for the yaw damper (Appendix III of Ref 8) is

$$\delta_r = \frac{-K_{aug}}{(\tau_{aug}\, s + 1)}\,\dot{r}$$

III. PILOT RATING EXPRESSION

The pilot rating expression was assumed to be of the form

$$PR = k\sigma_\phi + f(T_L) \qquad (1)$$

where σ_ϕ is the rms roll angle and $f(T_L)$ in some function of the pilot lead time constant.

The relation between pilot rating and lead was taken to be

$$f(T_L) = 3.25\ (1 - e^{-.77T_L}),\ T_L \geq 0$$

This hokey function is an exponential approximation to the straight line function of lead used in the longitudinal hover and pitch tracking cases (Refs 2 and 5). The comparison is shown graphically in Fig. 3. It was assumed that $f(T_L)$ would not change from task to task. For those cases where ω_ϕ/ω_d* is not much more than one, the pilot lead time can be approximated by

$$T_L \doteq T_r \doteq -1/L_p'$$

where T_r is the roll time constant (Ref 10). This approximation was used as a first cut for values of T_L.

Data for PR and σ_ϕ was taken from the results of the moving base simulation described in Ref 8. The pilot rating,

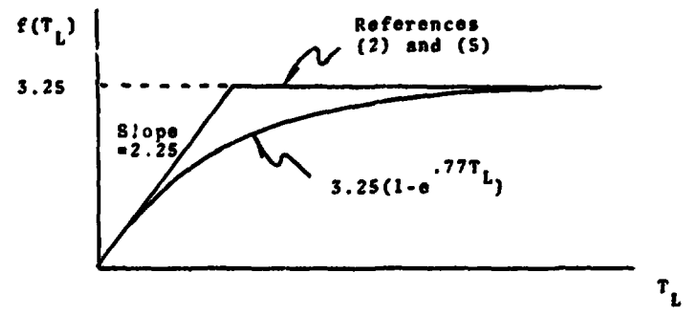

Fig. 3. Comparison of Functions Used to Determine Rating Degradation Due to Lead.

PR, is based on the Cooper rating scale (Ref 9) where a rating of 1 is optimal and a rating of 10 is unflyable. The values of σ_ϕ are in degrees.

With the data for PR and σ_ϕ and an approximation for T_L, the value of k in Eq (1), and hence the performance contribution to the pilot rating, can be estimated by plotting $PR - f(T_L)$ against the rms roll angle, σ_ϕ. This is done in Fig. 4 and a value of k = 1.3 was chosen. Having determined k, the pilot rating expression for the roll task is

$$PR = 1.3\sigma_\phi + 3.75\ (1 - e^{-.77T_L}) \qquad (2)$$

*ω_ϕ is the frequency of the second order numerator term in the ϕ/δ_a transfer function. ω_d is the frequency of the dutch roll mode.

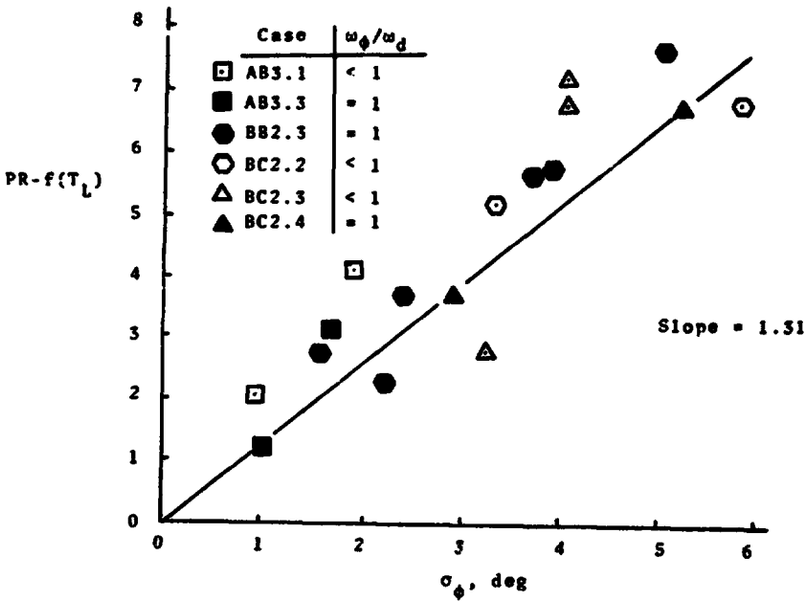

Fig. 4. Rating Degradation Due to RMS Roll Angle.

IV. ROLL PAPER PILOT

Basically the paper pilot rating is determined in the following way. The values of K_p and T_L that minimize the pilot rating expression (Eq (2)) for the closed loop system are determined. The resulting minimal value of Eq (2) is taken as the preliminary paper pilot rating.

There is however, an additional detail that must be considered and two adjustments are made to arrive at the final value of the paper pilot rating. To be specific:

1. The minimizing value of T_L is constrained to the range

$$0 \le T_L \le 5 \text{ sec}$$

2. Once the minimizing pilot parameters and the resulting closed loop performance is determined, the paper pilot rating is determined by the following formula.

$$PR = g(\sigma_\phi) + f(T_L) + h(\omega_\phi/\omega_d)$$

where

$$g(\sigma_\phi) = \begin{cases} 1 & , 1.3\,\sigma_\phi < 1 \\ 1.3\,\sigma_\phi, & 1 \le 1.3\,\sigma_\phi \le 6.75 \\ 6.75 & , 1.3\,\sigma_\phi > 6.75 \end{cases}$$

and

$$h(\omega_\phi/\omega_d) = 6.66|1 - \omega_\phi/\omega_d|$$

The constraint on T_L is imposed to account for the physical limitations of the pilot.

The modification on the rating contribution due to performance ($g(\sigma_\phi)$) can be justified in three ways: (1) the results are better, (2) it insures that paper pilot rating is in the same range as that of the actual pilot, between 1 and 10, and (3) it is reasonable to expect there is an upper and lower limit on the performance influence on the pilot's rating of the handling qualities of the aircraft.

The final modification to the paper pilot rating is a function of ω_ϕ/ω_d. A detailed explanation of the effect of ω_ϕ/ω_d on the pilot rating can be found in Ref 9 or Ref 10. The basic idea is that an aircraft with $\omega_\phi/\omega_d = 1$ is considered ideal by a pilot; and if there is a departure from $\omega_\phi/\omega_d = 1$, the resulting dutch roll oscillation is considered by the pilot to be a nuisance. The correlation of pilot rating with ω_ϕ/ω_d as reported in Ref 10 is shown in Fig. 5. The function $h(\omega_\phi/\omega_d)$ that is added on to the paper pilot rating is a straight line approximation to the data shown in Fig. 5. The primary reason for adding this function of ω_ϕ/ω_d to the paper pilot rating is that it improves the correlation of paper pilot ratings with the actual ratings. Whether or not this function of ω_ϕ/ω_d detracts from the paper pilot concept depends upon the point of view. The party of the second part believes that this term represents a failure of the pilot rating expression to adequately express the pilot rating as a function of the characteristics of the closed loop system. The party of the first part, on the other hand, considers this modified rating as the proper blend of the closed loop

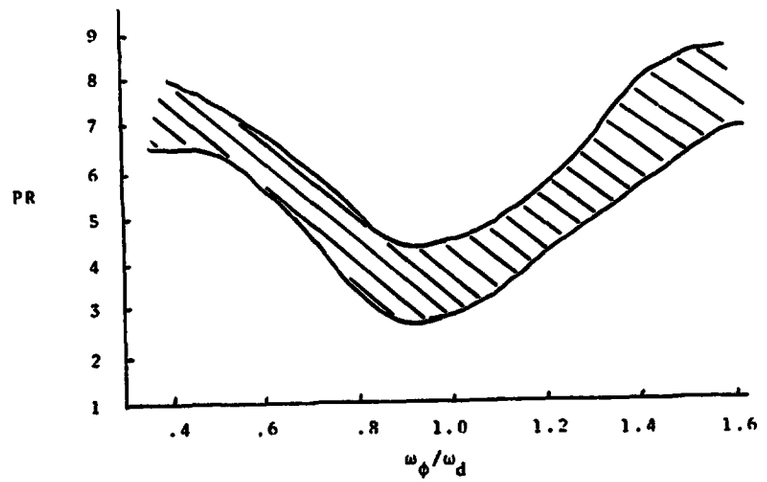

Fig. . Correlation of Pilot Rating with ω_ϕ/ω_d. (From Ref 10).

and open loop characteristics of the aircraft in the evaluation of aircraft handling qualities.

V. RESULTS

The roll paper pilot resul· .ere computed for the 25 aircraft-gust intensity configurations of Ref 8. The digital computer program used to compute the roll paper pilot results is described in Ref 11. The aircraft simulated was the T-33 and the detail data is given in both Refs 8 and 11.

The actual pilot's rating, roll paper pilot's rating, actual rms roll angle, and predicted rms roll angle are tabulated in Table I by configuration. A comparison of the results is shown in the scatter diagrams of Fig 5 and 7.

The correlation in pilot rating appears [illegible] In fact, the paper pilot results may be better than Fig 6 indicates, especially in the ratings below 4.5 or in the acceptable range. In this range there are two data points that lie outside of the one rating unit boundary. Both of these points are for the AB2.6 aircraft configuration with nearly the same gust intensity inputs. The simulation that resulted in an actual rating of 2 had a gust input of 13.03 ft/sec and that with an actual rating of 5 had a gust input of 16.50 ft/sec. Also note that two other simulations of the AB2.6 configuration resulted in a rating of 2.5 for a gust input of 9.46 ft/sec and a rating of 5 for a gust input of 34.27 ft/sec. Perhaps these two ratings should have been somewhat closer to the paper pilot rating.

Table I

Comparison of Actual and Paper Pilot Results

Configuration	Gust Intensity	Actual σ_ϕ, deg	Paper Pilot σ_ϕ, deg	Actual PR	Paper Pilot PR
AB2.6	13.03	1.59	1.57	2.0	3.17
AB2.6	23.55	3.33	2.65	4.0	4.81
AB2.6	34.27	4.16	3.66	5.0	6.33
AB2.6	9.46	1.59	1.17	2.5	2.[illegible]2
AB2.6	16.50	1.73	1.95	5.0	3.[illegible]5
AB2.7	12.46	1.43	1.55	3.0	3.44
AB2.7	21.05	2.37	2.50	6.5	4.80
AB2.7	33.41	2.66	3.70	8.0	6.63
AB3.1	11.58	.97	.9[illegible]	3.0	3.03
AB3.1	27.09	1.88	1.70	5.0	4.36
AB3.3	12.26	1.01	.98	2.0	2.20
AB3.3	23.33	1.69	1.67	4.0	3.29
BB2.3	5.79	2.28	2.11	4.0	3.74
BB2.3	11.24	3.92	3.88	6.5	6.31
BB2.3	15.54	5.04	5.19	8.5	8.17
BB2.3	7.37	2.42	2.66	4.5	4.53
BB2.3	4.69	1.60	1.72	3.5	3.22
BB2.3	14.08	3.75	4.75	6.5	7.47
BC2.2	10.31	5.83	4.76	9.0	9.19
BC2.2	5.89	3.39	3.40	7.5	7.04
BC2.3	10.50	4.09	4.97	9.5	9.11
BC2.3	10.51	4.09	4.57	9.0	9.26
BC2.3	5.72	3.29	3.03	5.0	5.91
BC2.4	12.39	5.21	6.20	9.0	9.01
BC2.4	5.12	2.92	2.90	6.0	5.45

ORIGINAL PAGE IS OF POOR QUALITY

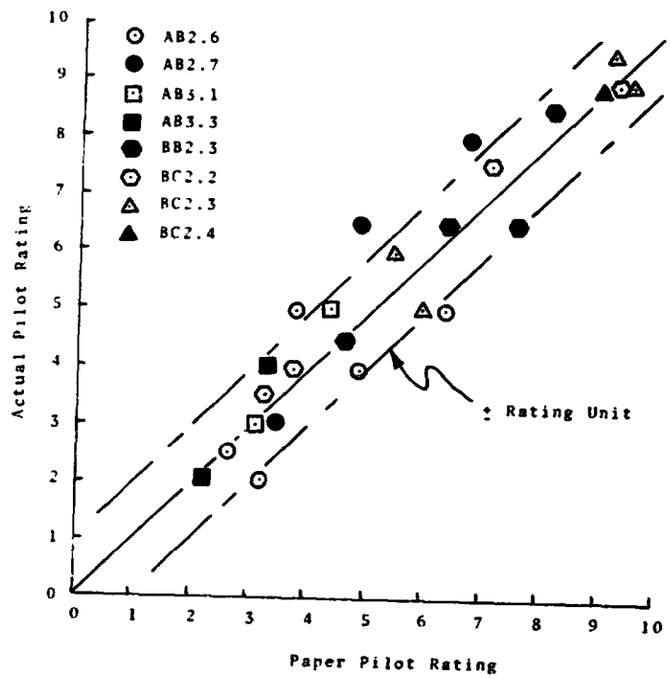

Fig 6. Comparison of Paper Pilot Rating and Actual Pilot Rating.

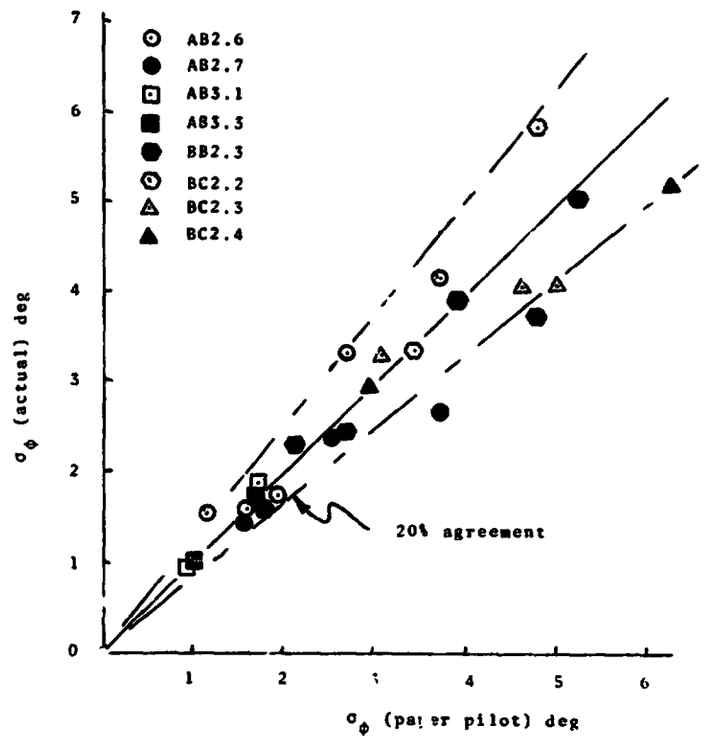

Fig. 7. Comparison of RMS Bank Angle Between Paper Pilot and Actual Pilot.

VI. CONCLUSIONS

The paper pilot predicted ratings agree well with actual ratings for those cases considered. However a better evaluation of the agreement could be made if there was some indication of the actual pilot rating spread for each aircraft-gust intensity configuration. Also, since there was only 25 data points available for comparison, it is premature to assert that the roll paper pilot is an unqualified success at predicting ratings.

The apparent success of the roll paper pilot to predict roll angle performance in the roll tracking task is also encouraging. As with the rating correlation, a better evaluation of the agreement could be made if some information in the actual spread were known and the results were compared to a larger data base.

Press on paper pilot--you done good.

REFERENCES

1. R. O. Anderson, A New Approach to the Specifications and Evaluation of Flying Qualities, AFFDL-TR-69-120, June 1970.

2. J. D. Dillow, The "Paper Pilot" - A Digital Computer Program to Predict Pilot Rating for the Hover Task, AFFDL-TR-70-40, March 1971.

3. D. P. Miller and E. W. Vinje, Fixed Base Flight Simulator Studies of VTOL Aircraft Handling Qualities in Hovering and Low Speed Flight, United Aircraft Research Laboratories, AFFDL-TR-67-152, January 1968.

4. E. W. Vinji and D. P. Miller, Analytic and Flight Simulator Studies to Develop Design Criteria for VTOL Aircraft Control Systems, United Aircraft Research Laboratories, AFFDL-TR-68-165, April 1969.

5. R. O. Anderson, A. J. Conners, and J. D. Dillow, Paper Pilot Ponders Pitch, AFFDL-TM-70-1, November 1970 (Revised January 1971).

6. I. A. M. Hall, Effects of Controlled Element on the Human Pilot, Princeton University, WADC-TR-57-509, August 1958.

7. R. P. Denaro and G. L. Greenleaf, "Selection of Optimal Stability Augmentation System Parameters for a High Performance Aircraft Using Pitch Paper Pilot," AFIT Thesis, GGC/EE/73-7, Oct 1972.

8. E. D. Onstott and E. P. Salmon, Airplane Flying Characteristics in Turbulence, Northrup Corporation, AFFDL-TR-70-143, February 1971.

9. C. R. Chalk, T. P. Neal, T. M. Harris, F. E. Pritchard, and R. J. Woodcock, Background Information and Users Guide for MIL-F-8785B (ASG), "Military Specification-Flying Qualities of Piloted Airplanes," Cornell Aeronautical Laboratories, AFFDL-TR-69-72, August 1969.

10. I. L. Ashkenas, A Study of Conventional Airplane Handling Qualities Requirements, Part II. Lateral-Directional Oscillatory Handling Qualities, Systems Technology, Inc., AFFDL-TR-65-138, November 1965.

11. F. R. Naylor, Predicting Roll Task Flying Qualities with Paper Pilot, Air Force Institute of Technology, GAM/MA/73-1, September 1972.

NASA - Langley

RIDE QUALITY SIMULATION USING DATA RECORDED FROM COMMERCIAL AIRLINE FLIGHTS

By Hugh P. Bergeron

Abstract of Paper Proposed for
Ninth Annual Conference on Manual Control
May 23-25, 1973
Cambridge, Massachusetts

Ride quality tests are being performed at NASA Langley Research Center using various motion base simulators. The low frequency range (0.2 to 1.0 Hz) is being examined on Langley's Real-Time Dynamic Simulator (RDS).

Accelerations measured on commercial aircraft during normal flight operations were recorded for all six degrees of freedom. These accelerations were then analyzed and shaped to drive the simulator. Extensive shaping was necessary to compensate for the fairly low response capability and limited translation inherent to the RDS. Several shaping techniques including drift compensation, washout, and forward feed were combined to optimize response reproduction in the 0.2 to 1.0 Hz frequency range. The output of the simulator, obtained from accelerometers, was compared directly to the measured aircraft signals. Comparisons were made using time histories and power spectral densities. (A short film clip demonstrates the motions involved.)

The results show a good match of acceleration characteristics but with a nearly constant time lag. The ride quality tests, however, use recorded data that drives the simulator in an open loop configuration. Therefore, the constant time lag does not present a problem in matching the input/output signals. Further, by not having to compensate for this lag, more freedom is allowed in the manipulation of the simulator drive signals to insure a better match.

ABSTRACT

Edward D. Onstott

Vehicle Dynamics and Control Research

Aircraft Division, Northrop Corporation

PILOT MODEL SENSITIVITY GRAPHS AND FLYING QUALITIES PARAMETERS

Previously reported flying qualities prediction and evaluation methods for flight in atmospheric turbulence have been based on the minimum of predicted tracking error versus pilot model gain graphs. The physical interpretation of these minimum values is discussed and further flying qualities parameters are identified. In particular, not only the minimum of the tracking error versus pilot model gain graph has significance, but the entire shape of the graph as well. The minimum value turns out to be a tradeoff between control over low frequency disturbance power and resonance of the short period system dynamics. Furthermore, this tradeoff determines the slope of the prediction graph, a flying qualities parameter that has proved to be of considerable importance in a number of development and research programs completed at Northrop.

N75 19135

ORIGINAL PAGE IS OF POOR QUALITY

PRECEDING PAGE BLANK NOT FILMED

PAPER PILOT PONDERS SUPERSONIC TRANSPORTS

John R. Stone
Flight Dynamics Laboratory
Wright-Patterson AFB, Ohio

ABSTRACT

This paper describes the application of the digital program Pitch Paper Pilot to a presimulation analysis of a large delta wing aircraft similar to the Concorde supersonic transport. Pilot acceptance (in terms of Cooper-Harper ratings), pilot model parameters, and pilot-vehicle performance were predicted by Paper Pilot and compared to actual inflight measures. Results are good and illustrate the value of using the Paper Pilot concept during the planning stages of simulation.

I. INTRODUCTION

The technical community relies heavily on simulation to test complex systems. New ideas can be examined and questions can be answered during simulation that would prove very costly to study on actual systems. However, for the simulation to be most efficient careful planning is necessary. This paper presents an example of an automated analysis that can predict important pilot-aircraft information for planning purposes. The information includes predictions of pilot-vehicle performance, pilot rating, and pilot model parameters; in addition, critical experimental parameters can be derived. The analysis is accurate, fast, economical, and can accommodate complex systems.

To test the presimulation planning capabilities of the technique, which is based on the digital computer program Pitch Paper Pilot (Ref. 1), data for an inflight simulation of a supersonic transport (Ref. 2) was analyzed before the results of the simulation were available. The predictions were generated and then compared to the actual inflight measurements.

II. PRESIMULATION ANALYSIS

PITCH TASK

The inflight simualtion modeled the landing approach task of a supersonic transport. For this task it has been well established that the primary pilot function for transport-type aircraft is the maintenance of pitch attitude (Refs. 2 and 3). Thus, the use of the Pitch Paper Pilot program, which only models the longitudinal pitch tracking task, was reasonable in this investigation, especially since the lateral configuaration remained constant

A brief review of the Pitch Paper Pilot program shows that the pitch tracking task is modeled by a single closed-loop system with pilot control of elevator (Fig. 1). Included are a commanded pitch input, pilot model Y_p, airframe dynamics, and stability augmentation system (SAS). The commanded pitch input is generated by passing white noise through a first order filter with a break frequency equal to one radian per second. The pilot model is of the form:

$$Y_p = k_p(T_L s + 1)e^{-\tau s} \approx \frac{-k_p(T_L s + 1)(s - 2/\tau)}{(s + 2/\tau)}$$

where

s = Laplace transform notation

k_p = pilot gain

T_L = pilot lead, seconds

τ = effective pilot central processing delay, seconds

The aircraft dynamics are the standard three degree-of-freedom longitudinal equations of motion with dimensional stability axis derivatives.

PROGRAM DESCRIPTION

To use the Pitch Paper Pilot program the aircraft stability derivatives, longitudinal airspeed, commanded input model parameters, pilot time delay, initial guess of pilot gain and lead, SAS gains, control system lags, and data used in the minimization routines are input. The first computational step in the Paper Pilot rating scheme finds a stable set of pilot parameters. The cost functional J is minimized with respect to the pilot parameters; subject to the constraint T_L = 5 seconds. J is given as

$$J = \text{Perf} + R_1 + R_2 + 1.0$$

where

$$\text{PERF} = \begin{cases} .1/(.974 - \sigma), & \sigma < .974 \\ 10^{11}(.974 - \sigma)^2 - 3 \times 10^7(.974 - \sigma) + 3 \times 10^3, & \sigma \geq .974 \end{cases}$$

$\sigma = \sigma_e/\sigma_i$ = root mean square (rms) tracking error normalized by the rms commanded input

$$R_2 = \begin{cases} -2.5T_L, & T_L < 0 \\ 2.5T_L, & 0 \leq T_L \leq 1.3 \\ 3.25, & T_L > 1.3 \end{cases}$$

$$R_3 = \begin{cases} 0, & T_L \leq 5.0 \\ 100(T_L - 5)^3, & T_L > 5.0 \end{cases}$$

The minimizing pilot parameters are then used to compute a closed-loop Pitch Paper Pilot rating in Cooper units as given by

$$PR = \begin{cases} R_1 + R_2 + 1.0, & \text{PERF} + R_2 + 1 \leq 10 \\ 10, & \text{PERF} + R_2 + 1 > 10 \end{cases}$$

where

$$R_1 = .1/(.974 - \sigma).$$

The Cooper ratings are converted to Cooper-Harper ratings which will be used in this paper. A rating of one is excellent; ten may be catastrophic.

APPLICATION OF PITCH PAPER PILOT

Pitch Paper Pilot was used to analyze the longitudinal flying qualities of fourteen supersonic transport configurations in landing approach. The stability derivatives were those used for the simulation, the break frequency was selected to equal one radian per second, and the pilot time delay was chosen to be 0.3 seconds. This value includes a mental processing delay of about 0.2 seconds and a neuromuscular delay of 0.1 seconds.

III. SIMULATION

FLYING QUALITIES EXPERIMENT

In the summer of 1972 an inflight simulation program was conducted by the Air Force Flight Dynamics Laboratory (AFFDL) and CALSPAN Corporation to establish flight characteristics criteria for airworthiness certification of supersonic transports during landing approach (Ref. 2). This program dealt specifically with the static longitudinal stability of the bare unaugmented airframe and required pilot ratings of the aircraft's handling qualities, and, thus provided an excellent example to test the Paper Pilot concept as a presimulation analysis tool. The method for obtaining

ORIGINAL PAGE IS OF POOR QUALITY

the needed inflight handling qualities data to fly actual landing approaches in the Total In-Flight Simulator (TIFS) (Fig. 2) on which were programmed the equations that described various longitudinal configurations of a large delta-wing jet transport of the Concorde class. The simulation included statically unstable configurations ($C_{m_\alpha} > 0$), and those on the backside or bottom of the thrust-required curve ($1/T_{h_1} < 0$). In most cases the short period mode had degenerated to two real roots, one of which was unstable. Three stable configurations with conventional dynamics were also tested. The Paper Pilot program was able to accurately rate the flying qualities of twelve of the fourteen unconventional configurations inspite of the fact that no written specifications exist for such configurations. After all, to define the specifications was the purpose of the TIFS experiment.

PILOT DESCRIBING FUNCTION EXPERIMENT

To help validate the predicted pilot model parameters and performance, a limited pilot describing function experiment was performed. Two pilots were instructed to fly a stable configuration of an inflight compensatory pitch tracking task with simulated turbulence. After a brief training period (both pilots were already familiar with the configurations because of the earlier TIFS evaluations), five experimental runs of one hundred-second duration were analyzed using a Describing Function Analyzer (Ref. 4). The pilot describing function and pilot performance data were than compared to the predicted values. The pilots also gave comments which were helpful in comparing the describing function experiment to the flying qualities experiment.

It is important to note the differences between the vertical gust input used in the describing function experiment and the commanded input used in the Paper Pilot predictions. First of all, the gust input entered the system directly through the aircraft equations. Consequently, the aircraft equations appeared as a higher order filter operating on the gust. Futhermore, the gust input was shaped to resemble the Dryden gust spectrum, with a break frequency of about one-half radian per second. On the other hand, the Paper Pilot commanded input was generated by passing white noise through a first order filter with a break frequency of one radian per second. Thus, the Paper Pilot predictions, compared to the describing function experiment, were based on an input which had a higher break frequency and energy content for the same tracking task. Inspite of these differences, both inputs approximated heavy turbulence.

As a footnote to the pilot describing function experiment, the digitally recorded inflight data is currently being analyzed at AFFDL with a parameter identification routine based on L. W. Taylor's work (Ref. 5). Pilot parameters identified with Taylor's method should provide interesting comparisons to those measured with the describing function analyzer.

IV. RESULTS

The findings of the TIFS study indicated that the pilots rated the configurations differently depending on the amount of training and the gust level. Consequently, the TIFS researchers attempted to eliminate training and gust effects and thereby derived "compensated" pilot ratings. Table 1 shows the very good comparison of the Paper Pilot predictions to the compensated ratings, as well as to the "raw" pilot ratings. In only two cases, where the actual ratings were 10, were the predictions notably different.

The pilot describing function experiment yielded measurements to validate the predicted performance and pilot model parameters. Table 2 shows good comparison between predictions and measurements, except for pitch rate. And the Bode plot of Figure 3 indicates that the predicted pilot model is very similar to the models of the actual pilots, especially in the vicinity of the crossover frequency which is about five radians per second.

The above results in terms of pilot rating, performance, and model parameters can indicate good and bad aircraft configurations which should be known in planning a simulation. However, additional information in terms of critical experimental parameters should also be known. The use of the Paper Pilot program indicated that the important parameter was the static stability Cm_α, the induced drag C_{D_α} and the pitch damping (Cm_q + $Cm_{\dot\alpha}$) were not as important. The inflight evaluations confirmed these predictions.

In summary the Pitch Paper Pilot program, which was developed from a base of fighter data, can analyze the handling qualities of large transport-type aircraft. Perhaps the form of the commanded pitch input, as opposed to a gust input through the aircraft equations, has a normalizing effect with respect to aircraft size. On the negative side of the picture, the Paper Pilot had difficulty in stabilizing and then finding the minimum pilot rating for some of the unstable configurations. Besides the problem of identifying the proper stabilizing gain (Fig. 4), there are preliminary indications that more than one set of pilot gain and lead would satisfy the minimization requirements. This leads to the interesting possibility of two ratings for the same configuration, and may explain why different pilots sometimes rate the same configuration quite differently, for example, Configurations 1 and 3 of Table 1. Such observations will be clarified as more complete simulations and data reductions are accomplished, in particular, if the measurement of pilot model parameters is emphasized.

REFERENCES

1. Anderson, R. C., A. J. Connors, and J. D. Dillow, "Paper Pilot Ponders Pitch, AFFDL-TM-70-1, January 1971.

2. Wasserman, R. and J. F. Mitchell, "In-Flight Simulation of Minimum Longitudinal Stability for Large Delta-Wing Transports in Landing Approach and Touchdown," AFFDL-TR-72-143, February 1973.

3. Gerken, G. J., F. Unfried, et al, "A Piloted Power Approach Sumulation," AFFDL-TR-73-27, March 1973.

4. Peters, R. A. and R. W. Allen, "Operational Manual for Describing Function Analyzer," W-P-406-2, Systems Technology, Inc., October 1970.

5. Taylor, L. W. and K. W. Iliff, "Systems Identification Using a Modified Newton-Raphson Method--A Fortran Program," NASA TN D-6734, May 1972.

TABLE 1

COMPARISON OF PILOT RATINGS

Conf	P Pilot	TIPS Pilots A	B	C	D	Compensated Ratings	T_2 sec
BL	6.1	-	-	-	-	-	5
1	5.6	-	2C	2B	5D	-	stable
2	6.0	4D	7(5)	-	6-7	6	60
3	6.1	6-7D	6	9	5	6	8
4	6.5	5C	5	-	7-8E	6.5	4
5	6.5	10E	-	10	7D	10	2
10	6.0	5D	5	-	7D	6	9
11	6.2	5D(6B)	-	-	6D	6	5
12	8.0	10F	6-7	-	-	8.5	2
13	5.3	3C	1-2	-	-	-	stable
14	5.3	4C	-	-	6D	5	8
15	5.3	6B	-	5C	7.5D	7.5	4
16	5.8	10E	-	-	10F	10	2
20	5.3	3C	-	-	4C	-	stable

TABLE 2

RMS VALUES, CONFIGURATION 20

	σ_{θ_e} (deg)	σ_θ (deg)	σ_q (deg/sec)	σ_α (deg)	σ_u (ft/sec)
PPP	.78	.71	1.52	.7	2.1
SC	.5	.5	.4	.8	2.2
DFA	.62	-	-	-	-

PPP - Pitch Paper Pilot predictions

SC - Approximate rms values from strip chart, averages of five runs, (rms = 1/3 x max value)

DFA - Describing Function Analyzer measurement

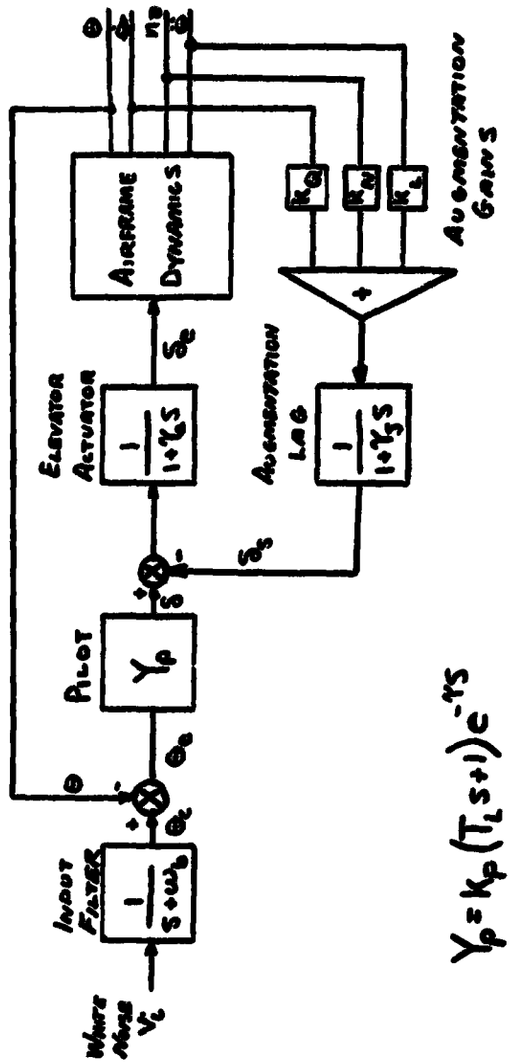

$$Y_p = K_p(T_L s+1)e^{-\tau s}$$

$$Y_p \doteq -K_p(T_L s+1)(s-2/\tau)/(s+2/\tau)$$

PITCH TRACKING TASK

FIGURE 1

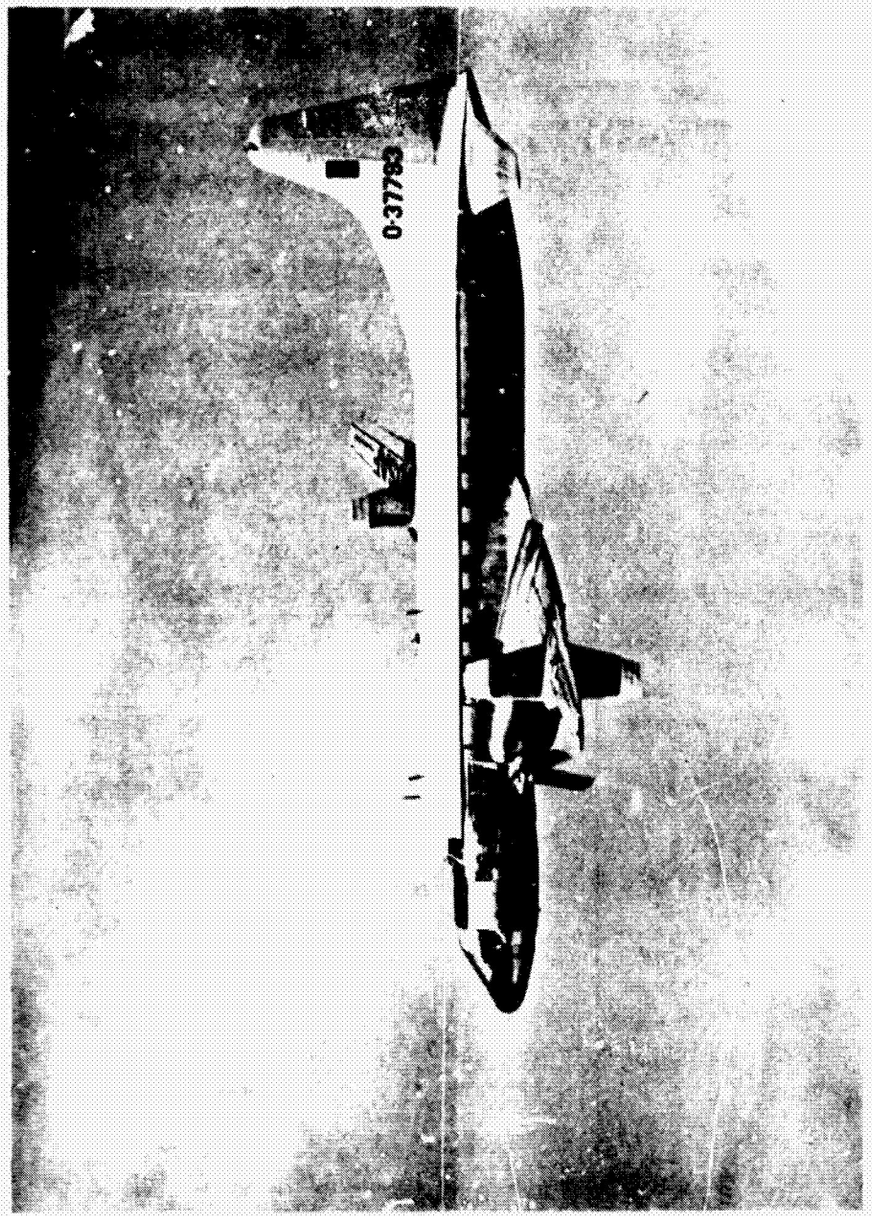

TOTAL IN-FLIGHT SIMULATOR (TIFS)

FIGURE 2

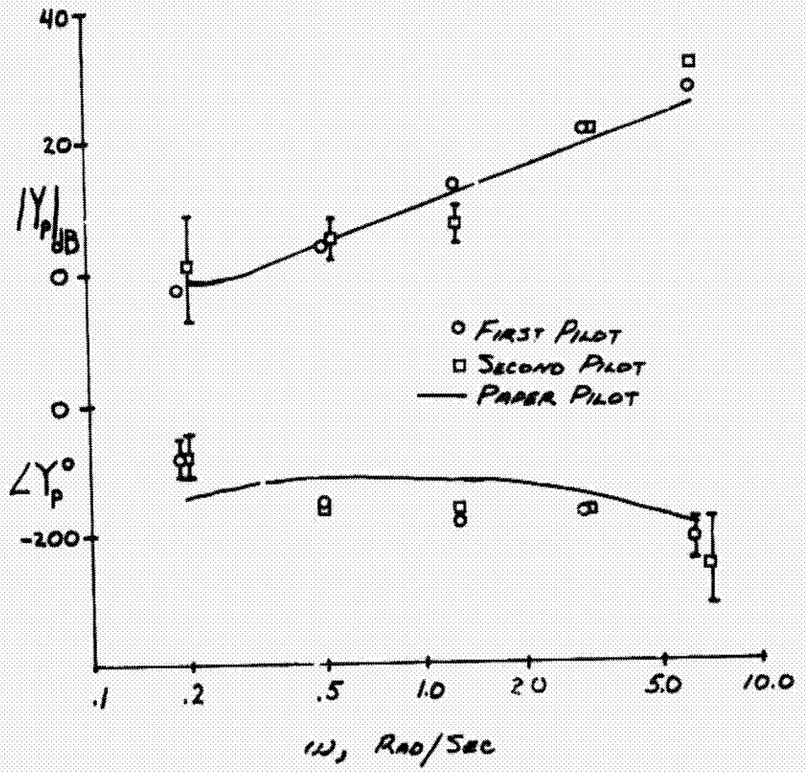

PILOT MODELS

FIGURE 3

SST BASELINE CONFIGURATION

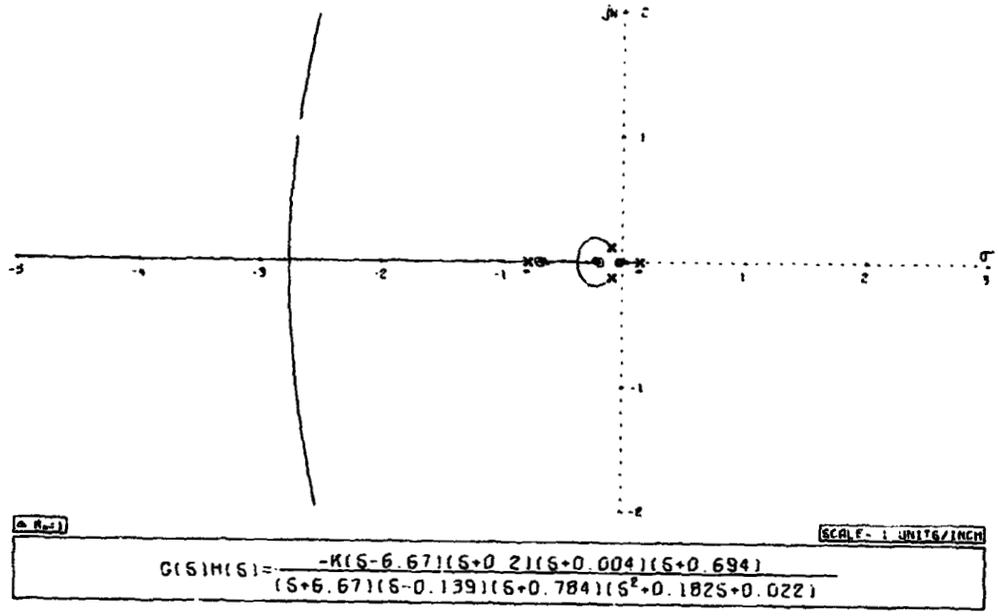

$$G(S)H(S) = \frac{-K(S-6.67)(S+0.2)(S+0.004)(S+0.694)}{(S+6.67)(S-0.139)(S+0.784)(S^2+0.182S+0.022)}$$

FIGURE 4 - ROOT LOCUS

ORIGINAL PAGE IS
OF POOR QUALITY

PRECEDING PAGE BLANK NOT FILMED

HANDLING PROPERTIES OF DIVERSE AUTOMOBILES AND CORRELATION WITH FULL SCALE RESPONSE DATA*

Roger H. Hoh and David H. Weir†
Systems Technology, Inc., Hawthorne, California

ABSTRACT

Driver/vehicle response and performance of a variety of vehicles in the presence of aerodynamic disturbances are discussed. Steering control is emphasized. The vehicles include full size station wagon, sedan, compact sedan, van, pickup truck/camper, and wagon towing trailer. Driver/vehicle analyses are used to estimate response and performance. These estimates are correlated with full scale data with test drivers and the results are used to refine the driver/vehicle models, control structure, and loop closure criteria. The analyses and data indicate that the driver adjusts his steering control properties (when he can) to achieve roughly the same level of performance despite vehicle variations. For the more disturbance susceptible vehicles, such as the van, the driver tightens up his control. Other vehicles have handling dynamics which cause him to loosen his control response, even though performance degrades.

INTRODUCTION

Past reports of driver/vehicle studies at STI have emphasized system structure, dominant (inner loop) driver control properties, and correlations with simulator and full scale response and performance data (e.g., Refs. 1-5). Recent driver/vehicle analyses have involved a wider range of vehicle handling properties, and the corresponding full scale data have provided a better appreciation of the factors involved in estimating outer loop closure and path performance properties. These results are illustrated here following a brief background summary.

Assumptions and Analytical Approach

The analyses involve the application of an empirically-founded theory of driver control which is based on the more general manual control theory. These theories and models take into account a combination of:

*This work was accomplished in part under DOT Contract FH-11-7570.

†Senior Research Engineer and Principal Research Engineer, respectively.

N75 19136

- Guidance and control requirements related to good stability and path following, regardless of the type of controller
- Driver-centered requirements which account for the preferences and limitations of the human driver

The driver responds to a composite of visual stimuli derived from the full visual field. These stimuli are selected such that the driver's control action serves to fulfill the guidance and control needs of the driver/vehicle system. Typically this means that more than one feedback loop will operate simultaneously (e.g., heading angle and lateral position), resulting in multiloop control.

The driver's response can be modeled using a quasi-linear model which consists in general of three components: a set of describing functions with parameters which depend on the system and situation; a set of rules which tell how to adjust the parameters; and an additive remnant.

The rationale of driver equalization can be discussed most simply by using an approximate "crossover model" (e.g., Ref. 6). Experimental data for a wide variety of both single and multiloop situations lead to the conclusion that the driver adjusts his describing function, Y_p, in each loop such that the open loop function, Y_pY_c, comprising the effective vehicle dynamics, Y_c, and the driver in the vicinity of the gain crossover frequency, ω_c, for that loop has the approximate form:

$$Y_pY_c = \frac{\omega_c e^{-j\omega\tau}}{j\omega} \qquad (1)$$

Here τ is an effective pure time delay which includes the neuromuscular dynamics as well as any net high frequency vehicle lag. The crossover frequency (ω_c) is the product of the driver and vehicle gains. In multiloop situations the effective controlled element dynamics, Y_c, will include the effects of all the other loops closed. The form of Eq. 1 emphasizes that the driver characteristics in each loop are tailored to the specifics of the control situation and the vehicle.

The remnant is that part of the driver's output which is not linearly correlated with the input, and its major source appears to be nonstationarity in the driver's behavior. When the driver's output is treated as a power spectrum the remnant can be considered as a driver-induced broadband random "noise" injected at the driver's output. For vehicle control situations involving reasonable handling dynamics the remnant will be small compared to that part of the driver's response involved in regulating against the external disturbance. For that reason it can often be neglected in making performance estimates and comparisons. Some evidence of remnant is seen in the full scale comparisons, shown subsequently.

As noted, multiloop control involving more than one feedback stimulus is appropriate to satisfying guidance and control, and driver-centered, requirements. Prior research (e.g., Refs. 1-5) has shown that the system of Fig. 1 is representative. This involves a primary feedback loop of vehicle heading angle (ψ), plus an outer loop of lateral deviation (y_I). These perceptual cues are operated on by the driver describing functions (Y_{p_y} and Y_{p_ψ}) to produce a steer angle correction (δ_w).

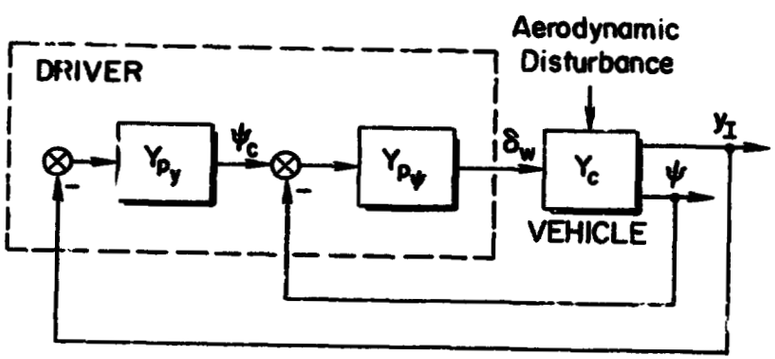

Figure 1. Driver/Vehicle System Block Diagram

The driver describing functions in Fig. 1 can be quantified by using a sequential application of the crossover model; beginning with $Y_{p_\psi}Y_c$ in the inner loop and then considering $Y_{p_y}Y_c'$ in the outer loop, where Y_c' denotes the effective vehicle dynamics with the heading angle feedback closed.

Vehicle Dynamics

The controlled element (vehicle) dynamics are a major task variable. The lateral-directional properties pertinent to steering control were modeled using 3 degree of freedom linear equations of motion. For a single vehicle the variables are:

- Lateral velocity (v)
- Heading rate (r)
- Roll angle (p)

Two additional degrees of freedom result when a towed trailer is added, i.e.:

- Trailer tow angle (η)
- Trailer roll angle (φ_t)

The equations of motion and corresponding transfer functions were quantified using chassis and tire data and verified by full scale tests. The resulting heading angle and lateral position transfer functions are given in Table 1. The transfer functions are:

$$\frac{\psi}{\delta_w} = \frac{sN^{\psi}_{\delta_w}}{s\Delta}$$

$$\frac{y_I}{\delta_w} = \frac{s^2N^{y_I}_{\delta_w}}{s^2\Delta}$$

Note that the denominator free s terms are not shown in the table for simplicity. Further details on the equations and vehicle properties are given in Ref. 7.

TABLE 1. SUMMARY OF VEHICLE TRANSFER FUNCTIONS

VEHICLE	TRANSFER FUNCTION POLYNOMIAL		
	HEADING NUMERATOR, $sN^{\psi}_{\delta_w}$	LATERAL DEVIATION NUMERATOR, $s^2N^{y_I}_{\delta_w}$	DENOMINATOR, Δ
1972 Wagon	22(3.8)[.22, 10.7]	11(7.0)[.30, 8.0][.01, 8.7]	.55[.70, 4.4][.24, 11.3]
1972 Wagon Plus Trailer	92(3.1)[.26, 4.4] × [.16, 8.3][.18, 10.2]	710[.27, 4.7][.29, 6.9] × [.07, 8.2][.15, 8.3]	4[1.0, 3.2][.24, 4.1] × [.16, 8.3][.23, 11.0]
Compact Sedan	2.6(2.2)[.53, 15.2]	21[.13, 7.5][.20, 7.5]	.24(.73)(4.1)[.62, 16.6]
Truck/Camper	21(4.1)[.21, 4.7]	14(5.0)[.17, 4.7][.15, 6.3]	.75[1.0, 4.0][.15, 4.6]
1972 Sedan	31(4.0)[.2, 9.8]	270[.33, 7.7][-.03, 8.1]	.41[.53, 6.2][.43, 15.9]
Imported Van	6.7(4.8)[.52, 13.4]	74[.17, 9.0][.18, 9.2]	.37[.64, 4.6][.48, 13.3]

The shorthand notation for polynomial factors is: $A(s + a)$ is written $A(a)$;
$A[s^2 + 2\zeta\omega s + \omega^2]$ is written $A[\zeta, \omega]$

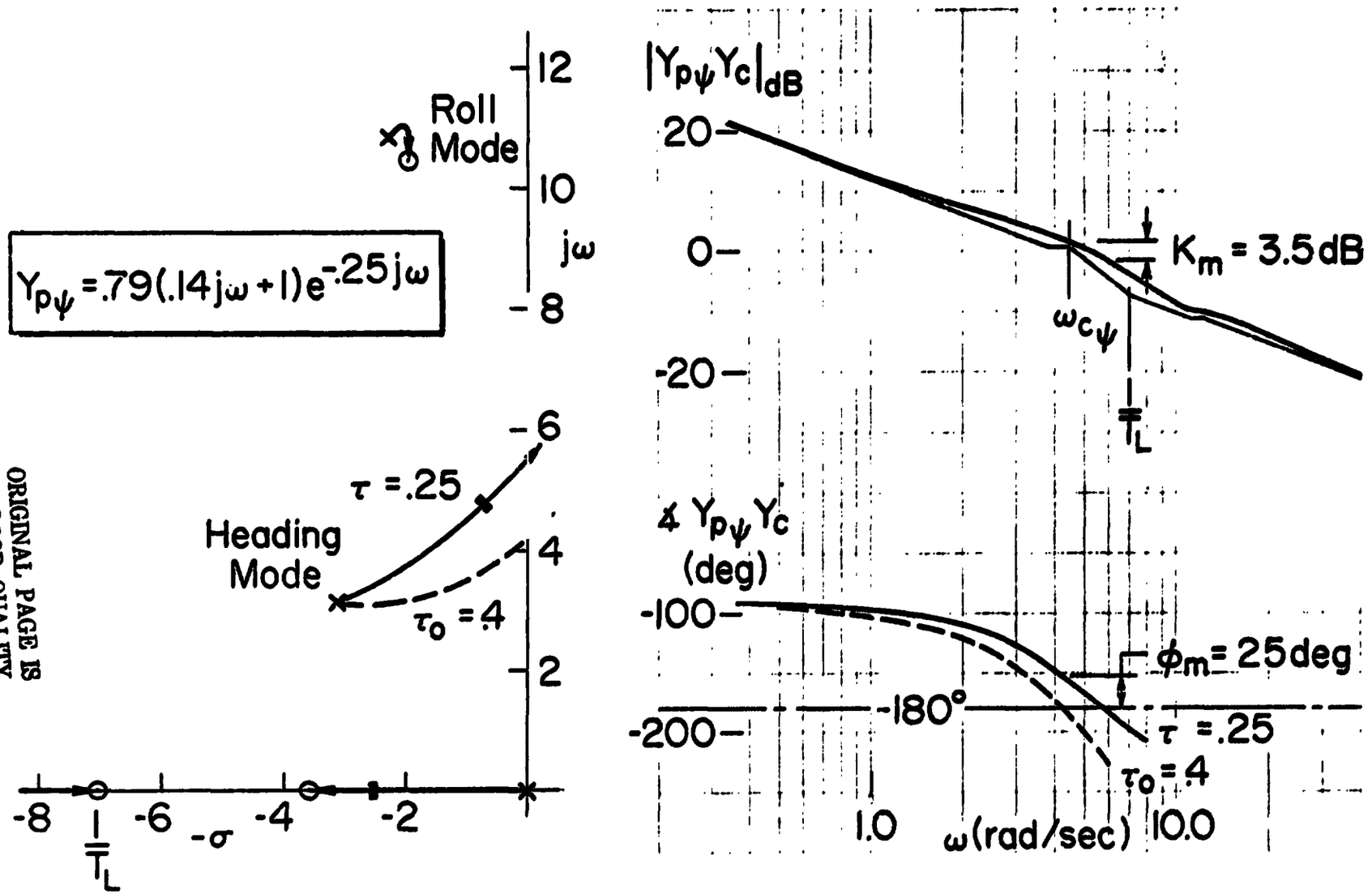

Figure 2. Driver/Vehicle Response Properties for Heading Control, 1972 Station Wagon at 60 mph

ORIGINAL PAGE IS OF POOR QUALITY

For the vehicles shown in Table 1 the required equalization can be accounted for in Y_{p_ψ}, and the driver time delay, τ, can be included there, also, by virtue of the "series" structure in Fig. 1. The effective forcing function bandwidth resulting from a typical aerodynamic disturbance is about 1 rad/sec for the vehicles shown in Table 1.

Driver/Vehicle Response Analyses and Full Scale Comparisons

The procedures and models outlined above were used to estimate the response and performance of the several driver/vehicle systems in the presence of a bus-induced aerodynamic disturbance. In the discussion the analytical results are shown, then the computed performance results are compared with the recorded full scale time responses. The 1972 station wagon is treated first in some detail, as the base case. This is followed by the results for the other vehicles.

<u>1972 Station Wagon</u> — The driver/vehicle response properties ($Y_{p_\psi}Y_c$) for the heading loop are shown in Fig. 2. A root locus plot is on the left and a frequency response (Bode) plot is on the right. The vehicle dynamics ($Y_c = \psi/\delta_w$) are taken from Table 1. A suitable Pade approximation is used for the driver time delay term, $e^{-\tau j\omega}$. The nominal result in Fig. 2 is for driver lead equalization (T_L) of 0.14 sec and a net driver time delay of 0.25 sec. The amplitude ratio of the frequency response plot shows that the lead of 0.14 sec satisfies the equalization needs of Eq. 1 and makes the slope −20 dB/dec (corresponding to $|K/j\omega|$) in the mid frequency region. For this amount of driver lead equalization and no disturbance input the driver time delay (τ_o) is about 0.35 to 0.4 sec; and the corresponding zero phase margin crossover frequency, ω_{c_o}, is about 4.2 rad/sec. The presence of the disturbance increases the driver's neuromuscular tension and reduces τ to about 0.25 sec; resulting in about 25 deg phase margin (ϕ_m) and 5 dB gain margin (K_m) for the same crossover frequency, $\omega_{c_\psi} = 4.2$ rad/sec. The nominal driver describing function in the heading loop for the 1972 station wagon becomes:

$$Y_{p_\psi} = .79(.14j\omega + 1)e^{-.25j\omega} \qquad (2)$$

In practice, a high frequency lag ($T_I \doteq 0.01$, say) can be used to complete the equalizer.

Heading and roll "modes" are shown on the root locus of Fig. 2. These refer to the roots of the vehicle characteristic equation, and they are associated with the corresponding heading and roll dynamics of the basic vehicle. For example, the natural frequency and damping ratio of the roll mode is determined largely by the springs, shock absorbers, and sprung mass inertial properties of the vehicle.

The effect of changing the driver's response properties can be inferred from Fig. 2. Decreasing driver lead equalization will result in a decrease in crossover frequency for constant stability margins. This will reduce closed loop system bandwidth and degrade performance. Similar results occur for increased driver time delay, or with increased lag from the vehicle's dynamics.

Closing the heading loop, above, is the first of two analytical steps. It results in an open "outer loop" effective controlled element (Y_c') which is to be combined with the driver's describing function for lateral deviation control (Y_{p_y}). Closing this outer loop by again applying the crossover model of Eq. 1 is the second step. The open outer loop system block diagram is shown in Fig. 3. The driver/vehicle response properties for lateral deviation control are shown in Fig. 4.

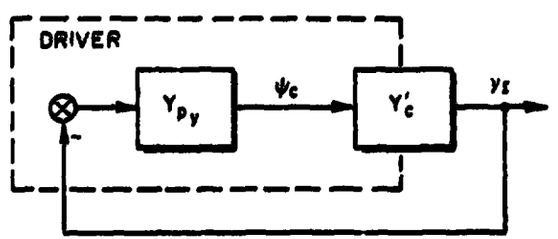

Figure 3. Block Diagram for Analysis of Lateral Deviation Control

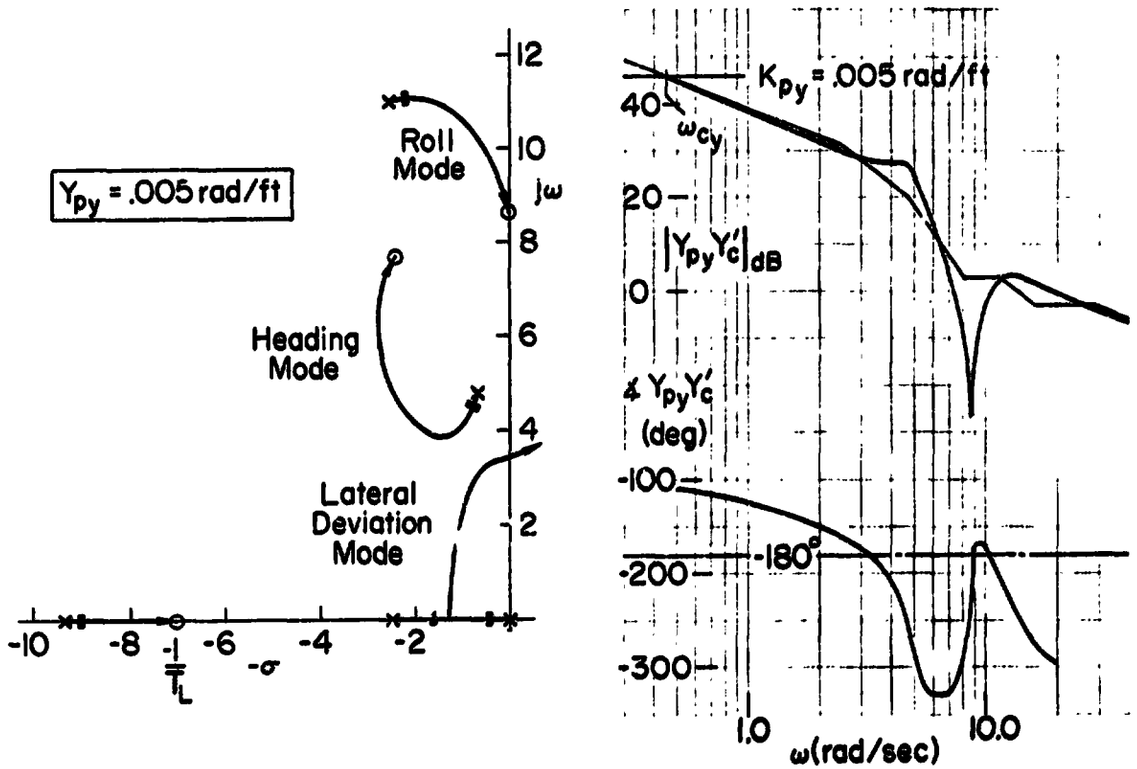

Figure 4. Driver/Vehicle Response Properties for Lateral Deviation Control, 1972 Station Wagon at 50 mph

The frequency response shows a broad region of $K/j\omega$-like amplitude ratio which will allow the driver to use a proportional control and vary his lateral deviation loop gain (K_{p_y}) over a considerable range depending on his closure criteria.

Selection of the outer loop crossover frequency (ω_{c_y}) in Fig. 4 can depend on several factors. Within limits, higher crossover frequencies give a wider driver/vehicle system bandwidth which improves performance by reducing lateral deviation error. The penalty associated with this is an increase in driver workload, and he will (when he can) adjust to some level of control which gives acceptable lane keeping performance. If the crossover frequency becomes too high performance will deteriorate because of reduced path damping and stability margins. For some vehicle handling dynamics, the quality of the response becomes poor for crossover frequencies well below the stability limit, as a result of undesirable interaction between the directional modes. In summary, the driver will increase his level of activity (crossover frequency) to achieve the desired level of performance, as long as he does not encounter undesirable vehicle handling properties in the process.

In view of these factors, the estimated value of ω_{c_y} becomes 0.46 rad/sec, which corresponds to $Y_{p_y} = 0.005$ rad/ft for this vehicle. Larger values of ω_{c_y} would not reduce the stability margins but they would result in poor response qualities, as follows. Consider the effect of increasing the crossover frequency in Fig. 4. For low values of ω_{c_y}, the lateral deviation and heading mode roots are well separated on the root locus, resulting in relatively simple response qualities which are dominated by the lateral deviation mode. As ω_{c_y} is increased, the closed-loop roots of the lateral deviation and heading modes approach each other. This results in a more complex, fourth order disturbance response, consisting of a combination of the two modes. Physically this means that the practical region of control is restricted by an undesirable interaction of lateral deviation and heading loop modes, although the region of stable control is large.

The disturbed vehicle's sensitivity to aerodynamic inputs also affects the driver's outer loop control effort. More sensitive vehicles require higher crossover frequencies to maintain a given range of performance. The station wagon is relatively insensitive so this factor did not override the response quality considerations described above.

The estimated driver/vehicle response characteristics, plus the aerodynamic disturbance data of Ref. 8, were used to compute the driver control and vehicle motion time responses for a given situation. Comparisons of such computed results with corresponding full scale data are given in Fig. 5. The test conditions involved the 1972 station wagon passing an intercity bus in about a -20 deg crosswind at a speed of 7 mph (bus 56 and wagon 63). The nominal (undisturbed) bus-vehicle centerline separation was about 12 ft. In the full scale data of Fig. 5, the mean front wheel steer angle is given by δ_w, U_C is the station wagon speed, r is the heading rate, and $|WV|$ and $\measuredangle WV$ are the magnitude and angle of the wind relative to the moving car. The lateral deviation of the station wagon relative to its nominal lane centerline is given by y_I. The data derive from the Ref. 7 study.

The lateral deviation results show excellent agreement, as do the low frequency variations in driver steer angle. The higher frequency remnant in steer angle, δ_w, and heading rate, r, occurs at the inner loop crossover frequency. As discussed, driver remnant can be included in the driver model when desired, but its effects on performance are minimal, as illustrated by the good match between the analytical and full scale lateral deviation time histories. This agreement in the lateral deviation comparison confirms the choice of outer loop crossover frequency shown in Fig. 4, $\omega_{c_y} = 0.46$ rad/sec.

<u>Station Wagon Plus Trailer</u> — Addition of the single axle travel trailer to the station wagon had a considerable effect on both the basic handling dynamics and the response of the driver/vehicle system to a bus-induced disturbance.

Root locus and frequency response plots of the heading loop driver/vehicle dynamics are shown in Fig. 6. Compared to the station wagon alone, the main effect of adding the trailer is to increase the mid frequency phase lag of the vehicle dynamics (Y_c) which tends to reduce the attainable driver

ORIGINAL PAGE IS OF POOR QUALITY

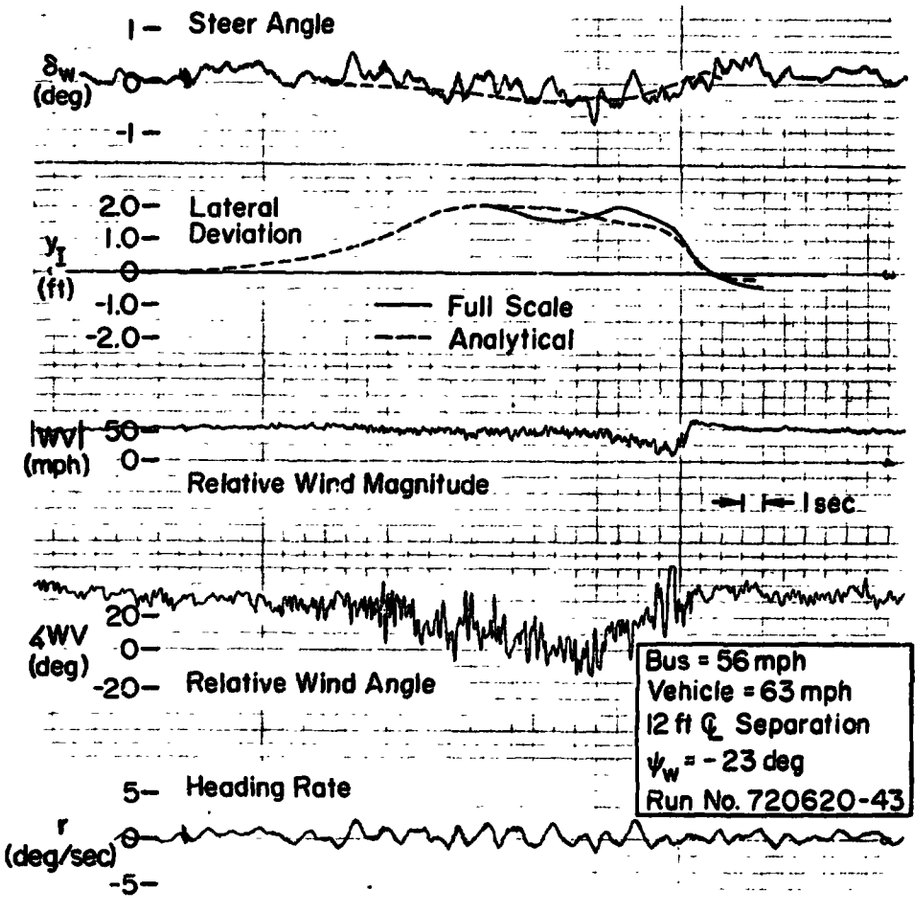

Figure 5. Comparison of Analytical and Full Scale Results, 1972 Station Wagon Passing Intercity Bus

crossover frequency. [The difference in speed between 60 and 65 mph has only a small effect on the vehicle dynamics.] Application of the previously discussed driver model rules resulted in a heading loop driver lead (T_L) at 0.33 sec, and a driver time delay (τ) of 0.25 sec. Comparison of the open loop heading roots of the station wagon (Fig. 2) with the wagon plus trailer (Fig. 6) shows that the trailer results in two additional modes (trailer roll and tow angle). The trailer tow angle mode is seen to be lightly damped, and this causes the initial instability as the driver increases his inner loop crossover frequency. Note that the station wagon heading mode remains quite well damped for all values of driver gain. Physically this means that the driver may be relatively unaware of large oscillations of the trailer. This analytical interpretation was borne out in the full scale tests where the driver comments indicated he was unaware of the typically large trailer oscillations.

The characteristics of the outer loop driver/vehicle response properties for the wagon plus trailer are shown in Fig. 7. Again, simple gain control (K_{py}) is adequate in the outer loop, and the crossover frequency (ω_{c_y}) is limited by the vehicle's handling dynamics.

An example comparison of full scale data and analytical results for zero crosswind is shown in Fig. 8, and the agreement is seen to be quite good. The tow angle is η. The lateral deviation trajectory* (y_{I_t}) in Fig. 8 shows that the trailer tends to move towards the bus in a zero crosswind condition, while the station wagon alone (and all other tested vehicles) tended to move away from the bus in this wind condition. This difference results from the aerodynamic disturbance of the trailer.

<u>Truck/Camper</u> — The driver/vehicle response properties of the truck/camper are given in Figs. 9-11. The system surveys of the heading and lateral deviation loops are presented followed by a time history of an analytical/full scale comparison. The truck/camper heading loop closure (Fig. 9) is similar to the wagon plus trailer (Fig. 6). The basic vehicle dynamics

*y_{I_t} refers to deviation of a point on the rear bumper of the trailer. This is done to account for the effect of trailer tow angle on lateral deviation.

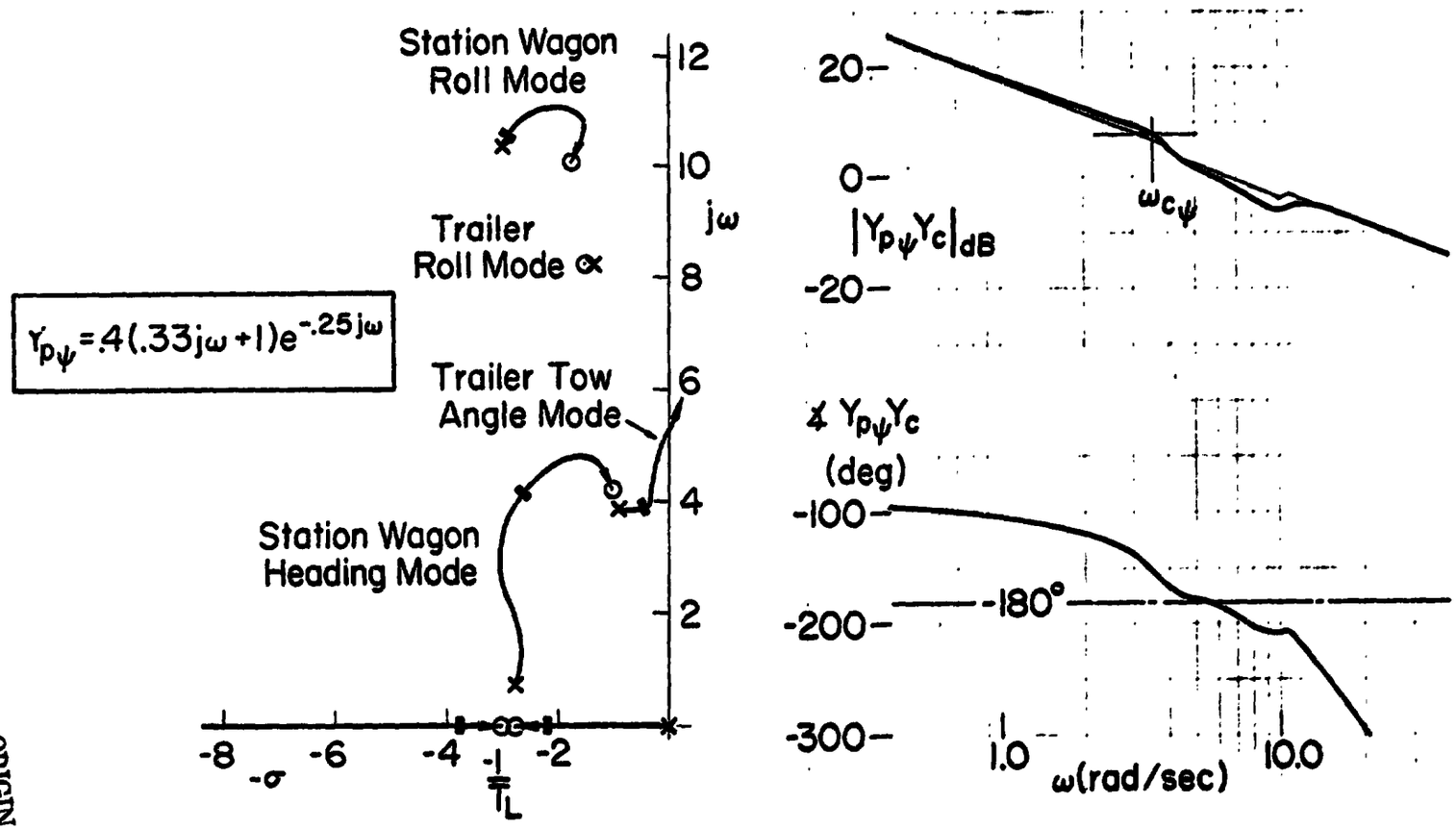

Figure 6. Driver/Vehicle Response Properties for Heading Control, Station Wagon Plus Trailer at 65 mph

ORIGINAL PAGE IS
OF POOR QUALITY

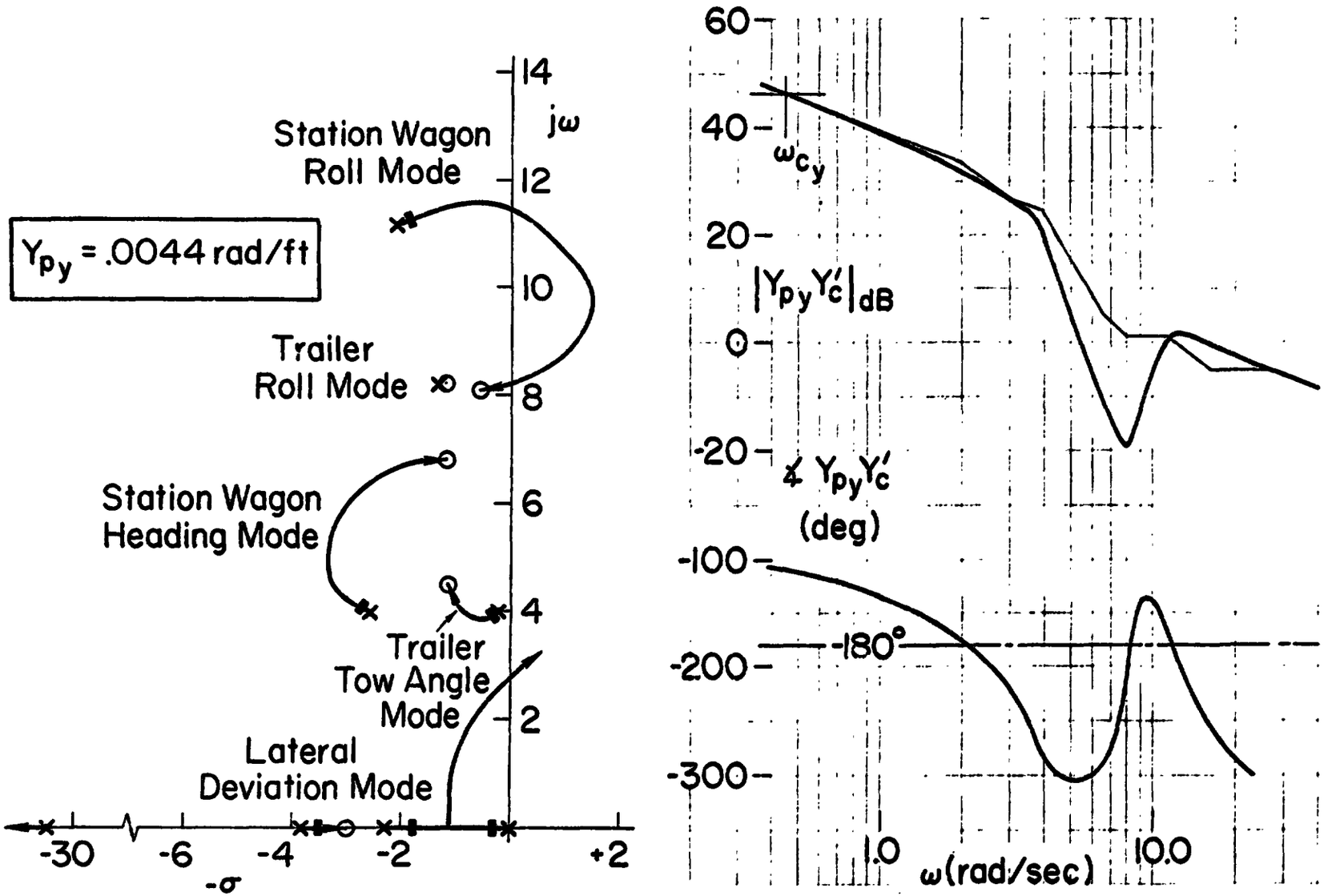

Figure 7. Driver/Vehicle Response Properties for Lateral Deviation Control, Station Wagon Plus Trailer at 65 mph

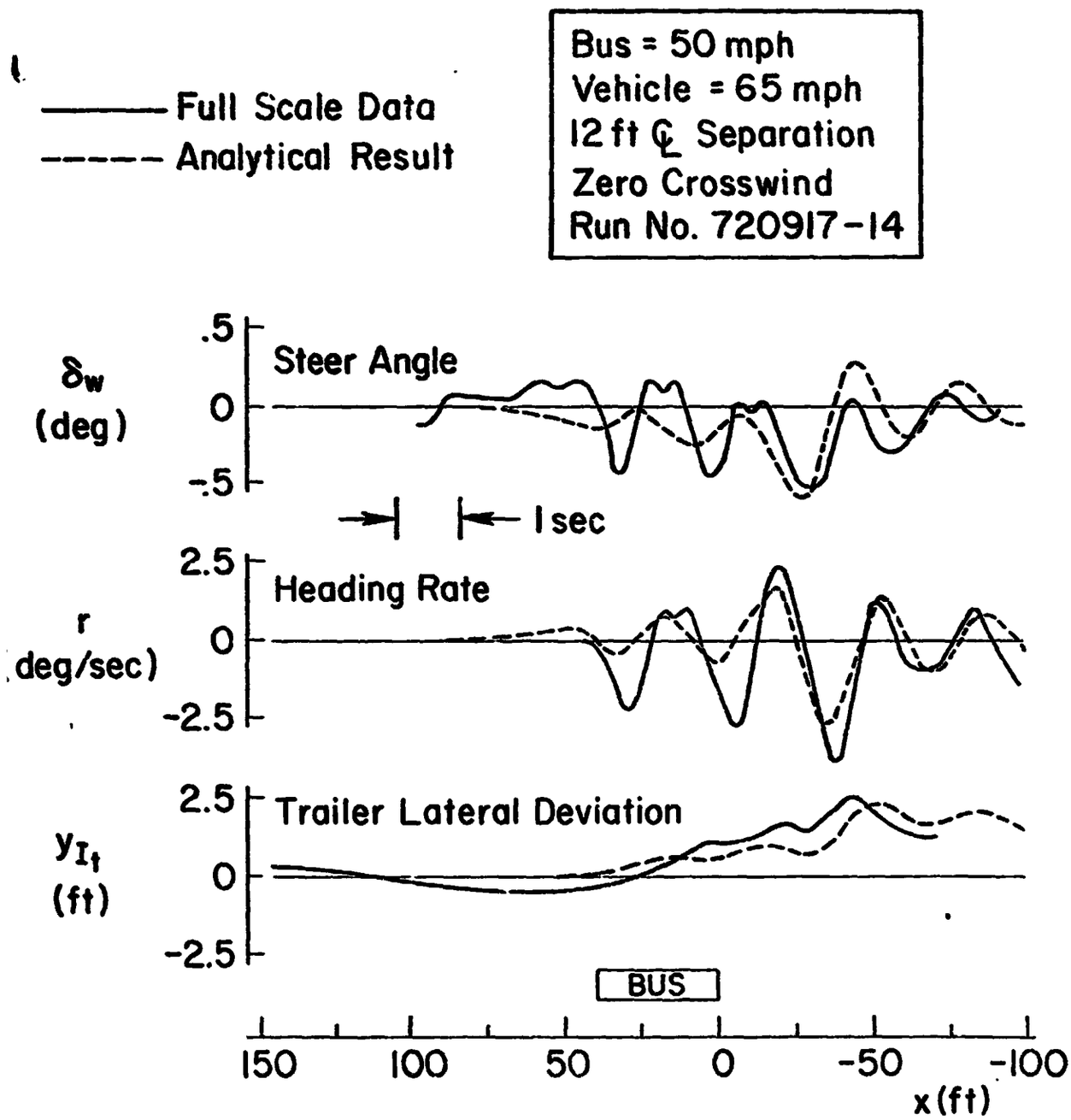

Figure 8. Comparison of Analytical and Full Scale Results, Station Wagon Plus Trailer Passing Intercity Bus

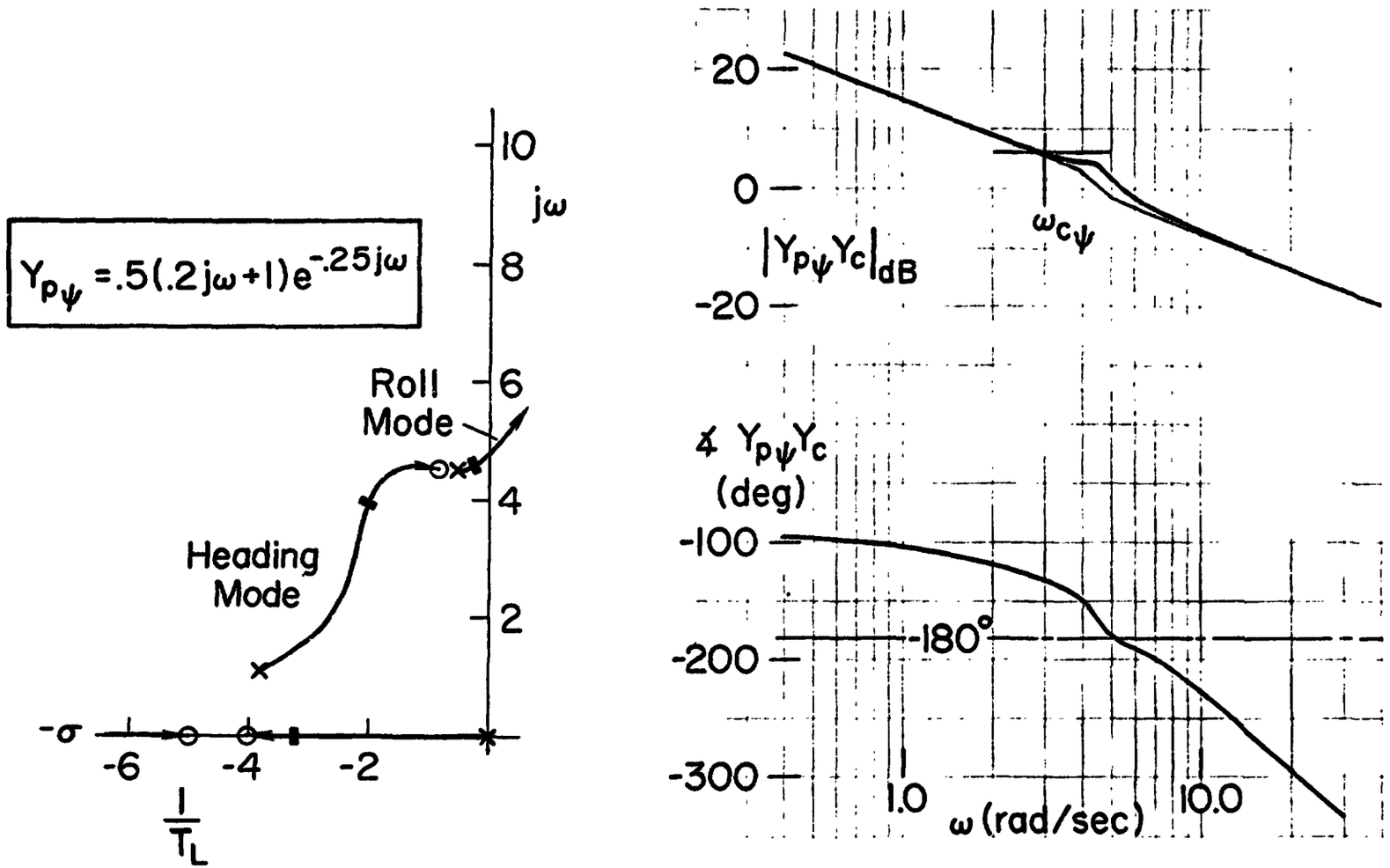

Figure 9. Driver/Vehicle Response Properties for Heading Control, Truck/Camper at 60 mph

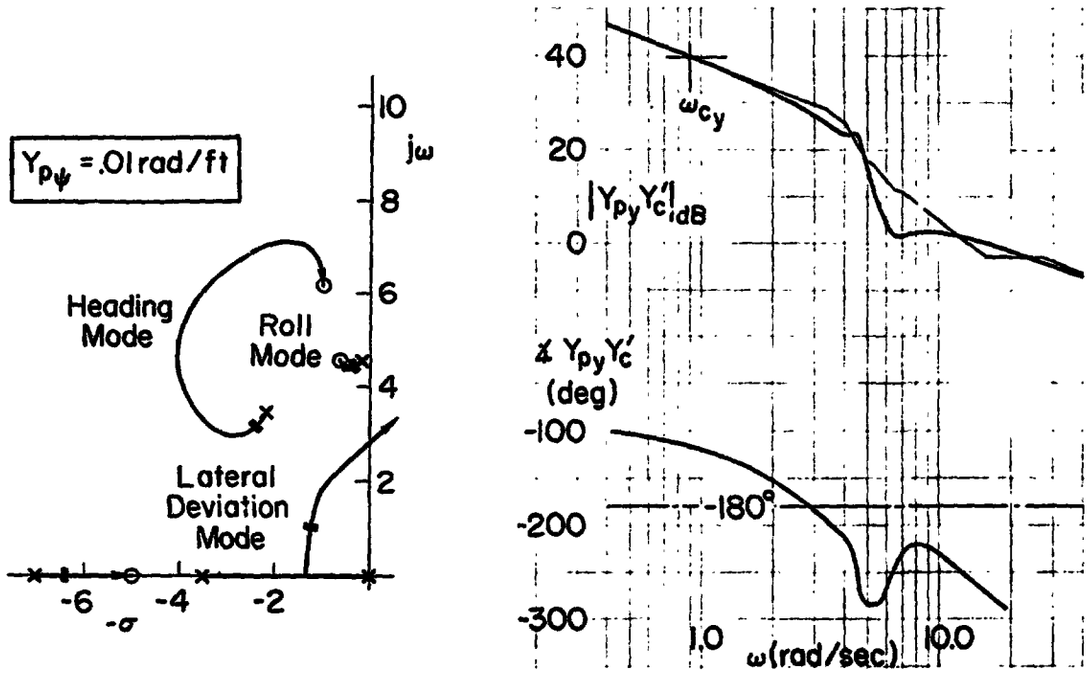

Figure 10. Driver/Vehicle Response Properties for Lateral Deviation Control, Truck/Camper at 60 mph

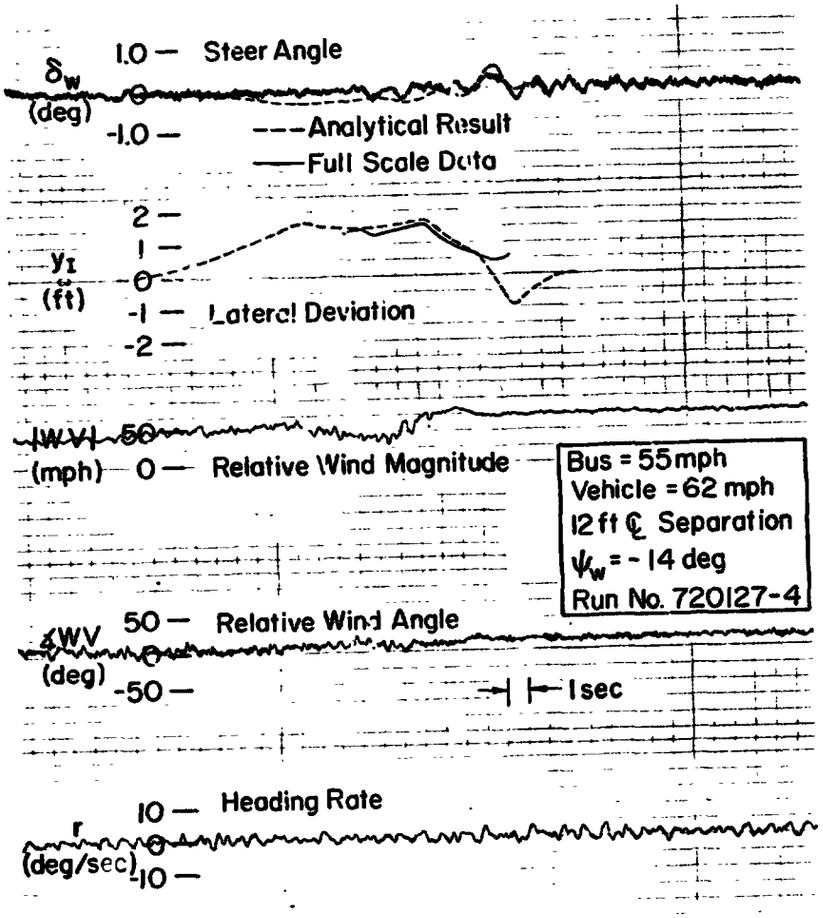

Figure 11. Comparison of Analytical and Full Scale Results, Truck/Camper Passing Intercity Bus

exhibit a lightly damped mode which tends to go unstable as a result of the heading loop closure. In the case of the truck/camper it is the roll mode which is critical. This is probably a result of the high c.g. location and large mass to roll stiffness ratio of the camper.

Discussion — The driver/vehicle heading loop response of the van, compact sedan, and 1972 full size sedan are all similar in form to the 1972 station wagon. The driver response properties for the other vehicles are summarized in Table 2. Details are given in Ref. 7. The lateral deviation response properties of the van, compact sedan, and 1972 sedan are similar to each other. Unlike the 1972 station wagon, their lateral deviation and heading modes are well separated; hence the driver can use a higher crossover frequency without producing undesirable qualities in the response. The outer loop closures were based on considerations discussed previously, and this was consistent with the full scale lateral deviation data. The driver/vehicle heading loop closures are seen to reflect fairly constant stability margins, in accordance with the driver model and analysis procedures. The crossover frequencies and lead equalization vary somewhat, depending on the handling dynamics of the vehicle.

The lateral deviation response properties shown in Table 2 vary considerably. The van shows low stability margins and high crossover frequencies, while the 1972 station wagon is just the opposite. As previously discussed, these variations depend on the aerodynamic and handling properties and reflect an effort on the part of the driver to achieve a desired level of performance. The performance of the several driver/vehicle systems is given in Fig. 12a for a bus disturbance in a 90 deg crosswind condition, in terms of peak lateral deviation ($\hat{y}_I$). The differences in performance among the several vehicles generally follow the trend of the vehicle-alone gust susceptibility (Fig. 12b), although the variation is not as large. With two exceptions, the peak lateral deviations are all in roughly the same performance band for a given crosswind. This relative insensitivity of overall performance to changes in the control task and situation is a familiar result in the field of manual control. It reflects a constancy of skill. The performance insensitivity is usually achieved by the human controller's adjustment of his response to offset deficiencies in the vehicle dynamics (as well as other changes in task

TABLE 2

SUMMARY OF ESTIMATED DRIVER/VEHICLE RESPONSE PROPERTIES

VEHICLE	HEADING RESPONSE					LATERAL DEVIATION RESPONSE			
	ω_{c_ψ} rad/sec	T_L sec	K_{p_ψ}	φ_m deg	K_m dB	ω_{cy} rad/sec	K_{py} rad/ft	φ_m deg	K_m dB
1972 Wagon	4.3	0.14	0.79	28	3.5	0.46	0.005	75	18
1972 Wagon Plus Trailer	3.6	0.33	0.40	25	7	0.45	0.0044	80	16
Truck/Camper	3.0	0.2	0.50	48	4	0.75	0.01	65	10
Imported Van	4.2	0.2	0.71	35	4	2.3	0.03	30	5
Compact Sedan	3.6	0.33	0.45	25	5	1.3	[illegible]	58	17
1972 Sedan	2.8	0	0.80	60	4	0.8	[illegible]	60	13

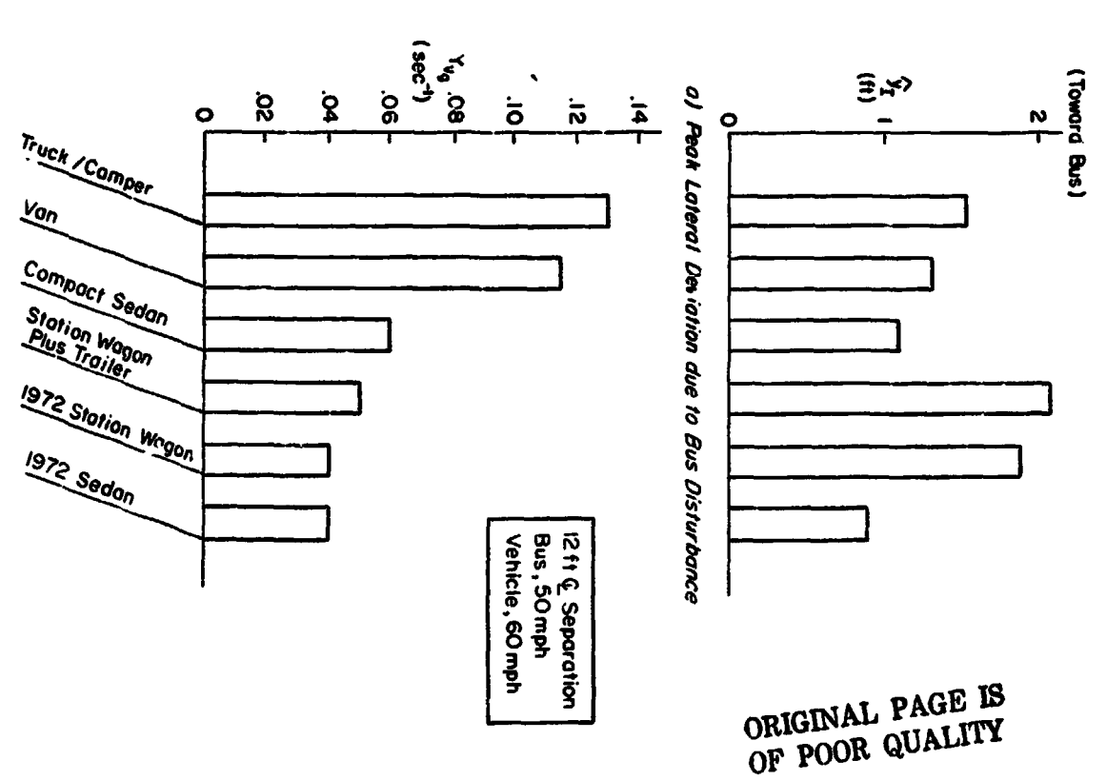

Figure 12. Effect of Disturbed Vehicle Properties on Estimated Performance

ORIGINAL PAGE IS OF POOR QUALITY

variables). The path performance (e.g., peak lateral deviation) is not the only element in the driver's "performance criterion," however, and other factors are taken into account. Hence variations in performance do occur, such as those evidenced in Fig. 12a by the 1972 station wagon and the station wagon plus trailer.

In the cases where these characteristics are reasonably nominal, the closures in Table 2 exhibit crossover frequencies about 1 rad/sec and phase margins of about 60 deg (truck/camper, compact sedan, 1972 sedan). These outer loop closures (with 60 deg phase margin) give good path mode stability and overall performance, simple response qualities with constant closed loop damping ratio across vehicles, and a relative insensitivity to changes in driver gain. The performance is proportional to driver control effort (crossover frequency). Departures from the nominal lateral deviation response properties for the remaining three vehicles can be summarized as follows:

- The 1972 station wagon estimates exhibit a somewhat lower crossover frequency and larger phase margin in the lateral deviation loop. This is due to the undesirable interaction between the lateral deviation and heading modes which results as the crossover frequency is increased.

- The large phase margin for the station wagon plus trailer also results from an undesirable interaction between the lateral deviation and trailer tow angle modes as the driver increases the outer loop crossover frequency (see Fig. 7).

- The reduced phase margin and increased crossover frequency seen in the van estimate is due to the large gust disturbance sensitivity which results in a high yawing moment. The analyses showed that aggressive closure of the lateral deviation loop tends to stabilize the heading mode which is being excited by the yaw disturbance.

The driver/vehicle characteristics in Table 2 represent nominal results which are consistent with the full scale data.

REFERENCES

1. Weir, David H., and D. T. McRuer, "A Theory for Driver Steering Control of Motor Vehicles," Road User Characteristics, Highway Research Record No. 247, 1968, pp. 7-28.

2. Weir, David H., and Duane T. McRuer, "Models for Steering Control of Motor Vehicles," Fourth Annual NASA-Univ. Conf. on Manual Control, U. of Mich., 21-23 Mar. 1968, NASA SP-192, pp. 135-169.

3. Weir, David H., and Duane T. McRuer, "Dynamics of Driver/Vehicle Steering Control," Automatica, Vol. 5, No. 1, Jan. 1970, pp. 87-98.

4. Weir, David H., and Charles K. Wojcik, "The Measurement of Driver Describing Functions in Simulated Steering Control Tasks," Seventh Annual Conf. on Manual Control, USC, 2-4 June 1971, NASA SP-281, pp. 209-218.

5. Weir, David H., and Duane T. McRuer, Measurement and Interpretation of Driver Steering Behavior and Performance, SAE Paper No. 730098, presented at the SAE International Automotive Engineering Congress and Exposition, Detroit, Mich., Jan. 1973.

6. McRuer, D. T., D. Graham, and E. S. Krendel, "Manual Control of Single-Loop Systems: Parts I and II," J. Franklin Institute, Vol. 238, No. 1, Jan. 1967, pp. 1-29; and Vol. 238, No. 2, Feb. 1967, pp. 145-168.

7. Weir, David H., Roger H. Hoh, Robert K. Heffley, and Gary L. Teper, An Experimental and Analytical Investigation of the Effect of Bus-Induced Aerodynamic Disturbances on Adjacent Vehicle Control and Performance, Systems Technology, Inc., Tech. Rept. 1016-1, Nov. 1972.

8. Heffley, Robert K., The Aerodynamics of Passenger Vehicles in Close Proximity to Trucks and Buses, SAE Paper No. 730255, presented at the SAE International Automotive Engineering Congress and Exposition, Detroit, Mich., Jan. 1973.

SESSION III

DISPLAYS II

N75 19137

A DISPLAY EVALUATION METHODOLOGY APPLIED TO VERTICAL SITUATION DISPLAYS*

Sheldon Baron
William H. Levison

Bolt Beranek and Newman Inc.
Cambridge, Massachusetts

1. INTRODUCTION

In spite of vast efforts in display design and evaluation, there do not appear to be standardized procedures for evaluating aircraft displays. Instead, a variety of techniques are employed in the several stages leading to an acceptable display configuration, with man-in-the-loop real-time simulation experiments playing a central role. While there are a number of valid reasons for the techniques that have been used [1], it seems fair to say that there exists a need for unifying concepts and approaches.

Analytical models of the pilot-vehicle-display system appear to offer the possibility of a systematic, well-defined and comprehensive approach to display evaluation. Such models allow one to examine the interactions of displayed information with vehicle dynamics, disturbances, mission criteria and human performance. They may be used to provide early and preliminary evaluation of competing configurations without the necessity for expensive simulation; in later stages of display development, the models can serve as powerful diagnostic and extrapolative adjuncts to the necessary simulations.

The advantages of analytical models for display evaluation have been well-understood for some time and considerable effort has been expended in their development. Perhaps the most extensive effort to date is represented by the work of Allen, Clement and Jex [2] and McRuer, et al. [3]. They attempted to synthesize the human operator scanning model of Senders [4], multi-loop describing function theory [5] and Clement's theory of human signal reconstruction [6] into a theory for displays in manual control.

In this paper, an approach to display evaluation based on the optimal-control or state-variable model of the human operator [7-10] is described. The approach has evolved over the past several years [11-14] and we believe it has significant advantages for display evaluation. In the remainder of the paper, we describe

*This work was supported under Contract NAS2-6652 for the NASA, Ames Research Center, Man-Machine Integration Branch.

PRECEDING PAGE BLANK NOT FILMED

briefly the foundations of the methodology* and present results of its application to the analysis of vertical situation display for STOL approach. This analysis includes the effects of both status and command displays on pilot workload and system performance. More detail concerning the results and ideas presented here can be found in [15].

2. DISPLAY EVALUATION METHODOLOGY

The following four steps are fundamental in the application of the display evaluation methodology:

1. Specification of system dynamics, disturbances, and task requirements in terms of a linear-quadratic-gaussian optimization problem suitable for application of the optimal control model of the human operator [8, 10].

2. Analysis of proposed display configuration with respect to display characteristics and their relation to parameters of the human operator model.

3. Determine performance with given configuration and investigate the effects of elimination of display limitations.

4. Analyze display workload-performance tradeoffs via sensitivity analysis.

System Specification

System dynamics are approximated by the following linear state equation:

$$\dot{\underline{x}} = \underline{A}\,\underline{x} + \underline{B}\,\underline{u} + \underline{E}\,\underline{w} \qquad (1)$$

where $\underline{x}(t)$ is the vector of system states, $\underline{u}(t)$ the vector of pilot control inputs and $\underline{w}(t)$ the vector of linearly independent white gaussian noises. If external forcing functions are rational gaussian noise spectra of first order or higher as is the case for most turbulence models [16], they are represented by white noise ($\underline{w}$) passed through a linear filter and the system dynamics are augmented by those of the filter. Disturbances such as constant winds or wind-shears are modelled, essentially, by adding non-zero mean components to $\underline{w}$ [14, 15].

*A detailed description of the optimal control model of the human operator is not given as it has already been well-documented [7-10, e.g.].

The display-variables are assumed to be linear combinations of the state and control variables and are given by the "display-vector"

$$\underline{y}(t) = \underline{C}\ \underline{x}(t) + \underline{D}\ \underline{u}(t) \tag{2}$$

As with the input, display dynamics are included by introducing additional system states and augmenting the matrices in Equation (1). Such is required, for example, in analyzing certain flight director configurations.

Task requirements are stated in terms of "cost weightings" associated with various system variables in a quadratic cost functional of the form

$$J(\underline{u}) = E\ (\underline{y}'\ \underline{Q}\ \underline{y} + \underline{u}'\ \underline{R}\ \underline{u} + \dot{\underline{u}}'\ \underline{G}\ \dot{\underline{u}}) \tag{3}$$

It is assumed that the pilot selects his control response to minimize the appropriate J. For relatively simple, single-variable control situations, good approximations to experimental measurements have been obtained with a cost functional consisting simply of a weighted sum of system error variance plus control-rate variance [5]. The cost on control-rate represents, in part, a subjective penalty imposed by the controller on making rapid control motions and may account, indirectly, for physiological limitations on the pilot's bandwidth.

For complex multi-input, multi-output tasks, the cost weightings may not be chosen in so simple a fashion. One approach is to select values for the weightings so as to keep mean-squared output levels within prescribed tolerances [17]. A unit amount of "cost" is associated with a given variable when the magnitude of the "error" equals the nominal limit, and the weighting coefficient for each variable is simply the inverse of the square of the corresponding limit. This approach was used in the application to be discussed later.

For the present paper, the matrices introduced in Equations 1-3 are assumed constant. This corresponds to a condition for which we have the most validation data but it is not a necessary restriction. For example, in a companion paper [18] and in [15], range (time)-varying display gains and cost functional weightings are included in the analysis.

Analysis of Display Configuration

A basic assumption of the optimal control model of the human operator is that the human perceives a noisy, delayed version of the displayed variables; i.e., if $\underline{y}_p(t)$ is the vector of perceived variables, then

$$\underline{y}_p(t) = \underline{y}(t-\tau) + \underline{v}_y(t-\tau) \tag{4}$$

where $\underline{y}$ is defined by Equation 3, and $\underline{v}_y$ is a vector of white, gaussian observation noises.* When the displays have been optimally designed as is the case in many laboratory situations, central processing sources of pilot randomness appear to be the principal determinant of $\underline{v}_y$. Thus, we find for manual control situations in which the displayed signal is large enough to negate the effects of visual resolution ("threshold") limitations, the autocovariance of each observation noise component appears to vary proportionally with mean squared signal level and may be represented as

$$\begin{aligned} V_{y_i}(t) &= \pi\ P_i \cdot E(y_i^2(t)) \\ &= \pi\ P_i\ \sigma_{y_i}^2(t) \end{aligned} \tag{5}$$

where P is the "noise/signal ratio" and has units of normalized power per rad/sec. Numerical values for P_i of 0.01 (i.e., -20 dB) have been found to be typical of single-variable control situations [9, 10].

When display characteristics are not ideal it is necessary to modify the expression for the observation noise covariance associated with a particular display variable. In this study, two display limitations were important under certain circumstances, namely threshold limitations and the lack of a zero reference. We account for these phenomena by letting the autocovariance for each observation noise process be

$$V_i(t) = P_i \left(\frac{\sigma_i^2}{K_i^2\ (\sigma_i, a_i)} + \sigma_{i_o}^2 \right) \tag{6}$$

where the subscript i refers to the ith display-variable. The quantity $K(\sigma_i, a_i)$ in Equation 6 is the describing function gain associated with a threshold device

$$K(\sigma, a) = \frac{2}{\sqrt{\pi}} \int_{-\infty}^{-\frac{a}{\sigma\sqrt{2}}} e^{-x^2}\ dx$$

where "a" is the threshold and σ is the standard deviation of the "input" to the threshold device.** This factor is used primarily to account for threshold-type phenomena associated with viewing

*The human's time delay, τ, is a parameter of the model; typically, τ = .15 - .2 sec.

**For non-zero mean signals this expression must be modified [14].

the display, but "indifference" thresholds will have an indistinguishable effect. Essentially, its effect is to cause the observation noise covariance to become greater as the signal becomes smaller relative to the threshold.

The term $\sigma_{1_0}^2$ in (6) is a residual-noise covariance and, in many cases, is similar in effect to a threshold. However, it can be viewed as a separate parameter and used to account for observed degradation in tracking performance that results from lack of reference indicators [15].

Performance Evaluation

Once the system and human parameters have been chosen, performance can be evaluated. Although, for model development, task requirements are specified in terms of the quadratic cost functional J of Equation 3, other measures of performance are important in problem analysis. For many problems a useful system metric relates to performance reliability, or the probability of achieving mission objectives successfully. The success of a mission (segment) can often be stated in terms of constraints that the system states (or outputs, or controls, or functions of these variables) must satisfy. In other words, mission success may be equated with $\underline{x} \in X$. Then, the probability of success is, simply,

$$\Pr(\underline{x} \in X) = \int_{\underline{x} \in X} p(\underline{x})\,d\underline{x} \qquad (7)$$

where $p(\underline{x})$ is the probability density function for $\underline{x}$. An example where such a specification of success is meaningful is approach to landing (see below). Because of the linearity and gaussian assumptions, $p(\underline{x})$ (and $p(\underline{y})$, $p(\underline{u})$, etc.) is obtained in a single run of the optimal control model for the human operator.

The probability of success, as defined in Equation 7, is for the total man-machine system and the particular mission segment being analyzed. This probability is, in fact, a conditional one in that its computation depends on the particular system and model parameters chosen in Equations 1-6. Thus, through model analyses, success or failure probabilities may be determined as functions of any parameter(s) of interest. In particular, for display evaluation, one can investigate systematically the effects on performance reliability of changes in display characteristics. Because of the structure of the model, one can also compute the performance that could be attained with an idealized display; this provides a useful basis for comparison and analysis.

Workload Analysis

As noted earlier, the observation noise/signal ratio, P_i, seems to be associated with the operator's central processing capabilities. This association leads to a relatively straightforward model for task interference and operator workload. The details of this model are given in [19]. Very briefly, we consider, for convenience, that attention-sharing may be required at three levels: between manual control and non-control tasks; between sub-tasks within the manual control task; and between displays associated with performing a given sub-task. For example, a pilot might share attention between control and communication, between longitudinal and lateral control and between flight path and attitude displays. Thus, we define

f_t = fraction of attention devoted to the control task as a whole
f_s^t = fraction of attention devoted to sub-task s
f_i^s = fraction of attention devoted to i^{th} display in sub-task s

Then, the effects of attention-sharing are modelled by an increase in the "nominal" noise/signal ratio, i.e., by

$$P_i = P_o \cdot \frac{1}{f_t} \cdot \frac{1}{f_s} \cdot \frac{1}{f_i} \qquad (8)$$

where P_i is the noise/signal ratio associated with the ith display when attention is being shared and P_o is the noise/signal ratio associated with full attention to the display.

To predict the effect on specific tasks of sharing attention, Equation 8 is used to establish the appropriate observation noise-signal ratios and the model equations are solved using this value. If the pilot's allocation of attention is unknown beforehand, model solutions may be used to determine the optimum allocation of attention, which, in line with the fundamental optimality hypothesis, may be taken as a prediction of the pilot's allocation.

Building on the model for attention, we define a "workload index" as the fraction of attention required to achieve a specified criterion level of performance on the control task. Thus,

$$\text{Workload Index} = f_{t_c}$$

where f_{t_c} is the minimum fraction of attention for which performance can be maintained within the criterion level. In order to predict the workload index, it is necessary to specify a relevant performance measure, the required level of performance, and the "reference" noise/signal ratio P_o. Ideally, we would like P_o to correspond to full attention, but we cannot conduct an experiment in which the pilot is guaranteed to use his total information-processing capability. Therefore, we let P_o correspond to the

noise/signal ratio (namely, .01 or -20 dB) obtained in a standardized laboratory situation in which the pilot is motivated to minimize his tracking errors. We know that this value does not correspond to "full capacity", because significantly lower noise-ratios have been found experimentally [19]. However, based on our laboratory experience, P_o = -20 dB does appear to correspond to a high workload condition, and "operation" at this level for any prolonged time would undoubtedly be unacceptable. Of course, when we are interested primarily in the relative *change* in workload requirements from one situation to the next, the value for P_o is not too critical.

3. ANALYSIS OF VERTICAL SITUATION DISPLAYS FOR STOL APPROACH

The display evaluation methodology has been used to analyze basic status displays and director displays for the steep (7.5°) approach to landing of the Augmentor Wing Jet STOL Research Aircraft (AWJSRA). The displays were analyzed primarily with respect to steady-state, gust regulation performance at the decision height (approximately 30m), though other supporting studies were also conducted [15, 18]. Here, we describe the basic display configuration that was investigated and present some of the more interesting and more important results. Performance predictions are presented for lateral control and for combined lateral-longitudinal control. Results for the longitudinal control case are given in [5]. Details concerning vehicle dynamics, turbulence spectra, cost-functional weightings, and other parameters of the system-human operator model are given in [15], where more extensive presentation and discussion of results may also be found.

An abstraction of the relevant features of the STOLAND-EADI status display [20] considered here is shown in Figure 1. This display provides the pilot with glide path and localizer errors as well as attitude information. From such a display the pilot can also obtain the rates of change of these variables. Although an airspeed error indicator is not shown in Figure 1, the pilot is displayed this quantity with the STOLAND-EADI and we will assume that airspeed error is available in our analysis.

Effective visual thresholds were computed for the aircraft at the 30-meter decision height. On the basis of previous analysis of approach performance [14], an "indifference threshold" of 0.1 degrees visual arc was associated with perception of height error. Previous analysis of pilot remnant data [13] suggested thresholds of 0.05 degrees visual arc for other indicator displacements and 0.18 arc-degrees/second for indicator-rate quantities. Display gains given in [20] were used to convert thresholds into units related to system quantities.

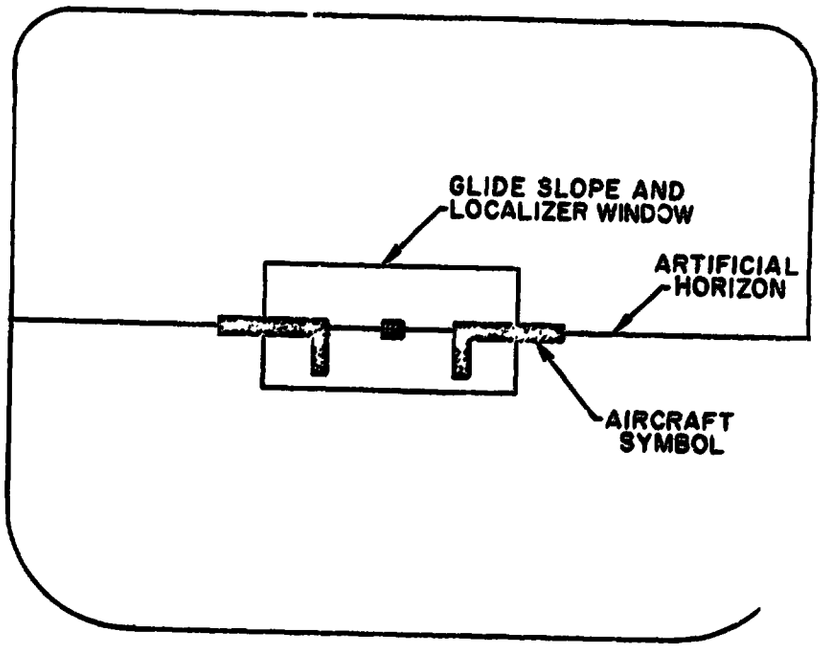

FIGURE 1. Display of Status Information

Non-zero rms residual noise terms were associated with height and sink-rate information. Because the display shows the height "window" of ±3.7 meters, a residual noise on height perception was needed to account for the lack of an explicit zero reference. To approximate the effects of the non-zero reference, the value of the residual noise was set equal to the amount of the reference offset (i.e., 3.7 meters). The residual noise on sink-rate information was included to account, in a rough way, for the resolution limitations of a Scanning Beam Instrument Landing System. However, the latter noise term was found to have no appreciable effect on predicted performance. A non-zero rms residual noise term was also associated with lateral offset error. This was set to a value of 5.4 meters, corresponding to the lateral dimensions of the "window". Studies of longitudinal control showed that the thresholds on attitude could be ignored, so in the analysis of lateral performance the thresholds associated with viewing the bank angle indicator were set to zero. Thresholds and residual noises for all displayed variables are summarized in Table 1.

Table 1

DISPLAY-RELATED PARAMETERS

Variable	Threshold	RMS Residual Noise
Altitude error (m)	0.48	3.7
Sink-rate (m/s)	0.85	1.1
Pitch (deg)	0.22	0.0
Pitch-rate (deg/s)	0.78	0.0
Airspeed error (m/s)	0.14	0.0
Lateral error (m)	.28	5.4
Lateral error rate (m/s)	.52	0
Bank angle (deg)	0	0
Roll rate (deg/s)	0	0

To evaluate various display configurations it was necessary to choose a performance metric. Although rms error scores were used as raw measures, it was decided to evaluate the displays in terms of the probability of not meeting Category II, approach window specifications, i.e., in terms of probability of a "missed approach". Of course, the missed approach probability is a function of gust intensity. Both, a worst-case wind- and a median-wind-condition, were investigated.* Because the relationship between rms performance and gust intensity is nearly linear [15] and the

*Given that turbulence occurs (P_T=.8), winds of intensity equal to or greater than that of the worst-case (median) wind will be encountered 1% (50%) of the time.

probability density for turbulence intensity is known [16], one can use the results for the two wind conditions to predict a measure of system performance that is averaged over all possible wind conditions. Such an overall system performance measure was also obtained in many cases.

Longitudinal and lateral displays were first analyzed separately. This was possible because of the decoupling inherent in the assumed linearized perturbation equations. Of course, the pilot must share his capacity between the longitudinal and lateral tasks, which implies some interference and a degradation in performance on each task. This interference was treated within the framework of the model of attention presented earlier.

To account for the interference, we define a combined cost functional

$$J_{TOT} = J_{LONG} + J_{LAT}$$

where J_{LONG} and J_{LAT} are the cost functionals for the longitudinal and lateral cases, respectively. The combined cost functional is meaningful because of the manner in which the weightings in the separate cost functionals were chosen. Now, if f_{LONG} is the fraction of attention devoted to the longitudinal task, then for control

$$f_{LAT} = 1 - f_{LONG}$$

It is therefore possible to determine how attention should be shared between the two control modes so as to minimize J_{TOTAL}.

Status Display

The first stage of the analysis of the lateral displays was a sensitivity study to determine the optimal allocation of attention between localizer and bank angle displays.* It was found that performance was not very sensitive to allocation of attention between these displays. Nevertheless, about 75% attention to localizer, 25% to bank angle indicator was best in a high workload situation [15] and this attention-split was assumed for the remainder of the analysis.

Lateral tracking performance was computed for the worst-case and median winds and these rms scores were used to compute a composite score for an "all-winds" average. This was done for several levels of total attention devoted to the lateral task. The results in terms of missing the lateral approach window (5.4m) are given in Figure 2. They reveal that the lateral control task, even with the SAS-on, is very difficult. (The probability of missing the lateral window when averaged across all winds is 1.5 - 3 times as great as that for missing the longitudinal window at all levels of attention investigated.) If a 95%

*Because of the nature of the EADI overt visual scanning was not considered.

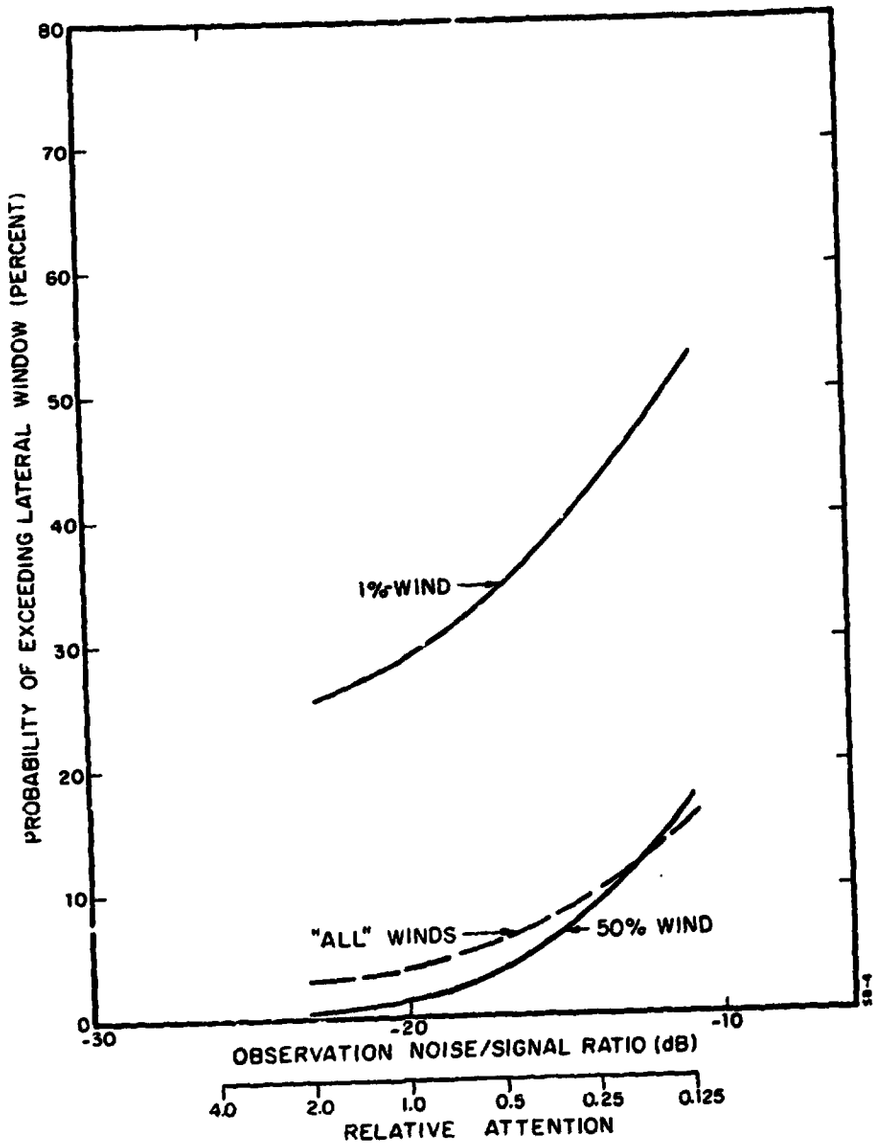

FIGURE 2. Effect of Attention on Lateral Window Performance

probability of a successful lateral approach is selected as a criterion level, the Workload Index for the lateral task for the 50% wind is about .4, and it is about .7 when the average of all winds are considered. For the 1% wind, it does not appear that a success probability of 95% is achievable within the limits of human behavior that we have observed heretofore.

The effects of sharing attention between longitudinal and lateral control tasks on window performance, averaged over all winds is shown in Figure 3. Using the probability of a missed approach as the measure of performance leads to the conclusion that approximately a 40/60 split of attention between longitudinal and lateral tasks is optimal. The corresponding overall probability of a missed approach (i.e., a miss on height or airspeed or lateral position) is about 8%. We can use these results and those for longitudinal control to obtain missed approach probabilities as functions of the relative attention devoted to the tracking task as a whole (assuming, for convenience that the pilot splits attention equally between the two tasks and that "full" attention = -20 dB). The result is plotted in Figure 4. This figure emphasizes the difficulty of the task. When all winds are considered, it does not appear possible to achieve a 95% approach success probability, at least within the range of pilot workload that is assumed acceptable. Even for the 50% wind condition, a success probability of 95% implies a Workload Index of about .9, hardly a desirable situation.

In an attempt to determine potential improvements in the lateral display, an analysis of the sensitivity of performance to changes in display parameters was conducted (for the worst-case wind and a high workload (P_o = -20 dB) condition). The following display improvements were considered in cumulative fashion: A) nominal EADI-Status Display; B) removal of residual noise associated with lateral error (providing a zero-reference); C) zero threshold for lateral error-rate; D) zero threshold for lateral error; E) no modification of noise/signal ratios for attention-sharing (display integration). The results of the analysis are given in Table 2.

Table 2

EFFECT OF DISPLAY PARAMETERS ON LATERAL PERFORMANCE

Condition	A	B	C	D	E
σ_y (m)	5.09	5.05	4.89	4.87	4.59
$\sigma_{\dot{y}}$ (m/s)	2.0	1.99	1.96	1.95	1.88
σ_ϕ (deg)	5.04	5.03	4.97	4.96	4.71
σ_{δ_W} (deg)	10.6	10.6	10.4	10.4	9.8

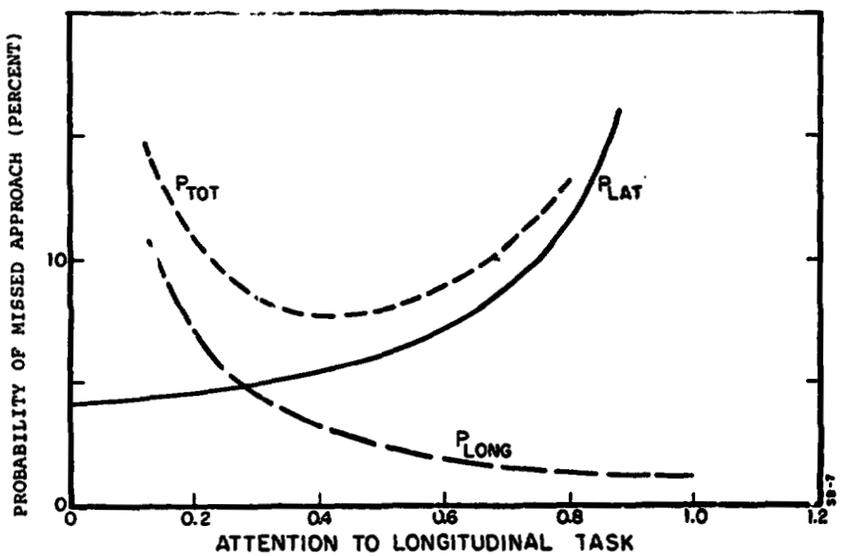

FIGURE 3. Effect on Approach Performance of Attention Sharing Between Longitudinal and Lateral Tasks

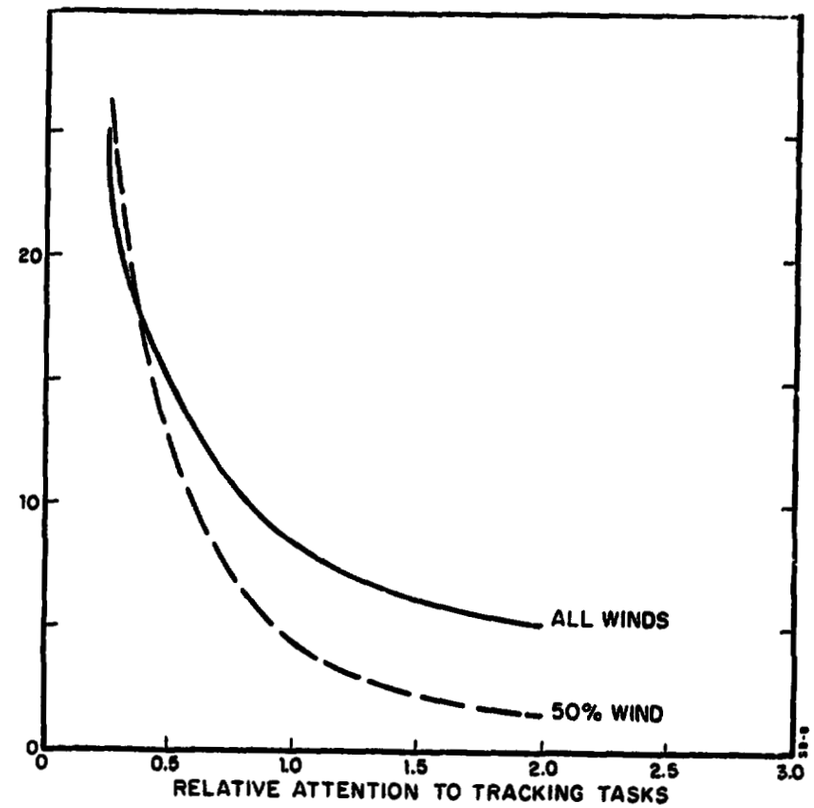

FIGURE 4. Effect of Attention on Missed Approach Probability

Performance improvements with display changes are not too dramatic, with the cumulative improvement in tracking performance being about 10%. Of the changes made, only two had any significant effect; namely, removing the lateral error rate threshold and removing the necessity for attention-sharing.

Director Display

A flight director display could remove threshold limitations and alleviate the requirement for display integration and, thus, realize the performance improvement possible with the *idealized* display of condition E. The actual performance improvement attained might not be substantial in terms of lateral error (about 10% according to Table 2). However, the flight director might allow achievement of similar performance at reduced workload, i.e., it might reduce the workload index.

An "interim" lateral flight director system for the AWJSRA has been described in [21]. We analyzed an approximate version of that system, as shown in Figure 5. It should be noted that we assume here that lateral flight path angle may be obtained directly rather than by means of the complementary filtering techniques of [21]. Although this assumption is somewhat unrealistic, the idealization should provide a bound on the performance improvements that can be expected of the more practical system. The gains for the lateral director system correspond to case 2F of [21].

The effects on rms performance of sharing attention between the lateral flight director and the lateral displays of the EADI-Status display (considered as an entity) were investigated. It was assumed that the portion of attention devoted to the status display was allocated between the localizer and bank angle indicators in the approximately optimal 3:1 ratio mentioned earlier. The results indicated that about 80-90% attention to the flight director is "optimal", but performance was very insensitive to changes in attention [15]. Results for the 80% division of attention were quite close to those for the idealized display; lateral error was about 3% greater for the flight director-status display combination and other variables were virtually identical. Even when only the flight director is available, there is not a significant increase in lateral error. In general, then, the attention-sharing results indicate that the "interim" lateral flight director comes close to achieving the improvements implicit in an idealized display. On the other hand, the improvements at the level of attention (-20 dB) and wind-condition (1%) investigated were not large indicating that, when working hard at the task, one can perform almost as well with the status displays as with the director.

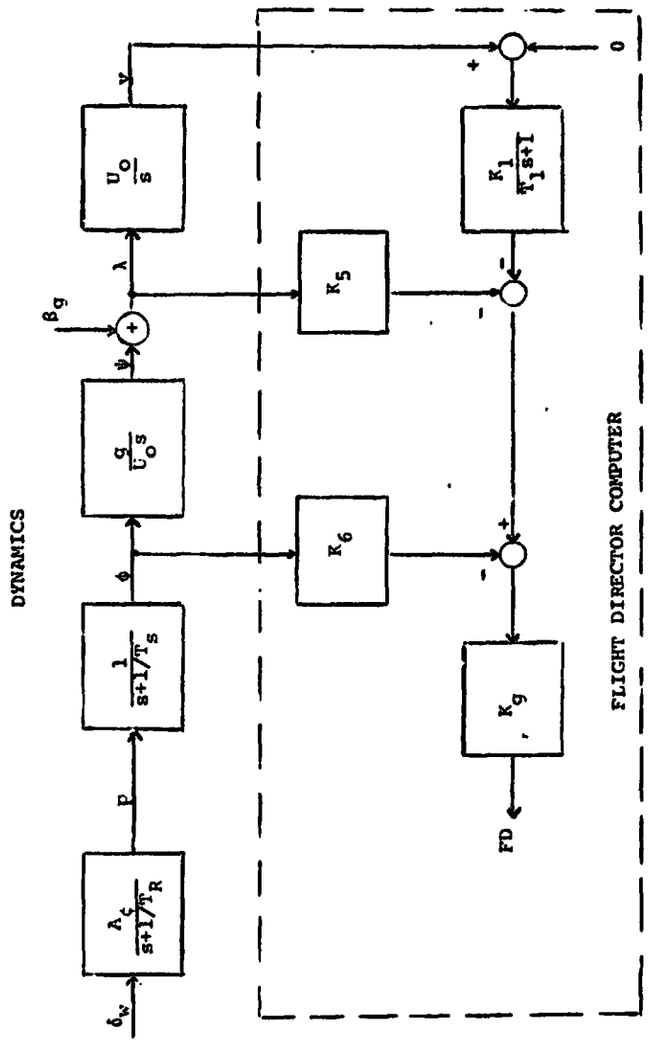

FIGURE 5. "Interim" Lateral Director System

The improvement provided by adding the lateral flight director to the status display at various "levels" of attention is shown in Figure 6. Averaged over all wind conditions, the probability of a missed approach without the flight director is 1.5 to 2 times greater than with it — at all levels of attention. Moreover, the improvement is greatest in the range of operation (attentions of .5 to .125 that are likely to be most important. For the 50%-wind (also shown in Figure 6), the flight director provides even more substantial improvement.

In terms of workload, an approach success probability of 99% is unattainable, with reasonable workload, when all winds are considered; for the 50%-wind, the flight director reduces the Workload Index from about 1.4 to about .3. For the all-winds average, a 95% success probability requires a workload index of about .7 in the no-director case as opposed to about .25 when the director is available. In general, the curves of Figure 6 indicate that addition of the flight director will reduce the lateral workload by a factor of 2-4 for success probabilities that can be achieved, with greatest improvement in the range of most interest.

The total longitudinal-lateral approach task with flight directors for both control tasks* was analyzed in exactly the same fashion as for the status display configuration. The results are presented in Figure 7. When the average of all-winds is considered, the addition of the flight-directors reduces the miss probability by about a factor of two, with the most improvement in the lower attention levels. Even greater improvement (4-7 times better) is evidenced for the 50%-wind condition. The missed approaches, for the all-winds average, are due largely to the lateral task; although not shown, this is even more true for the 50%-wind condition.

Figure 8 shows the tradeoff between workload and performance for the 50%-wind condition. The directors cut the workload by at least a third in the range of success probability of 95-99%. A similar reduction in workload is possible for the all-winds average, but the probability of success is much reduced. (The workload index for a 95% success probability is about .7 with the directors as opposed to 2 without them.)

4. CONCLUSIONS

A display evaluation methodology based on the optimal control model of the human operator has been described and applied to the analysis of vertical situation displays for STOL approach. The methodology appears to provide a powerful means for analyzing

*The "Interim" longitudinal directors for nozzle and elevator control were approximations [15] to those proposed in [21].

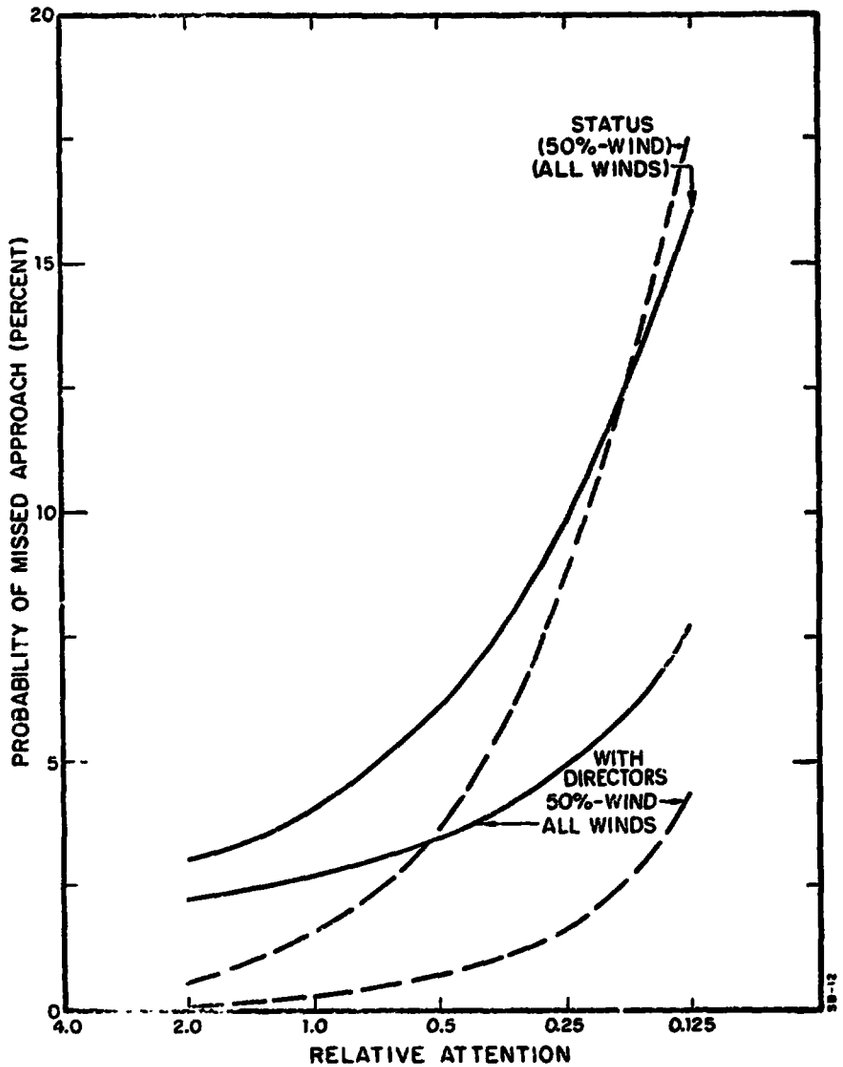

FIGURE 6. Effect of Lateral Director on Missed Approach Probability

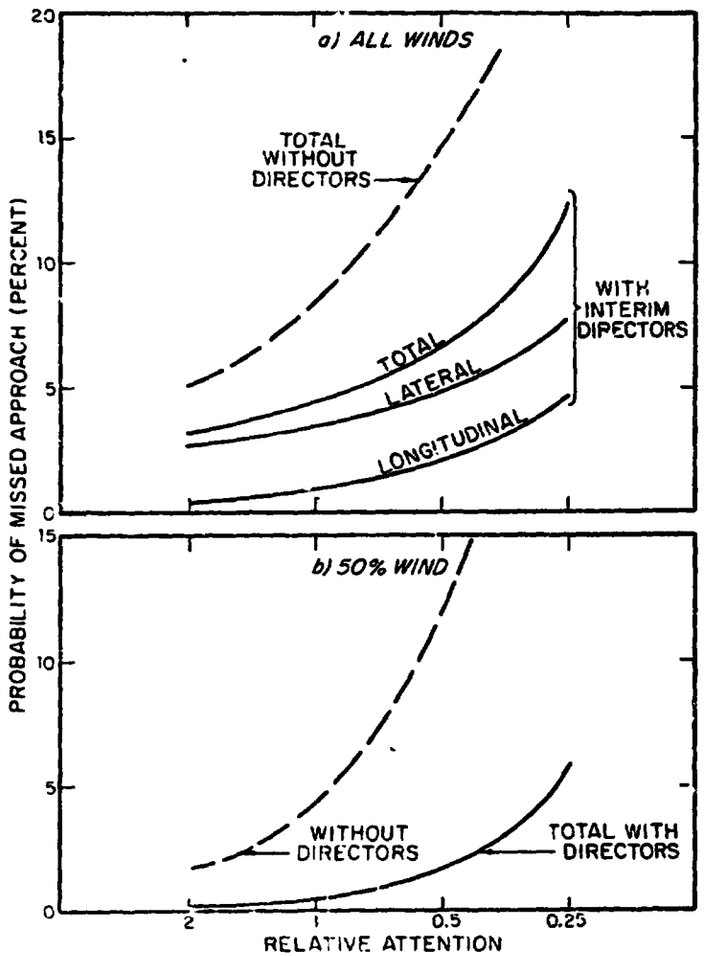

FIGURE 7. Effect of Director Systems on Combined Longitudinal/Lateral Approach Performance

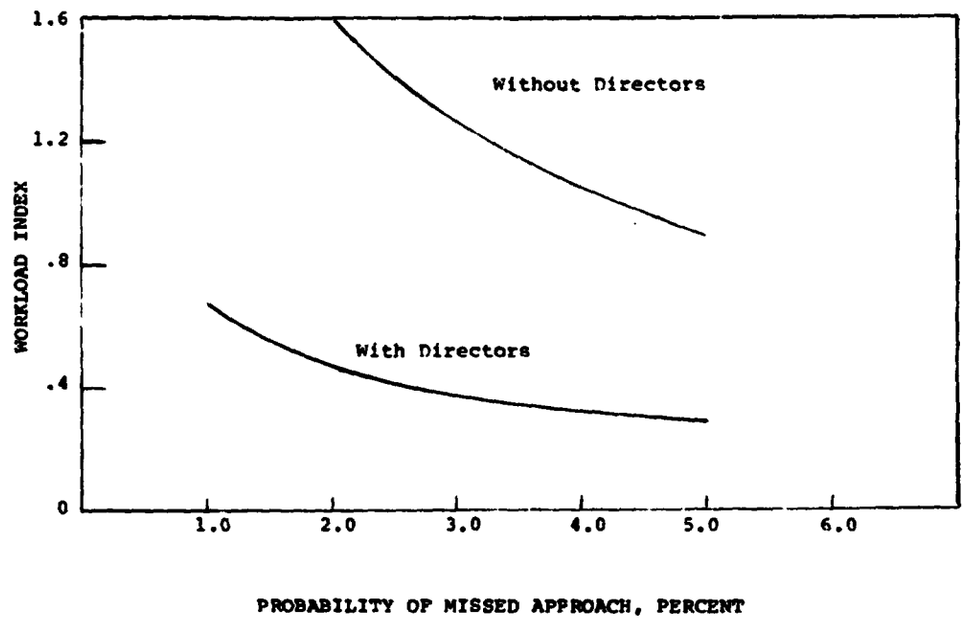

FIGURE 8. Effect of Flight Directors on Workload Index, 50%-Wind

displays and their effect on system performance and reliability. It may be used to determine bounds on expected display improvements via analysis of "idealized" displays. The model for task interference and workload permits linearized analysis of combined longitudinal and lateral performance in a rational and consistent manner. Interaction between axes is introduced via the limited capacity of the pilot and not through any vehicle coupling. The analysis techniques can also serve as a basis for director design. Such a (preliminary) procedure for design of a longitudinal director system, that considered only the gust-regulation problem, yielded a configuration that resulted in substantially reduced workload [22].

The performance of the AWJSRA with an "unaugmented" EADI-Status display was analyzed with respect to both "window" performance and pilot workload, for a range of turbulence conditions. The results indicate that with the basic display the overall task is quite difficult. When the median wind level is considered, a 95% success probability for approach requires a high workload. If performance is averaged over all possible winds, such a success-probability does not appear to be attainable within a reasonable range of workload. The lateral-directional task seems to be considerably more difficult than the longitudinal control task, even though stability augmentation is provided for lateral control. For a 95% probability of being within the respective approach window, the lateral task has a workload index about 2.5 times that for longitudinal control.

Potential improvements to the basic display were also explored. The greatest effects were observed when better error-rate (sink-rate, lateral error-rate) information was assumed, as might be provided, for example, by a display of longitudinal and lateral flight path angles. Significant effects were also observed when the requirements for attention-sharing were removed. These improvements, as well as a reduction in pilot workload, may be realizable with suitable flight-directors.

Analysis of suggested longitudinal and lateral flight director systems confirms that performance is improved and pilot workload is reduced by a significant amount. When the average of all-winds is considered, reducing the probability of a missed approach to 5% still requires a high workload. However, for a median-wind condition the directors reduce workload requirements to values that seem well within capabilities.

REFERENCES

1. "Space Vehicle Displays Design Criteria", NASA SP-8086, (March 1972).

2. Allen, R.W., W.F. Clement, and H.R. Jex. "Research on Display Scanning, Sampling and Reconstruction Using Separate Main and Secondary Tracking Tasks", NASA CR-1569 (July 1970).

3. McRuer, D., H.R. Jex, W.F. Clement, and D.Graham, "A Systems Analysis Theory for Displays in Manual Control", STI Technical Report 163-1, (June 1968).

4. Senders, J.W., "The Human Operator as a Monitor and Controller of Multi-Degree of Freedom Systems", IEEE Transactions on Human Factors in Electronics, HFE-5, No. 1, pp. 2-5, (Sept. 1964).

5. McRuer, D.T., D. Graham, E.S. Krendel, and W. Reisner,Jr., "Human Pilot Dynamics in Compensatory Systems: Theory, Models and Experiments with Controlled-Element and Forcing Function Variations", AFFDL, TR-65-15;(July 1965).

6. Clement, W.F., "Cardinal Reconstruction Theory - A Tool for Estimating Effects of Display Scanning", Proceedings of Fourth Annual NASA-University Conference on Manual Control, NASA SP-192, 1969.

7. Baron, S., and D.L. Kleinman, "The Human as an Optimal Controller and Information Processor", IEEE Trans. Man-Machine Systems, Vol. MMS-10, No. 1 (March 1969).

8. Kleinman, D.L. and S. Baron, "Manned Vehicle Systems Analysis by Means of Modern Control Theory", NASA CR-1753 (June 1971).

9. Levison, W.H., S. Baron, and D.L. Kleinman, "A Model for Human Controller Remnant", IEEE Trans. Man-Machine Systems, Vol. MMS-10, No. 4 (December 1969).

10. Kleinman, D.L., S. Baron, and W.H. Levison, "An Optimal-Control Model of Human Response, Part 1: Theory and Validation", Automatica, Vol. 6, pp. 357-369 (1970).

11. Elkind, J.I., P.L. Falb, D.L. Kleinman and W.H. Levison, "An Optimal Control Method for Predicting Control Characteristics and Display Requirements of Manned-Vehicle Systems", Wright-Patterson Air Force Base, AFFDL-TR-67-187 (June 1968).

REFERENCES

12. Baron, S., Kleinman, D.L. et al., "Application of Optimal Control Theory to the Prediction of Human Performance in a Complex Task", AFFDL-TR-69-81 (March 1970).

13. Levison, W.H., "The Effects of Display Gain and Signal Bandwidth on Human Controller Remnant", Wright-Patterson Air Force Base, AMRL-TR-70-93 (March 1971).

14. Kleinman, D.L. and S. Baron, "Analytic Evaluation of Display Requirements for Approach to Landing", NASA CR-1952 (November 1971).

15. Baron, S. and Levison, W.H. "A Manual Control Theory Analysis of Vertical Situation Displays for STOL Aircraft", Bolt Beranek and Newman Inc. Rept. No. 2484, April 1973.

16. Chalk, C.R., T.P. Neal, T.M. Harris, and F.E. Pritchard, "Military Specifications - Flying Qualities of Piloted Airplanes", AFFDL-TR-69-72 (August 1969).

17. Bryson, A.E. and Y.C. Ho, "Applied Optimal Control" Blaisdell Publishing Co., Waltham, Massachusetts (1969).

18. Baron, S., "Analysis of Response to Wind-Shears Using the Optimal Control Model of the Human Operator", Proceedings of the Ninth Annual NASA-University Conference on Manual Control, May 1973.

19. Levison, W.H., J.I. Elkind, and J.L. Ward, "Studies of Multivariable Manual Control Systems: A Model for Task Interference", NASA CR-1746 (May 1971).

20. Decker, D.W., "Display Requirements Specification for STOLAND EADI Display System".

21. Klein, R.H., "AWJSRA Flight Director Simulation Program", Systems Technology, Inc., Working Paper No. 1015-8 (March 1972).

22. Levison, W.H., "A Model-Based Technique for the Design of Flight Directors", Proceedings of the Ninth Annual NASA-University Conference on Manual Control, May 1973.

ORIGINAL PAGE IS
OF POOR QUALITY

N75 19138

A CONFORMAL HEAD-UP DISPLAY FOR THE VISUAL APPROACH

By

J. M. Naish

Douglas Aircraft Company
McDonnell Douglas Corporation
Long Beach, California

ABSTRACT

The degree of conformity used in matching a superimposed display to its visual background is considered in relation to the information available for vertical guidance and control during a purely visual approach. The information may be represented by individual symbols or combined in a single symbol, and the relative merits of these methods are discussed. A fully conformal display format is developed for the purpose of showing both the position and direction of the flight path, with provision for the effects of disturbances, HUD compatibility, and control needs.

The field of view needed for all conditions and phases of the visual approach with fully conformal display is studied in relation to the limitations of conventional collimator systems. Two methods are discussed which depend on deviation of the sight line, and on windshield reflection of the uncollimated image of a simple pointer. Limited flight tests show some promise for the uncollimated method.

INTRODUCTION

In this head-up method of presenting information, the display field is superimposed on the forward view by means of a reflecting collimator. In consequence, the user has occasion to move between information fields which may or may not be similar, depending on the way the symbol format is designed, and this may be expected to affect the control process. When the Head-Up Display (HUD) is used as a flight director with no requirement for aligning symbols with the external world, it is sufficient if the two fields are made only partly conformal, being understood by rules which are similar but not identical. The same is not necessarily true of the visual approach because another kind of information is involved. The first purpose of the enquiry is to examine the degree of conformity needed for this flight mode.

If the information available within the aircraft during a purely visual approach is used in a fully conformal manner, the corresponding symbols are always seen in their correct relation to the external world. This condition can be expected to influence both the form and movement of symbols, and thus exert a powerful effect on the display format. It may also demand of the optical system a field larger than is required for modes in which alignment is not essential, and it is to be asked whether sufficient field can be realized with known techniques of presentation. It is desirable also to consider the effects of providing HUD compatibility, and of operating in conditions of crosswind shear and turbulence.

ORIGINAL PAGE IS
OF POOR QUALITY

CONFORMITY OF DISPLAY AND BACKGROUND

GENERAL PRINCIPLES

Conformity exists in a superimposed display, such as a head-up display, when the symbols bear a resemblance to the background against which they are seen. The resemblance may not be complete. For example, the superimposed fields may only be alike in their orientation, to the extent that a direction of movement has the same meaning in each field. Figure 1 shows a simple attitude display in which the artificial horizon always remains parallel with the horizon visible in the external world, during changes in pitch attitude and bank angle, but this condition can be obtained without using a common scale of elevation, and without a common origin for the two fields. On the other hand, the resemblance may be more complete, such that all positions and all movements have the same meanings in each field, and there is one-to-one correspondence. It is thus possible to distinguish between displays which are partly or fully conformal.

The advantage of a conformal display is in reducing workload, for the user is not required to adapt to different rules of interpretation for each of the superimposed fields. And the best advantage is expected when the fields are fully conformal. There are practical difficulties in achieving this end, however, and full conformity cannot always be justified on grounds of workload alone. A more compelling reason is to be found in the information requirements for the visual approach.

VISUAL APPROACH INFORMATION

The need for a conformal display is not particularly strong when HUD is used to present command information, which is usually independent of the position in which it is shown, and has no natural scale in the external world when the control law embodies derivatives of angular displacements. The situation is different in the purely visual approach. The natural forward view is then the source of information about the approach path, and if HUD is used to support or augment this source, the displayed information is likely to be closely related to the background.

Two kinds of information are available in an aircraft which are independent of ground sources, and which may be used in HUD to maintain an approach path in the vertical plane, where help is most needed.[1] First, position can be shown with respect to a given path, such as A'T, Figure 2, where A is the aircraft's position, by a symbol depressed from the horizontal by a fixed angle, γ_k, which is made equal to the inclination of the given path, to true scale. The position of the symbol in relation to the touchdown zone then represents the offset from the given path, that is, TS is proportional to AA'. Second, the direction in which the aircraft is moving can be shown by a symbol depressed from the horizontal by the flight path angle, γ, again in true scale, so that the symbol shows the end point of the flight path in the ground plane, at F. Since the scale of presentation is the same as in the external world, in both cases, and since the position of each symbol is interpreted in relation to the visual background, the presentation is fully conformal and the superimposed fields are understood by the same rule.

INDIVIDUAL OR COMBINED REPRESENTATION

It has so far been assumed that individual symbols are needed to show position and direction of the flight path. But it is also possible for both kinds of information to be combined in a control law which is then applied to a single symbol, as described by Bateman.[2] The format is simplified by this arrangement, and simplicity is generally desirable, but the individual character of contributing components is naturally lost. And the display is no longer fully conformal, although conformity is

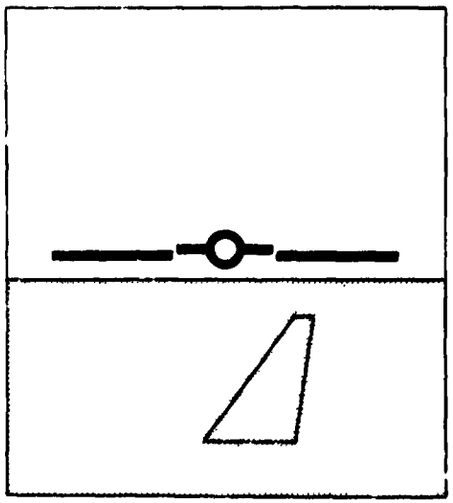

FIGURE 1. PARTLY CONFORMAL DISPLAY

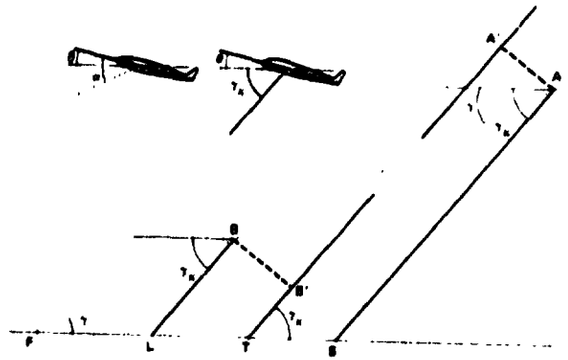

FIGURE 2. METHODS OF AIDING VISUAL APPROACH

to some extent maintained by zeroing the control law with respect to the touchdown zone. It has to be judged whether the loss of information implicit in combined representation, and the loss of conformity, are penalties which can be accepted in the interest of a simplified format.

An important feature of the situation is the complementary nature of the two classes of information each contributing to, but neither entirely sufficient in itself for the purpose of following a given path The fixed depression symbol shows whether the aircraft is above or below the given path, which the flight path symbol does not show, and the flight path symbol shows where the present path terminates, which the fixed depression symbol only allows to be inferred, from its change of position When the flight profile needs to be known, as in deciding when to start an approach or in deciding whether energy has to be lost or gained in order to wash out an offset, the fixed depression symbol appears to be indispensable On the other hand, this symbol gives poor information about the rate at which the given path is joined, though this is shown directly by the flight path symbol

When both symbols are shown they are used in conjunction in the manner shown in Figure 3. The flight path AF is chosen to reduce the offset AA' at a suitable rate, which is then adjusted by altering the flight path to BF' when the offset has been reduced to BB' It can be seen that the positions of the two symbols, which are represented by the figures in parentheses, lie on opposite sides of the touchdown zone, T, when the operation is correctly performed, and this condition is maintained by the user The same result would be achieved by a suitable control law applied to a single symbol backing off displacement by rate in the usual way, but without awareness of the magnitudes of the contributing components Individual representation thus allows the same control as combined representation but a better grasp of the total situation.

Another aspect of the situation is that the two symbols are affected differently by errors, noise, and wind [1] Both symbols are subject to errors, but the flight path symbol is more sensitive in the way errors affect longitudinal touchdown dispersion As regards noise, both symbols are subject to whatever disturbances affect their data sources, so that the flight path symbol is adversely affected if no inertial platform is available and it has to be driven by an angle of attack signal, whereas the fixed depression symbol is not significantly affected The influence of longitudinal wind is shown by both symbols, either as a change in offset or as a change in flight path, but the situation is again complicated in the case of the flight path symbol by the nature of the data source. The fixed depression symbol is thus less influenced, or at least influenced in a less complex manner, by disturbances and errors and may with advantage be shown independently.

The question of individual versus combined representation is also affected by control considerations in the vertical plane While it may not be desirable always to separate the effects of thrust and attitude on the path and speed of an aircraft, there are circumstances when it is advantageous to do so It may be possible to achieve change of speed, at fixed thrust, primarily by the use of the elevator and to change the direction of the flight path, at fixed speed, primarily by using thrust. In such a case, there is good reason to associate speed control with an attitude symbol, and to link height control (through flight path direction) with a symbol related to thrust. Clearly, this is less easily done if the flight path symbol loses its identity

Finally this issue is affected by the desirability of compatibility with ILS procedure, for although the display is intended for the purely visual approach, there will be occasions when ILS signals are available in visual flight conditions At such times, it will be convenient if the display continues to function in the same manner, while showing the correct relationship to the glideslope origin. This

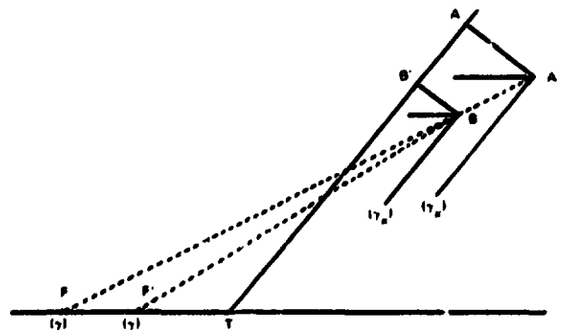

FIGURE 3. REDUCTION OF OFFSET BY PATH CONTROL

can be achieved quite simply by adding a symbol to represent the glideslope origin and by displacing it from the fixed depression symbol by the glideslope deviation, β. Then, as shown in Figure 4, the symbol will always coincide with the glideslope origin (here assumed situated at the touchdown zone) because the aircraft's elevation is $\gamma_k + \beta$.

Operation of the display with ILS compatibility can be illustrated by the special cases shown in Figures 5 and 6. In the case when the aircraft approaches with β constant, along the path AB, Figure 5, the touchdown zone remains at the same angular distance from the artificial horizon. As range decreases, the runway appears to grow and the position of the fixed depression symbol is interpreted as showing a smaller linear offset from the beam, the constant angle β representing a smaller ground run at the enlarged scale. In the case when the approach is made with constant linear offset from the beam, along the path AB in Figure 6, the fixed depression symbol remains at the same linear distance from the touchdown zone. This corresponds to an increased angular subtense at shorter range, the fixed depression symbol appearing to move away from the touchdown zone but at the same rate as the runway appears to grow. It is not difficult to see that these cases have their analogs in night operations when the touchdown zone is illuminated, and it is clear that the part played by the fixed depression symbol in all of them is only possible if it remains an individual entity.

The issues which have been discussed allow a good case to be made for individual representation. It seems reasonable to assume that it will generally be desirable to know both position and direction of the flight path, that it will be advantageous in balancing rate against displacement to know the magnitudes involved, which may be interpreted in the context of the visual background; that noise and error effects should be eliminated as much as possible, and wind effects estimated accurately, that control will be simplified in many cases by establishing separate pitch and thrust information channels, and that ILS compatibility is desirable. In what follows, it is assumed that these factors, which operate in the fully conformal display, are sufficient to justify the loss of simplicity resulting from the use of individual symbols to represent fixed depression and flight path angles.

CONFORMAL DISPLAY FOR VISUAL APPROACH

BASIC FORMAT

A fully conformal display for the visual approach, with the features which have been discussed, can be developed from the basic format of Figure 7, where the visual background is shown in schematic form. It is assumed that the framework of the format is fixed with respect to the airframe, and that its visible extent is limited by a simple rectangle. All components of the display format are shown as thick lines, to indicate their visual prominence in the actual display, but these are much broader than the lines as they appear to the user. The convention is used that when a symbol is displaced from its usual position, on a long-term basis, it is drawn with a broad dotted line. Features of the visual background are shown by thin lines.

The longitudinal axis of the aircraft is represented by the circular symbol with stub wings, as in previous practice. It has a fixed position on the midline of the format and thus moves with the aircraft it represents. For special purposes it may be moved into a displaced position, when it is shown in dotted form. Flanking this symbol are the two halves of a horizontal bar, which form the artificial horizon symbol. It is displaced vertically from the aircraft symbol by the pitch attitude angle, θ, in true scale and in the appropriate sense, and thus shows the position of the true (gyro) horizon in the external world. The aircraft and horizon symbols together form the attitude display, in the usual way, but it will be noted that the middle of the horizon bar is removed to avoid interference.

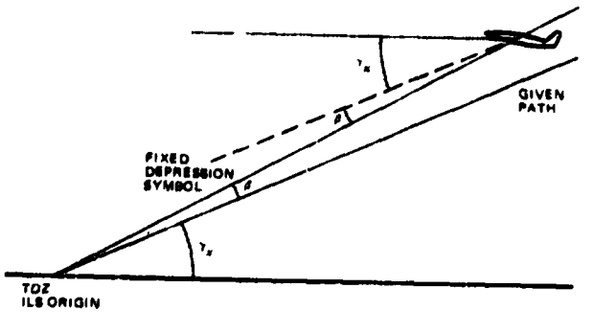

FIGURE 4. ILS COMPATIBILITY

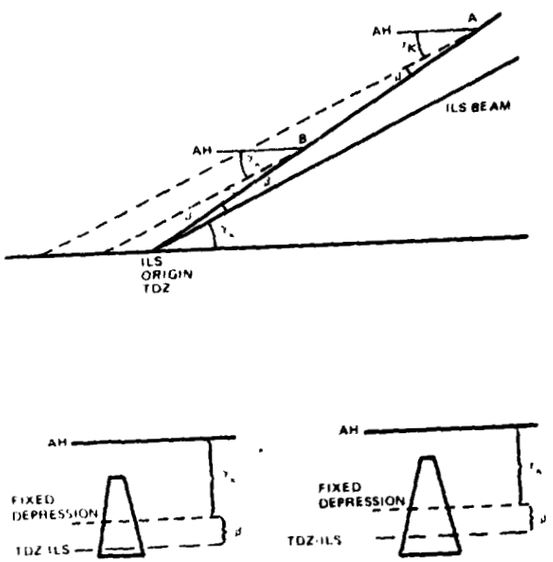

FIGURE 5 APPROACH WITH CONSTANT DEVIATION

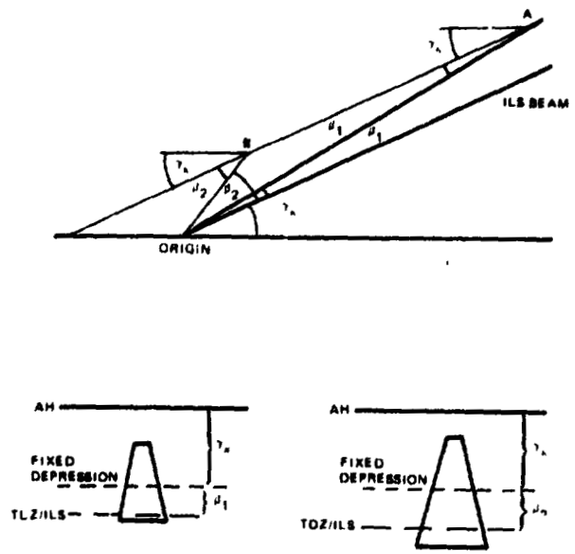

FIGURE 6. APPROACH WITH CONSTANT OFFSET

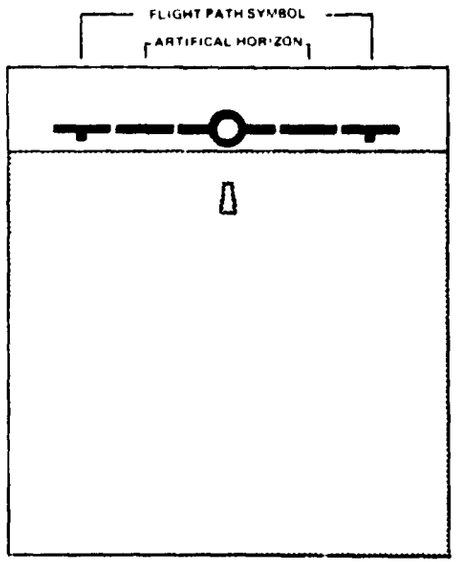

FIGURE 7 BASIC FORMAT

The artificial horizon is in turn flanked by the two halves of another bar, to which vertical bars of variable length are attached below. It is displaced from the artificial horizon by the flight path angle, in true scale, and thus shows the *position of the flight path in the external world*. In the approach configuration, the vertical bars are lengthened to form the letter T, suggestive, also, of association between thrust and flight path direction, and therefore height. As the symbols appear in Figure 7, the aircraft is in level flight with zero pitch attitude. It will be noted that the horizon bar does not coincide with the visible horizon because of the angle of dip (and perhaps also because of *effects of visibility and terrain*).

APPROACH TRANSITION

Development of the format for the approach transition, or for ILS capture, is shown in Figure 8. The main difference is in the addition of the fixed depression symbol which has the same form as the horizon bar but is dotted to show long-term displacement. It is set below the artificial horizon by the desired approach path angle or by the glideslope angle, in true scale, so that $\gamma_k = 3$ degrees, say. When the desired flight path is horizontal ($\gamma_k = 0$), the fixed depression symbol is concealed by the horizon bar. The situation shown in Figure 8 corresponds to a position such as A in Figure 2 where the desired path has not yet been intercepted, and this is shown by the symbol lying short of the runway.

Another difference is the addition of an ILS datum mark, the two halves of which lie outside the flight path symbol, where they serve the minor purpose of showing coincidence with the ILS origin in perfect conditions, be n_k displaced from the fixed depression symbol by the angle β in true scale as previously described. This symbol does not appear in the absence of a valid ILS signal, nor is it shown in the glideslope extension. Figure 8 shows that the aircraft is in a landing configuration and that the flight path is being held level, by means of thrust. This condition lasts until reaching the desired path, or glideslope, which occurs when the fixed depression symbol is aligned with the touchdown zone. By this time the glideslope deviation is reduced to zero, and the convention is preserved of the ILS datum moving downward (toward the fixed depression symbol in this case) as the glideslope is intercepted from below. The diagram also shows a nose-up change of attitude.

FINAL APPROACH

The appearance of the display format during the final approach is shown in Figure 9. The horizon bar is moved downward in the format as the nose rises to the full approach attitude, and there is a smaller separation between the true and visible horizons as height decreases. At this time, attention needs to be transferred to the touchdown zone in the lower part of the format, so a duplicate aircraft symbol is introduced in a displaced position, in dotted form. The downward displacement is $\theta_k + \gamma_k$ in true angular scale, where θ_k is the ideal pitch attitude for the approach, so that the angle between the displaced aircraft symbol and the fixed depression symbol is given by

$$\Delta\theta = (\theta_k + \gamma_k) - (\theta + \gamma_k)$$

The two dotted symbols thus form a pitch attitude error display and are available for the control of speed. The displaced aircraft symbol is added by manual selection.

In the situation shown, the aircraft is above the glideslope since the fixed depression symbol is above the touchdown zone (represented here by a single lateral line on the runway). This displacement is being reduced by aiming the flight path at the other side of the touchdown zone. Speed is a little low since the pitch attitude error is in the nose-up sense. The ILS datum mark remains aligned with the touchdown zone.

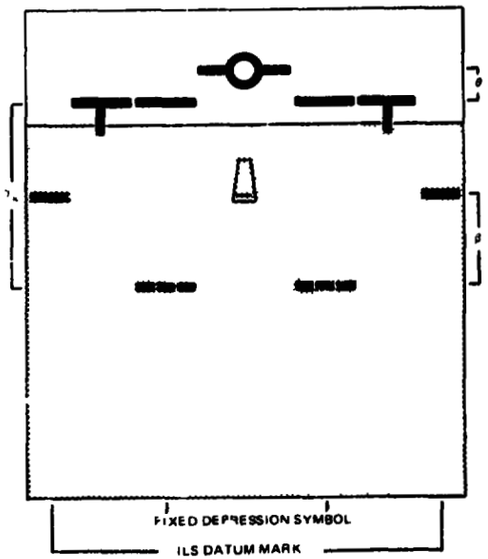

FIGURE 8. APPROACH TRANSITION

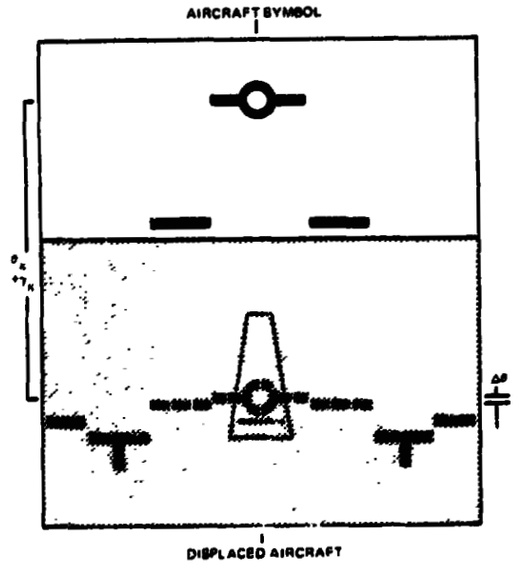

FIGURE 9. FINAL APPROACH

FIELD OF VIEW

EFFECT OF FULL CONFORMITY

Fully conformal development of HUD has an important effect on the field of view of the optical system. As the discussion has shown, it is necessary in this type of presentation for symbols to have a range of angular position. Thus, fixed depression, flight path, and ILS datum symbols need to be seen in the vicinity of the touchdown zone, which tends to move further away from, and below the longitudinal aircraft axis as the approach proceeds. For an optical system fixed in the airframe, the field of view, ω, must be of sufficient vertical extent to accommodate pitch attitude and fixed depression angles, as in Figure 9, so that

$$\omega < \theta_x + \gamma_k$$

This condition can be met in shallow approaches with only slightly nose-up attitudes, but is easily violated in other circumstances. For example, a 6-degree approach in a 4-degree nose-up attitude requires more than the 9-degree instantaneous field provided by a 4-inch aperture collimator when it is installed at a viewing distance of 25 inches, especially if room has to be found for peripheral symbols and allowance made for disturbed conditions.

The lateral extent of the field may need to be even greater, for although the display is only intended for vertical guidance, setting errors in the vertical plane will be smaller if the symbols are kept from moving to either side of the runway, which means accommodating the full range of drift angles. The format may thus need to be moved laterally about 30 degrees, and this cannot be achieved by standard techniques except through changing the eye position. The amount of head movement needed for this purpose, at a viewing distance of 25 inches, is 5-1/4 inches in each direction (allowing for an interpupillary distance of 2-1/2 inches) and this is unlikely to be acceptable.

It would be possible to enlarge the field by reducing the viewing distance. But experience shows that 25 inches is about the smallest value acceptable, in operating conditions, when using the present type of reflecting collimator in a typical commercial jet transport. The alternative is to increase the aperture of the optical system, thus increasing the instantaneous field and avoiding the need for head movement. The likelihood of success then depends on being able to install the larger, heavier system.

INSTALLATION STUDIES

If the collimator aperture is increased to 8 inches, the length of the collimator barrel becomes about 17 inches, and the weight about 65 pounds. Using a space model of these dimensions, installation studies have been made for the cockpit of a large commercial jet transport, with the results shown in Figures 10, 11, and 12. In the arrangement of Figure 10, which is seen from eye datum, the collimator is placed outboard and to the side, at the first officer's station, and the reflector is mounted separately on the glareshield. In this case, the instantaneous monocular field is 21 degrees. Unfortunately, the face clearance is reduced by the reflector plate, which is rather large and overhangs the glareshield by some 4 inches. Also, there is interference with the pilot's right shoulder and loss of downward view on this side.

Another arrangement is with the collimator mounted overhead, as shown in Figure 11 for a viewpoint behind the first officer's seat. There is little significant change in this case: the field is reduced slightly, to 20 degrees, the reflector plate again protrudes by 4 inches, while there is a loss

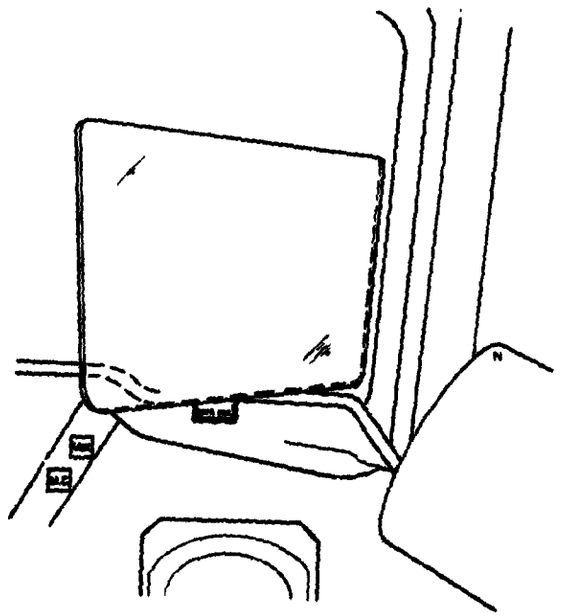

FIGURE 10. SIDE INSTALLATION OF LARGE COLLIMATOR

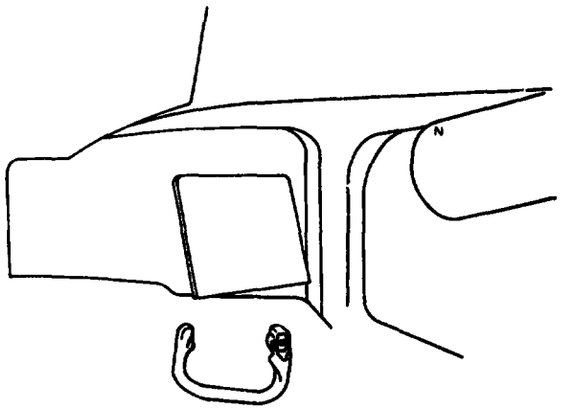

FIGURE 11. OVERHEAD INSTALLATION

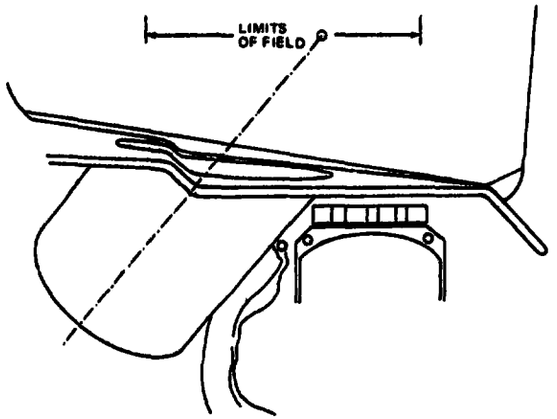

FIGURE 12. GLARESHIELD INSTALLATION

of head clearance and a restricted upward view On the other hand, there is now less chance of sunlight falling directly into the collimator.

These arrangements are scarcely satisfactory for production purposes, and since there is insufficient space for the conventional type of gunsight mounting, it does not appear possible to install such large equipment unless the windshield itself is used as the reflector. The barrel is then mounted in the glareshield, as shown in Figure 12, where the view point is eye datum at the first officer's station. Head and face clearances are not affected in this case, nor is the external view reduced, but these advantages are achieved at the expense of panel space. And there is now interference with wheel and hands, sufficient to require modification of the control column. Moreover, the instantaneous field is no more than 14 degrees, and is centered to the left of the forward sight line, as shown by the small circle at the top of the (chain dotted) collimator axis, which is to the left of the panel instrument Unfortunately, there is no flexibility in locating the collimator axis, and this has to be accepted with other disadvantages of the windshield as a reflector, which may arise from effects of bending, heating, lack of reflectivity, and multiple reflections. Of these, the latter may well prove to be the most serious because of low tolerances on wedge angle, typically, a wedge angle of 7 minutes of arc leads to displacement of the secondary image by about 7 times the width of line used in drawing the display symbols. For these reasons, windshield reflection does not offer much promise as an installation method for the type of cockpit considered, and there seems little hope of enlarging the field of view by the techniques so far described

ALTERNATE METHODS

The problem of enlarging the optical field can be approached by different methods. A simple technique, which is admissible when plenty of space is available, consists in moving the entire optical system to a new position and adjusting the axis to pass through eye datum It is then unnecessary to use a large collimator. However, the swept volume is bound to include large part of the space between eye datum and the windshield One way out of this difficulty may be to devise a scheme in which it is only necessary to move the reflector

Another method is by optical displacement of the external sight line, as shown in Figure 13. A collimator, c is mounted below the glareshield, g, and the display is seen in the reflector, r, in a conventional manner But the sight line is turned from the usual direction, ss', to the direction, d, by means of the prism, p. The deviation of the sight line is made equal to the drift angle, so that the view centered on the flight path is shown centered on the longitudinal axis of the aircraft. In this way, moderately sized equipment can be used to deal with quite large field angles, but at the expense of a discontinuity in the external field Clearly, this method could only be used after careful study of the disorientation potential

Finally, it is possible to avoid a large part of the problem by abandoning collimation, using an out-of-focus presentation in the line of sight This method appears suitable when the displayed information is very simple, so that it can be understood without detailed inspection, and it is well known that an open gunsight can be used with some accuracy. Clearly, a major advantage of HUD is sacrificed, for there is no longer any protection against effects of shortsightedness induced by an empty visual field, but this is acceptable for the visual approach.

Equipment previously used to explore this method is indicated in Figure 14 It consists of a simple link mechanism, ABCDF, which is used to keep crossbars mounted at F and C in line with eye datum, E This equipment allows a direction in the external field to be maintained if the link mechanism is altered to compensate for aircraft movements Unfortunately, it is difficult to mount in the space above the glareshield if the windshield is steeply inclined.

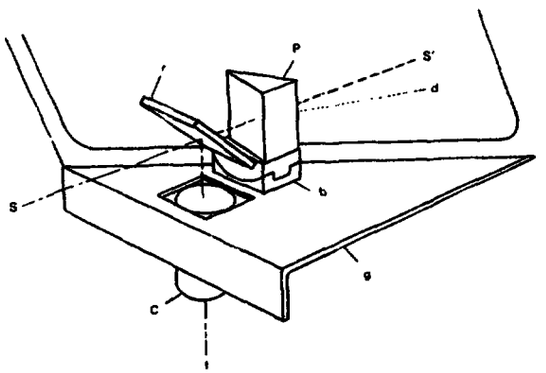

FIGURE 13. DEVIATION OF SIGHT LINE

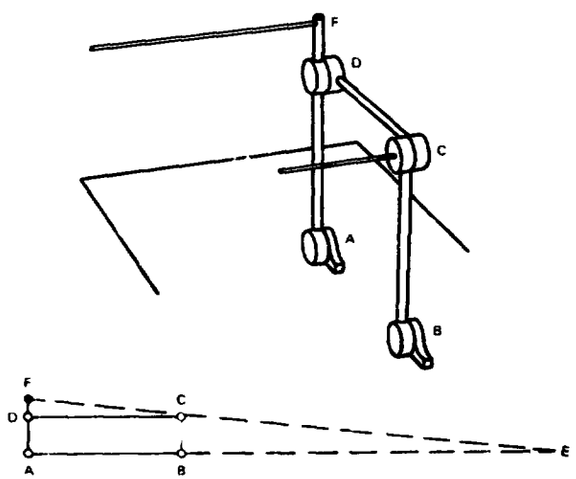

FIGURE 14. OPEN SIGHT LINK MECHANISM

A later development is shown in Figure 15. In this case, a single crossbar of arbitrary length is designed to be moved in the plane of the glareshield by an elementary lead screw drive. It is illuminated by ambient light so that its image may be seen by reflection in the windshield. The orientation of the lead screw is arranged to be such that the image of the bar moves up and down in the external field, in a manner representing changes in angle of attack, attitude, or related quantities. With this equipment, it is necessary to define the viewing position, and this has to be done by independent means.

The cockpit arrangement in a DC-9 is shown in Figure 16, where the captain's windshield is seen from eye datum. The baseplate of the experimental equipment is attached to the upper surface of the glareshield and cannot be seen because it is end-on to the viewer, but the crossbar, which is painted white, is evident at the lower edge of the windshield. The primary image of the crossbar appears as a white line running across the middle of the windshield. At some distance above is a secondary image of less brightness. The primary and secondary images are accompanied by much fainter images in close attendance. The images all lie in a horizontal plane but appear to converge slightly because they are closer than infinity.

Test flights were made with the equipment by two experimental test pilots, with the following results. About twelve approaches were carried out, mostly in fine weather but occasionally in poor external lighting conditions. The equipment was not driven by an input signal but used in a passive condition, simply to evaluate the uncollimated crossbar image as a means for conveying information in conditions of an active external scan. It was found somewhat distracting not to have the image at infinity and it was felt that the initial reaction of other users would be unfavorable. Multiple images, though annoying, were not unduly bothersome. It was convenient that the brightest image was also the lowest, suggesting an association with the nearer end of the runway, and leaving no doubt about which image to use. If desired, the two brightest images could be used as a bracket. The apparent inclination of the lines did not trouble the user. The primary image was visible under a range of lighting conditions, with the bar painted gloss white, but local illumination would naturally be needed by night. The travel of the bar was adequate, when moved up and down by hand, but the image needed to extend further toward the centerline of the aircraft. It was felt that the device had some merit and was worth developing as a flight aid, using an angle of attack, or a fixed depression drive.

CONCLUSION

A fully conformal display is desirable for head-up presentation on the general grounds of reduced workload, because it enables geometrical relationships in the superimposed fields to be understood by the same method of interpretation. It is more particularly desirable in the purely visual approach, for which two kinds of information available within the resources of an aircraft need to be understood in the context of the external visual world, each being represented by its own symbol. A simpler format results from a combined representation, but this precludes knowledge of the flight profile and of the rate used in reducing an offset. Also, individual representation is preferable for the elimination of noise and error effects, for the estimation of wind effects, for linking stick and throttle with individual elements of the display, and for the realization of ISL compatibility.

A fully conformal display can be developed from an attitude display by adding symbols showing fixed depression and flight path angles in true scale, which give information about the position and direction of the flight path. Another symbol can be added to show the position of the ILS glideslope origin, and a simple modification allows attitude to be used in controlling speed.

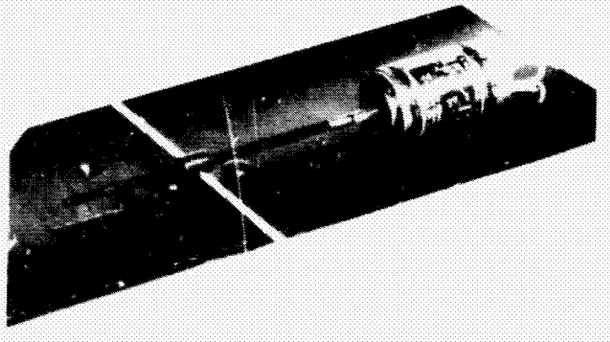

FIGURE 15. REFLECTED CROSSBAR MECHANISM

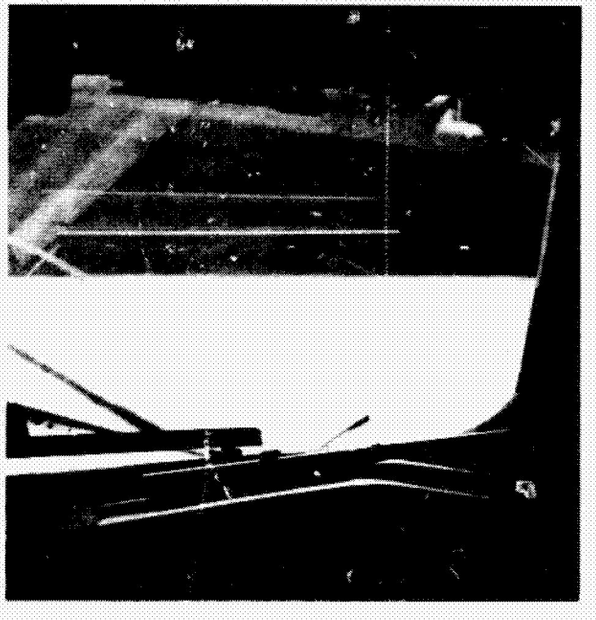

FIGURE 16. COCKPIT PRESENTATION OF REFLECTED CROSSBAR

But difficulties are met in trying to provide an adequate field of view, which is needed because of large relative movements of the center of interest in the external world during the course of a visual approach. New developments are needed to enlarge the field of the present type of display system, as may be used in commercial jet transports, since viewing distance cannot be decreased without loss of face clearance, and aperture cannot readily be increased without introducing other clearance problems and reducing the external view. Some of these difficulties are alleviated by the method of windshield reflection, but new problems arise, especially the problem of multiple images, and the field of view is only moderately large.

One possibility is that the external sight line may be deviated by means of a prism. This method allows the field to be enlarged while using quite small equipment, but a discontinuity is introduced in the external field, the seriousness of which is hard to assess. Another possibility is that collimation may be dispensed with by using some form of open sight, a method which is admissible when presenting simple information in visual approach conditions. If space is available, a mechanical linkage can be mounted above the glareshield and used to define an external direction by the alignment of pointers. An easier way is to move a pointer in the plane of the glareshield and use the ambient illumination to form an image by reflection in the windshield, in which case the head position needs to be defined. Flight tests of the latter method showed that adequate field could be obtained with a pointer of sufficient length, and that the method was worth developing as a simple flight aid despite obvious limitations of image quality.

The investigation shows that fully conformal head-up presentation, though suitable for guidance and control in the vertical plane during a visual approach, and though capable of realization in a format of symbols, depends for its success on the further development of techniques for enlarging the field of view.

REFERENCES

1. Naish, J. M., "Head-Up Display for the Visual Approach," 8th Annual NASA-University Conference on Manual Control, University of Michigan, Ann Arbor, Michigan, May 1972; Douglas Paper 6033.

2. Bateman, C. D., "The Single Task. A Flyability Improvement to the Visual Landing Aid," United Control, Redmond, Washington, January 1971.

DOUGLAS AIRCRAFT COMPANY

3855 Lakewood Boulevard Long Beach, California 90846 (213) 593 5511

MCDONNELL DOUGLAS CORPORATION

PRINTED IN USA MAY 1973

N75 19139

PILOT PERFORMANCE DURING A SIMULATED STANDARD INSTRUMENT PROCEDURE TURN WITH AND WITHOUT A PREDICTOR DISPLAY

John G. Kreifeldt[1] , Thomas Wempe[2]

(1) Tufts University
Medford Mass. 02155

(2) Ames Research Center, NASA
Moffett field, Calif. 94035

PRECEDING PAGE BLANK NOT FILMED

SUMMARY

A simulator study was conducted to measure the effectiveness of predictor information incorporated into a CRT display of a computer simulated aircraft's horizontal and vertical situation. Professional pilots served as subjects for the task of executing a standard instrument procedure turn at constant altitude in constant crosswinds with and without their predicted ground track displayed.

The results showed that the display with the predicted ground track was markedly and significantly superior to the display without this information and that the subjects were generally satisfied with this type of information. Mean rms lateral path error was independent of the crosswind velocity with the predictor information, and increased without it with increasing wind velocity. Rms stick activity decreased with the predictor display which also "uncoupled" aileron and elevator activity.

This research is part of a general investigation into the effectiveness of pictorial displays for manual control and monitoring at NASA-Ames, Man/Machine Integration Branch.

INTRODUCTION

It is sure that the future of commercial aviation will be marked by increasing pressure for tighter spatial and temporal flight constraints on individual aircraft as well as introduction of complex trajectories particularly for V/STOL aircraft. This pressure will be necessary for reasons of density, economy, safety and consideration of public human factors such as noise abatement and area exclusions.

The human's role in the aircraft in the coming decades is still to be determined but clearly it may vary from direct manual involvement in piloting to a flight management type of position in which the human may, among other functions, monitor automatic systems and operate as a goal setter and multiperformance evaluator. (For discussion of such possibilities see Warner[1][2].) It is sure that the total flight system will be optimized by researching and exploiting the best man-machine match.

A primary difficulty in man-machine system design is providing adequate information to the human in an easily assimilable form. This is true whether the human has direct ("inner-loop") manual involvement or system monitoring responsibility. Complete operational man-machine systems have a tendency to meet acceptable performance standards until they fail catastrophically with a very steep transition between these two phases. Much of this characteristic can be traced to man's limited mental information processing capabilities and limited prediction ability.

It has been shown numerous times that the Ziebolz-Paynter[3] philosophy of predicting the behavior of an operating dynamic system and feeding this information back for use in the system can radically improve total system performance. Kelley has extended this technique to feeding back to the human a visual display of the predicted performance of the dynamic system. This has resulted in marked and significant improvements in controlling systems such as submarines and aircraft. Much of the use of this technique and philosophy is discussed by Kelley[4].

This report discusses a simulation experiment in which professional pilot-subjects flew a standard procedure turn in crosswinds using horizontal and vertical attitude information presented on a CRT. The turn was "flown" with and without predicted ground path information displayed on the CRT in order to gain objective and subjective evaluation of the effect of a predictor display in a simple routine task. (Work along this line is also being pursued at Boeing by Warner[5].)

The predicted path consisted of a solid line extending from the aircraft symbol center out to a time length of 30 seconds. The physical length of this line depends upon the aircraft attitude, velocity and the strength of the crosswinds. The path shape is determined by the equations used to compute each predicted position but generally is responsive to winds and aircraft attitude also. As in all predictor displays, the farther forward in time the prediction is made, the more sensitive it becomes to operator and environmental influences incorporated into the prediction equations. Thus the "tail" of the predicted path can have disturbing movements. However, the thirty second prediction span used in this experiment did not seem to be excessive given the generally smooth control used by the subjects. The thirty second span was chosen so that its length under zero crosswind conditions was sufficient to "fair-in" the flight path through regions in which the actual path was inferable but not actually displayed.

Altitude and elevator control was available but not rudder nor throttle control.

PREDICTOR MATHEMATICS

As originally formulated by Ziebolz & Paynter, the behavior of a "plant" can be predicted over some time span or at some interval by modeling the plant dynamics and (by suitable scaling) running this simulation plant in fast-time (or "speeded-up") with the same inputs to both actual and fast-time plant. Actually, a number of subtle approximations enter into this philosophy such as the assumed behavior of the plant inputs over the future time being predicted and the plant dynamics model used.

This may be put into context by considering the functional block diagram of the A/C and display system equations as used in this experiment. Figure 1 shows the system in its essential form of human operator, A/C dynamics, Euler transformations and ground coordinate transformations. Notice for example that gusts are input to the A/C :constant crosswinds are input to the ground coordinate transfo... ions.

In this experiment, only the x, y, values were predicted and combined to display a future ground track. Any of the output quantities could be predicted and displayed, in principle.

PREDICTOR EQUATIONS

There are several ways of predicting the ground coordinates. The most direct method is to consider a series like expansion of the outputs assuming that, in fact, this is possible. The Taylor series expansion for x using t as the present time and τ as the future time would look like:

$$x(t,\tau) = x(t) + x'(t) \cdot \tau + x''(t) \cdot \frac{\tau^2}{2!} + \ldots$$

$$x''(t) = \text{initial condition at time } t \qquad (1)$$

$$x(t,\tau) = \text{predicted value at time } (t + \tau)$$

In principle this assumes $x(t)$ to be analytic. It is not clear without experiments how far to carry out the expansion in order for the displayed values of $x(t,\tau)$ to be useful as a prediction. This approach has, in fact, been used by Dey[6][7] in single point predictions with the series terminated after the squared term: the advantage of this method is the avoidance of any A/C dynamics modelling and direct measurability of the coefficients. A disadvantage is that direct knowledge of the environment and its future behavior such as winds is not used to best advantage.

A next approach would be to move further back along the path and express x as a function of the winds (W_x) and the inputs to the ground coordinate transformations. At this point either Taylor series approximations to θ, ψ, ϕ, could be used or assumptions made about their behavior. Again, if series approximations are used, knowledge about the A/C dynamics, wind gusts and controller movements is not utilized.

Therefore, at any stage, one has the choice of basing output predictions on:

(1) (Taylor) series approximation (extrapolation) of the outputs
(2) assumed behavior of the inputs with consequent transformation
(3) expression of the inputs as a function of inputs to the previous block
(4) assumed behavior of the output.

Obviously, option (3) simply moves consideration of (1) and (2) back to a prior block.

In order to be more specific and reveal some similarities and differences in (1) and (2), the specific A/C dynamics and approximations of the experiment will be used. To simplify matters and to correspond to the actual experiment which did not use z (altitude) prediction, only prediction of x and y will be considered.

The equations used in the experiment to simulate the dynamics of a Navion single-engine, four-place light aircraft are given below.

$$\dot{p} = L_p \cdot p + L_{\delta_a} \cdot \delta_a$$

$$\dot{t} = (g/U_o) \cdot p$$

$$\begin{bmatrix} \dot{u} \\ \dot{w} \\ \dot{q} \end{bmatrix} = \begin{bmatrix} X_u & X_w & -g/S \\ Z_u & Z_w & U_o \\ 0 & M_w & M_q \end{bmatrix} \cdot \begin{bmatrix} u \\ w \\ q \end{bmatrix} + \begin{bmatrix} 0 \\ Z_{\delta_e} \\ M_{\delta_e} \end{bmatrix} \cdot \delta_e \qquad (2)$$

The main approximations in this simulation were:

(1) Throttle control not used.
(2) Wind gusts not present.
(3) Coordinated turns for small bank angles.
(4) Rudder control not used.
(5) Pitch angle (θ) generally less than 20°.

Thus the pilot-subject always made coordinated turns, and only had aileron (δ_a) and elevator (δ_e) control.

The numerical coefficients can be found in the Appendix and are the same as used by Palmer and Wempe[8] in a previous report.

The Euler transform approximations and ground coordinate transforms are shown in Equation 3 producing only pitch rate ($\dot{\theta}$) and yaw rate ($\dot{\psi}$) needed for x, y positions. These x, y coordinates were displayed as the instantaneous position of the A/C on the horizontal situation display (HSD).

APPROXIMATE EULER TRANSFORMS

$$\dot{\theta} = q \cdot \cos\phi - r \sin\phi$$

$$\dot{\psi} = q \cdot \sin\phi + r \cos\phi$$

$$\dot{\phi} = p = \frac{U_o}{g} \cdot \dot{r} \qquad (3)$$

APPROXIMATE GROUND TRANSFORMS

$$\dot{x} = U_o \cdot \cos\theta \cdot \cos\psi + W_x$$

$$\dot{y} = U_o \cdot \cos\theta \cdot \sin\psi + W_y$$

$$\dot{z} = U_o \cdot \sin\theta + (W + 0.05236\, U_o) \cdot \cos\psi$$

Predictor Equations for Simulation

Two further simplifying assumptions were made in establishing the predictor equations. The pitch angle (θ) in inertial coordinates was assumed small enough that Cos θ was nearly unity. This is not a severe restriction since a pitch angle of 20° produces only a 6% deviation from unity. In addition, the bank angle (ϕ) was also assumed to be less than 20° with the same result. In the actual dynamic simulation, the bank angle for a standard turn rate of 3°/sec would be about 16°. With these approximations made for the predictor equations, the set of equations in (3) reduces to the following necessary set.

$$\dot{\psi} = r \qquad \dot{x} = U_o \cdot \cos\psi + W_x$$

$$\dot{r} = p \cdot g/U_o \qquad \dot{y} = U_o \cdot \sin\psi + W_y \qquad (4)$$

$$\dot{p} = L_p \cdot p + L_{\delta_a} \cdot \delta_a$$

The predicted results will be in error to the extent that these assumptions are violated in the simulation.

Assuming δ_a as the input and $\dot{\psi}$ as the output, ψ can be written in Laplace and time domain form as:

$$\psi(s) = \frac{\psi_o}{s} + \frac{r_o}{s^2} + \frac{g}{U_o} \cdot \frac{p_o}{s^2(s-L_p)} + L_{\delta_a} \cdot \frac{g}{U_o} \cdot \frac{\delta_a(s)}{s^2(s-L_p)}$$

$$\psi(t) = \psi_o + r_o \cdot t + \frac{g \cdot p_o}{U_o}\left[\frac{e^{L_p t}}{L_p^2} - \frac{1}{L_p^2} - \frac{t}{L_p}\right] + \mathcal{L}^{-1}\left\{L_{\delta_a} \cdot \frac{g}{U_o} \cdot \frac{\delta_a(s)}{s^2(s-L_p)}\right\} \qquad (5)$$

The first three terms depend only upon initial conditions of yaw angle (ψ_o), yaw rate ($r_o = \dot{\psi}_o$) and roll rate (P_o). The last terms depend upon the behavior of the aileron control (δ_a). For demonstration purposes, the simplistic assumption can be made that δ_a does not change but maintains a value of D over the prediction interval. Then after gathering terms together, and noting that prediction intervals will be longer than 1 second:

$$e^{L_p t} \cong 0 \qquad t > 1 \text{ sec.} \quad (L_p = -8.402 \text{ sec}^{-1}) \qquad (6)$$

then

$$\psi(t) = \psi_o - \frac{g/U_o}{L_p^2}\left[p_o + \left(\frac{L_{\delta_a}}{L_p}\right)D\right] + t \cdot \left[r_o - \frac{g/U_o}{L_p}\left(p_o + \left(\frac{L_{\delta_a}}{L_p}\right)D\right)\right] - \frac{t^2}{2}\left[\frac{g}{U_o}\left(\frac{L_{\delta_a}}{L_p}\right)D\right] \qquad (7)$$

It is instructive to compare this exact terminating equation for $\psi(t)$ with the taylor series approximation based upon its instantaneous derivatives.

$$\psi(t) = \psi_o + \psi_o' \cdot t + \psi_o'' \cdot \frac{t^2}{2} + \psi_o''' \cdot \frac{t^3}{3} + \ldots \tag{8}$$

A direct term-by-term identity of (7) and (8) is not obviously possible.

One could make nearly any assumption about aileron controller movement (δ_a) over the prediction interval. The more complicated it becomes the higher the order terms in (7). However, a fairly reasonable assumption made for this experiment was that δ_a is zero over the prediction interval, or in other words, the pilot would fly in a zero stick position. Thus the actual equation used for prediction extrapolation was

$$\psi(t) = \psi_o - \frac{g/U_o}{L_p^2} \cdot P_o + t\left[r_o - \frac{g/U_o}{L_p} \cdot P_o\right] \tag{9}$$

ψ_o = initial yaw angle

P_o = initial roll rate

r_o = initial yaw rate

It may be puzzling that in the above equation (9)

$$\psi(o) \neq \psi_o \tag{10}$$

however, (9) is not valid at $t = 0$ because of neglect of the exponential term (equation (6)). Equation (9) is equivalent to assuming that the yaw rate is constant.

Displayed Equations.

Equation (9) was used to predict the values of x, y from time t (now) to $(t + \tau)$ by obtaining the initial condition values at t and transforming to ground coordinates.

$$\psi(t,\tau) = \left[\phi(t) - \frac{g/U_o}{L_p^2} \cdot p(t)\right] + \tau \cdot \left[r(t) - \frac{g/U_o}{L_p} \cdot p(t)\right] \tag{11}$$

$$\triangleq a_o(t) + a_1(t) \cdot \tau$$

$$\dot{x}(t,\tau) = W_x + U_o \cdot \mathrm{Cos}\,\psi(t,\tau) \qquad x(t,o) = X(t)$$

$$\dot{y}(t,\tau) = W_y + U_o \cdot \mathrm{Sin}\,\psi(t,\tau) \qquad y(t,o) = Y(t) \tag{12}$$

yielding

$$x(t,\tau) = W_x \cdot \tau + \frac{U_o}{a_1} \cdot \mathrm{Sin}\left[a_o(t) + a_1(t) \cdot \tau\right] + \left[x(o) - \frac{U_o}{a_1}\,\mathrm{Sin}\,a_o(t)\right]$$

$$y(t,\tau) = W_y \cdot \tau - \frac{U_o}{a_1} \cdot \mathrm{Cos}\left[a_o(t) + a_1(t) \cdot \tau\right] + \left[y(o) + \frac{U_o}{a_1}\,\mathrm{Cos}\,a_o(t)\right] \tag{13}$$

In order to reduce computation, the predicted path coordinates (x, y) were computed and displayed for every other second into the future from $\tau = 2$ to $\tau = 30$ seconds with straight lines connecting the points. These predictions were updated 20 times per second with the effect that the assumption of zero aileron control was offset by picking up new initial conditions frequently enough.

These approximations and display conditions seemed to produce a satisfactory looking result inasmuch as the predicted path always started from the present position, had no "kinks" in it and moved smoothly. A very slight ripple could sometimes be discerned in the path due to the updating frequency and the amount of deviation of each temporal path point from its previous position.

It is clear from the equations used in (11) and (12) that if $\psi(t,\tau)$ is non-zero constant over the prediction interval, a straight line predicted path results while if $\psi(t,\tau)$ is a non-zero constant, second order curves will result. In general, the higher the order of $\psi(t)$, the higher the path order.

EXPERIMENTAL DESCRIPTIONS

Instrumentation

The basic instrumentation used for the experiment was a two axes fingertip side arm displacement controller with spring centering, a start-stop button, a SEL 816A CRT and SEL 840MP computer. Figure 2 shows the CRT and controller at the subject's position. During a test, a 6' high screen enclosed the subject and display.

The digital computer calculated the A/C dynamic responses, the predictor information, all display elements and transformations and recorded the raw data for later analysis. A functional block diagram of the experimental setup is shown in Figure 3.

Task and Display Elements

The task to be performed was the execution of a 180° procedure turn at constant altitude with a crosswind of 0%, 10%, or 20% of the nominal A/C forward velocity. This task was executed with and without predicted path information so that each subject received 6 different conditions (3 × 2). The crosswind always blew at constant velocity in the direction shown in Figure 4.

A map-like display of the desired A/C path projected onto a horizontal ground plane was displayed along with the A/C symbol and predicted path (when used). This information constituted the horizontal situation display (HSD). The vertical situation display (VSD), positioned directly above the HSD, contained the following 6 information display elements: an A/C wing symbol stationary in the middle of the VSD with the movable artificial horizon in an inside-out configuration; an error box centered on the A/C symbol in compensatory fashion for zero lateral and altitude error when on the correct course; a turn rate indicator with bars marking 0°, ±3°/sec.; and altitude and velocity information. Figure 4 is a labeled photograph of the HSD and VSD information display elements.

A brief word about the standard turn path. The circular arcs that should actually be flown between the linear portions are suppressed in order to decrease the computation and display required. Instead, the curved portions were boxed by their tangent lines and both the A/C symbol and the error box flashed on and off briefly when the A/C (projected back to the path) entered the turning point.

The map was stationary and the A/C moved so that the A/C was primarily head-down over most of the flight. Thus, there were times of control-display incompatibility for the HSD inasmuch as a right bank hand motion would produce a left turning display motion of the head-down A/C.

Since the procedure turn is flown by time rather than distance, the actual size of the map is relatively immaterial and was made as large as feasible within the HSD.

The predicted future path of the A/C was added as a projected ground track 30 seconds long. Inasmuch as the crosswind was also entered into the prediction equations, the predicted path changed in length and curvature in response to the wind as well so that it might appear very short or very elongated. Figures 5a, b, and c show sample appearances of this predicted path. Notice in Figure 5b the yaw angle of the A/C while still on the path. The dynamics were adjusted to make only coordinated turns.

Subjects and Test Procedure

Six experienced airline pilots served as subjects. Their flight experience is summarized in Table I. None had used predictor displays before.

TABLE I
PILOT EXPERIENCE

PILOT	POSITION	AIRCRAFT	Experience (hours)	
			Simulator with Visual & Hood with Inst. Only	Total Flight Time
1	Captain	B747	210	8,350
2	Co-Pilot	B707	1,150	3,600
3	Captain	B720	325	15,350
4	1st Officer	B707	150	4,070
5	Flight Officer	B707	500	6,350
6	2nd Officer	B727	(No data reported)	3,000

A subject would, on his test day, fly either with or without the predictor receiving four runs of each wind condition in a randomized order for a total of 12 runs per day, with a short rest after every 4 runs. Each subject received one day of practice without the predictor and one day of practice with the predictor with three runs each of the randomized wind conditions for practice. Three subjects practiced with the predictor first. The test days were likewise balanced for predictor-no predictor use. Practice and test conditions were independent.

Performance Measures

(1) The main performance measures were the mean and rms values of the lateral and altitude path errors; (2) elevator and aileron stick activities in the form of rms deflections were also recorded with (3) the total flight time also taken as secondary item of interest. (4) A short pilot-opinion questionnaire about the experiment was given to each subject to fill out after his series of tests was completed. (5) The actual lateral paths were also recorded for visual inspection later in order to study the efficacy of the predictor information.

RESULTS AND DISCUSSION

Lateral and Height RMS Errors

[All results are based upon data from 5 subjects. The sixth subject's data which conformed to the trends shown had several extremely large error scores for the no predictor case and was judged atypical in several other ways and was, therefore, eliminated from the comprehensive results.]

The major results can be seen in Figure 6 which compares the rms lateral offset and rms height error with and without the ground track predictor display.

Two results are apparent in Figure 6.

1. While the average values of the rms errors tend to increase in the no predictor case with increasing winds, the average rms errors are lower and are independent of the crosswinds with the predictor display.

2. The variation about each mean value also appears smaller with the predictor display.

This figure indicates that when the predicted horizontal ground track was displayed, performance on the altitude holding task improved as well even though no altitude prediction was displayed. There was an average decrease in rms lateral error of 110% and an average decrease of 64% in the rms height when using the predictor display. Table II summarizes the reduced data for these two error scores.

TABLE II

Reduced Data for the Lateral and Altitude Offset Errors With and Without the Predictor Display During a Standard Instrument Procedure Turn

	Crosswind Velocity ÷ Aircraft Velocity						
	0.0		0.1		0.2		
Predictor Display	On	Off	On	Off	On	Off	
Mean rms score (ft)	149.2	285.9	149.9	301.4	143.3	343.2	Lateral Offset
% Difference Significance Level(1)	91 >99.0		101.1 >99.0		139.5 >99.9		
S.D. of the rms scores (ft)	29.0	76.2	48.4	105.1	40.1	120.5	
Significance of S.D.(2)	>99.9		>99.9		>99.9		
Mean rms score (ft)	14.0	18.4	14.9	22.6	13.9	28.8	Altitude Offset
% Difference Significance level(1)	31.4 <90.0		51.7 >90.0		107.2 >99.0		
S.D. of the rms scores (ft)	4.2	6.7	7.3	10.2	5.8	23.0	
Significance of S.D.(2)	Not Significant		Not Significant		>99.0		

Data based on 5 subjects
(1) Fisher F Test - 13 D.F.
(2) X^2 Test - 1 D.F.

Thus, there is a beneficial carry over of the horizontal predictor display element to the vertical situation as well. It is probably safe to conclude that the improvement in altitude performance using

the horizontal predictor display is attributable to both decreased attention loading on the horizontal display and less horizontal maneuvering leading to less vertical interaction. In the first case, more attention can be directed toward the vertical situation display and in the second case, fewer corrective actions need to be taken.

The correlation (ρ) between the lateral and height errors was .91 and .88 for the predictor - no predictor case respectively with no significant difference and each correlation was significant past the 99.9% level. Thus, a high lateral error score corresponded to a high height error score with and without the predictor element.

One could conclude, that if the predicted ground track is displayed, lateral offset information on the VSD could most likely be eliminated with a consequent savings in computation/display requirements and an uncluttering of the VSD.

Stick Activity

Aileron (δ_a) and elevator (δ_e) movements of the controller were also sampled during the flights and the mean and rms values obtained. The rms values (in arbitrary units) measure a pilot's stick activity and are an indirect indication of the sizes and frequency of corrective actions and the "smoothness" of the flight.

Figure 7 shows the general behavior of the two activities with and without the predictor element.

As with the lateral and height errors, both the average activities and the variance of the activities were significantly lower where the predicted ground track was displayed. Aileron activity dropped by 64% while elevator activity dropped by 42%. The reduced data for the stick activities are shown in Table III.

TABLE III

Reduced Data for the Elevator and Aileron RMS Stick Activity During a Standard Instrument Procedure Turn

	Crosswind Velocity / Aircraft Velocity						
	0.0		0.1		0.2		
Predictor Display	On	Off	On	Off	On	Off	
Mean rms score (ft)	.61	.85	.61	.87	.59	.85	Elevator Activity δ_a
% Difference (1) Significance level	3.95 <90.0		41.4 <90.0		45.2 >90.0		
S.D. of the rms scores (ft)	.12	.38	.25	.39	.21	.45	
Mean rms score	.79	1.20	.73	1.25	.69	1.17	Aileron Activity δ_e
% Difference (1) Significance level	51.1 >90.0		71.2 >90.0		70.6 >95.0		
S.D. of the rms scores	.22	.53	.16	.54	.21	.49	

Data based on 5 subjects
(1) Fisher F Test - 13 D.F.

As Figure 7 indicates, there was no apparent wind effect on stick activity with or without the predictor display and a reduction in activity with the horizontal predictor element carried over from the horizontal to the vertical situation.

The average correlation between aileron and elevator stick activities was surprisingly high for the no predictor case (ρ = .97, significant at the 99.9% level) and rather lower (ρ = .67, significant at the 99% level) with the predictor. Introduction of the predictor element, therefore, seems to "uncouple" somewhat the two tasks of maintaining altitude and path. This decrease in correlation in the stick activities with the predictor display is unexpected since the lateral

and height errors were fairly highly correlated with each other with and without the predictor display.

Stick Activities and Errors

As might be expected, rms height error and elevator stick activity are strongly correlated with and without the predictor (ρ = .94 and .92, significent beyond the 99.9% level) with no significant difference between the two conditions. This is reasonable since an altitude error is either introduced or corrected by elevator stick movement generally.

On the other hand, rms lateral error and aileron stick activity were weakly correlated with and without the predictor (.26 and .39 respectively, not significant at the 95% level). This also is expected since following the turn exactly would still require appreciable aileron activity.

Flight Times

The flight times increased linearly with increasing crosswind velocity as would be expected. The theoretical minimum time to fly the path would be 225 seconds as the course was displayed. The average time, using the predictor display, ranged from 230.9 seconds in zero wind to 248.5 seconds in a 20% wind. The times were slightly longer without the predictor display, being 234.8 sec. to 249.5 for the above wind conditions. The relatively small dependence on the wind can be attributed to its direction relative to the path. The wind generally aided as much as delayed the flight except for the very initial leg. The extra time without the predictor can be attributed to the error path generally being longer than the actual one.

Anecdotal Information

The subjects were generally more relaxed using the predictor display which was easily observed by noting the set of their shoulders, and their body distance from the display. With no predictor, the subjects tended to lean in to the CRT and also raise their shoulders, denoting a stressful condition. The subjects seemed also to show more forearm muscle stiffness after the no predictor flights.

One subject, an experienced airline pilot, had difficulty flying the simulation without the predictor element. However, with the predictor element his performance was typical of the group's.

All the subjects were highly cooperative and generally enthusiastic about participating. Several expressed a desire to have similar predictor elements incorporated into their actual flight displays.

SUMMARY OF RESULTS

The major results may be summarized as follows:

1. Introduction of the predicted ground track into the HSD decreased mean rms error scores and their variances for both lateral offset and altitude deviation.

2. The predictor element caused the mean rms lateral offset and altitude error scores to be constant and independent of the crosswinds.

3. Aileron and elevator stick activity decreased significantly as well with introduction of the predictor element. Stick activity remained essentially constant for the different crosswinds with and without the predictor element.

4. The predictor element "uncoupled" the aileron and elevator activities by nearly half.

5. Because of the nature of the task, altitude rms error and elevator stick activity were strongly correlated while lateral offset rms error and aileron stick activity were not significantly correlated.

In general, the percentage improvement in performance was greatest for the situation for which the predictor element was primary (HSD). Beneficial improvements carried over to the secondary situation (VSD) as well.

FUTURE WORK SUGGESTIONS

While the experimental results unequivocably show the superiority of the predictor display in this type of simulation, it still remains to demonstrate its superiority in actual flight conditions and the relative magnitude of performance improvement there.

The apparent reduction in stress level and work load which can be attributed to use of the predictor display should also be determined. It is reasonable to assume that decreased stress and work loads are desirable and beneficial to optimum performance in either inner or outer loop control for dealing with a wider range of contingencies than would otherwise be possible.

Altitude prediction should be evaluated in conjunction with the ground path prediction. Integration of altitude and track predictions would be useful in simplifying eye scan and permitting more rapid evaluation of attitude and control corrections. Data of eye scan while using the predictor display elements would also be valuable information leading to an understanding of how they are used.

Better theoretical and practical understanding of the human's use of predictor information would allow more efficient design of predictor displays with the possibility of designing task-adaptive features to the displays. Man-Machine system modeling incorporating predictor elements should, therefore, be pursued. An early model of the human as a predictor can be found in Reference (9).

Use of predictor information in probability assessment should also be studied because of its relevance to the flight management situation.

APPENDIX

AIRCRAFT SIMULATION

The following equations and coefficients were used for the Navion aircraft dynamic simulation.

Airframe Dynamics

$$\begin{bmatrix} \dot{u} \\ \dot{w} \\ \dot{q} \end{bmatrix} = \begin{bmatrix} X_u & X_w & -g/s \\ Z_u & Z_w & U_o \\ 0 & M_w & M_q \end{bmatrix} \cdot \begin{bmatrix} u \\ w \\ q \end{bmatrix} + \begin{bmatrix} o \\ Z_{\delta_e} \\ M_{\delta_e} \end{bmatrix} \cdot \delta_e$$

$$\dot{p} = L_p . p + L_{\delta_a} . \delta_a$$

$Z_{\delta_e} = -8.45\ ms^{-2}$ $\qquad$ $U_o = 53.0\ s^{-1}$

$M_{\delta_e} = -11.1897\ s^{-2}$ $\qquad$ $L_p = 8.402\ s^{-1}$

$X_w = 0.03607\ s^{-1}$ $\qquad$ $L_{\delta_a} = 23.984\ s^{-2}$

$X_u = -0.0451\ s^{-1}$ $\qquad$ $M_w = -0.0166\ ms^{-1}$

$Z_w = -2.0244\ s^{-1}$ $\qquad$ $M_q = -2.0767\ s^{-1}$

$Z_u = -0.03697\ s^{-1}$

The yaw rate (r) was approximated for small bank angles by

$$\dot{r} = p \cdot \frac{g}{U_o}$$

ACKNOWLEDGEMENT

This research was supported through a NASA-ASEE 1971 Summer Faculty Fellowship with Mr. Thomas Wempe as the Research Supervisor. This support is very gratefully acknowledged as well as all the assistance provided by the Ames Research Center.

REFERENCES

1. Warner, J. D., "Advanced Controls and Displays for Future Commercial Aircraft Operations," AIAA 2nd Aircraft Design and Operations Meetings, Los Angeles, July 20-22, 1970. Paper No. 70-938.

2. Warner, J. D., "Advanced Display Systems for New Commercial Aircraft," Human Factors Society 14th Annual Meeting. San Francisco, California, October 12-16, 1970.

3. Ziebolz, H. and Paynter, H. M., "Possibilities of a Two-Time Scale Computing System for Control and Simulation of Dynamic Systems," Proceedings of the National Electronic Conference. Vol. 9, February 1954, pp. 215-223.

4. Kelley, C. R., "Manual and Automatic Control," Wiley & Sons, New York, 1968.

5. Warner, J. D. and Fadden, D. M., "Computer-Generated Map Displays," FAA Symposium on Area Navigation. Washington, D.C., January 24-25, 1972.

6. Dey, D., "Prediction Displays: A Simple Way of Modeling," Control Engineering, 8, July 1969, pp. 82-85.

7. Dey, D., "Results of the Investigation of Different Extrapolation Displays," Advanced Study Institute on Displays and Controls. Berchtesgaden, March 15-26, 1971.

8. Palmer, E. and Wempe, T., "Pilot Performance With a Simulated ILS-Independent Pictorial Display." 7th Annual Conference on Manual Control. NASA SP-281, 1971.

9. Kreifeldt, J. G., "Analysis of a Predictor Model," NASA CR 62006, July 1964.

PILOT QUESTIONNAIRE

The responses to each question are paraphrased without altering their intent. Replies that appeared basically the same are reported as one entry. The number of replies if greater than one is noted next to each entry.

Replies were quite extensive in some cases with supporting pencil illustration.

(1) Did you use the predictor display to a significant degree?

All pilots answered affirmatively.

(2) What difficulties (if any) did it help you to cope with?

Eased turning and crosswind complications, provided instantaneous heading corrections, could anticipate turns and maintain track. Solved intercept angle and wind crab correction, prevented correcting in the wrong direction, aided in determining the correct bank angle.

(3) What did you <u>like</u> about the PD?

Allowed an ease-off on scan while flying on heading. Convenience. Could see future course under present control action. Removed guesswork in track interception. Permitted easy navigation of a prescribed course.

(4) What did you <u>dislike</u> about the PD?

Length of predicted path too long for display aircraft. Nothing. Requires too much scan away from horizon. Initial "whipping" (due to large, frequent control motions) initially disturbing. However, excellent behavior with gentle control. Aircraft symbol should always appear to move toward the top of the CRT.

(5) What was your strategy in using the PD (i.e., how did you use it)?

Keep predicted path on the course to be flown. Fly the far end, once on track, on straight sections. On turns, keep the predictor going <u>through</u> the desired point until the aircraft arrives. Anticipated turns to rollout on proper course in order to maintain or correct track.

[2] To remove control-display incompatibility in head-down positions.

The tip of the predicted path was used for its error magnification properties.

In turns, the far end of the predictor was set tangent to or coincident with the course line.

(6) What information did the PD make available?

[4] Advance track information under present control action. Future error.

(7) How would you improve the PD?

Shorten predicted path to 1/4 length. Feed changing drift information into the predictor. No changes. Make it a command function at pilot's discretion. Larger A/C symbol on map. Rotatable map area.

(8) What additional information would you want for flying the simulator

(a) <u>Without</u> the PD?

(b) <u>With</u> the PD?

Suggestions common to both (a) and (b) are so noted

(a,b) - Different colors for both A/C wings and error box in VSD. Hack marks at turn points on track. Curved track.
[2] Rotatable map.

(a) - Differently colored "single scan" display of altitude indicator command and steer indicator command.
[2] Heading indicator.
Bank angle in degrees.
Crab angle indicator.

(b) - Nothing.

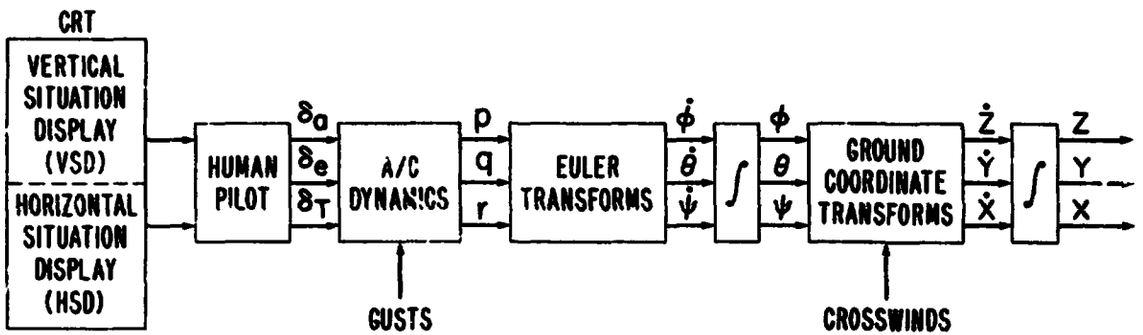

ACTIVITY	RATE	ANGLE
δ_a = AILERON	p = ROLL	ϕ = BANK
δ_e = ELEVATOR	q = PITCH	θ = PITCH
δ_T = THROTTLE	r = YAW	ψ = YAW
	(SHIP COORDINATES)	(INERTIAL COORDINATES)

Figure 1. Functional block diagram of the human operator and the system transformations.

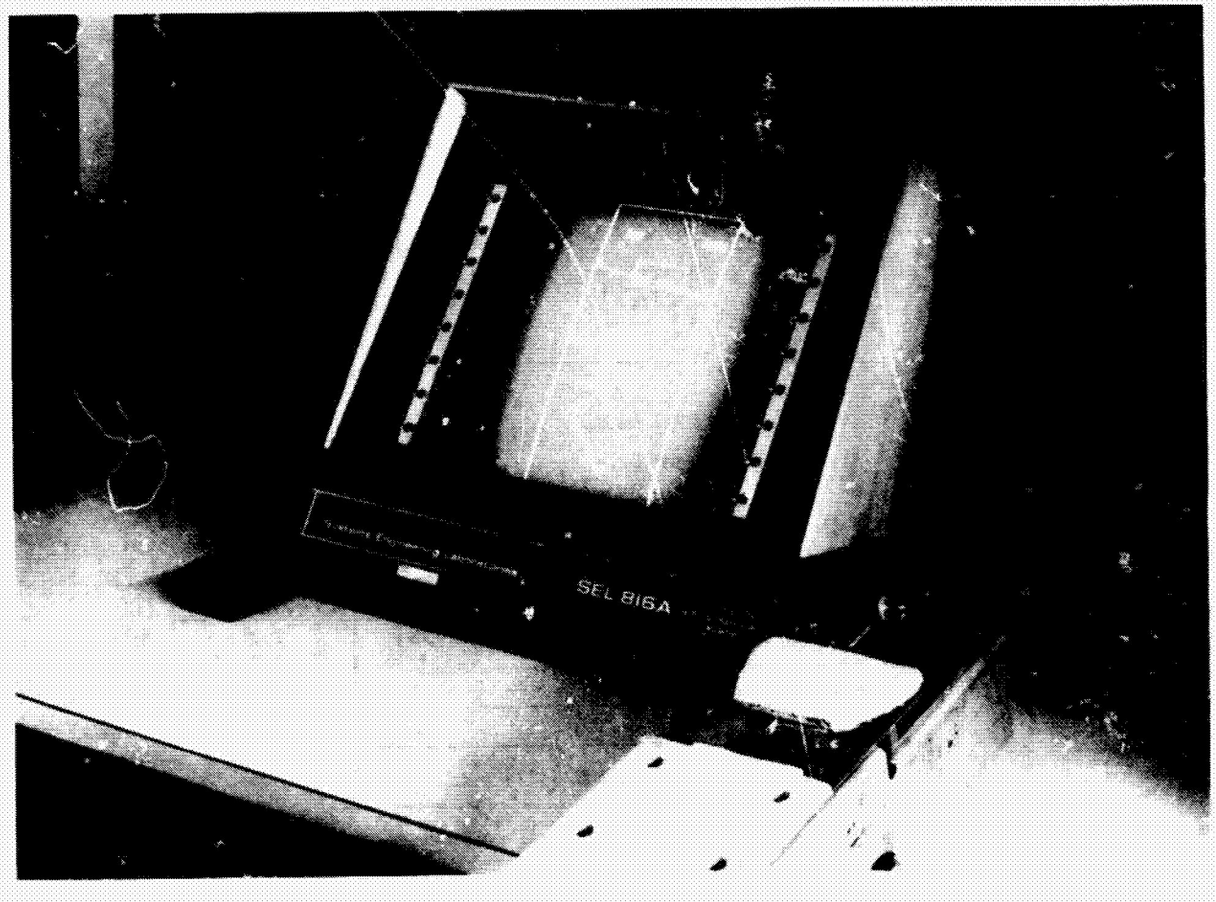

Figure 2. Photograph of the basic simulation configuration.

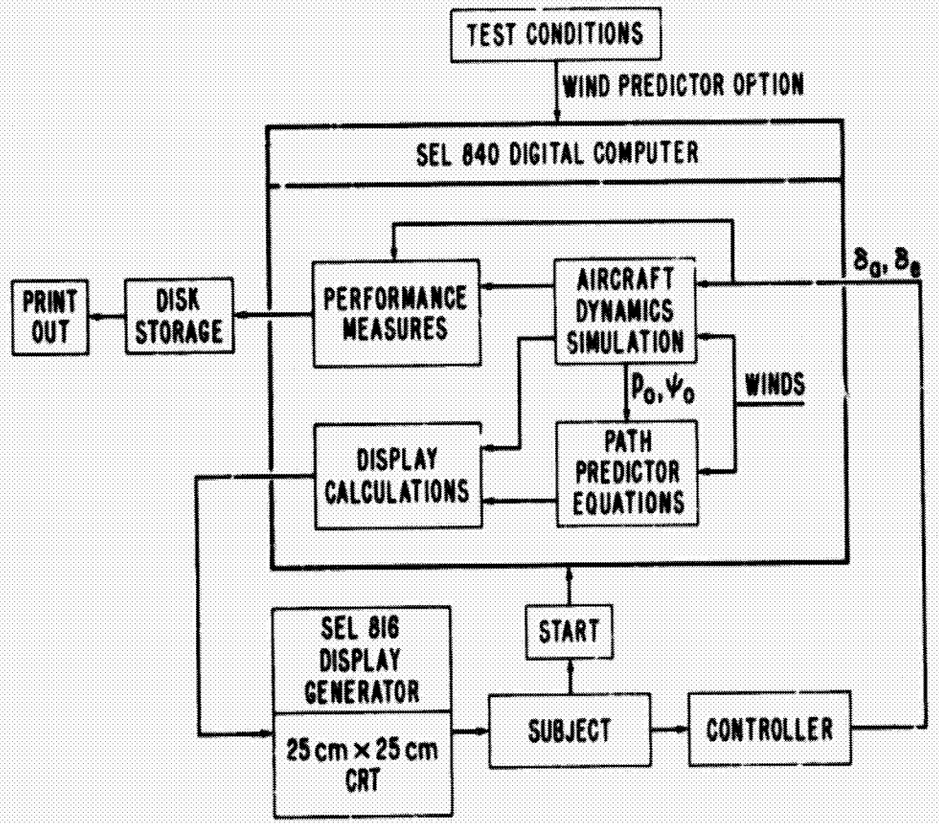

Figure 3. Functional block diagram of the experimental configuration.

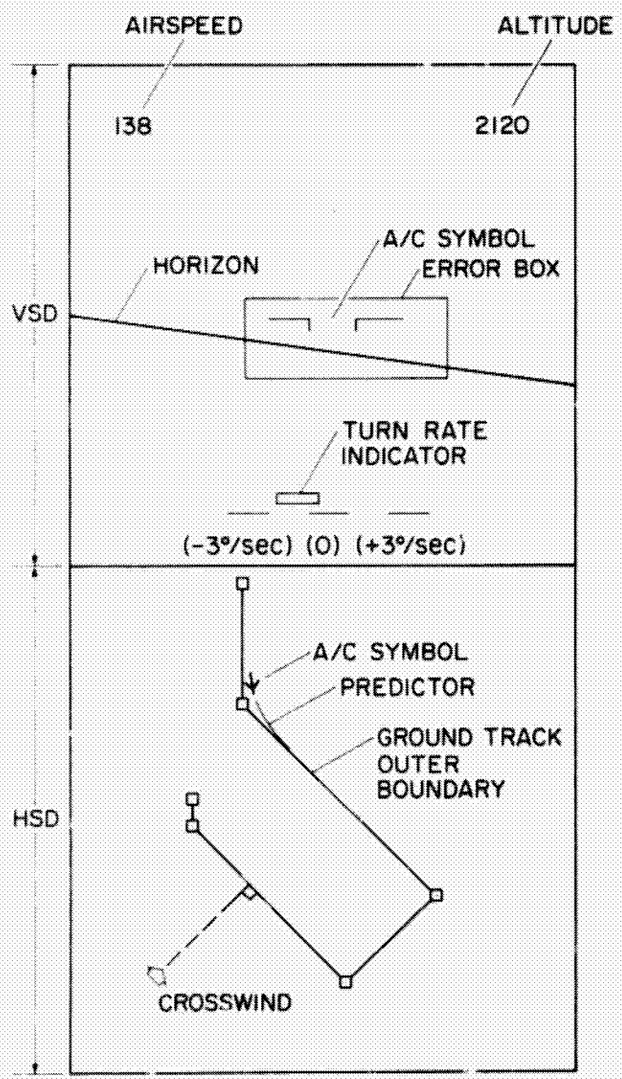

Figure 4. A labeled photograph of the CRT display showing the horizontal and vertical situation displays and the crosswind direction.

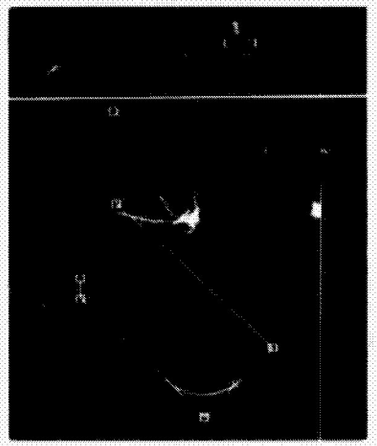

(a) Aircraft and predicted path in a turn.

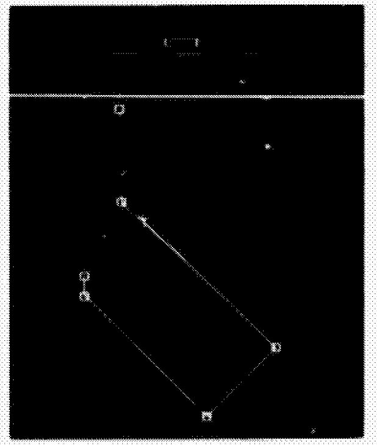

(b) Aircraft on course with predicted path. Note aircraft yaw angle in wind.

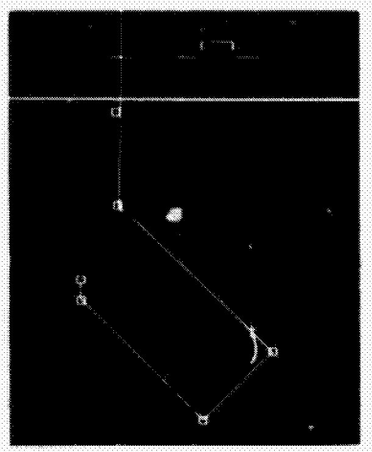

(c) Predicted path with a 50 percent crosswind shown for demonstration purposes.

Figure 5. Horizontal situation display

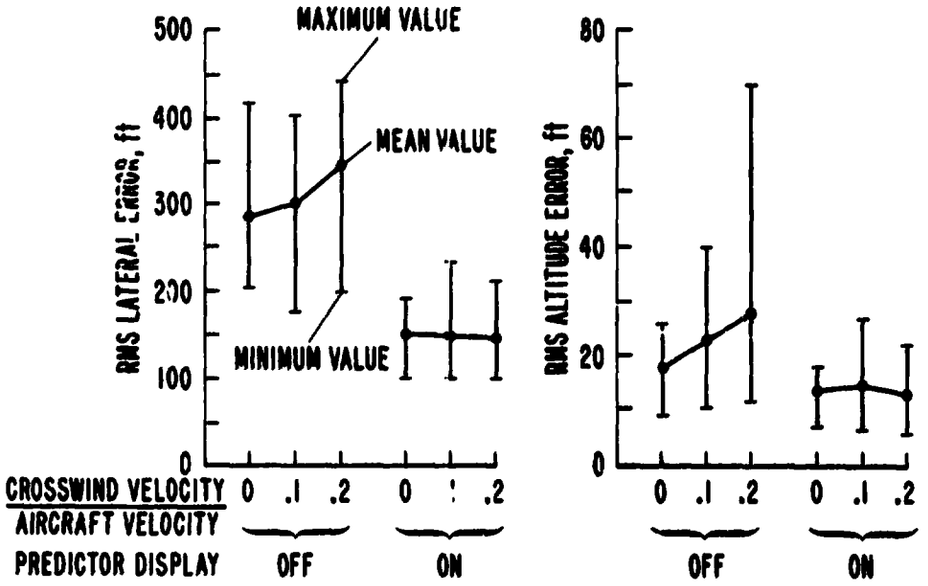

Figure 6. Pilot performance during a standard instrument procedure turn with and without a ground track predictor display. RMS lateral and altitude error.

N75 19140

A MODEL-BASED TECHNIQUE FOR THE DESIGN OF FLIGHT DIRECTORS*

William H. Levison

Bolt Beranek and Newman Inc.
Cambridge, Massachusetts

Presented at the Ninth Annual Conference on Manual Control, May 1973

ABSTRACT

A new technique for designing flight directors is discussed. This technique uses the optimal-control pilot/vehicle model to determine the appropriate control strategy. The dynamics of this control strategy are then incorporated into the director control laws, thereby enabling the pilot to operate at a significantly lower workload.

A preliminary design of a control director for maintaining a STOL vehicle on the approach path in the presence of random air turbulence is evaluated. By selecting model parameters in terms of allowable path deviations and pilot workload levels, one achieves a set of director laws which allow improved system performance at reduced workload levels. The pilot acts essentially as a proportional controller with regard to the director signals, and control motions are compatible with those appropriate to status-only displays.

INTRODUCTION

Aircraft instrument panels often include a "flight director", so called, the purpose of which is to provide acceptable levels of system performance at reduced levels of pilot workload by providing the pilot with one or two display variables which combine the sensor variables in an optimal fashion. In this way, the pilot's visual scanning and attention-sharing requirements are substantially reduced. Furthermore, the pilot can obtain, from the velocity of the director indicator, derivative information (such as acceleration) not otherwise available from visual displays.

The objective of this paper is to outline a proposed new technique for determining flight director laws. This design procedure is based on application of the state-variable (or "optimal-control") model for pilot/vehicle systems (Refs. 1, 2). Application of the procedure is illustrated by the derivation of director laws for a STOL vehicle in the final approach configuration.

The proposed technique (hereinafter referred to as the "model-based procedure) offers certain important computational advantages over alternative procedures. The model-based techniques would appear to allow the derivation of a full set of director gains with a minimum number of iterations of the design procedure. (Only a single iteration is needed for the example presented later in this paper.) Other procedures, whether they be based on analog simulation or on other forms of pilot/vehicle analysis (Ref. 3), generally require a number of iterations on the proposed director feedbacks to arrive at an acceptable design. This is especially true for situations involving multiple control variables in a single axis of control.

The model-based technique also appears to require fewer a priori assumptions relating to pilot behavior than other techniques. In order to minimize the computational effort required to carry out other design procedures, it is usually desirable to pre-specify loop closures (i.e., which sensor variables should influence which director variables). Using the state-variable procedure suggested here, one may simply assume that all sensor variables influence all control variables and proceed to compute the full matrix of director feedbacks. Such an assumption does not increase computational complexity (which depends only on the dynamical order of the system) and, as we shall show, adds only minimally to the complexity of the director design itself.

The model-based technique is not without its own judgemental requirements. The designer must postulate desired performance levels, and the available sensory variables must be specified. These considerations are common to all director design procedures, however, and do not represent a limitation peculiar to the proposed scheme.

*This effort was supported by the Man-Machine Integration Branch of the NASA-Ames Research Center under Contract NAS2-6652.

DIRECTOR DESIGN PHILOSOPHY

Certain constraints are imposed on the design of flight-director laws that will allow improved performance at reduced levels of pilot workload. The director variables must be composed of signals that can be generated by available aircraft measurement devices. These signals are commonly combined in such a way as to make the combined director/vehicle dynamics approximate a K/s-like behavior so that the need for pilot lead is minimized. Considerations of pilot acceptance also suggest that required control inputs and resultant vehicle motions be similar to those that are appropriate to flight with conventional displays. In addition, the director signal should provide the pilot with a good indication of instantaneous flight-path and attitude errors so that frequent reference to status displays is not required.

If the director is a control director (i.e., if it provides the pilot with an explicit indication of the desired control response), a director signal must be generated for each control variable. An ideal design should require little or no pilot coupling so that a given director variable commands a control response along a single dimension.

The preliminary design procedure outlined below allows one to approach many of the above design goals in a relatively straightforward manner. The following design steps have been followed in deriving the control-director for the numerical example presented in this page.

1. Define the control situation in terms of system dynamics, input characteristics, sensory information, performance requirements, and pilot parameters.

2. Use the pilot/vehicle model to predict the pilot-generated feedbacks between each display variable and each control variable.

3. Approximate each of the transfers by a first- or second-order filter. (This approximation simplifies both analytical evaluation and implementation of the resulting director laws.)

4. Derive the commanded control signal by summing the outputs of the transfers between all sensor variables and the control variable appropriate to the director. The director signal is thus expressed as

$$D_i(s) = \sum_j T_{i_j}(s) \cdot Y_j(s)$$

where D_i is the director signal appropriate to the i_{th} control variable, Y_j is the j_{th} sensor variable, and T_{ij} is the approximate describing function between the j_{th} sensor variable and the i_{th} control variable.

5. Evaluate the proposed director laws using the pilot/vehicle model. If an inappropriate "mix" of flight-path errors, attitude errors, and control motions is predicted, repeat the design with a revised set of cost weighting coefficients. If performance is still inadequate, additional sensory variables may be have to be considered.

In essence, the flight director laws are designed to perform the equalization and cross-coupling that the pilot would otherwise have to do. With the director in the system, the pilot's task is basically that of generating a control response proportional to the deflection of the corresponding director indicator. Thus, cross-coupling shoul be at a minimum, and the pilot's response strategy should be approximately that of a pure gain at low and mid frequencies.

If the sensor variables and performance requirements assumed for the director design are the same as would apply to the control task with a more conventional display panel, the characteristics of control and vehicle motions should not be appreciably changed by the use of the director. Nevertheless, the consequent reduction of pilot-related "noise" associated with scanning, attention-sharing, and visual resolution limitations should allow a substantial improvement in performance and/or a reduction in pilot workload. If additional sensory information (such as linear or rotational accelerations) is used in generating the director signal, further improvement may be expected.

NUMERICAL EXAMPLE

The following numerical example is presented to demonstrate the model-based design procedure outlined above. Control-director laws are derived for longitudinal-axis control of an augmentor-wing jet STOL aircraft (C8-M) in a steep (7.5 deg) approach-to-landing configuration. Longitudinal and vertical random-wind disturbances are considered, and linearized perturbation equations are used to describe aircraft dynamics. Two control variables are considered: the elevator control, and the "nozzle" control which regulates the direction of the thrust vector.

The director laws derived below are intended only as a preliminary flight director design — not one that would necessarily be implemented without modification. For example, a realistic design effort would involve consideration of additional factors such as wind-shears, beam capture, and random fluctuations of the signal which generates the desired glide slope ("beam noise"). In addition, the director laws would have to prohibit the possibility of "stand-off" errors in which a steady-state error in one variable compensates for a steady-state error in another variable to yield a zero reading on the director. Nevertheless, the following example does illustrate the essence of the design procedure, and we consider the predicted improvements in performance and workload to be representative of the benefits that would be obtained in practice.

Definition of the Control Situation

The control situation used in this example has been described in considerable detail in Reference 4 and to a lesser extent in a companion paper (Ref. 5). Accordingly, only those aspects of the situation critical to an understanding for the director design procedure will be elaborated upon here. The reader is directed to the above references for a description of the vehicle dynamics and wind-gust characteristics assumed in this example.

No description of the pilot/vehicle model is given here, as this model has been well documented in the literature (Refs. 1, 2). The rationale for selecting model parameters will, however, be discussed.

The sensory information available to the flight director was assumed to be the same as the flight-control information available to the pilot through his status displays; namely, (a) height error, (b) sink-rate error, (c) pitch deviation from trim, (d) pitch rate, and (e) airspeed error. (Lateral-directional variables are not considered in this example.)

Performance requirements were specified in terms of a (scalar) quadratic cost functional that combined deviations associated with flight-path, attitude, and control variables. Weighting coefficients for this cost functional were selected on the basis of maximum allowable deviations (or "limits") for the various problem variables. A unit amount of "cost" was associated with a given variable when the magnitude of the "error" (i.e., deviation from trim) was equal to the nominal limit. Thus, the weighting coefficient for each variable was computed simply as the inverse of the square of the corresponding limit. Height-error and airspeed limits were based on Category II "window" specifications; control and control-rate limits were determined largely from physical considerations, and the remaining limits were based on assumed pilot preferences.

The limits assumed for this analysis and the resulting weighting coefficients are shown in Table 1.

Table 1

"LIMITS AND COST FUNCTIONAL WEIGHTINGS"

Variable	"Limit"	Weighting
h	3.7 (m)	0.073
$\dot{h}$	1.1 (m/s)	0.83
θ	6.0 (deg)	0.028
q	(none specified)	0.0
u_i	2.6 (m/s)	0.15
δ_e	9.0 (deg)	0.012
δ_N	29. (deg)	0.0012
$\dot{\delta}_e$	50. (deg/s)	0.0004
$\dot{\delta}_N$	100. (deg/s)	0.0001

On the basis of previous analysis of manual control behavior (Refs. 1, 2), pilot time delay was assumed to be 0.2 seconds. Pilot-related "noise" levels, on the other hand, were set at levels considerably greater than those found in the laboratory. The rationale for choosing noise levels is as follows.

The selection of model noise/signal ratios for flight director design depends on whether one views the benefit of the director as primarily the reduction of system errors or the reduction of pilot workload.* If the pilot is expected to maintain a high level of workload so that he can minimize errors, low noise/signal ratios appropriate to maximal effort should be used in the analysis. On the other hand, if the director is intended mainly to allow the pilot to maintain performance with reduced workload, then the director should be optimized for substantially larger noise/signal ratios.

*The basis for relating noise parameters of the model to attentional workload is discussed in Refs. 6 and 7.

Although a director designed for a low-noise situation will allow better performance under conditions of maximal effort, the alternative design will be less sensitive to pilot noise and should thus be more "forgiving" of non-optimal pilot behavior. Accordingly, the director laws designed and evaluated in this study have been obtained by computing predicted pilot describing functions for a high-noise situation.

Specifically, levels of -10 dB were used for both motor and observation noise/signal ratios (as opposed to levels of -20 dB for observation noise and -25 dB for motor noise typically derived from laboratory tracking data). Attention-sharing was not specifically considered – the large noise/signal ratios already took this factor into account – and display-related thresholds and resolution limitations were ignored.

Derivation of Director Laws

Pilot describing functions were obtained from a steady-state analysis of pilot/vehicle performance. Wind gust intensities corresponded to the "1-percent" wind condition. That is, gust intensities greater than these levels would be encountered in practice only 1% of the time. Thus, a "worst-case" analysis was performed.

Predicted pilot describing functions (magnitudes only) relating the elevator and nozzle controls to each of the five display variables are shown in Figures 1 and 2.* Since the frequency-dependencies of the five transfers associated with a given control variable were nearly identical, only two shaping filters were required to generate the director laws.

Specifically, each of the predicted pilot transfers was approximated by the transfer function of a second-order, critically-damped low-pass filter. The critical frequencies of all responses corresponding to a given control variable were made identical. Thus, each of the two director signals was represented as follows:

$$D_i(s) = \sum_j K_{ij} \cdot \left[\frac{1}{1+s/\omega_i}\right]^2 \cdot y_j(s)$$

where ω_i is the critical frequency of the filter associated with the i_{th} control variable and K_{ij} is asymptotic low-frequency behavior of the approximate transfer function relating the i_{th} control variable to the j_{th} sensory input.

*For the purposes of this design exercise, velocity variables (pitch rate and sink rate error) were considered to be sensory variables distinct from the corresponding position variables. Hence, five pilot describing functions were computed for each control variable.

Approximations to the predicted internal describing functions were obtained by visual inspection. The resulting director parameters are shown in Table 2. The units of the low-frequency gains are in terms of relevant display and control variables. For example, the gain associated with the contribution of height information to the elevator director has units of degrees (of control surface deflection) per meter (of height error). Critical frequencies are in radians/second.

Table 2

PARAMETERS FOR MODEL-BASED LONGITUDINAL DIRECTOR LAWS

Director	Sensory Variable	Critical Frequency	Low-Frequency Gain
Elevator	Height		0.25
	Sink Rate		1.8
	Pitch	5.0	0.9
	Pitch Rate		0.8
	Airspeed		0.5
Nozzle	Height		1.1
	Sink Rate		6.3
	Pitch	3.5	0.8
	Pitch Rate		1.0
	Airspeed		6.3

The ability to approximate each set of five pilot describing functions with a single shaping filter is an encouraging result, for it shows that the complexity of the problem is negligibly affected by the number of display-to-control closures that are considered. That is, two shaping filters are needed whether there is one closure per control variable or whether there are five. Additional closures merely add additional gain coefficients which contribute minimally to the design complexity of the director. Furthermore, these additional coefficients do not increase the computational effort involved in analyzing the proposed design with the state-variable model.

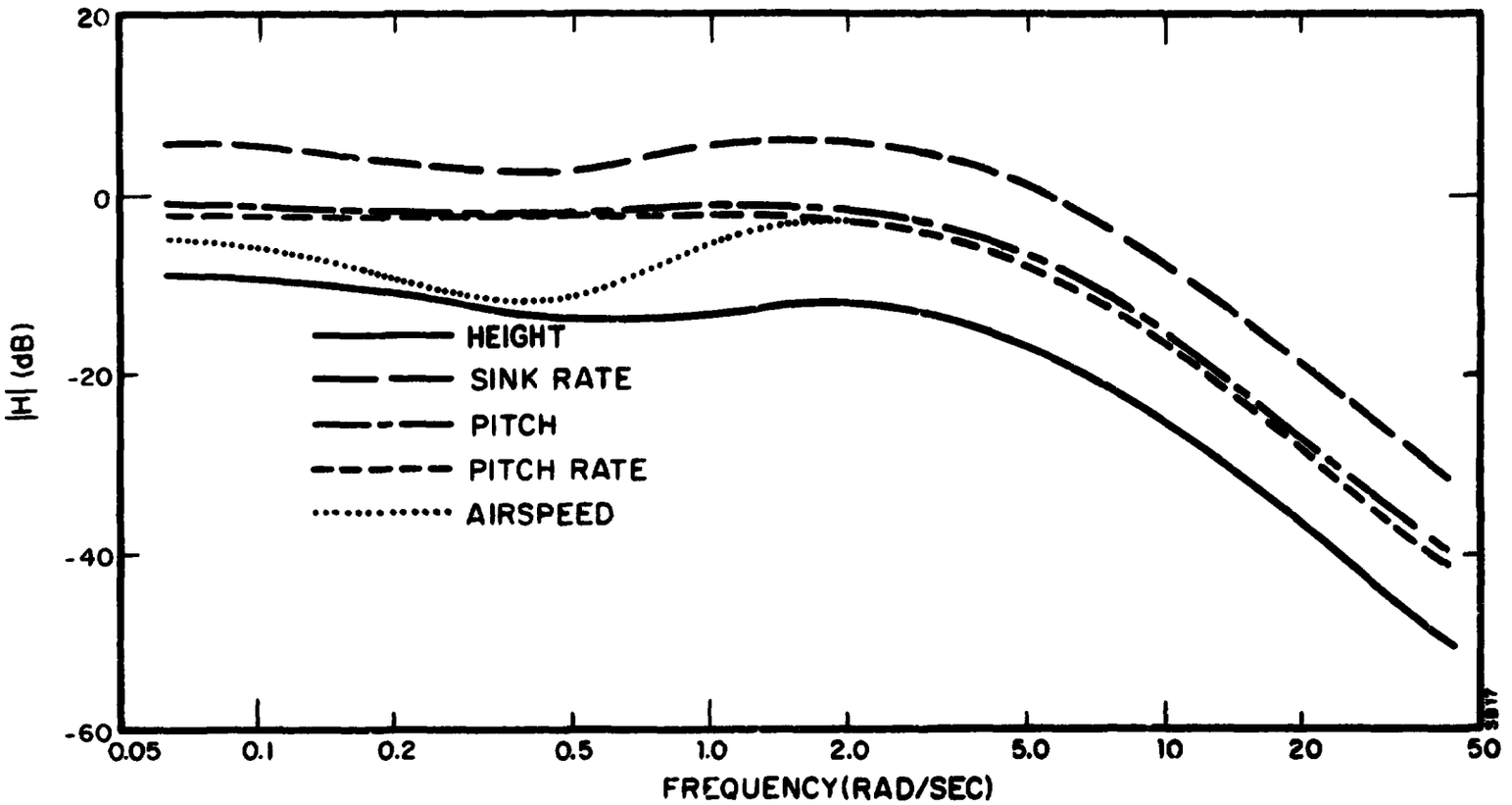

FIGURE 1. Magnitudes of Internal Pilot Describing Functions for Elevator Control

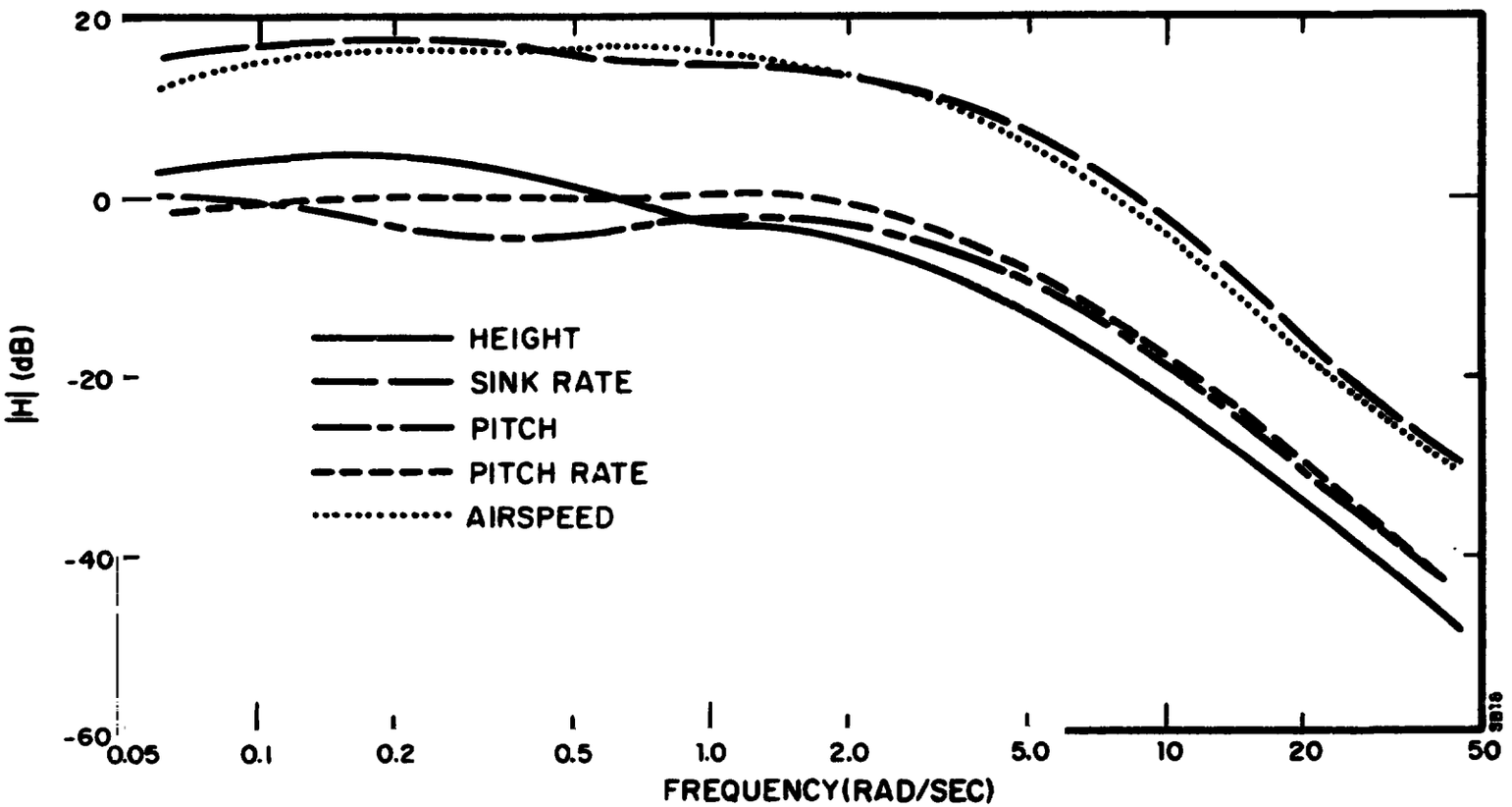

FIGURE 2. Magnitudes of Internal Pilot Describing Functions for Nozzle Control

Further experience with the proposed technique is needed to determine whether such simplifications can be made in general. If such is found to be the case, then we have demonstrated a very powerful technique for designing a control director of minimal complexity.

Evaluation of the Director Laws

For the purpose of evaluating the proposed control-director laws, pilot-related model parameters were selected to correspond to a high level of pilot effort. Parameters not related to pilot randomness were set to the same values used in the design procedure. The motor noise/signal ratio was set to approximately -25 dB, and, in order to perform a workload analysis (Refs. 6, 7), the observation noise/signal ratio was varied from a minimum of -20 dB to a maximum of about -10 dB.

Performance. — Predicted rms performance scores for the 1%-wind condition and an observation noise/signal ratio of -20 dB are shown in Table 3. Also shown for comparison are the scores predicted for the status displays without a flight director and the scores associated with an idealized display condition which ignores most of the display-related limitations (Refs. 4, 5).

The performance variable most effected by display parameters is the rms height error. The score predicted with the flight director is about 26% less than the score predicted for the status display. (The idealized display yields about a 35% reduction with respect to the status display.) A similar reduction is predicted for the sink rate error score. A reduction of about 10% is predicted for rms stick and stick rate. Other performance scores are virtually unchanged. Except for improved flight-path performance, then, vehicle motions and control responses are essentially the same with and without the flight director.

Workload. — In order to assess the degree to which workload can be reduced by the use of the flight director, we examine the relationship between the probability of a "missed approach" and "attention". A missed approach is defined as the situation in which either height or airspeed error exceeds its respective "limit" of 3.7 meters or 2.6 meters/second. Attention is related inversely to the observation noise/signal ratio, with a relative attention of unity associated with a ratio of -20 dB.

Table 3

COMPARISON OF PREDICTED RMS PERFORMANCE WITH VARIOUS DISPLAY CONFIGURATIONS

(1%-wind, P_o = - 20 dB)

Variable	Display Condition: Without Flight Director, Status	Without Flight Director, Idealized	With Flight Director
σ_h (m)	2.3	1.5	1.7
$\sigma_{\dot{h}}$ (m/s)	.68	.55	.55
σ_θ (deg)	1.8	1.8	1.8
σ_q (deg/s)	1.2	1.2	1.1
σ_u (m/s)	1.3	1.3	1.3
σ_{δ_e} (deg)	2.1	2.0	1.9
$\sigma_{\dot{\delta}_e}$ (deg/s)	7.4	7.0	6.6
σ_{δ_N} (deg)	12.	12.	12.
$\sigma_{\dot{\delta}_N}$ (deg/s)	21.	21.	21.

The relation between predicted performance and attention is shown for the 1%-wind condition in Figure 3a. Curves for both the status and director displays are shown for comparison. For the 1%-wind condition performance is still poor for the director display, but it is appreciably better than for the status display configuration. In particular, the flight director reduces significantly the sensitivity of performance to observation noise (both display-related and human related) and, therefore, shows relatively greater improvement at lower levels of pilot attention.

ORIGINAL PAGE IS OF POOR QUALITY

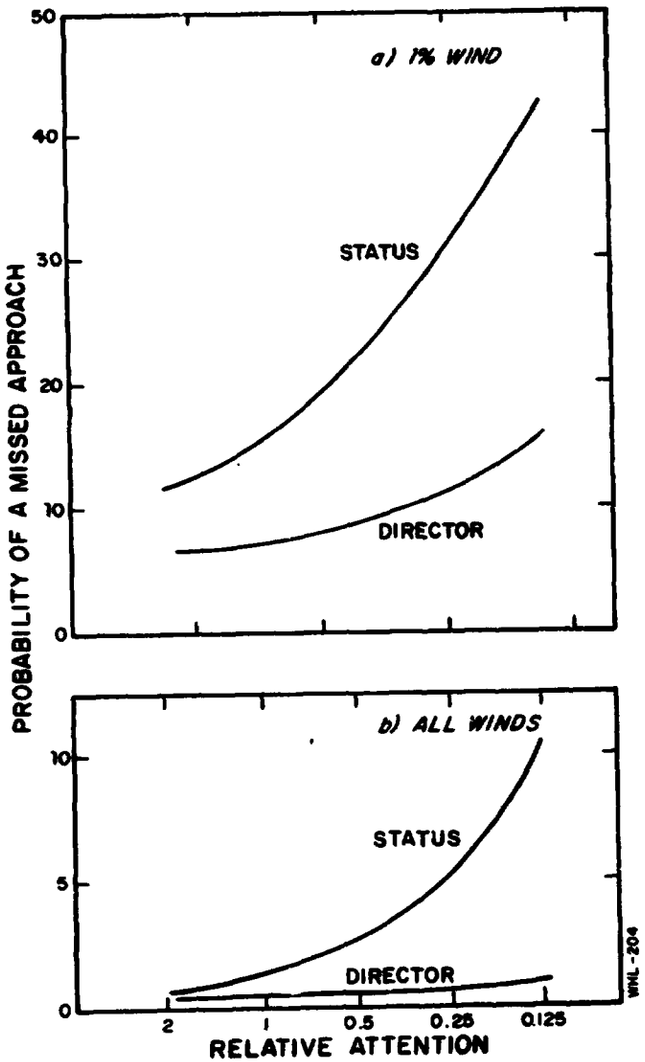

FIGURE 3. Relation Between Predicted Performance and Attention

In order to provide a more meaningful comparison of the workload/performance relationships for the two display configurations, a probability-weighting procedure was employed to derive a set of curves corresponding to "average" gust conditions (Refs. 4, 5). The value of the flight director is now even more apparent. The predicted workload requirements are substantially lessened even for relatively stiff performance demands. For example, if we require a 99-percent probability of a successful approach, a relative pilot attention of slightly greater than unity is required when no director is provided. With the proposed director, however, predicted attention requirements are reduced by about a factor of 10. Conversely, performance is improved for a pilot operating at a constant level of attention. For a relative attention of 0.25, the predicted probability of a missed approach is reduced from about 5 percent for the status display to around .6 percent for the "model-based" director.

Predicted Pilot Describing Function. — One of the design goals set forth earlier was that the flight director should allow the pilot to adopt a control strategy that resembles a simple gain at low and mid frequencies. We expected that the design procedure adopted in this study would meet this requirement by allowing the director laws to perform the required equalization. It was also anticipated that cross-coupling in the pilot's response strategy would be unnecessary with a properly designed set of flight directors.

Inasmuch as the model for the pilot is relatively "free form", pilot transfers will in general be predicted between all display and all control variables. Thus, for the control situation investigated here, there are two sets of predicted pilot describing functions to consider: the "direct" transfers which relate each control response to the corresponding director command, and the "cross" transfers which relate control responses to commands on non-associated directors. In cases where pilot cross-coupling is unimportant, the magnitudes of the predicted cross transfers should be numerically small.

The predicted direct transfers are shown in Figure 4. As expected, these transfers approximate a pure gain at frequencies up to about 4 rad/sec (which is beyond gain-crossover for flight-path and attitude control). The high-frequency peaks in the amplitude ratios are typical of actual pilot response behavior obtained in K/s tracking situations.

Predicted cross transfers are shown in Figure 5. The frequency-dependency of the phase-shift indicates that both describing functions are non-minimum-phase.

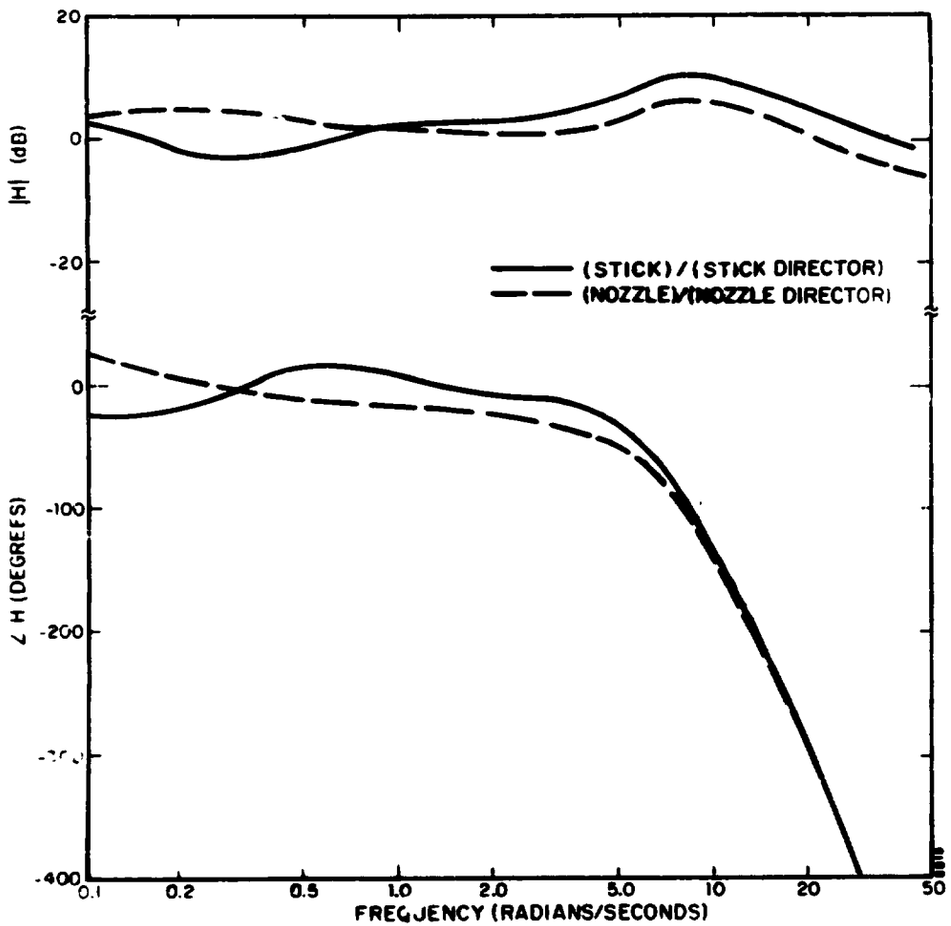

FIGURE 4. Predicted "Direct" Pilot Transfers

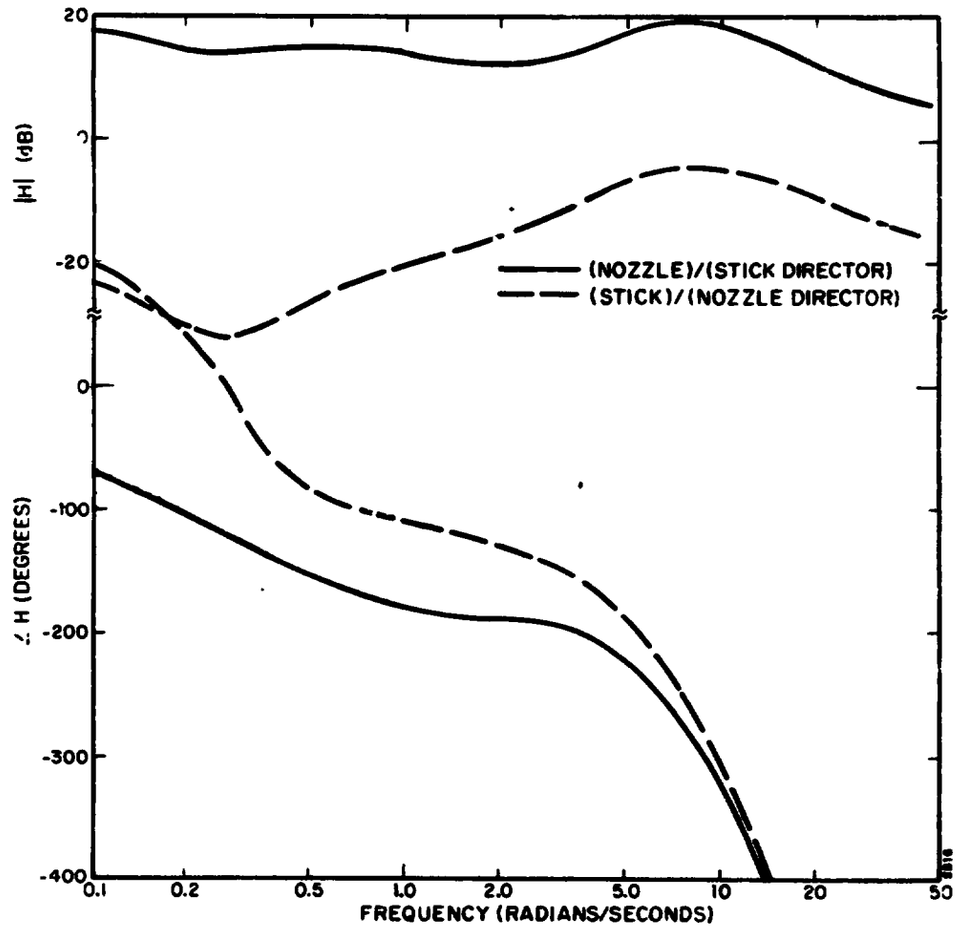

FIGURE 5. Predicted "Cross" Pilot Transfers

In order to determine whether or not the magnitude of the cross transfers are small enough to be neglected, we must compare the open-loop describing functions for the direct and cross paths. (The open-loop transfer is defined as the cascade combination of a predicted pilot describing function and the corresponding vehicle transfer function.) Such a comparison (not shown here) reveals that the magnitudes of the cross control paths are not substantially less than the magnitudes of the direct paths at all frequencies. Thus, we cannot claim that the predicted pilot cross couplings are numerically small.

A true test of the importance of cross-coupling would be to determine the levels of performance and workload that would be obtained if cross coupling were prohibited. There is no simple way to make this test at present, however, because current implementation of the pilot/vehicle model does not allow for such a constraint on the predicted control strategy.

SUMMARY

An approach to designing flight director laws based on the "optimal-control model" of the human operator was suggested. Director laws for longitudinal control of a STOL vehicle were developed using this approach. Analysis of system performance with status displays and with the proposed director display led to the prediction that the director would provide improved system performance at reduced workload levels. Thus, the proposed design technique achieved its major objectives. On the other hand, the results did not substantiate the belief that the need for control cross-coupling would be reduced by this design procedure. Further work is necessary to evaluate this aspect of the design.

It should be re-emphasized that the illustrative example presented in this paper resulted in only a preliminary design of director laws and an analytic (not experimental) evaluation thereof. A number of factors such as steady-state winds, sensor noise, and stand-off errors were not considered, and design compromises that are perhaps inevitable in practice were unnecessary here. Nevertheless, the author believes that the results presented here are highly encouraging and warrant both further development and experimental evaluation of the design technique proposed in this paper.

REFERENCES

1. Kleinman, D. L., S. Baron, W. H. Levison, "An Optimal Control Model of Human Response, Parts 1 and 2", Automatica, Vol. 6, May 1970.

2. Kleinman, D. L., S. Baron, W. H. Levison, "A Control Theoretic Approach to Manned-Vehicle Systems Analysis", IEEE Transactions on Automatic Control, Vol. AC-16, No. 6, December 1971.

3. Klein, R. H., D. T. McRuer, D. H. Weir, "A Pilot-Vehicle Systems Approach to Longitudinal Flight Director Design", Proceedings of the Sixth Annual Conference on Manual Control, April 1970.

4. Baron, S. and W. H. Levison, "A Manual Control Theory Analysis of Vertical Situation Displays for STOL Aircraft", Bolt Beranek and Newman Inc., Report No. 2484, April 1973.

5. Baron, S. and W. H. Levison,"A Display Evaluation Methodology Applied to Vertical Situation Displays", presented at the Ninth Annual Conference on Manual Control, May 1973.

6. Levison, W. H., "A Model for Task Interference", Proc. IEEE, International Symposium on Man-Machine Systems, Vol. 3, September 1969.

7. Levison, W. H., J. I. Elkind, J. L. Ward, "Studies of Multivariable Manual Control Systems: A Model for Task Interference", NASA CR-1746, May 1971.

SOME EFFECTS OF A QUANTIZED DISPLAY FORMAT ON HUMAN OPERATOR TRACKING PERFORMANCE

by

Ronald A. Hess and Walter M. Teichgraber
Naval Postgraduate School

an informal paper

Abstract

An investigation was made of the effects of quantizing the displayed error in a series of compensatory tracking tasks. In the first part of the study, two subjects completed over 1900 single and dual-axis critical tracking task runs using three critical task controlled elements and eight separate degrees of quantization coarseness. Both first and second order critical task controlled elements were utilized as well as an intermediate "1.5" order element. The quanta levels ranged from 0 cm (a continuous format) to 1.7 cm on a 10 by 10 cm display.

In the second part of the study, a single well trained subject participated in a series of cross-adaptive tracking tasks. These tasks were aimed at determining the display format effects in terms of a single performance index which reflected both operator workload and tracking error. Three main task controlled elements were used: K/s, $K/s(s+2)$ and K/s^2. Three degrees of quantization coarseness were utilized with quanta levels ranging from 0 to 0.5 cm.

The critical tracking task experiments indicated that the operators' critical instability scores deteriorated almost linearly with increasing quanta level magnitude. The cross-adaptive experiments indicated increasing operator workload and error scores with increasing quanta level magnitude.

ORIGINAL PAGE IS
OF POOR QUALITY

N75 19141

Improvements in Pilot/Aircraft-Integration by Advanced Contact Analog Displays

by

V. Wilckens *)

PRECEDING PAGE BLANK NOT FILMED

An extract of this paper was presented under the more general title "New Aspects in Man/Machine-Integration; Recommendations for Research Priorities" at the 9. Annual Conference on Manual Control, Massachusetts Institute of Technology, Cambridge, Mass., May 1973

*) Dipl.-Ing., Research Engineer and Experimental Test Pilot, Zentralabteilung Luftfahrttechnik in the "Deutsche Forschungs- und Versuchsanstalt für Luft- und Raumfahrt" (DFVLR), Oberpfaffenhofen, Bavaria, Germany.

Abstract

Several expert statements selected from literature and concerning the qualities of modern information displays lead to the definition of a number of requirements which should be covered by the displays of the future.

It is shown that abstract displays principally cannot fulfill all these demands and that simply superimposing abstract symbols with the natural view of the outside world or with its artificial equivalent will not result in an optimum solution.

On the other hand, the natural visual contact information has some shortcomings too, some of which are identified.

All requirements can be, or will have the best chance to be, fulfilled by pictorial displays which contain the image of real outside world elements, as far as they are useful for information, and of their imaginary extensions into the airspace. The Channel Display is designed according to these rules.

Some test results are shown for confirmation of the concept; special and general problems are touched.

Content

	Page
Preface	3
Introduction	5
On the evolution of the problem to be solved	6
Visual Contact Information	10
Remarks on Quantification	11
Orientation	12
Disorientation	15
Confidence	16
Problems of Monitoring, Decisionmaking and Manual Take-Over	17
Resulting Remarks on Basic Suitability of Contact Analog Displays due to Human Characteristics	19
Concluding Problem Definition	21
Test Results	22
Conclusions	31
Literature	34

Preface

Our activities, as far as reported here, are primarily viewed from the standpoint of economic increase of Flight Safety. Not only because this is an officially delegated duty of our group but because it should be wise to base the orientation of each research effort more and more on fundamental human needs.

Flight Safety belongs to these.

It seems to be generally accepted that - due to the high contribution in aircraft accidents believed to be human errors - the main branches of the manyfold roots of Flight Safety are found in the area of human engineering.

On the other hand, the general title 'Flight Safety' is closely related, for instance, to many aspects of economy as well. Thus neither the various complex problem areas nor their more or less complicated details can be separated without raising the probability for deterioration of the quality of the progress, for example, in Flight Safety Research.

Since it is a natural human tendency to concentrate on detail and to disregard the whole, every effort should be supported which tends to correlate detail knowledge with the intention of improving the chance to s e e weak points as well as desirable trends, and to respect them.

In other words, problem definition of today should be "system-oriented" - and we see that this is very well known in the USA.

There is another general point of view related to the more or less specific content of this paper:

The efforts to correlate details within the whole are necessary as a preparation of sound decisions for the future. Lack in overall view tends to produce only small steps towards progress, even when a big step is required. Decisions must be made much more "cautiously" than desirable, and their quality does not necessarily rise with the degree of caution, or more precisely: of hesitation.

The complexity of the overall problem requires thinking and speaking about details which belong to very different disciplines of science. Thus, experts in very different fields should closely cooperate in order to evaluate the possible fruitful relations between those; but, we know how difficult it is to achieve this.

A provisionary, but possibly very useful, substitute for direct cooperation is an evaluation of experts' knowledge already available in literature. In many cases sufficient, assured detail 'know-how' is already available for synthesizing a new concept.

Thus, as indicated in the abstract, relatively numerous statements selected from literature are used in order to point out relevant characteristics of the "state of the art", some of it's shortcomings and the main desires for progress. Secondary reasons for making use of these are twofold:

- Many of the facts they describe can not be said in s h o r t more precisely,
- it is only fair to revive again thoughts others expressed before but which are buried in the avalanche of later papers.

But argumentation with literature extracts is sometimes - if it proves to be unconventional and thus inconvenient - tried to be neutralized by the comment: "... *separated from the context.*"
Although there can be a risk of modifying the meaning of an original text this does not necessarily imply falsification. An extract describing a complete notion will not falsify, and drawing conclusions from it which had not been drawn by the originator should not effect a distortion. Last not least, recognizing the risk is an important presupposition for discriminating cases of wrong interpretations from evasive comments.

In research on aircraft displays, their valuation is often exclusively concentrated on measurement and statistical processing of parameters concerning 1. guidance precision and 2. workload. A general aspect of this paper will be to demonstrate that these topics are very important, but nevertheless can be presuppositions only for further deciding proof for suitability in the future. This suggests, too, that the two quality measures are insufficient and new additional valuation criteria and methods are needed.

Introduction

Fig. 1 shows possibilities for research and improvement reduced to six ways along which, in principle, the problems of Flight Safety as far as influenced by All Weather Operations can be and are attacked.

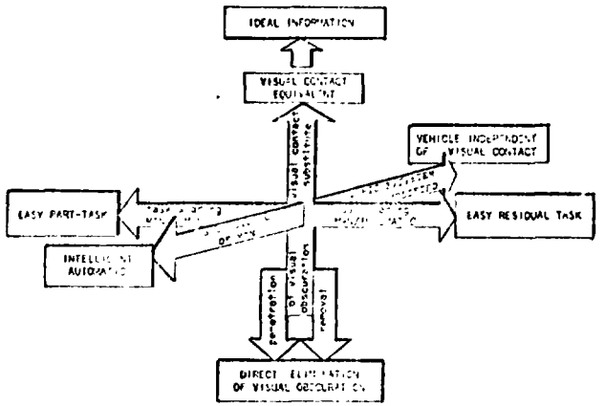

Fig. 1: Possible Ways to Attack the Critical All Weather Flight Problem.

The fundamental reason for the unsolved problems of the critical phases of All Weather Flight is the more or less impaired visual contact to the outside world [1]. Therefore, trials which intend to disperse or penetrate the obscuration or which offer an artificial substitute for the visual contact are considered, as far as they are successful, to be real s o l u t i o n s in the strict sense. These ways are indicated in the vertical axis of Fig. 1, and they include, in principle, all types of visual information display.

All other ways try to e l u d e the problem by reducing the difficulty level of the critical task or by providing technical means which are independent of visual information. *)

Today all the different ways are used in aeronautics to a more or less high degree. It can be shown, however, that a sound overall solution which is to remarkably raise the safety level needs much better visual contact substitutes than are available today.

Insofar, the paper primarily deals with display and mental processing of information.

*) Details of the different ways are evaluated in a separate paper [2].

ORIGINAL PAGE IS OF POOR QUALITY

On the evolution of the problem to be solved

When improvements are proposed, their valuation can be facilitated if the things to be improved are specifically processed for comparison. Although you are well familiar with the 'state of the art', a very condensed abstraction of it may be allowed here (Fig. 2).

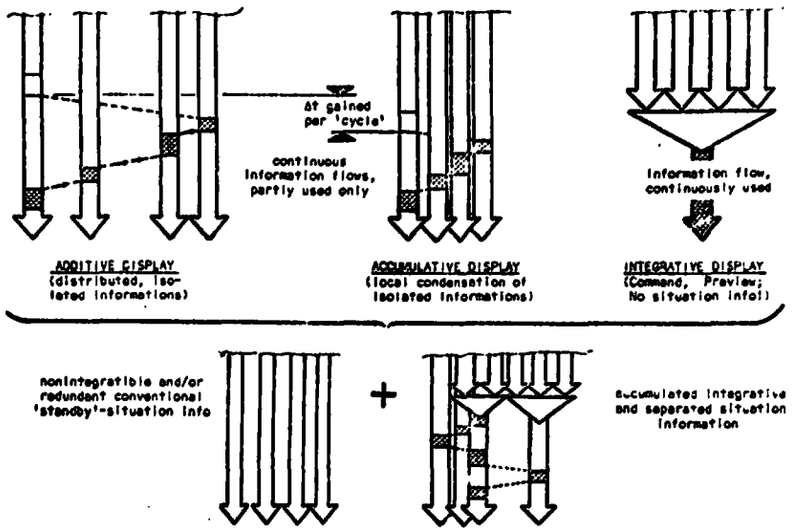

Fig. 2 Main Steps in Evolution of Information Gathering from Conventional Displays.

The ADDITIVE Display which consists of a number of isolated indicators, the number of which increased with time and progress, emerged from the growing importance of limitations of the natural visual contact. The 'single channelness" of the human brain [3, 1] requires that the favourable

continuity of the different information flows be broken by intermittent information scanning. Thus, the precentage of the actually used part of the several continuous information flows decreased during display evolution due to the process of extension and completion - certainly an undesirable trend.

You know that one action against this problem was the local condensation of some indicators in the "combined" or, as it is called here, the "ACCUMULATIVE Display". The advantage: There is some gain in the time needed per - simplified - scanning cycle which in truth has multiloop character.

One of the most important advances in aircraft control was obtained with the introduction of command signals necessary for automatic control and useful for manual control if displayed for instance, with a 'Flight Director'. These types of instruments are collected here, together with others, under the group "INTEGRATIVE Displays".

This information is - under certain presuppositions - a dynamically correct combination of a set of variables which is - on a first view - completely sufficient for the "precision control"-part of the task. With it, the human controller could, in principle, concentrate as the autopilot does on one single control signal per axis. The result, in general, is a more or less remarkable improvement in regularity of guidance precision combined with a reduction in the pilot's mental load under the more or less critical environmental operating conditions.

A command that satisfies completely an automatic control system may, however, not necessarily be sufficient for the human pilot. The autopilot does, in general, not take care of the situation, and would for example - without any fears - precisely follow a false command into a crash.

Most human pilots on the other hand n e e d to know the situation in order to be confident. But from the command they cannot derive an overall view, because the conventional command information is not "transparent".

It is stated in two of the latest AGARD-Reports of a joint working group concerned with V/STOL Displays:

"... the pilots expressed a lack of confidence in directors alone ..." [4, p. 4].

" ... the pure flight director that has to be nulled can be flown very accurately. Unfortunately without the inclusion of situation information the pilot is extremely uncomfortable, since he is unaware of how close he is to disaster. In addition, instruments which can fail to a zero position - like the conventional abstract needle instruments (remark of the author) - *are particularly dangerous ..."* [5, p. 8] or:

" ... the lack of situation information may lead to a condition in which the command display shows all commands satisfied - while the aircraft actually flies in ... a dangerous situation which cannot be detected ..." [5, p. 6].

Since these statements on V/STOL are related to general display problems and not to aircraft characteristics they should be applicable to CTOL, too.

Due to these problems, we have all historical stages of display evolution in the modern cockpit: An accumulation of primary command and situation indications (in the ADI/HSI-Instruments) and a number of non-integratible, or redundant, 'standby'-instruments for emergency control and confidence-crosscheck, respectively. *)

However, this introduced again the dynamically unfavourable scanning:

" ... in (tests) with the pilot instructed to share his attention between directors and situation displays, the accuracy was only half as good as when the flight director received full attention" [4, p. 4].

In addition, these disadvantages in guidance precision are accompanied by a fundamental lack of spontaneous confidence caused by the high degree of abstraction of the conventional situation instruments, not only of the 'non-transparent' command information.

Among others, a statement of ANAST [7] may describe the problem:

"We are all aware that a flight director does not meet the overall needs of a psychologically satisfying display. ... The pictorial s i t u a t i o n display ... is a firm requirement before automatic landings will be considered completely acceptable".

This and other similar remarks mean a realistic outside world equivalent and not the reduced "pictorial" presentations used in today's head down instruments, the Horizontal Situation Indicators (HSI) for example.

*) The research groups of STI, for instance, have studied the problems of this operational modern display and have created many ideas which seem useful for extended application [e.g. 6].

we know that recent display concepts try to solve the problem by superimposing "precision control symbols" like scales, digits, needles on the or artificial - according to ANAST: *"psychologically needed"* - image of the outside world, head up or head down, respectively.

But even this solution which can - without doubt - introduce a further remarkable improvement, compared to the visual display technique up to now, s t i l l l e a v e s something to be d e s i r e d .

There are, too, arguments to confirm this:

"Pilots like to dim the light intensity of HUD-symbols down to the minimum usable level, because - as they reported - they want to make them transparent and look through or behind them" [8, p. 18]. *)

"A superimposed display can not naturally be interpreted simultaneously with the underlying real world view. The pilot still retains an attention-switching task ..." [5, p. 11].

The final root for such statements - which all, more or less directly, criticize the superimposition principle - is expressed, for example, by the following text extract:

" ... superimposition will not promote combination and fusion (of the different information fields) unless the head up display conforms correlatively with the visual field external to the cockpit." [6, p. 97].

We can find statements which even suggest that support for the abstract "precision control" information is expected to come from the outside world image:

Again a free translation:

" ... the danger of 'short landings' ... and the touch down spread ... are reduced, if the runway threshold is visible (in a head down TV-monitor) ..." [8, p. 23].

Wouldn't this mean that duties of precision control are delegated to the visual contact or its' analog - which is sometimes believed to be useful for qualitative quick orientation only - and that the abstract information is considered to be insufficient even for the duties it is primarily designed for?

*) a translation

In my opinion, at least the following four arguments can be derived from these very remarkable statements:

- the abstract symbols disturb the perception of the "psychologically needed" outside world information,
- collimation (focussed at infinity) does not provide the required true integration of the information components,
- the information content of the abstract "precision control" symbology is - intuitively - considered by the pilots to be insufficient and needs to be supported by the "information behind", by the VISUAL CONTACT,
- the citation of ANAST (p. 7) indicates, that the residual display problems are not always primarily concerned with controllability but with the pilot's CONFIDENCE - a generally agreed upon but not yet very precisely defined term.

Therefore, the natural 'visual contact' information and the phenomenon 'confidence' should attract further attention in specific chapters.

Visual Contact Information

As far as precision and ease of control is concerned, the several thousand landings per day successfully performed by the "pictorial situation display" VISUAL CONTACT are no problem for well educated pilots in good visual conditions. But after reading, or listening to, some of the papers on these matters one often has more or less the impression that it is not yet completely understood why.

An extract from german literature [8, p. 19] says in free translation:

" ... The conflict between ... superimposed information ... and the pure visual contact ... will, perhaps, be better understood when in future improved knowledge about information requirements of the pilot in visual flight is available."

The question might arise, whether any reasonable valuations of contact analog displays and decisions on preferable display progress can be tried, b e f o r e the most habitual, obviously very important, visual contact information is - at least believed to be - completely understood.

Thus, intensive effort with high priority seems to be necessary to fill this gap of basic knowledge.

One reason for the difficulty in evaluating the quality of the visual contact information is probably the apparent contradiction between the obviously high success rate and the ease of control on one hand and the wide scatter of visual approach paths which seems to uncover lack of precision qualities on the other.

However, this lack of precision can, under certain circumstances, be misunderstood as lack of display quality; while in truth it expresses highly desirable "flexibility".

Precision in terms of any deviation measures of the time functions of a set of relevant variables can be a valuation criterion only if the respective variables are definitely indicated, and it is requested of and accepted by the pilot that he should closely track them.

In fact, there is no definite indication of a glide path.

In addition, a landing aircraft actually only needs to meet certain touchdown requirements, no matter, which approach path it flies along, provided it always proceeds reliably safe and according to the intentions of the pilot.

Straight or otherwise prescribed approaches are in many cases basically neither a necessity nor desirable, but an excuse for poor dynamic stability, i.e. poor guidance and display systems which do not allow VMC-like flexibility. In best visual contact, that is: where best transparency of the atmosphere and optimum habitual texture of the outside world features are available, reliably safe visual contact landings can be performed with enormous flexibility - and without relevant height perception difficulties.

Remarks on Quantification

The aversion to the "difficult-to-analyse" visual contact information is sometimes based upon the argument that height perception in terms of estimated meters or feet - whichever quantification units are preferred - is inaccurate. It is indeed; but in landings under optimum visual contact conditions, it doesn't mean very much in terms of the relevant quality measures "landing-success" and 'safety'.

Accurate perception of height, for example, is necessary only - and then the visual contact information really needs supplementation - if safe vertical distance to the not reliably visible fixed or moving environment (obscured mountains, obstacles and other traffic) must be maintained.

But this does not necessarily require abstract quantitative information elements like scales, digits and needles, nor are these very advantageous. Although, with good reasons, one units system was selected by a majority from the many possibilities to be applied in aeronautics, some pilots who don't use these units in everyday-life have to apply some extra effort to translate them into their most habitual units in order to be really informed.

Quantification by the generally usable measures: meters, feet, degrees etc., is sometimes overemphasized by far in aircraft guidance displays; perhaps because it is not understood or accepted everywhere that other directly task-oriented pictorial units can be used to give the environment meaningful dimensions. The oddity of the situation is demonstrated, if we try to imagine, for instance, that the car driver's information - the field of view in front of his vehicle - were painted with meter or feet scales and digital data for improvement of position and heading information.
Probably, this would not result in an improvement.

Problems of interpretation of transfer between different units systems do not exist at all if natural outside world units are used - necessarily in pictorial form - which are and should be very habitual to all human beings. This would give the best guarantee that orientation is immediate and reliable.

Orientation

It is generally accepted that the most familiar visual contact information is intuitively and immediately understood, in other words: there is a spontaneous orientation.

Is this really true to the full extent or are there any restrictions and if so, where precisely?

If a well-textured level plane - of the earth's surface - is seen from an altitude which is very small compared with the diameter of the globe, and the horizon lies within the field of view, we can say that attitude orientation - i.e. pitch (θ) and roll (ϕ) - is immediately achieved.

However, the orientation in azimut, and much more in the translational degrees of freedom, very much depends on the individual texture of, and on the height above, the earth's surface. High altitude gives wide-scaled "undistorted" impressions of the environment below This view is very useful for raw orientation in terms of relative distances and directions between individual locations - if these are clearly identified.

The unaided natural texture must be very familiar to the man if a fairly spontaneous orientation is to be effected. In most cases of pure VMC aircraft operation, some time-consuming observation and comparison with maps are required before the pilot is completely oriented. Therefore, well defined artificial navigational symbols will enhance quick orientation, preferably in the form of the new electronic map displays.

Simple perspective line or checkerboard patterns representing the surface do not offer any plan position information, rather only qualitative impressions of motion and height. Nevertheless, some support for attitude perception relative to the horizontal may be expected.

In addition, spatial orientation must include orientation in relation to the "moving environment" which is particularly problematic in VMC operation [21, p. 80].

We would assume high foveal sensitivity and continuous attention abilities of the pilot's visual system over the whole spheric field of view if we expect this part of the orientation problem to already be satisfactorily solved by painting aircraft tails and wingtips with bright orange colour and by installation of strobe lights.

Plan position map displays do not provide integrated vertical position information which is necessary for complete spontaneous orientation as well as for control. On the other hand, a profile view would be incomplete and therefore not sufficient as well but now in the lateral axis. Besides, the latter cannot be available in the natural visual contact for a pilot since it is, in principle, an "outside-in" display.

Immediate spontaneous attitude and position orientation is very important, as far as it's influences in manual control as well as monitoring are considered. Based on the findings of the first chapter, we must assume that full integration of all 6 degrees of freedom is required.

The unaided ' f o r w a r d ' visual contact clearly offers simple sensitive integrated directional information - simple, because the image of the environment, whatever it momentarily contains, is simply shifted transversally in the field of view. Together with the attitude angles the position is also offered fully integrated. However, in many cases it suffers from lack of typical texture. This problem is amplified by perspective distortion and by the low sensitivity and it's very nonlinear change due to motion.

Height perception for touch down is completely left to intuitive judgment.

Thus, precise visual contact approaches and landings are not as easy to learn d teach, as skilled pilots make believe; and even in best atmospheric transparency, the pure visual contact information can be dangerously misinterpreted. During night approaches, lack of foreground texture and sloping runways can cause early catastrophic ground contact [9, 10, 11]. Therefore the different attempts in simulating the pure visual contact for aircraft control have not been very successful [8, p.22].

All these shortcomings of orientation by the natural visual contact in it's different modifications require a prescribed flight path to be visible. Such a path would be <u>desirable</u> for economy because it can show the shortest/fastest connection between departure and destination. It is <u>necessary</u> for safety because it provides safe trajectories which reliably avoid dangerous interference (collision) with the environment. A prescribed path can only be made by imaginary means, since - in opposition to the hard earth's surface - space, in general, can not practically contain a real prescribed path for an aircraft. (The condensation trail of a preceding liner on an airway may be considered as an exception.)

Such a path can and should offer the most suitable sensitivity, preferably constant during each typical phase of flight, in order to enable sufficient precision. In the central perspective forward view presentation, for instance, of a street - which is the most familiar form of a prescribed path on the earth's surface - deviation sensitivity changes with the distance between the observer and the street surface. The more sensitivity desired, the more closely parallel should be the imaginary street to the prescribed path of the pilot's eyes.

With a sufficiently realistic image of a prescribed path of such a type, in addition to the pictorial attitude information, any human pilot will be completely oriented, probably as spontaneously as at all possible.

In addition, symbols similar to a street offer a tolerance limits indication for path deviations by their natural pictorial quantification.

Disorientation

Recent expert statements say the following:

"The ... displays ... have not eliminated disorientation. ... Disorientation in flight is not only a current problem; it promises to be a continuing problem... I do not think that instruments, no matter how good, will ever completely prevent disorientation." [12, pp. 5, 7].

Indeed, the present modern instruments - although some are beautifully painted in order to stimulate convincing impressions - do not prevent that even very skilled pilots sometimes have illusions which, per definition, do not correlate with the true attitude and/or position oriertation and the motion within the airspace.

The drift of the human inertial orientation system requires this system to be updated by the visual orientation. If the visual inputs for the perception of the vertical - for instance from the artifical horizon - are poor in comparison to dominating cockpit references, or if vague external cues excite misleading impressions, orientation conflicts known as 'vertigo' occur.

Under certain circumstances strong illusions can happen even in excellent visibility in flight. This is possible, for instance, on high altitude flight above flat untextured haze layers with some reference marks (cumulonimbus) at the horizon.

In turns under such conditions the horizon texture sometimes seems to move and the aircraft appears to be the fixed reference. Some pilots even can intentionally produce the illusion of fast lateral or even backward translational motion! *) Psychological background to such experiences is explained in a book of BEATY [21].

*) observations of the author

Such experiences should not be treated as an illness of the pilot but as naturally explainable reactions of the human (visual) orientation system to the sometimes ambiguous visual contact information:

The absence of distributed near-by texture - which is necessary in order to sense changes of position - allows the eye and brain to interpret the far-away azimutal turn motion as a fast unnatural translational motion of the aircraft.

There will be no doubt that the orientational disturbances are definitely avoidable if the presentation of the environment contains sufficient elements of vertical and/or horizontal orientation which are about as urgent and sensitive as in everyday visual contact of human beings.

The presentation of the prescribed path which, in the previous chapter, was found to be necessary, could be designed so as to reinforce to a convincing degree the impression of a vertically and horizontally oriented fixed outside world reference.

It seems to be realistic that a display with such characteristics has a good chance of completely eliminating disorientation. But strictly speaking, confirmation is still left for experimental research in real flight.

Confidence

The dominating significance of the display quality 'confidence' was mentioned in some earlier papers [e.g. 1], and confirmed in one of the cited AGARD-Reports:

"Pilot's confidence is probably the most important single factor in achieving operational all-weather landing." [5, p. 3]

Obviously, there are different contributions to the phenomenon 'Confidence':

- speed and reliability of orientation,
- ease and precision of control,
- flexibility of flight path selection,
- the - display dependent - proficiency of the pilot
- and the functional reliability of the electronics

All these more or less remarkably influence the pilot's confidence in the overall system and situation.

Build-up of confidence in some new All Weather Systems is almost exclusively based on the - without doubt very important - last component. But in my opinion, confidence produced only by extremely reliable equipment, is very expensively purchased because very much of the unactivated human abilities have to be substituted. There is no question that pilots will fly such systems because they have no choice [1, 13]. According to their human tendency to adapt to almost everything, they will develop a substitute for confidence which is sometimes said to be a psychological progress [11, p.966], but should be better called fatalism.

The following general remark applies to confidence as well as to the orientation problems:

The pictorial display should have a high degree of realism, a highly sensitive perspective which always seems to be a true undistorted, although possibly simplified, visual contact. There appears to exist a threshold in realism resulting in a respective discontinuity in human acceptance. As soon as sufficient realism is offered, human imagination automatically completes the "picture of the situation" and unequivocally integrates it with the inputs of the other orientation sensors. If this threshold is not reached, however, imagination is not exited and the pseudo-pictorial presentation is felt to be not much more than a specific arrangement of symbols. The psychologically rooted components of confidence don't seem to be activated by displays with too limited realism.

Therefore, too, permutation of abstract symbols, colors and other means for information coding, does not seem to be a very effective tool for achieving desirable progress in display research and technique.

In my opinion, here are also some chances for further efficient research.

Problem of monitoring, decision making and manual take-over

Some papers could make one believe that the man/vehicle-cooperation problem could be characterized with headlines such as:

- "reduce the workload of the man in the cockpit",
- "the pilot's task should be kept as simple as possible" [5, p. 2]
- "the pilot must progress from being the operator to becoming the manager" [15].

That the root of the problem would be missed by such a progress seems to be indicated by the following translated remarks:

" ... It is the question, how far man may be supported by complex subsystems, without causing hazards for the whole in case of any failure. Too much "foolproof" systems wouldn't maintain the pilot sufficiently trained ..." [16]

"The step from ... an extremely easy monitor task ... to the more complex ... (one which requires mental) ... measurement and interpretation of information (as well as) manual control must remain acceptably small." [17]

Of course, the step from extremely easy monitoring to the m o s t complex basic form of a manual control task requires a jump over the maximum possible difference of difficulty levels!

Therefore, it can only be m u c h too demanding, particularly because it would have to be mastered in very rare and unexpected cases and because even the already continuously trained manual task is too difficult - <u>as far as instrument landings in critical cases are considered!</u>

If the statements above are true, this conclusion seems to be permitted:

A reasonable monitoring task

- includes fully competent manual take-over by the pilot, and this
- requires the best possible information display, which must be by far much more capable than the 'state of the art'.

The tendency to confront pilots with a more or less arbitrary collection of different command, situation and monitoring instruments or electronic drawings and, being discontent with his necessarily inconsistent resulting performance, to push him into the pseudo-active role of a monitor and "go automatic or overshoot"-decisionmaker will hardly lead to optimum solutions.

It is unrealistic to derive human dynamic skills from observations of conventional instrument flight. Since the extremely wide step mentioned above is well within human pilot's capabilities as soon as he flies in good visual conditions, the assumption is justified that a display which could offer information really equivalent to visual contact and including the necessary and desirable improvements would allow him to perform at least as well.

However, manual take-over needs manual skill, necessarily based on training, which will be more and more reduced by automatic operation. Since man usually applies no more than the effort which is requested from him, the manual skill is not developed within human limits to the desirable degree by the information principles used today.

Insofar, it is doubtful that the pilots' task should be made "as easy as possible". Manual skills should be kept high by a reasonably demanding task presented by respective display qualities.

Resulting Remarks on Basic Suitability of Contact Analog Displays due to Human Characteristics

Referring to the shortcomings of the visual contact there are numerous comments in literature which condemn this natural information source as a model for display development.

The well known fact that the use of the visual contact i n f l i g h t is not so easy to teach and to learn as it seems to be when observing experienced pilots is basically caused by the deteriorations of information content as soon as the pilots' eyes are raised high above the surface.

But this does not necessarily postulate the so caused deficiencies of the visual contact to the ground to be unavoidably associated with the other, the doubtless superb qualities of this natural display. The possibilities of today's artificial electronic image generation would allow an interruption if such an undesirable compromising connection would exist. In other words, it cannot be prohibited in using, extending and amplifying the favourable pictorial elements and in deleting the superfluous or even unfavourable ones.
Abstraction of information, as well as destroying it's natural integration by a break down into single parameters, and a mixture of different display principles should be abandoned because much or all of the unique qualities of the environment view model are lost. It c a n be abandoned because a l l the necessary information - in quantity and quality - can be presented in a p u r e pictorial form.

An interesting remark, received in a discussion, and it's analysis will probably further contribute to clear the "difficult-to-measure" problems:

"A very habitual information, like the perspective outside world view, is not necessarily an optimum."

To me, this appears to be very true even in general and neither restricted to one type of information only, nor to vehicle control alone.

The appearance of the environment as picked up not only by the visual system but also by other closely correlated sensory modalities obviously reaches an absolute "familiarity maximum" for almost every individual during his evolution from childhood. Beyond this it is highly probable that, due to the "principle of amplifying selection" in the evolution of mankind, human sensors should have adapted to the appearance of the environment. This particularly because the appearance and it's change in human motion remained the same during the very long time of the evolution process.

Probably therefore, the eyes in their normal 'zero' attitude, looking in the direction of motion, became very able to sense shifts of the path-stabilizing attitude angles due to foveal sensitivity and/or due to very precise eye tracking ability. This is supported by peripheral view which, in addition, became very sensitive to streamer vectors and asymmetries indicating transversal deviations.

This should be one strong, although not the only, argument for the visual contact on earth's surface being preferable in comparison to other more or less artificial information principles.

Other - to engineers probably more convincing - arguments should come from considerations dealing with the suitability of the information content under control dynamics aspects. These matters are discussed in the next chapters.

Due to the finding that weaknesses of poor information (display) qualities are principally the roots of the problems, human pilots should not be treated as underdeveloped subjects as far as the task of stabilization and control of dynamic systems is concerned. This became almost common habit in argumentations which claim for superiority of automatic control systems. It should be surprising that in such cases it is not tried to explain the discrepancies between this attitude on one hand and the admirable precision of the well known close formation flight acrobatics controlled by a "purely pictorial" visual contact information on the other. The argument that those are performed by rare exceptionally talented individuals does not fit. Very many, if not all of the thousands of fighter pilots for instance, were, are or will be able to reach similar skills because they are all human controllers "designed" and selected, educated and trained by the same principles.

However, then it must also be accepted that some remarkable "rest" of dynamic adaptation is left to learn for many very experienced pilots who primarily have to manage instead of flying their aircraft.

Without doubt it is conceded that the 'combat ready' fighter pilots have to be fit in the precision task formation flight for normal service. Thus it won't be unreasonable to request adaptation of pilots to a similarly demanding task given by a pure pictorial display if this display would be highly desirable from an overall standpoint.

Concluding Problem Definition

As an output from the preceding chapters, the design targets for future displays would in short be:

1. Spontaneous reliable orientation, eliminated disorientation; (realized by →): → deviation-sensitive advanced contact analog;
2. Easily controllable precision: → fully integrated command qualities;
3. VMC-like flexibility: → advanced contact analog;
4. Maximum and economic development of manual skill: → demanding advanced contact analog;
5. Best monitoring qualities: → deviation sensitive advanced contact analog;
6. Satisfaction of all confidence components: → results from point 1 through 5.

Thus, a 'demanding deviation-sensitive advanced contact analog display with fully integrated command qualities' would be required. Or, returning to the described limits of the 'state of the art' (p. 10), the problem to be solved could be defined by the following overlapping questions:

- How could information for spontaneous confidence and for precision control be combined, "integrated" command be achieved, without the disadvantages of superimposition of different types of information?
- Is there a type of display which offers all simultaneously?
- How could the contact analog information which obviously is necessary to amplify confidence artificially be improved in order to offer the precision control aids which are not available in the visual contact in the natural or, much less, in simulated form?

Test Results

We tried to answer at least parts of these questions in an experiment last year, where we compared simulator tests, flown with three different stages of conventional display evolution (Fig. 2) and with the Channel-Display, which was described in earlier papers [18, 1, 13]. The latter was especially developed to fulfill the design targets mentioned before.
Figure 3 shows the display arrangement which includes a relatively poor realization of the channel display due to very limited computer capacity.

ORIGINAL PAGE IS OF POOR QUALITY

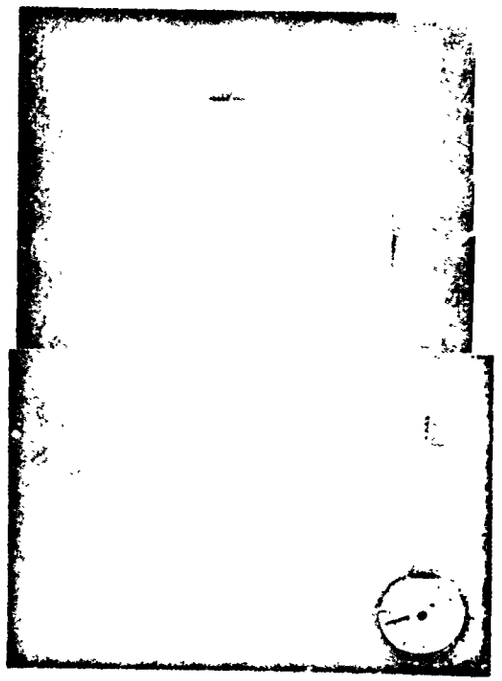

Fig. 3 Conventional Instruments and Channel Display

Fig. 4 shows graphs of the lateral offset and of the bank angle command C_ϕ for three typical test runs flown in a fixed base simulator with the Flight Director (FD), the Channel Display and the conventional ILS.

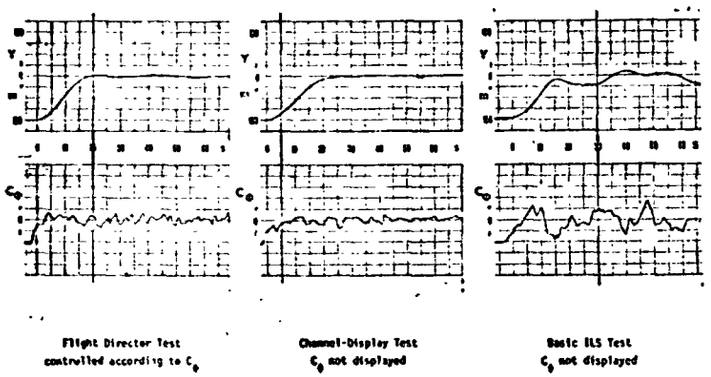

Fig. 4: Comparison of test graphs

There are comparable flight path traces in the FD and Channel tests in the interception as well as tracking phases. It is worth being mentioned that the C_ϕ- signal reaches zero after a similar time lapse from the start of the channel-run as well as the FD-test.

The FD-test was controlled by zeroing the C_ϕ-Signal resulting in the time function of the residual alternating command error. In the channel test no command signal was of course visible for the pilot. In spite of that there is a comparable quality in the command traces, the FD showing higher frequencies only caused by the direct response of the pilot to the command needle which is deflected under the influence of gust-induced motions.

The natural or artificial visual contact is considered to be a pure situation information. Insofar, it should be surprising that the Channel-Display, which is evaluated from this model, exhibits a guidance precision and path error smoothness which is comparable to that of the FD, and much better than that of the abstract situation instruments.

ORIGINAL PAGE IS
OF POOR QUALITY

Fig.5 depicts a more detailed processing of C_ϕ-traces of FD- and Channel/Tunnel-runs *) and additional traces from basic ILS, distributed as well as accumulated.

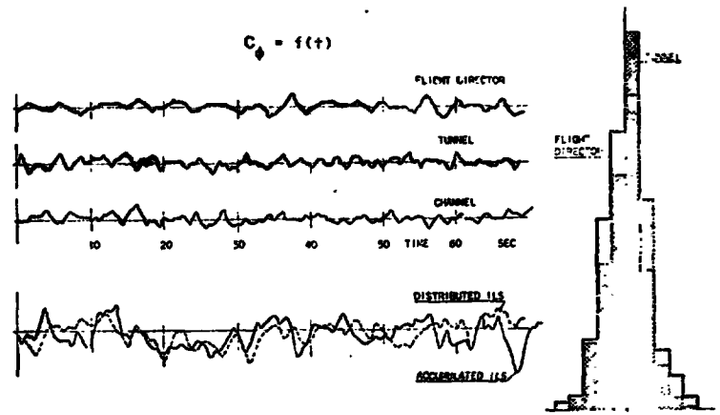

Fig.5: Comparison of evaluated C_ϕ- traces**) histograms

The histograms of C_ϕ, superimposed for comparison,***) belong to the first 2, the FD and Tunnel traces, respectively. Obviously, the results are even better with the Tunnel than with FD in this case.

Channel and Tunnel traces are similar in frequency and amplitude. The tasks with raw distributed and accumulated ILS had identical gust time functions and show much higher C_ϕ-error functions which are similar, too.

To me, such results suggest that the channel display inherently contains a sort of command characteristic comparable to that of the typical FD.

---

*) Tunnel = a closed channel (see Fig. 6)

**) These traces were taken from another type of analog record than those of Fig. 4. With regard to this, it will be recognized that the dominating frequency of the traces of the FD tests is the same in Figs. 4 and 5.

***) Of course, single test graphs do not seem to be very convincing. But a very laborious manual processing had to be done because the magnetic tapes became unusable after a fire in our simulator rooms. However, the analog records selected are typical.

And, indeed, we find the analog of the FD-equation in the perspective picture of a Tunnel. (Fig. 6)

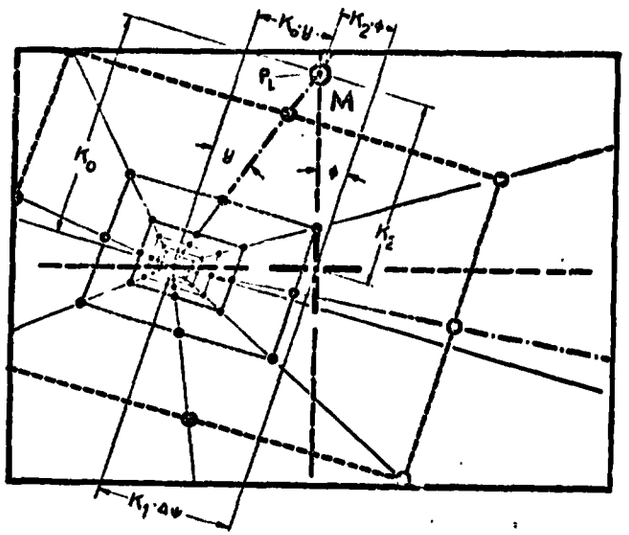

Fig. 6: The Director in the Tunnel Display

The lateral deviation is transformed into an angle y due to the laws of central perspective projection, while the heading difference ψ is represented by a lateral offset of the tunnel's vanishing point from the reticle. The bank angle ϕ is of course given by a corresponding rotation. Finally, the view angle magnification ratio defines the coefficients K_0, K_1 and K_2, so that the simplified FD-equations can be derived from Fig. 6:

$$C_\phi = K_0 \cdot y + K_1 \cdot \Delta\psi + K_2 \cdot \phi = 0$$

The equation $C_\phi = 0$ is satisfied as soon as a point M at the upper end of the reticle coincides with another point P_L on the upper centerline of the Tunnel.

Of course, this does not mean that pilots will focus their attention on these two markings and closely track them. Instead they probably learn in a modified type of 'Successive Organization of Perception' [6] to perceive the correct progress peripherally and to apply the "command characteristic" intuitively in a favorable flexible manner.

There was a remarkable difference in the control strategies of the Channel/Tunnel tests and the FD-runs. The Channel/Tunnel display enables the pilot in discriminating between bank, yaw and displacing disturbances and in reacting individually with the respective control. Control inputs were applied well coordinated or independently, whichever was preferable [18]. With the "nontransparent" FD the pilot has no choice but to react with the aileron only although, in case of a ψ-disturbance, the most reasonable direct action would be with the rudder.

Since the stability of a command control system depends on the magnitudes of the coefficients and since the coefficient K_0 is a function of the cross-section size of the channel, it is desirable to know which channel calibration would be optimum with respect to precision and ease of control.

Fig. 7 is a qualitative diagram of the relations between the channel size and the tracking accuracy.

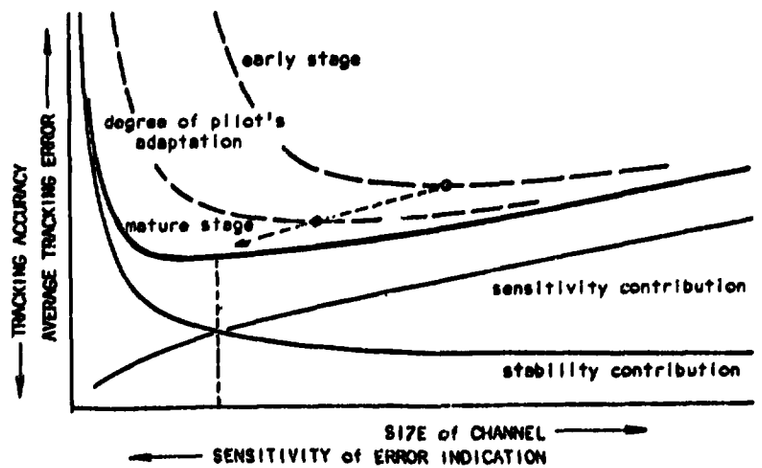

Fig. 7: Average tracking errors VS size of channel

In general, we can expect an increase in the tracking errors with a growing size of the channel due to the reduction of signal sensitivity. On the other hand, there will be a hyperbolic contribution because the closed loop dynamic stability will progressively decrease if the channel is tightened; and thus deviation sensitivity (or K_0) grows beyond favourable values and causes increasing oscillatory overshoots.

The sum of both will necessarily have an optimum at a certain channel size. Further the optimum will be a function of other parameters like vehicle dynamics, type and level of the disturbances, and degree of adaptation of the pilot. Since the stability contribution will be more influenced by the pilot's skill level than the sensitivity contribution, the optimum will drift towards smaller size during the adaptation process.

The position of the optimum is particularly important, because the channel shall additionally provide inherent motion tolerance information where necessary; for instance, during the final phase of the landing. This will help to avoid superfluous precision and control activity, and will allow more flexibility, all being factors which contribute to confidence.

In a series of test runs with one pilot at an approximately constant level of adaptation the influence of channel size was investigated (Fig. 8).

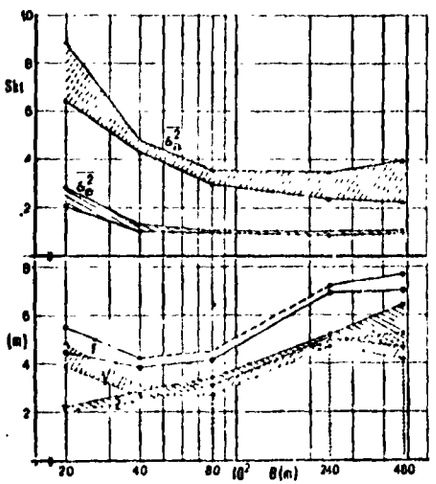

CONTROL ACTIVITY

$$\bar{\delta}_i^2 = \frac{1}{T}\int |\delta_i^2|\, dt$$

i = e → elevator
= a → aileron

TIME AVERAGE ABSOLUTE ERRORS

$$\bar{y} = \frac{1}{T}\int_0^T |y|\, dt \qquad \bar{r} = \sqrt{\bar{y}^2 + \bar{z}^2}$$

$$\bar{z} = \frac{1}{T}\int |z|\, dt$$

Fig. 8: Tracking Error and Control Activity as a Function of Channel Size

ORIGINAL PAGE IS OF POOR QUALITY

The time average absolute errors in the lateral (y) and vertical (z) direction as well as their vector sum r and the respective control activities are drawn as functions of the channel width B at a constant ratio H/B = 3/8.
The results reproduce the functions as they were expected according to Fig. 7.

The spread of values was not, or not only, caused by stochastic influences. With one exception, the upper limit represents the early, the lower limit the later tests. Apparently, there was still an adaptation process going on.

It seems to be important to mention here that statistical evaluation of such tests with many subjects would hardly exhibit these very important results. They would probably be masked by undetermined influences like different unknown adaptation levels of the subjects. With other words, such and other traditional "laboratory rituals" [5, p.12] should be applied with caution. Otherwise, misleading conclusions could be encouraged.

While there is a minimum of $\bar{y}$ (Fig. 8) at 70 < B < 80, $\bar{z}$ continues to drop with decreasing B. This difference was obviously caused by the lower difficulty level of the control task in the vertical axis in comparison to the lateral. This results partly from the higher order of the lateral task, partly from the difference in χ-sensitivity (B/2 > H; Fig. 9).

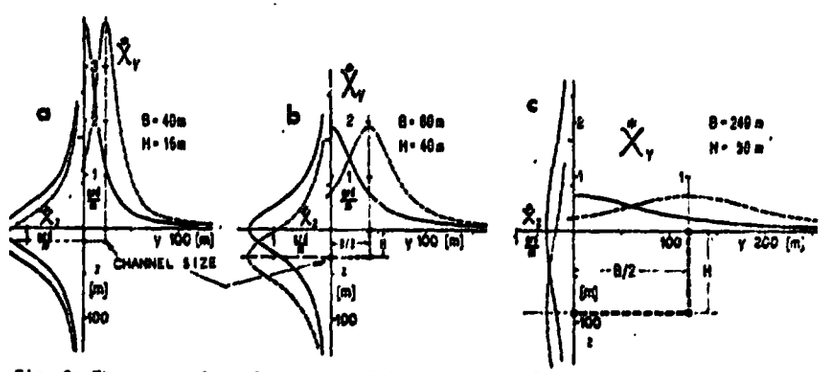

Fig. 9: Three examples of vertical ($\bar{\chi}_z$) and lateral ($\bar{\chi}_y$) deviation sensitivity as functions of the resp. deviations .(Derived in [20]).

The control difficulty differences are recognizable (Fig. 8) from the control activity functions, as well. The δ_a^2-activity has a wider "scatter" - i.e. the pilot still continued to adapt - and starts to increase at a larger B. Especially the consistency of the elevator activity is believed to be an indication of the reliabilty of the results.

The differences in control activity partly originated from the different control sensitivities and partly from the extraordinarily poor lateral control characteristics of the simulator.

The most important overall result, however, appears to be that the minimum of the resultant average error $\bar{r}$ lies at a channel width B which approximately coincides with the width of a typical runway!

Thus, for the conditions selected, we had coincidence of the optima of three of the most important display characteristics: Ease (1) and presision (2) of control and tolerance information (3).

A further interesting observation during the tests confirmed by the results was that the stability of the closed-loop system, including a well adapted pilot and the Channel/Tunnel display, was much less dependent on "variation of coefficients" than a flight director controlled system in principle is.

BEYER et al. [19] have shown that the coefficients can be selected to effect either a high precision control aid with an oversensitive, "high workload" indicator or a less demanding, less precise control task. They stated that, therefore, "no really optimum selection of the coefficients is possible" [19, pp. 20, 21].

A performance restricting compromise is needed. Although this paper deals with the "quickened display" *) for a heading control task, and not for the more critical flight path control which is the relevant type of operation today, the problem would principally correspond with the findings derived from the simpler system in [19].

With the conventional "nontransparent" FD any human pilot is necessarily condemned to operate as a poor constant amplifier. When using the inherent command characteristic of the Channel/Tunnel display, he is able to develop and apply his intelligence-based high adaptability. He can thereby compensate the changes of system dynamics caused, for instance, by variations of display and control sensitivities or of aircraft characteristics.
In Fig. 8 the increasing control activity, with decreasing error, indicates the compensating ability of the human pilot.

*) in this respect the "quickened display" may be considered to be the same as the flight director

There are still some questions concerning, for instance, the computer sophistication for realizing the Channel Display, it's information content in cases of large deviation, the suitability of the available guidance systems for feeding the display and it's failure warning and survival abilities. These points are very important from the operational standpoint and their evaluation depends very much on less provisionary realization and flight testing.
Although there are many favourable arguments which already seem to be convincing, these should now be retained until they can be reliably confirmed.

Conclusions

1. As long as pilots are able to fly and land an aircraft manually in good visual conditions, and there is any deterioration in performance as soon as the visual conditions get worse, the root of the problem is a poor display.

2. It is recognized that man must scan when provided with a number of single information sources. Thus, he can unfavourably use small asynchronous sections of the continuous information flows only. Therefore, it is necessary to derive that scanning should definitely be avoided for the dynamically demanding task of attitude and flight path stabilization.

3. Although local condensation and superimposition of different information allow some improvement, these methods do not completely eliminate the need for some undesirable "attention switching".

4. A dynamically complete and correct pure single command indicator would allow the removal of scanning, but it is not "transparent" for orientation which the human pilot needs for confidence. Observing the command needle, for instance zeroed by the autopilot, does not sufficiently satisfy this need.

5. Neither additional abstract basic conventional data nor the pseudo-pictorial situation displays, especially such in the plan position or profile view, provide sufficient confidence in critical cases. In addition, they distract attention from the primary control information, which distraction conflicts with the item 2.

6. It is necessary to fully understand the visual contact information before successful comparing valuations of present display principles and reliable decisions for desirable future development can be made.

7. Selfexplanatory, complete visual contact to habitual environment fully satisfies the human need for confidence. But in most cases the visual contact in flight, even in good visual conditions, does not contain sufficiently sensitive three dimensional position information, especially in the vertical.

8. The deficiencies can be overcompensated, the superb qualities amplified, by the presentation of a - necessarily imaginary - prescribed flight path. This should be calibrated in intuitively obvious pictorial elements of preferably horizontal and vertical orientation which provide sensitive vertical, lateral and longitudinal position information. A prescribed path eliminates ambiguity and attention-demanding mental processing.

9. Especially for the use of precision control (item 2.) and complete immediate orientation, this prescribed path can only be presented in fully integrated form, together with the three rotational degrees of freedom, by central perspective projection of the 'forward' view. Only this single format emphasizes the information components approximately according to their importence. An additional "inside-out" map display is desirable for raw orientation.

10. The Channel/Tunnel-Display is designed according to the findings 1. to 9.

11. Furthermore it has been shown by test results that this display contains inherent command characteristics which - in contrast to the conventional "nontransparent" flight director - leaves situation information available and thus can be used in an extremely flexible manner.

12. The pictorial integration used in the channel display allows an increase of the sensitivity of deviation information beyond that which is acceptable in "abstract integration" (deviation coefficient in the command equation) in order to maintain dynamic stability.

13. The acceptance for high deviation sensitivity allows the use of channel dimensions as meaningful tolerance limit indications even in the - generally most critical - landing phase. It was shown by test results that optimum tracking precision can be achieved with a channel calibrated for standard runway width.

14. Thus, an objective measure is possibly achieved for the momentary performance level of a pilot, for the dynamic aptitude of student pilot candidates or for sufficient runway width.

15. Although it does not agree with the philosophy of offering a display which is "as easy to control as possible", two pilots expressed that they felt relaxed when changing over from modern conventional instruments in simulator tests. Director tracking appeared to be a comparatively stultifying primitive task.

16. In any case there was no problem of manual take over from a failing autopilot in simulator tests with the channel display. The channel, which simultaneously allows quick orientation and manual precision control, was felt to be optimum for the monitoring and decision task, too. In general, monitoring and manual control should be most convenient with one and the same display.

17. With the Channel/Tunnel-Display spontaneous orientation and VMC-like flexibility will be achieved, disorientation problems - very probably - completely eliminated.

18. Regard for different display quality requirements does not necessarily require a compromise in the strict sense which includes reductions in the performance of the conflicting components. There are combinations - additive and superimposed displays, for instance - which suffer from such reductions. Other combinations, the channel display for example, can offer qualities which are more than the sum of the components.

19. The problem of safely overcoming the extraordinary demands for dynamic capability in case of a necessary unexpected take-over under adverse conditions cannot be solved by separation of the pilot from these basic demands. Instead of artificially "making his task as easy as possible" only - with the attitude stabilization (which is very useful), higher sophisticated flight directors etc. - the reserves of human dynamic adaptability should be activated by better displays in order to achieve an efficient and economic increase of safety.

Literature

[1] WILCKENS, V. — On the Dependence of Information Display Quality Requirements upon Human Characteristics and 'Pilot/Automatics'-Relations. NASA SP-281, 7. Annual Conference on Manual Control, USC Los Angeles, June 1971

[2] WILCKENS, V. — Ober die verschiedenen Wege zur Lösung des Problems der Wetterabhängigkeit des Flugzeugs. Interner Bericht (Vorabdruck) Nr. 019-72/8 der DFVLR-Zentralabt. Luftfahrttechnik, Oberpfaffenhofen

[3] SENDERS, J.W., ELKIND, J.I., ORIGNETTI, M.C., SMALLWOOD, R. — An Investigation of the Visual Sampling Behaviour of Human Observers. NASA CR-434, April 1966

[4] Displays for Approach and Landing of V/STOL Aircraft. AGARD-AR-51, November 1972

[5] V/STOL Displays for Approach and Landing AGARD-R-594, July 1972

[6] McRUER, D., JEX, H.R., CLEMENT, W.F., GRAHAM, D. — A Systems Analysis Theory for Displays in Manual Control. STI-Technical Report 163-1, Oct. 1967, revised June 1968

[7] ANAST, J.L. — All Weather Landing Developments. AGARDograph 55, Oct. 1960, Istanbul, p. 400 - 406.

[8] BEYER, R. — Elektronisch erzeugte Informationsdarstellung in Flugzeugen. DLR-FB 72-43, Juli 1972

[9] KRAFT, C.L. — Flight Deck Workload and Night Visual Approach Performance. AGARD-Symposium "Aircraft Landing Systems", Natick/Mass. May 1969, Conference Proc. No. 56

[10] PALMER, E. — Night Visual Approaches - Pilot Performance with and without a Head Up Display. NASA TMX-62, 188, Ames Research Center, Oct. 1972

[11] BOURQUIN, K.
PALMER, E.
COOPER, G.
GERDES, R.
Initial Flight and Simulator Evaluation of a Head Up Display for Standard and Noise Abatement Visual Approaches.
NASA TMX-62, 187, Ames Research Center, Febr. 1973

[12] CLARK, B.
Disorientation Incidents Reported by Military Pilots Across 14 Years of Flight.
AGARD-CP-95-Part I, Aerospace Medical Panel Spec. Meeting, Luchon, France, Sept. 1971

[13] WILCKENS, V.
Pilot/Automatic Relations, Confidence, Displays.
Paper at Society of Experimental Test Pilots - Europe, Zurich/Lucerne, Aug. 1971 SEPT-'COCKPIT', April 1972; SEPT Techn. Review, Vol. 11, No. 3

[14] PRICHARD, H.C.
The Problems of Blind Landing.
Journal of Royal Aeronautical Society, Bd 50, 1946

[15] ST. JOHN, O.B.
All-Weather Landing.
AGARD Guidance and Control Panel Symposium, Aircraft Landing Systems, May 1966

[16] STEININGER, K.
Das Maß der Dinge ist der Mensch.
Flugwelt 8/1964, p. 601

[17] DOETSCH, K.H.
Mensch und Maschine in der Flugführung.
Flugwelt 3/1966

[18] SCHATTENMANN, W.
WILCKENS, V.
Vergleichende Simulatorstudien mit dem kontaktanalogen KANAL-Display und mit konventionellen Instrumentierungen.
Paper No 72-100, DGLR-Conference, Berlin, Oktober 1972

[19] BEYER, R.
ZIETLOW, E.
Beitrag zur analytischen Behandlung der qualitativen Vorausanzeige in Führungssystemen.
DLR FB 69-30, February 1969

[20] WILCKENS, V.
Zur Lösung der Flugführungsprobleme vornehmlich bei der Nullsichtlandung mit der echt perspektivischen, bildhaft-quantitativen Kanal-Information.
Prepared for printing.

[21] BEATY, D.
The Human Factor in Aircraft Accidents.
Secker & Warburg, London 1969

N75 19142

VISUALLY INDUCED SENSATIONS OF MOTION

L.R. Young*, J.M. Dichgans**, and C.M. Oman*

As early as 1875, Mach noted that under appropriate visual conditions, a large visual field, moving uniformly around a subject, could produce a sensation of self-rotation or self-translation which can be extremely powerful, and nearly indistinguishable from body motion. These phenomena, often referred to as Circularvection (CV) and Linearvection (LV), have subsequently been studied by a number of different investigators.

From the point of view of flight simulator design, it has been generally found that appropriate visual scenes can be used to influence subjective spatial orientation, and minimize the actual linear and angular motions required.

In the past year, our laboratory has been conducting a collaborative research program with the Department of Neurology in Freiburg, Germany, and the Psychology Department at M.I.T. Our work has been specifically aimed at modelling the visual and vestibular information integration process in humans, and determining the implications of these models with respect to requirements for flight simulation. This paper reviews our findings with respect to visually induced motion sensation.

Working with a subject seated on a rotating chair inside a cylindrical, closed, rotating drum whose inner walls were painted with vertical alternating black and white stripes,

*Man-Vehicle Laboratory, Department of Aeronautics and Astronautics, Massachusetts Institute of Technology, Cambridge, Mass.
**Department of Neurology, Freiburg i Br., Germany

Dichgans and Brandt (1972) found that subjects were not able to distinguish rotation of the drum at constant velocity from rotation of the chair at the same rate but in the opposite direction. The strength of the stimulus to the peripheral retina appeared to be of primary importance in determining the strength of apparent rotation. Brandt and Dichgans (1972) showed CV strength to be essentially independent of the stimulus strength to the central retina (± 20 degrees), and also independent of the strength and direction of optokinetic nystagmus, such as might be generated by a separate display in the central portion of the field of view.

Dichgans, Held, Young, and Brandt (1972) have shown that an analogous effect can be produced for CV about horizontal as well as vertical axes. They found that a rolling visual field produced tilts of the apparent vertical up to 40 degrees, depending on the angular velocity of the visual roll stimulus. Subjects report feeling the paradoxical sensation of being tilted at a constant angle, but continuing to experience a sensation of roll angular velocity, due to the continuing stimulus. Apparently, this is due to the inherent conflict of the visual information with that from the otolithic graviceptors. Presumably, this conflict is not present when CV is produced about an earth vertical axis. Some of our recent studies using the projection system in the NASA Langley Dual Maneuvering Simulator indicate that CV can also be produced in pitch, although apparent tilt responses induced appear somewhat smaller than in roll. Occasionally, vertical linearvection is also experienced simultaneously, possibly because the axis of rotation of the scene is less visable. The Langley studies indicated that the strength of the apparent tilt induced in pitch and roll was substantially increased when the subject's head was tilted.

With respect to design of displays for flight simulation, it is particularly interesting to note that Dichgans and Brandt (1972) have found that head movements about horizontal axes by a subject experiencing CV about a vertical axis elicit perceptual effects (such as apparent tilt and nausea) subjectively indistinguishable from the well known Coriolis Phenomenon (Guedry and Montague, 1961)- even though the body is not undergoing actual rotation. Our attempts to elicit this phenomenon with CV about non-vertical axes in the Langley simulator have so far been equivocal, however.

More recently, our efforts have been specifically aimed at studying the interaction between visual CV effects and vestibular responses. Young and Henn (1973) have found that CV produces a short term direction specific habituation of nystagmus response to vestibular stimuli. Tang (1973) has studied the combined effects of body tilt and roll CV using an appropriately modified Link GAT-1 simulator, and has found that the effects of tilt and CV seem additive, at least for the small tilt angles studied thus far. Using the same device with CV and actual cab rotations ocurring about a vertical axis, Young, Dichgans, Murphy, and Brandt (1973) found that CV in a given direction produced a corresponding rise in subject's angular acceleration thresholds. Magnitude estimates of angular velocity showed the effects of a CV induced offset, which were increased slightly by vestibular responses in the same direction, and decreased markedly for vestibular responses in the opposite direction. However, rapidly occuring conflicts between visual and vestibular sensation, especially those involving direction disparities, resulted in a precipitous decline in CV and temporary domination by the vestibular response.

Current efforts are aimed at optimizing display configurations appropriate for simulation; extending current studies to include linearvection effects; continuing investigations of the visually induced "pseudocoriolis" effect; attempting to incorporate these results into a hierarchical model for visual and vestibular interaction; and the application of this model to the simulator design process.

REFERENCES

Brandt, Th. and Dichgans, J., 1972: Circularvektion, optische Pseudocoriolis-Effekte und optokinetischer Nachnystagmus: Eine vergleichende Untersuchung subjektiver und objektiver optokinetischer Nacheffekte. Albrecht v. Graefes Arch. Klin. Exp. Opthal., 184, 42-57.

Dichgans, J. and Brandt, Th., 1972: Visual-Vestibular Interaction and Motion Perception. Bibliotheca Ophthalmologica, No. 82: Cerebral Control of Eye Movements and Motion Perception. Streiff, E.B. (Ed.) S. Karger, Basil.

Dichgans, J., Held, R., Young, L.R., and Brandt, Th., 1972: Moving Visual Scenes Influence the Apparent Gravity. Science: 178, 1217-1219.

Guedry, F.E., and Montague, E.K., 1961: Quantitative Evaluation of the Vestibular Coriolis Reaction. Aerospace Medicine, 32, 487-500.

Tang, J.T.Y., 1973: MIT, Man-Vehicle Laboratory Progress Report. Unpublished.

Young, L.R., Dichgans, J., Murphy, R., and Brandt, Th.,1973: Interaction of Optokinetic and Vestibular Stimuli in Motion Perception. In press.

Young, L.R., and Henn, V., 1973: Selective Habituation of Vestibular Nystagmus by Visual Stimulation. In press.

FLIGHT-TEST EXPERIENCE WITH A SNAP-SHOOT DISPLAY

A.E. Preyss, J. L. Meiry, J.E. Potter, and R.E. Curry

ABSTRACT

This paper will report on some of the flight test experience with a heads-up pursuit tracking display proposed several years ago (Gilbert, Preyss, and Wills, 1969 Conference on Manual Control). The primary advantages of this display over conventional lead angle computing displays was thought to be a better allocation of tasks between man and machine: the man should be able to perform a more accurate prediction of target motion, whereas the computer is able to do the rote ballistic computations. Although the display has an inherent delay of one time of flight, the pilot should, nevertheless, be able to predict the convergence of the impact point and the target. The flight test data confirm these hypotheses, in general. Problems associated with timing cues, pilot-computer interactions, dynamic bore sighting, symbology, tracking problems, learning experience and contradictory simulation results will be discussed.

APPLICATION OF DESCRIBING FUNCTIONS FOR EVALUATION OF SPACE SHUTTLE LANDING AID DISPLAY CONCEPTS

Wendell D. Chase
NASA-Ames Research Center

ABSTRACT

The Space Shuttle Orbiter is a sophisticated vehicle designed to reenter the atmosphere essentially unpowered and expected to land on a conventional runway. During the final phase, the pilot may monitor the approach or manually perform the unpowered terminal area flight maneuvers. As an aid to the terminal area operations, a promising approach to improved pilot display support for approach management and flight path control has been identified. This display concept provides a more direct "see-through" pictorial representation of key flight situation parameters. These parameters, controlled by the pilot, are expected to enhance the management of the Orbiter recovery for manual flight control operations.

Three of five levels of increasing display aid were evaluated in simulated Orbiter approach sequences. Data was obtained to support the relative effectiveness of each display for pilot monitoring and assessment throughout an unconventional two segment final approach. In addition to some of the usual performance measures, special application of human operator describing function measurements were computed from a modified Fast Fourier Transform. This method is used in the analysis of increasing display aid and to help identify the aid obtained with a heads-down panel mounted or heads-up windscreen positioned display. The most significant feature of this paper is a comparison of pilot describing function analysis as applied

for more effective man-vehicle display design. The results are useful to support conventional performance measures as they are considered in the evaluation of each display format.

This paper summarizes the display requirements for the terminal area space shuttle type vehicle landing operations, and illustrates the supporting describing function-analytical performance measure techniques.

PRECEDING PAGE BLANK NOT FILMED

ORIGINAL PAGE IS
OF POOR QUALITY

PRECEDING PAGE BLANK NOT FILMED

SESSION IV

DRIVING AND PSYCHOMOTOR SKILLS

N75 19143

SENSITIVITY OF A CRITICAL TRACKING TASK TO ALCOHOL IMPAIRMENT

PRECEDING PAGE BLANK NOT FILMED

Jean A. Tennant
Project Manager, Driver Physiological Systems

Richard R. Thompson
Senior Project Engineer

General Motors Engineering Staff

Ninth Annual Conference on Manual Control
Massachusetts Institute of Technology
May 24, 1973

ABSTRACT

A first order critical tracking task is evaluated for its potential to discriminate between sober and intoxicated performances. Mean differences between predrink and postdrink performances as a function of BAC are analyzed. Quantification of the results shows that intoxicated failure rates of 50% for blood alcohol concentrations (BACs) at or above 0.1%, and 75% for BACs at or above 0.14%, can be attained with no sober failure rates.

A high initial rate of learning is observed, perhaps due to the very nature of the task whereby the operator is always pushed to his limit, and the scores approach a stable asymptote after approximately 50 trials. Finally, the implementation of the task as an ignition interlock system in the automobile environment is discussed. It is pointed out that lower critical performance limits are anticipated for the mechanized automotive units because of the introduction of larger hardware and neuromuscular lags. Whether such degradation in performance would reduce the effectiveness of the device or not will be determined in a continuing program involving a broader based sample of the driving population and performance correlations with both BACs and driving proficiency.

TABLE OF CONTENTS

		Page
I	INTRODUCTION	1
II	PREDRIVING PERFORMANCE TESTS	4
	A. Objectives and Desired Characteristics	
	B. Operational Modes	
III	A CRITICAL TRACKING TASK (CTT) AS AN ALCOHOL INTERLOCK SYSTEM	6
IV	EXPERIMENTAL DESIGN	8
	A. Subjects	8
	B. Test Protocols	8
	C. Administration of Alcohol	9
V	SOBER VS INTOXICATED PERFORMANCE	12
	A. Sober Performance	12
	B. Intoxicated Performance	12
	C. Group Comparisons	15
	D. Test Results Summary	15
VI	DISCUSSION	21
	References	23

I INTRODUCTION

It has become common knowledge that alcohol is involved in the majority of traffic fatalities (1), (2)*, and that casualties in terms of both human lives and material losses have reached phenomenal levels. Consequently, General Motors has been actively pursuing means of alleviating the problem through an alcohol countermeasures program.

Several technological approaches to the "driving while intoxicated" problem were discussed in Reference 3, having for common objectives the identification of the intoxicated driver through performance or chemical (breath) tests (4), (5). Two philosophies were distinguished: one where the identification process takes place prior to driving by a test,-behavioral or chemical,-of short duration, and the other involving the continuous monitoring of driver performance. The latter approach could involve warning mechanisms (e.g., hazard flashers), and the predriving test could involve the actual inhibition of the vehicle's starting through ignition interlocks.

A discussion of some of the drawbacks and advantages of the above approaches is in order. In the case of direct BAC measurement, it is well accepted that great individual variability in capabilities exists at equal BACs; and, although it is well established that as blood alcohol concentration rises basic performance capabilities deteriorate, the relationship between BAC and driving performance is not a perfect one. It is, for instance, often argued that experienced drinkers are less impaired than inexperienced drinkers at lower blood alcohol

*Numbers in parentheses designate References at end of paper.

concentrations, and, that indeed, large individual differences do exist in tolerance to alcohol. On the other hand driving is a behavioral task, and a behavioral testing procedure seems, therefore, more logical than a chemical one for examining an individual's current ability to drive. This would be true even if alcohol were the only agent or condition that produced temporary driving impairment. It is not, of course, and to devise automatic chemical means of detecting other possible agents or any large subset of them has major technical drawbacks.

In the case of a predriving performance test, however, the intoxicated driver might on some occasions be able to "pull himself together" sufficiently to pass the predriving test even though his blood alcohol level exceeds legal limits and though his driving capability is impaired to the point of gravely increasing his probability of involvement in an accident.

The time involved for the absorption and metabolism of alcohol and the resulting delay in its effects on driving performance also deter from this approach. In addition, the implicit assumption that the performance task will be degraded by alcohol consumption in a similar fashion to driver performance must be justified. Nevertheless, an interlock system is designed not to keep people from drinking, but to keep them from driving when their abilities are impaired to the extent that their risk of having an accident is greatly increased.

Indeed, no predriving behavioral or psychomotor test provides the utopian system that could continuously monitor driving performance and bring the vehicle to a safe halt when performance impairment is detected (6). While it is believed necessary to devote efforts towards gaining a better understanding of the perceptual, decision, and motor response processes that comprise the driving task, and towards establishing quantitative means of assessing them on a continuous and passive monitoring basis, it is felt that the predriving identification of the unfit individual and temporary inhibition of his vehicle from starting by virtue of an interlock system promise more immediate benefits. Indeed, a recently completed Accident Causation Study at General Motors showed that an effective behavioral predriving task would be one of the highest payoff accident countermeasures available. Although General Motors has put more emphasis on this type of countermeasure, we are also pursuing the alternative approaches mentioned, namely, those based on breath test and on the continuous monitoring of driver performance.

ORIGINAL PAGE IS
OF POOR QUALITY

II PREDRIVING PERFORMANCE TESTS

A. Objectives and Desired Characteristics

The main objectives for a predriving performance test implemented as an alcohol ignition interlock can be stated simply as follows:

- Large discrimination against intoxicated individuals (*positive rejection rates*).
- No discrimination against sober individuals capable of driving* (false rejection rates).

While most programs to date were conducted primarily with the goal of quantifying individual test sensitivities to BAC by assessing the above rejection rates, the following additional characteristics are desired and must be considered in any comparative analysis:

- High correlation with driving ability.
- Short duration of test.
- *Rapid learning rate.*
- Easy integration in vehicle.
- Insensitivity to age, sex, intelligence, and social and educational backgrounds.
- Not easily compromised.
- Low cost.

Although the correlation between traffic accidents and rising BACs is well established, large variabilities in driving capabilities are attributed to different tolerances to alcohol. Therefore, performance on the predriving task should be correlated with driving ability, the main variable of interest. Consequently, the collection of such data would allow one to compare legal restrictions sought by many states, namely, *having a cutoff for driving according to BAC* (e.g., passing all below 0.10%) with having a performance check implying that one who is too intoxicated to pass should not be driving.

*Tolerable false rejection rates would depend on the application, with higher rates permitted if applied only to those with a driving while intoxicated record.

B. Operational Modes

There exist two distinct philosophies in selecting the design or test parameters for any behavioral task to be used as an alcohol interlock. One approach calls for universal thresholds, that is, fixed parameters for the entire driving population; the other allows for the individualization of the test parameters for each subject. The tradeoff here is primarily between cost and effectiveness.

It is clear that unless interlocks are to be directed only to a selected few offenders, individualization on a universal basis would be costly and complicated, since the baseline performance of each driver would have to be established. In most instances, however, the effectiveness of the test is greatly enhanced by individualization since the variability in performance between subjects is eliminated.

III A CRITICAL TRACKING TASK (CTT) AS AN ALCOHOL INTERLOCK SYSTEM

The CTT device as implemented in the automotive environment (7) utilizes existing systems on the car; namely, the steering wheel and a meter mounted on the instrument panel (the meter use could be shared with other systems, such as fuel measurement). The test consists of steering to keep the needle within a bounded area, just as one would steer his car on a bounded road. Figure 1 shows the current experimental system.

The test resembles somewhat the steering of a car on a slippery surface, such as ice, while the speed of the car gradually increases (without the driver's control). It involves controlling an unstable system which gradually becomes more unstable (8). If control is successfully maintained up to a preset level of instability (λ_f), i.e., in the analogy of driving on ice up to a certain speed, a green light comes on and the car can be started. If the needle wavers outside of the designated area, a red light comes on and the starter is immobilized. In this event he may be allowed additional trials. That is, whether the threshold value, λ_f, is reached or not determines whether the trial is a <u>success</u> or a <u>failure</u>. It appears that the initial value for the unstable mode, λ_{ic}, and $\overset{o}{\lambda}$, can be selected to limit the duration of the test to approximately 10 seconds. The development and characterization of "critical tasks" are well documented in the literature (8), (9), and (10).

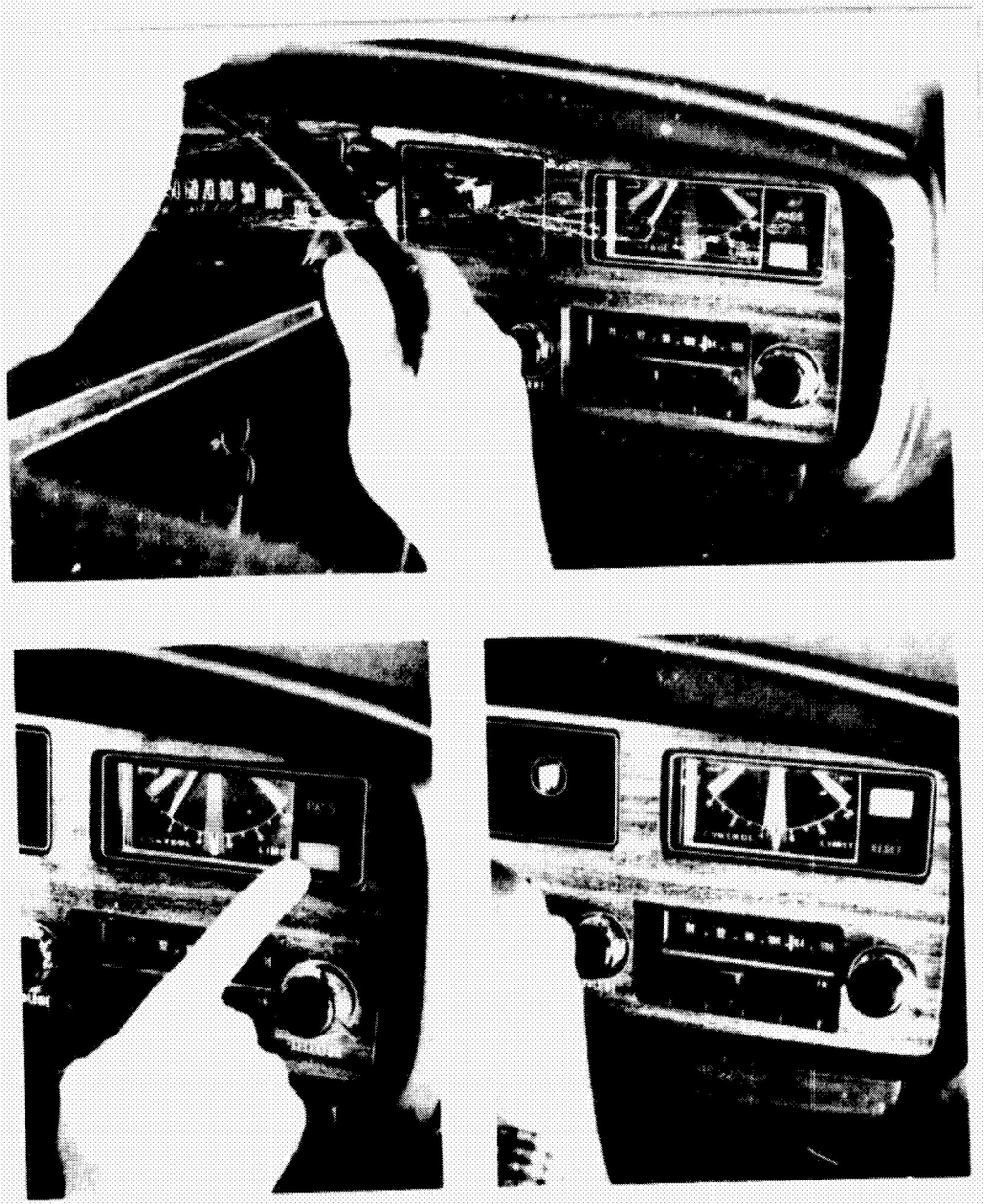

Figure 1 CTT - Current experimental installation in a car. The meter could be time-shared with some other function such as fuel measurement.

IV EXPERIMENTAL DESIGN

A. Subjects

Seventy-six subjects (47 males and 29 females) ranging in age from 17 to 65 participated in the study. The subjects were part of a larger study on the effects of alcohol conducted at Beaumont Hospital under General Motors sponsorship.

In order to avoid any potential complications from the ingestion of alcohol, the volunteers were selected by medical personnel at Beaumont following a study of their medical history.

Those under medication, which if combined with alcohol could prove harmful, and those with diabetes or past liver problems, etc., were eliminated from the studies.

B. Test Protocols

All training and testing were conducted at the hospital on a first order Critical Tracking Task mechanized with an oscilloscope display. The room provided by the hospital was located in a nonmedical building of the hospital complex. During the training and test sessions the room was furnished and arranged to provide an informal, nonclinical setting.

The score, or value of λ at which control was lost, was indicated to the subject at the end of each trial by the location of the line on the face of the oscilloscope. The score was read directly off the markings on the oscilloscope and reset to the center position for the next trial.

During the training and test period the subjects could rest briefly between each trial at their discretion, and they controlled the start of each trial.

Two sessions were used for training on the Critical Tracking Task. In Session 1 the subject was first familiarized with the equipment and the nature of the task. Following this the subject was given 30 trials on the task, and the scores were recorded. Two weeks later the subject returned for the second session. Session 2 consisted of 20 additional training trials, followed by alcohol consumption and 10 test trials. Table I illustrates the overall Testing Plan.

During Session 1, subjects were given training on the CTT on an individual basis. In order to provide a more social, informal setting, four subjects participated together in the training and test phase during Session 2.

The schedule for Session 2 was as follows: Upon arrival each subject was given a Breathalyzer test, followed by 20 trials on the CTT. Next, the subject received four drinks, evenly spaced, in an 80-minute period. Following a 40-minute interval after the last drink, the subject was given 10 test trials on the CTT. A breathalyzer test to determine BAC level was then given, and a blood sample was taken.

C. Administration of Alcohol

One-hundred-proof vodka mixed with either orange juice or tomato juice was used in the study. The total volume of vodka administered to each subject was based on the subject's body weight and his reported drinking habits. Based on his report, each subject was identified as to one of the following four categories and received the corresponding volume of vodka indicated.

Very Light Drinker	- 1.00ml/lb body weight
Occasional Drinker	- 1.25ml/lb body weight
Average Drinker	- 1.50ml/lb body weight
Above Average Drinker	- 1.75ml/lb body weight

TESTING PROGRAM

SESSION 1	2 WEEK INTERVAL	SESSION 2	
30 TRIALS (at BAC = 0)		20 TRIALS (at BAC = 0)	10 TRIALS (at Peak BAC)

Table 1

During the drinking period changes were occasionally made in the amount of vodka given per subject, based upon visual evidence of intoxication, or lack of it, and on verbal reports of nausea.

All drinks were administered by an attending physician, and the Breathalyzer measurements were taken by a trained operator. Calibration of the Breathalyzer was checked after each session.

V SOBER VS INTOXICATED PERFORMANCE

A. Sober Performance

The overall performance of the subjects during the two training sessions is presented in Figure 2. For summary purposes the mean score on the CTT of successive five trial blocks for all subjects and the standard deviation of the scores for each trial block are presented.

Trial blocks 9 and 10 reveal that performance has reached or approached a asymptote by the end of session 2. A stable baseline such as this is a requirement for quantifying the deterioration in performance following the consumption of alcohol.

B. Intoxicated Performance

Of the 76 original subjects, seven were unable to complete the test phase of the study as a result of illness which developed during or following the drinking session.

Figure 3 shows the terminal performance at the end of training and the performance of the remaining subjects on the 10 test trials. Here the mean score has been plotted for each trial. BAC levels obtained by Breathalyzer readings ranged from 0.056 to 0.19%, with a mean level of 0.11%.

As indicated in the figure, the mean performance of the group on the test trials is considerably below that of the predrink performance.

A t-ratio for the difference between the means of the last five training trials and the first five test trials was highly significant. ($t=11.03$, $P < 0.0005$)

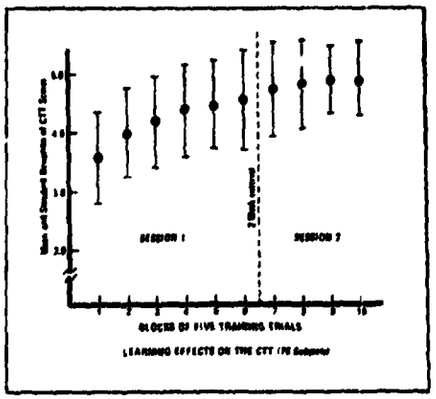

Figure 2

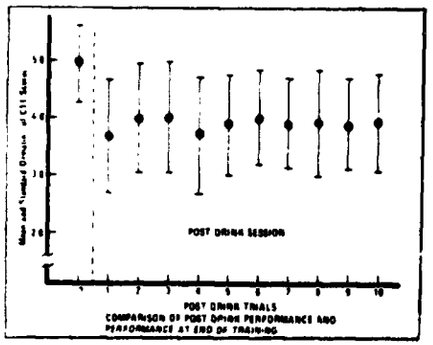

Figure 3

C. Group Comparisons

The range of BAC levels obtained in the test session provided an opportunity to examine the degree of deterioration on the task as a function of various BAC levels. For this analysis the subjects were assigned to one of the five groups indicated below according to the BAC level they reached.

Group 1	BAC 0.05 to 0.08%	N=9
Group 2	BAC 0.081 to 0.099%	N=16
Group 3	BAC 0.10 to 0.119%	N=19
Group 4	BAC 0.120 to 0.149%	N=21
Group 5	BAC 0.150 to 0.20%	N=4

The mean decrement in CTT scores for the five groups between the last block of training trials and the first block of five test trials for each subject is presented in Figure 4.

As indicated in Figure 4, all groups showed a deterioration in performance in the postdrink test session. The mean difference in performance between the last block of five training trials and the first five postdrink trials ranged from 15.4% for the low BAC Group 1 to 48.9% for the high BAC Group 5.

A t-ratio for the difference between the means of the last five training trials and the first five test trials was computed for each of the five groups and is presented in Table II. As indicated, the difference in performance for each group was significant at the 5.0% level.

D. Test Results Summary

This section presents the experimental data in a form that illustrates the effectiveness of the Critical Tracking Task as a potential alcohol ignition interlock device when the universal threshold approach is used. In particular, the data are analyzed by answering the two following questions:

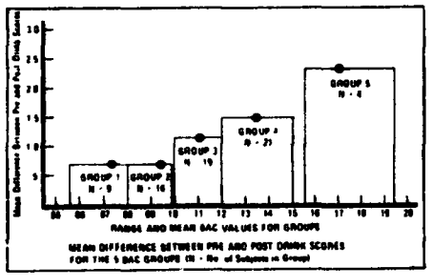

Figure 4

T-RATIOS FOR THE DIFFERENCE BETWEEN PRE AND POST DRINK CTT SCORES FOR THE FIVE GROUPS

GROUP	BAC RANGE	MEAN DIFFERENCE	SD	T RATIO	df	P
1	.056 - .081	.71	.219	3.24	8	< .05
2	.089 - .099	.76	.220	3.16	15	< .05
3	.109 - .119	1.15	.176	6.53	18	< .05
4	.129 - .149	1.48	.132	11.22	20	< .05
5	.156 - .192	2.30	.577	3.98	-	< .05

Table II

(a) If the CTT were mechanized as an ignition interlock, and a maximum limit on the percentage of sober failures (false rejection rates) that would be tolerated were stated, what would be the corresponding intoxicated failure rate at various BACs?

The answer to this question is given by Table III for ascending values of sober failure rates ranging from 0% to 3.0%. In addition, Table III stipulates the answers for:

(i) several test criteria (ratio of number of number of required successes to number of trials allowed) given in decreasing order of difficulty and involving the following: 1/1, 2/3, 1/2, and 1/3.

(ii) corresponding threshold values, λ_r, required.

As indicated, all trial criteria and λ_r conditions resulted in 100% failures for BACs equal to or greater than 0.15%, with decreasing intoxicated failure for lower BAC levels and lower λ_r threshold levels.

(b) If the CTT were mechanized as an ignition interlock, what would be the sober and intoxicated failure rates for various threshold values, λ_r, for:

(i) the following test criteria: 1/1, 2/3, 1/2, 1/3, in decreasing order of difficulty?

(ii) various blood alcohol concentrations?

The answer to this question is given by Table IV, where the data are presented as a function of increasing threshold levels (λ_rs) As expected, both the sober and intoxicated failure rates decrease with decreasing criterion difficulty.

As indicated in the tables the data presented are for experiments involving 67 sober subjects and 40 subjects at BACs at or above 0.10%.

Table III

SOBER VS INTOXICATED FAILURE RATE SUMMARY
FOR UNIVERSAL THRESHOLDS

SOBER FAILURE RATE (%)	THRESHOLD (λ_r)	CRITERION		INTOXICATED FAILURE RATE (%)				
		No. of Passes Required	No. of Trials Allowed	BAC ≥ 0.1%	BAC ≥ 0.12%	BAC ≥ 0.13%	BAC ≥ 0.14%	BAC ≥ 0.15%
0	3.7	1	1	57.5	62.5	68.8	81.8	100
0	3.7, 3.8, 3.9	2	3	55.0	62.5	75.0	81.8	100
0	4.0	1	2	50.0	54.2	62.5	72.7	100
0	4.0	1	3	42.5	50.0	56.3	63.6	100
1.5	3.8	1	1	57.5	62.5	68.8	81.8	100
1.5	4.1 & 4.2	1	3	47.5	58.3	68.8	72.7	100
3.0	4.0	1	1	62.5	66.7	75.0	81.8	100
3.0	4.1 & 4.2	1	2	60.0	66.7	75.0	81.8	100
3.0	4.4	1	3	62.5	70.8	87.5	90.9	100
N = 67				N = 40	N = 24	N = 16	N = 11	N = 4

N = No. of Subjects

Table IV

SUBJECT FAILURE RATES FOR THE CTT USING UNIVERSAL THRESHOLDS

UNIVERSAL THRESHOLD (λr)	CRITERION		BLOOD ALCOHOL CONCENTRATION (%)					
	No. of Passes Required	No. of Trials Allowed	0	0.10	0.12	0.13	0.14	0.15
3.8	1	1	1.5	57.5	62.5	68.8	81.8	100
	2	3	0	55.0	62.5	75.0	81.8	100
	1	2	0	45.0	50.0	66.3	63.6	100
	1	3	0	32.5	37.5	50.0	54.5	100
3.9	1	1	3.0	60.0	66.7	75.0	81.8	100
	2	3	0	55.0	62.5	75.0	81.8	100
	1	2	0	47.5	50.0	56.3	63.6	100
	1	3	0	37.5	41.7	50.0	54.5	100
4.0	1	1	3.0	62.5	66.7	75.0	81.8	100
	2	3	1.5	55.0	62.5	75.0	81.8	100
	1	2	0	50.0	54.2	62.5	72.7	100
	1	3	0	32.5	50.0	56.3	63.6	100
4.2	1	1	13.4	72.5	75.0	81.3	81.8	100
	2	3	4.5	65.0	70.8	81.3	90.9	100
	1	2	3.0	60.0	66.7	75.0	81.8	100
	1	3	0	47.5	58.3	68.8	72.7	100
4.4	1	1	16.4	75.0	79.2	87.5	90.9	100
	2	3	11.9	67.5	75.0	87.5	90.9	100
	1	2	7.5	65.0	75.0	87.5	90.9	100
	1	3	3.0	62.5	70.8	87.5	90.9	100
NO OF SUBJECTS			67	40	24	16	11	3

VI DISCUSSION

The data from the present study indicate that the CTT is a sensitive measure for detecting behavioral impairment resulting from alcohol (Tables III and IV). In fact, the data indicate that intoxicated failure rates of 50% for BACs at or above 0.1% and failure rates of 75% for BACs at or above 0.14% can be achieved with no sober failures. Perhaps one of the greatest assets of the task is that only a few parameters are involved in the test configuration, thus simplifying the optimization of the task and tending to minimize variability in performances. As mechanized in the study the task was readily learned, and most subjects approached an asymptotic level of performance in the unimpaired state within a relatively short time (Figure 2). Fast learning of the task is expected, since the operator is always pushed to his limit when the task is pursued until control is lost.

In addition to the use of existing vehicle hardware, the mechanization of the CTT in the automobile environment appears to correlate readily with the driving task, since it resembles the road-tracking portion required of driving. This is an important issue in the development of a performance test to be implemented as an ignition interlock system. Any such task should exercise those faculties that are considered dominant in driving and therefore have a significant correlation with the driving task.

Perhaps the most significant change between the laboratory unit used in the experiments reported herein and a vehicle integrated unit is the dynamic response of the Driver/CTT System. While the laboratory unit involved a small hand-control stick requiring only slight movements of the fingers and wrist, the steering wheel requires larger motions of the hand and arms, thus including large neuromuscular lags in the system. An additional hardware lag would undoubtedly be included

when replacing the oscilloscope display with a meter. The net expected effect of these time delays is a decrease in the critical limits (λ_{cr}) reached, but not necessarily a reduction or increase in the effectiveness of the task. Equivalent degradation in performance for the sober and intoxicated states would not affect the expected effectiveness of the device; however, the relative decrement in proficiency would have to be reevaluated. It will be important also to assess the relative performance decrement on a broader based sample of subjects statistically representing the driving population.

The dilemma faced in the development of any alcohol ignition interlock system is that under present laws the legal criterion for impairment resulting from the consumption of alcohol is based upon a BAC measure rather than a measure of behavioral impairment. While there exists a relationship between the two, there is obviously wide variability in proficiency among individuals both in a nonimpaired state and in the degree of impairment which develops under the same BAC. It is the area of overlap of these two distributions of behavior at the legally defined BAC level which complicates the development of a behavioral ignition interlock test. As a result, correlations of performance on the Critical Tracking Task with both BACs and driving proficiency will be included in a following program.

REFERENCES

(1) R. E. Allsop, Alcohol and Road Accidents. A Discussion of the Grand Rapids Study, Road Research Laboratory, Ministry of Transport, RRL Report No. 6, Harmondsworth Road Research Laboratory, 1966.

(2) Alcohol Safety Countermeasures Program, Nat. Hig.. Safety Bureau, June 8, 1970.

(3) T. O. Jones, J. A. Tennant, A Critical Evaluation of the Phystester: A Test for Dr ·er Impairment, American Association for Automotive Medicine, Chapel Hill, North Carolina, October 20, 1972.

(4) C. B. Gibbs, The Effect of Minor Alcohol Stress on Decision Processes in a Step-Tracking Task, IEEE Transactions on Human Factors in Electronics, Vol. HFE-7, No. 4, December, 1966.

(5) Alcohol and the Impaired Driver. A Manual on the Medicolegal Aspects of Chemical Tests for Intoxication. American Medical Association, 1968.

(6) P. W. Davis, E. D. Sussman, A. Warner, W. Z. Leavitt, Alcohol Safety Interlock Systems - A Status Report. Presented at the OECD International Symposium on Countermeasures to Driver Behavior, September, 1971, London, England.

(7) J. A. Tennant, and R. R. Thompson, A Critical Tracking Task as an Alcohol Interlock System, SAE 730095, January, 1973.

(8) H. R. Jex, J. D. McDonnell, and A. V. Phatak, A Critical Tracking Task for Man/Machine Research Related to the Operator's Effective Delay Time, 7th IEEE Symposium on Human Factors in Electronics, May 5, 6, 1966.

(9) R. W. Allen, and H. R. Jex, Visual-Motor Response of Crewmen During a Simulated 90-Day Space Mission as Measured by the Critical Task Battery, Seventh Annual NASA-Univ. Conference on Manual Control, USC, Los Angeles, California, June, 1971.

(10) L. R. Young and J. L. Meiry, Manual Control of an Unstable System with Visual and Motion Cues, IEEE Intern. Conven. Record, Vol. 13, Part 6, 1965, pp. 123-127.

EFFECTS OF ALCOHOL ON CONTINUOUS DRIVER CONTROL DYNAMICS*

Duane T. McRuer, Henry R. Jex, and R. Wade Allen†
Systems Technology, Inc., Hawthorne, California

Abstract

The nature of lateral control in elementary lane maintenance and regulation steering tasks is considered as a multiloop control system with the driver acting on heading and path deviations. A measurement methodology is evolved to permit the separation of path, heading, and neuromuscular components within the driver.

Experimental results for drunk and sober subjects are given. Path, heading, and neuromuscular properties all show some degradation associated with alcohol impairment. The sensitivity to path deviations usually degrade more than sensitivity to heading errors, indicating some difference in the control pathways involved and indirectly justifying the multiloop nature of the driver's guidance and control processes assumed.

Preliminary results are also given for the same driving task associated with a secondary detection, recognition, and response task, involving small discrete "command signs" presented randomly at ±20 and ±40 deg from the central view. The results support existing theories of scanning-while-tracking behavior. Some concurrent eye-scanning data are presented, showing sober/drunk differences and giving insight into the detailed nature of such discrete tasks.

*This work was sponsored by the National Highway Traffic Safety Administration under Contract DOT-HS-227-2-388, 1972-7 .

†President and Technical Director, Principal Research Engineer, and Senior Research Engineer, respectively.

PRECEDING PAGE BLANK NOT FILMED

Performance Assessment via the Critical Task and Dowel Balancing

Richard W. Pew
The University of Michigan

The visual motor coordination of 25 men and 25 women in each of two daily sessions was assessed by means of the critical task λ values and by the length of time each could balance 24-, 18-, and 12-inch dowels on the tip of his finger. Reliability from day to day fo both measures was respectably high (.88, .93), but the correlation between the critical task and dowel balancing scores was only .50. Although both tasks required control of unstable plants, it appears that the difference in physical conditions between manipulating a small joy stick in response to a CRT error display and using the whole arm in a standing position to correct for a tilting dowel are more important than might be expected a priori.

N75 19144

MEASUREMENT OF DRIVER/VEHICLE MULTILOOP RESPONSE PROPERTIES WITH A SINGLE DISTURBANCE INPUT

Duane T. McRuer, David H. Weir, Henry R. Jex,
Raymond E. Magdaleno, and R. Wade Allen*
Systems Technology, Inc., Hawthorne, California

ABSTRACT

Multiloop response properties of controllers are, in general, very difficult to obtain because an independent forcing function is needed for each describing function to be measured, and interpolation procedures may be required to obtain intermediate describing functions at common frequencies. Even then, a certain amount of untangling is required before the final results are obtained. When the loops which are closed and the nature of the describing function forms adopted in each loop are known or hypothesized, matters can be made much simpler. Then, the quantitative values of the individual describing functions can readily be identified using appropriate closed-loop describing function measures and decomposition procedures. Two examples are provided for the measurement of driver/vehicle multiloop response properties using a single disturbance input. The validity of the procedure is based on current multiloop operator adjustment rules and is made plausible by comparison with experimental data.

INTRODUCTION

The most common man/machine system in use today is a driver and an automobile, yet remarkably little is known empirically about the details of driver dynamic responses and how these interact with the vehicle dynamic characteristics. For instance, only one study of lateral control has been reported where driver describing functions were measured in an actual car (Ref. 1), and less than half a dozen studies have even been concerned with measurements in a simulator situation. A primary reason for this lack of attention resides in measurement difficulties due to the multiloop nature of most driver/vehicle system control situations of interest. The difficulties stem from the need for one independent input for each describing function to be measured, to the many couplings between the vehicle's state variables, to signal-to-noise problems, and last but not least, to data manipulation

*President and Technical Director, Principal Research Engineer, Principal Research Engineer, Senior Research Engineer, and Senior Research Engineer, respectively.

PRECEDING PAGE BLANK NOT FILMED

difficulties which include fairing and interpolation with already low confidence, dubious data and small differences between large uncertain numbers (Ref. 2). In spite of these difficulties, enough measurements now exist to support some key rules for multiloop human operations (Refs. 2-4). When these rules can be applied to specific situations, the fundamental difficulties can be bypassed and much simpler measurements can be made which nonetheless reflect the signficant multiloop human control characteristics (Refs. 5-6). In this paper these techniques are applied to the problem of driver steering control.

VEHICLE AND DRIVER SUBSYSTEM DYNAMICS

The object of control in the driver/vehicle system is the automobile. Its dynamic characteristics for essentially constant speed steering maneuvers can adequately be described by equations of motion involving side velocity, v, heading rate, r, and roll angle, φ. The roll mode is least important in nominal maneuvers and many of the roll effects, such as roll steer and camber thrust, can be partially accounted for in the lateral velocity and heading degrees of freedom. Accordingly, the constant velocity lateral-directional characteristics can often adequately be approximated by the two-degree-of-freedom set:

$$\begin{bmatrix} s - Y_v & U_o - Y_r \\ -N_v & s - N_r \end{bmatrix} \begin{bmatrix} v \\ r \end{bmatrix} = \begin{bmatrix} Y_\delta \\ N_\delta \end{bmatrix} \delta \qquad (1)$$

Approximate values for the stability derivatives in terms of vehicle parameters and the key vehicle transfer functions for control inputs are summarized in the appendix. More complete automobile descriptions in six degrees of freedom are provided in Ref. 7.

Turn now to the driver. Driving tasks are often multiloop in nature. That is, the driver responds to more than one vehicle motion quantity. The key to multiloop driver models is the fundamental concept of manual vehicular control analysis: that the operator constructs feedback loops about the effective controlled element. The feedback quantities available to him for possible use consist of those:

- Directly sensed within the general visual field.
- Observable via visual displays.
- Directly sensed using modalities other than vision.

Quantities which can be perceived from the fixated visual field will show no scanning penalties, whereas those which require instrument scan or modification of the fixation point will introduce decrements in some driver dynamic features. For lateral steering control the feedbacks are derived from the general visual field and possibly supplemented by non-visual modalities. The feedback quantities actually selected by the driver will be those needed to satisfy the guidance and control needs and certain driver-centered requirements. The guidance and control needs are situation-specific. In the steering case, they involve an outer loop for lateral position control and an appropriate inner loop to provide damping for the low-frequency mode formed by virtue of closing the lateral position loop. These requirements are, of course, essentially independent of whether the controller is animate or inanimate.

The driver-centered requirements are central to the manual control, as opposed to the general control, problem. The human propensities and behavior associated with these requirements must be discovered by experiment. From the data available (Refs. 2-4), a series of adjustment rules similar to those for single-loop manual control systems can be stated. These include:

1. The feedback loops preferred are those which:
   a. Can be closed with minimum operator equalization.
   b. Require minimum scanning.
   c. Permit wide latitude in variation in the operator's characteristics.
2. Where distinct inner- and outer-loop closures can be defined by ordering the bandwidths (i.e., the higher the bandwidth, the more inner the loop), a series multiloop structure applies.
3. The adjustment of the variable gains in each of the loops is, in general, similar to that which would be used by a skilled automatic control designer who has available the same feedback entities. To a first approximation:
   a. The crossover model is directly applicable to many inner loop closures.

   b. The crossover model also holds for the outer loop with the proviso that the effective controlled-element transfer function includes the effects of all the inner-loop closures.
4. When scanning is not present, the remnant is primarily associated with the inner loop and is essentially the same as that for a single-loop system equivalent to the inner loop alone.

Other rules apply to situations where scanning is present; these are not pertinent here.

DRIVER/VEHICLE SYSTEM STRUCTURE

The combination of driver and vehicle into an appropriate control system for lateral position can conceivably be accomplished using a wide variety of feedback quantities. A number of these have been investigated theoretically in Refs. 8 and 9. One of the most likely possibilities when guidance and control requirements, driver-centered requirements, availability of cues in the visual field, and interpretation of such experimental evidence as driver eye movements are considered is an outer loop in lateral position, y, and an inner loop involving either path angle or heading angle. Additionally, path rate and heading rate are pertinent for higher-frequency control action. When all evidence is taken into account, a very likely structure for many driving tasks is that shown in Fig. 1. In equation form, the quasilinear model for the driver is:

$$\delta_s = Y_y(j\omega)Y_\psi(j\omega)y_e(j\omega) - Y_\psi(j\omega)\psi(j\omega) + Y_\psi(j\omega)n(j\omega) \qquad (2)$$

The describing function, Y_yY_ψ, characterizes the driver's operations on functions of the position error, whereas Y_ψ alone represents the driver's operations on functions of heading angle. The portion of the driver's output which is not linearly correlated with any disturbance or command inputs is modeled by the remnant, n.

It is important to note that the above presumed structure in no way implies direct perception of either lateral position or heading angle as such, but only that the driver responds in part to some function of these

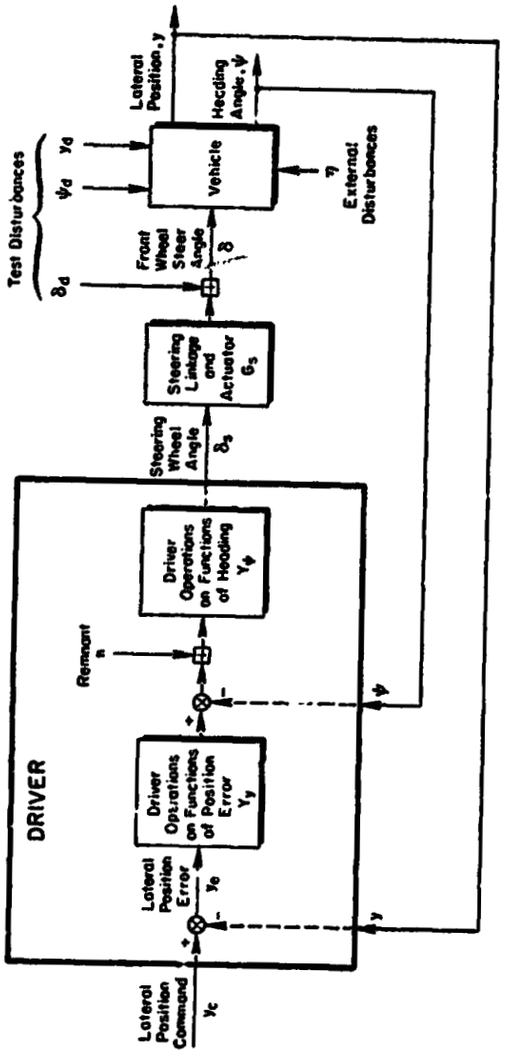

Figure 1 Block Diagram of Driver-Vehicle System for Lateral Steering Control

variables as sensed from the available visual field and non-visual modalities. In other words, although Eq. 2 is expressed explicitly in terms of lateral position and heading angle, any other possible feedbacks which are linear functions of y and ψ are also handled implicitly.

When y and ψ actually are the direct functions used by the driver in the experimental situation of interest, then in the light of the multiloop principles listed above heading should be an inner and lateral position an outer loop, and the low- and mid-frequency characteristics of Y_y should be a simple gain and those of Y_ψ a gain plus time delay. Since some vehicle dynamics present challenges which are readily overcome with heading rate, the higher-frequency portion of Y_ψ should include a lead. This can be considered as either high-frequency lead generation on ψ (with little or no degradation in effective time delay) or direct sensing of yawing velocity. The latter is pertinent for supra-threshold values of yawing velocity, r, as sensed by the vestibular system. Thus, the driver dynamics which we will ultimately use are given by:

$$Y_y = K_y$$
$$Y_\psi = K_\psi e^{-j\omega\tau}(T_L j\omega + 1) \qquad (3)$$

More extensive high-frequency characterization can be used with appropriate changes in τ. For example, when distinctions are to be drawn between different power steering systems, or when the effects of alcohol on the neuromuscular system are to be considered, a more extensive analytical description of the neuromuscular system can be added to Y_ψ with τ adjusted accordingly.

If interpretation of data obtained using these specific forms are in reasonable accord with analytical implications, then this would be strong indirect evidence that the driver used ψ and y feedbacks directly in accomplishing the particular driving task considered. If, on the other hand, Y_y or Y_ψ as deduced from the task-specific data are much more complex dynamic forms, then alternate feedbacks should be considered.

GENERAL SYSTEM EQUATIONS

In the study of driver/vehicle interaction in steering tasks, a number of system inputs require consideration. The most obvious are the lateral positional command, y_c, and external disturbances, η, because they are representative of actual roadway conditions. As shown in Fig. 1, y_c is actually present in the driver component of the closed-loop system, i.e., the lateral position command actually acting on the system is to some extent driver induced. The general character of the command is, however, determined by the roadway, lane pattern, obstacles to be avoided, etc. It can be as simple as a prescribed pathway with narrow tolerances and as complex as a tortuous way through freeway traffic. The external disturbances can arise from the atmosphere, such as yawing velocity, r_g, or side velocity, v_g, gusts, from roadway-induced disturbances, or from specially-contrived force and/or moment generators attached to the vehicle (e.g., a rocket). In addition to these inputs into the driver/vehicle system, various test disturbances are of interest for special measurement applications. The three most common are indicated in Fig. 1. The first, δ_d, is a front wheel steer angle applied in series with the driver's steering wheel input. The δ_d input is readily applied in actual or simulated cars by the addition of an extensible link or other differential device into the steering system. The heading and path disturbances, ψ_d and y_d, are primarily of values in simulator applications, where these signals are readily added within the equations of motion. These test disturbances enter the equations of motion at the locations shown in Fig. 2. They can, for example, be readily applied to the servo drive of a television camera used to generate the visual scene from a model landscape, as in Refs. 10 and 11 .

The equations of motion for lateral position and heading with these forcing functions and disturbances and using Y_y and Y_ψ for generality are given by:

$$\begin{bmatrix} (1+Y_yY_\psi G_s G_\delta^y) & Y_\psi G_s G_\delta^y \\ Y_yY_\psi G_s G_\delta^\psi & (1+Y_\psi G_s G_\delta^\psi) \end{bmatrix} \begin{bmatrix} y \\ \psi \end{bmatrix} = \begin{bmatrix} 1 & U_o/s & G_\delta^y & Y_yY_\psi G_s G_\delta^y & Y_\psi G_s G_\delta^y & G_\eta^y \\ 0 & 1 & G_\delta^\psi & Y_yY_\psi G_s G_\delta^\psi & Y_\psi G_s G_\delta^\psi & G_\eta^\psi \end{bmatrix} \begin{bmatrix} y_d \\ \psi_d \\ \delta_d \\ y_c \\ n \\ \eta \end{bmatrix}$$

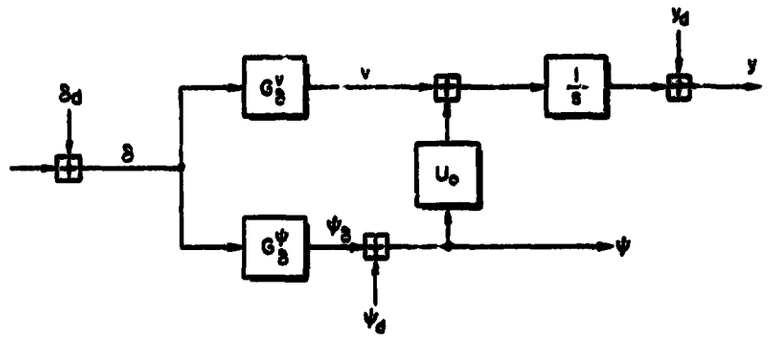

Figure 2. Test Disturbance Entry Locations in Vehicle Dynamics

The front wheel steer angle is provided by the auxiliary equation:

$$\delta = \delta_d + Y_yY_\psi G_s(y_c - y) + Y_\psi G_s(n - \psi) \qquad (5)$$

The closed-loop system responses of heading, lateral position, and front wheel steer angle are given as functions of the forcing function and disturbances in Table 1. The multiloop character of this system is indicated by the sum of $Y_\psi G_s G_\delta^\psi$ and $Y_yY_\psi G_s G_\delta^y$ in the denominator and the presence of the coupling numerator terms, $G_{\eta\delta}^{y\psi}$ and $G_{\eta\delta}^{\psi y}$, shown in the ψ and y numerator expressions (Ref. 12). The two primes on the denominator indicate that two loops are closed.

Closed-loop describing function measurements can be made using any of the forcing functions or disturbances, or combinations of these which are independent. Because the remnant acts as a continuous power spectral density, it will tend to contaminate any such measurements as a noise. However, if input power is large w compared with the remnant when both are reflected to a point of interest in the system, this contamination will be negligible. In any event, it can generally s assessed directly by consideration of the

TABLE 1

CLOSED-LOOP SYSTEM DYNAMICS

Denominator:

$$D'' = 1 + Y_\psi G_s (G_\delta^\psi + Y_y G_\delta^y) = 1 + Y_\psi G_s G_\delta^y \left[1 + \frac{U_o Y_y}{s} + \frac{Y_{\dot{y}}}{s} G_\delta^y \right]$$

y Numerator:

$$D''y = Y_y Y_\psi G_s G_\delta^y y_c + (1 + Y_\psi G_s G_\delta^\psi) y_d + Y_\psi G_s G_\delta^y n + G_\delta^y \delta_d + (G_\eta^y + Y_\psi G_s G_{\eta\delta}^{y\psi}) \eta + \left(\frac{U_o}{s} - Y_\psi G_s \frac{G_\delta^y}{s} \right) \psi_d$$

ψ Numerator:

$$D''\psi = Y_y Y_\psi G_s G_\delta^\psi y_c - Y_y Y_\psi G_s G_\delta^\psi y_d + Y_\psi G_s G_\delta^\psi n + G_\delta^\psi \delta_d + (G_\eta^\psi + Y_y Y_\psi G_s G_{\eta\delta}^{\psi y}) \eta + \left(1 + Y_y Y_\psi G_s \frac{G_\delta^y}{s} \right) \psi_d$$

δ Numerator:

$$D''\delta = Y_y Y_\psi G_s y_c - Y_y Y_\psi G_s y_d + Y_\psi G_s n + \delta_d - Y_\psi G_s (Y_y G_\eta^y + G_\eta^\psi) \eta - Y_\psi G_s \left(1 + \frac{U_o Y_y}{s} \right) \psi_d$$

relative power at the frequencies involved. One of the tricks in multiloop measurement is to select a family of describing functions which indicate high signal-to-noise ratios over particular (different) frequency ranges.

The fundamental measurement problem is to determine Y_y, Y_ψ, and remnant power spectral densities, Φ_{nn}. In principle, to obtain Y_y and Y_ψ separately, two independent inputs will be required. As noted already, the early work on multiloop human operator measurements had to use several independent inputs because the general nature of quantities such as Y_y and Y_ψ were to be discovered. Now that we have some appreciation for at least the likely form of these quantities, as given in Eq. 3, a simpler procedure can be used with only one input. The inputs to be considered should satisfy two fundamental criteria:

- The closed-loop describing functions should have a large frequency range over which signal to noise is high, i.e., remnant power should be small compared to forcing function or disturbance power at common points with the system.
- The closed-loop describing functions should be differentially sensitive to Y_y and Y_ψ in different frequency bands so that the properties of Y_y and Y_ψ can be readily untangled.

For these reasons, the principal disturbances and forcing functions that have been used are y_c, δ_d, ψ_d, and y_d. The first two are applicable to both actual vehicles on the road and simulator operations, whereas the latter two are suitable only in a simulator. Measurements with a disturbance, while having great value in peculiar situations, tend to be extraordinarily muddled because of the coupling features introduced via the coupling numerators. It is better to stay with inputs acting directly within one of the loops rather than a disturbance which is diffused into both loops via complex vehicular couplings.

Two particular examples will be illustrated in more detail below. These are describing functions measured with a steering or with a heading disturbance as the test input.

TYPICAL DESCRIBING FUNCTIONS WITH STEERING DISTURBANCES

The front wheel steer angle response with a steering disturbance as the system forcing characteristic and remnant is given by specialization of Table 1, i.e.:

$$\delta = \frac{1}{1 + Y_\psi G_s\left(G_\delta^\psi + Y_y G_\delta^y\right)}\left[\delta_d + Y_\psi G_s n\right] \tag{6}$$

At frequencies where remnant effects can be considered negligible, an effective open-loop system can be formed by considering δ_d as the input and δ the error. Then the quantity $\delta_d/\delta - 1$ parallels the quantity $(I/E) - 1$, which is equivalent to the open-loop transfer function in a single-loop system. Performing this operation gives:

$$\begin{aligned}
\frac{\delta_d}{\delta} - 1 &= Y_\psi G_s(G_\delta^\psi + Y_y G_\delta^y) \\
&= Y_\psi G_s\left[G_\delta^\psi\left(1 + \frac{U_o Y_y}{s}\right) + \frac{Y_y}{s} G_\delta^y\right] \\
&= Y_\psi\left[1 + \frac{U_o Y_y}{s} + \frac{Y_y}{s}\frac{G_\delta^y}{G_\delta^\psi}\right] G_s G_\delta^\psi \\
&= Y_p^* G_s G_\delta^\psi
\end{aligned} \tag{7}$$

where

$$\begin{aligned}
Y_p^* &= Y_\psi\left[1 + \frac{U_o Y_y}{s} + \frac{Y_y}{s}\frac{G_\delta^y}{G_\delta^\psi}\right] \\
&= Y_\psi\left[1 + Y_y \frac{G_\delta^y}{G_\delta^\psi}\right]
\end{aligned} \tag{8}$$

Here the quantity Y_p^* is seen to be obtained by taking the closed-loop response measurement, δ/δ_d, inverting it, subtracting 1, dividing out the known transfer function of the steering linkage and vehicle, $G_s G_\delta^\psi$. Y_p^* is particularly simple in form in that the driver's heading describing function, Y_ψ, is a multiplicative factor, while Y_y enters into the bracketed expression in a relatively simple way.

At this point, let us examine the properties of the bracketed expressions in Eq. 8. In terms of the lateral equations of the automobile, this is given by:

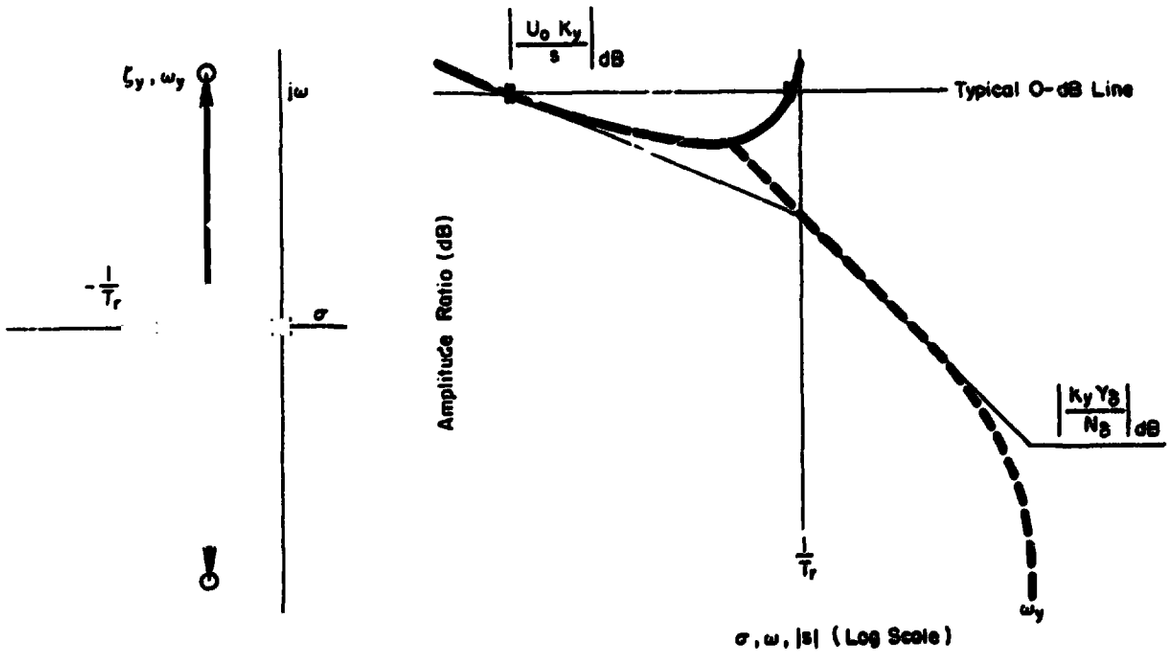

a) Conventional Root Locus *b) Bode Root Locus*

Figure 3. System Survey of Roots of $1 + K_y(G_\delta^y/G_\delta^\psi)$

$$1 + Y_y \left\{ \frac{G_\delta^y}{G_\delta^\psi} \right\} = 1 + Y_y \left\{ \frac{Y_\delta}{N_\delta} \; \frac{\left[s^2 + 2(\zeta\omega)_y s + \omega_y^2 \right]}{s(s + 1/T_r)} \right\} \tag{9}$$

Using the relationships developed in the appendix for the two-degrees of freedom equations this becomes:

$$1 + Y_y \left\{ \frac{G_\delta^y}{G_\delta^\psi} \right\} = 1 + Y_y \left\{ \frac{a}{k_z^2} \; \frac{\left[s^2 + \left(\frac{1}{T_r}\right)s + \frac{aU_o}{k_z^2}\left(\frac{1}{T_r}\right) \right]}{s\left(s + \frac{1}{T_r}\right)} \right\} \tag{10}$$

The roots of Eq. 9 can be readily evaluated if it is viewed as the result of a loop-closing operation in which the transfer function, $Y_y\{\;\}$, is the open-loop transfer function. At this point, we bring to bear the multiloop operator adjustment rules previously described and substitute for the general outer-loop driver describing function, Y_y, the much more specific form, K_y. A system survey which shows the roots of $1 + K_y\{\;\}$ is given in Fig. 3. The Bode root locus there indicates the closed-loop roots as the driver gain, K_y, is varied. The conventional root locus, which shows the same effects, is remarkable in that it is an example from practice of an academic anomaly, i.e., the damping of the quadratic zeros is approximately the same as the heading transfer function numerator inverse time constant, $1/T_r$. This approximation is exact for the two-degree-of-freedom lateral-directional equations when the z axis radius of gyration, k_z, is equal to the geometric mean between the car dimensions, a and b.

The path loop is the outer loop, so typically the gain, K_y, is relatively low. Then, a nominal zero dB line on the Bode root locus would be as shown in Fig. 3. The σ-Bode (locus of all real roots) is essentially on the low-frequency asymptote at this point; consequently, one of the roots will be given almost exactly by:

$$\sigma_1 = -U_o K_y \tag{11}$$

Because of the peculiar approximate relationship between $2(\zeta\omega)_y$ and $1/T_r$, the sum of the closed-loop roots is constant in spite of the variation in

gain (this is not, of course, true for a general open-loop system with a quadratic numerator and denominator). Under these special circumstances, the second root will be given by:

$$\begin{aligned} \sigma_2 &= -(1/T_r - U_o K_y) \\ &= -1/T_r' \end{aligned} \tag{12}$$

With these literal approximate factors, the value of $1 + K_y(G_\delta^y/G_\delta^\psi)$ becomes:

$$1 + K_y \frac{G_\delta^y}{G_\delta^\psi} \doteq \frac{U_o K_y \left(\frac{j\omega}{U_o K_y} + 1\right)\left(T_r' j\omega + 1\right)}{j\omega(T_r j\omega + 1)} \tag{13}$$

When the form for Y_ψ provided by the multiloop adjustment rules is used in conjunction with Eq. 13, the total describing function, Y_p^*, is seen to have the form:

$$Y_p^* \doteq \frac{U_o K_y K_\psi \left(T_L j\omega + 1\right)\left(\frac{j\omega}{U_o K_y} + 1\right)\left(T_r' j\omega + 1\right) e^{-j\omega\tau}}{j\omega(T_r j\omega + 1)} \tag{14}$$

An asymptotic Bode plot of this is shown in Fig. 4. Here, it will be noted that the low-frequency asymptote defines the outer-loop gain uniquely, while the mid-frequency horizontal asymptote is just the gain, K_ψ. The breakpoint between the very low-frequency and mid-frequency asymptotes is $U_o K_y$. The high-frequency breakpoint gives the indication of any inner-loop lead. Actual data are presented on Fig. 5. They show the same characteristic concave-upward basket-like shape of the sketch of Fig. 4. Quick approximations to the values of K_y, K_ψ, and $1/T_L$ are readily obtained by fairing in the asymptotic plot. By keeping in mind the shape and functional relations involved in the asymptotes, comparative describing function data and parameters can be directly assessed by eyeball.

Precise values for the driver characteristics are most easily determined with an optimal curve-fitting routine. The routine adjusts the Y_p^* parameters

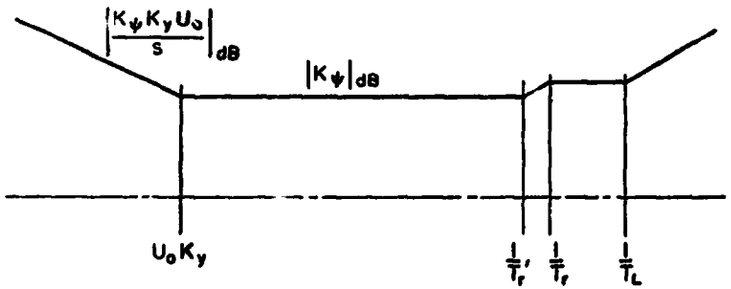

Figure 4. Asymptotic Bode Plot for $|Y_p^*|$

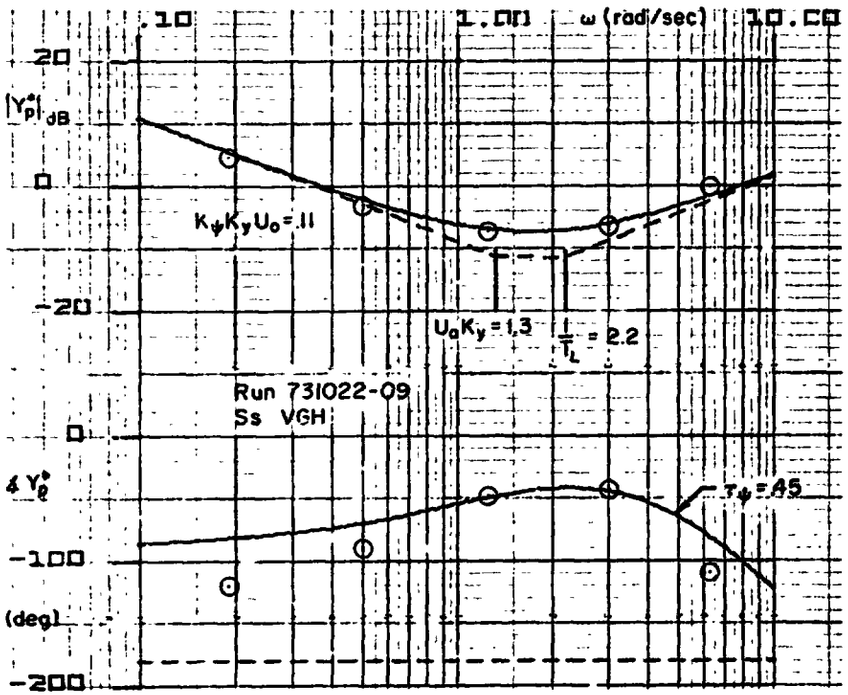

Figure 5. Example Y_p^* Data and Curve Fit

including the effective time delay, τ, to simultaneously fit amplitude and phase. An example curve fit is also shown on Fig. 5 (although the T_r, T_r' dipole in Eq. 14 was not included for simplicity).

As a practical matter, the measurements are quite simple to obtain with sums of sinusoids and on-line describing function measurements. These are then inexpensively reduced and curve-fitted on a routine basis. Thus, the previously highly-complex multiloop reduction procedures are reduced to an elementary and inexpensive set of operations. The shape of the data further confirms the multiloop describing rules presented earlier, in that the data behave according to the predictions.

Y_p^* data can be interpreted in alternate ways which are helpful when considering actual perceptual structures which the driver may be using. For example, excellent single-loop driver/vehicle systems result when the driver is assumed to act on the "time-advanced lateral deviation," $y(t+T)$, or the "aim-point-heading" error, ψ_L. Both are shown in Fig. 6 and both involve an aim point at a distance, R, down the road. With the first:

$$y(t+T) \doteq y + U_o \gamma T = (Ts+1)y \qquad (15)$$

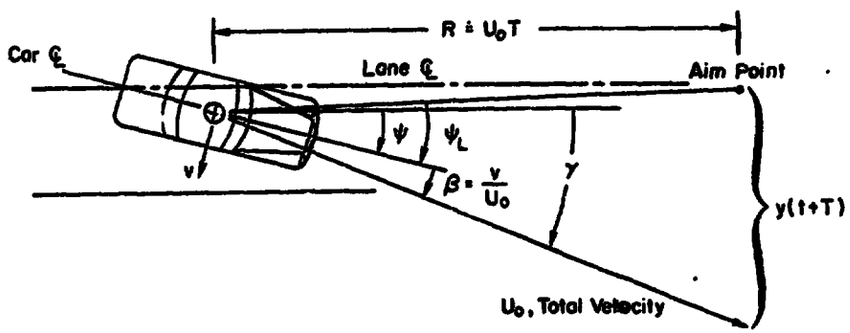

Figure 6. Motion Quantities for Directional Control

In this interpretation, the low-frequency lead breakpoint in Fig. 4 is just $1/T$. Thus:

$$1/T = U_o K_y \doteq U_o/R \tag{16}$$

Note that:

$$K_y \doteq 1/R \tag{17}$$

the inverse of the aim point distance down the road. With ψ_L, the aim point heading error:

$$\psi_L \doteq \psi + y/R \tag{18}$$

If the composite feedback quantity, $Y_\psi(\psi + K_y y)$, in Eq. 2 is identified with ψ_L, then K_y is simply $1/R$, just as above. With either of these variables as the basis for control, there is an effectively single-loop closure, with the kinematic relation $1/R$ corresponding to K_y, and $1/U_o K_y$ or R/U_o to the low-frequency lead time constant.

MULTILOOP DESCRIBING FUNCTIONS WITH HEADING DISTURBANCE

The closed-loop heading-to-heading-disturbance transfer function as obtained from Table 1 is:

$$\frac{\psi}{\psi_d} = \frac{1 + Y_y Y_\psi G_s \frac{1}{s} G_\delta^y}{1 + Y_\psi G_s \left[G_\delta^\psi \left(1 + \frac{U_o Y_y}{s} \right) + \frac{Y_y}{s} G_\delta^y \right]} \tag{19}$$

When this is considered in a fashion similar to that above, i.e., when ψ_d is taken as an input and ψ as the error of an equivalent single-loop feedback system, then the effective inner-loop describing function, $(\psi_d/\psi) - 1$, becomes:

$$\frac{\psi_d}{\psi} - 1 = Y_\psi G_s G_\delta^\psi \left[\frac{1 + \frac{U_o Y_y}{s}}{1 + Y_y Y_\psi G_s \frac{G_\delta^y}{s}} \right]$$

$$= Y_\psi G_s [G_\delta^\psi]' \tag{20}$$

where

$$[G_\delta^\psi]' = G_\delta^\psi \left[\frac{1 + \frac{U_o Y_y}{s}}{1 + Y_y Y_\psi G_s \frac{G_\delta^y}{s}} \right]$$

Here, the effective vehicle transfer function, $[G_\delta^\psi]'$, is the transfer function for the vehicle as seen by the heading loop as an outer loop, i.e., it reflects the lateral position loop closure. If, now, we insert the appropriate forms for vehicle and driver multiloop characteristics, Eq. 20 becomes:

$$\frac{\psi_d}{\psi} - 1 = \frac{U_o K_y K_\psi \left(\frac{j\omega}{U_o K_y} + 1 \right) \left(T_L j\omega + 1 \right) e^{-j\omega\tau_\psi}}{j\omega} \left[\frac{G_\delta^\psi(j\omega)}{1 + \frac{K_y K_\psi (T_L j\omega + 1) e^{-j\omega\tau_\psi} G_\delta^y(j\omega)}{j\omega}} \right] \tag{21}$$

An asymptotic Bode plot of this function is shown in Fig. 7. Here again the path loop dominates the low-frequency characteristics, while the heading inner loop is more significant at higher frequencies. In Fig. 7 note that the pole at very low-frequencies is non-minimum phase; hence, the phase curve starts at −270 deg. This pole arises from the terms in brackets in Eq. 21. This function can be used directly to fit data, as with the steering input considered previously. Typical data from Ref. 11, as well as some unpublished data from that series of experiments, is shown in Fig. 8. These data indicate a value of $U_o K_y$ of about 0.37 rad/sec whereby the low-frequency lead time constant is about 2.8 sec and, for a speed of 88 ft/sec (60 mph), the "aim point distance" would be about 240 ft.

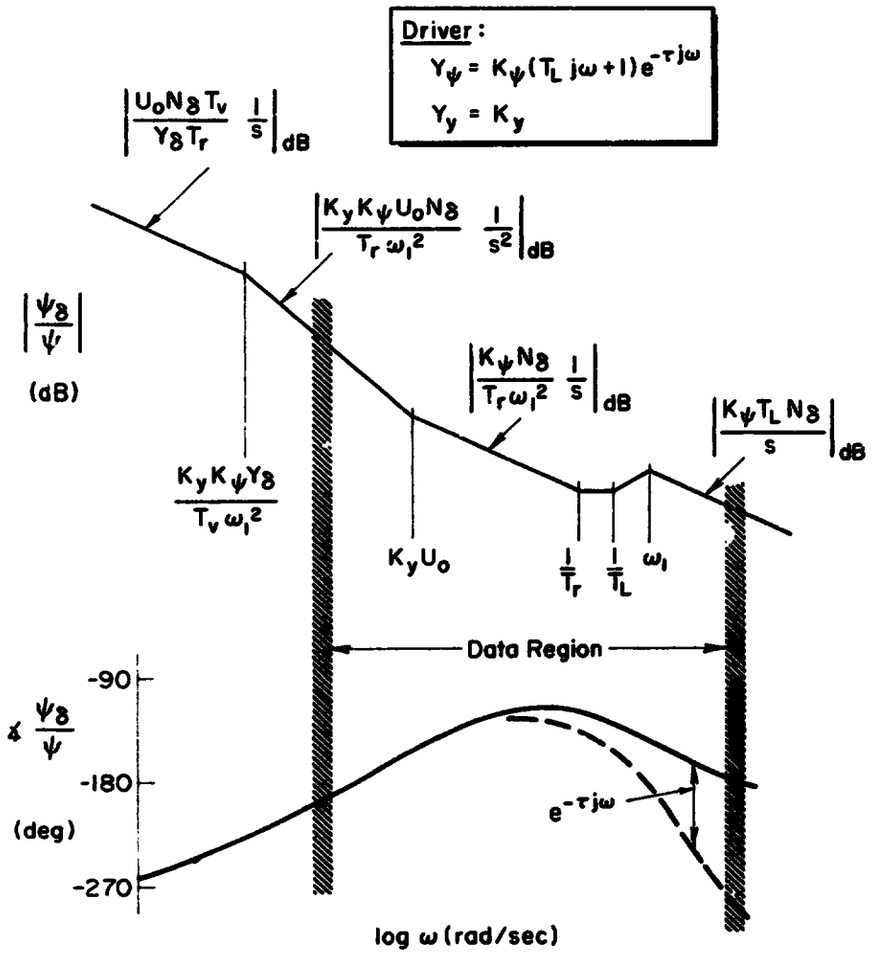

Figure 7. Open-Loop Driver/Vehicle Describing Function for Heading

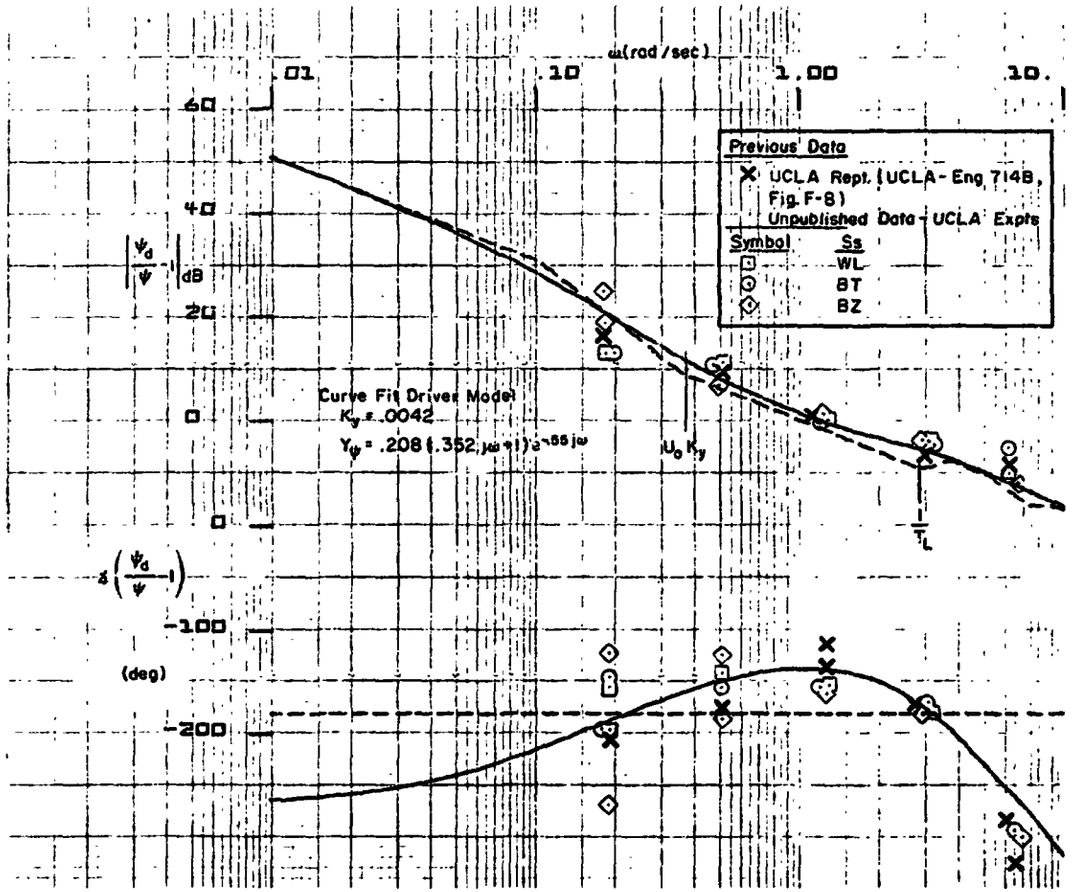

Figure 8. Effective Inner-Loop Describing Function Data and Curve Fit

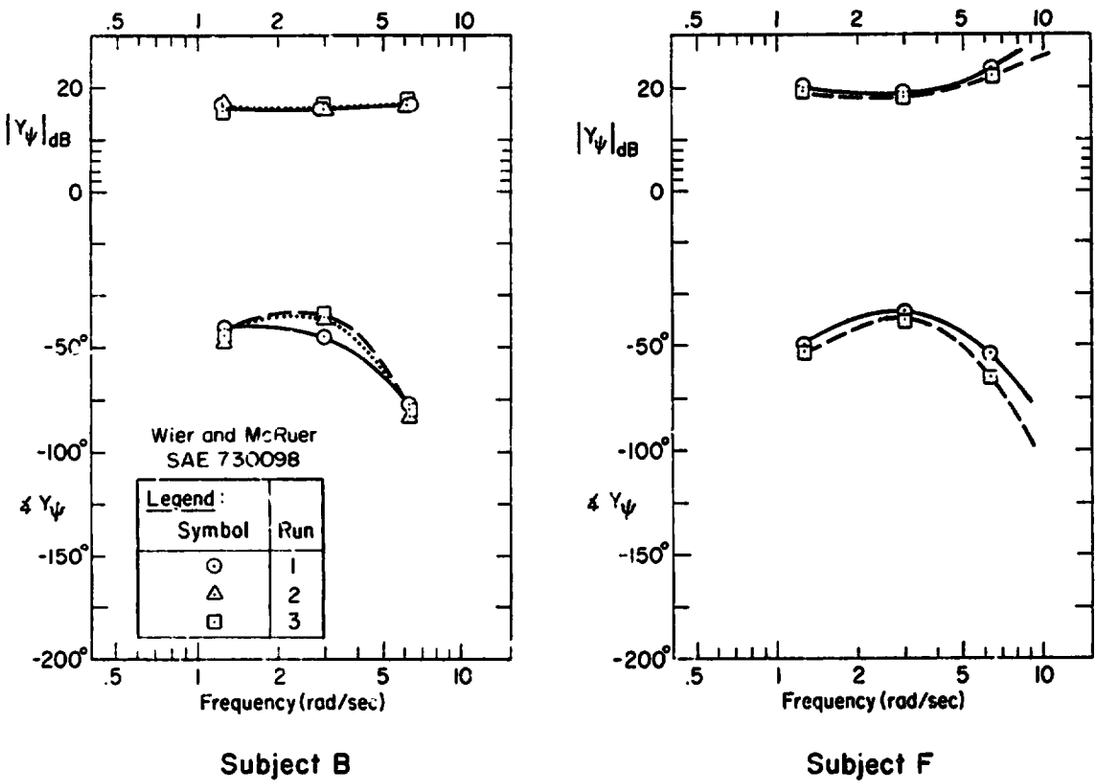

Figure 2. Interpreted Driver Alone Describing Functions for Inner Loop, Y_ψ (Ref. 13)

At upper middle to high frequencies, the effective vehicle transfer function, $[G_\delta^\psi]'$, is hardly affected by the path closure. Thus, at these frequencies:

$$[G_\delta^\psi]' \doteq G_\delta^\psi$$

and (22)

$$\frac{\psi_a}{\psi} - 1 \doteq Y_\psi G_s G_\delta^\psi \qquad \text{at higher frequencies}$$

The driver's heading response describing function, Y_ψ, can then be isolated from the equivalent open-loop system high-frequency properties by removing the known vehicle and steering subsystem dynamic characteristics, $G_s G_\delta^\psi$. Typical data, from Ref. 13, are shown in Fig. 9. These demonstrate clearly the difference between Subject B and Subject F in that only the latter uses high-frequency lead generation. Again, the fact that data, such as shown in Figs. 8 and 9, tend to follow the trends predicted using the multiloop adjustment rules provides further verification.

Finally, an interesting comparison of the features of describing functions obtained from heading vs. steering disturbances can be seen in the low-frequency regions of Figs. 9 and 8. The Y_p^* steering disturbance case has K_y effects changing the low-frequency amplitude while the phase is insensitive (starting at −90 deg for any value of K_y). Just the opposite occurs for the heading disturbance case in Fig. 8 where the amplitude is relatively insensitive, while the phase curve moves directly with K_y.

CONCLUSIONS

The point of view taken in this paper permits the simple and routine estimation of the more significant driver characteristics in steering control tasks. The fundamental difficulties of multiloop measurements are avoided by tailoring the driver loop structure per the currently understood multiloop human operator adjustment rules. The simplifications so obtained permit multiloop car/driver situations to be analyzed as easily as systems which are essentially single loop and single input.

NOMENCLATURE

a	Distance of mass center aft of the front axle
b	Distance of mass center forward of the rear axle
G_s	Steering linkage transfer function
G_δ^v	Vehicle transfer function between steer angle and lateral velocity
G_δ^ψ	Vehicle transfer function between steer angle and heading angle
I_{zz}	Vehicle yaw moment of inertia
k_z	Vehicle radius of gyration, $\sqrt{I_{zz}/m}$
K_y	Driver gain for lateral position control
K_ψ	Driver gain for heading control
m	Vehicle mass
n	Driver remnant
r	Yawing velocity (heading angle rate)
s	Laplace transform complex variable
U_o	Nominal forward velocity
v	Side velocity
y	Lateral position of mass center (relative to an inertial frame)
y_c	Lateral position command to driver
y_d	Lateral position disturbance
Y_y	Driver describing function for lateral position control
Y_{α_1}	Side force due to front tire slip angle
Y_{α_2}	Side force due to rear tire slip angle
Y_ψ	Driver describing function for heading angle control
γ	Path angle
δ	Front wheel steer angle

δ_d Steer angle disturbance

δ_s Driver steering wheel angle

η General external disturbance

τ_e Effective time delay

ψ Heading angle

ψ_d Heading angle disturbance input

ω Frequency

REFERENCES

1. Delp, P., E. R. F. W. Crossman, and H. Szostak, "Estimation of Automobile-Driver Describing Functions From Highway Tests Using the Double Steering Wheel," Seventh Annual Conf. on Manual Control, USC, 2-4 June, 1971, NASA SP-281, pp. 223-236.

2. Stapleford, R. L., S. J. Craig, and J. A. Tennant, Measurement of Pilot Describing Functions in Single-Controller Multiloop Tasks, NASA CR-1278, Jan. 1969

3. Stapleford, R. L., D. T. McRuer, and R. Magdaleno, Pilot Describing Function Measurements in a Multiloop Task, NASA CR-542, Aug. 1966.

4. Weir, D. H., and D. T. McRuer, Pilot Dynamics for Instrument Approach Tasks: Full Panel Multiloop and Flight Director Operations, NASA CR-2019, May 1972.

5. Teper, G. L., "An Effective Technique for Extracting Pilot Model Parameter Values From Multi-Feedback, Single-Input Tracking Tasks," Eighth Annual Conf. on Manual Control, U. of Mich., 17-19 May 1972, pp. 23-34.

6. Teper, G. L., An Assessment of the "Paper Pilot" — An Analytical Approach to the Specification and Evaluation of Flying Qualities, AFFDL-TR-71-174, June 1972.

7. Weir, D. H., C. P. Shortwell, and W. A. Johnson, Dynamics of the Automobile Related to Driver Control, SAE Paper 680194, Feb. 1967.

8. Weir, D. H., and D. T. McRuer, "A Theory for Driver Steering Control of Motor Vehicles," Highway Res. Record No. 247, 1968, pp. 7-28.

9. Weir, D. H., and D. T. McRuer, "Dynamics of Driver/Vehicle Steering Control," Automatica, Vol. 6, No. 1, 1970, pp. 87-98.

10. Weir, D. H., and C. K. Wojcik, "Simulator Studies of the Driver's Dynamic Response in Steering Control Tasks," Driving Simulation, Highway Res. Record No. 364, 1971, pp. 1-15.

11. Wojcik, C. K., and R. W. Allen, Studies of the Driver as a Control Element, Phase 3, UCLA-ENG-7148, July 1971.

12. McRuer, D., D. Graham, and I. Ashkenas, Aircraft Dynamics and Automatic Control, Princeton Univ. Press (forthcoming).

13. Weir, D. H., and D. T. McRuer, Measurement and Interpretation of Driver Steering Behavior and Performance, SAE Paper No. 730098, Jan. 1973.

APPENDIX

LATERAL-DIRECTIONAL VEHICLE DYNAMICS

The two-degree-of-freedom lateral-directional equations for a car are given in Eq. 1. The stability derivatives are defined in terms of vehicle and tire design parameters by the expressions below.

$$Y_v = \frac{-2}{mU_o}(Y_{\alpha_1} + Y_{\alpha_2})$$

$$N_v = \frac{2}{I_{zz}U_o}(bY_{\alpha_2} - aY_{\alpha_1})$$

$$Y_r = \frac{2}{mU_o}(bY_{\alpha_2} - aY_{\alpha_1})$$

$$N_r = \frac{-2}{I_{zz}U_o}(a^2Y_{\alpha_1} + b^2Y_{\alpha_2})$$

$$Y_\delta = \frac{2}{m}Y_{\alpha_1}$$

$$N_\delta = \frac{2a}{I_{zz}}Y_{\alpha_1}$$

ORIGINAL PAGE IS OF POOR QUALITY

The transfer functions of interest are:

Heading Angle:

$$\frac{\psi}{\delta} = G_\delta^\psi = \frac{1}{s} G_\delta^r = \frac{N_\delta (s + 1/T_r)}{s[s^2 + 2\zeta_1\omega_1 s + \omega_1^2]}$$

Side Velocity:

$$\frac{v}{\delta} = G_\delta^v = \frac{Y_\delta (s + 1/T_v)}{[s^2 + 2\zeta_1\omega_1 s + \omega_1^2]}$$

Lateral Position:

$$\frac{y}{\delta} = G_\delta^y = \frac{Y_\delta (s^2 + 2\zeta_{y,y} s + \omega_y^2)}{s^2[s^2 + 2\zeta_1\omega_1 s + \omega_1^2]}$$

where

$$2\zeta_1\omega_1 = -(Y_v + N_r) \quad ; \quad \omega_1^2 = N_v(U_o - Y_r) + Y_v N_r$$

$$1/T_r = -Y_v + \frac{Y_\delta}{N_\delta} N_v \quad ; \quad 1/T_v = -N_r - \frac{N_\delta}{Y_\delta}(U_o - Y_r)$$

$$2\zeta_{y,y} = -N_r + \frac{N_\delta}{Y_\delta} Y_r \quad ; \quad \omega_y^2 = \frac{U_o N_\delta}{Y_\delta}\left(-Y_v + \frac{Y_\delta}{N_\delta} N_v\right) = \frac{U_o N_\delta}{Y_\delta}\left(\frac{1}{T_r}\right)$$

In terms of the vehicle parameters:

$$\frac{1}{T_r} = \frac{2}{mU_o}\left(\frac{a + b}{a}\right) Y_{\alpha_r}$$

$$2\zeta_{y,y} = \frac{2b}{I_{zz}U_o}(a + b)Y_{\alpha_r} = \frac{mab}{I_{zz}}\left(\frac{1}{T_r}\right) = \frac{ab}{k_z^2}\left(\frac{1}{T_r}\right)$$

If the radius of gyration in yaw, k_z, is the geometric mean of the c.g. to axle dimensions, a and b, then $2\zeta_{y,y}$ will be equal to $1/T_r$.

ABSTRACT

AN EXPERIMENTAL STUDY OF THE MOTORCYCLE ROLL STABILIZATION TASK

David J. Eaton

The stabilization task of the motorcycle rider has been studied experimentally, using data from actual road tests. In each experiment, the test subject, whose upper body was restrained by a rigid brace, controlled the motorcycle roll angle by applying a steering torque to the handlebars. Roll angle, roll rate, steering torque, and steering angle were recorded for three test subjects. Experiments were restricted to the steady-state, straight path, constant forward speed (usually 30 mph) situation.

The strongest source of excitation to the man-motorcycle system was found to be the rider's remnant. To minimize bias errors in identifying a linear transfer function representing the rider, a technique developed by Wingrove and Edwards of the NASA Ames Research Center was employed. The results are consistent with a theoretical analysis of the man-motorcycle system, using classical automatic control theory.

N75 19145

AN EXPERIMENTAL STUDY OF THE MOTORCYCLE ROLL STABILIZATION TASK

David J. Eaton
Highway Safety Research Institute
The University of Michigan
Ann Arbor, Michigan

April, 1973

AN EXPERIMENTAL STUDY OF THE MOTORCYCLE ROLL STABILIZATION TASK

1. INTRODUCTION

Although the literature concerning motorcycle and bicycle dynamics is not large, such research usually has been concerned with the uncontrolled single-track vehicle. The work of Sharp [1] represents the most complete theoretical analysis of the uncontrolled motorcycle presently available, and serves as a theoretical basis for the study described herein. Sharp's analysis included roll, yaw, lateral translation, and steering degrees of freedom, and the resulting equations are linear with constant coefficients. For use here, tire aligning moments due to tire sideslip have been added to Sharp's equations.

Of the few existing studies of a man and single-track vehicle as a closed-loop control system, the most significant are Van Lunteren, et al. (e.g., [2, 3]) and Weir [4]. While the former research represents a pioneering effort in obtaining rider transfer functions experimentally (with a bicycle simulator), it should be pointed out that Van Lunteren's major interest was the performance of the human operator under various conditions (drugs, etc.) and not the dynamics of the bicycle. Thus, the accuracy of the simulator dynamics with respect to real bicycles and the validity of the assumption of steering angle control (rather than steering torque) are questionable. On the other hand, the work of Weir, although strictly theoretical, was based upon the motion equations and motorcycle parametric data of Sharp, and represents a comprehensive study of the man-motorcycle system.

It is the purpose of the work described here to present experimental results and relate them to the theoretical studies of Sharp and Weir.

2. DESCRIPTION OF EXPERIMENTS

The particular rider task under consideration here is stabilization of the vehicle roll angle by means of steering torques applied to the handlebars. Path following and control by body movements are not being studied. From theoretical considerations, Weir [4] has shown that roll stabilization is best accomplished by steering torque control and that body lean control is more suited to the path following task. An "inner loop" of the multi-loop man/motorcycle control system postulated by Weir is shown in Figure 1, in which ϕ is the roll angle, t_δ is the rider-applied steering torque, i includes wind and road disturbances, and n is the rider's remnant. The block diagram of Figure 1 represents the man-motorcycle system model that is used in the present study.

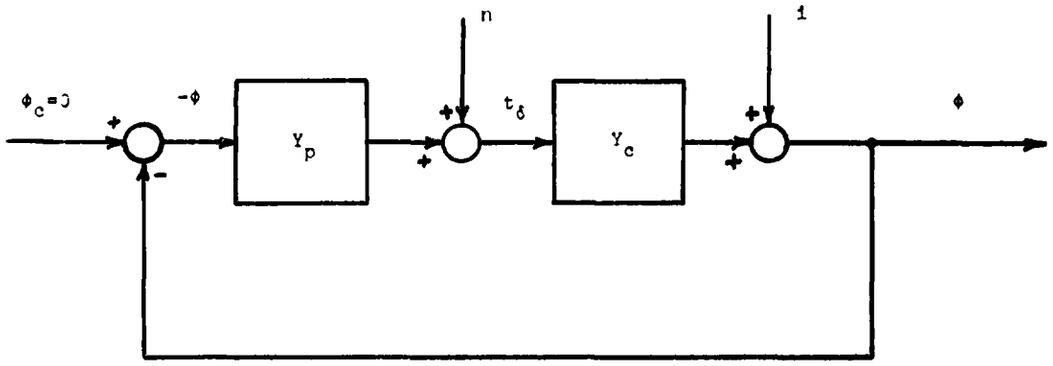

Figure 1. Block diagram of the man-motorcycle system.

The motorcycle transfer function, or controlled element, $Y_c(j\omega)$, can be calculated from the equations of motion of Sharp [1]. It will be shown that both $Y_c(j\omega)$ and the rider transfer function, $Y_p(j\omega)$, can also be obtained experimentally.

To restrict the experiments to the roll stabilization task, road tests were performed on a 0.5-mile section of essentially straight paved road in good condition. The test motorcycle was operated next to an automobile, which carried the power supplies and recording equipment. Figure 2 shows the experimental situation, including the rigid brace mounted on the motorcycle to reduce rider body lean, and the third wheel that was used to measure roll angle. (Also visible is a horizontal arm supporting two weights which was removed for these experiments.) Additional instrumentation included a rate gyro to sense roll rate, a steering angle potentiometer, and a strain-gaged bar to record steering torques. With this torque bar, it was necessary for the rider to steer with one hand. Throttle control was relocated to the rear frame. The effect of this unusual control arrangement upon the generality of the results is not known, but it is felt that any such effects were small and, at least, considerably smaller than they would have been if the rider had been using position control instead of torque control.

Three experienced riders, denoted Rider A, Rider B, and Rider C, were tested. These riders were chosen to be of approximately the same weight (170-196 lb.) to minimize changes in $Y_c(j\omega)$ due to variations in rider mass and mass distribution.

A total of fifteen experiments were performed with Rider A (the author). These experiments took place on two days about four months apart. On the first day, experiments began with a 30 mph test, followed by a 15 mph test, followed by a 30 mph test, etc., until eleven total were recorded, with three of each speed being suitable for analysis. The remaining nine tests were selected from a group of ten (all at 30 mph) performed on the second day.

On a single day, a total of thirteen tests were carried out with Rider B, with twelve of these being suitable for analysis. Similarly, on a single day, twelve tests were recorded with Rider C, eleven tests being suitable for analysis. Both riders were instructed to ride at a constant 30 mph while minimizing body movements with the aid of the brace attached to the motorcycle. A few practice runs were made before recording was begun.

The duration of each 30 mph test was about 50-60 seconds, while the 15 mph tests lasted about 65 seconds.

A major objective of the experiments was to identify the rider transfer function, $Y_p(j\omega)$. Since the wind/road disturbance i is unknown, it is necessary to estimate $Y_p(j\omega)$ by an open-loop method. To reduce bias errors arising from a correlation between n and ϕ, a method developed by Wingrove and Edwards [5, 6, 7, 8] must be employed. When the remnant autocorrelation function is sufficently small for lags less than or equal to the rider's time delay, τ_p, this method can remove most of the bias errors by first identifying $e^{\lambda j\omega}Y_p(j\omega)$, the transfer function having $-\phi(t-\lambda)$ as input and $t_\delta(t)$ as output, where $0 < \lambda \leq \tau_p$, since there is much less correlation between $\phi(t-\lambda)$ and $n(t)$ than between $\phi(t)$ and $n(t)$. The Wingrove-Edwards method must be coupled with an identification procedure that is constrained to identify only physically realizable systems. The impulse response method [6, 9], which first identifies a discrete form of the impulse response function of the unknown system, and then determines the transfer function by Fourier transformation, is such a procedure and has been used in this study.

3. DISCUSSION OF RESULTS

Preliminary analysis of the experimental data for 30 mph tests indicated that the theoretical controlled element, $Y_c(j\omega)$, could be accurately identified with the following relationship:

$$\hat{Y}_c(j\omega) = \frac{\hat{S}_{\phi t_\delta}(\omega)}{\hat{S}_{t_\delta t_\delta}(\omega)}, \qquad (1)$$

where $\hat{Y}_c(j\omega)$ is the estimate of $Y_c(j\omega)$, $\hat{S}_{\phi t_\delta}(\omega)$ is the estimated cross-spectrum between ϕ and t_δ, and $\hat{S}_{t_\delta t_\delta}(\omega)$ is the estimated power spectrum of t_δ. An example of such an identification is shown in Figure 3. The theoretical $Y_c(j\omega)$, calculated from the equations of motion and the motorcycle parametric data measured for the test vehicle (Appendix A), is shown for comparison. The identification is seen to be the closest to the theoretical controlled element for frequencies of about 1-4 radians/second, where most of the power of the roll angle and steering torque records is located.

The fact that the theoretical $Y_c(j\omega)$ can be identified experimentally provides support for the motorcycle equations of motion and also indicates that the rider's remnant, n, is a much greater source of excitation to the man-machine system than the wind/road disturbance, i. When the remnant is the primary disturbance to the system, the Wingrove-Edwards method is required to identify $Y_p(j\omega)$.

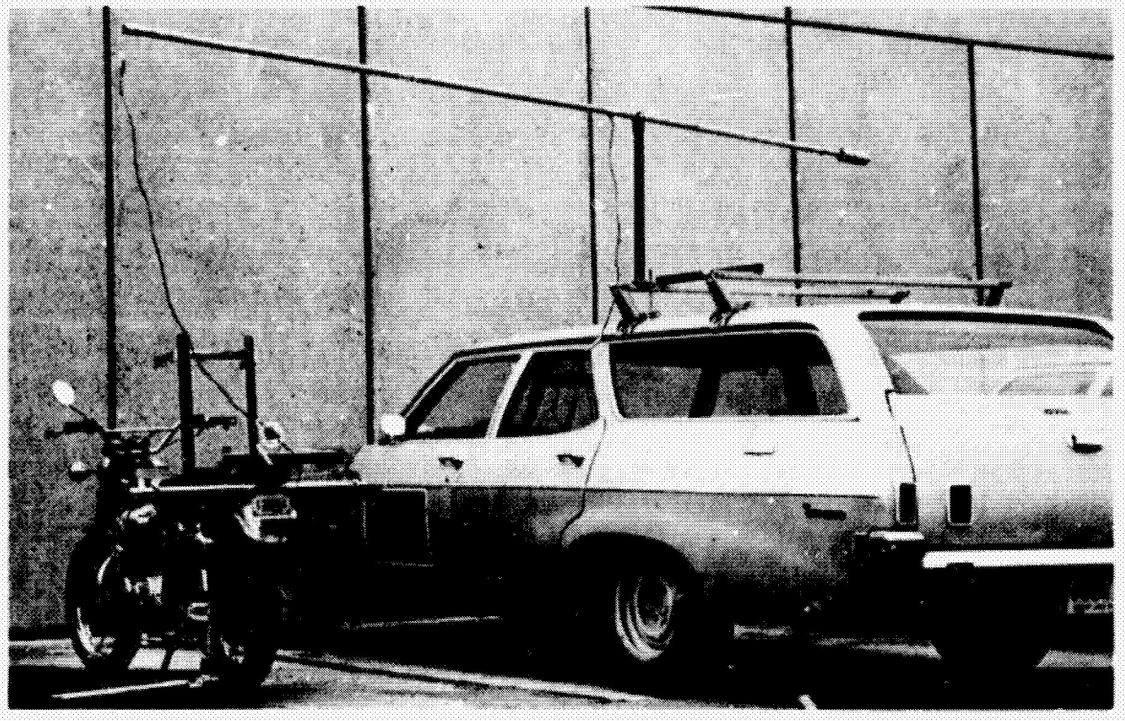

Figure 2. Test motorcycle and instrumentation car.

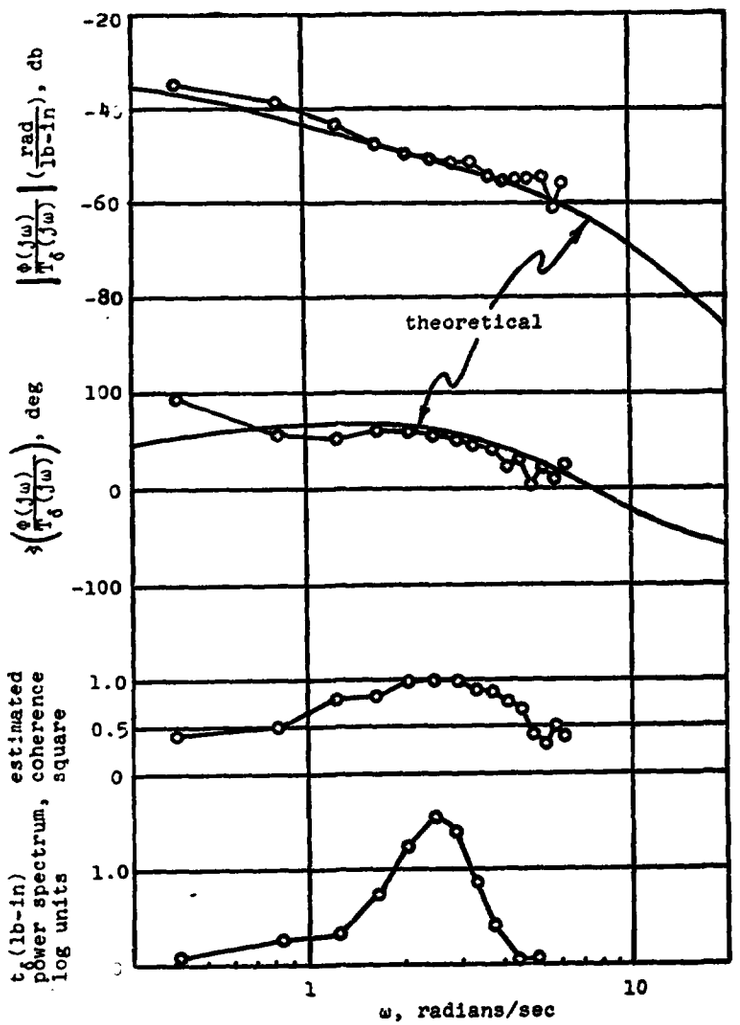

Figure 3. Identification of $Y_c(j\omega)$, 30 mph.

Since the impulse response and Wingrove-Edwards methods are not nearly as well documented in the literature as spectral analysis techniques, some rules regarding the interpretation of Bode diagrams of $\hat{Y}_p(j\omega)$ were derived from applying the methods to the identification of known systems from artificially created data, as outlined in Appendix B. A further aid to the interpretation of $\hat{Y}_p(j\omega)$ Bode diagrams was obtained by assuming the remnant power spectrum to be "white" and calculating the expected power spectrum of t_δ, based on the estimate of $Y_p(j\omega)$ and the theoretical $Y_c(j\omega)$ (including the effect of the analog filter applied to the data).

Two example identifications of $Y_p(j\omega)$ are shown in Figure 4. In general, the form of $Y_p(j\omega)$ for the 30 mph tests was found to be

$$Y_p(j\omega) = -K_p e^{-\tau_p j\omega}(T_\ell j\omega + 1). \tag{2}$$

The value of T_ℓ was negligibly small, except for the tests carried out with Rider A on the second day. Thus, for most of the 30 mph tests, a rider transfer function of the form,

$$Y_p(j\omega) = -K_p e^{-\tau_p j\omega}, \tag{3}$$

fits the data. In the three 15 mph tests the rider transfer function was of the form

$$Y_p(j\omega) = -K_p j\omega e^{-\tau_p j\omega}(T_\ell j\omega + 1). \tag{4}$$

Estimated mean values of the parameters in Equations (2-4) are presented in Table 1. The confidence intervals for the true mean values were calculated on the assumption that the estimates of the means were unbiased. Since this assumption may not be valid, more certainty may be attached to the width of the confidence interval than its midpoint.

The resulting rider transfer functions were found to be consistent with the crossover model, which was employed by Weir [4] in his theoretical analysis of the man-motorcycle system. The crossover model requires that

$$Y_p(j\omega)Y_c(j\omega) \doteq \frac{\omega_c e^{-\tau_e j\omega}}{j\omega}, \quad \omega \doteq \omega_c,$$

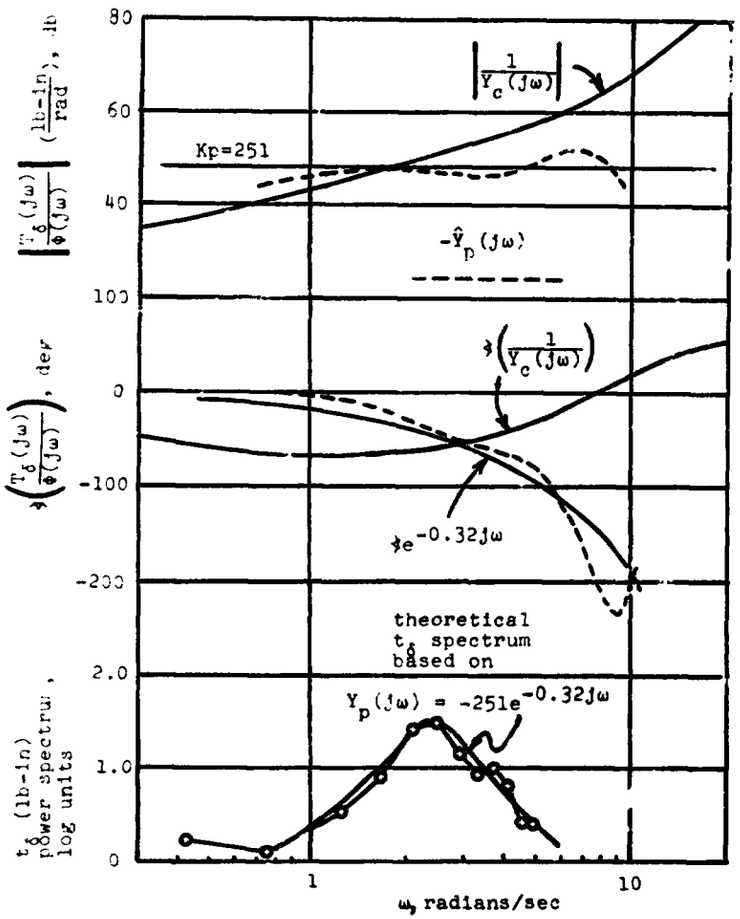

Figure 4a. Identification of $Y_p(j\omega)$ for a single test (Rider A, 30 mph, first day).

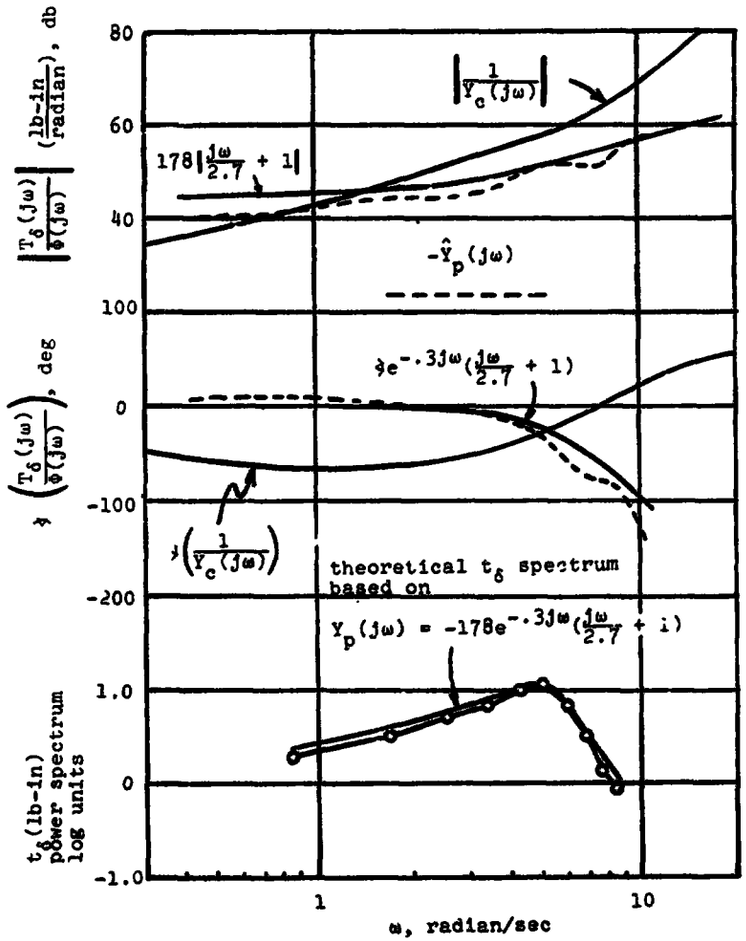

Figure 4b. Identification of $Y_p(j\omega)$ for a single test (rider A, 30 mph, second day; the case in which $\hat{Y}_p$ evidenced the most lead).

TABLE 1

SUMMARY OF RIDER TRANSFER FUNCTIONS

	Day of Test	1	1	2	3	4
	Speed, mph	15	30	30	30	30
	Rider	A	A	A	B	C
	Form of $\hat{Y}_p(j\omega)$	$-K_p j\omega e^{-\tau_p j\omega} \cdot (T_\ell j\omega + 1)$	$-K_p e^{-\tau_p j\omega}$	$-K_p e^{-\tau_p j\omega} \cdot (T_\ell j\omega + 1)$	$-K_p e^{-\tau_p j\omega}$	$-K_p e^{-\tau_p j\omega}$
Mean Values of Estimated Quantities	K_p, $\frac{\text{lb-in}}{\text{radian}}$	75.6	277	261	167	206
	τ_p, seconds	0.300	0.298	0.300	0.328	0.299
	$1/T_\ell$ $\frac{\text{radians}}{\text{second}}$	9.04		6.45		
	ϕ_m, degrees	25	28.3	48.6	41.4	39.1
90% Confidence Intervals	K_p, $\frac{\text{lb-in}}{\text{radian}}$	(53.6, 97.6)	(219, 335)	(236, 286)	(152, 182)	(185, 227)
	τ_p, seconds	(.216, .384)	(.260, .336)		(.287, .369)	(.276, .322)
	$1/T_\ell$ $\frac{\text{radians}}{\text{second}}$	(3.37, 11.42)		(5.27, 7.41)		
	ϕ_m, degrees		(15.2, 41.4)	(42.4, 54.8)		(36.7, 41.5)
Parameters for Cross-over Model, Based on Average $\hat{Y}_p(j\omega)$	ω_c, $\frac{\text{radians}}{\text{seconds}}$	3.2	2.0	1.9	1.3	1.5
	τ_e, seconds	0.370	0.533	0.393	0.572	0.533

where ω_c is the crossover frequency. Figure 5 shows a Bode diagram of $\bar{Y}_p(j\omega)Y_c(j\omega)$, where $\bar{Y}_p(j\omega)$ is the average of the estimated rider transfer functions from the second test day (from Table 1), and a Bode diagram of $\bar{Y}_p(j\omega)\bar{Y}_c(j\omega)$ for the 15 mph tests. In the 15 mph situation, it was necessary to use the average of $Y_c(j\omega)$, as estimated from Equation (1), because there was noticeably less agreement between the theoretical Y_c and the experimental Y_c, as compared with the 30 mph tests. It can be seen that, with appropriate values of ω_c and τ_e, the crossover model closely fits the experimental results near the crossover frequency. The values of ω_c and τ_e that were selected for each group of data are included in Table 1.

As shown in Figure 3, $|Y_c(j\omega)|$ at 30 mph has a br d region of a -20 db/decade slope, with a steeper drop-off near 0 radians/second. As speed decreases, this drop-off moves to lower frequencies. Thus, to fit the crossover model, increasing amounts of lead equalization are required as speed decreases. At 30 mph, however, lead is optional.

Estimates of the remnant power spectra were made from the estimated rider impulse response functions. These calculated spectra, which, precisely speaking, were based on the estimates of $Y_p(j\omega)$ before they were fitted by Equations (3-4), were generally of the form

$$S_{nn}(\omega) \approx \frac{\text{Constant}}{25 + \omega^2} ,$$

the form that would be obtained if "white" noise were passed through a first order filter having a break frequency of 5 radians/second, which, in fact, was the filter applied to the data before digitizing. Thus, to at least about 10 radians/second, the actual unfiltered remnant is apparently "white", as was assumed earlier.

The estimated remnant consists of all the steering torque output of the rider that is not related to the roll angle by the linear transfer function $-Y_p(j\omega)$. The remnant contains (1) rider output which is nonlinearly related to the roll angle, (2) path correction steering torques not linearly related to the roll angle (such as corrections needed due to the real road not being perfectly straight, obstacle or bump avoidance, etc.), (3) miscellaneous steering torques, voluntary or involuntary (including direct mechanical transmission of road shocks through the rider's arms to the handlebars, although road shocks are high frequency phenomena and would not be included in the estimated remnant), (4) any time variation in $Y_p(j\omega)$, and (5) errors in identifying $Y_p(j\omega)$. Since the rider is using torque control for purposes other than roll stabilization, it was found that the mean square remnant was a large proportion of the mean square steering torque: from 30-95%. It is

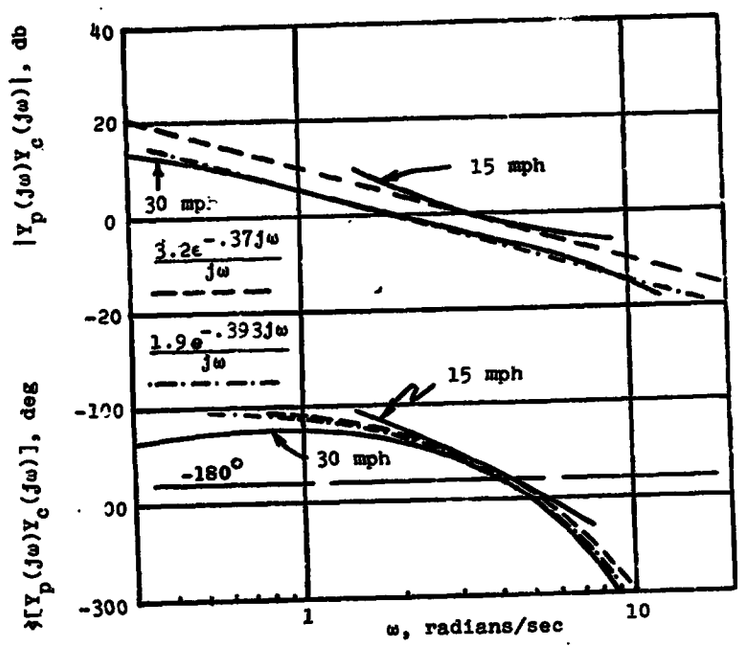

Figure 5.

Crossover model approximations to $\bar{\hat{Y}}_p(j\omega)Y_c(j\omega)$ (rider A, 30 mph, second day average, $\bar{\hat{Y}}_p(j\omega) = -26.1e^{-.3j\omega}(\frac{j\omega}{6.45} + 1)$), and $\bar{\hat{Y}}_p(j\omega)\bar{\hat{Y}}_c(j\omega)$ (rider A, 15 mph, first day average, $\bar{\hat{Y}}_p(j\omega) = -75.6j\omega e^{-.3j\omega}(\frac{j\omega}{9.0} + 1)$).

not known how much of this is due to errors in estimating $Y_p(j\omega)$. Probably the identification errors increased with the remnant, since a large remnant tended to make accurate identification of $Y_p(j\omega)$ more difficult.

4. CONCLUSIONS

1. During normal operation on a paved road in good condition, the primary excitation to the man-motorcycle system is the rider's "remnant". This fact allows accurate identification of the controlled element ($Y_c(j\omega)$) by open-loop cross-spectral analysis, at least for the frequency range in which there is substantial amplitude of the records being analyzed. Agreement between the theoretical and experimental $Y_c(j\omega)$ is better at 30 mph than at 15 mph.

2. The Wingrove-Edwards method [5] can be used to identify $Y_p(j\omega)$, the transfer function of the rider for the task studied. The experimental steering torque power spectra were helpful in interpreting Bode diagrams of $Y_p(j\omega)$.

3. At 30 mph, the rider transfer function $Y_p(j\omega)$ was found to be a constant gain and time delay, with the optional inclusion of lead equalization having a break frequency in the neighborhood of 5-10 radians/sec. Time delays were about 0.3 second for all the tests, and gains were about 250-350 lb-in/radian.

4. Only three experiments were performed at 15 mph, but the results of these indicated that a combination of rate control and lead equalization (break frequency, 5-10 radians/second) was required on the part of the rider. Here the time delays were about 0.25-0.35 second, and the gains were about 60-90 lb-in/radians.

5. The experimental results agree with the crossover model, which has been used to theoretically study the man-motorcycle system [4].

6. Most of the rider's steering torque output was remnant. The power spectrum of n(t) was found to have about the same shape as that of "white" noise passed through the same filter that was applied to the original analog records.

REFERENCES

1. Sharp, R.S., "The Stability and Control of Motorcycles," Journal Mechanical Engineering Science, Vol. 13, No. 5, 1971.

2. Van Lunteren, A., and Stassen, H.G., "Investigations on the Characteristics of a Human Operator Stabilizing a Bicycle Model," Intern. Symp. on Ergonomics in Machine Design, Prague, 1967.

3. Van Lunteren, A., and Stassen, H.G., "On the Variance of the Bicycle Rider's Behavior," 6th Annual Conference on Manual Control, Wright Patterson AFB, Ohio, 1970.

4. Weir, D.H., "Motorcycle Handling Dynamics and Rider Control and the Effect of Design Configuration on Response and Performance," Ph.D. Thesis, University of California (L.A.), 1972.

5. Wingrove, R.C., and Edwards, F.G., "Measurement of Pilot Describing Functions from Flight Test Data with an Example from Gemini X," 4th Annual NASA - University Conference on Manual Control, The University of Michigan, March 1968.

6. Wingrove, R.C., and Edwards, F.G., "A Technique for Identifying Pilot Describing Functions from Routine Flight-Test Records," NASA TN D-5127, May 1969.

7. Wingrove, R.C., "Comparison of Methods for Identifying Pilot Describing Functions from Closed-Loop Operating Records," NASA TN D-6235, March 1971.

8. Edwards, F.G., "Determination of Pilot and Vehicle Describing Functions from the Gemini-10 Mission," NASA TN D-6803, May 1972.

9. Taylor, L.W., Jr., "A Comparison of Human Response Modeling in the Time and Frequency Domains," Third Annual NASA-University Conference on Manual Control, University of Southern California, L.A., March 1-3, 1967.

10. Jenkins, G.M., and Watts, D.G., Spectral Analysis and Its Applications. Holden-Day, San Francisco, 1969.

APPENDIX A

MEASUREMENT OF MOTORCYCLE PARAMETERS

To calculate the theoretical $Y_c(j\omega)$ from the motorcycle equations of motion [1], it was necessary to make a number of measurements of the test vehicle.

In addition to geometric measurements, mass and mass distribution estimates were made for the front wheel, fork and handlebar assembly, and the total motorcycle with Rider A in place on the seat. (The brace in Figure 2 was used.) The following quantities were measured:

1. Masses
2. Center of gravity locations
3. Roll moments of inertia (x-axis)
4. Yaw moments of inertia (z-axis)
5. XZ products of inertia

It was necessary to attach the front frame assembly and the entire vehicle to fixtures to measure mass distribution. Moments of inertia were measured with cable-suspended torsional pendula, except for the roll moment of inertia of the man-motorcycle combination, for which measurements were made by swinging the assembly on knife edges.

Additionally, wheel polar moments of inertia were measured with a torsional pendulum arrangement. An effective polar moment of inertia for the engine and transmission was calculated from data supplied by the manufacturer.

Tire properties were obtained from the HSRI flat bed tire tester. Measurements included the dependence of tire lateral force and aligning moments on slip and inclination angles, and the tire relaxation length.

Friction in the steering head was estimated and found to be negligible, on the basis of analog computer studies not discussed here.

APPENDIX B

IDENTIFICATION OF KNOWN TRANSFER FUNCTIONS

Artificial data were prepared by digital computer as follows: a subroutine generated a series of random numbers $z(kh)$, $k=1,2,\ldots 500$, $h=0.1$ second, where $z(kh)$ was normally distributed with mean zero. The artificial remnant was calculated from

$$n(kh) = \alpha_1 n[(k-1)h] + z(kh), \quad k=1,2,\ldots 500$$

The theoretical autocorrelation function of $n(kh)$ is [10]

$$r_{nn}(k'h) = \alpha_1^{\,|k'|}, \quad k'=0,\pm 1,\pm 2,\ldots \quad .$$

The "rider" and "motorcycle" transfer functions were taken to be

$$Y_{p_1}(j\omega) = e^{-0.4j\omega},$$

$$Y_{p_2}(j\omega) = 1.5e^{-0.4j\omega},$$

and

$$Y_c(j\omega) = \frac{1}{j\omega} \quad .$$

The degree of bias in estimating $Y_p(j\omega)$ by the Wingrove-Edwards method is increased by increasing $r_{nn}(\tau_p) = r_{nn}(0.4)$ [5], or, in this case, by increasing α_1. Zero bias results if $r_{nn}(\tau)=0$ for $\tau > 0.4$.

Figure 6 shows the identification of Y_{p_1} when $\alpha_1 = 0.3$ ($r_{nn}(0.4) = .0081$) and Y_{p_2} when $\alpha_1 = 0.8$ ($r_{nn}(0.4) = 0.41$). In general, $|\hat{Y}_{p_2}|$, which is more biased, tends more toward $1/Y_c(j\omega)$ at the higher and lower frequencies than $|\hat{Y}_{p_1}|$. Further, $\measuredangle(Y_{p_2})$ is underestimated for $\omega > 2$ radians/second. If the bias is increased further, it has been found that both $|\hat{Y}_p|$ and $\measuredangle(Y_p)$ tend to be underestimated. On the other hand, it is seen that $|\hat{Y}_{p_1}|$ and $\measuredangle(\hat{Y}_{p_1})$, which should not be strongly biased, tend to be slightly overestimated.

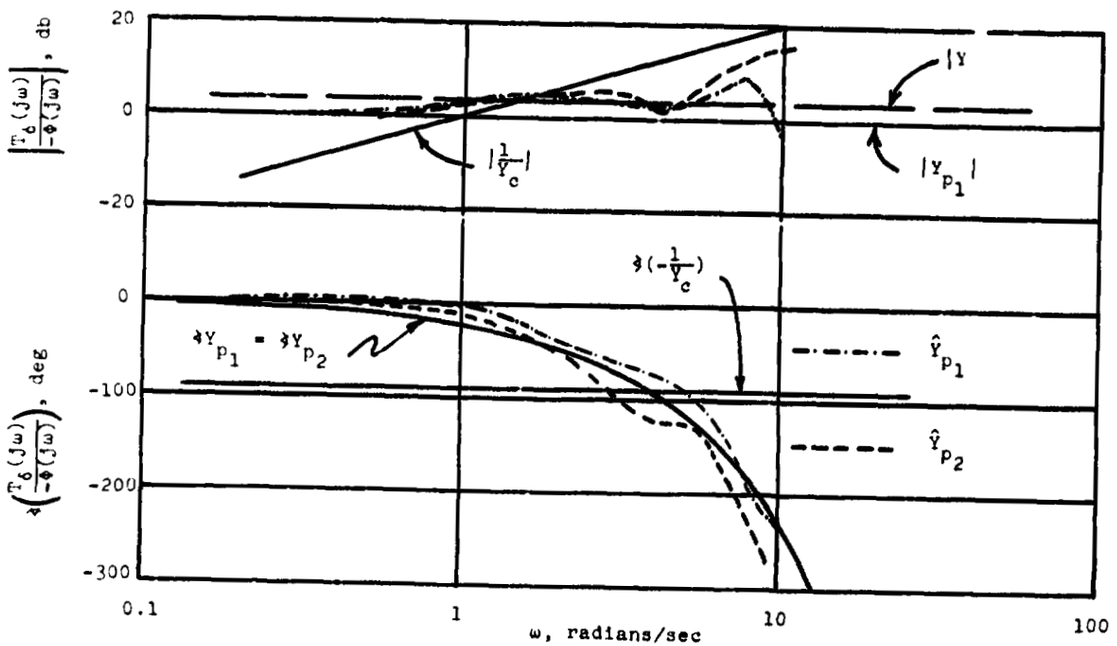

Figure 6. Identification of known "rider" transfer functions from artificial data by the time shifting method.

ORIGINAL PAGE IS
OF POOR QUALITY

N75 19146

COMPARISONS OF POPULATION SUBGROUPS PERFORMANCE ON A KEYBOARD PSYCHOMOTOR TASK

R[illegible]ert L. Stapleford*
Systems Technology, Inc., Hawthorne, California

ABSTRACT

Response time and pass/fail data were obtained from 163 subjects performing a psychomotor task. The basic task comprised a random five digit number briefly displayed to the subject at the start of each trial, and the keyboard on which the subject was to enter the number as fast as he could accurately do so after the display was extinguished. Some tests were run with the addition of a secondary task which required the subject to respond to a displayed light appearing at a random time.

Matched pairs of subjects were selected from the group to analyze the effects of age, sex, intelligence, prior keyboard skill, and drinking habits. There was little or no effect due to age or drinking habits. Differences in response time were: average IQ subjects faster than low IQ subjects by [illegible] to [illegible].6 sec; subjects with prior keyboard skill faster by 0.4 to 0.5 sec; and female subjects faster by [illegible] to 0.3 sec. These effects were generally insensitive to the presence of the secondary task.

TASK

At the initiation of the task, a random five digit number was displayed to the subject for [illegible] sec. After the light was extinguished the subject was to enter the number on an adding-machine-like keyboard. He was instructed to enter the number as rapidly as he could without making an error.

The task was done with and without a divided attention task (DAT). For the DAT [illegible] light came on at a random time within a window of 1.0 to 4.0 sec after the five digit number was extinguished. The subject then had 3.0 sec to extinguish the DAT light by pressing a foot pedal.

For each trial the following data were recorded:

- Primary reaction time — time to enter five digit number
- Secondary reaction time — time to respond to DAT if present
- Pass or fail — failures were due to entering the wrong number, not completing the DAT in time, or starting to enter the number too [illegible]

* Principal Research Engineer.

PRECEDING PAGE BLANK NOT FILMED

Subjects were recruited at offices of the California Motor Vehicle Department and Human Resources Development. Each subject who was accepted was given a drinking-profile test (based on NIMH-HEW studies) and a short IQ test. They were then briefed on the purpose of the experiment and the details of the task. They were then given approximately 63 trials on the task without the DAT. The first 15 trials were excluded from the subsequent data analysis. They were then briefed on the operation of the DAT and given another 63 trials on the task with the DAT. The first 10 trials of this second set were also excluded from the data analysis.

GROUP COMPARISONS

This section describes the analysis of the differences among various subsets of the subject population. The analysis was specifically done to determine if there are any systematic effects of differences in subject intelligence, keyboard skill, sex, drinking habits, and age. For each of the five comparisons, matched pairs of subjects were selected. For example, in the comparison of average and low IQ subjects the low IQ subjects were isolated first, as this was the smaller subset of the population. We then attempted to match each low IQ subject with an average IQ subject. The matching was done on the basis of the other four factors, i.e., keyboard skill, sex, drinking habits, and age. Low IQ subjects which could not be matched on the other four factors were dropped from the comparison. Thus for each comparison we had matched pairs of subjects, where the matching was done over four factors and the effects of the fifth were then tested.

In each group comparison several parameters were analyzed. These included mean reaction times and standard deviations for the group. Here we considered the primary reaction time with and without the DAT and also the DAT reaction time. In addition to the mean and standard deviation, a histogram of the group reaction time was obtained. Examples of these histograms are shown in Fig. 1.

While the group histograms are interesting as an indication of population characteristics, they are not too informative about the population members. The problem is whether the group distribution is due to the

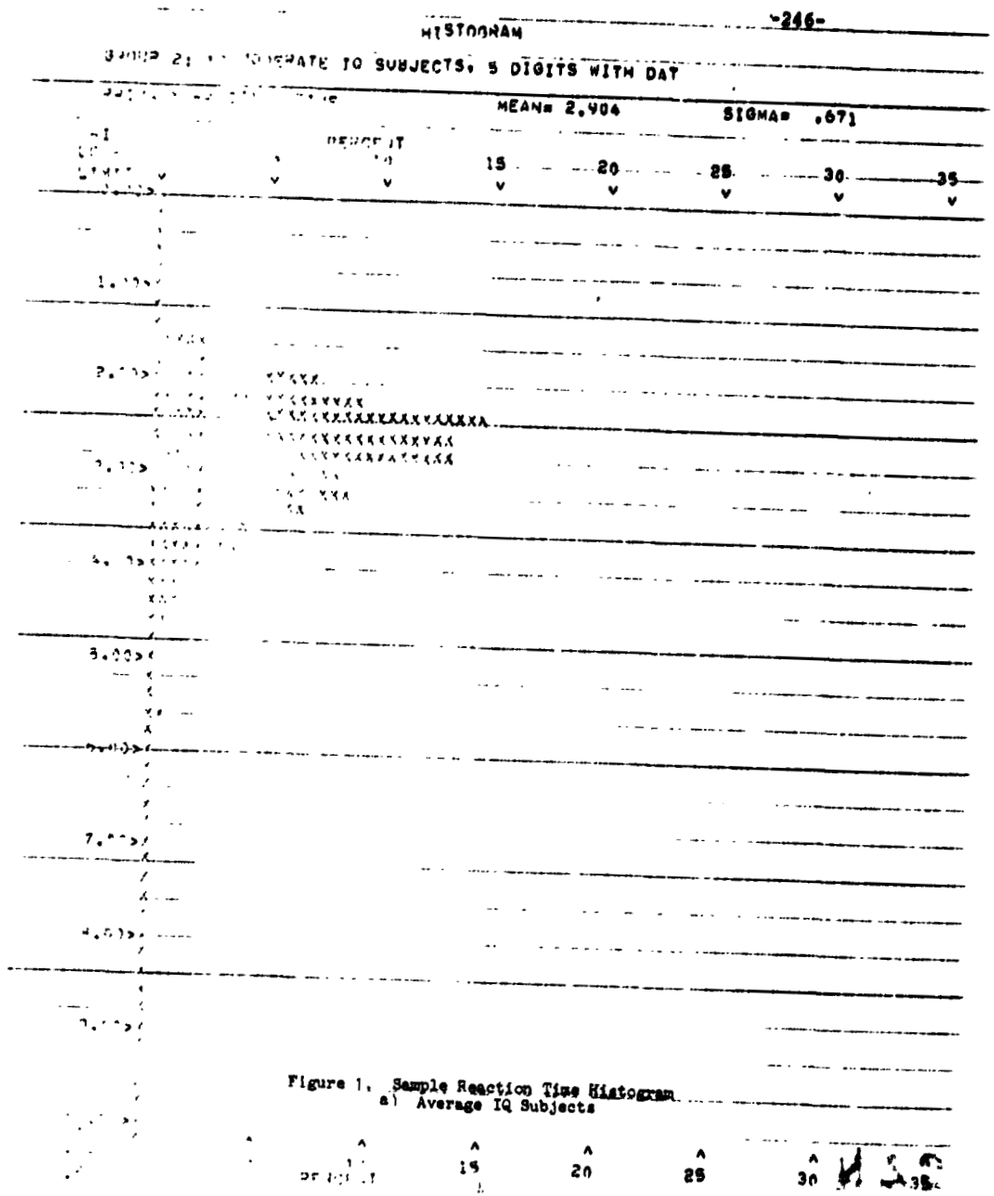

Figure 1. Sample Reaction Time Histogram
a) Average IQ Subjects

ORIGINAL PAGE IS
OF POOR QUALITY

HISTOGRAM

GROUP 1: 10 LOW IQ SUBJECTS, 5 DIGITS WITH DAT

PRIMARY REACTION TIME MEAN= 3.495 SIGMA= .841

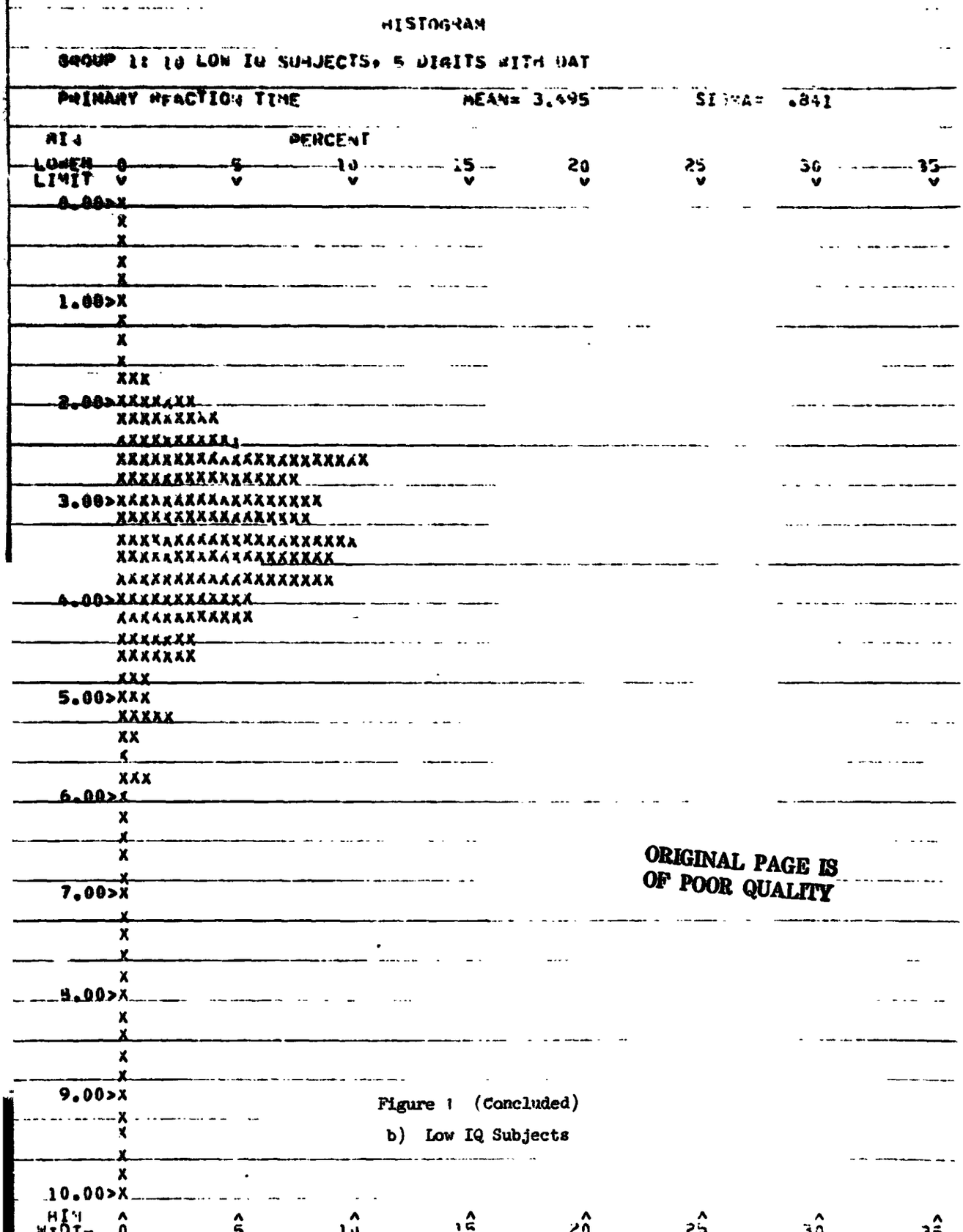

ORIGINAL PAGE IS OF POOR QUALITY

Figure 1 (Concluded)

b) Low IQ Subjects

HISTOGRAM

GROUP 2: [illegible] MODERATE IQ SUBJECTS, 5 DIGITS WITH DAT

PROB. ALL DIGITS CORRECT MEAN= .925 SIGMA= .059

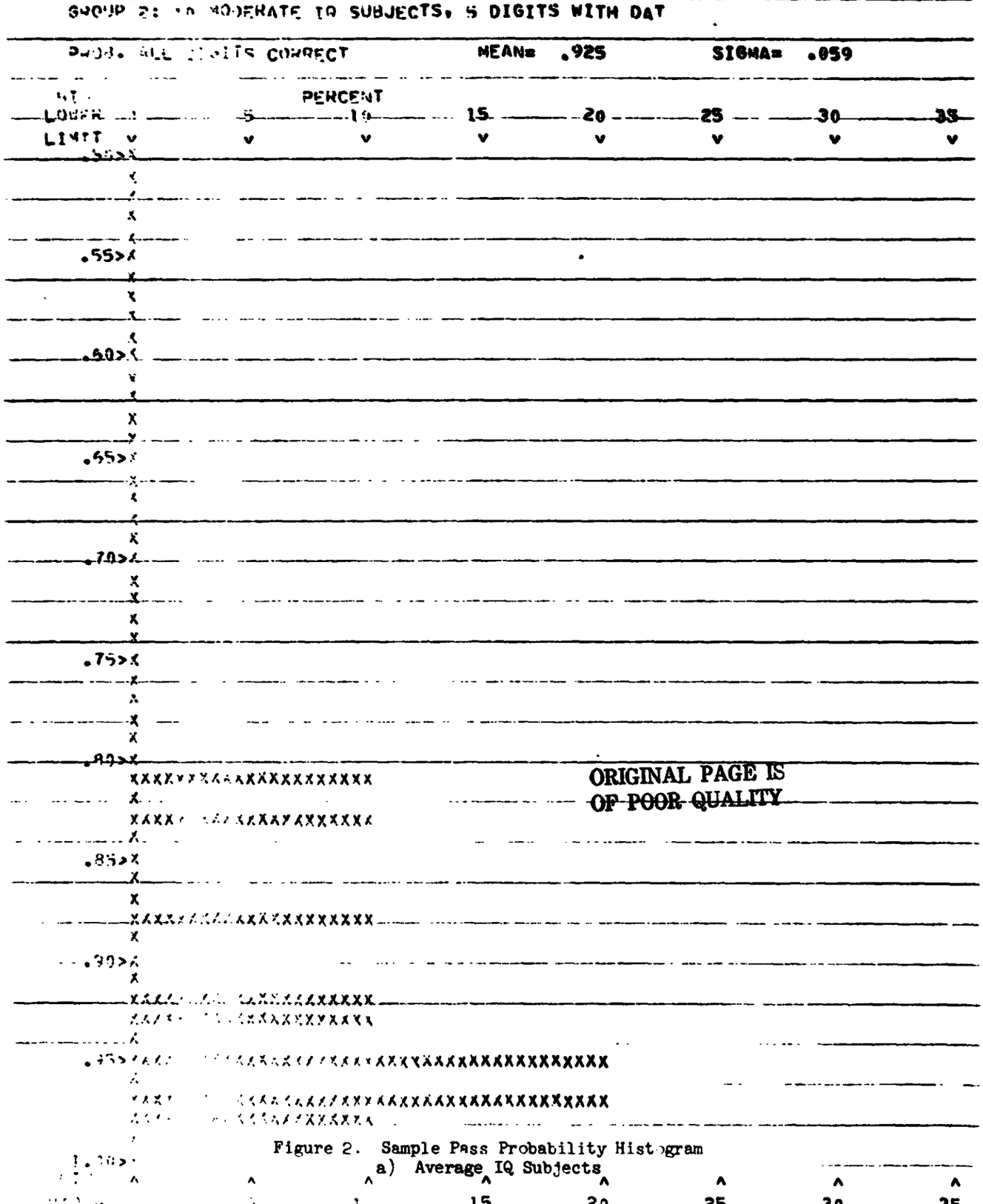

ORIGINAL PAGE IS
OF POOR QUALITY

Figure 2. Sample Pass Probability Histogram
a) Average IQ Subjects

HISTOGRAM

GROUP 1: 10 LOW IQ SUBJECTS, 5 DIGITS WITH DAT

PROB. ALL DIGITS CORRECT NEAN= .033 SIGMA .060

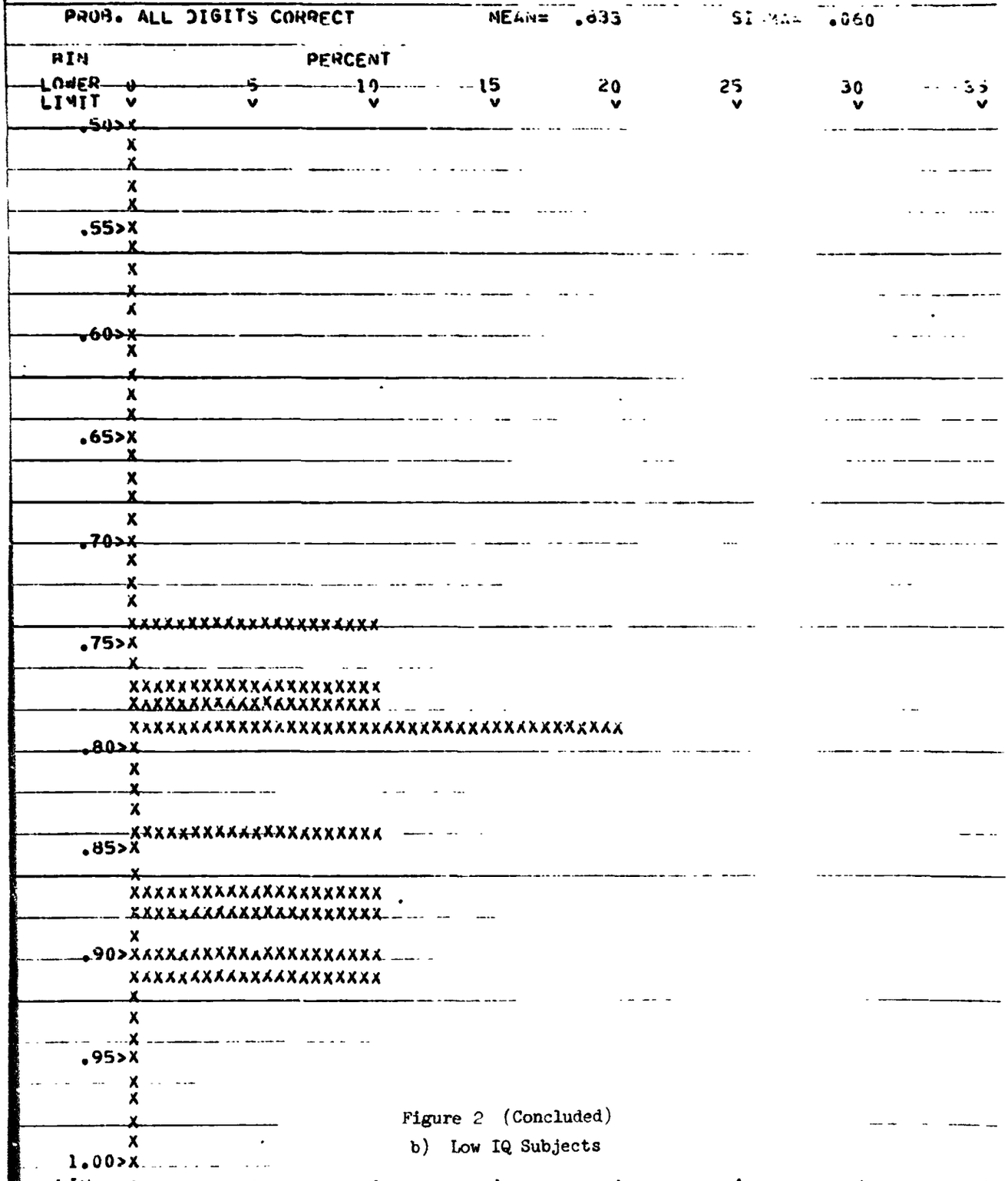

Figure 2 (Concluded)

b) Low IQ Subjects

TABLE 1

PERFORMANCE COMPARISON

QUALIFIER	COMPARED SUB-GROUPS	NUMBER OF SUBJECTS	MEAN PRIMARY RESPONSE TIME, T_{R_p}		PERCENTAGE PASSED		MEAN SECONDARY RESPONSE TIME, T_{R_s}	COMMENTS
			WITHOUT DAF	WITH DAF	WITHOUT DAF	WITH DAF		
INTELLIGENCE	AVERAGE IQ	20	3.03	2.90	92	93	0.70	1. Average IQ S's faster on primary, by 0.3-0.6 sec on the average. 2. Average IQ S's have high pass percentage. 3. Difference in pass percentage with DAF is significant at 1%. 4. DAF* increases differences in pass percentage.
	LOW IQ		3.55	3.50	85	83	0.76	
KEYBOARD SKILL	HIGHLY SKILLED	32	2.68	2.50	92	88	0.68	1. Skilled S's faster on primary, by 0.4-0.5 sec on the average. 2. T_{R_p} differences with DAF significant at 5%. 3. Skilled S's more homogeneous on primary. 4. DAF* reduces differences in pass percentage.
	NON-SKILLED		3.05	2.97	88	87	0.72	
SEX	FEMALE	54	2.74	2.70	91	89	0.69	1. Female S's faster on primary, by 0.04-0.34 sec on the average.
	MALE		3.08	2.94	91	87	0.71	
DRINKING HABITS	NON-HEAVY DRINKERS	60	3.03	2.95	91	88	0.76	1. Non-heavy drinkers slightly faster on primary, by 0.13-0.15 sec on the average. 2. Non-heavy drinkers have slightly higher pass percentage. 3. Differences in T_{R_p} more apparent for faster response times. 4. Differences in pass percentages without DAF is significant at 1%.
	HEAVY DRINKERS		3.16	3.10	88	86	0.70	
AGE	YOUNG (<30)	56	3.04	2.98	90	86	0.69	1. Young S's slightly faster on primary, by 0.2 sec on the average. 2. Old have slightly better pass percentage.
	OLD (>40)		3.26	3.16	92	88	0.76	

*DAF effects include learning effects.

ORIGINAL PAGE IS
OF POOR QUALITY

summation of the subjects with different mean times and fairly narrow distributions or if all subjects have the same reaction time characteristics. Therefore, we also examined each subject's mean and standard deviation of the primary reaction time with the DAT. These will be shown later in cumulative histograms. The differences between groups were subjected to the Kolmogorov-Smirnov test for statistical significance.*

Comparisons were also made on the basis of the pass percentage for each subject within the group. It should be recalled that the tests were conducted without any primary task time limits, and so the pass percentage is very nearly the probability of the subject's keying in the proper number. The pass percentage for each subject within a group was computed and a histogram was made for all the subjects within the group, see Fig. 2 for an example. Differences between the histograms were checked for statistical significance using the Kolmogorov-Smirnov test.

The results of the group comparisons are summarized in Table 1. The five comparisons have been arranged in order of the practical significance in group differences, the most significant listed first. In examining the data presented in Table 1 one must be careful about comparisons of the same subgroup with and without the DAT. Since the subjects were first tested without the DAT, the effects of the DAT are confounded with learning effects. This is obvious when one looks at the mean primary response times and notes that the times always decrease with the addition of the DAT. From this it appears that the learning effects on response time are stronger than the DAT effects, that is, the learning reduces the response time more than the DAT increases it.

In the first group comparison, we see that the average IQ subjects are considerably faster on the primary task than the low IQ subjects. The difference is about 0.5 to 0.6 sec. This is also indicated in Fig. 3 which is a cumulative histogram for the mean primary response times. In Fig. 3 we see a fairly constant time shift across all the subjects. The difference is not, however, statistically significant, at least at the 5% level, because of the relatively small number of subjects, i.e., 10 in each subgroup. Table 1 also shows a considerable difference in pass percentage, with the

*Siegel, Sidney, Nonparametric Statistics, McGraw-Hill, New York, 1956.

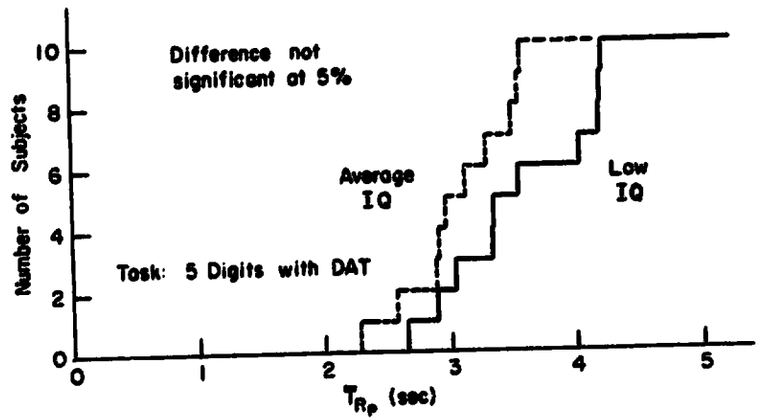

Figure 3. Group Comparison, Intelligence

average IQ subjects doing better. Note particularly that the difference is increased with the addition of the DAT (i.e., 92-83 < 93-83). In fact, with the DAT this difference in pass percentage becomes significant at the 1% level. Again, it is not certain whether this effect is due to the DAT or learning. However, it is interesting to note that going from the task without the DAT to that with the DAT, the average IQ subjects got better and the low IQ subjects got worse. This data trend could either be due to the average IQ subjects learning much more rapidly than the low IQ subjects, or because the low IQ subjects are much more adversely affected by the DAT than the average IQ subjects. In either event, it appears that intelligence has a very significant effect on performance, at least for the level of training employed here. If we look at only the data with the DAT we would conclude that the difference is significant for subjects who have had on the order of 75 practice trials.

In the second group comparison, the effects of keyboard skill are examined. The data shown in Table 1 indicate that skilled subjects are faster on the primary task by 0.4 to 0.5 sec. This large difference is statistically significant at the 5% level. Fig. 4 shows a fairly even shift in response time between the skilled and nonskilled subjects. It is interesting to note in Fig. 4 that the skilled subjects are a more homogenous group, that is, the cumulative histogram is more nearly a vertical line. On the other hand, some of the nonskilled subjects are also quite fast, but there is more variation within the group. On the basis of pass percentage, we see that there is a fairly small difference between the subgroups with the skilled being slightly better. Also note that the difference is diminished with the DAT. This might also be attributed to learning effects in that the nonskilled subjects may become as good as the skilled ones with sufficent practice. This theory seems to be supported by the pass percentage data but is not supported by the primary response time data. However, the difference in this case is only about 75 practice runs. We would conclude, therefore, that prior keyboard skill does have a significant effect at the training level of our subjects. Whether or not this difference would diminish or be eliminated with additional training is an unanswered question.

In the third group comparison we find that male-female differences are of marginal practical significances, the main difference being the female

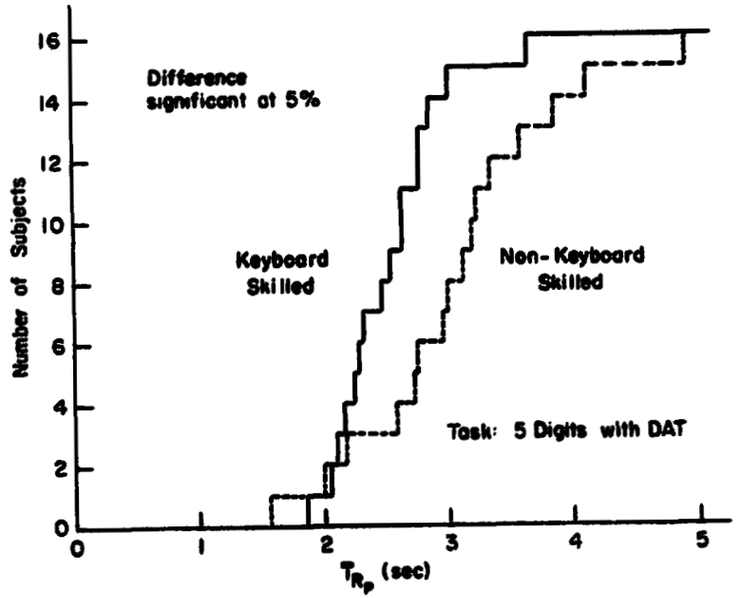

Figure 4. Group Comparison, Keyboard Skill

subjects are faster on the primary task by 1/4 to 1/3 of a second on the average. A more detailed view of this difference is shown in Fig. 5. Here we see no differences at the extremes, that is, for the fastest and slowest response times, but for the medium subjects the females are faster than the males.

The effects of drinking habits are seen in Table 1 to be quite small. The nonheavy drinkers are slightly faster on the primary task and have a slightly higher pass percentage. Fig. 6 shows that the difference in primary reaction time is not uniform but occurs only for the faster subjects. When we consider reaction times of more than 3 sec, Fig. 6 shows no difference at all between the heavy and nonheavy drinkers.

The results of the fifth group comparison were somewhat surprising. It showed a negligible effect of age. Young subjects were slightly faster on the primary task — on the order of 0.2 sec — but had a slightly lower pass percentage. Fig. 7 shows very similar distributions of primary reaction times.

There was some question as to whether this unexpected result was due to the fact that the old group wasn't old enough. Of the 28 "old" subjects only 9 were over 50 and 1 was over 60. To further explore the effects of age, we took each matched pair of subjects in the age comparison and subtracted their mean response times on the primary task. This was then plotted against the age of the older subject and is shown in Fig. 8. These data are very scattered and no trend with age is obvious. Clearly, within the test conditions of this experiment the effects of age are of no practical significance, at least up to roughly 60.

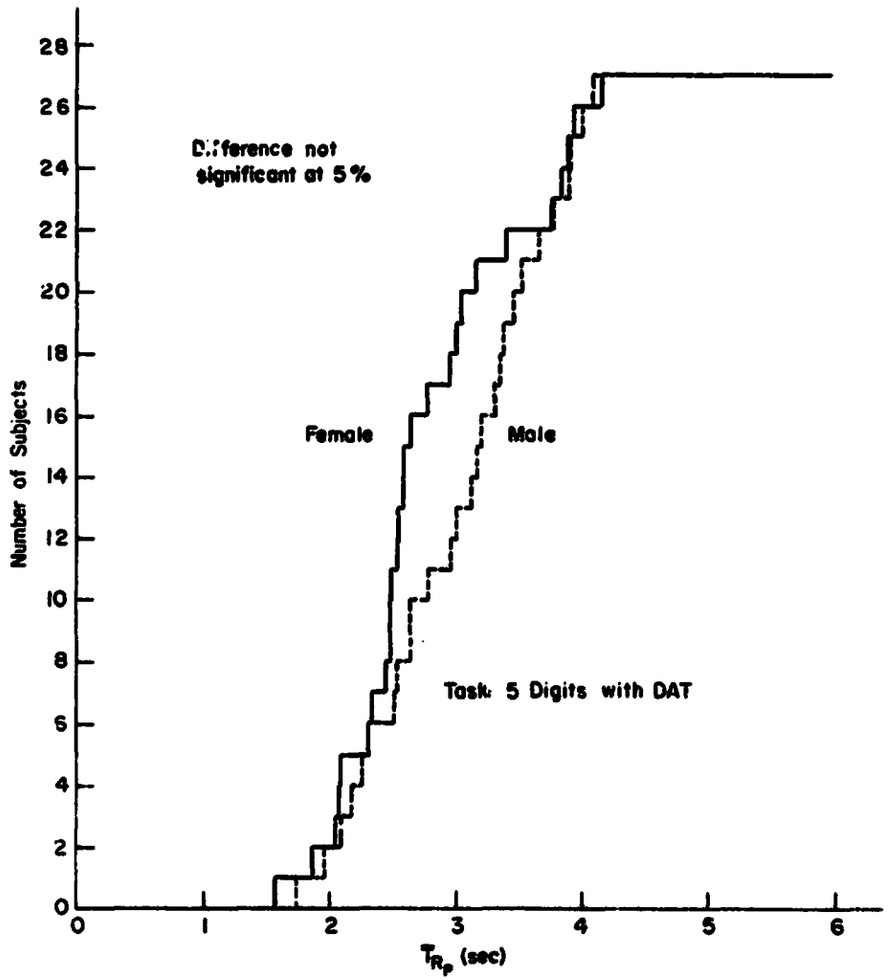

Figure 5. Group Comparison, Sex

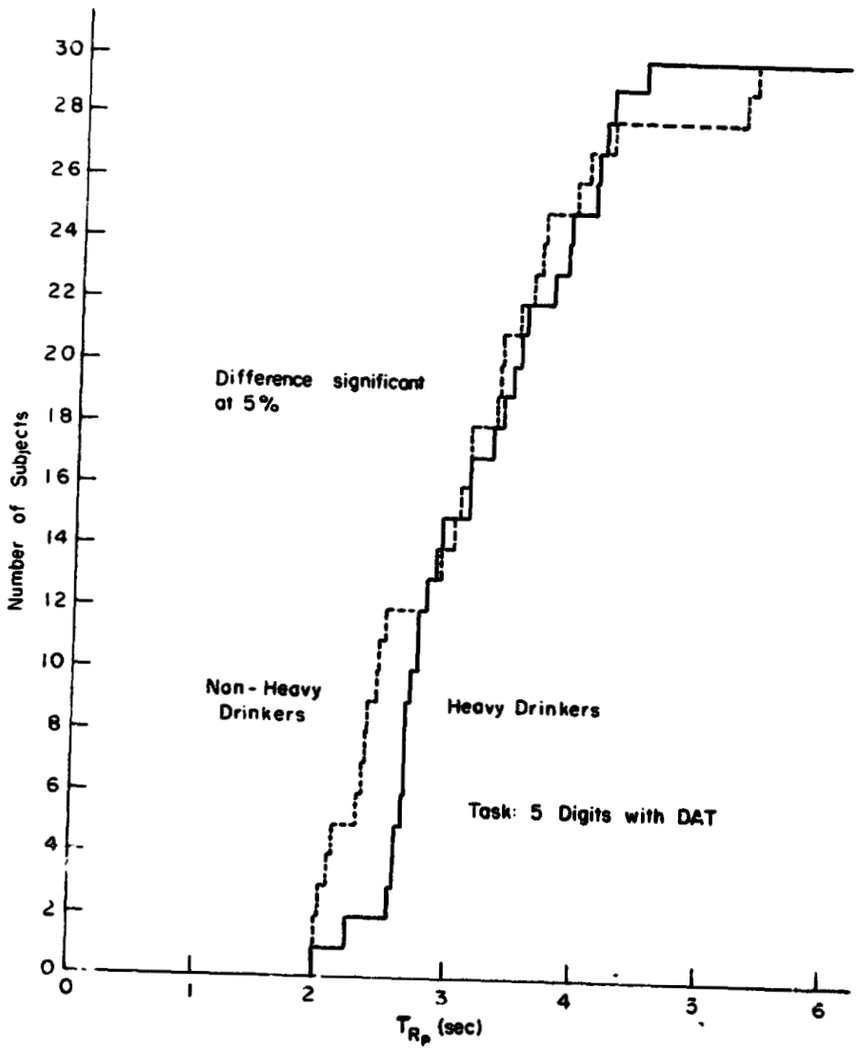

Figure 6. Group Comparison, Drinking Habits

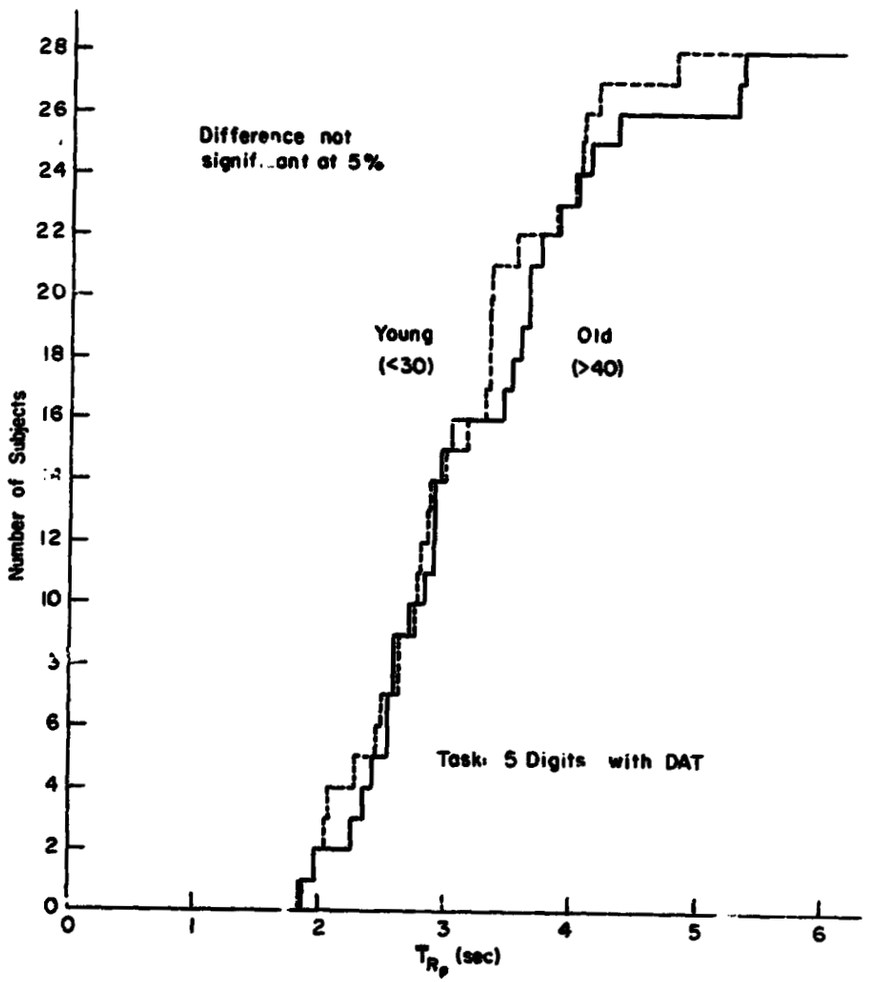

Figure 7. Group Comparison, Age

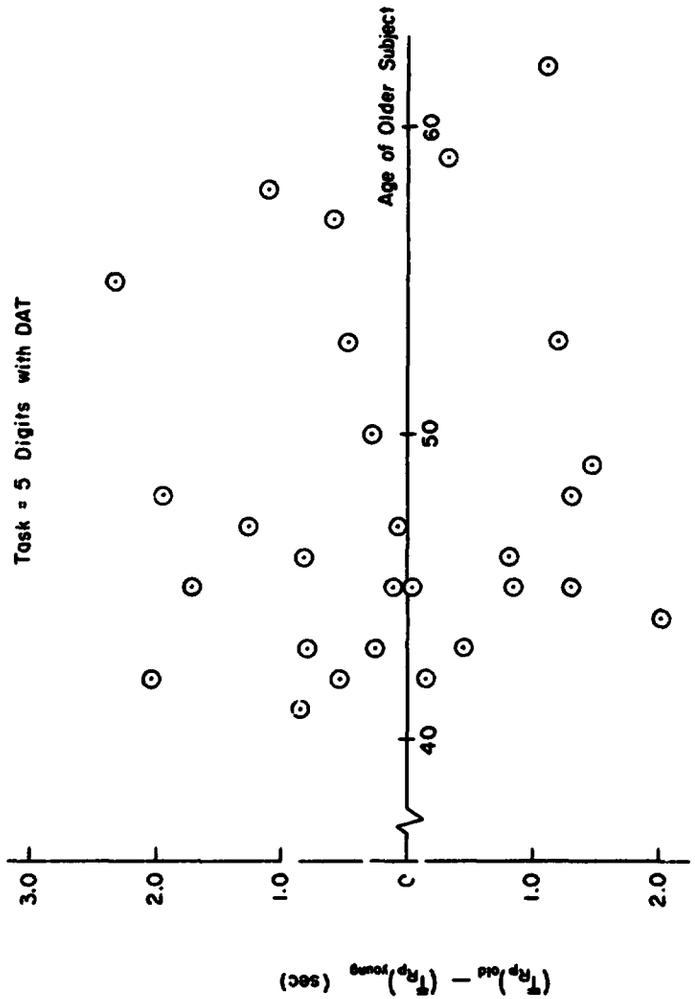

Figure 8. Reaction Time Differences for Old/Young Matched Pairs

EYE AND HEAD INTERACTION IN VISUAL SEARCH

*Peter Delp, Gordon Robinson, and John Ringenbach

ABSTRACT

A laboratory experiment provided quantitative data on transient responses of the eye and head to targets of unknown location and varying complexity. The objective was to provide correlative data for road test measurements of the visual search dynamics of vehicle drivers.

The location of the targets ranged from an initial straight forward fixation point to from 20 to 100 degrees to the right in horizontal plane only. Target complexity was varied from a four choice discrimination task to an eight choice task. A corneal-scleral boundary contrast technique was used to measure eye position relative to head, and the head position relative to the initial fixation point was measured by electro-mechanical means. Ten student subjects were employed.

The effect on the transients of alcohol was also measured.

The authors are with the Department of Industrial Engineering, University of Wisconsin, Madison, Wisconsin.

SESSION V

CONTROL

PRECEDING PAGE BLANK NOT FILMED

Optimization of Control Gain by Operator Adjustment

Kruse, W., Rothbauer, G.
Forschungsinstitut für Anthropotechnik
Meckenheim, West Germany

1. Introduction
2. Experimental Set-Up
3. Experimental Procedure
4. Experimental Results and Discussion

N75 19147

PRECEDING PAGE BLANK NOT FILMED

Abstract

Initially, an optimal gain was established by measuring errors at 5 discrete control gain settings in an experimental set-up consisting of a 2-dimensional, first-order pursuit tracking task performed with an isotonic fingerstick. This optimum gain was also judged least loading by subjects (S's). In addition, no significant experience effect on optimum gain setting was found in the first experiment. During the second experiment, in which control gain was continuously adjustable , high experienced S's tended to reach the previously determined optimum gain quite accurately and quickly. Less experienced S's tended to select a marginally optimum gain either below or above the experimentally determined optimum depending on initial control gain setting, although mean settings of both groups were equal. This quick and simple method is recommended for selecting control gains for different control systems and forcing functions.

Introduction

In complex high performance manual control systems, control can be performed sufficiently well only if the man-machine interfaces are designed with respect to the psychological and physiological characteristics and limitations of the human operator. For optimizing a man-machine system, we have to take into consideration two main aspects :

1. The performance of the entire system with regard to certain performance criteria, and
2. The workload of the human operator.

When an operator is part of a continuous control loop he tends to adapt to the machine system by adjusting his own describing function and gain in order to get the desired output. This adaptability is one of the advantages of the human controller. His adaptability, however, is not infinite. Considering that operator corrective movements and actions are performed by internal human control loop processes, real system optimization can only be attained if system control characteristics are adjusted to be compatible with human control characteristics. In a continuous tracking task e.g. VINCE found out that any adaptation difficulties by the operator lead to higher control frequency in order to keep control error within a certain range through increased operator effort.

In a machine system with a fixed describing function an optimization can most easily be done by adapting system gain to the human operator. With regard to the man-machine interfaces we make a distinction between display gain and control gain. Assuming display gain to be fixed, control gain remains an optimization variable. What are the influences of control gain on a pursuit tracking task ?

1. With low control gain settings a wide manipulation range is needed. Large control movements through this wide range result in relatively small changes in the controlled element. Such a control has low sensivity and high stability. It has the advantage of high accuracy, but the disadvantages of large amplitudes, long adjustment times and high velocities of motion.
2. A high control gain means high sensitivity and low stability so that slight control movements produce a big change of the output signal. Advantages are small manipulation area and slow velocities of motion. A disadvantage is reduced accuracy.

The choice of the right control gain should therefore be some compromise between accuracy and a convenient velocity of motion depending on the specific task or unique requirements on the system.

In earlier experiments where tracking errors were measured with various control gains the curve of tracking errors as a function of control gain was found to be rather u-shaped, with a broad range of minimal errors. Since the operator adapted

regardless of workload it did not seem to be worthwhile to put much effort into the task of optimizing control gain.

In previous experiments, not reported here, only with the more difficult tasks were gain se optimized. It was necessary to consider both objective performance measurements and subjective ratings in determining optimum control gain settings. The method seemed to be rather complicated. Few proposals for control gain settings can be found in literature ; usually only for zero order systems.

Results of a previous experiment concerned with operator selection of alternate control gains in a step tracking task, indicated that the human operator is capable of selecting from two different control gains so as to improve his performance and reduce his workload. The experiment reported here was conducted to test the capability of the human operator of optimizing his own gain with a continuously adjustable control gain.

The following questions had to be examined :

1. Is there an optimal range of control gain for all S's ?
2. Do control gain optimization results obtained with objective error measurements agree with subjective rating results ?
3. Are the individual optimal gains obtained by repeated adjustments of control gain by the S himself within a narrow range (sharp or broad optimum) ?
4. Is there a relationship between operator experience and his choice of an optimal control gain setting ?

Experimental Set-up

A two-dimensional continuous first-order pursuit tracking system was designed for this experiment (see figure 1).

Gaussian noise was filtered to .3 Hz and used as the forcing function. This was done to avoid the possibility of operators learning and anticipating the forcing function, and perhaps affecting optimum control gain settings. The used frequency is near .5 Hz, which HAMMERTON proposes is the maximum frequency for unpredictable signals that human operators can follow. The resulting high difficulty level should also lead to a narrow range of optimal control gain.

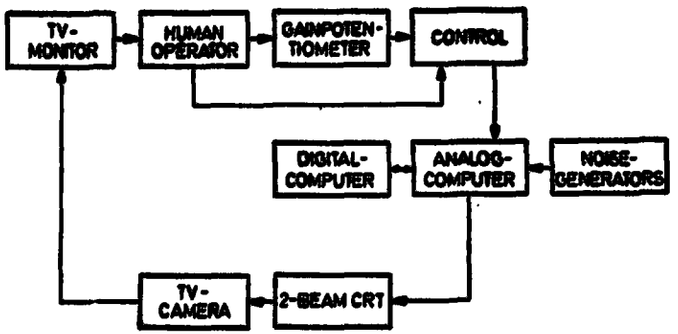

Figure 1 : Flow diagram of the experimental set-up

Target and cursor were displayed on a 24 " tv-monitor. The target was displayed as a small circle, the cursor as a dot. A light centering fingerstick with nearly no friction was used for control. Maximum stick deflection in all directions was 16 °.

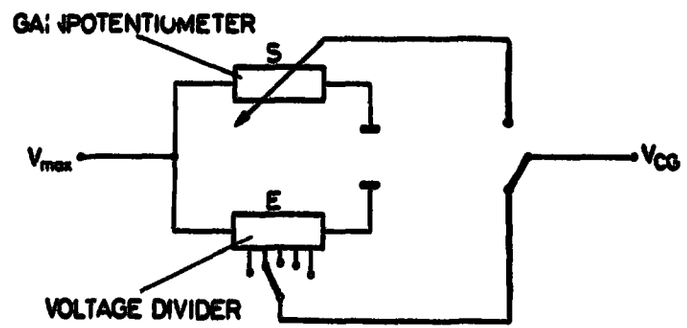

Figure 2 : Circuit for adjustment of control gain

To investigate question 2, listed above, an apparatus (see figure 2) was designed to permit control gain to be set either by the experimenter or by the operator. Settings were first fixed by the experimenter to generate performance curves. In later procedures , a 10-turn potentiometer was used by the operator himself.

Control of the experiments, data collection and processing was done by a hybrid computer.

Experimental Procedure

The experiment was performed with two groups of S's. The first group consisted of 10 low ranking enlisted men from a communications batallion. They had nearly no tracking experience. The second group consisted of 5 engineers with extensive tracking experience. During a training time of 15 minutes, S's became aquainted with their task and practised the self-adjustment of control gain with the potentiometer.

The experiment was divided into two parts :

1. Recordings of performance curves, characterized by RMS-tracking errors and TOT-measurements, were made in 5 trials of 2 1/2 minutes each with different control gain settings in a range of 1 to 10. After each trial, subjective data were collected using rating scales and questionaires of operator workload and controllability of each setting.
2. During these trials, S's could adjust their control gain to any value they wanted by turning the potentiometer knob. After initial maximum setting by the experimentor, S's were able to select control gain settings during the first 2 1/2 minutes which were adjusted more finely during the next trial. The same experimental sequence was repeated with an initial setting of minimum gain.

Experimental Results

a) Control gain - error characteristics

RMS-Tracking error was used as the performance criteria. In figure 3 control gain-error curves of both groups are shown. Although typical u-shaped curves resulted, a significant minimum error was seen with the unexperienced group.

The rather big standard deviations did not result from different individual optimum gain values as it could be demonstrated with the TUKEY-test of non-additivity. That test showed : There is an optimum range of control gain for all members of this group.

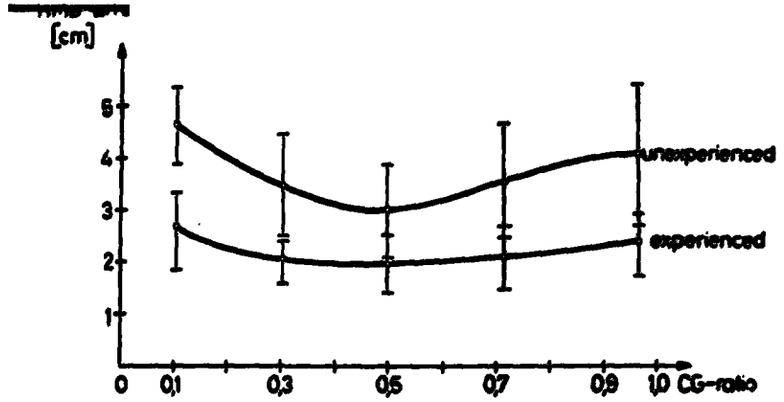

Figure 3 : RMS-error as a function of control gain ratio and tracking experience

The results of the experienced S's were similar. A control gain range of minimum error was demonstrated as well, but there is no significant difference between the 3 middle settings due to the higher degree of experience.

In answer to experimental question 1 these experiments showed that with objective measures there is almost no difference in optimal gain settings between the two groups.

Subjective judgements were obtained from S's after each control gain setting using Cooper rating scales and direct comparison ratings of each setting with preceding ones. The Cooper rating scale, developed for experts, was too finely subdivided for our S's. Therefore all ratings were transformed to rank orders by which the mode of each setting was computed. A comparison of the modes of subjective and objective ranks is shown in figure 4.

	Modes of ranks for each CG-setting				
CG-setting	I	II	III	IV	V
objective error measurement	5	2	1	3	4
subjective rating	5	1	2	3	4

Figure 4 : Modes of ranks for each control gain setting determined by subjective rating and error measurement

Results obtained with direct comparisons with respect to controllability between each setting are similar. The difference between each setting is shown in figure 5.

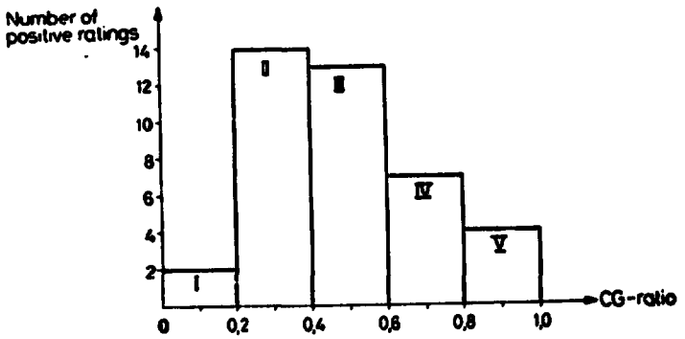

Figure 5 : Comparative controllability ratings of given control gain settings

The preference of S's for control gain settings II and III is pointed out very clearly. Operator's workload ratings show similar results (see figure 6).

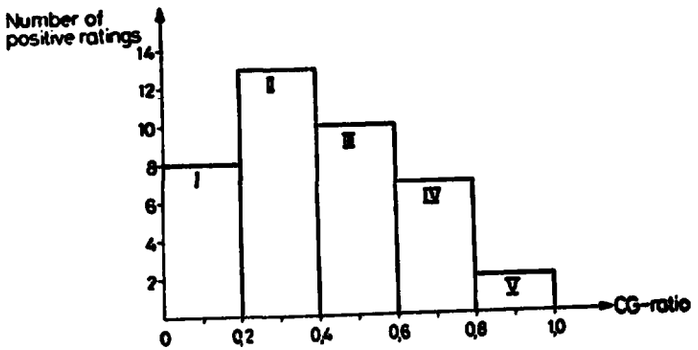

Figure 6 Comparative workload ratings of given control gain settings

There is a slight but insignificant shifting of the optimum gain to lower control gains with the subjective ratings, but the question about agreement of objective with subjective optimum gain settings can be answered positively.

b) Continuous adjustment of control gain by the operator

In figure 7, means and standard deviations of final adjusted control gains are to be seen. These values are given for the different initial setting conditions and degrees of experience.

Subjects	Initial CG-setting		mean
	CG_{max}	CG_{min}	
experienced	0,53±0,175	0,48±0,125	0,505
unexperienced	0,62±0,254	0,38±0,125	0,500

Figure 7 : Operator adjusted control gain settings as a function of initial control gain settings and experience

Contrary to unexperienced S's there is no significant influence of initial gain setting. Less experienced S's tend to adjust to the margins of the optimal range of the performance-optimized control gain settings determined in the first experiment (see figure 8).

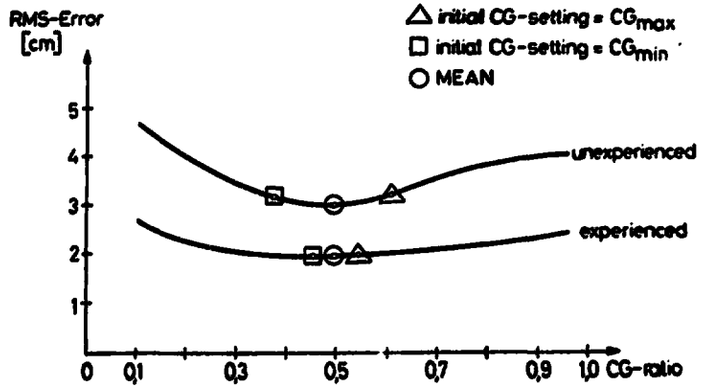

The main result of this experiment is the congruency of the overall means of self-adjusted control gains of both groups with the experimentally determined optimal control gain setting.

The human operator seems to be capable of optimizing the control gain of a man-machine system by means of a simple additional manual device.

The essential advantages of this method are simplification of the measuring system and shortening of experimental time. Only the final value of the gain adjustment needs to be recorded, and it takes only about 1 minute for each adjustment. Subjective questioning may be omitted. The task can be done by experts, and the result will fit all persons.

It should be possible to determine optimal gain settings for various controls, systems and forcing functions by using this method, to help manufacturers design their products and to help operators in performing their tasks.

Bibliography

1. HAMMERTON, M — "An investigation into the optimal gain of a velocity control system" Ergonomics 5 , 1962, 539-543

2. ROTHBAUER, G. KRUEGER, W. KRUSE, W. — "A fingerstick with binary selectable control gain" Proc. of the 8th annual conference on manual control, 1972, 81-88

3. TIPTON, C.L.& BIRMINGHAM, H.P. — "The influence of control gain in a first-order man-machine control system" Human Factors 3, 1959, 69-71

4. VINCE, M.A. — "Corrective movements in a pursuit task" J. of experimental psychology, 1948, 85-103

N75 19148

THE EFFECTS OF DISPLAY VARIABLES & SECONDARY LOADING ON THE DUAL AXIS CRITICAL TASK PERFORMANCE*

George M. Swisher
Wright State University
Dayton, Ohio

S. Nataraj
Sinclair Community College
Dayton, Ohio

ABSTRACT

Jex, Jewell and Allen (3) discussed the development of the dual-axis critical tasks and the effects of display format and control stick variation. This paper investigates the effects of scanning displays for separated instruments, separated versus combined displays and the effects of secondary loading. In addition an operator rating scale for handling qualities is established analogous to the Cooper Harper Scale.

PRECEDING PAGE BLANK NOT FILMED

* This research was made possible by the loan of analog computing equipment from the Air Force Directorate of Airframe Engineering, Flight Control Division, Wright-Patterson Air Force Base, Ohio. The authors acknowledge the help received from Bill Bohrer, M. J. Cook and John M. Howard. This paper was presented at the 9th Annual Manual Conference held at M.I.T., Boston During May 23, 24, and 25.

INTRODUCTION

Jex and McDonnell (4,5,6,7) developed a "critical" tracking task for man/machine research related to the operator's effective delay time. The auto paced single axis critical task mechanization yields consistent, reliable and very low variance measurements of the critical levels of instability. Swisher and Maher (10) investigated the degradation of human operator psychomotor performance and human information processing due to secondary loading and environmental stresses of heat and noise. Swisher, Bethke and Cook (11) studied the operator performance of critical tracking task due to intermittent display.

Jex, Allen & Jewell (3) have worked on dual axis critical task and have investigated different symbol formats and different control sticks (force stick and a softly-sprung finger control stick). The same autopacing principle and parameters as used for the single-axis critical instability tasks were used.

This paper investigates further the dual axis critical task for variations of number of controls and displays and also investigates the stress sensitivity of critical tracking tasks for secondary loading.

METHOD

Subjects

Six male college students were used as subjects. All the subjects reported 20/20 (un)corrected vision and freedom from auditory and psychomotor deficiencies. Subject age ranged from 20 to 23 years of age.

Apparatus

Figure 1 shows the block diagram and Figure 2 shows the analog mechanization of the no input dual axis critical task using two EAI-TR-20 10-volt analog computers in a slaved configuration. The displays used were two Hewlett Packard 122 A scopes set at 0.366 cm/volt sensitivity. The control sticks were identical U.S.A.F. type number C-1 Formation Sticks with ± 10.0 volt output. The stick was calibrated for a sensitivity of 4.16 volts/Newton. The C-1 formation stick was cascaded with a 0.58 potentiometer to make it compatible to the control stick used by Jex. The resulting stick system had a sensitivity of 2.413 volts/Newton.

Testing

A repeated Latin-Square design was used to assign the order of presentation for the different conditions (Table I).

The distance between the centers of the two displays was 10". The displays were at a height of 40" from the floor and 84" away from the subject. The distance between the controls was 20". The displays are listed in Table II.

Each subject was briefed concerning the experiment and his task prior to training. The subject was first given one set of telephone test (24 trials). The subject was then given 3 trials of the test task for training, followed by 3 trials of tracking alone, 6 trials of tracking and telephone and 3 trials of tracking alone for each of the eight conditions. The telephone test alone was given only once.

TABLE I

ORDER PRESENTATION OF EXPERIMENTAL CONDITIONS

Subject	Sequence							
	Line Display					Dot Display		
1	1	2	3	4	5	6	7	8
2	2	3	4	5	1	7	8	6
3	3	4	5	1	2	8	6	7
4	4	5	1	2	3	6	7	8
5	5	1	2	3	4	7	8	6
6	1	2	3	4	5	8	6	7

Instructions to the Subjects

You will be given either a line or a point display on one or two oscilloscopes. You are also given one or two joystick controls. For each trial, the display is brought to the center by the experimenter. You are told "Ready, go", and then the display will tend to get away from the center. Your primary task is to keep the display on the oscilloscope centered for as long as possible by manipulating the joystick motion forward and backward, or sideward, depending on the display motion. When you lose control of the display the trial is completed. The duration for which you hold the display within the range is the criterion.

For some trials you will be given a telephone test simultaneously with the tracking task. You are asked to listen to a series of messages which are logical statements. The letters used are P, Q, R and S and the words used are

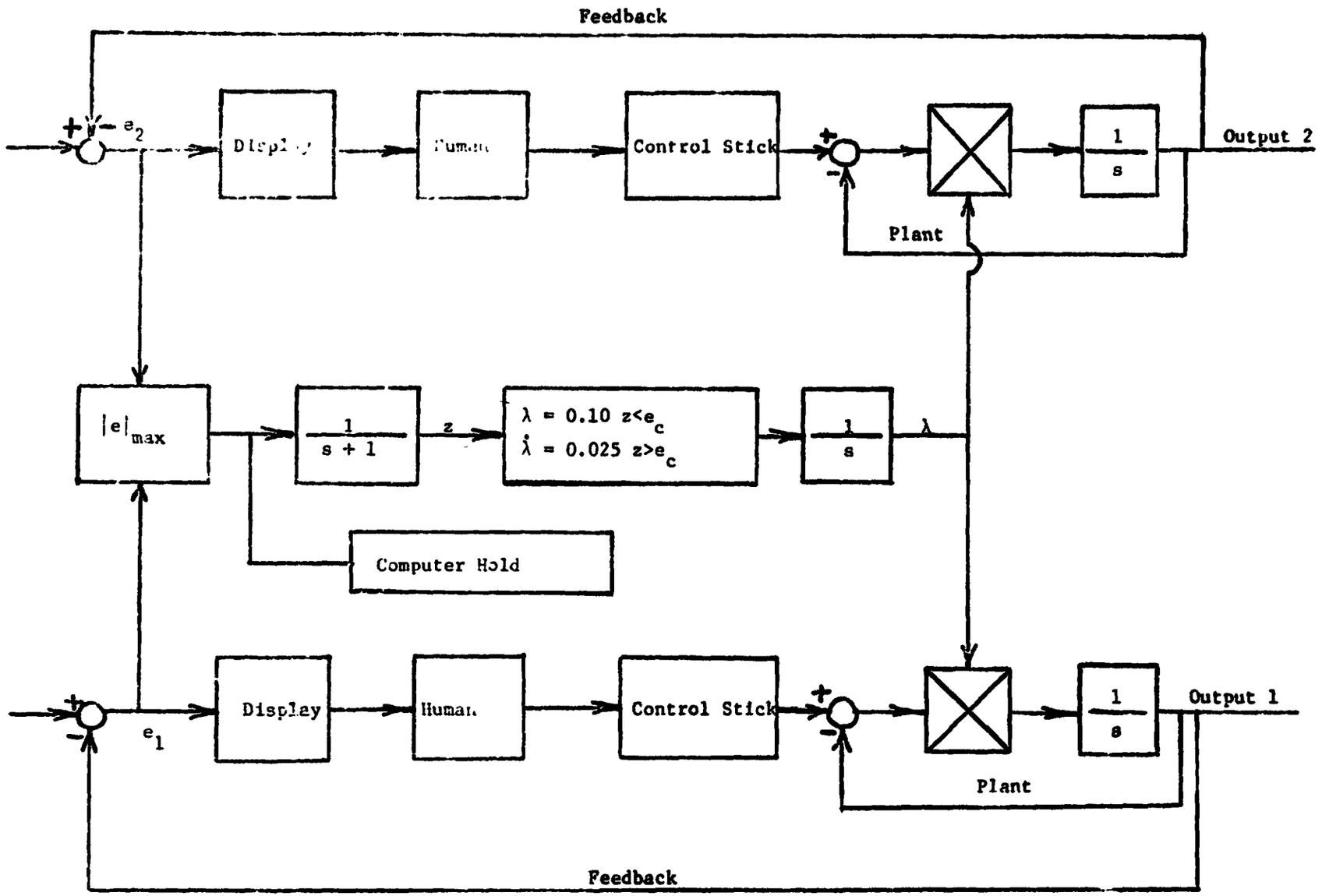

Figure 1. Block Diagram of Dual Axis Critical Task.

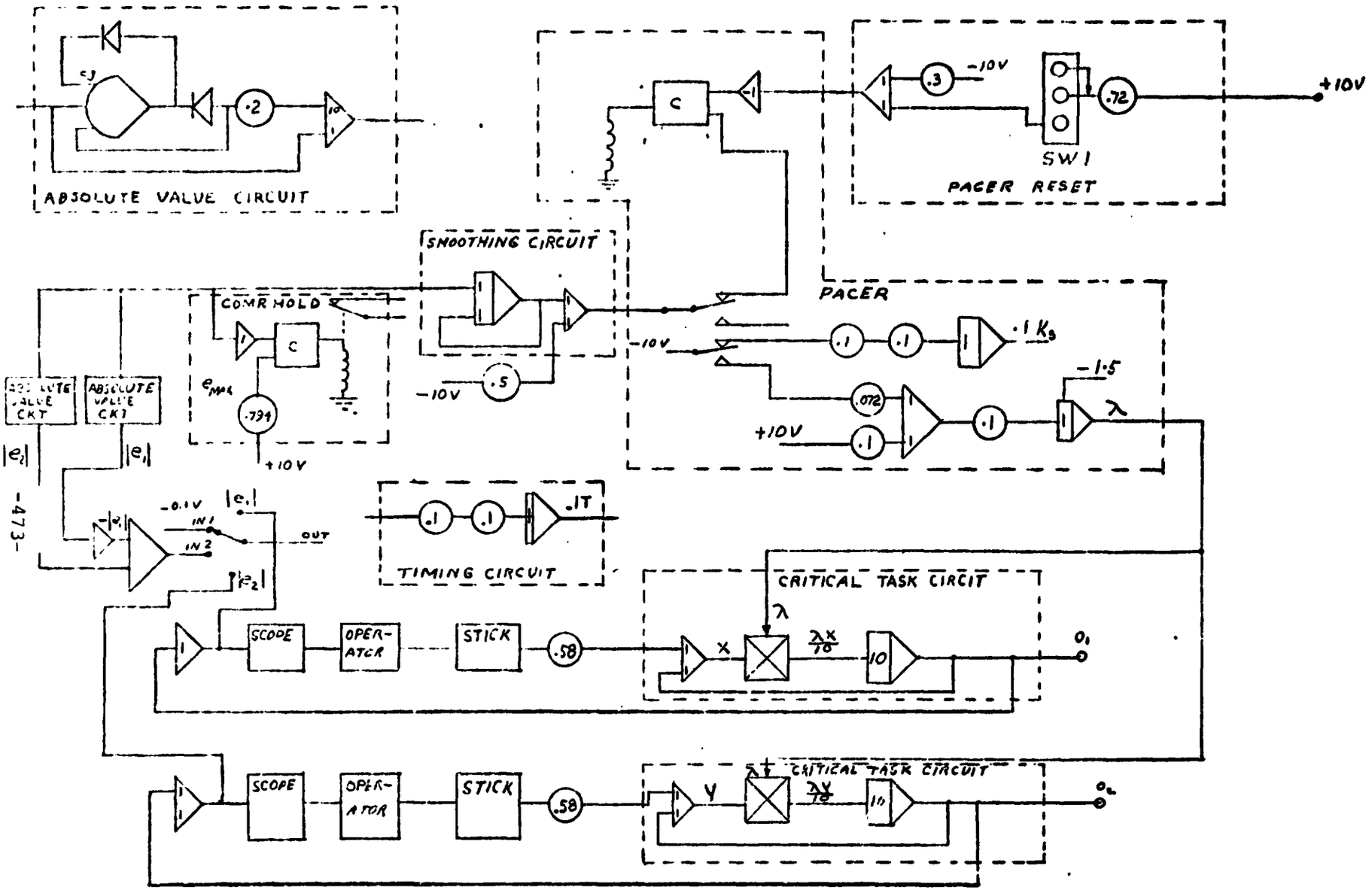

Figure 2. Analog Computer diagram of task.

TABLE II

TRACKING DISPLAY CONDITIONS

CONDITION 1	
CONDITION 2	
CONDITION 3	
CONDITION 4	
CONDITION 5	
CONDITION 6	
CONDITION 7	
CONDITION 8	

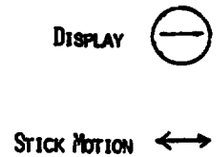

"precedes" and "follows". Note that the order in which the letters come in the alphabet is of no importance in this test. We are concerned only with their order in the statement. Your task is to listen carefully to each statement and decide promptly whether it is right (yes) or wrong (no), then call out your decision. Provide an answer for each statement, even if you doubt it. Are there any questions?

Secondary Task

Th secondary cognitive test used was a modification of the Baddeley Telephone Test reported by Guignard (12). The subject listens to a series of purportedly logical statements, some of which are in fact logically absurd. The task was paced at one statement every 5 seconds and the number of errors were scored. Omissions of answers were considered as errors.

The tracking performance measurer recorded for each tracking run were T (total run time), λ (critical divergence frequency), and t_s (time of rate shift on autopaced task). These voltages were read on a Fluke 8000 A Digital Multimeter.

RESULTS

The descriptive statistics are presented in an integrated tabular and graphic form. The graphs show the mean and the standard deviation of scores. The tables, located below the graphs, present numerical values of mean and standard deviation.

Critical Divergence Frequency (Lambda, λ)

The critical divergence frequency λ is defined as that divergence frequency when the subject loses control. The results shown in Figure 3 indicate that the mean λ did not vary much and the largest variability was observed in condition 6 (both tracking alone and combined). All but condition 1 showed a degradation in performance with the secondary test added.

Total Tracking Time (T)

The total tracking time (T) is defined as the time from the onset of tracking until one of the errors exceeds the display. The results are shown in Figure 4. The highest tracking times were recorded in condition 6 with no telephone test. This condition also had the highest variability. All conditions showed a degradation in performance with the secondary test added (except condition 1 and 2).

Rate Switching Time (t_s)

Switching time t_s, represented the time from the onset of a trial until the instantaneous absolute system error reached the level at which the instability rate switched from high to low rate. Group performance as defined by the switching time score is shown in Figure 5. Condition 3 4 and 6 yielded high scores but condition 6 had the highest variability. Secondary loading caused a degradation in performance for all conditions except condition 1 and 2.

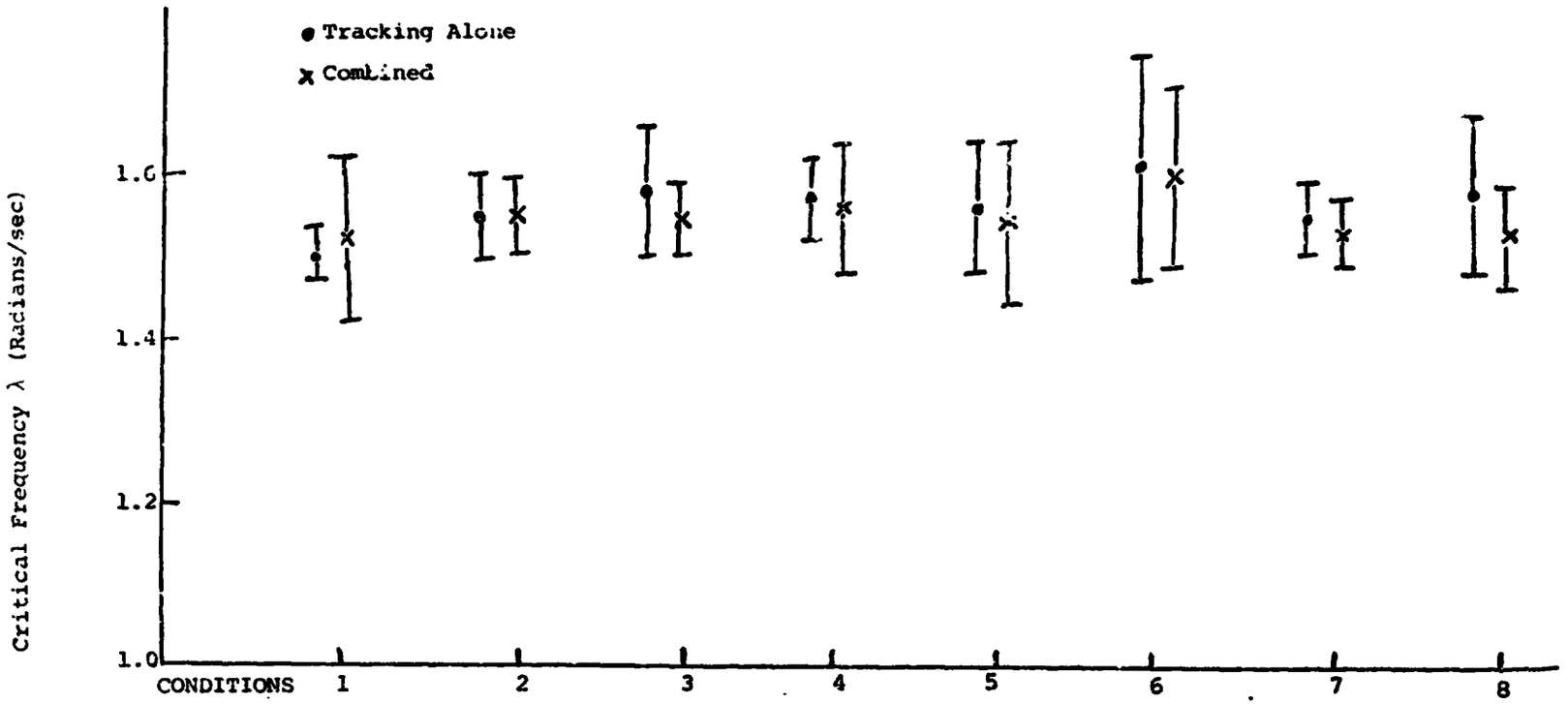

		1	2	3	4	5	6	7	8
Mean	Tracking Alone	1.500	1.560	1.579	1.577	1.562	1.616	1.552	1.578
	Combined	1.544	1.552	1.545	1.560	1.540	1.601	1.535	1.534
St. Dev.	Tracking Alone	.03217	0.04941	.07919	.04838	.07908	.13911	.04141	.09402
	Combined	.1035	.04805	.04795	.08111	.10402	.11438	.03391	.05366
	N	36	36	36	36	36	36	36	36

Figure 3. Critical frequency for tracking with and without secondary loading

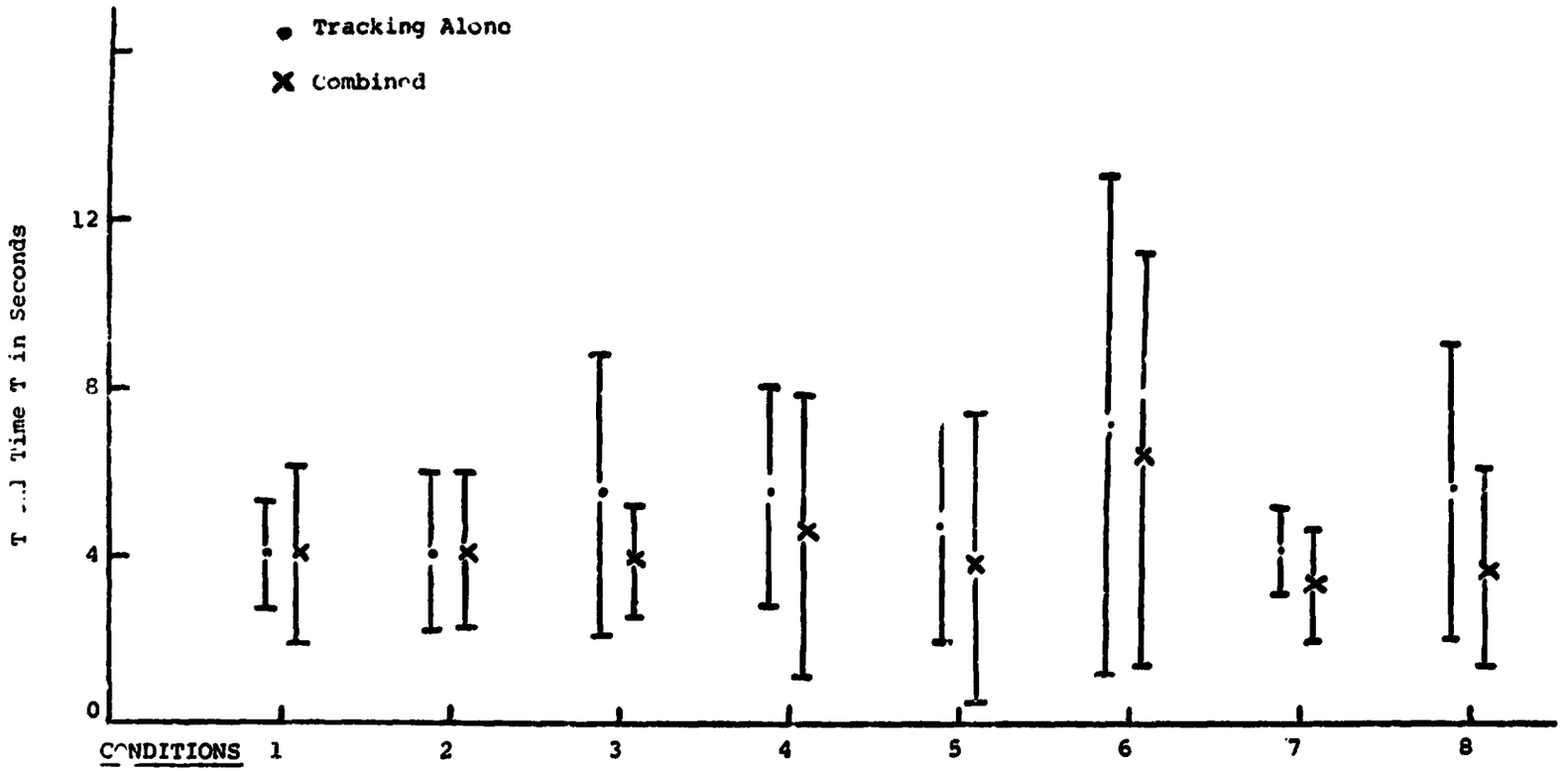

Mean Tracking								
Alone	4.09	3.98	5.35	5.3	4.74	6.97	3.93	5.47
Combined	3.91	4.02	3.80	4.48	4.03	6.30	3.26	3.52
Std. ..v. Tracking								
Alone	1.388	2.0316	3.433	2.9305	2.8361	5.944	0.8597	3.555
Combined	2.222	2.1363	1.8633	3.475	3.736	4.8861	1.3962	2.567
N	36	36	36	36	36	36	36	36

Figure 4. Total time for t· ·cing with and without secondary loading

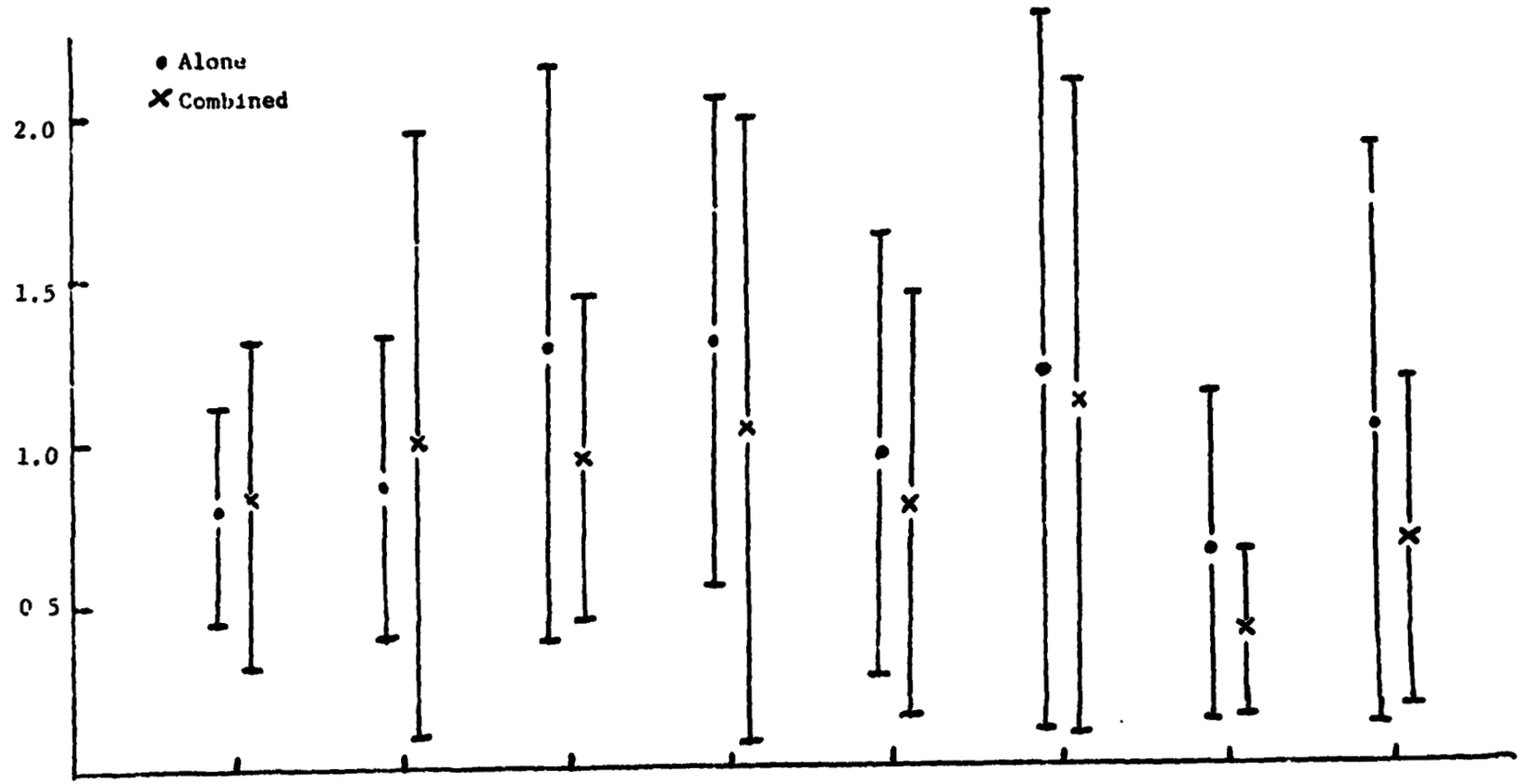

Conditions	1	2	3	4	5	6	7	8
Mean Tracking	0.8083	0.8639	1.233	1.3028	0.9583	1.2139	0.6417	1.022
Combined	0.8305	1.008	0.8472	1.0194	0.7972	1.1	0.4170	0.6772
Std. Dev. Tracking	0.3236	0.4564	0.9011	0.7644	0.6806	1.1208	0.5117	0.9
Combined	0.5333	0.9528	0.5028	0.8556	0.6722	1.0694	0.2555	0.4902

Figure 5. Rate Switching Time for Tracking With and Without Secondary Loading

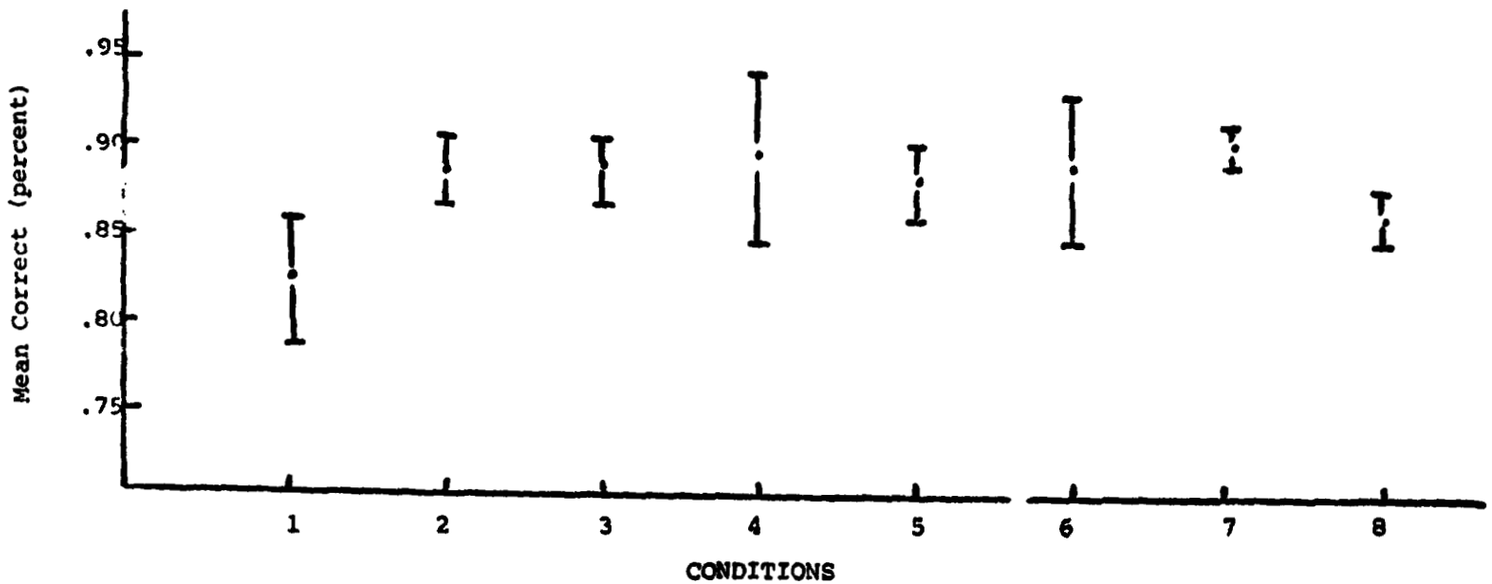

Mean (percent)	.825	.880	.883	.890	.878	.888	.895	.866
Std.Dev. (percent)	.042	.032	.021	.049	.026	.042	.017	.016
Correct/Total	152/184	174/196	175/198	170/191	151/172	183/206	162/181	123/142

Figure 6. Correct Responses (percent) on Telephone Test

TABLE III

NUMBER OF TIMES AN OPERATOR LOST A PARTICULAR DISPLAY FIRST

	CONDITIONS							
	1	2	3	4	5	6	7	8
LEFT								
Tracking Alone	24	25	26	25	24	22	24	21
Tracking Combined	24	22	24	25	23	23	25	22
RIGHT								
Tracking Alone	12	11	10	11	12	14	12	15
Tracking Combined	12	14	12	11	13	13	11	14
N	36	36	36	36	36	36	36	36

TABLE IV

PERFORMANCE RATING SHEET

Please indicate by circling your choice rating in the scale 1 through 7, as to the ease of operation. Number 1 indicates "least comfortable" and number 7 indicates "most comfortable".

1.	Two Controls, Two Displays (line) in vertical direction, Two Oscilloscopes	1 2 3 4 5 6 7
2.	" " " " (Dot) " " " " "	1 2 3 4 5 6 7
3.	" " " " (line) " horizontal " " "	1 2 3 4 5 6 7
4.	" " " " (line) at right angles to each other Two Oscilloscopes	1 2 3 4 5 6 7
5.	One " " " (line) at right angles to each other " "	1 2 3 4 5 6 7
6.	Two " " " (dot) One Oscil. scope	1 2 3 4 5 6 7
7.	One " " " (dot) One Oscilloscope	1 2 3 4 5 6 7

Name: _____

Date: _____

Performance Rating Scale:

A performance rating scale (Table IV) was given to the subjects to indicate their preference of each condition on a "one" to "seven" scale with "one" indicating the least comfortable and "seven" indicating the most comfortable. Table V shows the mean scores for each condition. Conditions 1 and 6 were rated best and the total tracking time for condition 6 agrees with this result. The total tracking time for condition 8 was the least and the subjects rated condition 8 as the most uncomfortable. Conditions 2 and 3 were rated low because the anthropometric motions involved in moving the sticks were perpendicular to each other.

Loss of Display

All the subjects used were right handed. It was noted (Table III) that the display controlled by the left hand was lost first in approximately an order of 2 to 1 compared to the display controlled by the right hand.

Telephone Test

Figure 6 shows the subject consistently paid attention to the secondary loading. The mean correct response to the telephone test in all conditions did not vary much in its range. The largest variability in mean correct response, occurred in conditions 1, 4, and 6, in which the direction of motion of the two displays was the same.

TABLE V

SUBJECTIVE RATING OF TRACKING CONDITIONS

Condition	Individual Ratings	Mean Rating
1	6, 7, 6, 5, 7, 6	6.1667
2	2, 4, 1, 4, 3, 4	2.8333
3	2, 4, 1, 2, 3, 3	2.5
4	4, 3, 3, 4, 3, 4	3.5
5	3, 3, 3, 7, 3, 1	3.3333
6	6, 7, 6, 7, 5, 6	6.1667
7	3, 2, 3, 4, 2, 3	2.8333
8	3, 3, 3, 1, 2, 1	2.1667

CONCLUSIONS

e critical divergence frequency (lambda λ) was not affected by ery loading. The secondary loading produced a degraded performance in total tracking time and also in rate switching time (except n condition 2) for all conditions. A large variability was noticed in condition 6 which may be due to the fact that this condition was rated to be the most comfortable one. The subjects showed a preference to the dot display with the display moving in the vertical axis. The subjects showed a high correction percentage in the telephone test showing that they were well motivated for the task.

RECOMMENDATIONS

The results of this research support that Jex's critical task can be used in evaluation of operator's performance measures in dual-axis critical tracking task. In experiments of this type, it is recommended that a mixed hand dominant population be used because as exemplified in this research the left display was lost in a 2 to 1 ratio compared to the right display.

REFERENCES

1. Anderson, R. O., Westbrook, C. B. and Pietrasek, P. E. "Handling Qualities and Pilot Work Load," W-PAFB, F.D.L., TRFDCC TM 66-5. September 1966.

2. Harper, R. P., Cooper, G. E. "The Use of Pilot Rating in the Evaluation of Aircraft Handling Qualities", NASA TN D-5153.

3. Jex, H. R., Jewell, W. F. and Allen, R. W. "Development of the Dual Axis and Crosscoupled Critical Tasks," Proceedings of the 8th Annual Conference on Manual Control, 1972.

4. Jex, H. R., McDonnell, J. D. and Phatak, A. V. "A Critical Tracking Task for Man/Machine Research Related to the Operator's Effective Delay Time," Part I and II NASA CR-616 and CR-674. November 1966/ January 1967.

5. Jex, H. R., Allen, R. W. and Magdaleno "Display Format Effects on Precision Tracking Performance Describing Functions, Remnant," AMRL TR-71-63, W-PAFB, Ohio. 1971.

6. Jex, H. R., "Two Applications of a Critical Instability Task to Secondary Work Load Research," S.T.I., TR-155-1, February 1967.

7. Jex, H. R., Allen, R. W. "Research on a New Human Dynamic Response Test Battery," 6th Annual Conference on Manual Control, April 1970.

8. Kelley, C. W. "The Measurement of Tracking Proficiency," Human Factors, Vol. 11, No., February 1969.

9. McDonnell, J. D. "Pilot Rating Techniques for the Estimating and Evaluation of Handling Qualities," AFF DL-TR-68-76, December 1968.

10. Swisher, G. M. and Maher, F. "The Degradation of Tracking Performance as a Function of Environmental Stresses of Heat and Noise," Proceedings of the 8th Annual Conference on Manual Control, 1972.

11. Swisher, G. M., Bethke, R., and Cook, M. J. "The Effect of Intermittent Error Displays on the Operator Critical Tracking Performance." Proceedings of the 8th Annual Conference on Manual Control, 1972.

12. Guignard, J. C., "A Telephone Test for Use in Combined Stress Experiments," Wright State University Environmental Stress Research Unit Internal Memo 70-6, December, 1970.

MANUAL CONTROL OF VEHICLES WITH SLOWLY-VARYING DYNAMICS

by

T. E. Moriarty, R. M. Howe, R. W. Pew
Department of Aerospace Engineering
&
Department of Psychology
The University of Michigan

ABSTRACT

Manual control of a simulated task representing the angle of attack of a lifting reentry vehicle has been studied while the plant gradually changes characteristic[illegible] n. a pure inertia to a damped second-order system. Transition in characteristic[illegible] fast enough so that autocorrelation functions of the tracking error mu[illegible] be computed by taking ensemble averages rather than time averages. Practical considerations limit the number of runs for each case to ten, so that considerable variance is evident in the correlation functions. However, the bandwidth of the pseudo spectrum corresponding to each correlation function can be estimated by direct examination of the correlation function shape. This new technique appears to give good bandwidth estimates with relatively small variance even when the ensemble-average correlation functions are based on very few samples.

A Multi-Axis Side-Arm Controller for the Tactical Aircraft Guidance System (TAGS) Program

M. Gordon-Smith

ABSTRACT

The prime objectives of the joint Canadian Government/U.S. Army sponsored TAGS program are to define, design, develop and flight test an Advanced Flight Control System which

- Incorporates a triply-redundant, "Fly-by-Wire", digital flight control system.
- Permits pilot command of the vehicle through a specially developed multi-axis side-arm controller
- Demonstrates a viable redundancy management scheme
- Substantially reduces pilot workload
- Provides safety throughout the flight test program

This paper will briefly discuss the development of the multi-axis side-arm controller and the results of the simulator and flight test evaluations. The problems encountered with the four-axis controller during the flight test program will be reviewed. These problems were partially resolved by reverting to a three-axis side-arm controller with a separate control for the vertical axis.

VIBRATION FEEDTHROUGH TO MANUAL CONTROL SYSTEMS*

R. Wade Allen, Raymond E. Magdaleno, and Henry R. Jex†
Systems Technology, Inc., Hawthorne, California

Abstract

Vibrational motions applied to a manual control system can "feed through" to the control stick as a result of dynamic couplings among the seat, the human operator's body and limb, and the stick. Measurements of sinusoidal vibration-input-correlated stick motions show that this vibration feedthrough can dominate control stick activity under various circumstances, but may not appear to any significant extent at the visual display if the vibration frequencies are heavily filtered by the controlled element. It was found that feedthrough characteristics are profoundly affected by control stick characteristics and the direction of vibration.

Based on these measurements, linearized biodynamic models are presented which give further insight into the feedthrough phenomenon and allow extrapolations to operational problems such as the effect of vibration isolation seats and different control stick configurations.

PRECEDING PAGE BLANK NOT FILMED

*This work was sponsored by the 6570th Aerospace Medical Research Laboratory under Contract F33615-71-C-1487, 1972.

†Senior Research Engineer, Senior Research Engineer, and Principal Research Engineer, respectively.

Flight investigation of pilot describing function for lateral directional control of airplane in turbulent air

Goro Beppu

Chief of Stability and Control Section
Flight Test Division
National Aerospace Laboratory, Japan

The investigation was carried out using a variable stability airplane. Pilot behaviors how to use aileron and rudder for lateral directional control of airplane in turbulent air, were made clear in describing function form which was estimated by spectral analysis of time series data (r, p, δ_a, δ_r). These data were measured during the flight whose environment of natural atmopheric turbulence has been imulated by the variable stability equipment. The experiments have been done for the case in which the coupling between roll and yaw motion is large. The aileron is deflected mainly proportional to p and . The gains of the aileron derlections are determined by pilots such that phase margines are about 50° - 90°. The usage of rudder depends upon pilot flight careers. The pilot who has the experience of helicopter control, uses quite well the rudder proportional to r so that the pilot works like a yaw damper.

On the Dynamics of Human Pilots in Marginally Controllable Systems

Norihiro Goto* and Kyuichiro Washizu**

In designing V/STOL and high speed flight vehicles, knowledge of the human pilot's controllability limit may be needed. Measurement of the pilot's describing function for his control of the system with marginal levels of static stability or damping, or both, is important to determine the controllability limit. This report includes the results of describing function measurement for dynamically or statically unstable second-order systems. Also included is a brief explanation of an improved time domain analysis method.

When the system is dynamically unstable, the results show that the pilot employs a modified describing function that contains a second-order lead term with a particular time constant associated with the undamped natural frequency of the system. For the statically unstable case, the results indicate that the pilot pays attention only to the unstable first-order mode so that the describing function coincides with that for the first-order unstable system control.

The full paper is contributed to AIAA Journal.

* Associate Professor, Department of Aeronautical Engineering, Kyushu University, Fukuoka, Japan

** Professor, Department of Aeronautics, University of Tokyo, Tokyo, Japan

PRECEDING PAGE BLANK NOT FILMED

PRECEDING PAGE BLANK NOT FILMED

SESSION VI

SYSTEM IDENTIFICATION AND
SIGNAL DETECTION

IDENTIFICATION OF THE OPTIMAL CONTROL MODEL FOR THE HUMAN OPERATOR

A. V. Phatak*, R. K. Mehra**, and C. Day***

PRECEDING PAGE BLANK NOT FILMED

One of the more important problems in manual control theory concerns the identification of human operator model parameters from input-output data. This paper considers the identifiability properties of the optimal control model structure. Typically the parameter vector to be identified is given by

$$\theta = [\tau, T_N, \underline{L}, V_y, V_m]$$

where τ = delay time

T_N = "motor" time constant

$\underline{L}$ = optimal gain vector

V_y = observation noise covariance matrix,

and V_m = motor noise covariance matrix.

Preliminary results indicate that θ may not be globally and/or locally identifiable in some cases. In such examples modifications to the optimal control model, including reduced order modeling, may be required to guarantee identifiability. These concepts are illustrated by way of a simple example. Finally the relationship between the optimal control model and the classical describing function model is discussed from the system identification viewpoint.

* - Systems Control, Inc., Palo Alto, Calif.
** - Harvard University, Cambridge, Mass.
*** - Wright Patterson AFB, Ohio

N75 19149

PARAMETER ESTIMATION IN LINEAR MODELS OF THE HUMAN OPERATOR IN A CLOSED LOOP WITH APPLICATION OF DETERMINISTIC TEST SIGNALS.

A. van Lunteren and H.G. Stassen
Man-Machine Systems Group
Laboratory for Measurement and Control
Department of Mechanical Engineering
Delft University of Technology
The Netherlands.

PRECEDING PAGE BLANK NOT FILMED

Abstract

The human operator can be described by a linear model and a remnant added to the output of this model. In practical cases this remnant is always non-zero. Therefore the presence of this remnant has to be taken into account in any identification method applied in human operator research.

Parameter estimation techniques are discussed with emphasis on unbiased estimates in the presence of noise. A distinction between open and closed loop systems is made. A method is given based on the application of external forcing functions consisting of a sum of sinusoids; this method is thus based on the estimation of Fourier coefficients and is applicable for models with poles and zeros in open and closed loop systems.

1 Introduction

To describe the behavior of the human operator controlling time invariant linear system with time constants up to the order of seconds, the Describing Function Method is a powerful too [1]. This DFM says that the system to be considered, in this case the human operator's behavior, can be assumed to consist of a linear time invariant system given by a transfer function and a remnant uncorrelated with the system input and added to the ouput of the system. The methods of estimating the parameters of these quasi-linear models can be devided into two main groups [2].

- o General Methods: From the observation of input-ouput of a system, the impulse response or the transfer function is determined. These methods deal with classical identification techniques, such as the determination of Bode or Nyquist plots from sinusoidaltest signals. More recent additions are correlation techniques, power density analyses, FFT's and averaged response techniques.
- o More Specific Methods: By observing the input-output of a system, the parameters of a defined mathematical model can be estimated. Therefore both the system to be analyzed and the mathematical model are given the same input. From the differences between the outputs of system and model the parameters can be determined according to a certain performance criterion and by means of a well considered strategy.

The fundamental difference between both the methods is that in a General Method only knowledge of the bandwidth of the input of the system to be analyzed is required (to choose a proper test signal), while for a More Specific Method the structure of the model itself must be known as well. This paper will deal with the discussion of a More Specific Method applied to the description of the human operator in open and closed loops.

2 Identification in an open loop

As pointed out before, a system in an open loop can be described by a linear transfer function H(p) and a remnant n(t) uncorrelated with the system input. For a known transfer function H(p) the parameters of a model based on this transfer function can be calculated from a set of equations which results from minimising a function E(ε(t);t) [3], where the quantity ε(t) is the difference between system output y(t) and model output $y^m(t)$ (see Fig. 1).

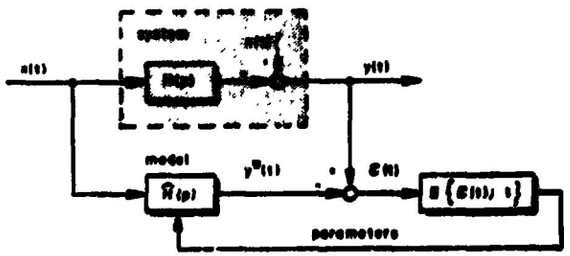

FIGURE 1:
Block diagram of system identification by means of parameter estimation; p denotes the Heaviside operator d/dt.

If the function E(ε(t);t) is equal to the mean squared error $\frac{1}{T}\int_0^T [\varepsilon(t)]^2 dt$ then also the error ε(t) will be uncorrelated with the system input x(t). In the special case that the model output can be written as:

$$y^m(t) = \sum_{i=1}^{n} a_i f_i(x(t)), \qquad (1)$$

the parameters a_i can be calculated from a set of linear equations; models having this property are called "linear in the parameters". A system having a transfer function with zeros only is an example of such a model; systems described by a transfer function with poles and zeros are not linear in the parameters. However, for these systems a so-called "generalised model" [2] can be defined (see Fig. 2). Here, not the difference ε(t) between system output y(t) and model output $y^m(t)$ is minimised according to a given criterion E(ε(t);t),

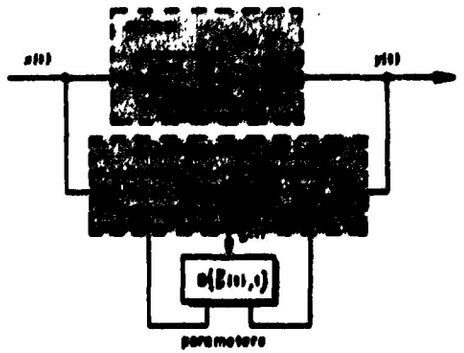

FIGURE 2:
Parameter estimation by using a generalised model.

but the difference ξ(t) is minimised according to the criterion E(ξ(t);t). The quantity ξ(t) is defined as the difference between two signals, which are obtained by modifying the system input x(t) with the transfer function N(p) and the output y(t) with the transfer function D(p); the transfer functions N(p) and D(p) possess only zeros. However, it can be shown that the estimates of the parameters obtained in this way will be biased if the error signal ξ(t) is non-white [3]. Therefore, this method can be applied only if the

remnant n(t) is zero or very small in relation to the system output y(t). If an unbiased estimate is required in most practical cases either the parameters of a set of filters for the signals x(t) and y(t) have to be estimated which whiten the signal $\xi(t)$, and this has to be accomplished iteratively [3], or the model parameters have to be estimated from the original criterion $E(\varepsilon(t)|t)$ which leads to a set of nonlinear equations. In practice these equations have to be solved by hill-climbing techniques, either analog or digital, which is also an iterative procedure.

3 Identification in a closed loop

For a system in a closed loop the remnant n(t) is no longer uncorrelated with the system input x(t), because it circles around by way of the feedback. This means that the application of open loop methods in a closed loop will lead to a bias in the estimation of the parameters. There are two possibilities to solve this problem.

3.1 Transformation of the closed loop system into an equivalent open loop system (see Fig. 3)

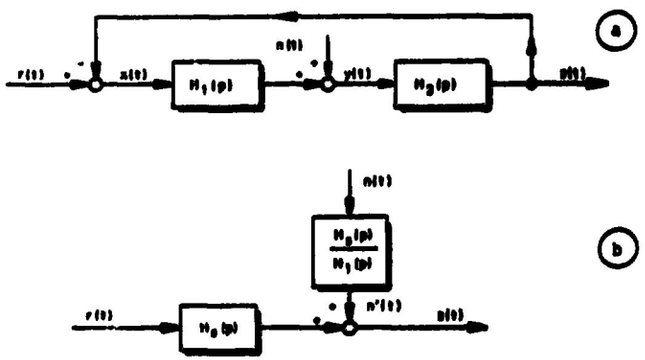

FIGURE 3:
System in a closed loop (a) and the equivalent open loop system (b).

If $H_1(p)$ is the unknown transfer function, and $H_2(p)$ is a known transfer function, then the closed loop transfer function $H_0(p)$ is:

$$H_0(p) = \frac{H_1(p)H_2(p)}{1+H_1(p)H_2(p)} \quad (2)$$

this transfer function can be estimated by means of an open loop method as illustrated in Fig. 1. The transfer function $H_1(p)$ then follows from:

$$H_1(p) = \frac{H_0(p)}{H_2(p)(1-H_0(p))} \quad (3)$$

Based on Eq. (3) a model of $H_0(p)$ can be built as a closed loop system with a known transfer function $H_2(p)$ and an unknown transfer function $H_1(p)$. In such a system a parameter estimation technique can be accomplished according to Fig. 4 or according to Fig. 5.

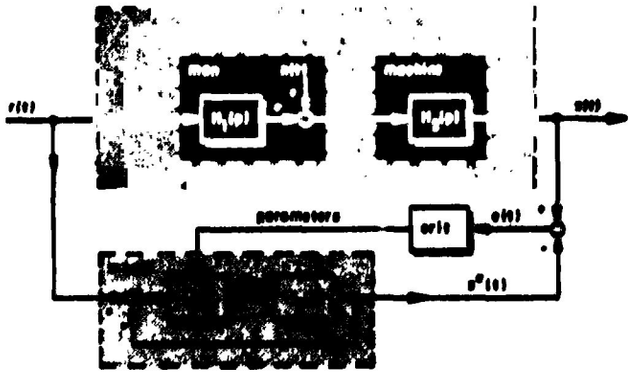

FIGURE 4:
Parameter estimation in a closed loop where $H_2(p)$ is a known system.

The latter method, for instance, is applied by Johannsen [4]. The method mentioned before implies that knowledge of the transfer function $H_2(p)$ of the machine is required. However, in many practic-

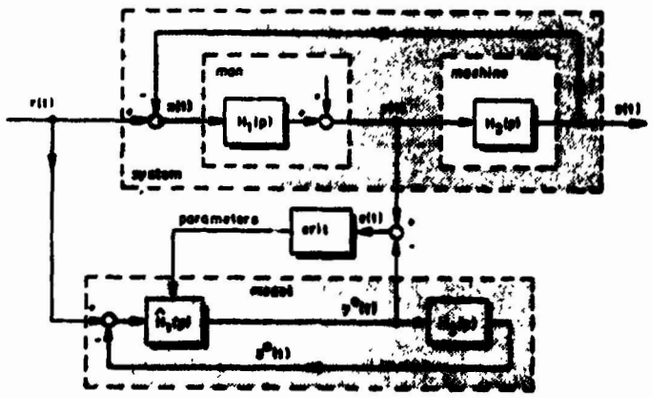

FIGURE 5:
Modified version of the method of Fig. 4.

al situations this knowledge is not available, at least not to the degree of accuracy required to get a reliable estimate of the transfer function $H_1(p)$.

3.2 Application of filtering techniques to closed loop systems

In a closed loop an unbiased estimate can be obtained only if the remnant is zero or if the remnant can be separated from the signals used for the identification; this can be achieved by applying filters. Fig. 6 shows a block diagram of a method to obtain unbiased estimates. The input x(t) and the output y(t) of the unknown system $H_1(p)$ are filtered in such a way that only those components of the signals x(t) and y(t) which originate in the external forcing function r(t) contribute in the parameter estimation. If the forcing function r(t) is a stochastic signal, the filter operation consists of the computation of the cross-covariance functions of the forcing function r(t) with the input x(t) and with the output y(t) respectiv-

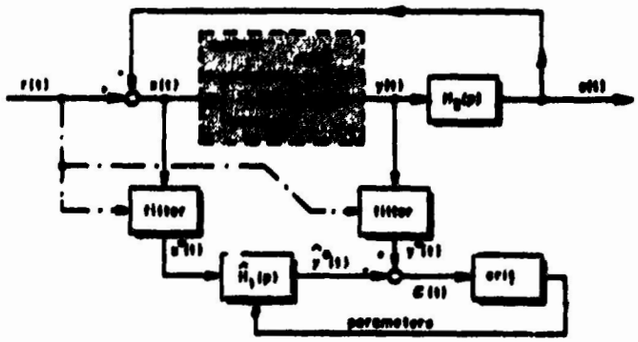

FIGURE 6:
Unbiased parameter estimation for a system in a closed loop where both the transfer functions $H_1(p)$ and $H_2(p)$ are unknown.

ely. A more attractive way of filtering can be achieved if the external forcing function r(t) consists of a sum of sinusoids. Now the application of the filters is equivalent to the estimation of a set of Fourier coefficients. Therefore, many investigators [5; 6; 7] apply a sum of sinusoids as a forcing function in experiments to identify the transfer function of the human controller. In this class of investigations it is important to choose the number of sinusoids in the forcing function sufficiently high, so that the input appears as a random signal to the human controller.

3.3 A closed loop method using a deterministic test signal

Starting from a different background, viz. the application of binary multi-frequency test signals for system identification [8], van den Bos arrived independently at the method just indicated. Moreover, he also showed that it could be applied to the generalised model in an open loop system as well as in a closed loop one without

getting biased estimates [9]. Hence the method just mentioned can be treated as a method for a system in an open loop with zero remnant. This outline will be followed in the next derivation.

Consider a system having a transfer function H(p):

$$H(p) = \frac{\alpha_0+\alpha_1 p+\ldots+\alpha_l p^l}{1+\beta_1 p+\ldots+\beta_m p^m} e^{-\tau_v p} , \tag{4}$$

in which p is the Heaviside operator p=d/dt. The input x(t) to this system is described by

$$x(t) = \sum_{k=1}^{n} (a_k \cos\omega_k t+b_k \sin\omega_k t) + n_1(t) = x^*(t) + n_1(t); \tag{5}$$

the output y(t) is described by:

$$y(t) = \sum_{k=1}^{n} (c_k \cos\omega_k t+d_k \sin\omega_k t) + n_2(t) = y^*(t) + n_2(t). \tag{6}$$

The estimates $\hat{a}_k$ and $\hat{b}_k$ of the Fourier coëfficients a_k and b_k can be obtained from:

$$\hat{a}_k = \frac{2}{T} \int_0^T x(t) \cos\omega_k t \, dt = a_k + \frac{2}{T} \int_0^T n_1(t) \cos\omega_k t \, dt; \tag{7}$$

$$\hat{b}_k = \frac{2}{T} \int_0^T x(t) \sin\omega_k t \, dt = b_k + \frac{2}{T} \int_0^T n_1(t) \sin\omega_k t \, dt \tag{8}$$

In these formulas the observation time T is the period of the fundamental frequency of the signals x(t) and y(t). Similar expressions are valid for the estimates $\hat{c}_k$ and $\hat{d}_k$ of the coëfficients c_k and d_k. The filtered signals $\hat{x}^*(t)$ and $\hat{y}^*(t)$ can be defined as:

$$\hat{x}^*(t) = \sum_{k=1}^{n} (\hat{a}_k \cos\omega_k t+\hat{b}_k \sin\omega_k t); \tag{9}$$

$$\hat{y}^*(t) = \sum_{k=1}^{n} (\hat{c}_k \cos\omega_k t+\hat{d}_k \sin\omega_k t). \tag{10}$$

Hence the larger part of the disturbances $n_1(t)$ and $n_2(t)$ is filtered out from the signals x(t) and y(t); only the small part around the circular frequencies ω_k remains. The relation between the deterministic parts $x^*(t)$ and $y^*(t)$ of the input x(t) and output y(t) respectively can be described by:

$$(1+\beta_1 p+\ldots+\beta_m p^m)\, y^*(t) = (\alpha_0+\alpha_1 p+\ldots+\alpha_l p^l)\, x^*(t-\tau_v). \tag{11}$$

In a model with parameters $\hat{\alpha}_0, \hat{\alpha}_1, \ldots \hat{\alpha}_l, \hat{\beta}_1 \ldots \hat{\beta}_m, \hat{\tau}_v$ and with an input $\hat{x}^*(t)$ a similar relation is given by

$$(1+\hat{\beta}_1 p+\ldots+\hat{\beta}_m p^m)\hat{y}^*(t) = (\hat{\alpha}_0+\hat{\alpha}_1 p+\ldots+\hat{\alpha}_l p^l)\hat{x}^*(t-\hat{\tau}_v) + \xi(t). \tag{12}$$

A more general way of writing this equation is:

$$\xi(t) = y(t) - \underline{a}^T \underline{g}(t,\tau) = y(t) - \underline{g}^T(t,\tau)\underline{a}. \tag{13}$$

In Eq. (13) the function y(t) corresponds to $\hat{y}^*(t)$ in Eq. (12). The vector $\underline{a}$ consists of the estimates $\hat{\alpha}_i$ and $\hat{\beta}_j$ of the unknown parameters, and the vector $\underline{g}(t,\tau)$ consists of the negatives of all sensitivity functions

$\frac{\partial f(t)}{\partial \alpha_i}$ and $\frac{\partial f(t)}{\partial \beta_j}$, which in this case are equal to $-p^i(\hat{x}(t-\tau))$ and $p^j(\hat{y}^*(t))$ respectively. The optimal value of τ corresponds to the estimated time delay $\hat{\tau}_v$. Now, consider the criterion function

$$E(\underline{a},\tau) = \frac{2}{T} \int_0^T \xi^2(\underline{a},\tau,t) \, dt. \tag{14}$$

Minimisation of this criterion function with respect to the parameters to be estimated yields a set of equations from which these parameters can be solved. Figure 7 which is in fact a combination of the Figs 2 and 6 shows the general idea of this method. The method is elaborated in more detail as follows. Define the scalar

$$n = \frac{2}{T} \int_0^T y^2(t) \, dt; \tag{15}$$

the vector

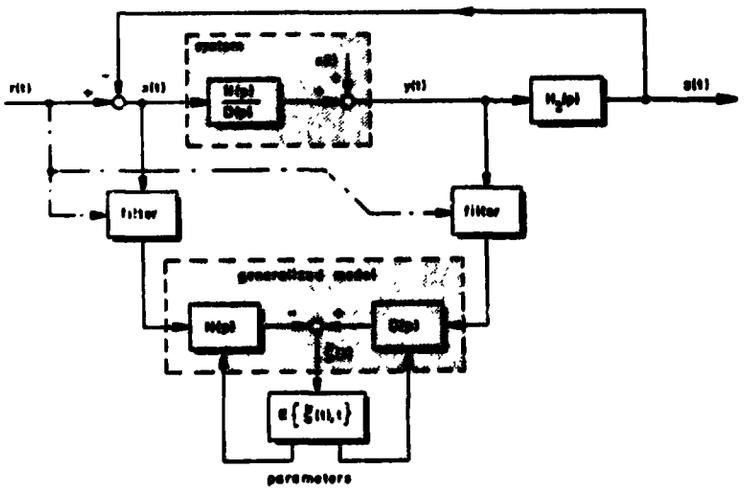

FIGURE 7:
Unbiased parameter estimation in a closed loop with a generalized model.

$$\underline{u}(\tau) = \frac{2}{T}\int_0^T \underline{z}(t,\tau)\, y(t)\, dt; \tag{16}$$

and the matrix

$$Z(\tau) = \frac{2}{T}\int_0^T \underline{z}(t,\tau)\, \underline{z}^T(t,\tau)\, dt. \tag{17}$$

Then

$$Z(\tau) = Z^T(\tau), \tag{18}$$

and

$$E(\underline{a},\tau) = \eta - \underline{a}^T\underline{u}(\tau) - \underline{u}^T(\tau)\underline{a} + \underline{a}^T Z(\tau)\, \underline{a}, \tag{19}$$

where

$$\underline{a}^T\underline{u}(\tau) = \underline{u}^T(\tau)\underline{a}, \tag{20}$$

so that $E(\underline{a},\tau)$ can also be written as:

$$E(\underline{a},\tau) = \eta - 2\underline{u}^T(\tau)\underline{a} + \underline{a}^T Z(\tau)\underline{a}. \tag{21}$$

Minimisation of $E(\underline{a},\tau)$ with respect to the parameter vector $\underline{a}$ yields:

$$\mathrm{grad}_{\underline{a}}\, E(\underline{a},\tau) = -2\underline{u}^T(\tau) + 2\underline{a}^T Z(\tau) = \underline{0}^T, \tag{22}$$

from which follows:

$$\underline{a} = Z^{-1}(\tau)\, \underline{u}(\tau). \tag{23}$$

Denote the criterion $E(\underline{a},\tau)$ which is minimized with respect to $\underline{a}$, as $E_0(\tau)$, then insertion of Eq. (23) into Eq. (21) leads to:

$$E_0(\tau) = \eta - \underline{u}^T(\tau)\, Z^{-1}(\tau)\, \underline{u}(\tau). \tag{24}$$

This means, that the parameter τ can be solved even before the parameter vector $\underline{a}$ is known. The solution follows from:

$$\frac{\partial E_0(\tau)}{\partial \tau} = -f_1(\tau) = 0, \tag{25}$$

which can be written more explicitly as:

$$f_1(\tau) = \frac{\partial}{\partial\tau}(\underline{u}^T(\tau))\, Z^{-1}(\tau)\, \underline{u}(\tau) + \underline{u}^T(\tau)\frac{\partial}{\partial\tau}(Z^{-1}(\tau))\, \underline{u}(\tau)$$
$$+ \underline{u}^T(\tau)\, Z^{-1}(\tau)\frac{\partial}{\partial\tau}\, \underline{u}(\tau) = 0, \tag{26}$$

where

$$\frac{\partial}{\partial\tau}(\underline{u}^T(\tau))Z^{-1}(\tau)\underline{u}(\tau) = \underline{u}^T(\tau)Z^{-1}(\tau)\, \frac{\partial}{\partial\tau}(\underline{u}(\tau)). \tag{27}$$

By writing $Z^{-1}(\tau)$ as:

$$Z^{-1}(\tau) = \frac{\mathrm{Adj}\, Z(\tau)}{|Z(\tau)|}, \tag{28}$$

and by multiplying both sides of Eq. (26) with $|Z(\tau)|^2$ this equation can be transformed into:

$$f_2(\tau) = |Z(\tau)|^2\, f_1(\tau) = |Z(\tau)|\,[2\underline{u}^T(\tau)\, \mathrm{Adj}\, Z(\tau)\frac{\partial}{\partial\tau}(\underline{u}(\tau))$$
$$+ \underline{u}^T(\tau)\frac{\partial}{\partial\tau}(\mathrm{Adj}\, Z(\tau))\underline{u}(\tau)] - \frac{\partial}{\partial\tau}(|Z(\tau)|)\underline{u}^T(\tau)\, \mathrm{Adj}\, Z(\tau)\, \underline{u}(\tau) = 0 \tag{29}$$

Eq. (29) can be solved by an iteration procedure such as the Newton-Raphson algorithm. In order to apply this algorithm, the derivative of $f_2(\tau)$ has to be known. The derivative of $f_2(\tau)$ is given by:

$$\frac{\partial f_2(\tau)}{\partial \tau} = |Z(\tau)|\Big[2\frac{\partial}{\partial\tau}(\underline{u}^T(\tau))\ \mathrm{Adj}\ Z(\tau)\frac{\partial}{\partial\tau}(\underline{u}(\tau))$$

$$+ 4\underline{u}^T(\tau)\frac{\partial}{\partial\tau}(\mathrm{Adj}\ Z(\tau))\frac{\partial}{\partial\tau}(\underline{u}(\tau)) + 2\underline{u}^T(\tau)\mathrm{Adj}\ Z(\tau)\frac{\partial^2}{\partial\tau^2}\underline{u}(\tau))$$

$$+ \underline{u}^T(\tau)\frac{\partial^2}{\partial\tau^2}(\mathrm{Adj}\ Z(\tau))\underline{u}(\tau)\Big] - \frac{\partial^2}{\partial\tau^2}(|Z(\tau)|)\underline{u}^T(\tau)\ \mathrm{adj}\ Z(\tau)\underline{u}(\tau). \tag{30}$$

Eq. (29) will have an infinite number of solutions, but owing to the fact that in practice the range of possible solutions for the value of τ can be given, normally an unambiguous solution can be found. The starting point for the iteration procedure can be chosen by solving Eq. (24) for a small number of values of τ in the range of interest, so that Eq. (29) can be solved. Finally, the parameter vector $\underline{a}$ can be computed from Eq. (23).

For a given model and for known estimates of the Fourier coefficients of the signals $x(t)$ and $y(t)$, all elements of the vectors and matrices mentioned in Eqs (29) and (30) can be computed. For example, if:

$$H(p) = \frac{a_0+a_1p}{1+a_2p}e^{-\tau_v p}, \tag{31}$$

then Eq. (12) can be written as:

$$\xi(t) = \hat{y}^m(t) - [\hat{a}_0\hat{x}^m(t-\hat{\tau}_v) + \hat{a}_1p(\hat{x}^m(t-\hat{\tau}_v)) - \hat{a}_2p(\hat{y}^m(t))]; \tag{32}$$

which means that in this case the elements $\zeta_i(t,\tau)$ of the vector $\underline{z}(t,\tau)$ in Eq. (13) are:

$$\zeta_0(t,\tau) = \hat{x}^m(t-\tau) = \sum_{k=1}^{n}\{\hat{a}_k\cos\omega_k(t-\tau) + \hat{b}_k\sin\omega_k(t-\tau)\}; \tag{33}$$

$$\zeta_1(t,\tau) = p(\hat{x}^m(t-\tau)) = \sum_{k=1}^{n}\omega_k\{\hat{b}_k\cos\omega_k(t-\tau) - \hat{a}_k\sin\omega_k(\tau-t)\}; \tag{34}$$

$$\zeta_3(t,\tau) = -p(\hat{y}^m(\tau)) = \sum_{k=1}^{n}\omega_k\{\hat{a}_k\sin\omega_k t - \hat{b}_k\cos\omega_k t\}. \tag{35}$$

The elements of the vector $\underline{u}(\tau)$ and the matrix $Z(\tau)$ can be calculated in a way similar to the one given below:

$$z_{12}(\tau) = \frac{2}{T}\int_0^T \zeta_1(t,\tau)\ \zeta_2(t,\tau)\ dt =$$

$$= -\frac{2}{T}\int_0^T p(\hat{x}^m(t-\tau))\ p(\hat{y}^m(t)),$$

$$z_{12}(\tau) = -\sum_{k=1}^{n}\omega_k^2((\hat{a}_k\hat{c}_k+\hat{b}_k\hat{d}_k)\cos\omega_k\tau + (\hat{a}_k\hat{d}_k-\hat{b}_k\hat{c}_k)\sin\omega_k\tau). \tag{36}$$

From the foregoing it follows that all information necessary for the estimation of the parameters is available if the estimates of the Fourier coefficients of the signals involved are known.

4 Multiloop systems

For systems having more than one input and more than one output, the identification of unknown transfer functions is less straightforward. Consider, for instance, the system of Fig. 8 which represents a man-bicycle system where the rider has to perform two tasks viz. the stabilisation of the bicycle and the following of a given track. In this system inputs and outputs of the unknown transfer functions $H_1(v)$, $H_2(v)$, $H_3(v)$ and $H_4(v)$ are coupled, not only within the human operator, but also within the bicycle simulator. The signals $R_1(v)$ and $R_2(v)$ are introduced externally as forcing functions. If the relations between inputs and outputs of the bicycle simulator are linear, then all signals in the system can be described as linear functions of the forcing functions $R_1(v)$, $R_2(v)$ and the remnants $N_1(v)$ and $N_2(v)$. For instance:

$$W(v) = F_1(v)R_1(v) + F_2(v)R_2(v) + F_3(v)N_1(v) + F_4(v)N_2(v); \tag{37}$$

$$X(v) = G_1(v)R_1(v) + G_2(v)R_2(v) + G_3(v)N_1(v) + G_4(v)N_2(v), \tag{38}$$

where the transfer functio $F_1(v)$, $F_2(v)$, $F_3(v)$, $F_4(v)$, $G_1(v)$, $G_2(v)$,

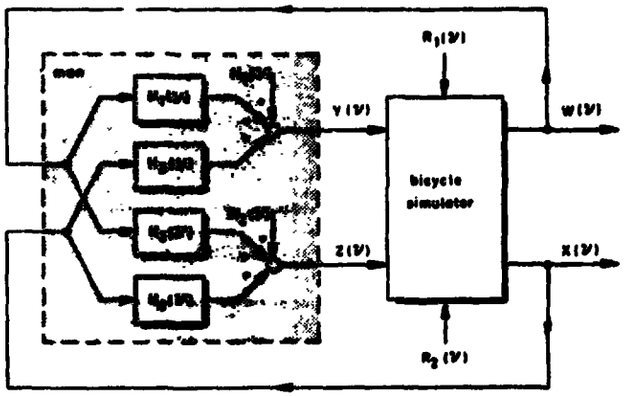

FIGURE 8:
Example of a multiloop system.

$G_3(\nu)$ and $G_4(\nu)$ describe the relations between the external inputs $R_1(\nu)$ and $R_2(\nu)$ on the one hand and the signals $W(\nu)$ and $X(\nu)$ on the other. From Fig. 8 and Eqs (37) and (38) it follows that:

$$Y(\nu) = \{H_1(\nu)F_1(\nu)+H_2(\nu)G_1(\nu)\}R_1(\nu) + \{H_1(\nu)F_2(\nu)+H_2(\nu)G_2(\nu)\}R_2(\nu)$$
$$+ \{1+H_1(\nu)F_3(\nu)+H_2(\nu)G_3(\nu)\}N_1(\nu) + \{H_1(\nu)F_4(\nu)+H_2(\nu)G_4(\nu)\}N_2(\nu); \tag{39}$$

$$Z(\nu) = \{H_3(\nu)F_1(\nu)+H_4(\nu)G_1(\nu)\}R_1(\nu) + \{H_3(\nu)F_2(\nu)+H_4(\nu)G_2(\nu)\}R_2(\nu)$$
$$+ \{H_3(\nu)F_3(\nu)+H_4(\nu)G_3(\nu)\}N_1(\nu) + \{1+H_3(\nu)F_4(\nu)+H_4(\nu)G_4(\nu)\}N_2(\nu). \tag{40}$$

Suppose that for each of the signals $W(\nu)$, $X(\nu)$, $Y(\nu)$ and $Z(\nu)$ the components $W_1(\nu)$, $W_2(\nu)$, $X_1(\nu)$, $X_2(\nu)$, $Y_1(\nu)$, $Y_2(\nu)$, $Z_1(\nu)$ and $Z_2(\nu)$, originating in the external test signals $R_1(\nu)$ and $R_2(\nu)$ can be

separated. Then a set of filtered signals can be distinguished, viz.:

$$\left.\begin{aligned}
W_1(\nu) &= F_1(\nu)R_1(\nu);\\
W_2(\nu) &= F_2(\nu)R_2(\nu);\\
X_1(\nu) &= G_1(\nu)R_1(\nu);\\
X_2(\nu) &= G_2(\nu)R_2(\nu);\\
Y_1(\nu) &= \{H_1(\nu)F_1(\nu) + H_2(\nu)G_1(\nu)\}R_1(\nu);\\
Y_2(\nu) &= \{H_1(\nu)F_2(\nu) + H_2(\nu)G_2(\nu)\}R_2(\nu);\\
Z_1(\nu) &= \{H_3(\nu)F_1(\nu) + H_4(\nu)G_1(\nu)\}R_1(\nu);\\
Z_2(\nu) &= \{H_3(\nu)F_2(\nu) + H_4(\nu)G_2(\nu)\}R_2(\nu).
\end{aligned}\right\} \tag{41}$$

By eliminating $F_1(\nu)$, $F_2(\nu)$, $G_1(\nu)$ and $G_2(\nu)$ the set of Eqs (41) can be reduced to a set of 4 equations from which the 4 unknown transfer functions $H_1(\nu)$, $H_2(\nu)$, $H_3(\nu)$ and $H_4(\nu)$ can be solved. As an example:

$$H_1(\nu) = \frac{X_2(\nu)Y_1(\nu)-X_1(\nu)Y_2(\nu)}{X_2(\nu)W_1(\nu)-X_1(\nu)W_2(\nu)}, \tag{42}$$

or

$$H_1(\nu) = \frac{Y_1(\nu)-\frac{Y_2(\nu)}{X_2(\nu)}X_1(\nu)}{W_1(\nu)-\frac{W_2(\nu)}{X_2(\nu)}X_1(\nu)} = \frac{Y_1'(\nu)}{W_1'(\nu)}. \tag{43}$$

Separation of the components of the signals originating in the two forcing functions is possible when both these test signals are composed of a number of sinusoids. In order to distinguish between the components originating in each of the two test signals it is necessary that no common frequencies occur in both test signals. However, now the problem arises that application of Eqs (42) or (43) is not possible because for a given frequency either the signals with the index 1 or those with the index 2 or both are zero. In general the transfer functions considered here are sufficiently smooth, i.e. the transfer functions can be considered to be constant within a frequency range $\Delta\nu = 1/T$. Now the problem can

be solved as indicated below.

Choose a test signal $R_1(\nu)$ consisting of a set of sinusoids with frequencies ν_k $(k=1,2,\ldots n)$ and choose the signal $R_2(\nu)$ which has the same number of sinusoids with frequencies $\nu_k+\Delta\nu (k=1,2,\ldots n)$. Then if it is assumed that:

$$\frac{Y_2(\nu_k+\Delta\nu)}{X_2(\nu_k+\Delta\nu)} \approx \frac{Y_2(\nu_k)}{X_2(\nu_k)}, \tag{44}$$

and if the same approximation can be applied to all quotients in the equations for the transfer functions $H_1(\nu)$, $H_2(\nu)$, $H_3(\nu)$ and $H_4(\nu)$, it is now possible to compute the decoupled inputs and outputs like $W_1'(\nu)$ and $Y_1'(\nu)$ in Eq. (43). These decoupled inputs and outputs can then be used in the parameter estimation method described under Par. 3. Another possibility to obtain the decoupled inputs and outputs at the frequencies desired is to apply an interpolation procedure. This method, for instance, is used by Stapleford et al [10].

Finally, it should be mentioned, that the number of parameters to be estimated should be chosen as small as possible, i.e. the structure of the model should be as simple as possible. A redundancy in the number of parameters means an increase in the number of near optimal solutions in the parameter space. Small disturbances due to noise may have the effect that for the same unknown system different sets of solutions can be found which lie far apart.

5 References

1. McRuer, D.T.; Jex, H.R.: "New approaches to human pilot/vehicle dynamics analysis", S.T.I., Report AFFDL-TR-67-150 (1968), pp. 1-188.
2. Eijkhoff, P.; Grinten, P.M.E.M. van der; Kwakernaak, H.; Veltman, B.P.Th.: "Systems modelling and identification", Survey paper Third IFAC Congress, London (1966), pp. 1-17.
3. Clarke, D.W.: "Generalized-least-squares estimation of the parameters of a dynamic model, IFAC Symp. on Identification Techniques, paper 3.17, Prague (1967), pp. 1-11.
4. Johannsen, G.: Development and optimization of a Non-linear Multiparameter Model for the Human Operator. Proceedings of the seventh Annual Conference on Manual Control, Los Angeles, (1971), NASA SP-281, pp. 15-21.

5. Elkind, J.J.: Characteristics of simple manual control systems, MIT, Lincoln Laboratory, TR 111 (1956).
6. McRuer, D.T.; Graham, D.; Krendel, E.S.; Reisener, W.: Human pilot dynamics in compensatory systems, AFFDL-TR-65-15 (1965), pp. 67-75.
7. Shirley, R.S.: Application of a modified Fast Fourier Transform to calculate human operator describing functions, IEEE Trans. on Man-Machine Systems, Vol. MMS-10, No. 4 (1969), pp. 140-144.
8. Boe, A. van den: Construction of binary multi-frequency test signals, IFAC Symposium on Identification in Automatic Control Systems, Paper 4.6, Prague (1967), pp. 1-6.
9. Boe, A. van den: Estimation of linear system coefficients from noisy responses to binary multi-frequency test signals. Second IFAC Symposium on Identification and Process Parameter Estimation, Paper 7.2, Prague (1970), pp. 1-6.
10. Stapleford, R.L.; Craig, S.J.; Tennant, J.A.: Measurement of pilot describing functions in single-controller multiloop tasks, NASA CR-1238 (1969), pp. 5-11.

ORIGINAL PAGE IS OF POOR QUALITY

AN ADAPTIVE APPROACH TO NONLINEAR SYSTEM IDENTIFICATION

Ralph Mekel, member IEEE

The City College of The City University of New York
New York, N. Y.

ABSTRACT

A nonlinear technique that shows promise as a parameter identifying scheme is presented. The technique permits one to derive control laws that provide identification dynamics for a model's parameters. An important feature of these identification dynamics is their "learning" capability. This feature provides a means for determining when a set of model parameters has been identified. As it can be observed from digital computer printouts, during the initial segment of a "learning" interval, the model parameters usually fluctuate over a wide range of values. In the latter portion of the "learning" interval, as the parameters approach the correct values, the fluctuations diminish. Therefore, once the fluctuations have ceased, one may assume that a set of model parameters has been identified.

The "learning" capability of the identification dynamics has another important feature. It permits one to establish a correspondence between parameter value changes in the model and disorders or malfunctions in the system that is being modeled. If a change occurs in the system that is being modeled, the model parameters begin to fluctuate again and a new "learning" interval is initiated. The fluctuations cease when the model assumes new parameter values that correspond to the changed condition of the system being modeled.

This adaptive property of the nonlinear identification technique offers a theoretically consistent approach for identifying a model's parameters from experimental data of the system being modeled. This is illustrated via an example, where the system being modeled is a nonlinear physiological process. The necessary data of the physiological process is recorded on tape and the model is constructed initially as an approximate mathematical representation of the physiological process. A digital computer program and the printouts are presented and discussed.

This research was supported by NASA, Langley Research Center, under Grant NGR-33-013-053

PRECEDING PAGE BLANK NOT FILMED

N75 19150

IDENTIFICATION OF HUMAN OPERATOR PERFORMANCE MODELS UTILIZING TIME SERIES ANALYSIS

by Frank M. Holden, M.D.
Aerospace Medical Research Laboratory
Wright-Patterson AFB, Ohio 45433

Stanley M. Shinners
Sperry Systems Management Division
Sperry Rand Corporation
Great Neck, New York 11020

I. INTRODUCTION

One of the missions of the Aerospace Medical Research Laboratory (AMRL) is to define the effects of stress encountered in Air Force missions upon man, and to use this understanding to develop means to alleviate the harmful effects of the stresses or to advise aircraft designers of the limits of man's capacity to withstand these stresses. A second mission of the Laboratory is to develop an understanding of how a man achieves control of a complex, dynamic system, such as an aircraft, in order that aircraft designers can use this understanding to build work space environments, display systems, and control systems which optimize man's control capability.

Until recently, accomplishment of both of these mission goals has been achieved through the classic disciplines of environmental medicine and physiology on the one hand and performance and engineering psychology on the other hand. Both of these approaches have contributed a substantial amount of information and data to the aerospace vehicle designer and have also advanced the state of our understanding of man as a subsystem of a larger, complex system. Neither of these approaches, however, provides data or information concerning man as a subsystem of a larger system which can be directly equated to the type of information which an engineer uses in the design and development of an airframe.

To design a control system for an aircraft, an engineer needs to know the performance specifications of the aircraft, the variables available to him for control of the airframe, the equations of motion to the aircraft and the associated stability coefficients, and the characteristics of the signals which will be used to provide inputs to the controller. For example, consider building a control system with one or more of these pieces of information unspecified or unavailable. Consider further the possibility of not having accurate information about the effects of the flying environment upon the integrity or stability of the components which must be used in building the controller or the components of the airframe.

Man, as a subsystem in a larger system, is usually a controller. He uses information available to him to effect changes in the controls available to him in order to achieve some level of performance of the whole system. He must cope with both dynamic changes in the characteristics of the controlled system due to environmental effects and with changes in himself due to the effects of the environment and the motion of his vehicle. The primary hypothesis recently advanced by the AMRL is that adequate descriptions of man as a controller, expressed in equations usable by the design engineer, can be used to understand how man is affected by stress and how man achieves control of complex, dynamic systems. Further, these equations can be used to optimize the performance capability of the entire system by lessening the stress effects and creating a more efficient man-machine division of labor.

In an attempt to describe man as a subsystem in manned weapon systems, several approaches to the modeling of the human operator have been tried. This paper presents the results of an effort performed by Sperry Systems Management Division (SSMD) for AMRL in applying time series analysis as a tool for modeling the human operator. In addition, it indicates how this technique can be utilized for determining the variation of the human transfer function under various levels of stress. The approach is useful as it does not require the postulation of a model and then checking its adequacy or inadequacy with actual performance. Instead, the method determines the human operator's model based on actual input and output data from a tracking experiment.

II. HUMAN OPERATOR PERFORMANCE MODELING

a) Previous Human Modeling Efforts

A multitude of mathematical models exist to describe human operator performance[1]. Although a study of these models leads one to conclude that they look at the problem from relatively narrow viewpoints, previous modeling efforts served to provide knowledge and greater understanding of this complex problem. The approach of these previous models has been to postulate models, and then to check their predictive capability against actual data. Analysis of these previous efforts has resulted in the use of "remnant components" which represent those portions of the actual data which the model cannot account for. The remnant represents primarily the components due to nonstationarity, nonlinearities, and time variability of the human response. In many cases, the remnant represents the major portion of the output. This shortcoming of previous human modeling approaches is overcome with time series analysis which determines the human operator's model based on actual input and output data from a tracking experiment.

b) AMRL Modeling Efforts

AMRL has been involved in human operator modeling efforts for the past eight years. The Crossover model (AFFDL 65-15) and its adjustment rules have been exercised by several divisions in the Laboratory and at the School of Aerospace Medicine at Brooks AFB, Texas, to measure the effects of motion and drugs upon humans. Further, as an indirect measure of the parameters of a model for a human controller, the first and second order Unstable Tracking Task has been widely used. The development efforts of the laboratory have included research into analog parameter trackers, frequency and time domain methods for identification of human operators. Specific models of anti-aircraft gunners have also been developed under sponsorship of AMRL based upon the Optimal Control Model representation of human operators. The Laboratory has, therefore, participated in the entire range of human operator modeling, from the basic research into identification techniques to the development of models to be used by the design and analysis engineering communities.

The major reason for such a broad involvement in human operator modeling by AMRL is that the existing state-of-the-art in modeling capability is on the edge of providing significant breakthroughs in achieving the goals identified previously. In the laboratory setting, existing modeling approaches appear to be adequate. In the operational environment, however, the existing methodologies account for an insufficient amount of the output power of the human operator or do not effectively deal with the complex mixture of multiple discrete and continuous control paths used by man.

PRECEDING PAGE BLANK NOT FILMED

c) Effects of Stress on the Human Controller

Stress (an ill-defined word but a usable concept) can affect man physically, such as by acceleration forces; physiologically, such as by altered central nervous system function in response to drugs; and psychologically, by anxiety and fear. The modeling of human transfer functions which can account for stress is of great interest. Physical stresses can have a direct effect upon manual control capability. Physiologic and psychologic stress, however, can indirectly affect man's control capability. The manifestation of these indirect effects in changes in the human operator can be extremely subtle. There are tests, which can be given to a stressed man, which are more sensitive in exposing altered human performance due to the stress than can be currently developed by the manual control community. Rather than being an affront to the methodologies used by the manual control community, this fact is an accolade to man's capability to compensate for the indirect effects of the stresses. Total system performance may not measurably change until the physiologic and psychologic structure of the man cannot sustain intelligent responses on his part.

That man, as a controller, is changing under mild physiologic stress is assumed to be true; and the fault with existing methodologies for human operator identification is assumed to be their lack of sensitivity in elucidating these changes. The study which is reported upon here was designed to expose the veracity of the above statement.

d) The Experiment Analyzed

AMRL has the facilities to expose man to a number of differing kinds of stress and combinations of stress. Acceleration stress, as one of its effects upon man, causes both local tissue and system c hypoxia. In order to separate the physical effects of acceleration stress from the hypoxic effects, a short study was run using three subjects and breathing mixtures representative of sea level and 15,000 feet altitude ($PA_{O_2} \approx 60\%$ saturation). The subjects were instructed to perform a single axis compensatory tracking task consisting of a random forcing function and a third order representation of the pitch axis dynamics of a high performance aircraft. Randomization of the sequence of altitude exposures and multiple replications of the runs were accomplished to maximize the accuracy of the measurement of the error variance. The study concluded with the observation that the variance and mean of tracking error for the two minute task was not affected by the changes in altitude. The data acquired during the two minute runs consisted of the forcing function, the tracking error, and the control stick output sampled at 20 msec intervals. This data was subsequently analyzed using time series analysis.

Figure 1 illustrates the experimental compensatory tracking configuration utilized. The forcing function, n(t), represented the resultant output of a noise generator. The transfer function of the plant, H, was set at 1, 1/s, and $1/s^2$. The human operator was attempting to track the input of a compensatory tracking display in a simulated F-4 cockpit.

For purposes of this report, the three subjects utilized for this study will be referred to as subjects A, B, and C. In order to gain flexibility in analyzing the experiments, several runs were repeated the same day and on other days in order to determine variations due to time, learning, adaptability, etc.

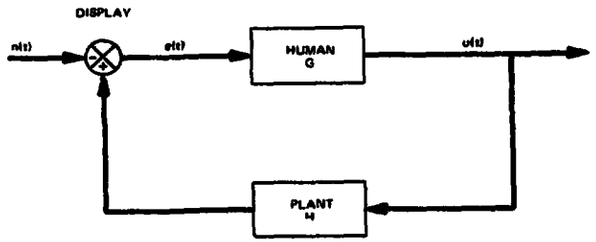

Figure 1. Experiment Block Diagram

III. DATA REDUCTION USING TIME SERIES ANALYSIS

a) Time Series Representation

Time series representation of discrete linear random processes consists of linear difference operations which relate the time series data x_t to a white noise process, z_t. A purely white noise process is represented by

$$x_t = z_t \tag{1}$$

An autoregressive (AR) model of order p is represented by

$$x_t = \phi_1 x_{t-1} + \phi_2 x_{t-2} + \dots + \phi_i x_{t-i} + \dots + \phi_p x_{t-p} + z_t \tag{2}$$

where ϕ_i for $i = 1, \dots, p$ are the model coefficients. By defining the backward shift operator

$$Bz_t = z_{t-1} \tag{3}$$

then the general AR equation can be given by

$$(1 - \phi_1 B - \phi_2 B^2 - \dots - \phi_i B^i - \dots - \phi_p B^p)\, x_t = z_t \tag{4}$$

A moving average (MA) process of order q is represented by

$$x_t = z_t - \theta_1 z_{t-1} - \theta_2 z_{t-2} - \cdots - \theta_i z_{t-i} - \cdots - \theta_q z_{t-q} \tag{5}$$

In terms of the backward shift operator B, this equation is given by

$$x_t = (1 - \theta_1 B - \theta_2 B^2 - \cdots - \theta_i B^i - \cdots - \theta_q B^q) z_t \tag{6}$$

A general mixed AR/MA process is given by

$$x_t = \phi_1 x_{t-1} + \phi_2 x_{t-2} + \cdots + \phi_p x_{t-p} + z_t - \theta_1 z_{t-1} - \theta_2 z_{t-2} - \cdots - \phi_q z_{t-q} \tag{7}$$

In terms of the B operator, this equation is given by

$$(1 - \phi_1 B - \phi_2 B^2 - \ldots - \phi_i B^i - \cdots \phi_p B^p) x_t = (1 - \theta_1 B - \theta_2 B^2 - \cdots - \theta_i B^i - \ldots - \theta_q B^q) z_t \tag{8}$$

Differencing of the data is necessary to induce stationarity, if the data is comprised of nonstationary processes such as a ramp or random walk in addition to a stationary process. The representation of one difference of data is given by

$$x_t - x_{t-1} = (1 - B) x_t \tag{9}$$

The representation of d differences of data is given by

$$(1 - B)^d x_t \tag{10}$$

b) Model Building Approach

Data reduction using time series analysis produces a mathematical model by reducing a wave form to white noise while identifying the correlated portion of the time series. The mathematical model is obtained by a three stage iterative procedure based on identification, estimation, and diagnostic checking. The identification process is concerned with the generation of the series in order to determine a class of models that should be investigated. The estimation phase uses the data to make inferences about parameters conditioned on the sufficiency of the model chosen. Diagnostic checking analyzes the fitted model with the data in order to determine any model inadequacies and obtaining model improvements.

c) Identification

In the identification stage of model building, the observations x_t are differenced as many times as required to induce stationarity. The resulting AR/MA process is then identified by analyzing the autocovariance function (ACVF), the autocorrelation function (ACF), and the partial correlation function (PCF)[1]. These functions are also useful for

obtaining approximate estimates of the parameters which are useful in the estimation stage for providing initial values needed by the iterative estimation procedures. As shown in Figure 2, the pure AR and MA processes are duals of one another, and opposite behavior of ACF and PCF indicates a pure AR or MA process.

d) Estimation

The estimation technique for determining the ϕ and θ parameters used Marquardt's Algorithm[3]. This nonlinear estimation approach performs an optimum interpolation between two traditional nonlinear estimation techniques - the Gauss (Taylor Series) method and the method of steepest descent. The algorithm combines the advantages of the ability of the steepest descent to converge from an initial guess which may be far from the final value, and the ability of the Gauss method to close in on the converged values quickly once the vicinity of the final value has been reached. In addition, Marquardt's algorithm overcomes the disadvantages of the slow final convergence of the steepest descent and the possible divergence of the successive iteration with the Gauss method.

e) Diagnostic Checking

The diagnostic checking step is concerned with examining the white noise residuals, z_t, from the fitted models in order to determine any lack of randomness. Analysis of z_t can indicate whether the model is adequate or inadequate, and yield information on how to better describe the series. Modified models would then be refitted and resubjected to diagnostic checking.

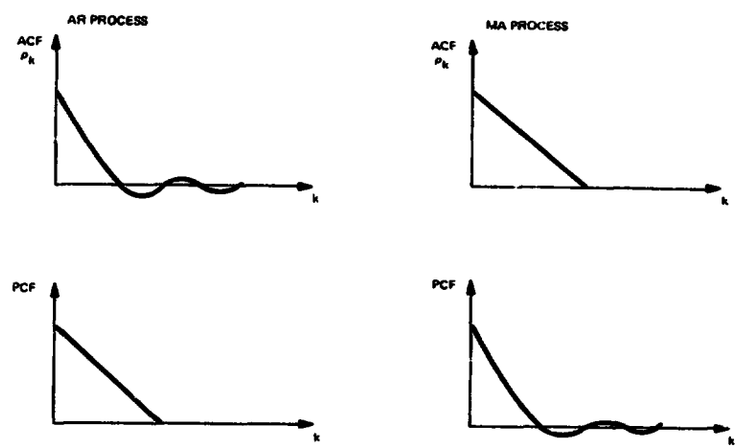

Figure 2. Comparison of ACF and PCF for Pure AR and MA Processes

f) Transfer Function Development

Time series analysis techniques can be extended to obtain discrete linear transfer functions of systems having an input time series x_t and an output time series y_t. For the system illustrated in Figure 3, it is assumed that the system can be adequately represented by the impulse response parameters, v_0, v_1, v_2, v_3, v_4, and v_5. Therefore, y_t is related to x_t by

$$y_t = (v_0 + v_1 B + v_2 B^2 + v_3 B^3 + v_4 B^4 + v_5 B^5)\, x_t \tag{11}$$

In general, for a dynamic system containing input observations x_t and output observations y_t,

$$y_t = v(B)\, x_t \tag{12}$$

where v (B) represents the impulse response function of the system.

The input/output relationship of the type of system represented by Figure 3 can also be represented by the following general linear difference equation:

$$(1 - \delta_1 B - \cdots - \delta_R B^R)\, y_t = (\omega_0 - \omega_1 B - \ldots - \omega_S B^S)\, x_{t-b} \tag{13}$$

or

$$\delta(B)\, y_t = \omega(B)\, x_{t-b} \tag{14}$$

Solving for y_t, the following expression is obtained:

$$y_t = \delta^{-1}(B)\ \omega(B)\ x_{t-b} = \delta^{-1}(B)\, \omega(B)\, B^b\, x_t \tag{15}$$

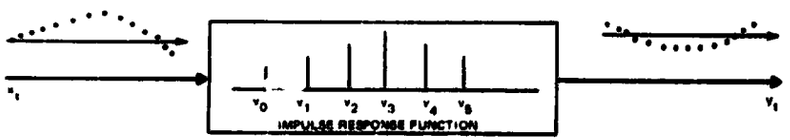

Figure 3. The Input/Output Model

By defining

$$\Omega(B) = \omega(B)\, B^b \tag{16}$$

Equation 15 can be written as

$$y_t = \delta^{-1}(B)\, \Omega(B)\, x_t \tag{17}$$

Comparing Equation 17 with 12, we find that

$$v(B) = \delta^{-1}(B)\, \Omega(B)$$

Using the definition of Equation 12 for the discrete transfer function of the system and substituting this into the difference Equation 13, the following identity is obtained:

$$(1 - \delta_1 B - \cdots - \delta_R B^R)(v_0 + v_1 B + v_2 B^2 + \ldots) = (\omega_0 - \omega_1 B - \cdots - \omega_S B^S) \tag{18}$$

The following set of equations is obtained by equating like powers of B:

$$v_j = 0,\ j < b \tag{19}$$

$$v_j = \delta_1 v_{j-1} + \delta_2 v_{j-2} + \cdots + \delta_R v_{j-R} + \omega_0,\ j = b \tag{20}$$

$$v_j = \delta_1 v_{j-1} + \delta_2 v_{j-2} + \cdots + \delta_R v_{j-R} - \omega_{j-b},\ j = b+1, \ldots, b+S \tag{21}$$

$$v_j = \delta_1 v_{j-1} + \delta_2 v_{j-2} + \cdots + \delta_R v_{j-R},\ j > b+S \tag{22}$$

The relationship of the v_i parameters from the impulse response function to the δ and ω parameters of the difference equation representation are illustrated in Equations 19 through 22.

The transfer function model identification process is greatly simplified if the input to the system is white noise since the cross correlation function between a white noise input and the system output represents the impulse response function of the system. If the input is some other stochastic process, simplification is possible by performing an operation denoted as "prewhitening".[2] This approach was used in this study.

The estimation technique used for obtaining the δ and ω parameters for difference Equation 15 is analogous to that given for the one dimensional modeling case. After applying Marquardt's Algorithm, the resulting model is of the form

$$y_t = \delta^{-1}(B)\, \omega(B)\ B^b x_t + R_t \tag{23}$$

where R_t represents the residual signal not correlated with the input. Solving equation 23 for R_t, the following expression is obtained:

$$R_t = \left[\, y_t - \delta^{-1}(B)\ \omega(B)\ B^b\ x_t \,\right] \tag{24}$$

The procedure determines the ζ and ω parameters by attempting to minimize the following sum of squares function:

$$S(\zeta, \omega) = \sum_{t=1}^{N} R_t^2 \tag{25}$$

The diagnostic checking procedure is analogous to that given for the one dimensional case.

g) Transfer Function Development in a Feedback Loop

This study was concerned with modeling the human operator in a compensatory tracking system[1] as shown in Figure 1. The human transfer function G cannot be obtained directly by only considering the time series e_t and u_t, since the residual R_t must be independently distributed of e_t. For example, its cross correlation function must be zero for all lags:

$$E\left[(R_t - \bar{R})\ (e_{t+\tau} - \bar{e})\right] = 0 \tag{26}$$

If this is violated, then the parameter estimates obtained are not consistent. Unfortunately, when a dynamical system as the human transfer function, is located within a feedback loop, the independence assumption between e_t and R_t does not hold.[4] In order to overcome the problem, the signals e_t and u_t must be analyzed with respect to the input signal R_t. Since R_t is an externally generated random noise series, it is uncorrelated with any noise generated within the system and present at the output or error signal.

Based on classical control Technique,[5,6] the following equations can be defined relating u_t to n_t, and e_t to n_t:

$$u_t = \frac{G(B)}{1 + G(B)\,H(B)}\, n_t + z_{1,t} \tag{27}$$

$$e_t = \frac{1}{1 + G(B)\,H(B)}\, n_t + z_{2,t} \tag{28}$$

where

G (B) Human transfer function

H (B) Plant transfer function

$z_{1,t}$, $z_{2,t}$ Noise components on the output signals uncorrelated with the input signal n_t

By redefining the control ratios

$$T_u(B) = \frac{G(B)}{1 + G(B)\,H(B)} \tag{29}$$

$$T_e(B) = \frac{1}{1 + G(B)\,H(B)} \tag{30}$$

the human transfer function G(B) can be obtained using the following equation:

$$G = \frac{T_u(B)}{T_e(B)} \tag{31}$$

Therefore, the pilot transfer function in this experiment was obtained from transfer functions relating output/input and error/input.

IV. HUMAN OPERATOR PERFORMANCE MODELS

The human operator transfer functions and residual characteristics for the various experiments analyzed in which H = 1 are shown in Figure 4. Based on these results, the following general conclusions can be made concerning the experiments:

- All of the pilots exhibited a time delay of 0.2 second with a second order denominator.
- Two of the three models had a zero in the numerator.
- The controlling functions for all of the operators modeled resulted in overdamped systems.

An important result obtained from analyzing the residual terms of these models was that the human is a generator of seasonality characteristics. This is a very significant conclusion reached on this study which is not obtainable by means of conventional methods.

Seasonality characteristics indicate that an observation at a particular time is related to observations from previous times in some periodic manner. In order to eliminate the seasonality characteristics from the observations, it is necessary to difference the data by the periods of the seasonality. This operation nullifies the seasonality pattern and emphasizes the actual response. Therefore, the operation $B^s z_t = z_{t-s}$ played a particularly important role in the analysis of the seasonality time series and it was found that the simplifying operation $\nabla_s z_t = (1-B^s)\, z_t$ was very useful.

Based on an analysis of the residuals for the three experiments shown in Figure 4, it was concluded that seasonalities were present. Figure 5 summarizes the results of the analysis of these seasonalities. Note that the seasonality periods determined, 0.4, 1.6, and 3.4 seconds, appear to be closely related to some multiple having a fundamental period of 0.4 seconds. It was concluded that the result is due to some "rhymic" motion of the subject operators in attempting to track the random inputs. It appears that the subjects were generating a seasonality variation which they were superimposing on their response in tracking the random inputs. This may be analogous to some of the "dither" inputs used by previous investigators who have postulated various models[7]. Verification of this rhymic effect is a very important result of this study and its origin needs to be investigated further.

The multivariate program was also applied to model experiments in which the plant's transfer function was given by

$$H = \frac{1}{s} \tag{32}$$

EXPERIMENT				PLANT (H)	HUMAN = $G = \frac{u_t}{e_t}$	FORM	RESIDUAL		SYSTEM CHARACTERISTICS
RECORD NO	RUN NO	DURATION (SECS)	SUBJECT				PARAMETERS	VARIANCE	
00000	00001	158.72	A	1	$G = \frac{0.488}{(1-0.548B)(1-0.548B)}$	(2,0,1)	$\phi_1 = 0.22$ $\phi_2 = 0.52$ $\theta_1 = 0.192$	0.167	OVERDAMPED
00007	00001	153.6	B	1	$G = \frac{0.74(1-0.928B)B}{(1-0.5378)(1-0.9448)}$	(1,0,1)	$\phi_1 = 0.205$ $\theta_1 = 0.107$	0.516	OVERDAMPED
00004	00001	243.2	C	1	$G = \frac{-0.65(1-0.803B)B}{(1-0.3868)(1-0.978)}$	(2,0,0)	$\phi_1 = 0.202$ $\phi_2 = 0.109$	1.05	OVERDAMPED

NOTE B = DELAY OF 0.2 SEC IN TIME (i.e., $Bx_t = x_{t-0.2}$)

Figure 4. Modeling Results for H = 1

in order to determine the change in the human transfer function when the plant changes. In order to compare performance, the experiment that subject C performed in Record No. 00014, Run No. 00001, was analyzed and compared with his performance when H = 1, in Record No. 00004, Run No. 00001, using the time series method. The results of the two models obtained are compared in Figure 6. Analysis of these two models indicates that the most significant difference with H = 1/s is that a transportation lag does not exist in the numerator, leading one to conclude that the integrator, H = 1/s, provides memory to the system from which the operator is better able to anticipate and predict future actions using the two numerator lead factors of (1-0.958B) and (1+8.75B). However, since the coefficient of the B term, 8.75, is very much greater than the coefficient of 1 in the term (1 + 8.75B), it is interpreted to mean that although there is a small instantaneous response, the predominant response is delayed by 0.2 sec. Therefore, the numerator does approximate a transportation lag with the following result:

$$G = \frac{-3.02\,(1 - 0.958B)B}{(1-0.872B)\,(1 + 0.64B)} \qquad (23)$$

The interpretation of the increase in operator gain from 0.65 in the original transfer function with H = 1, to 3.02 in the approximated new transfer function with H = 1/s is attributed to the decrease in open-loop gain caused by the H = 1/s. Thus, when the operator is controlling the plant H = 1/s, it is necessary that he increase his gain to compensate for the attenuation caused by the plant in order to achieve a desirable bandwidth. This problem was not present with H = 1. Therefore, it is seen that the change in the plant from H = 1 to 1/s supplies the operator with memory from which he is better able to anticipate future action, and also decreases the open-loop gain causing the operator to increase his gain in order to achieve a desirable bandwidth.

RECORD NO.	RUN NO.	SUBJECT	RUN LENGTH (SECS.)	PLANT H	SEASONALITY PERIOD PRESENT IN RESIDUAL (SECS.)
00000	00001	A	158.72	1	3.4
00007	00001	B	153.6	1	0.4
00004	00001	C	243.2	1	1.6

Figure 5. Seasonality Periods Generated by the Human Operator

	Human $G = \frac{u_t}{e_t}$
Model with H = 1 Record No. 00004, Run No. 00001	$G = \frac{-0.65\,(1-0.803B)B}{(1-0.3868)\,(1-0.978)}$
Model with H = 1/s Record No. 00014, Run No. 00001	$G = \frac{-0.248\,(1-0.958B)\,(1+8.75B)}{(1-0.872B)\,(1+0.64B)}$

Figure 6. Models of Subject C with Plants of H=1 and 1/s

Examination of the variability of the human transfer function was studied by analyzing experiments similar to those considered in Figures 4 and 5, where the three subjects A, B, and C repeated the compensatory tracking tasks. The program was also applied to examine 30-second "windows" (300 points spaced at 0.1 second intervals) over the duration of the three original experiments analyzed in Figures 4 and 5.

To check the repeatability of the human transfer function, the transfer functions for subject A repeating Record No. 00000, Run No. 00001, immediately, and for subject C repeating Record No. 00004, Run No. 00001, eleven days later were obtained. Figure 7 compares the two models obtained for subject A; Figure 8 compares the two models obtained for subject C.

	HUMAN $G = \frac{u_t}{e_t}$	DURATION (SECS)	RESIDUAL			
			FORM	PARAMETERS	VARIANCE	SEASONALITY
ORIGINAL MODEL (Record No 00000, Run No 00001, 11/4/71)	$G = \frac{0.48B}{(1-0.54B)(1+0.54B)}$	158.72	(2,0,1)	$\phi_1 = 0.22$ $\phi_2 = 0.52$ $\theta_1 = 0.19$	0.167	3.4 Secs
REPEATED MODEL (Record No 00000, Run No 00002, 11/4/71)	$G = \frac{(0.032-0.33B)}{(1+0.252B)}$	289.28	(1,1,0)	$\phi_1 = -0.575$	0.108	3.4 Secs

Figure 7. Repeatability of Subject A with H = 1

	HUMAN $G = \frac{u_t}{e_t}$	DURATION (SECS)	RESIDUAL			
			FORM	PARAMETERS	VARIANCE	SEASONALITY
ORIGINAL MODEL (Record No 00004 Run No 00001, 11/4/71)	$G = \frac{-0.66(1-0.66)B}{(1-0.386B)(1-0.97B)}$	243.2	(2,0,0)	$\phi_1 = 0.202$ $\phi_2 = 0.109$	1.05	1.6 Secs
REPEATED MODEL (Record No 00013, Run No 00002, 11/15/71)	$G = \frac{-0.51(1-0.974B)B}{(1-0.71B)(1-0.99B)}$	153.6	(1,0,0)	$\phi_1 = 0.565$	1.14	1.6 Secs

Figure 8. Repeatability of Subject C with H = 1

It is observed from Figure 7 that the model of subject A has changed considerably by having subject A immediately repeat the experiment. It is significant to note that a transportation lag does not exist in the numerator, leading one to initially conclude that the subject has learned the experiment very well and the numerator factor, (-0.032 - 0.33B), is behaving as an anticipation time constant. However, since the coefficient of the B term, -0.33, is very much greater than the coefficient -0.032, then it is concluded that the numerator approximates a transportation lag with the following result:

$$G = \frac{-0.33B}{(1 + 0.252B)} \tag{34}$$

Note that the denominator for the repeated experiment only contains one smoothing delay time constant, as compared to the original model. In addition, note the variance of the white noise residual was reduced from 0.167 to 0.108. It was therefore concluded that the subject A had learned the experiment very well and was trying to behave without a transportation lag and required only one smoothing time constant.

For the repetition of the experiment by subject C, whose results are analyzed in Figure 8, it is observed that the form of both the original and repeated models were the same when the experiment was repeated eleven days later. His gain is down and the variance of the white noise residual is up, which could be due to several factors. The only revealing factor concerned with his new model is that the numerator factor (1-0.974B) nearly cancels the denominator factor (1-0.99B) resulting in

$$G = \frac{-0.51B}{(1-0.71B)} \tag{35}$$

Therefore, it was concluded that there is some learning evidence here, since the subject now only needed one smoothing time constant. However, due to the long time delay between experiments, there isn't much evidence of learning in the set of experiments for subject C, as for the set of experiments for subject A.

Variability of the human transfer function over an entire run was also analyzed. Experimental data concerned with the tracking performance of subject B in Record No. 00007, Run No. 00001, was chosen for analysis (see Figure 4). Windows located over the first and last 30 seconds of the experiment were modeled and compared with that previously obtained over the entire experiment which lasted 153.6 seconds. Figure 9 compares the original model obtained over the entire length of the experiment with those models obtained by investigating the 30 second windows located at the beginning and at the end of the experiment. Note from this table that for the Model Number 1, the pole at (1-0.94B) is fairly close to the zero at (1-0.83B) and could be cancelled to obtain the approximate model shown. In the case of models numbered 2 and 3, however, notice that there are poles and zeros which are exactly equal, or extremely close, and can be cancelled very precisely resulting in very good, approximate models as shown.

Based on these results, it was concluded that the models for the 30 second windows can be approximated very well be first order transfer functions. In addition, the model for the entire run can be approximated as a first order transfer function with lesser accuracy. Analysis of the results for the continuous time equivalent of the approximate model is quite interesting. It indicates that the gain of the human operator is constant over the entire experiment. However, the time constant changes over a wide range: 0.5 seconds for the first 30 second window; .2 seconds for the final 30 second window; an average of .3 seconds over the entire experiment. This would appear to indicate that

ORIGINAL PAGE IS OF POOR QUALITY

		Sampling Interval (Secs)	Definition of B	Exact Model	Approximate Model	Continuous Time Equivalents of the Approximate Model
Model No 1	Model for Entire Experiment Lasting for 153.6 Seconds	0.2	$Bx_t = x_{t-0.2}$	Human $= G = \frac{u_t}{e_t}$ $\frac{0.74(1-0.83B)}{(1-0.54B)(1-0.94B)}$	Human $= G = \frac{K e^{-0.2s}}{(s+a)}$ $\frac{5e^{-0.2s}}{(s+3)}$	
Model No 2	Model for Window Located Over First 30 Seconds of Data	0.1	$Bx_t = x_{t-0.1}$	$\frac{0.82(1-0.978B)B^2}{(1-0.688B)(1-0.988B)}$	$\frac{0.828B^2}{(1-0.688B)}$	$\frac{5e^{-0.2s}}{(s+2)}$
Model No 3	Model for Window Located Over Last 30 Seconds of Data	0.1	$Bx_t = x_{t-0.1}$	$\frac{0.64(1-0.906B)B^2}{(1-0.368B)(1-0.908B)}$	$\frac{0.648B^2}{(1-0.368B)}$	$\frac{5e^{-0.2s}}{(s+5)}$

Figure 3. Window Sample Analysis of Subject B with H = 1

the human operator is applying much more smoothing during the earlier part of the experiment than at the end. Therefore, his response time is faster towards the later part of the experiment indicating that he has learned and can anticipate changes, with the result that he can respond faster.

Time series analysis has the capability of modeling human operator transfer functions under task and/or environmental stress conditions. As an illustration of its application in this manner, consider a human operator in a compensatory tracking situation. It is desired to determine the variations of his model's parameters under hypoxia stress and he is required to perform the tracking task under simulated oxygen levels corresponding to sea level, 12,000 feet and 22,000 feet. For each of these three experiments, the program can determine the human transfer function directly from the data very efficiently.

It might also be desired to determine the parameter variation of the human transfer function under combinations of stress. For example, the program could be extended and applied for determining the human operator model while he is tracking a target on a compensatory display with various combinations of stress including hypoxia, roll, pitch, vibration, heat, etc. The program could be further applied for determining the effect of these stresses on such physiological parameters as blood pressure, heart rate, etc.

Due to budget limitations the program was not extended to model stress data. For the same reason, the program was not applied to model pilot compensatory tracking data for areas where the element H was changed to $1/s^2$.

CONCLUSIONS

This pioneering effort for applying time series analysis to model the human operator represents the first time that time series theory has been applied to this problem and its results have been most illuminating. The foremost conclusion found on this study is that the time series method is a very efficient, effective, and powerful method for modeling any dynamical process having an input and output which contains noisy observations. Application of the time series technique to modeling the human operator in a compensatory tracking situation indicated that he can be adequately represented in the B domain by the B-transfer function having the following form.

$$G(B) = \frac{K(1-T_1B)B}{(1-T_2B)(1+T_3B)} \tag{36}$$

plus a residual containing a completely modeled mixed AR/MA structure and white noise.

It was also concluded that when the plant's transfer function was changed from 1 to 1/s, the integrator, H = 1/s, provided memory to the system, and the operator was better able to anticipate and predict future actions. The resultant model, therefore, did not contain a transportation lag. However, a good approximation to this transfer function contained a tranportation lag and it was found that the operator also had to increase his gain significantly. The interpretation of his increase in gain was caused by his compensation for the decrease in the open-loop gain due to the integrator H = 1/s. The operator basically increased his gain in order to achieve a desirable bandwidth.

It was also found that when an operator immediately repeated an experiment, he attempted to eliminate the transportation lag and one of the smoothing time constants.

This is a very significant result and is anticipated based on his ability to learn. However, due to the magnitude of the coefficient, the model still had an effective transportation lag from a practical viewpoint. It was also found that having an operator repeating an experiment several days later indicated very little learning ability.

Analysis of the variability of the human transfer function over the length of the experiment by means of analyzing a small number of points (window) indicated that the human operator is applying much less smoothing during the later part of the experiment. This was interpreted to mean that he has learned and can anticipate changes, with the result that he can respond faster.

A very significant result of this effort was measurements of a seasonality being generated by the operator. These seasonalities are interpreted as a rhymic effect that the operator is generating in order to track random noise.

REFERENCES

S. M. Shinners, Techniques of System Engineering, New York: McGraw Hill, Chap. 6, 1967.

G. E. P. Box and G. M. Jenkins, Time Series & Analysis Forecasting and Control, San Francisco: Holden - Day, 1970.

D. W. Marquardt, An Algorithm for Least Square Estimation of Nonlinear Parameters, SIAM Journal, Vol. II., No. 2, June 1962.

H. Akaike, Some Problems in the Application of the Cross-Spectral Method, Advanced Seminar on Spectral Analysis of Time Series, Edited by Bernard Harris, John Wiley and Sons, Inc., New York, 1967, pp. 81-107.

S. M. Shinners, Modern Control System Theory and Application, Reading: Addison - Wesley, 1972.

S. M. Shinners, Control System Design, New York: John Wiley and Sons, Inc., Chap. 9, 1964.

S. M. Shinners, Man-Machine Control Systems, Electro-Technology, Vol. 79, No. 4, pp. 59-76, April 1967.

N75 19151

IN-FLIGHT MEASURED HUMAN PILOT DESCRIBING FUNCTION AND REMNANT FOR PITCH ATTITUDE CONTROL

H.A. Mooij

National Aerospace Laboratory
Amsterdam, The Netherlands

ABSTRACT

Flight tests have been performed with a variable pitch-rate-command/attitude-hold flight control system in a Beechcraft Queen Air-80 aircraft. Some results of in-flight measured runs for two pilots controlling typical "easy" and "difficult" dynamics are presented together with the initial results of the same tracking experiment performed on a ground-based flight simulator. Results are compared with results of other investigators using fixed-base flight simulators.

1 INTRODUCTION

Twenty-five years of pilot modeling have passed since Tustin's initial efforts to describe the human controller and still there are good reasons for expanding the available knowledge, even for the most simple control situations such as single loop compensatory tracking.

The reason here, for performing some experiments in this area is the involvement in a program aimed at the formulation of design criteria for electrical primary flight control systems for transport aircraft. Longitudinal systems are studied and especially the approach and landing flight phases are considered. Pitch-rate-command/attitude-hold systems form the basis of all flight-control system mechanisations presently under study.

In the experimental phases of this particular research program, piloted moving base flight simulation plays an important role. Because it is planned to incorporate a compensatory tracking task experiment in the handling qualities evaluation program (to gain more insight into pilot ratings and commentary), hard- and software has been prepared to measure pilot dynamics and pilot-aircraft system performance.

At the moment a pilot-vehicle system analysis study is performed for

the prediction of total system behaviour; results of this study will be used to indicate ranges of parameters for the aircraft/flight control system combination which are worthwhile to be covered during piloted flight simulation. For this study we needed Analytical Verbal Describing Function Model (AVDFM) rules (Ref. 1) which are applicable to real pilots, normal piloting effect (rather than optimized behaviour after considerable practice) controlling the (simulated) aircraft with the type of manipulator which is typical for electrical flight control systems for advanced designs, which is a displacement side-stick controller with some viscous damping.

Relatively little systematic work has been reported on the correlation of flight and ground-simulator studies as far as pilot describing functions, remnant and pilot-aircraft system performance is concerned in order to determine the accuracy with which simulator studies of control problems can be extrapolated to the flight environment. On the subject of pilot's remnant no in-flight measured data could be traced in the literature.

A limited in-flight as well as moving/fixed base flight-simulation study of three dynamical configurations with three pilots has been performed. The results of these experiments have given basic information on models to be used in system analysis studies as well as more insight into the correlation of in-flight and ground based measured data.

After a short description of the experiment, some of the final results of the in-flight experiment are presented in this paper. Initial results of the measurements of the ground-based flight simulator counterpart of the in-flight experiment, which ended just two weeks ago, will be presented as well.

2 THE EXPERIMENT

The task was single axis compensatory pitch-attitude tracking with a small amplitude disturbance input. The random appearing forcing function was injected at the display. This "still air" task seems applicable for the study of pitch-attitude-stabilised aircraft.

(Although the longitudinal control task for approach and landing is typically multiloop, several investigators have shown that pilot dynamics of the pitch attitude inner loop in this multiloop situation are quite

PRECEDING PAGE BLANK NOT FILMED

similar to the pilot dynamics for the single-loop attitude tracking task, e.g. reference 5).

The forcing function should ideally have a power spectral density representative of the task under study, which is landing approach for transport type aircraft. However to be able to correlate results with those of many fixed-base experiments a rectangular spectrum formed by 10 sine waves with an effective bandwidth (6 sine waves) of 1.5 rad/sec has been used. The control system, display and manipulator were the same for flight- and ground experiments. Below a short out-line of the equipment used, is presented.

Vehicle: flight : - Beechcraft Queen Air Model-80
- Speeds 130 KIAS
- Normal acceleration characterized by the first order zero[m)] of the pitch attitude-to elevator deflection transfer function: value 1.26 sec^{-1}
- Roll control by safety-pilot.

ground : - 3-degrees of freedom, Moving Base Flight Simulator of the Delft University of Technology, also used "fixed-base".
- Pitch attitude motion identical to flight situation (no wash-out)
- Normal acceleration characterized by the first order zero, see above Wash-out, second order, with a time constant of 2 secs

Control system : Prefilter-Model-Following mechanization for a pitch-rate-command/attitude-hold system;

Controlled element (CE): General form $Y_c = \frac{K_c(S+1/T_c)}{S(S^2+2\zeta_c\omega_c S+\omega_c^2)}$

Parameters $1/T_c$ and ω_c selectable

m) Short-period approximation.

Dynamics used:

CE No.	$1/T_c$ sec^{-1}	ω_c $rad\ sec^{-1}$
1	1.5	4
2	0.6	4
3	0.6	0.8

$\zeta_c = 0.7$

Display : CRT (0.75 meter distance to the pilots eye)
Root-mean-square amplitude of forcing function: 1 cm

Manipulator : NLR-side-stick controller; gradient 2.5 kgcm/degree
Stick sensitivity near optimum for each Controlled Element.

3 DATA PRESENTATION

Fourier analysis of the recorded data has been performed on a Hewlett Packard 5450 A Fourier Analyzer. Run length was 200 secs and the data sampling rate was 10. Computed results are averages of 5 runs for each pilot-controlled element combination.

A least squares fitting procedure was used to determine the parameters of a mathematical model approximating the measured describing functions near cross-over frequency. Data weighting according to the frequency separation with respect to the cross-over frequency has been applied.

The derived numerical results for the pilots who controlled both "easy" and "difficult" dynamics during the in-flight experiments are presented in table form. Only the describing function data for CE-3 are in graphical form because this is possibly the most interesting controlled element tested.

4 DISCUSSION OF RESULTS

Flight

For the in-flight experiment the standard deviation for data

averaged over 5 runs as indicated in figure 1 and 2 for the system and human controller describing function is small. Minus 20 dB/dec slope for the amplitude ratio of the system describing function is measured in the region of cross-over.

Table 1, presenting cross-over frequencies and phase margins shows for pilot A, CE-1 a regressed situation. As indicated in table 2 high scores (score = 1 - variance of the error divided by variance of the forcing function) for "easy" dynamics relative to those for CE-3 have been measured. This table shows also that error-related relative remnant ($\rho^2_{a_e}$) is always higher than or equal to output-related relative remnant ($\rho^2_{a_o}$).

Regarding pilot models (table 3) the interesting observation can be made that near equal (-high)-values for the lead time constant have been obtained (table 3) and identical values for the effective time delay for control of CE-3.

When observing the in-flight measured input injected remnant, figure 3, for pilot B, or nearly flat spectrum up to 4 rad/sec is measured for the "easy dynamics" situation CE-2. The results for the CE-3 however indicate a -20 dB/dec slope over the same frequency band. The data above ω = 4 rad/sec should be disregarded because a neuro-muscular/manipulator mode existed around 5.7 rad/sec.

The probability density function of the pilot's output (Fig. 4) clearly illustrates the regressed situation of pilot A, CE-1, (peak-at-zero); for the CE-3 situation this pilot shows less bimodal character than pilot B.

A comparison of these results for pilot dynamics with the predictions of the AVDPM of reference 1, shows (table 4) lag (lead) equalization (CE-2) by the pilot as expected from the AVDPM "rules" with the location of the break frequency ($1/T_I$) in such a way that a long stretch of -20 dB/dec for the open loop system will exist. The cross-over frequencies measured, 3 respectively 1.8 rad/sec, are 60 % below the values of 5 respectively 3 rad/sec for K_c and K_c/S^2-forms as indicated by the AVDPM. However, the controlled statement form actually existing during the experiment differs from the simple expressions mentioned above. An additional 90° phase lag exists for CE-2 while an increased phase lag (in excess of 180°) exists for ω>2 rad/sec for CE-3.

Comparison of flight results with ground-simulator results

Moving-base experiments yielded higher cross-over frequencies and lower phase margins than comparable fixed-base experiments for the same pilot with an "easy" controlled element, pilot A, CE-1[m]. [A comparison for pilot B, CE-2, is not possible because for the moving-base situation too few practice runs were included.]
For CE-3 no appreciable changes in cross-over frequency and phase margin can be observed when comparing moving- and fixed-base results.

Approximately 30 % increase in the $1-\sigma$ value for the error can be observed when going from the moving-base to the fixed-base situation; this is also measured for the easy dynamics. This trend correlates well with the commentary of the pilots, stating that the task was easier when performed with motion. The score fore moving-base was always higher than either flight or fixed-base.

Trend in the output-related relative remnant shows a reverse in the relative numbers when comparing the easy and difficult dynamics; for the easy dynamics the relative remnant decreases when going from the MB to FB-situation while the inverse holds for the difficult dynamics.

Excluding the regressed control situation in-flight for pilot A, CE-1, good correspondence exists between in-flight and ground-based measured pilot-vehicle system performance.

The relation of moving-base and fixed-base simulator results show that motion cues have a definite effect on pilot's tracking behaviour.

Comparison with previous results

With respect to the in-flight results, no direct comparison of system performance with previous results is possible due to the lack of data in the literature.

A similar in-flight and ground-based study by Seckel and others, reference 2, presents no pilot-aircraft system data.

More recent in-flight data have been reported by Newell and Smith in reference 3; pilot-aircraft system data for a forcing function bandwidth of 1.5 rad/sec are given but the task here was a roll-tracking task. For the A-2+ configuration of this reference, a cross-over frequency of 1.8 rad/sec and a phase margin of 50 degrees were obtained for pilot A and B (Pilot C showed "regressed" control characteristics). A fitting of a simple mathematical model indicated a lead time constant of 2.3 seconds.

m) This same observation could be made from the data of another pilot participating in the ground-simulator program. (Pilot C, table 1).

In reference 2 and 3 no remnant data are presented.

Table 5 presents correlation of the current FB results with data of reference 4 and 5 (fixed-base also). In reference 4, data originally from NASA TND-2067 are presented (p.244) for high ω_c dynamics which are suited for a comparison with the current CE-2 dynamics. The estimate for system cross-over frequency (3.3 rad/sec) from data at lower frequencies reported herein seems on the optimistic side. The phase curve of the reference coincides completely with the current measured phase curve at lower frequencies. A phase margin of 35 degrees (as predicted in the reference) leads to a newly estimated cross-over at 3 rad/sec.
This agrees very well with the current measured 2.8 rad/sec (phase margin 40 degrees for CE-2.

In reference 5 results for a single axis experiment are presented which can be used for comparison with the current low ω_c dynamics (CE-3). The measured pilot-aircraft system describing functions for this experiment are presented however in reference 6.
The cross-over frequencies of 2.4/2.7 reported herein for two pilots corresponds to very low phase margins of 12 and 0 degrees respectively. Taking the liberty to question the correctness of the amplitude scaling in this case, a new estimate for the cross-over frequency can be made. Taking the lowest phase margin reported in the current program as well as in the experiments described in the literature for tasks where low frequency lead is generated, namely 20 degrees, a value of 2 rad/sec for both pilots results. Again this correlates very well with the results described here.

To summarize, the following can be said:

- The predictions of pilot's equalization (form and location of break points) and his effective time delay by the AVDPM (1965 status) holds for the in-flight pitch attitude tracking situation.
- The flight data correlate very well with results obtained during the ground-based experiment. Characteristic for "easy dynamics" are cross-over frequencies of 3.0 to 3.2 rad/sec with a phase margin of 20 to 30 degrees for flight and moving-base simulation conditions. Fixed-base, somewhat lower cross-over frequencies with higher phase margings have been measured.
  For control of the "difficult dynamics" cross-over frequencies of 1,8 to 2,0 rad/sec with phase margin 20 to 35 degrees are measured.

5 REFERENCES

1. McRuer, D.T. Jex, H.R. — A review of quasi-linear pilot models. IEEE Transactions on Human Factors in Electronics. Vol. HFE 8, number 3, September 1967.
2. Seckel, E. Hall, I.A. McRuer, D.T. Weir, D.H. — Human pilot dynamic response in flight and simulator. WADC Technical Report 57-520, 1958.
3. Newell, F.D. Smith, H.J. — Human transfer characteristics in flight and ground simulation for a roll tracking task. NASA TND-5007, 1969.
4. Sadoff, M. Dolkas, C.B. — Acceleration stress effects on pilot performance and dynamic response. Second Annual NASA-University Conference on Manual Control, NASA SP-128, 1966.
5. Stapleford, R.L. Craig, S.J. Tennant, J.A. — Measurement of pilot describing functions in single controller multiloop tasks. NASA CR-1238, 1969.
6. Weir, D.H. McRuer, D.T. — Pilot dynamics for instrument approach tasks: full panel multiloop and flight director operations. NASA CR-2019, 1972.

CE	Pilot	ω_c (rad/sec)			φ_m (degrees)		
		FLT	MB	FB	FLT	MB	FB
1	A	1.3	3.2	2.5	80	30	65
	C	-	3.0	2.5	-	20	45
2	B	3.0	2.5	2.8	30	45	40
3	A	1.8	2.0	2.0	35	35	20
	B	1.8	2.0	2.0	20	35	25

Table 1 Cross-over frequency ω_c and phase margin φ_m.

FLT = in-flight MB = moving-base simulator FB = fixed-base simulator

CE	Pilot	σ-error			Score			relative remnant $\rho^2_{a_c}$		
		FLT ')	MB ")	FB ")	FLT	MB	FB	FLT ($\rho^2_{a_e}$)	MB	FB
1	A	0.54	1.9	2.5	0.71	0.78	0.73	0.84 (0.93)	0.87	0.73
2	B	0.48	1.9	2.8	0.77	0.79	0.69	0.70 (0.70)	0.90	0.75
3	A	0.77	4.1	5.2	0.40	0.58	0.40	0.20 (0.63)	0.35	0.58
	B	0.85	3.5	4.7	0.27	0.62	0.49	0.50 (0.66)	0.40	0.48

Table 2 Performance measures and relative remnant. ') cm display
") and ") Volts

CE	Pilot	K_p deg/cm display	T_I	T_L	τ_e
			sec		
1	A	5.5	1.1	0.8	0.28
2	B	6.0	1.4	0.7	0.26
3	A	0.6	0.1	4.7	0.38
	B	0.6	0.05	4.3	0.38

$$Y_p = K_p \frac{(T_L j\omega+1)}{(T_I j\omega+1)} e^{-\tau_e j\omega}$$

Table 3 Model for pilot's describing function (FLT)

Form controlled element near cross-over frequency				
CE-2		CE-3		
K_c (based on amplitude ratio; phase lag $\approx -90°$)		K_c/s^2 (very good approximation for amplitude ratio; phase lag exceeds $-180°$ for $\omega > 2$ rad/sec)		
AVDPM	This study Pilot B	AVDPM	This study Pilot A	This study Pilot B
Lag(-lead)	Lag(-lead)	Low freq.lead	Low freq.lead	Low freq.lead
$1/T_I \approx 1/\tau_e = 0.6$	$1/T_I = 0.7$	$1/T_L \ll \omega_c = 1.8$	$1/T_L = 0.21$	$1/T_L = 0.22$
($\tau_e = 0.33$) $\tau_e = 0.22$	$\tau_e = 0.26$	($\tau_e = 0.50$) $\tau_e = 0.38$	$\tau_e = 0.38$	$\tau_e = 0.38$

Table 4 Correlation with pilot dynamics predicted by the AVDPM of reference 1. ω_i = forcing function bandwidth. ($\tau_e = \tau_o - 0.07\,\omega_i$)

Source	Pilot	Controlled Element $1/T_\theta$ sec^{-1}	ω_θ rad/sec	ζ_θ	ω_i rad/sec	ω_c rad/sec	φ_m deg.	$\rho^2_{a_c}$
Ref.4	A	0.4	3.35	0.53	1.5	3.3 1)	34 1)	-
This study (FB)	A	1.5	4.0	0.70	1.5	2.5	65	0.73
	B	0.6	4.0	0.70		2.8	40	0.75
Ref. 5	A	0.6	0.8	0.4	1.0	2.4 2)	small	0.30
	B					2.7 2)	small	0.36
This study (FB)	A	0.6	0.8	0.7	1.5	2.0	20	0.58
	B					2.0	25	0.48

1) Estimated from system describing function data at lower frequencies.
2) Estimated as indicated in reference 6.

Table 5 Correlation with previous results, fixed-base.

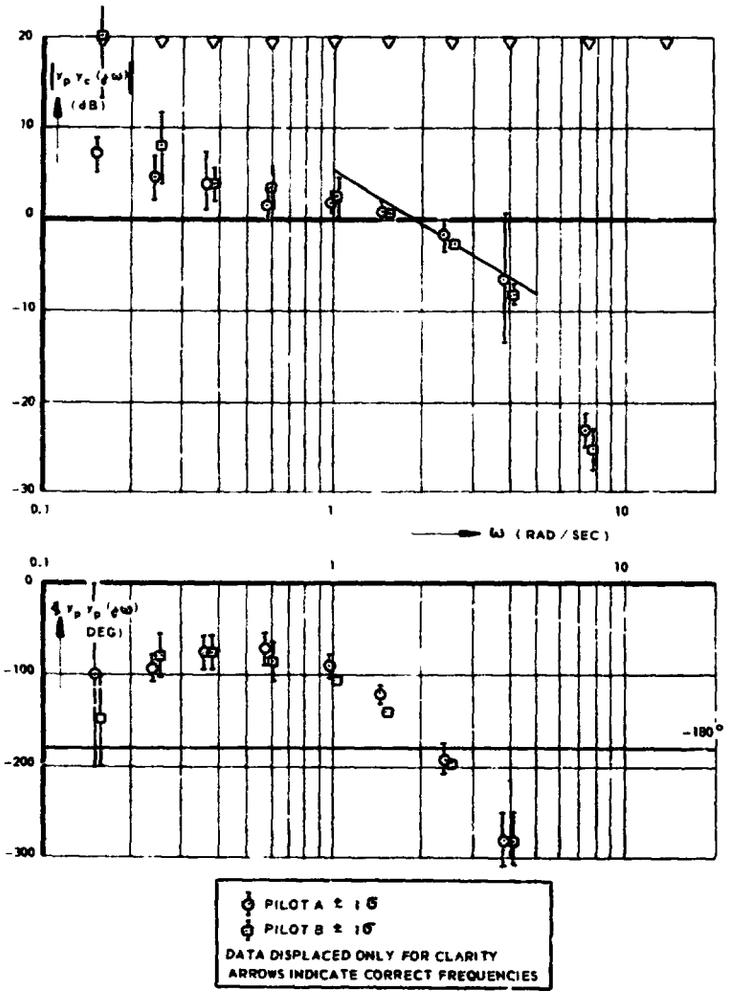

FIG 1. SYSTEM DESCRIBING FUNCTION CE-3 (FLIGHT)

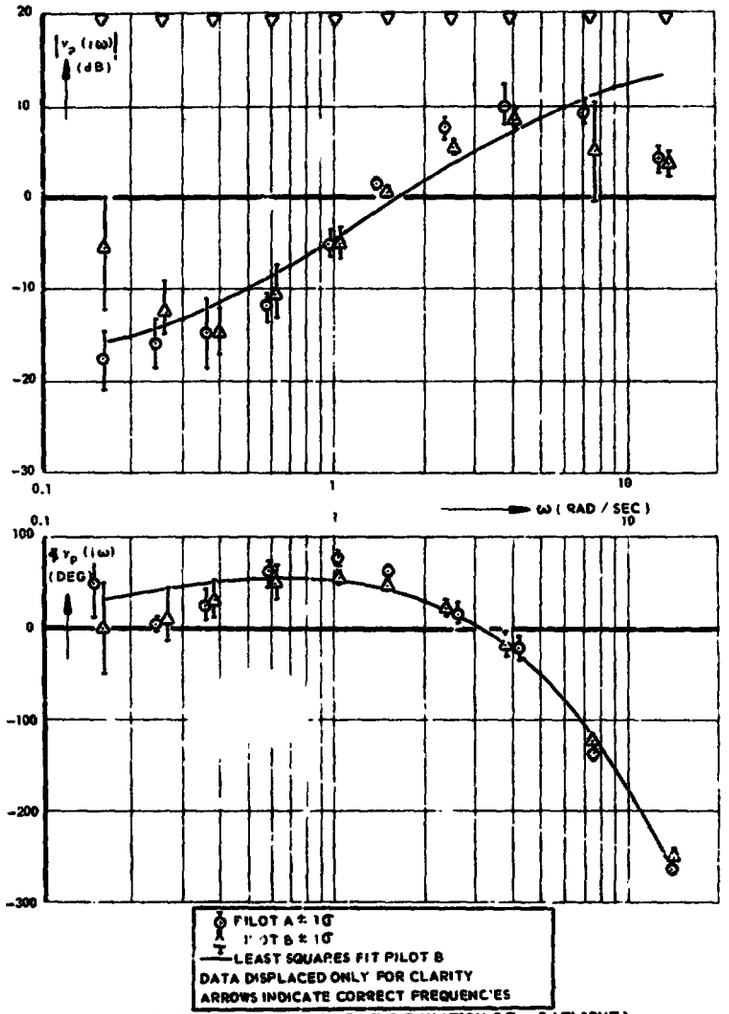

FIG. 2 HUMAN PILOT DESCRIBING FUNCTION CE-3 (FLIGHT)

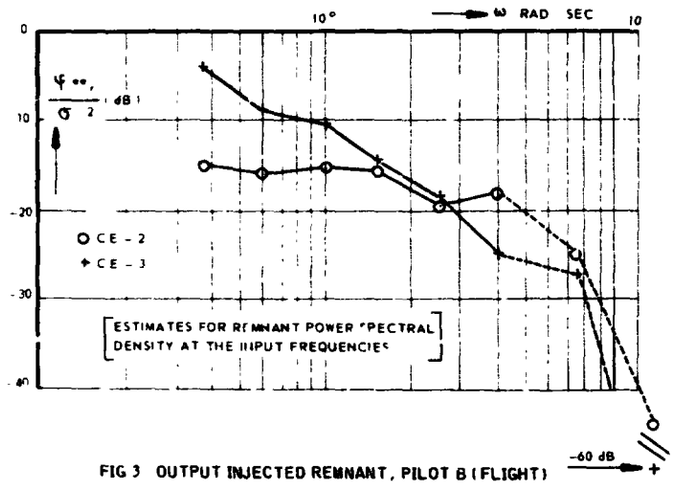

FIG 3 OUTPUT INJECTED REMNANT, PILOT B (FLIGHT)

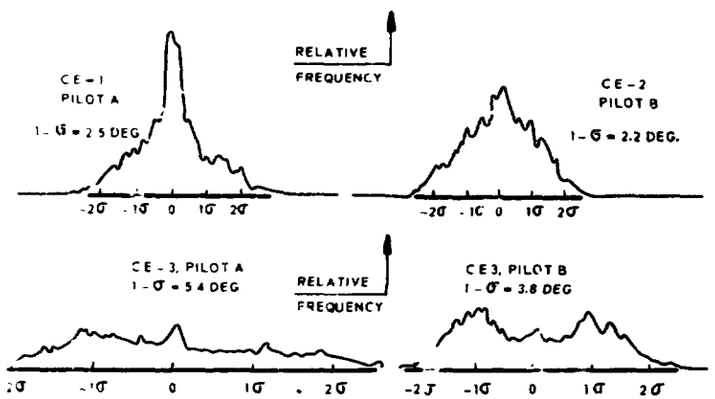

FIG 4 PROBABILITY (FLIGHT) DENSITY FUNCTION OF THE PILOT OUTPUT

N75 19152

A SIMPLIFIED SIGNAL ANALYSIS TECHNIQUE FOR OBTAINING OPTIMAL ESTIMATES OF SYSTEM DYNAMICS

by

R. P. Whitbeck
Calspan Corporation

Abstract

Given an unknown system with n inputs and m outputs, one possible modeling approach is to compute estimates of transfer functions using the mathematical methods of Wiener-Hopf (i.e., the steady state Kalman estimators). Unfortunately, all the computational methods for implementing the Wiener-Hopf approach require (or assume) an analytical expression for the determinant of the spectral matrix. These assumptions, in turn, pre-ordain the final form of the Wiener estimates and hence the approach tends to lose the "Free-Minimization" methodology which makes it attractive. Clearly, what is needed is an algorithm which operates on the finite length input and output signals in a manner which does not bias the results through the use of possibly unwarranted assumptions. The procedure set forth in this paper furnishes such an algorithm for the special case where n finite-length realizations, for each of the n input signals, are available.

1. Introduction

The Wiener-Hopf method leads to the formalization of a spectral matrix which must be factored into the product of two matrices, one of which is analytic in the right half of the complex frequency plane; the other analytic in the left half plane. Unfortunately, all methods for accomplishing this factorization, at one particular step or another, require (or assume) an analytical expression for the determinant of the spectral matrix. This assumption, in turn, pre-ordains the final form of the Wiener estimates.

For example, if it is assumed that the determinant of the spectral matrix is a rational polynomial in s, then the estimators are forced to be rational polynomials in s also. Clearly what is needed is a computational algorithm which operates on the finite-length input and output signals and furnishes optimal estimates without prejudicing the results through the use of possibly unwarranted assumptions. The procedure set forth in this paper furnishes such an algorithm for the special case where the unknown system has n inputs and n finite length realizations for each of the n input signals are available.

2. Theory

In the interests of brevity, the results will be developed for the case where the unknown system has the two-input and one-output configuration shown in Figure 1. After this, the extension to the case of n inputs and m outputs will be obvious.

*This work was supported by Calspan Corporation as an internal research project, No. 86-218.

PRECEDING PAGE BLANK NOT FILMED

FIGURE 1. TWO INPUT CASE

The Wiener-Hopf minimization procedure leads, for the ideal case of an infinite number of infinite length realizations of the signals, to Equation (1):

$$\begin{bmatrix} \phi_{xx} & \phi_{xy} \\ \phi_{yx} & \phi_{yy} \end{bmatrix} \begin{bmatrix} H_1 \\ H_2 \end{bmatrix} - \begin{bmatrix} \phi_{xz} \\ \phi_{yz} \end{bmatrix} = \begin{bmatrix} \mathcal{E}_1 \\ \mathcal{E}_2 \end{bmatrix} \tag{1}$$

In Equation (1),

$$\phi_{xy} = \lim_{T \to \infty} \frac{1}{2T} E\left\{ X(-s)\, Y(s) \right\}, \text{ etc.} \tag{2}$$

where, for example,

$$Y(s) = \int_{-T}^{T} y(t)\, e^{-st}\, dt \tag{3}$$

The $\mathcal{E}$ vector is unknown but must have the property of being analytic in the L.H.P. The $E\{\ \}$ denotes the ensemble average of the various auto and cross power spectra.

The solution to this equation, given that $\phi = \Theta_+ \Theta_-$ in

$$\phi H - \psi = \mathcal{E}$$

is

$$H = \Theta^{-1} \left[\Theta_+^{-1}\, \psi \right]_+ \tag{4}$$

$$H = \frac{\begin{bmatrix} \frac{Y_2}{2\sqrt{T}} & -\frac{Y_1}{2\sqrt{T}} \\ -\frac{X_2}{2\sqrt{T}} & \frac{X_1}{2\sqrt{T}} \end{bmatrix}}{\frac{1}{4T}\left[X_1 Y_2 - Y_1 X_2\right]} \left\{ \frac{\begin{bmatrix} \frac{\bar{Y}_2}{2\sqrt{T}} & -\frac{\bar{X}_2}{2\sqrt{T}} \\ -\frac{\bar{Y}_1}{2\sqrt{T}} & \frac{\bar{X}_1}{2\sqrt{T}} \end{bmatrix} \begin{bmatrix} \frac{1}{4T}\left(\bar{X}_1 z_1 + \bar{X}_2 z_2\right) \\ \frac{1}{4T}\left(\bar{Y}_1 z_1 + \bar{Y}_2 z_2\right) \end{bmatrix}}{\frac{1}{4T}\left[\bar{X}_1 \bar{Y}_2 - \bar{X}_2 \bar{Y}_1\right]} \right\}_+ \tag{8}$$

Carrying out the inner multiplication gives

$$H = \frac{\begin{bmatrix} \frac{Y_2}{2\sqrt{T}} & -\frac{Y_1}{2\sqrt{T}} \\ -\frac{X_2}{2\sqrt{T}} & \frac{X_1}{2\sqrt{T}} \end{bmatrix}}{\frac{1}{4T}\left[X_1 Y_2 - Y_1 X_2\right]} \left\{ \frac{\begin{matrix} \frac{1}{8T \cdot 4/2}\left[\bar{Y}_2 \bar{X}_1 z_1 + \cancel{\bar{Y}_2 \bar{X}_2 z_2} - \bar{X}_2 \bar{Y}_1 z_1 - \cancel{\bar{X}_2 \bar{Y}_2 z_2}\right] \\ \frac{1}{8T} \cdot 2\left[-\cancel{\bar{Y}_1 \bar{X}_1 z_1} - \bar{Y}_1 \bar{X}_2 z_2 + \cancel{\bar{X}_1 \bar{Y}_1 z_1} + \bar{X}_1 \bar{Y}_2 z_2\right] \end{matrix}}{\frac{1}{4T}\left(\bar{X}_1 \bar{Y}_2 - \bar{X}_2 \bar{Y}_1\right)} \right\}_+$$

or

$$H = \frac{\begin{bmatrix} \frac{Y_2}{2\sqrt{T}} & -\frac{Y_1}{2\sqrt{T}} \\ -\frac{X_2}{2\sqrt{T}} & \frac{X_1}{2\sqrt{T}} \end{bmatrix}}{\frac{1}{4T}\left[X_1 Y_2 - Y_1 X_2\right]} \left\{ \begin{matrix} \frac{z_1}{2\sqrt{T}} \\ \frac{z_2}{2\sqrt{T}} \end{matrix} \right\}_+$$

$$\therefore \begin{bmatrix} H_1 \\ H_2 \end{bmatrix} = \frac{\left[\begin{array}{c|c} Y_2 & -Y_1 \\ \hline -X_2 & X_1 \end{array}\right]}{X_1 Y_2 - Y_1 X_2} \begin{bmatrix} z_1 \\ z_2 \end{bmatrix} = \frac{\begin{bmatrix} Y_2 z_1 - Y_1 z_2 \\ X_1 z_2 - X_2 z_1 \end{bmatrix}}{X_1 Y_2 - Y_1 X_2} \tag{9}$$

The details of solving this equation analytically are discussed, for example, in Reference 1 and 2.

For the case where only a finite number of fixed length records are available, the various power spectra in Equation (1) are replaced by their estimates. For example, the estimate of ϕ_{XY}, call it $\hat{\phi}_{XY}$, is

$$\hat{\phi}_{XY} = \frac{1}{2Tn} \sum_{i=1}^{n} X_{i(-s)} Y_{i(s)} \tag{5}$$

Suppose now that only two realizations of each signal are available. Equation (1) becomes, using $\bar{X}$ to denote $X_{(-s)}$, etc.:

$$\left[\begin{array}{c|c} \frac{1}{4T}\left(\bar{X}_1 X_1 + \bar{X}_2 X_2\right) & \frac{1}{4T}\left(\bar{X}_1 Y_1 + \bar{X}_2 Y_2\right) \\ \hline \frac{1}{4T}\left(\bar{Y}_1 X_1 + \bar{Y}_2 X_2\right) & \frac{1}{4T}\left(\bar{Y}_1 Y_1 + \bar{Y}_2 Y_2\right) \end{array}\right] \begin{bmatrix} H_1 \\ \hline H_2 \end{bmatrix} - \begin{bmatrix} \frac{1}{4T}\left(\bar{X}_1 z_1 + \bar{X}_2 z_2\right) \\ \hline \frac{1}{4T}\left(\bar{Y}_1 z_1 + \bar{Y}_2 z_2\right) \end{bmatrix} = \begin{bmatrix} \varepsilon_1 \\ \hline \varepsilon_2 \end{bmatrix} \tag{6}$$

Because we have chosen to work directly in the frequency domain with the transform of the various signals, the factorization of the two input case becomes trivial when only two realizations of the inputs are available. Factor Equation (6) as

$$\hat{\phi} = \begin{bmatrix} \frac{\bar{X}_1}{2\sqrt{T}} & \frac{\bar{X}_2}{2\sqrt{T}} \\ \frac{\bar{Y}_1}{2\sqrt{T}} & \frac{\bar{Y}_2}{2\sqrt{T}} \end{bmatrix} \begin{bmatrix} \frac{X_1}{2\sqrt{T}} & \frac{Y_1}{2\sqrt{T}} \\ \frac{X_2}{2\sqrt{T}} & \frac{Y_2}{2\sqrt{T}} \end{bmatrix} = \theta_s \theta \tag{7}$$

Compute the inverses of the θ and θ_s given in Equation (7) and substitute into Equation (4)

Thus one need only work with the transforms of the signals when only two realizations are available. Note that no assumptions were necessary - the Wiener-Hopf theory guarantees that the H's computed according to Equation (9) are the best mean square fits possible under the stated conditions.

The extention to the n input case is now obvious but will require a double subscript notation (refer to Figure 2).

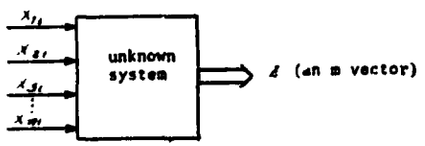

FIGURE 2. DOUBLE SUBSCRIPTED INPUTS

The factorization is now $\theta_o \theta$ where

$$\theta = \begin{bmatrix} \frac{x_{11}}{\sqrt{2nT}} & \frac{x_{21}}{\sqrt{2nT}} & \cdots & \frac{x_{n1}}{\sqrt{2nT}} \\ \frac{x_{12}}{\sqrt{2nT}} & \cdots & & \frac{x_{n2}}{\sqrt{2nT}} \\ \vdots & & & \\ \frac{x_{1n}}{\sqrt{2nT}} & \cdots & & \frac{x_{nn}}{\sqrt{2nT}} \end{bmatrix} \qquad (10)$$

3. Experimental Results

To develop some feel for the results given in Equation (9), the simple experiment shown in Figure 3 was set up as a digital simulation.

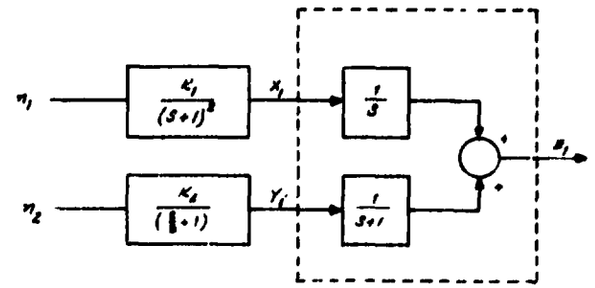

FIGURE 3. BLOCK DIAGRAM OF DIGITAL SIMULATION

In Figure 3, n_1 and n_2 are white noise sources fed through two different filters to produce the input signals X and Y. The estimates of $1/s$ and $1/s+1$ were then computed using Equation (9). The results are shown in Figure 4 for three different values of the ratio of K_1/K_2. As can be seen, the estimate of $1/s$ is excellent when the n_1 noise dominates while the estimate of $1/s+1$ is excellent when n_2 dominates. Somewhere in between, poorer estimates of both $1/s$ and $1/s+1$ are obtained.

The experiment also provided an opportunity to check out the effect of operating on the data with three different time windows. These are denoted as the square window (Π), the triangular data window (Δ) and the triangular window convolved with itself ($\Delta * \Delta$). The resulting magnitude plots for $1/s$ ($K_1/K_2 = 25$), shown in Figure 5, demonstrates the dramatic effect the time window has on the variability of the estimates.

4. Conclusion

Given an n input system and n experimental records for each input, it has been shown that the optimum Wiener filter is easily computed using only the experimental data. That is, no assumptions concerning the analytical structure of the spectral matrix are necessary.

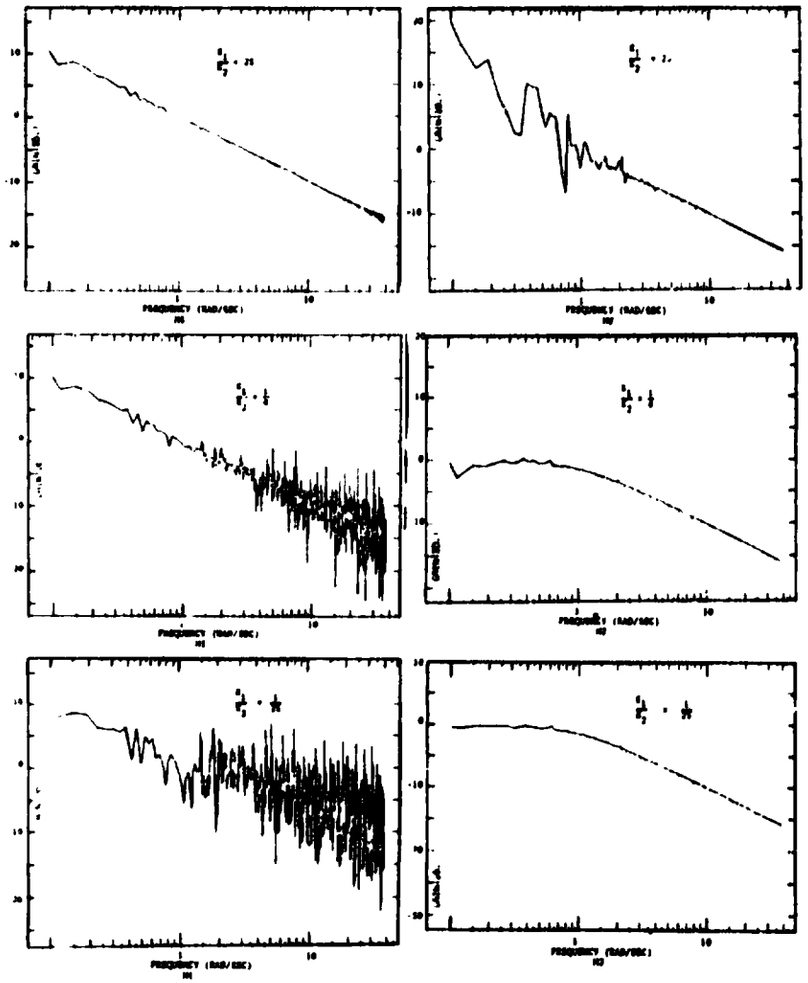

FIGURE 4. ESTIMATION OF H_1, H_2 WITH K_1/K_2 AS A PARAMETER

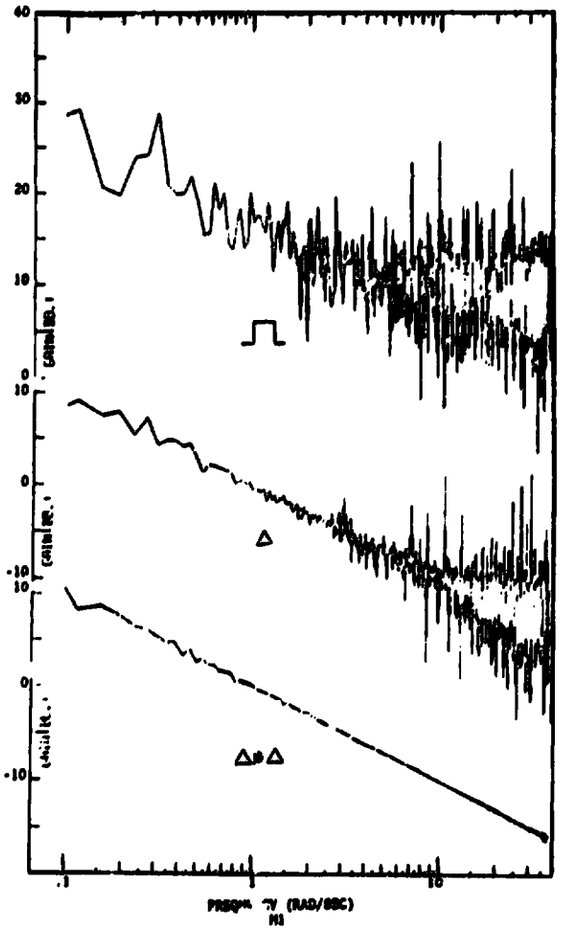

FIGURE 5. EFFECT OF TIME WINDOW ON $1/g$ ESTIMATES

References

1. Anderson, B. D., An Algebraic Solution to the Spectral Factorization Problem, IEEE Transactions on Automatic Control, Vol. AC-12, No. 4, August 1967.

2. Whitbeck, R. F., Knight, J. R., A Study of Pilot Modeling in Multi-Controller Tasks, Cornell Aeronautical Laboratory, Report IH-3037-J-1.

PRECEDING PAGE BLANK NOT FILMED

SESSION VII

ELECTROPHYSIOLOGICAL SYSTEMS ANALYSIS

N75 19153

A STOCHASTIC MODEL OF THE ELECTROMYOGRAM

Gyan C. Agarwal and Gerald L. Gottlieb
College of Engineering
University of Illinois at Chicago Circle
and
Biomedical Engineering Department
Rush-Presbyterian-St. Luke's Medical Center
Chicago, Illinois 60612

This work was supported in part by the National Science Foundation and the Presbyterian-St.Luke's R & E grants.

Ninth Annual Conference on Manual Control
May 23-25, 1973
Massachusetts Institute of Technology
Cambridge, Mass. 02139

PRECEDING PAGE BLANK NOT FILMED

Introduction

The electrical activity of muscle has long been studied by recording from the surface of a muscle and by recording the activity of individual motor units with concentric needle electrodes. Both techniques are simple and reliable enough to be used routinely in the kinesiology and in the diagnosis of many diseases of the muscles and their motor nerves [1].

The interference pattern electromyogram (EMG) which is observed when recording from the muscle's surface is a summation of action potentials of a number of motor units. The information about these motor units latent in it is not readily apparent because of the very complex pattern. Consequently, the surface EMG has not yet seen widespread clinical application. The purpose of this study is to investigate the quantitative regularities of interference pattern formation by motor unit action potentials. To this end, we have considered the parameters of a single motor unit and how they relate to the Fourier transform analysis of an EMG. The Fourier transform of the simulated electromyogram is compared with the Fourier transform of the actual EMG recorded from various human muscles using surface electrodes.

The Parameters of the Motor Unit

The steady state discharge of single neurons is often characterized by a probability density function for the intervals between successive nerve impulses called the Inter Spike Intervals (ISI).

Buchthal and his associates [2,3], Clamann [4], Leifer [5] and several other investigators have shown that the ISI of successive motor unit spikes are normally distributed. The rates

of steady state discharge in the cats are usaully between 5 to 30 pulses per second (pps) [6].

Clamann [4] has reported the firing rates between 7 to 25 pps in the human brachial biceps. The transient discharge rates may be higher, particularly in smaller muscles. A peak frequency of 150 pps has been reported in the adductor pollicis in the human hand [7]. In unfatigued human muscles, the mean and the standard deviation of the probability density function characterizing the ISI are functionally related [4], making it possible to completely specify the stochastic process by determining its mean. For the human brachial biceps muscle he arrives at the following functional relation between the mean (μ) and the variance (σ^2) of the ISI:

$$\sigma = 9.1 \times 10^{-4}\ \mu^2 + 4.0 \text{ msec} \qquad (1)$$

When successive intervals are uncorrelated, the probability density function and its mean and variance completely specify the statistical process generating the intervals. In the normal, unfatigued muscle, under conditions of low or moderate activation, the steady discharges of motoneurons generally do not show any dependence between successive intervals [4,5,8,9]. However, at high levels of muscular activity and particularly during fatigue, the discharges tend to be grouped so that successive intervals will no longer be uncorrelated.

The EMG of a single motor unit can be looked at as a time function defined by a convolution integral:

$$e(t) = \int_0^t h(t-\tau)\ p(\tau)d\tau \qquad (2)$$

where p(t) is a point process (i.e., a series of unit impulses

or Dirac delta functions) which passes through a filter whose impulse response is h(t) as in Fig. 1. The time function h(t) describes the shape of a single motor unit action potential. The width of the motor unit action potential is usually between 3 to 20 msec. [2]. The conduction process of the action potential along the muscle fiber is such that successive muscle action potentials recorded from the same motor unit cannot overlap. They remain distinct events. A typical EMG of a synthetic motor unit is shown in Figure 2. The time origin is arbitrarily fixed so that the first motor unit starts at $t = \ell$ msec. The Fourier transform (FT) of equation (2) is

$$E(jw) = H(jw)\ P(jw) \qquad (3)$$

where H(jw) is the FT of the impulse response and P(jw) is the FT of the random pulse train.

Let $t_i = \tau_1 + \tau_2 + \cdots + \tau_i$ and $t_0 = 0$. Then the ith pulse occurs at time $(\ell + t_{i-1})$. For a pulse train of $N + 1$ pulses, p(t) may be written as

$$p(t) = \sum_{i=0}^{N} \delta(t-\ell-t_i) \qquad (4)$$

and its FT is

$$P(jw) = \sum_{i=0}^{N} e^{-jw(\ell+t_i)}$$

$$= e^{-jw\ell} \left[\sum_{i=0}^{N} e^{-jwt_i}\right]. \qquad (5)$$

Without any loss of generality, we will from now on consider $\ell = 0$, i.e., the time origin is defined at the occurrence of the first pulse. Therefore,

$$P(jw) = \sum_{i=0}^{N} e^{-jwt_i} \tag{6}$$

where t_i is a sum of i normally distributed independent ISI.

Ensemble Average of P(jw)

The (i+1)th pulse occurs at time t_i which is a sum of i independent random variables

$$t_i = \tau_1 + \tau_2 + \ldots + \tau_i$$

The mean (μ) and variance (σ^2) of each ISI is assumed to be the same. Thus the mean and variance of t_i are given by:

$$E(t_i) = E(\tau_1 + \tau_2 + \ldots + \tau_i)$$

$$= \sum_{j=1}^{i} E(\tau_j) = i\mu \tag{7}$$

$$V(t_i) = V(\tau_1 + \tau_2 + \ldots + \tau_i)$$

$$= \sum_{j=1}^{i} V(\tau_j) = i\sigma^2 \tag{8}$$

The probability density function of t_i is given by

$$f(t_i) = \frac{1}{\sqrt{2\pi i}\,\sigma} \exp\left[\frac{-(t_i - i\mu)^2}{2i\sigma^2}\right] \tag{9}$$

The Fourier transform P(jw) is a random function of t_i, i = 1,2, ..., N. The ensemble average is given by

$$\overline{P(jw)} = E\,[P(jw, t_1, t_2, \ldots, t_N)]$$

$$= E\,[\sum_{i=0}^{N} e^{-jwt_i}]$$

$$= \sum_{i=0}^{N} E(e^{-jwt_i}) \tag{10}$$

The expected value of e^{-jwt_i} is given by

$$E(e^{-jwt_i}) = \int_{-\infty}^{\infty} e^{-jwt_i} f(t_i)\, dt_i$$

$$= \frac{1}{\sqrt{2\pi i}\,\sigma} \int_{-\infty}^{\infty} e^{-jwt_i}\, e^{\frac{-(t_i - i\mu)^2}{2i\sigma^2}}\, dt_i$$

Let $t_i - i\mu = x$. Then

$$E[e^{-jwt_i}] = \frac{2e^{-jwi\mu}}{\sqrt{2\pi i}\,\sigma} \int_{-\infty}^{\infty} \cos wx\, e^{\frac{-x^2}{2i\sigma^2}}\, dx$$

$$= e^{-jwi\mu} \cdot e^{\frac{-iw^2\sigma^2}{2}} \tag{11}$$

The ensemble average $\overline{P(jw)}$ from equations (10) and (11) is given by

$$\overline{P(jw)} = \sum_{i=0}^{N} e^{\frac{-iw^2\sigma^2}{2}} \cdot e^{-jwi\mu} \tag{12}$$

From equation (2) and (12), the ensemble average of the Fourier Transform of a single motor unit is given by

$$\overline{E(jw)} = \overline{P(jw)}\, H(jw) \tag{13}$$

and

$$|\overline{E(jw)}| = |\overline{P(jw)}|\, |H(jw)| \tag{14}$$

In Figure 3, the FT of the EMG given by equation 14 is plotted for μ = 20 msec, σ = 4.36 msec and N = 50 (which represents about 50 pulses on the average in one second interval). H(jw) is taken for a diphasic pulse with peak to peak height 2b and width 2c as shown in Figure 2. The FT for this pulse is

$$H(jw) = \frac{4b}{cw^2}\, e^{-jwc}\, [2\sin(\tfrac{wc}{2}) - \sin(wc)] \tag{15}$$

EMG Simulation

The EMG simulation was carried out on an IBM 1800 process computer. Our simulation is very similar to the work done by Person and Libkind [10,11]. Their studies were, however, limited to the symmetrical biphasic motor unit potentials.

In our model, M is the number of active motor units. The interspike intervals (ISI) are independent random values having a normal distribution with mean μ and standard derivation σ. Various shapes of motor unit potentials were used in this study with widths from 4 to 16 msecs. The pulse shapes were chosen to have a zero mean value. The ISI was always taken to be greater than the width of the pulse.

The first pulse for the ith motor unit was taken at a random interval uniformly distributed between zero and μ msec. All other ISI were normally distributed. The interference pattern was arrived at by summing up the action potentials of active motor units in the time interval from 0 to 1050 msec. The samples were 1 msec apart. The Fourier transform was obtained using 1024 samples and employing a fast Fourier transform algorithm.

Simulation Results

With a small number of motor units active, the pulses were frequently grouped with a "pile up effect". With an increase in the number of active motor units the time intervals free of impulses gradually diminished. A "saturation" level is reached with about 16 active motor units at mean frequency of 20 pps. Figure 4A shows that synthetic EMGs, especially the "saturated" ones, bears a close resemblance to the actual surface EMG, examples

of which appear in Figure 4B.

The theoretical analysis indicates that the average FT is the product of the FT of the motor units pulse shape and the ensemble average of the FT of a randomly occurring impulse train. Figure 5 shows the |FT| for one motor unit with a symmetric biphasic pulse of 8 msec width as shown in Figure 2 [μ = 20 msec, σ = 4.36 msec, M = 1]. Figure 6 shows the average |FT| for 15 such independent motor units. The smooth curve in Figure 6 is obtained from equation 14 for 10 spike sequence. The important point in this analysis is that average |FT| of several identical motor units approaches the FT of a single motor unit's pulse shape. Figure 7 shows some samples of the average |FT| of the surface EMG data recorded from the gastrocnemius-soleus muscle.

Discussion

In this analysis it has been assumed that mean and variance of the interspike interval remains constant and also that the shape of the various motor unit potentials in a muscle are the same. The theoretical analysis shows that the average |FT| of the synthetic EMG approaches the |FT| of the motor unit potential. This has been confirmed by simulation studies except at the very low end of the spectrum.

If one assumes that the mean and the variance of the ISI for the real EMG remain nearly stable over a short interval during constant force and also that the shape of the various motor unit potentials within the recording field of the electrodes are the same, then it is theoretically feasible to calculate the shape of the motor unit potential from the average FT. The practicality of this procedure is now being investigated.

References

1. J. V. Basmajian, Muscles Alive, The Williams and Wilkins Comp., Baltimore, 1967.

2. F. Buchthal, C. Guld, and P. Rosenfalck, "Action Potential Parameters in Normal Human Muscle and their Dependence on Physical Variables," Acta Physiol. Scand., Vol. 32, pp. 200-218, 1954.

3. F. Buchthal, P. Pinelli, and P. Rosenfalck, "Action Potential Parameters in Normal Human Muscle and their Physiological Determinants," Acta Physiol. Scand., Vol. 32, pp. 219-229, 1954.

4. H. P. Clamann, "Statistical Analysis of Motor Unit Firing Patterns in a Human Skeletal Muscle," Biophysical Journal, Vol. 9, pp. 1233-1251, 1969.

5. L. J. Leifer, "Characterization of Single Muscle Fiber Discharge During Voluntary Isometric Contraction of the Biceps Brachii Muscle in Man," Ph.D. dissertation, Stanford University, 1969.

6. E. Henneman, G. Somjen, and D. O. Carpenter, "Functional Significance of Cell Size in Spinal Motoneurons," Journal Neurophysiology, Vol. 28, pp. 560-580, 1965.

7. C. D. Marsden, J. C. Meadows, and P. A. Merton, "Isolated Single Motor Units in Human Muscle and their Rate of Discharge during Maximal Voluntary Effort," Journal Physiology, Vol. 217, pp. 12-13, 1971.

8. V. S. Gurfinkel, A. N. Ivanova, Ya.M.Kots, I. M. Pyatetskii-Shapiro, and M. L. Shik, "Quantitative Characteristics of the Work of Motor Units in the Steady State," Biophysics, Vol. 9, pp. 694-697, 1964. [English translation of Biofizika, Vol. 9, pp. 636-638, 1964].

9. W. S. Masland, D. Sheldon, and C. D. Hershey, "Stochastic Properties of Individual Motor Unit Interspike Intervals," American Journal Physiology, Vol. 217, pp. 1384-1388, 1969.

10. R. S. Person and M. S. Libkind, "Modelling of Interference Bioelectrical Activity," Biofizika, Vol. 12 (1), pp. 127-134, 1967. [English translation, pp. 145-153 by Pergamon Press].

11. R. S. Person and M. S. Libkind, "Simulation of Electromyograms Showing Interference Patterns," Electroencephal. Clin. Neurophysiol., Vol. 28, pp. 625-632, 1970.

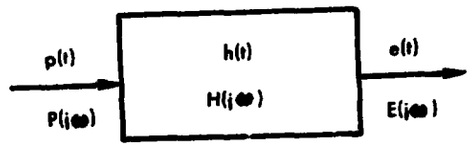

FIGURE 1: EMG Model as low pass filter

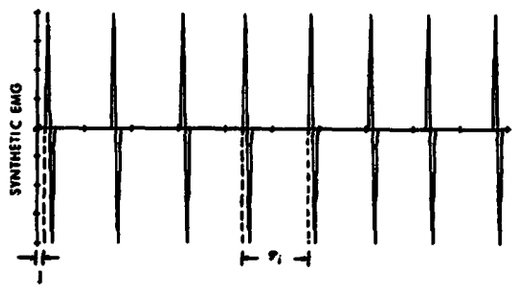

FIGURE 2: Synthetic EMG for a single motor unit with the parameters μ = 50 msec and σ = 6.27 msec. [Time = 400 msec]

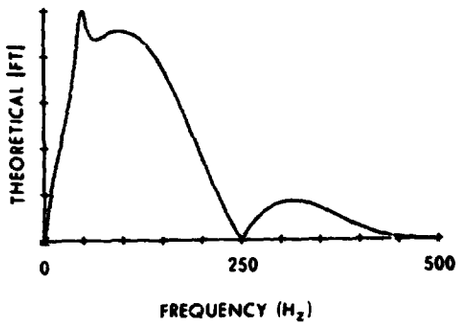

FIGURE 3: Theoretical absolute Fourier transform of the EMG for a symmetric biphasic pulse of 8 msec width, μ = 20 msec, σ = 4.36 msec and the number of pulses is 50.

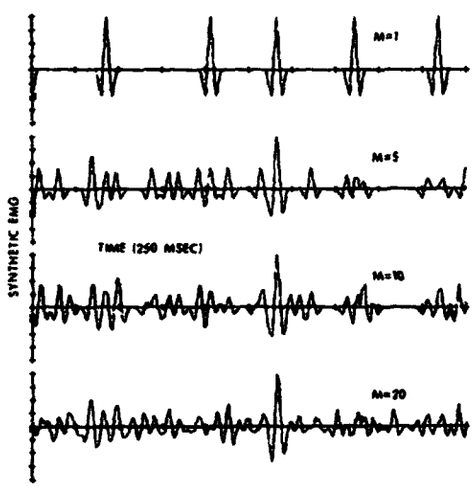

FIGURE 4A: Synthetic EMG generated for a symmetric triphasic pulse. The four traces are for 1, 5, 10 and 20 active motor units.

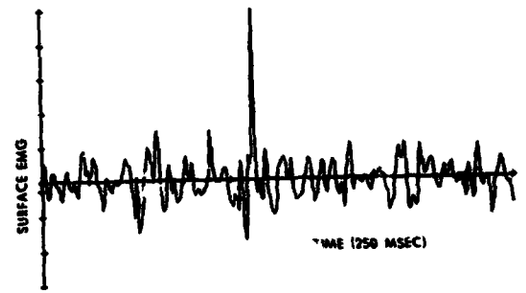

FIGURE 4B: Surface EMG from gastrocnemius-soleus muscle at low force level.

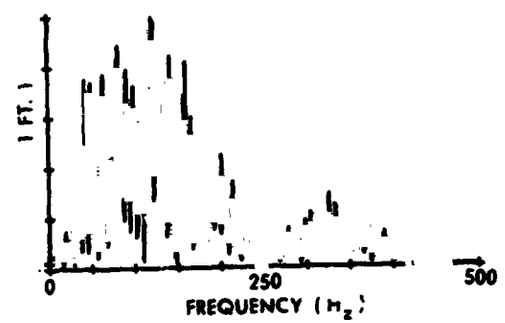

FIGURE 5: Absolute Fourier transform for a single active motor unit with biphasic pulse shape (μ = 20 msec and σ = 4.36 msec).

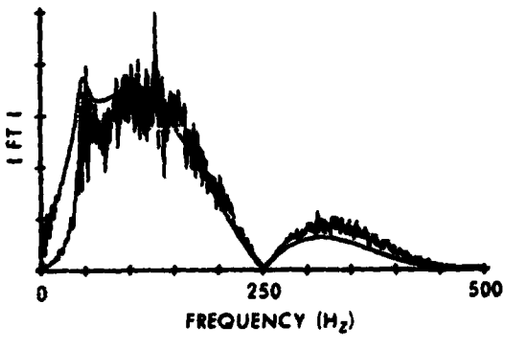

FIGURE 6: Average absolute Fourier transform for fifteen independent active motor units with biphasic pulse shape (μ = 20 msec and σ = 4.36 msec). The smooth curve is the theoretical absolute Fourier transform.

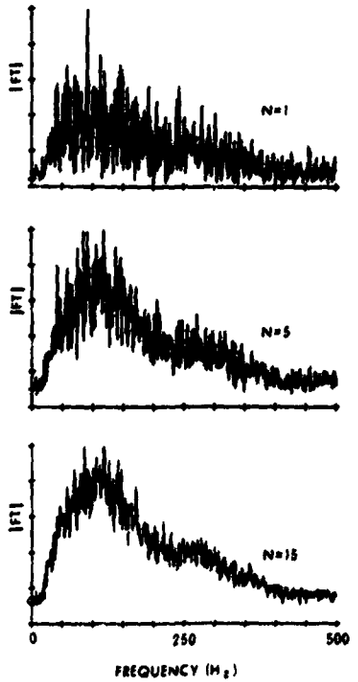

FIGURE 7: Average absolute Fourier transform of surface EMG data from gastrocnemius-soleus muscle. The three parts are average of 1, 5 and 15 samples.

N75 19154

MODELING AND MEASURING LIMB FINE-MOTOR UNSTEADINESS*

Raymond E. Magdaleno, Henry R. Jex, and R. Wade Allen
Systems Technology, Inc., Hawthorne, California

ABSTRACT

Threading a needle, pointing a flashlight, wielding a soldering iron, taking sextant readings, or aiming a handgun — all are tasks in which limb unsteadiness limits our finesse of visual-motor control. In this paper we examine such "fine-motor unsteadiness" — its properties, conceptual and analytical models, and experimental measurements.

Fine-motor unsteadiness (fluctuations of limb movement about a desired limb position) can have several oscillatory modes, which results in a multi-peaked spectrum and requires a fairly complex model. Based on a data review, the tentative model derived here includes: neuromuscular system (primarily muscles, spindles, tendons, and bones), grip interface, and control system dynamic elements. The properties of this model change with muscle tension and match a wide group of extant data. Particularly interesting is a tendon-compliance mode which seems dominant in the frequently observed "tremor mode" at 10-12 Hz and whose amplitude peak increases with force on the limb.

A simple experiment was performed to investigate the amplitude/force relationships of the "tremor mode." As the finger-pull force increased from [illegible] to 20 newtons, the tremor mode frequency for a given individual stayed within roughly ±1 Hz over a range from 9-12 Hz, while the average magnitude of the rms tremor acceleration increased tenfold.

A standardized test for making such measurements is given and applications in the fields of psychophysiological stress and strain measurements are mentioned.

INTRODUCTION

Threading a needle, pointing a flashlight, wielding a soldering iron, taking a sextant reading, or aiming a handgun — all are examples of fine-motor tasks in which hand unsteadiness limits our finesse of visual-motor control. To quote Marsden in Ref. 1:

*This work was sponsored by Lockheed Space and Missile Systems Co., as part of the NASA Manned Spacecraft Center's "Integrated Medical Biological Laboratory Measurement System," under Consulting Subcontract LCS7Z7920K.

PRECEDING PAGE BLANK NOT FILMED

"Our ability to perform tasks involving manual dexterity is limited by fluctuations in the force of muscle contraction and variations in the position of the hand and fingers which we term physiological tremor. If these fluctuations were totally asynchronous, delicate operations involving the use of both hands would be even more frustrated than if tremor of the two hands were synchronized. By holding a pencil in each hand and trying to keep the points in light contact, it is apparent that the involuntary movements of the two hands are not perfectly synchronous."

Such drift and fluctuations about a desired limb position are defined herein as fine-motor unsteadiness. Generally, these motions can have several oscillatory "modes," depending on the nature of the task. Before meaningful measurements can be made, it is important to understand these modes and their possible interactions. Putting the cart before the horse for tutorial clarity, we will first present our neuromuscular model for fine-motor tasks and then review the data on which it is based. This will lead to a set of simple measurements which can yield the salient characteristics of fine-motor unsteadiness. A brief experiment was made to optimize the proposed measures and procedures and to provide samples of typical data.

NATURE OF UNSTEADINESS

Conceptual and Analytical Models

Figure 1 shows a block diagram of a human operator performing a fine-motor task in which he attempts to minimize a perceived error by manipulating the controlled element in the correct direction.

The major internal functional elements in a human controller are: central sensing and equalization (Y_{CNS}), the muscle/manipulator dynamics (G_m), and the resulting proprioceptive feedback (G_p). Generally, the operator adopts equalization (anticipation lead or smoothing lag) so that the forward loop describing function for the combination of man and controlled element behaves like an integrator in the unity-gain crossover frequency region (i.e., from 0.1 to 1 Hz, Refs. 2 and 3). The man/machine system then has a dominant "visual-motor" closed-loop mode (denoted by subscript CL) just above these frequencies, i.e., f_{CL} = 1-2 Hz. At higher frequencies, other dynamic modes, due to internal neuromuscular system feedbacks, will also be present. These can often be

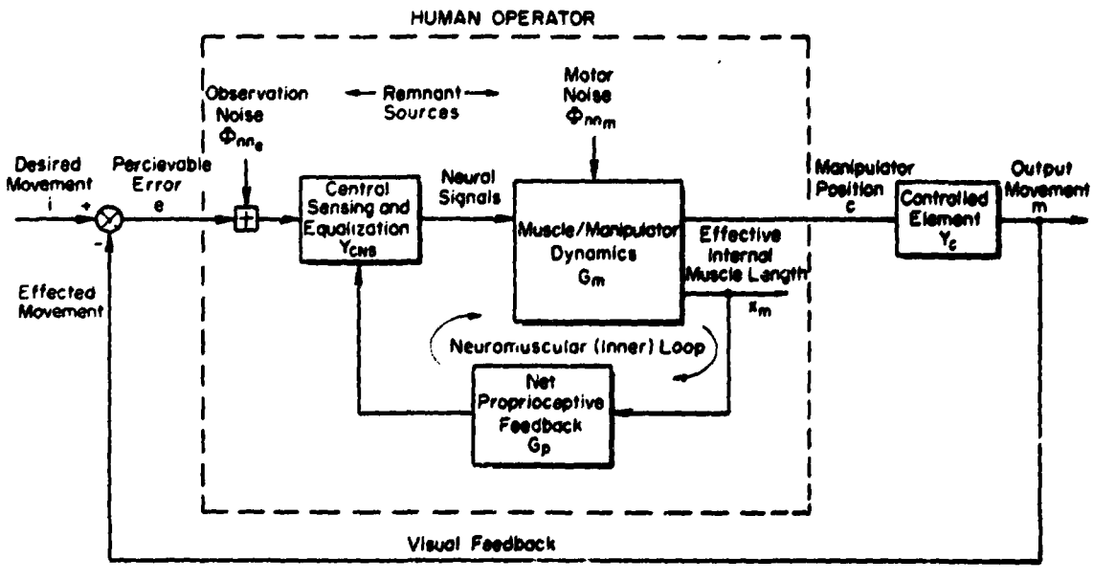

Figure 1. Block Diagram of Human Operator/Controlled Element During Fine-Motor Tasks

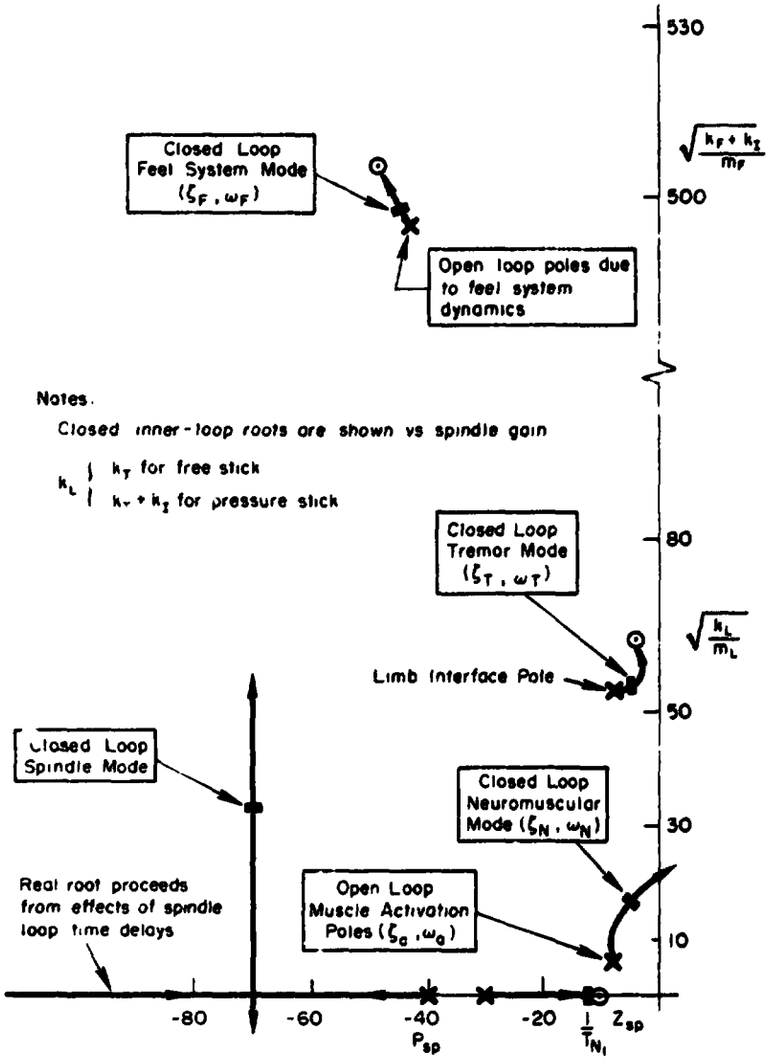

Figure 1. Root Locus Diagram Showing Modes for Spindle Closure of Neuromuscular Loop

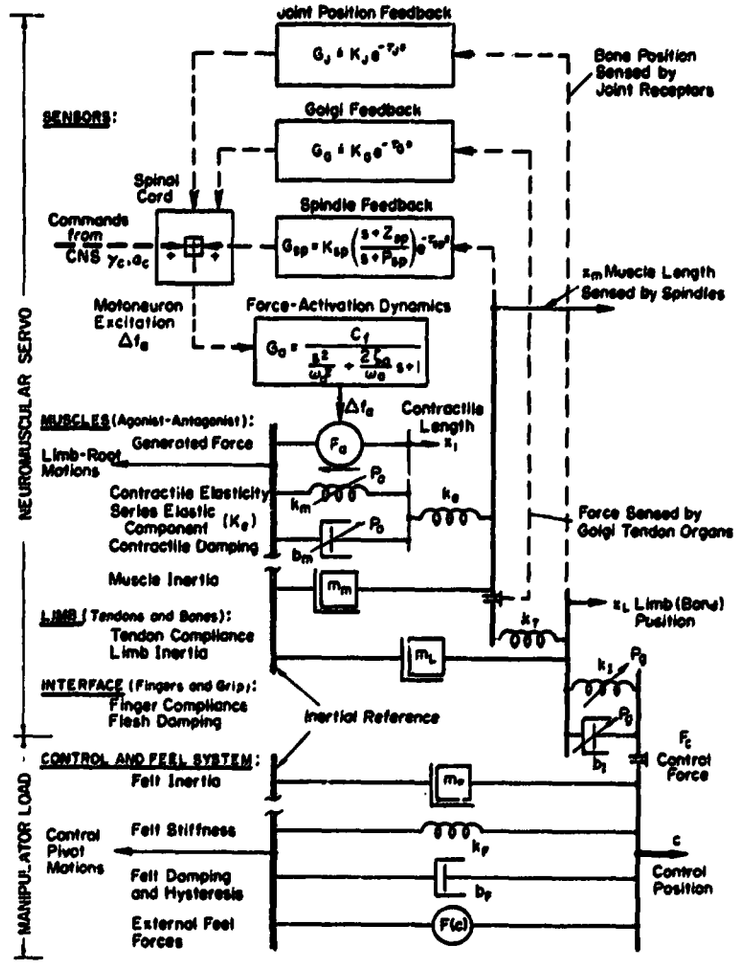

Figure 2. Network Diagram for Combined Neuromuscular Servo and Manipulator System (Shows Elements Required to Represent Neuromuscular and Tremor Modes)

ignored in modeling the manual control of vehicles, but become important during fine-motor tasks.

Proprioceptive information is shown feeding back an internal muscle length change rather than the manipulator position directly (Ref. 2); this has important effects as will be seen shortly. Muscle spindles are the dominant elements in the net proprioceptive feedback. These feed back a dynamically varying internal muscle length due to their location within the active muscle. Golgi tendon organs (force sensors) are also present; their dynamics are quite similar to those for spindles (Ref. 4). Joint angle sensors are present, too, but appear to play only a minor role in fine-motor tasks.

Also shown in Fig. 1 are two sources of remnant (noise) excitation: "observation and processing" noise, Φ_{nn_e}, (Refs. 5 and 6) and "motor remnant," Φ_{nn_m} (Refs. 3 and 5). The latter arises from muscle nonlinearities and irregularities in motor neuron firing rate.

The general form for the power spectral density of the manipulator position is given by:

$$\Phi_{cc} = |G_1|^2 \Phi_{nn_e} + |G_2|^2 \Phi_{nn_m} + |G_{1c}|^2 \Phi_{11}$$

i.e., each remnant excites some closed-loop transfer function. Note that a peak in Φ_{cc} could be due to either a lightly damped mode in the transfer functions or to a narrowband excitation process in the remnants, or both effects together. Because of the intrinsic nonlinearities in the muscle springiness, damping and neural firing rates, which vary with tension, the dominant modes may be different when tracking (with both agonist and antagonist muscles tensed) than when holding a steady force (with one or the other muscle slack).

To provide an appropriate conceptual and dynamical framework to interpret data, a lumped parameter model has been derived which fits the essential neuromuscular phenomena observed in fine-motor unsteadiness. This model, shown in Fig. 2, reflects a re-interpretation of the data and refinement of the model of Ref. 7, with more detail in representing the limb and muscle inertias, tendon compliance and grip interface compliance and damping. In addition,

we have added the "Activation Dynamics" which reflect the lag and attenuation in converting motorneuron firing rate into generated muscle force. This is the simplest model that can handle limiting cases such as isometric (fixed) and isotonic (free) controls, held objects (like flashlights, soldering irons, etc.), while reflecting the separate "neuromuscular" and higher frequency "tremor" and "manipulator" modes observed in the literature (see the following subsection, "Data on Unsteadiness Power Spectral Density"). Detailed numerical analysis has not yet been carried out for this model, but a brief series of "system surveys" using the systems analysis techniques of Ref. 3 has been made which shows that it yields modes and dynamic parameter trends which fit the large array of extant unsteadiness and tremor spectra.

Typical neuromuscular system modes for the neuromuscular "inner" loop of Fig. 1 are shown in the example root locus diagram of Fig. 3. The muscle spindle and force activation elements dominate the net proprioceptive feedback path. The "Closed-Loop Neuromuscular" mode near 20 rad/sec (4.3 Hz) has been shown (Ref. 7) to arise from the open-loop muscle force activation characteristics measured in experiments. The closed-loop "Tremor" and "Feel" System modes arise from the internal muscle-limb feedbacks and elastic elements, coupled with the control stick and grip compliance properties. It can be shown (e.g., Refs. 2 and 8) that the pole-zero dipoles arise from the spindles feeding back an internal muscle length rather than the manipulator position. This results in two sets of quadratic zeros near the imaginary axis which attract closed-loop roots. The closed-loop Tremor Mode arises from the Limb Interface dipole, which reflects the limb inertial interacting with the Interface, Tendon, and Contractile elements of Fig. 2. The closed-loop Feel System mode arises from the feel system inertia, spring rate, and damping interacting with the interface compliance.

The key feature of the dynamic situation depicted in Fig. 3 is that the natural frequency of the tremor mode at high-loop gain is heavily dependent on the limb inertia, m_L, and an equivalent spring, k_L, which is a combination of tendon and interface (flesh) compliances. Thus, the tremor mode frequency is relatively insensitive to the feel system restraints.

The frequency of the feel system mode depends primarily on the control stick inertia (m_F), spring rate (k_F), and interface compliance (k_I). This

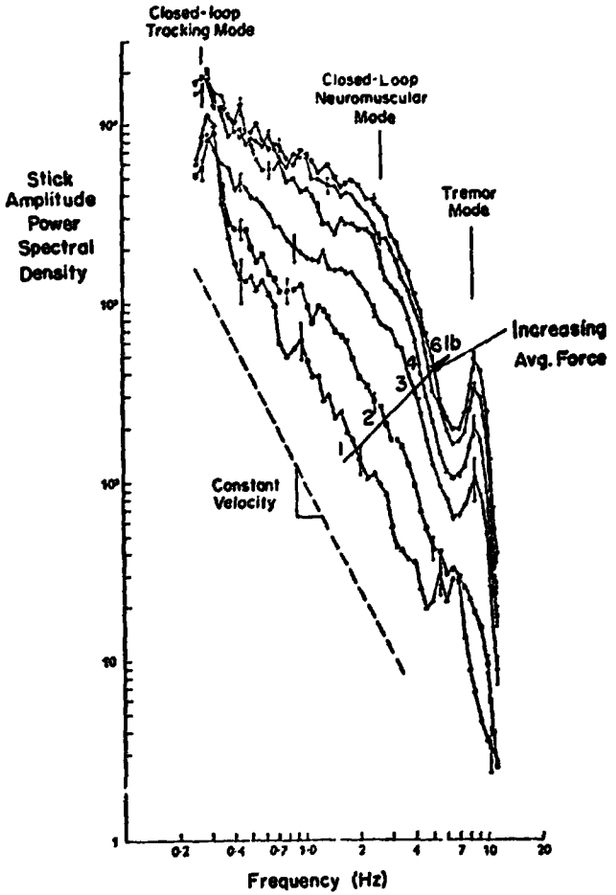

Fig. 1. Mean power spectra for six forces for subject M.D.
The error bars are of total length twice the standard error of the mean. 1 Lb. (0.45 kg) ▲, 2 Lb (0.91 kg) ■, 3 Lb (1.36 kg) +, 4 Lb (1.81 kg) ×, 5 Lb. (2.27 kg) ●, 6 Lb. (2.72 kg) ▼. The dashed line has a slope of 6 db/octave.

Figure 4. Typical Control (Error) Unsteadiness Power Spectra for Various Steady Forces on a Pressure Stick (From Sutton and Sykes, Ref. 9)

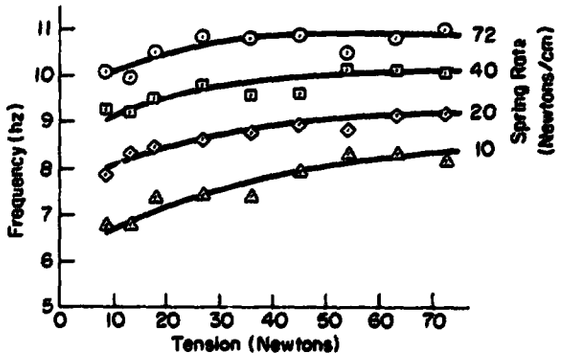

Figure 5. Effects of Set Force and Spring Stiffness on Forearm Flexor Tremor (Adapted from Robson, Ref. 11)

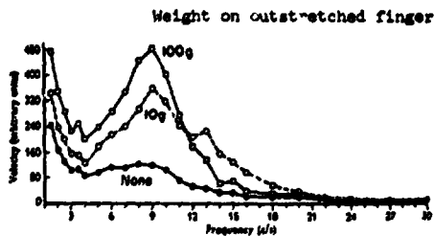

Plotting of tremor measured as velocity versus frequency in cycles per second averaged for the movements of the terminal phalanx of the fingers of 26 normal men. With the unloaded fingers (filled circles) and with 10 g (circle) and 100 g (square) strapped to the terminal phalanx. (Halliday and Redfearn, 1956, Ref. 12).

Figure 6. Effects of Load Weight on Velocity Power Spectral Density

mode may be beyond the frequency region of interest for extremely small inertia and stiff springs; while for large control inertias or weak springs, the feel system modes may be even lower than the tremor modes. Detailed analysis of these situations has yet to be done for this particular model and is beyond the scope of this brief survey.

Data on Unsteadiness Power Spectral Density

We will now re-examine the earlier experimental data on which this model is based from the standpoint of unsteadiness and tremor. The data to be reviewed are easier to interpret having digested the neuromuscular model and dynamics in Figs. 2 and 3.

An example of the error power spectral density for a pressure joystick is shown in Fig. 4 for a range of applied forces from Sutton and Sykes (Refs. 9 and 10). At larger forces the Neuromuscular and Tremor modes are quite distinct. The feel system mode is not within the data band since the feel system spring rate is nearly infinite. The closed-loop tracking mode is near 0.3 Hz (although it is not clearly defined for each curve in Fig. 4). Sutton and Sykes found, for four subjects, that the rms error increased linearly with the commanded (set) force. In addition, they found that as the set force increased the tremor frequency increased slightly but soon reached a limit of about 8.5 Hz.

Robson (Ref. 11) found the same trend in the tremor mode frequency with tension, and he took data for a range of stiff spring rates. In Fig. 5 forearm flexor tremor frequency is plotted as a function of the pressure force at the wrist. This force was exerted against a spring (attached to the wrist) which was oriented parallel to the upper arm. For each spring, increasing the force causes a slight increase in tremor frequency except at the higher tensions where the data level off. However, an increase in spring stiffness produces an incremental increase in tremor frequency which is essentially independent of the set force.

To emphasize tremor frequencies (5-15 Hz), Halliday and Redfearn (Ref. 12) used a lightweight accelerometer mounted on an outstretched (tensed) finger subject to various pressure forces while the hand was on a rest. Figure 6 gives their averaged finger tremor data which show that increasing the load

weight on the extended finger leads to more tremor at all frequencies and that the amplitude of the tremor mode near 9 Hz increases more than the surrounding spectra. This implies that a small finger-mounted accelerometer would not attenuate the tremor motions. Figure 7 shows spectra for, and cross-spectra between, the right- and left-hand index finger velocity for three subjects. The peaks are in the range of 7-11 Hz. Also shown is the coherence between right- and left-hand unsteadiness, which is very small, indicating that it is the uncorrelated motor noise in each separate limb rather than a common (central) excitation source which drives the tremor mode. These data indicate that the tremor mode is not just a closed-loop neuromuscular system response to an EEG driving signal, even though the EEG's alpha rhythm has the same frequency range.

Data indicating that the feel system mode can be driven to frequencies lower than the tremor mode can be found in Gydikov (Ref. 13) where the task was to track a ramp input (pursuit display). The subject gripped a handle in his fist and used wrist rotation about the forearm axis to generate his response. Four different load inertias were used, and grip tension was sensed. The dependence of dominant mode frequency on inertia and grip tension is given in Fig. 8. For each inertia there is an increase in frequency as tension increases, whereas for constant tension an increase in inertia causes a decrease in frequency. The low frequencies with the large inertia cases indicate that the feel system mode (Fig. 3) has been driven down and is interacting with muscle activation and closed (outer) loop visual-motor dynamics.

Additional results in Ref. 13 indicate that the dynamic modes of one hand are independent of the other. Specifically, if one hand is controlling a large inertia without pressure, then its dominant frequency can be much less than that of the other hand if it is controlling a small inertia with great pressure. This verifies that the Neuromuscular and the Feel System modes can be strongly dependent on the load and, further, that each limb's neuromuscular system has signal drives independent of the other.

The earlier work of Lippold, et al. (Ref. 14) interpreted the extant data at that time as indicating that tremor was <u>not</u> a response to alpha rhythm. In addition, Lippold, et al., found that fatigue increased and

ORIGINAL PAGE IS
OF POOR QUALITY

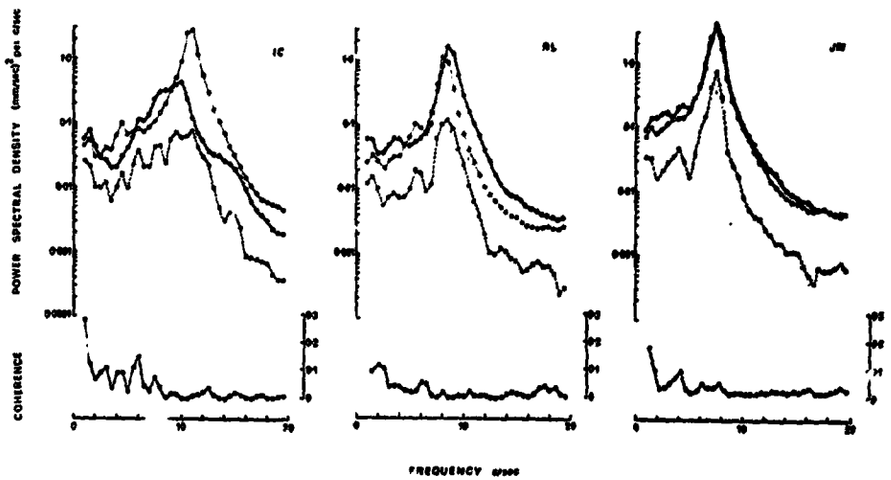

Fig. 4

Representative tremor spectra from three subjects, showing examples of marked difference (I.C. 40 years, female), slight difference (R.L. 37 years, male) and close similarity between the two heads (J.M. 28 years, male). Each spectrum shows: above, the spectra of tremor of the right (●) and left (○) hands; middle, the cross-spectrum between hands (□), and below, the coherence between hands (■). (From Marsden, et al., 1969, Ref. 1)

Figure 7. Effects of Right and Left Hand Index Finger on Velocity Power Spectral Density

0005 (1 cm)

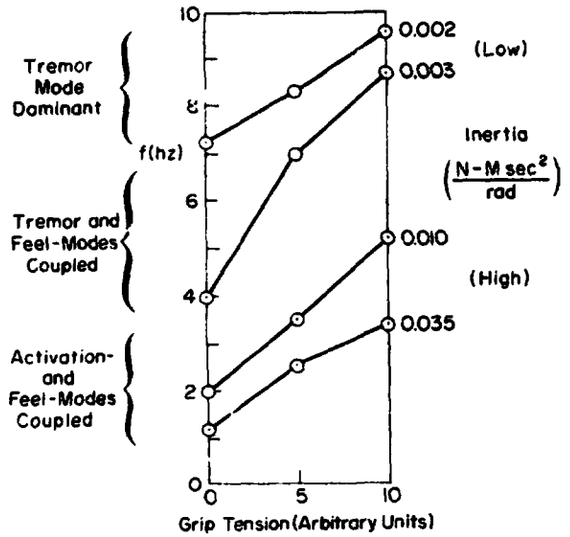

Figure 8. Dominant Frequency Shows Interaction of Feel System and Tremor Modes (Effects of Inertia and Grip Tension on Tremor During Constant Velocity Wrist Rotation, Adapted from Gydikov, Ref. 13)

cooling decreased the tremor frequency; further evidence that the peripheral neuromuscular system determines the tremor mode frequency rather than its being present in a central drive signal. An excellent example of tremor while tracking (involving fine control of position) is provided by some of our unpublished data taken during experiments reported in Ref. 13. This was a multiloop task in which the pilot's feet were controlling rudder pedals and his hand was controlling a stiff spring-restrained side stick. One of the subjects used a high tension technique, i.e., tensed both legs against the pedals and performed the rudder task with differential force changes. Simultaneously, his hand tracking displayed an intermittent tremor of 8 Hz, which was largest at the extreme stick excursions (which requires the largest tensions).

Factors Affecting Tremor

In normal subjects tremor is most often seen when only one muscle is being tensed. That is, for the experiments and data reviewed earlier, in all cases the pilot or subject was producing a force against a restraint (spring or inertia) such that only an agonist muscle was strongly active. Tremor while tracking has always occurred at the extremes of manipulator movement, i.e., where the pilot is pushing with much force against the stick such that only one muscle is being strongly activated, again giving the conditions as above. Tremor while tracking shows an intermittent nature; being easily perceivable only when the pilot is hardover one way or the other. This is readily evident from the time traces. Power spectral analysis of such a run would show some power at the high frequency regions where tremor has been observed, but it would tend to be smeared out due to the intermittent nature of the tremor onset and waning. Thus tremor properties are best measured for cases where the pilot holds a constant force or load weight.

Marsden (Ref. 15), in finger tremor studies, found that the relative size of the tremor peak was correlated with the total rms unsteadiness velocity for both right and left hands. (See Fig. 9.) Here the total rms velocity was evaluated from the total power between 1 and 20 Hz (Fig. 7

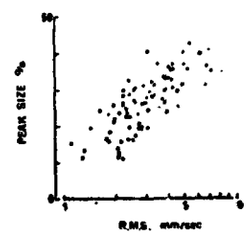

Fig. 9. Relation between the relative size of the peak (ordinate) and total RMS velocity (abscissa) obtained from C.M.'s right (■) and left (▲) hands, and that obtained from J.M.'s right (□) and left (△) hands. Relative peak size increases as tremor increased ($r = +0.33$, $P < 0.01$). (From Marsden, Ref. 15)

indicates that this region contains essentially all the power). The relative peak is defined as the ratio of the power in a 0.5 Hz band about the peak frequency to the total power. In Fig. 9 note that the tremor peak contains an increasing share of the total power as the rms level increases; this is consistent with the data in Figs. 4 a 7.

The influence of external factors on tremor per se has been summarized by Marsden (Ref. 15) as follows (underlines ours):

> "The fluctuations in tremor observed in two trained subjects during periods ranging from minutes to months were not great, and the shape of the tremor spectrum was very similar at different times. Many factors are known to contribute to fluctuations in tremor amplitude, including: anxiety (Graham, Ref. 16; Redfearn, Ref. 12), alcoholism (Carrie, Ref. 17), thyrotoxicosis (Lippold, et al., Ref. 18; Marsden, et al., Ref. 19), and fatigue (Eagles, et al., Ref. 20). Some of the fluctuation of tremor amplitude that occurs in the normal subject may be due to variations in catecholamine secretion, for adrenaline infusion has also been found to increase tremor considerably (Marsden, et al., Ref. 21). In addition, the amplitude of tremor is dependent upon the force exerted (Sutton and Sykes, Ref. 9) and, in certain tasks, upon visual feedback (e.g., Sutton and Sykes, Ref. 10); Merton, et al., Ref. 22). All these factors must be taken into account when planning experiments on physiological tremor and when evaluating the results."

In a series of approach and landings with a Boeing 707, Nicholson, et al. (Ref. 23) found significant increases in finger tremor (at 10 Hz) in "stressful" situations ("an unresolved problem persisting or a fresh problem of some magnitude") as evidenced by subjective reports and elevated heart rates (above 150 beats per minute). The finger tremor was measured by a lightweight accelerometer (less than 1 gram) on an outstretched index finger. Fig. 10 shows both pre-takeoff and immediately post-landing tremor spectrum for four of the most stressful cases, in which the dramatic increase in the 10 Hz peak is readily apparent.

Concluding this section on tremor mode properties, the following conclusions are emphasized:

1. The tremor mode is a distinct limb-muscle resonance phenomena, compared to the more highly coupled visual, neuromuscular and feel system modes. As such, it is not strongly correlated with the other visual-motor modes.

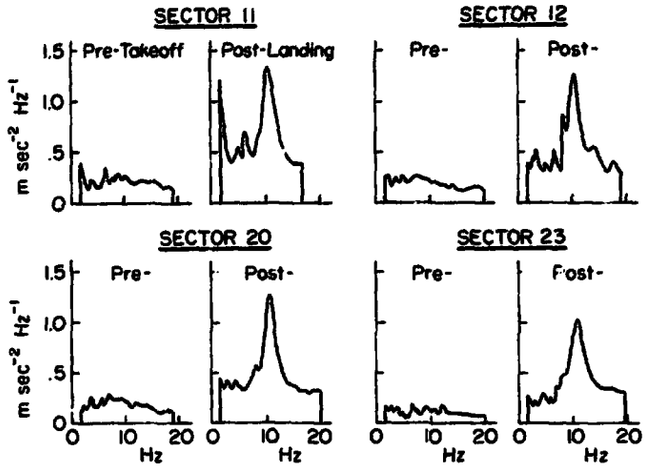

Figure 10. The Frequency Spectra of Finger Tremor for Takeoff (Controls) and for Stressful Landings in Four Letdowns in Which the Mean Heart Rate Exceeded 150 Beats/Min and Was Associated With a Peak Acceleration Around the 10 Hz Frequency Exceeding 1.0 msec^{-2} Hz^{-1} (From Nicholson, et al., 1970, Ref. 23)

2. Its frequency is not very sensitive to limb load and it primarily reflects neuromuscular system feedback lags and tendon compliance.

3. The tremor mode power spectral density is narrowband and its amplitude increases with applied force, as well as various external or internal operator stresses.

4. Tremor is most pronounced when only one muscle of an agonist/antagonist pair is tensed.

5. Tremor mode motions are clearly revealed by measuring the limb acceleration (rather than position) in the frequency range from 8-15 Hz.

Factors Affecting Low Frequency Unsteadiness

While the tremor mode is a distinct and isolatable mode, the low frequency control motion spectra have multiple peaks (e.g., closed-loop tracking and neuromuscular modes) which are very sensitive to the manipulator restraint as shown by the Gydikov data of Fig. 8 as well as control stick type. The pressure-stick displacement spectrum in Fig. 4 shows the closed loop tracking mode and the muscle/manipulator mode while these modes are not obvious in the unrestrained finger acceleration spectra (Fig. 7). In tracking tasks the controlled element has a strong effect on the pilot's equalization (Ref. 3) and thereby the frequency and damping of the closed loop tracking mode which results. Furthermore, the forcing function bandwidth, if large, may cause crossover regression thereby lowering the closed loop tracking mode frequency. Thus, the power spectral density of unsteadiness motions is multipeaked, and there is no single pair of frequency-amplitude parameters which can meaningfully describe the signal properties unless bandpass filtering is performed first. If information is desired about all the possible modes of unsteadiness, the best solution is to measure the complete power-spectral-density and carefully analyze it. However, a simpler metric of low frequency unsteadiness is the overall rms position excursions, because for force regulation (Fig. 4), the low frequency modes dominate the displacement PSD. In addition this metric is directly relevant to fine motor task performance, since this is a direct measure of the average closed loop unsteadiness magnitude.

An example of this metric is given by Marsden (Ref. 1). He investigated the correlation between the tremor peak size with low frequency unsteadiness and total rms control velocity (Figs. 11a and 11b). The data (in the range 1-5 Hz) has a small and negative correlation with the tremor mode peak. This indicates that the low frequency modes may have different trends from those of the tremor mode. The positive correlation for the total, Fig. 11b, is consistent with Fig. 9.

Thus, fine-motor task unsteadiness can be assessed separately from the tremor mode by filtering out the high frequency portion of the signal and measuring the rms position excursions in the non-tracking case.

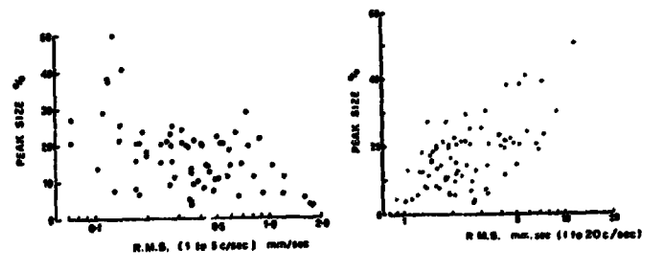

a) Low Frequency Unsteadiness b) Total RMS Unsteadiness

Figure 11. Correlation of Tremor Peak Size with Low Frequency and Wideband RMS Unsteadiness

EXPERIMENT TO VALIDATE RECOMMENDED MEASUREMENTS

Experimental Setup

A simple analog computer simulation was conducted in order to test various unsteadiness measurement concepts suggested in Sections A and B and to validate the tremor and unsteadiness tests recommended therein. A functional block diagram of the simulation is shown in Fig. 12. The subjects were required to rest their elbows on an arm rest and, pulling with the ball of their first finger, null out a command force using a nearly isometric (very stiff) control stick (MSI Model 435). The difference signal c_e represents the control unsteadiness. Force error feedback to the subject was provided by a 5-inch Dumont 304A Oscilloscope. The displayed error was smoothed by a first order filter with a 1.0 second time constant, to eliminate perception of the high frequency unsteadiness and to assure a tight loop closure to remove any residual force drift. The dc display/control gain was 2.5 cm on CRT/Newton on stick.

The low-frequency components of fine motor unsteadiness (visual/motor modes) were measured by the rectified and averaged control error signal, $\overline{|c_e|}$, as shown in Fig. 12.

The tremor mode signals were obtained by processing the control error signal (c_e). The rate and acceleration of c_e were obtained with a pseudo-differentiation circuit. The acceleration signal was additionally smoothed with a second order filter similar to the pseudo-differentiation circuit. The break frequency of both circuits was set at 100 rad/sec (16 Hz) with a damping ratio of 0.7. These settings give a 25% amplitude attenuation at 16 Hz with linear phase shift up to the break frequency. The phase shift characteristics cause minimal phase distortion in the signals up to the break frequency, and the signals appear as though they are merely time delayed by about 0.014 sec for $\dot{c}_e$ and 0.028 sec for the filtered $\ddot{c}_e$ signal. "Average tremor magnitude" was obtained by rectifying and smoothing the $\ddot{c}_e$ signal, as shown.

Ten subjects (including two females) were asked to hold command forces of 5, 10, 15 and 20 newtons (1.12, 2.25, 3.36 and 4.49 lb respectively) with their right forefinger. Data were recorded with a Brush Mk 200 strip chart recorder (100 Hz bandwidth).

Data

Tremor Frequency. A typical recording is shown in Fig. 13. The tremor frequency in the smoothed acceleration signal is clear at all four force levels. However, the 15 and 20 newton cases appear most suitable for measuring tremor frequency with a zero crossing detector.

The velocity trace shows evidence of the closed loop neuromuscular mode as well as the tremor mode. Closer inspection of the 10 newton trace reveals a 2 to 3 Hz frequency combined with the 13 Hz tremor mode, and past describing function measurements have shown the neuromuscular mode to fall into this frequency range (Ref. 2 and Fig. 3 herein).

It is apparent that the smoothed acceleration signal gives a good measure of the tremor mode frequency and amplitude. These data are shown on Fig. 14. The tremor frequency is remarkably constant while the tremor amplitude increases by an order of magnitude. The mean frequency over 40 trials (4 forces × 10 Ss) was 11.6 Hz (73 rad/sec) with a standard deviation of 0.9 Hz. The lowest frequency measured was 9.5 Hz and the highest was 13 Hz. Measurements with the left hand of two subjects gave frequencies

in the same range, but slightly different than their right hand. Thus it is apparent that the tremor mode occurs within a very restricted frequency region in most subjects over a significant range of applied forces. The low end of this frequency range for isometric-stick pulling also matches the finger-free data shown in the preceding section, "Nature of Unsteadiness."

Additional tremor frequency measurements were made to check the tremor mode of other limbs. These were:

- Free hand tremor measured by pointing a miniature flashlight at a photocell,
- Biceps tremor measured by pulling with the arm on a spring restrained bar,
- Leg muscle (quadraceps) tremor measured by pushing with the foot on a spring restrained pedal.

Frequencies measured in the above manner were within the forefinger tremor frequency range reported above. Also, left hand/right hand tremor was comparable for two subjects tested. Thus the tremor mode frequency of a normal human neuromuscular system seems to be a very fundamental physiological property. From the model and dynamics of Figs. 2 and 3, this implies that the ratio of limb inertia to tendon compliance and the neuromuscular loop lags are about the same for all of these cases, or that other limit-cycling phenomena are involved.

Tremor Magnitude. A time trace of the 1-second running average tremor magnitude signal for a typical run is given in the bottom of Fig. 13. Tremor mode magnitude is a direct function of the average applied force, as shown. It was also found to vary significantly from subject to subject. Average tremor magnitudes for each subject and force level were read off the strip chart recordings and are cross plotted in Fig. 14. These data suggest an exponential relationship between tremor intensity and applied force, with the high forces producing much higher tremor magnitude, e.g., $\sigma_T = \sigma_{T_o} + e^{rF}$, where σ_T, σ_{T_o} = total and residual tremor (rms) magnitudes; F = force, r is fitting constants. It seems that as the average muscle force is increased the tremor mode damping ratio drops and/or the motor remnant forcing function increases (a la Weber Law), while its frequency remains roughly constant. (This is consistent with Fig. 3.)

ORIGINAL PAGE IS OF POOR QUALITY

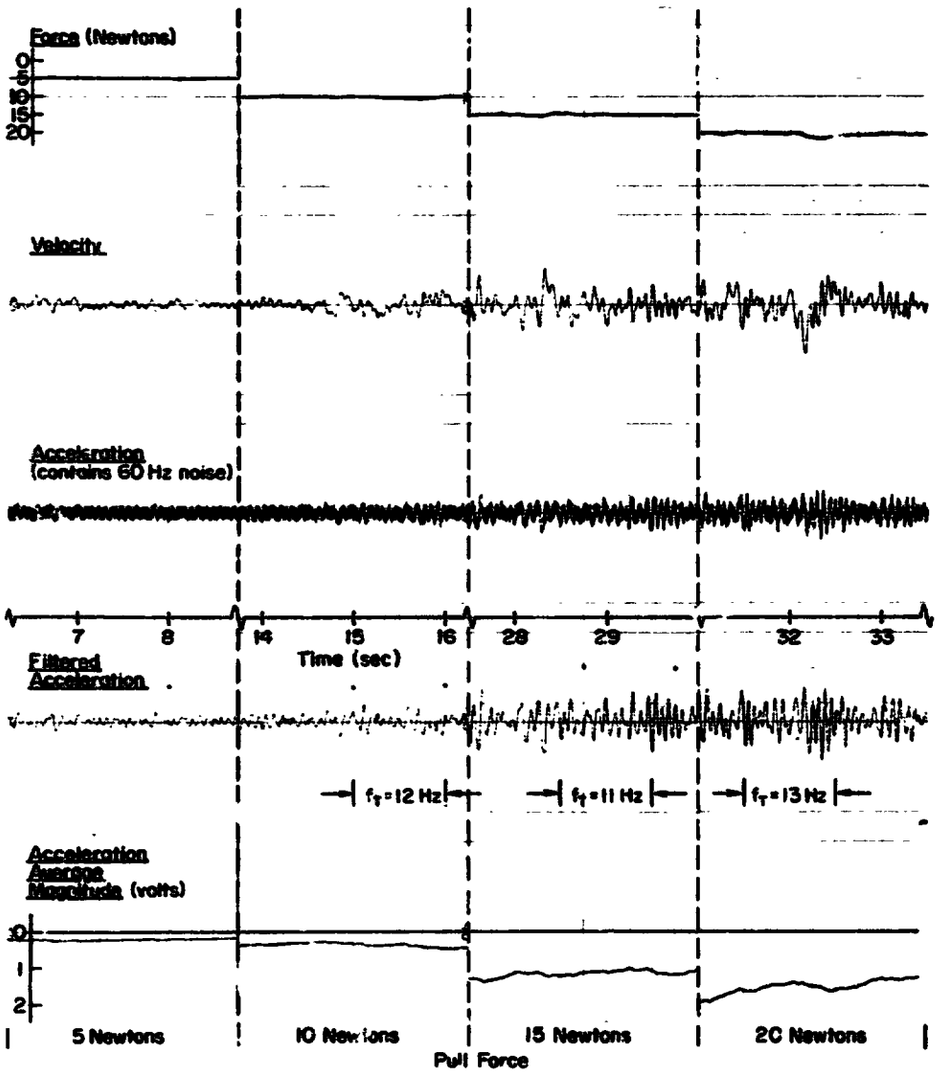

Figure 17. Tremor Test Time Traces for Various Command Forces

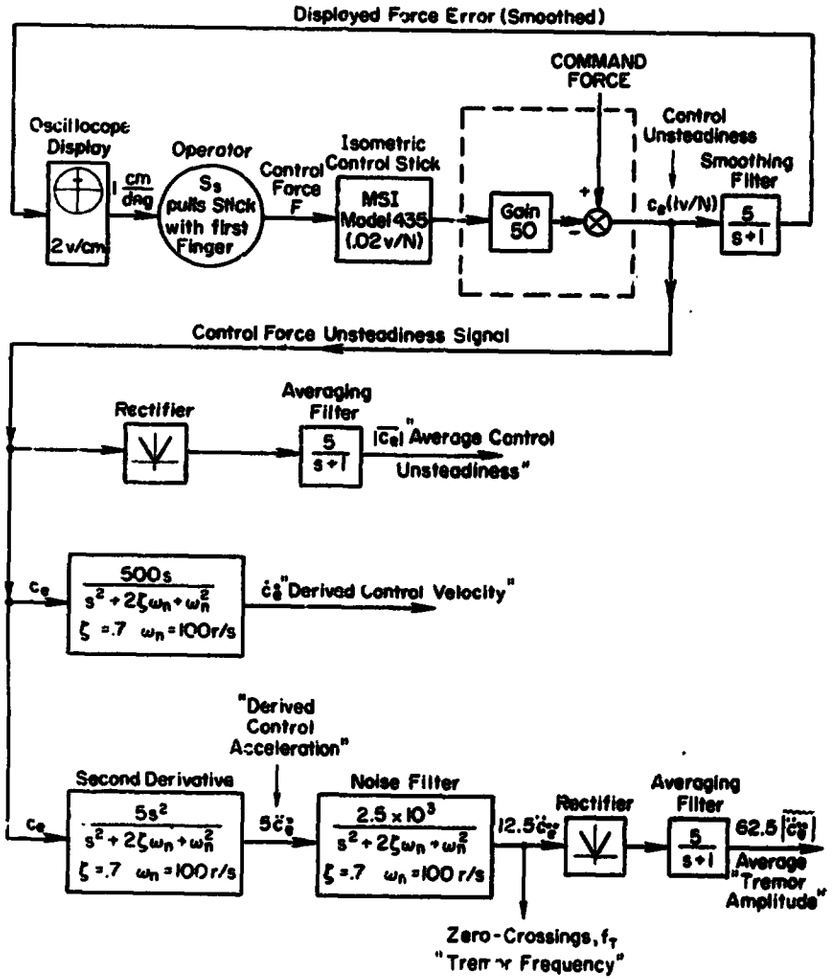

Figure 12. Experimental Setup for Unsteadiness and Tremor Measurements

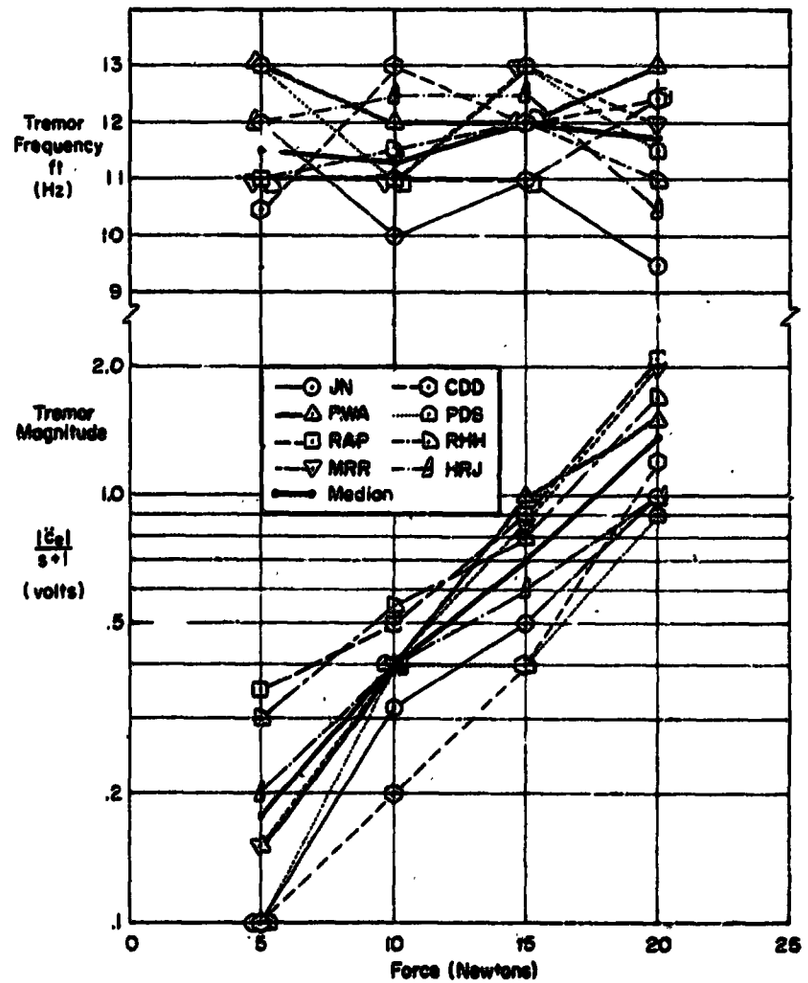

Figure 14. Tremor Intensity as a Function of Applied Force

Unsteadiness Magnitude. A preliminary test was conducted to determine the characteristics of the low-frequency control force unsteadiness signal $\overline{|\dot{c}_e^*|}$. This measure of unsteadiness magnitude seems to covary somewhat with tremor magnitude and to vary directly with applied force. Low frequency variations also apparent. Additional research will be required to further quantify the characteristics of this measurement.

Standardized Tremor Measures

Based on the success and ease of mechanizing these measures, we recommend the following standard test battery for unsteadiness properties:

- Mechanize the functional circuits shown in Fig. 12 for computing the force error and its derivatives, (omitting derived control velocity). The tremor bandpass filter for computer $\ddot{c}_e^*$ should have $\zeta = 0.7$ for minimal phase distortion and $\omega_n \approx 60$-80 rad/sec to peak near typical tremor frequencies of 9-13 Hz. ("Standard" $\omega_n = 63$ r/s = 10 Hz.)
- Subject presses on the pressure-stick with whatever limb is being investigated, with the limb root grounded (e.g., pull with forefinger; elbow braced). Command forces should be in the range of 5-25 Newtons (1-5 lb) with 15 Newtons (3.4 lb) as a "standard" value for finger pulling.
- Each trial should have a 10 second stabilization period, then 10-second measurement interval. (These periods are a good compromise, balancing measurement precision against muscle fatigue.)
- The test measurements are, in order of interest: "Average Tremor Amplitude" $\overline{|\ddot{c}_g^*|}$ (which is approximately 1.28 $\sigma_{\ddot{c}_g}$ for a Gaussian signal); "Average Control Unsteadiness," $\overline{|\dot{c}_e|}$ (roughly = 1.28 $\sigma_{\dot{c}_e}$); and the "Average Tremor Frequency" f_t (e.g., from the positive-going axis crossing of the $\ddot{c}_g^*$ signal).
- To make such measures of universal value, the values of c_e and $\ddot{c}_g$ should be given in terms of force or force acceleration (N, N/sec^2), respectively.

CONCLUDING REMARKS

This paper has summarized some recent work in developing a quasilinear model and measurements characterizing the neuromuscular control of a precisely manipulated device such as a: soldering iron, handgun, or various types of manual control sticks, wheels or pedals. The model given here is based on the dominant physiological components and phenomena involved, and it can cover all these cases. In addition, it clearly reveals the various modes of fine-motor unsteadiness, including the Neuromuscular mode at 1-3 Hz and the Tremor mode near 10 Hz. The data review and reexamination, upon which it is based shows good qualitative agreement with many phenomena observed by earlier experimenters, as well as our own work.

Nevertheless, we feel a little uneasy about the "cause" of the very stable-frequency tremor mode. Our brief experiment showed a tenfold increase in tremor amplitude for a fourfold increase in finger pull-force, while the tremor frequency remained within ±1 Hz of 11 Hz, all consistent with the model of Figs. 1-3. Nevertheless, there are other mechanisms, such as threshold-plus-delay-caused limit cycles which might be involved. Furthermore, we have not considered any of the tremor-symptomatic diseases such as Parkinson's Disease, nor have we separated the motor-remnant from the system dynamics. Clearly, more investigation is warranted, using this model as a guide to the appropriate measures and tests.

The proposed "standard" Unsteadiness Test Battery is recommended for clinical investigations of the effects on fine-motor unsteadiness of: various stressors such as work fatigue, lack of sleep, drugs, high-adrenalin situations, and febrile illness; on different limbs; for various ages; and with different manipulated devices. The authors would like to hear about any applications of these tests or modifications to the model.

REFERENCES

1. Marsden, C. D., J. C. Meadows, G. W. Lange, and R. S. Watson, "The Relation Between Physiological Tremor of the Two Hands in Healthy Subjects," Electroenceph. clin. Neurophysiol., 1969, Vol. 27, pp. 169-185.

2. Magdaleno, Raymond E., Duane T. McRuer and George P. Moore, Small Perturbation Dynamics of the Neuromuscular System in Tracking Tasks, NASA CR-1212, Dec. 1968.

3. McRuer, D., D. Graham, E. Krendel, and W. Reisener, Jr., Human Pilot Dynamics in Compensatory Systems — Theory, Models, and Experiments with Controlled Element and Forcing Function Variations, AFFDL-TR-65-15, Jan. 1965.

4. McRuer, D. T. and E. S. Krendel, Dynamic Response of Human Operators, WADC-TR-56-524, Oct. 1957.

5. Levison, William H., David L. Kleinman, and Sheldon Baron, A Model for Human Controller Remnant, Bolt Beranek and Newman, Inc., Rept. 1751, Job No. 11320, 15 Oct. 1968.

6. Clement, W. F., R. W. Allen, and H. R. Jex, Experiments in Controlled Display Scanning and Sampling, NASA CR-1569, July 1970.

7. Magdaleno, R. E., and D. T. McRuer, Experimental Validation and Analytical Elaboration for Models of the Pilot's Neuromuscular Subsystem in Tracking Tasks, NASA CR-1757, April 1971.

8. Magdaleno, R. E., and D. T. McRuer, "A Closed-Loop Neuromuscular System Explanation of Force Disturbance Regulation and Tremor Data," Fourth Annual NASA-University Conference on Manual Control, NASA SP-192, 1969, pp. 527-541.

9. Sutton, G. G., and K. Sykes, "The Variation of Hand Tremor with Force in Healthy Subjects," J. Physiol. (Lond.), 1967b, Vol. 191, pp. 699-711.

10. Sutton, G. G., and K. Sykes, "The Effect of Withdrawal of Visual Presentation of Errors Upon the Frequency Spectrum of Tremor in a Manual Task," J. Physiol. (Lond.), 1967a, Vol. 190, pp. 281-293.

11. Robson, J. G., "The Effect of Loading on the Frequency of Muscle Tremor," J. Physiol., 1959, pp. 29P.

12. Halliday, A. M., and J. W. T. Redfearn, "An Analysis of the Frequencies of Finger Tremor in Healthy Subjects," J. Physiol., Vol. 134, 1956, pp. 600-611.

13. Gydikov, A., "Sampling with Adjustable Frequency in the Hand Movement Control System," IEEE Trans., Vol. MFE-8, No. 2, June 1967, pp. 135-140.

14. Lippold, O. C. J., J. W. T. Redfearn, and J. Vuco, "The Rhythmical Activity of Groups of Motor Units in the Voluntary Contraction of Muscle," J. Physiol. (Lond.), 1957, Vol. 137, pp. 475-487.

15. Marsden, C. D., J. C. Meadows, G. W. Lange, and R. S. Watson, "Variations in Human Physiological Finger Tremor, with Particular Reference to Changes with Age," Electroenceph. clin. Neurophysiol, 1969, Vol. 27, pp. 169-178.

16. Graham, J. D. P., "Static Tremor in Anxiety States," J. Neurol. Neurosurg. Psychiat., 1945, Vol. 8, pp. 57-60.

17. Carrie, J. R. G., "Finger Tremor in Alcoholic Patients," J. Neurol. Neurosurg. Psychiat., 1965, Vol. 28, pp. 529-532.

18. Lippold, O. C. J., J. W. T. Redfearn, and J. Vuco, "The Frequency Analysis of Tremor in Normal and Thyrotoxic Subjects," Clin. Sci., 1959, Vol. 18, pp. 587-595.

19. Marsden, C. D., T. M. D. Gimlette, R. G. McAllister, D. A. L. Owens, and T. N. Miller, "Effect of β-Adrenergic Blockade on Finger Tremor and Achilles Reflex Time in Anxious and Thyrotoxic Patients," Acta endocr. (Kbh.), 1968, Vol. 57, pp. 353-362.

20. Eagles, J. B., A. M. Halliday, and J. W. T. Redfearn, "The Effects of Fatigue on Tremor," In W. F. Floyd and A. T. Welford (eds.), Symposium on Fatigue, Lewis, London, 1953, pp. 41-58.

21. Marsden, C. D., T. H. Foley, D. A. L. Owen, and R. G. McAllister, "Peripheral β-Adrenergic Receptors Concerned with Tremor," Clin. Sci., 1967a, Vol. 33, pp. 53-65.

22. Merton, P. A., H. B. Morton, and C. Rashbass, "Visual Feedback in Hand Tremor, Nature (Lond.), 1967, Vol. 216, pp. 583-584.

23. Nicholson, A. N., L. E. Hill, R. G. Borland and H. M. Ferres, "Activity of the Nervous System During the Let-Down, Approach and Landing: A Study of Short Duration High Work Load," Aero. Med., Vol. 4, pp. 436-466, April 1970.

EVALUATION OF FLIGHT SIMULATION DISPLAYS USING ELECTROPHYSIOLOGICAL TECHNIQUES

L.J. Leifer
Man-Vehicle Laboratory, MIT

G. Buckland
Man Machine Integration Branch,
NASA Ames Research Center

This paper presents preliminary experience with the use of evoked electroencephalographic (EEG) analysis of information display utilization by pilots. The theory and method attempt to apply recent findings in psychophysiology which demonstrate that low frequency components of the evoked EEG are related to cognitive functions such as: 1) attention, the selective processing of sensory information; 2) prediction, the expectation of sensory inputs; 3) conation, the preparation for behaviour contingent on sensory inputs.

In a feasibility study at NASA-Ames (June/July, 1972), direct coupled recordings of the scalp EEG and vertical electro-oculogram (EOG) were made while six commercial pilots performed a simulated night VFR approach (fixed base). Simplified aircraft dynamcis were those of a DC-8. The approach was begun 2.1 miles from the runway aim point, at an altitude of 510 feet. As the aircraft passed through the altitudes of 410, 295, 180, and 65 feet the display was temporarily blanked; manual control and dynamics simulation were uninterrupted. After 2.0 seconds the simulated VFR scene was reinstated with accumulated pilot and external disturbances.

Results indicate that: 1) pilot attention was strongly focused on the expected touchdown from the beginning of the approach sequence; 2) attention was heightened during display blanking; 3) this attention to information loss increased as the flight approached touchdown. A film, details, and implications will be presented.

PRECEDING PAGE BLANK NOT FILMED

N75 19155

THE MUSCLE SPINDLE AS A FEEDBACK ELEMENT IN MUSCLE CONTROL

Lee T. Andrews
Anthony M. Iannone
Medical College of Ohio
Department of Neurosciences
Toledo, Ohio

Donald J. Ewing
University of Toledo
Toledo, Ohio

PRECEDING PAGE BLANK NOT FILMED

ABSTRACT

The muscle spindle, the feedback element in the *myotatic (stretch) reflex*, is a major contributor to muscular control. Therefore, an accurate description of behavior of the muscle spindle during active contraction of the muscle, as well as during passive stretch, is essential to the understanding of muscle control. With this goal in mind, animal experiments were performed in order to obtain the data necessary to model the muscle spindle. Spectral density functions were used to identify a linear approximation of the two types of nerve endings from the spindle A model reference adaptive control system was used on a hybrid computer to optimize the anatomically defined lumped parameter estimate of the spindle. The derived nonlinear model accurately predicts the behavior of the muscle spindle both during active discharge and during its silent period. This model will be used in future research to determine the mechanism employed to control muscle movement.

INTRODUCTION

This paper is concerned with the derivation of a mathematical model which describes the behavior of the mammalian muscle spindle of the cat over its entire operating range. The muscle spindle is a subsystem of a larger system which is responsible for skeletal muscle control. One control loop within this system is known as the myotatic reflex arc.

Analyzing the myotatic reflex itself can be undertaken only when each of the subsystems and elements of this reflex are well defined. It is the goal of this paper to experimentally and mathematically analyze one of the subsystems of the reflex. The subsystem to be considered is the muscle spindle.

The muscle spindle is studied during active contraction as well as during stretch in order to determine the normal functioning of this essential subsystem in the myotatic reflex. An optimization scheme is utilized on an anatomical representation of the muscle spindle in order to ascertain the importance of its various properties. Because it is important to relate each mathematical term to real components within the biological elements themselves, the analysis of the muscle spindle is based on its anatomy rather than treating it as a "spectral fit" of the experimental data. This study utilizes engineering concepts to analyze and predict the normal functioning of the mammalian muscle spindle. These concepts lend themselves to the analysis of this type of biological system because it can be represented as a basic servo mechanism as Merton (1952) did in his well known presentation.

ANATOMICAL CONSIDERATIONS

The mammalian muscle spindle is a complex sensory organ connected in parallel with skeletal muscle fibers. It detects changes in the length of the muscle as well as in other parameters which are related to length, such as tension and velocity. The spindle is composed of several intrafusal muscle fibers contained within one envelope. The multiple fibers contained within this envelope fall into two distinct categories. Of the two fibers, the larger, called the nuclear bag fiber, reveals two different regions. The polar regions of this nuclear bag fiber consist of striated contractile tissue, while the central region is composed of a noncontractile tissue containing nuclei. The smaller fibers within the envelope are a uniform distribution of nuclei and striated regions. These fibers are called nuclear chain fibers due to their chain-like appearance.

Two types of nerve endings innervate the striated regions of the spindle. These are denoted as the γ_1 and γ_2 motor fibers. This gamma efferent system provides the necessary bias to the muscle spindle. Figure 1 shows the γ_1 and γ_2 motor fibers innervating the different types of intrafusal fibers. The afferent discharge from the muscle spindle is of two distinct types. The first, namely, the *Ia afferent* discharge, has its endings on both the nuclear bag and nuclear chain fibers. These afferent discharges are connected monosynaptically with alpha motoneurons. The second type of discharge, the type II, has its ending only on the nuclear chain fiber and is connected polysynaptically with the alpha motoneuron.

A more detailed discussion of the anatomy of the muscle spindle is available in the list of references: Matthews [2], Eldred [3], Granit [4] and others. Of particular interest are the proceedings of the first Nobel Symposium.

DATA AQUISITION

In order to model a given system, it must be fully defined by certain information. Knowledge of input-output relationships is required to formulate a mathematical description of the system being studied. Therefore, modeling of the muscle spindle requires the recording of input to the spindle as well as its output pulse train. Input to the muscle spindle consists of any mechanical change in the length of the extrafusal muscle fibers. This change

is transferred to the intrafusal fibers of the muscle spindle because the latter are anatomically placed in parallel with the extrafusal fibers. The output of the muscle spindle system includes the afferent discharge of both type Ia (primary nerve ending) and type II (secondary nerve ending) fibers. The following experimental procedures are utilized to obtain the input-output data necessary for modeling the system.

A simple schematic diagram of the experimental facility explains the arrangement of equipment. In Figure 2 the stimulating electrode and monitoring electrodes are shown on the appropriate nerve bundles. The stimulating electrode is driven by a constant current unit to provide uniform stimulus regardless of changes in resistance between the electrode and nerve bundle. The rate and duration of the stimulus pulses are controlled by a stimulator which drives the constant current unit.

Nerve conduction tests are performed in order to differentiate between type Ia and type II nerve fibers from the muscle spindle. A conduction velocity of less than 70 m/sec is generally a type II ending. Further identification of the nerve fibers is made by observing the dynamic sensitivity of the fiber output. The type Ia fiber shows greater sensitivity to velocity of muscle movement than the type II ending.

EXPERIMENTAL RESULTS

A majority of previous investigators have driven the muscle by means of a mechanical apparatus or external force. Such experiments tend to keep the muscle spindle afferent in the range of continuous discharge by controlling the gamma efferent bias and mechanical load. It is assumed that the only region of interest to the physiological system is that of active discharge. This study differs in that it treats the silent period of operation as well as the period of active spindle discharge. This is accomplished by leaving the normal nerve pathways intact and causing muscle contraction by stimulation of the peripheral nerve. The results of these experiments are discussed in detail in succeeding sections.

Isotonic Loading - Type Ia Ending

Isotonic loading of the medial gastrocnemius-soleus muscle group is accomplished by attachment of a constant tension spring. The measurement apparatus provides a low mass mechanism for measurement of muscle movement. After attachment of the spring, the muscle's length is allowed to stabilize. The spindle afferent is monitored in order to ascertain whether the discharge has reached steady state.

Once it has been determined that the muscle spindle and muscle are at steady state, the peripheral nerve to the muscle group is stimulated with a 0.5 millisecond pulse at an amplitude sufficient to cause a maximal twitch of the muscle fibers. This stimulus pulse and the post-stimulus spindle afferent discharge are recorded along with the positional translation of the muscle for

a period in excess of one hundred stimuli in order to insure a large enough sample to provide a statistical basis for data analysis.

The resultant positional translation and spindle discharge are shown in Figure 3. It can be seen that the spindle afferent discharge ceases, or is silent, immediately following the stimulus to the muscle. This silent period is maintained until the direction of the velocity component is reversed. Figure 3 also shows that the offset of the silent period is characterized by an apparent bursting or high frequency discharge of the spindle afferent.

The instantaneous frequency of the spindle afferent discharges provides output information to higher centers in the biological system. Therefore, it is an important variable which must be measured. Since each post-stimulus discharge is unique, a post-stimulus histogram of its instantaneous frequency is necessary (Figure 4). This figure illustrates the silent period, its offset, and the instantaneous frequency of the spindle afferent discharge.

Static Characteristics

Observation of static as well as dynamic results are important in understanding the normal function of the muscle spindle. Two types of loads, inertial and isotonic, are utilized to determine the properties of the spindle. These different types of loads affect only the muscle's dynamic response and consequently, the spindle's dynamic response, while the static characteristics of each experiment remain the same. Therefore, the static characteristics for both types of load can be discussed together.

The elastic properties of the muscle are determined by measuring the amount of elongation of the muscle relative to the amount of load. Figure 5 illustrates the results of this measurement for four cats. The four curves shown are displaced in the vertical axis but have similar shapes and appear as a family of curves. The vertical displacement is a natural result of normal differences between experimental animals. The important characteristics to be noted here are the nonlinear nature of the force-displacement curves and the similarity of the curves to each other. The results illustrated in Figure 5 are similar to those of previous investigators. Experiments of Wilkie, 1956; Ritchie and Wilkie, 1958; Zajac, 1968; and others show an exponential relationship between the length of the elastic element and the force applied. However, the results both of this study and the above works disagree with those of Rosenthal [5] who describes the length-tension relationship as one of a linear nature with or without the myotatic reflex present. The data he presented are apparently a result of the dynamic nature under which they were obtained. The nonlinear properties of the elastic element shown in Figure 5 are the result of measurements taken with the myotatic reflex intact.

The static discharge of the spindle, illustrated in Figure 6, has characteristics very similar to those of the length-tension curves graphed in Figure 5. The points plotted in Figure 6 represent the mean spindle discharge; the normal spindle output varies about a mean frequency. Both graphs appear to be logarithmic in nature due to the characteristics of a sharp initial slope followed by continual reduction of slope as the tension is increased.

Inertial Loading - Dynamic Characteristics

Although the static characreristics for both types of loads are the same, the dynamic characteristics are different. A mass is used to provide a load with inertia which more closely approximates the type usually encountered in the normal state. The muscle response and corresponding spindle afferent are shown in Figure 7. The muscle response to the stimuli shows a definite damped oscillation which results in a secondary silent period in the discharge of the spindle afferent. Figure 8 better illustrates the time sequence and duration of this secondary silent period. A family of post-stimulus histograms is illustrated in Figure 9. Whereas the initial silent period remains approximately constant in duration, the secondary silent period diminishes as the load increases and is extinguished by loads in excess of 3.4 kilos. Observation of the family of displacement curves in Figure 10 shows the secondary oscillation of the positional data decreasing as the load is increased. This measure, namely, the sensitivity to secondary oscillations, provides a valuable index of the sensitivity of the spindle afferent to displacement, velocity, and acceleration. Another important phenomenon is the relative constancy of the initial silent period, particularly since the muscle dynamics are grossly affected by increase in load.

The reduction and cessation of pulse discharge during muscle contraction or length decrement can be explained by interpretation of the physical parameters acting on the spindle. The initial silent period observed in Figure 9 cannot be explained simply as a response to the mechanical forces acting on the spindle. Observation of the large variation in muscle response, illustrated in Figure 10, indicates other factors must be present to account for the uniform duration of the silent period. Mechanical factors definitely contribute to the silent period observed in Figure 9. However, as the load is increased, the duration of the silent period does not decrease. The probable cause of the uniform silent period is inhibition of fusimotor neurones by an antidromic volley in adjacent neural roots (Ellaway, 1971; Holmgren and Merton, 1954). This inhibition of fusimotor neurones is shown to have a duration of approximately 50 milliseconds which coincides with the minimum duration of the silent period found in the experimental data. The inhibition of the fusimotor neurones causes the relaxation of the polar regions of the spindle, resulting in the silent period observed in the experimental data. Jansen and Rudjord [7] also noted the same phenomenon and stated, "The duration of the silent period of motoneuron was not appreciably changed even by large variations in the inital tension."

Isotonic Loading - Type II Ending

The exact role of the type II ending in the reflex system is not completely understood. It is thought, however, that the type II ending provides information to the gamma system which controls the efferent bias to the muscle spindle. The data presented in this section shows that the secondary ending of the muscle spindle has very little dynamic sensitivity. Instead, the secondary ending provides a measure of the static position of the muscle. Due to this characteristic, the bias control theory appears to have some validity. However, it is also known that the type II ending excites flexors and inhibits extensors and, therefore, plays additional roles in the overall control system.

Dynamic Characteristics

The spindle afferent discharge and corresponding positional translation are illustrated in Figure 11. Of interest here is the almost complete lack of the typical high frequency discharge noted in previous data at the offset of the silent period. The burst in the afferent discharge readily apparent in the type Ia afferent is drastically reduced in the type II ending. Its afferent discharge frequency decreases gradually as the muscle returns to steady state. Its range of the discharge from the maximum frequency to the steady state frequency is less than twenty percent, whereas the peak discharge rate for the type Ia ending is four to five times that of the steady state discharge.

Discussion of Experimental Results

The preceding sections presented a view of the data generated by the various experiments utilized in this study. This section describes the results and parameters derived from these experimental investigations and discusses them with reference to the results of previous investigators.

The silent period seen in the data presented in this paper demonstrates the nonlinear nature of the type Ia and type II endings. An important parameter to be determined is the sensitivity of the silent period to physical forces. Comparison of the velocity curve and the discharge occurrence histograms shows a relative offset and onset sensitivity of slightly less than 0.1 centimeters per second for offset and approximately 0.9 centimeters per second for onset. Utilizing this sensitivity parameter to determine the load required to extinguish the secondary silent period, a value of 2.7 kilos is determined from the velocity curve in Figure 8. Since only a finite number of loads is used in these experiments, interpolation is necessary to check on the validity of this value. The histograms displayed in Figure 9 show that the secondary silent period is beginning to be extinguished by afferent discharge for a load of 2.270 kilos and is completely extinguished for 3.4 kilos. This agrees very well with the calculated tension of 2.7 kilos. As Lennerstrand states, assessment of velocity response during length decrement cannot be determined. However, the relative values of onset and offset are important in determination of the type of nonlinearity in the spindle system. The relative values of these sensitivity parameters are necessary in the prediction of silent period occurrences and durations.

Holmgren and Merton found that an interjected muscle twitch during steady contraction caused a silent period in the electromyogram of the muscle. Before reflex action was developed, the motoneuron discharge was already arrested. This cessation of motoneuron activity was attributed to antidromic blocking, if the twitch was produced by excitation of motor fibers. Similarly, orthodromic stimulation produced a depression in motoneuron activity. In our experiments it is apparent that the silent period onset is attributable to this blocking phenomenon, since the onset of the silent period does not depend on the dynamics of the muscle system. Verification of this phenomenon is also given in the

experiments utilizing inertial loads by observation of the secondary silent period produced. Clearly the onset of the secondary silent period obeys the muscle system dynamics in that case.

Granit and van der Meulen investigated the duration of the silent period and the cause of the spindle afferent's firing after the cessation of activity. The long pause and short pause responses demonstrated were attributed to the large differences in length of the spindles contained within the muscles studied. The adaptation time of spindle length (approximately 10:1 for largest to smallest) to the dynamics of the muscle is described as the predominate cause of the variability in the spindle silent periods. This long pause, short pause phenomenon is not found in the present research. In contrast, the silent period described here is dominated by the dynamics of the muscle itself, with the exceptions already mentioned.

A relatively constant silent period of motoneuron firing was reported by Jansen and Rudjord during single shocks of maximal intensity to the muscle nerve. Three reflex mechanisms were studied in order to determine the cause of the silent period duration. These were: antidromic inhibition, Golgi tendon inhibition, and the pause in Ia excitatory afferent impulses. It was concluded that, under the experimental conditions utilized, the most important factor determining the concomitant silence of the electromyogram was the pause in Ia afferent activity. This agrees with the results shown in the present study as the constancy of the Ia afferent silent period agrees with the motoneuron silent period. However, this research also defines the overall cause of the Ia afferent and motoneuron efferent silent periods, since the motoneuron efferent is dependent on the Ia afferent.

Determination of the frequency of afferent discharge relative to the velocity of the muscle is found by measuring the peak velocity of the preparation and the corresponding peak in afferent discharge. The data for the isotonic and inertial load experiments reveal a nonlinear relationship between velocity and afferent discharge frequency. The probable cause of the differences between the two curves (other than those normally expected between experiments) is the much larger negative velocity of the muscle at the onset of active muscle contraction. This initial large negative velocity component apparently overdrives the system. The nonlinear curves indicate that the muscle spindle can respond only up to certain limits, after which the gain of the system rapidly decreases. This is probably due to depolarization of the nerve terminals in the spindle. Matthews and Stein also observed this nonlinear response in 1969 during sinusoidal changes in muscle length. Their experiments were accomplished through the use of mechanical oscillation of the muscle, however, and cannot be directly compared to this investigation.

THE MODEL

The previous section briefly presented the results of the experiments and analysis of the experimental data. This section utilizes these results in determination of an appropriate model which describes the behavior of the muscle spindle. The model derived is then tested against the experimental data already presented in order to determine the authenticity of its behavior.

Certain constraints, such as approximation of the analog components to the anatomical form of the biological elements, must be maintained. In addition, the model must be able to perform under the influence of forcing functions representing both stretch and contraction. It is with these constraints in mind that the following models are proposed and developed.

Logically, the input or forcing function to the muscle spindle is the displacement of the muscle in which it is contained. Therefore, the muscle itself must be modeled in order to simulate the input in the biological system. The model of the muscle is then used as the input for the model of the muscle spindle.

Analysis of the spectral density function for the muscle shows that a differential equation of at least second order is necessary to describe the response of the muscle. This is determined from the increase in spectral content prior to the decline of the spectral density function. This behavior denotes a complex pair of roots which implies a second order differential equation. Taking this into consideration, the following equation describes such a system.

$$a\ddot{x} + b\dot{x} + cx = f(t)$$

Using mechanical analysis, it is apparent that the three elements in the differential equation represent mass, elasticity, and viscosity. The mass is the lumped sum of the muscle mass and the load to the muscle. Elasticity is the elastic property of the muscle and its interconnecting fibers, and viscosity refers to the viscous properties of the same elements. A model is formulated from these parameters.

Elastic Elements

A reasonable place to begin the modeling process is with the elastic elements of the system. Since the elastic properties of the muscle exhibit their characteristics statically as well as dynamically, the identification scheme can be either static or dynamic. Since static characteristics are described in the previous section and evaluation of the static properties of the element eliminates other dynamic characteristics of the muscle, static evaluation of the muscle fiber is used. Elasticity is analogous to a spring; therefore, it is a simple matter to model the elastic properties with a spring which has the same characteristic behavior as the experimental data. Observation of the data, however, indicates that a linear spring is insufficient to provide an accurate description of the muscle's elastic properties. Therefore, several nonlinear equations are evaluated as to their goodness of fit to the experimental data. The choice of the function for evaluation is somewhat arbitrary, and perhaps other selections would suffice. However, the functions described appear reasonable when observed in relation to the experimental data.

Linear regression techniques are utilized to determine the optimal values of the parameters. Three functions are tested as possible representative lumped parameter estimates of the elastic properties of the muscle fibers. The three choices are as follows:

STRAIGHT LINE ESTIMATE

$$y = ax + b \quad \text{straight line estimate}$$

$$Q = \sum_{i=1}^{n} [Yi - (axi + b)]^2 \quad \text{the cost function}$$

To minimize Q with respect to a and b, the partial derivatives of Q with respect to a and b are equated to zero.

$$1)\ \frac{\partial Q}{\partial a} = -2\sum_{i=1}^{n} [Yi - (ax_i + b)]X_i = 0$$

$$2)\ \frac{\partial Q}{\partial b} = -2\sum_{i=1}^{n} [Yi - (ax_i + b)] = 0$$

from these equations are obtained

$$a = \frac{\sum_{i=1}^{n} XiYi - \bar{y}\sum_{i=1}^{n} Xi}{[(\sum_{i=1}^{n} Xi)^2 - \bar{x}\sum_{i=1}^{n} Xi]} \quad \text{optimal parameter estimate}$$

POWER ESTIMATE

$$y = ax^b \quad \text{power estimate}$$

$$\ln y = \ln a + b\ln x$$

$y' = a' + bx'$ by using this transformation the previous estimate can be used to determine the transformed parameters.

EXPONENTIAL ESTIMATE

$$y = ae^{bx}$$

$$\ln y = \ln a + bx$$

$y' = a' + bx$ the same technique is utilized to determine the transformed parameters.

The optimal estimates representing the elastic properties of the muscle and its interconnecting tissues are shown in comparison with experimental data in Figure 12. Observation of the graphs shows that the exponential estimate represents the best fit of the experimental data. The power estimate yields a good fit and can also be used as an estimate of the lumped equivalent of the elastic elements. The straight line estimate does not represent a close enough approximation for use in later work.

The estimates derived here are used later in the modeling of the muscle spindle, since it is assumed that the striated regions of the spindle possess properties similar to those exhibited by the muscle itself. The optimal estimates determined are as follows:

$F = 1523.8\,X + 0.27$		straight line estimate
$F = 1041.3\,X^2$		power estimate
$F = 168.25\,(e^{1.91X} - 1)$		exponential estimate

One term of the differential equation has been determined and results in a non-linear differential equation. The second term to be determined is the viscous element in the differential equation.

Viscous Elements

After determination of the elastic properties of the muscle, the next element to be determined represents the viscous property. Viscosity can be represented mechanically by a dash pot. Since the viscous properties of the muscle can only be exhibited during muscle dynamics, the parameter optimization scheme used must be dynamic in nature.

The method used to analyze the viscous properties of the muscle is the gradient search technique. By implementing the differential equation of the system described earlier on the analog portion of the hybrid computer, a dynamic search can be accomplished. Since the properties of the elastic element have been defined, one term of the differential equation is fixed. The term to be optimized is β in the following equation:

$$\alpha\ddot{x} + \beta\dot{x} + cx^2 = f(t)$$

To accomplish this end, experimental data is compared with the data generated by the mathematical model on the analog computer. By summing the square of the difference between the experimental data and the generated data, the error squared cost function is minimized so that the parameter beta (β) is optimized. The cost function is defined as:

$$J = \sum_{i=1}^{n} (XE_i - XM_i)^2 \quad \text{where } XE = \text{experimental data}$$

$$XM = \text{model data}$$

Since the optimal solution is the point where the cost function (J) equals zero, the best estimate of β occurs when the cost is minimized. The value of the model generated data (XM_i) is the voltage sampled by the analog to digital converter at a sample rate determined by the real time clock and the number of clock counts between samples. The sampling rate is a critical factor. If the sample rate of the digital computer deviates too far below the required rate necessary to accurately reconstruct the sampled waveform, the minimized value of the cost function would never approach zero. Taking these factors into account, the following algorithm is implemented in the digital computer:

$$\beta_{i+1} = \beta_i + \lambda \nabla J_i$$

Using the above algorithm, a single parameter search is performed in order to determine the optimal value of beta (β). The results of the optimal search are illustrated in Figure 13. An observation of the graphs shows that an excellent approximation to the experimental data is determined by the following nonlinear differential equation:

$$m\ddot{x} + \beta\dot{x} + cx^2 = f(t) \qquad \text{where } m = 1.0$$

$$\beta = 0.093$$

$$c = 0.915$$

A closer approximation can be obtained by replacing the elastic term with the exponential estimate previously determined. However, due to considerations of ease of implementation on the analog computer, the power estimate is used. The resultant accuracy of the differential equation in relation to the experimental data justifies the deviation from the more optimal estimate of the elastic element in the system.

Muscle Spindle Model

One of the original constraints of the modeling approach previously stated is adherence to anatomical relationships within the structure of the model. Since some of the elements of the model are already defined, the relationship of these elements is determined by referring to the anatomical representation of the muscle spindle shown in Figure 1.

Properties similar to those of striated fibers are assumed and, therefore, the elastic elements are represented by the same nonlinear spring previously derived. The viscous elements are also assumed to possess similar properties to those derived for the muscle in which the spindle is contained. The non-contractile portions of the spindle have been shown to have elastic constants three times greater than that of the striated regions and, therefore, the coefficients of those parameters reflect this difference.

The force generators represented in the lumped parameter model of the spindle are assumed to behave in a manner similar to that already demonstrated by the muscle containing the spindle. However, since the force generators $f_i(t)$ generally provide a bias to the system, a steady state level is used to simulate the force of the striated regions of the spindle. By modification of the model, this force generation system can interact with the model in a manner similar to the muscle itself.

Secondary Ending

The lumped parameter model of the nuclear chain fiber of the muscle spindle is shown in Figure 14. The behavior, or input-output relationships, should correspond to the results elicited by the experimental data. In order to verify these results a comparison of the experimental and mathematical data is a necessity.

The comparison of experimental results with those obtained from the mathematical model is a better test of the model's validity, since the correlation techniques yield only a linear approximation of the nonlinear behavior of the secondary ending. The instantaneous frequency histograms and comparison of actual and artificial unit potentials provide sufficient basis for verification of the model performance.

Instantaneous frequency histograms of experimental and artificial data are shown in Figure 17. The characteristic behavior of the secondary ending is repeated quite accurately by the model for the range of load utilized in the experiments. The artificial data is much more predictable as the random variable of fluctuating γ efferent is not present in the model. This parameter can be added to the model for future studies.

Figure 15 illustrates the similarity of the unit action potential post stimulus firing patterns for the actual and experimental situation. The deviation of the firing pattern of the action potentials of the model is very small in comparison with that of the experimental data. The reasons for this difference are the same as those discussed earlier. The actual sensitivity of the secondary ending to muscle dynamics and to γ efferent bias is easily adjustable in the model and is one of the features which makes the model useful in studying muscle spindle behavior under a variety of system constraints.

Primary Ending

Figure presents the lumped parameter model of the nuclear bag fiber of the muscle spindle. The following differential equations are derived from the model illustrated in Figure 16.

a) $C_1(X - X_1) = C_1(X_1 - X_2)^2 + B(\dot{X}_1 - \dot{X}_2)$

b) $C_1(X_1 - X_2)^2 + B_1(\dot{X}_1 - \dot{X}_2) = 3C_1X_2^2 + B_1X_2$

now solving for X_1 from equation (a) yields

$$B_1\dot{X}_1 = B_1\dot{X}_2 + C_1(X - X_1) - C_1(X_1 - X_2)^2$$

$$\dot{X}_1 = \dot{X}_2 + \frac{C_1}{B_1}(X - X_1) - \frac{C_1}{B_1}(X_1 - X_2)^2$$

equation b yields $\dot{X}_2$

$$2B_1\dot{X}_2 = C_1(X_1 - X_2)^2 + B_1\dot{X}_1 - 3C_1\dot{X}_2^2$$

$$\dot{X}_2 = \frac{C_1}{2B_1}(X_1 - X_2)^2 \bullet \frac{\dot{X}_1}{2} - \frac{3C_1}{2B_1}X_2^2$$

The third term shown represents a unindirectional term in the transfer function in as much as the elements represent no load to the system, but are directly responsible for the derivative term in the transfer function of the type Ia ending.

$$\text{(c)} \quad KX_3 = B_1(\dot{X}_2 - \dot{X}_3)$$

$$B_1\dot{X}_3 = B_1\dot{X}_2 - KX_3$$

$$\dot{X}_3 = \dot{X}_2 - \frac{KX_3}{B_1}$$

Instantaneous frequency histograms of the model response and experimental response are shown in Figure 17. As can be seen, the behavior of the model closely follows that of the actual biological system. As in the case of the type II ending, the variability of the post stimulus discharge is markedly reduced due to the elimination of the pseudo random variations in the discharge frequency of the biological system.

The post stimulus occurrence histograms shown in Figure 18 also illustrate the ability of the model to approximate the behavior of the muscle spindle primary ending. The sensitivity of the model to variations in velocity is adjustable and, therefore, allows the model to depict wide ranges of conditions normally found in the physical system. This ability of the model to permit adjustment of parameters allows simulation of a great variety of experimental conditions and restrictions.

The Silent Period

One of the goals of this study is to investigate the silent period and to predift its occurrence and behavior. With this purpose in mind, the following silent periods shown in Figure 19 are predicted by the mathematical model. Comparison of the predicted silent periods in Figure 19 with actual silent periods in Figure 20 illustrates the accuracy of the projected calculations.

The explanation for the behavior of the silent period illustrated in Figure 19 is that, once the spindle activity is extinguished, it will remain in this state until it is forced to resume firing. The cause of the resumption in spindle activity shown in illustration is a positive velocity vector greater than 0.9 centimeters per second. This explains why the duration of the silent period increases rather than decreases with load. Initially, it was thought that the silent period would decrease in duration with load until it extinguished due to a reduction in muscle dynamics. However, because of antidromic stimulation, the spindle is initially caused to be silent, regardless of load. · spindle will remain silent for a considerable time (approximately 200 milliseconds) unless something causes it to resume firing. As load is increased, the positive velocity vector exceeds the threshold level with increasing latency. This shift in the time at which the velocity vector exceeds threshold is the cause of the longer duration of the silent period for increased load.

The secondary silent periods for the inertial load experiments illustrated in Figure 9 do not exhibit the phenomenon of increasing duration described in the previous paragraph. The reason for this deviation in the spindle discharge pattern is that the onset of the secondary silent period is due only to the dynamics of the muscle and is not initiated by antidromic stimulation. The model is able to predict these silent periods as well, since both onset and offset of the spindle activity follow the dynamics of the system.

IMPLICATIONS OF THE MODEL

The mathematical model presented, which was derived from experimental data, possesses several capabilities not incorporated in previously published models. Consideration of the entire range of muscle functioning allows the spindle afferent discharge to be predicted both during stretch and active contraction. Additionally, since the elements comprising the model adhere to the anatomy of the muscle spindle, individual parameter contributions to output of the muscle spindle can be studied. Also, sensitivity of the silent period is evaluated and permits the study of the silent period in relation to control of muscle movement.

Since both the muscle and the muscle spindle have been modeled, the control law which governs muscle activity can now be investigated. We can now study the effects of various parameters, such as gamma efferent bias on reflex activity.

Merton's follow-up length servo hypothesis [1], which has been widely accepted as an explanation of muscle control, does not account for phasic muscle movements. His servomechanism can be an adequate mechanism for postural regulation.

Considering the information described in previous sections and by other investigators, spindle discharge mediated by γ activity is inadequate to control muscle movement. In addition, the delays of the γ route due to the propagation time of neural transmission are obvious. A follow-up servo would require a high gain in order to maintain its steady state length, regardless of load. However, the ease with which limb position is varied by application of load verifies the fact that the servo mechanism which controls reflex activity has low gain.

A concept which is taking the place of the follow-up servo theory of muscle control is that of servo-assistance proposed by Matthews [2]. The servo-assistance scheme suggests a system which initiates movement by co-activation of the α and γ pathways. This provides a type of "power steering" whereby contraction of muscle is assisted by increased spindle discharge. However, acceptance of this more plausible explanation of the mechanism of motor control still leaves many factors obscure.

How does the CNS process these and the other sensory inputs such as the Golgi tendon organ and joint receptors? The overall control mechanism appears to utilize all of these inputs to formulate the control strategem.

Given adequate estimators of all of the peripheral receptors and actuators, investigation of the role of the central nervous system plays in tonic and phasic control of muscle movement can be investigated.

1. Merton, P.A.: "Speculations on the Servo-Control of Movement." The Spinal Cord. 1953. Malcom, J.L.; Gray, J.A.B. ed. Ciba Foundation Symposium. Little, Brown & Co., Boston.

2. Matthews, P.B.C.: Mammalian Muscle Receptors and Their Central Actions. Williams & Williams Co. 1972, Baltimore.

3. Eldred, E.: The Dual Sensory Role of Muscle Spindles. Physical Therapy. 1965, Vol. 45, p. 290-313.

4. Granit, R.: The Basis of Motor Control. Academic Press, 1970, London, New York.

5. Rosenthal, N.P.: "A Linear Systems Analysis of the Myotatic Reflex and Its Component." Ph.D. Dissertation, Univ. of Minnesota, 1969.

6. Ellaway, P.H.: "Recurrent Inhibition of Fusimotor Neurones Exhibiting Background Discharges in the Decerebrate and the Spinal Cat." J. Physiol., 1971, Vol. 216, p. 419-439.

7. Jansen, J.K.S.; Rudjord, T.: "On the Silent Period and Golgi Tendon Organs of the Soleus Muscle of the Cat." Acta Physiol. Scand., 1964, Vol. 62, p. 364-379.

8. Gottlieb, G.; Agarwal, G.; Stark, L.: "Studies in Postural Control Systems, Part III: A Muscle Spindle Model." I.E.E.E. Trans. System Science and Cybernetics, Vol. SSC-6, No. 2, April 1970.

9. McRuer, D.T.; Magdaleno, R.E.; Moore, G.P.: "A Neuromuscular Actuation System Model." I.E.E.E. Trans. Man-Machine Systems, Sept. 1968, Vol. MMS-9, p. 61-71.

10. Zajac, F.E.: "The Mathematical Formulation of the Kinematic Properties of Muscle Derived From an Experimental Investigation." Ph.D. Dissertation, Stanford University, 1968.

11. Houk, J.C.; Cornew, R.W.; Stark, L.: "A Model of Adaptation in Amphibian Spindle Receptors." J. Theoret. Biol., 1966, Vol. 12, p. 196-215.

12. Rudjord, T.: "A Second Order Mechanical Model of Muscle Spindles Primary Endings." Kybernetic, 1970, Vol. 6, p. 205-213.

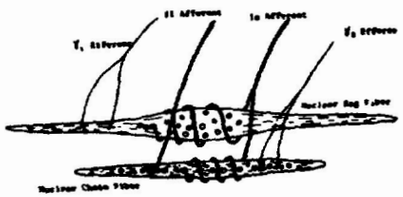

Figure 1

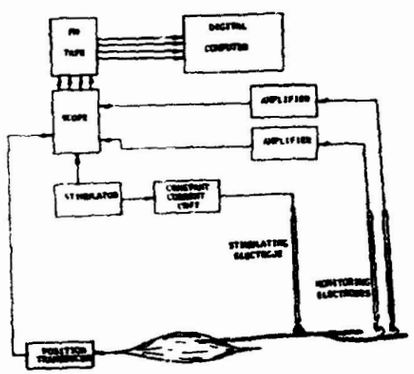

Figure 2

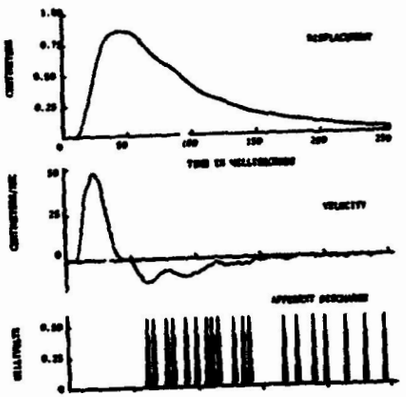

Figure 3

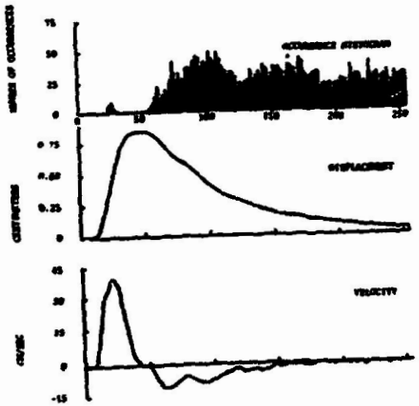

Figure 4

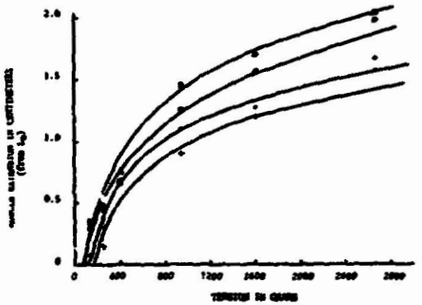

Figure 5

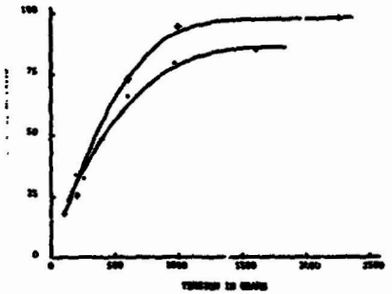

Figure 6

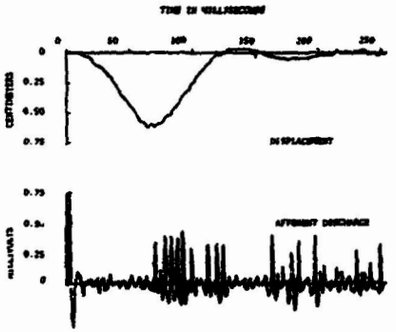

Fifure 7

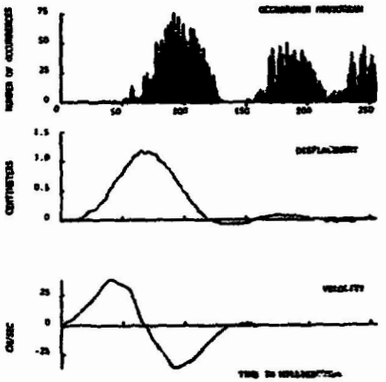

Figure 8

Figure 9

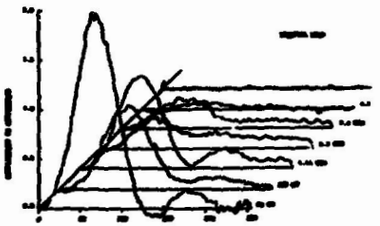

Figure 10

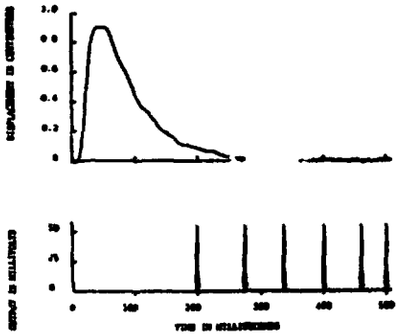

Figure 11

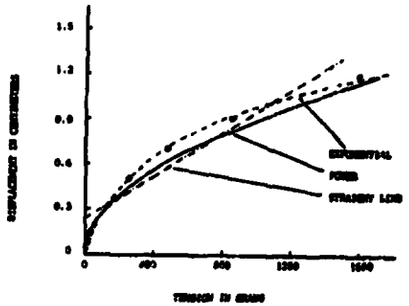

Figure 12

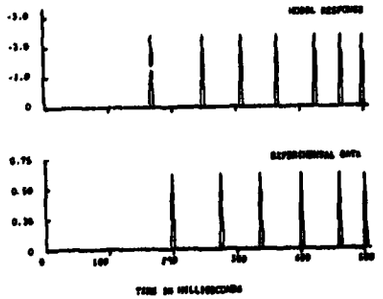

Figure 15

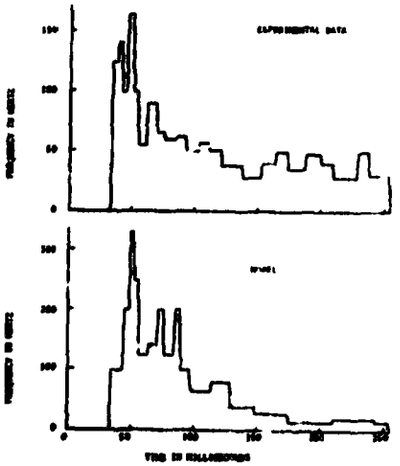

Figure 17

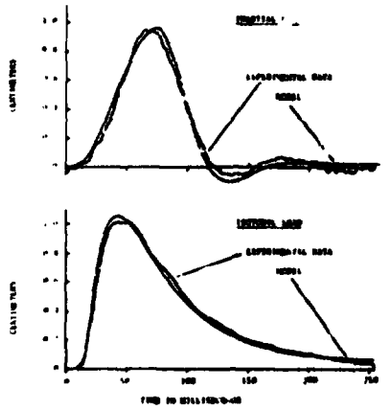

Figure 13

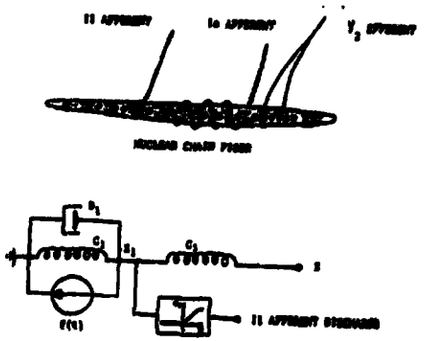

Figure 14

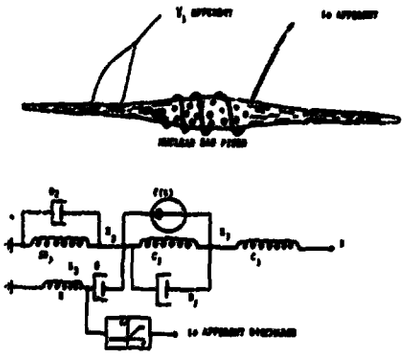

Figure 16

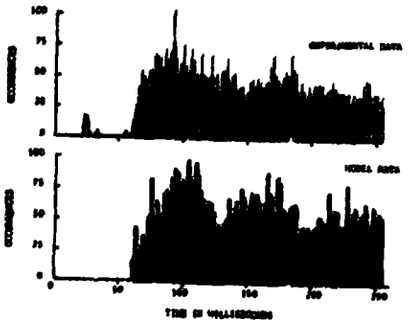

Figure 18

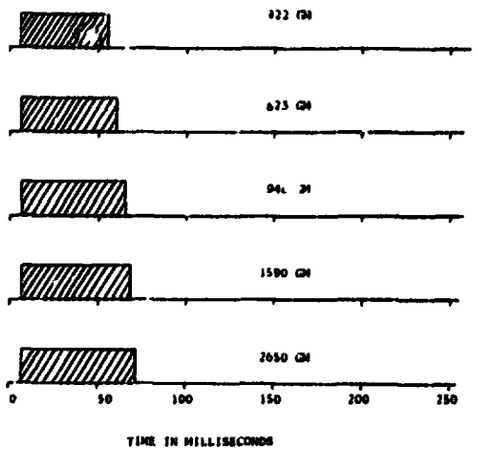

Figure 19

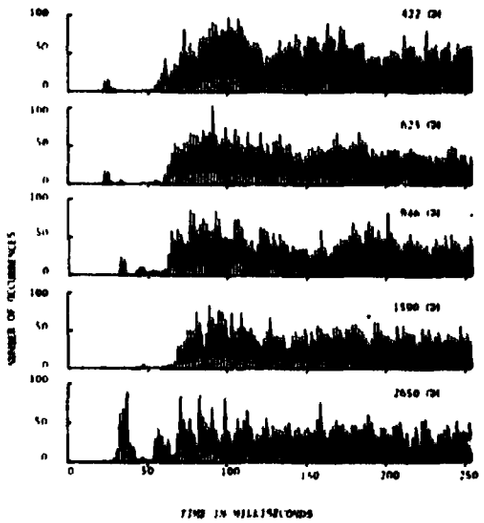

Figure 20

N75 19156

PRECEDING PAGE BLANK NOT FILMED

CONTINUOUSLY VARYING SKIN POTENTIALS ELICITED BY SINUSOIDALLY VARYING ELECTRIC SHOCK POTENTIALS

J.W. Senders, V.L. Senders, and B. Tursky

Although the electrodermal responses, GSP and GSR, have been extensively studied, and have been used as indices of autonomic functioning and of emotion over a period of many years, their basic nature is still not well understood. The stated aim of the investigation carried out under this grant was to determine whether a form of quasi-linear systems analysis can be applied to these response measures to yield new insights into the nature of the underlying response mechanisms and their interrelationships. It was originally proposed that the principal response to be investigated should be the electrodermal response (galvanic skin potential, GSP) as elicited by an electric shock stimulus applied to the skin. The experimental procedure involves a change from the usual method of applying electric shock stimulation, which has been to apply brief pulses of electric current of approximately one second duration and with a modulation envelope essentially square. The response subsequent to this stimulation has been examined and its [illegible]teristics measured in terms of latency, magnitude, rate of [illegible], and its characteristic of being unipolar or bipolar. Following one such elicitation, an interval of time, typically averaging 30 sec., was allowed to elapse before the next stimulus was applied. In the investigation reported here, the stimulus was to have been a continuously varying shock current in which the modulation envelope was eiher 1) that of a sinusoid of some fixed frequency, or 2) that of a random or quasi-random time function. The response, then, would not be a discrete response to a discrete stimulus application, but rather a continuous, driven response which would be correlated with the modulation envelope applied to the stimulus.

Most of the desired experimental goals were reached. Limitations of time and funding did not permit the investigation of random or quasi-random modulation envelopes. However, a series of experimental runs on three Ss (two runs on one S, one on each of the other two) was accomplished, using sinusoidal modulation envelopes of frequencies of .05, .10, .15, .20, .30, .40, and .80 hz. In all cases results showed that it was possible to drive the GSP and to achieve relatively high coherence between the driving frequency and the response itself. The analysis was laborious, and because of practical considerations was limited to Fourier analysis of the response in order to determine the relative energies at the driving frequency and at successive harmonics of that driving frequency, and correlational analysis in order to determine the degree of linear relationship between the driving frequency and the driven response.

Results:

The most significant findings and conclusions of the preliminary study were as follows:

1. The skin potential response is capable of continuous driving, without habituation, between frequencies of .1 to .4 hz.
2. The GSP has an insignificant to vanishingly small response to frequencies of 0.05 hz. and 0.80 hz.
3. The response is relatively flat over the range from .10 hz. to .40 hz.
4. There is a suggestion that a natural resonance phenomenon can be triggered by driving in the range from .10 to .20 hz.
5. The linearity of relationship between the driving frequency and the driven response can go as high as .9 or as low as .1 for different Ss or for the same S at different times and for different frequencies.
6. The shape of the response function, while periodic, nonetheless exhibits significant and reliable harmonic content.
7. The reliability of the response, in the case of two Ss, suggests that the original goal of the research, that of demonstrating that quasilinear analysis could be applied successfully to these measures has been achieved. Applications of the technique to improve our understanding of the bases of such response systems are feasible and desirable.

8. The electrodermal response system of one S was sufficiently strongly entrained by the driving frequency that a nearly pure sinusoidal response was generated with a peak-to-peak magnitude of 80 mv. This response was sustained at the rate of .1 hz. for a period of more than 2 minutes without apparant dimunition.

9. There is a suggestion in some of the records that very low frequency variations, or possibly beats, do occur, which could be analysed by more elaborate recording and computer-analysis techniques.

10. Breathing, heart-rate, and blood-volume all demonstrated driving by the sinusoidally-modulated shock-stimulus, but in varying degrees for the different Ss. In all Ss there was a clear relationship between blood-volume and electrodermal response such that the electrodermal response appeared in its driven form only when blood-volume was markedly reduced. There was, however, no report of apparent intensity difference or change in discomfort produced by the stimulus.

SESSION VIII

HUMAN MODELLING

N75 19157

PRECEDING PAGE BLANK NOT FILMED

MODELLING THE BEHAVIOR OF THE HELMSMAN STEERING A SHIP

W. Veldhuyzen and H.G. Stassen
Man-Machine Systems Group
Laboratory for Measurement and Control
Department of Mechanical Engineering
Delft University of Technology
The Netherlands.

Abstract

A supertanker can be considered as a nonlinear system which responds very slowly to changes in the rudder position. Moreover this type of ships is often unstable in loaded condition, i.e. it has a tendency to start turning either to the left or to the right. These properties make the supertanker very hard to handle.

In order to model the helmsman's behavior, a number of tests has been performed using a ship maneuvering simulator. The trained subjects had to steer a 200,000 tons tanker along a varying course. The results obtained from these trials are encouraging. A discussion of the further research is given.

1. Introduction

Most of the investigations concerned with the behavior of the human operator as a controller have been executed with reference to pilots of aircraft or spacecraft; some work has been done on the control of submarines. The human operator as a controller of surface ships, however, did not get very much attention until recently.

In the Netherlands in 1968 the Institute TNO for Mechanical Construction (TNO-IWECO) at Delft built a ship maneuvering simulator [1] in order to study among other things ship maneuverability, the design of nautical instruments and the training of ship crews. In the same year Stuurman [2] executed a series of trials in which he showed that for small ships the control behavior of the helmsman could very well approximated by means of a Describing Function Model. He also found evidence that for larger ships a nonlinear model probably would give a more realistic description of the helmsman's behavior.

In consult with TNO-IWECO it was decided to continue the work of Stuurman as a joint activity of the Shipbuilding Laboratory of the Delft University of Technology and the Man-Machine Systems Group. Special emphasis was to be laid on modelling the helmsman of a supertanker with the following goals in mind: To provide data on which the maneuvers of this type of ships under human control can be predicted in a number of situations as well as to enable an evaluation of the employment of a human pilot. The results of some preliminary experiments have been reported at last year's Annual Conference on Manual Control [3].

2 Ship dynamics

The dynamics of a ship depend not only on the properties of the ship itself but also on the topology of the surrounding water. The motions of a ship in the horizontal plane can be described by a set of nonlinear differential equations. These equations describe the translations of the ship in a direction corresponding to the longitudinal axis of the ship and in a direction perpendicular to this axis as well as the rotation about a vertical axis through the center of gravity. Fig. 1 gives an indication of the variables concerned.

In 1957, Nomoto [4] showed that for a ship sailing at constant speed the relation between rudder angle δ and rate of turn r can be described by means of a second order linear differential equation. For most of the smaller ships this equation gives an adequate description of the ship's behavior in a number of standard maneuvers. For a supertanker, however, it was found that the behavior was essentially nonlinear. Based on full scale trials, Bech [5] proposed to extend Nomoto's equation with a nonlinear term. This leads to the following relation [6]:

$$T_1T_2\,\ddot{r}(t)+(T_1+T_2)\dot{r}(t)+a_1 r(t)+a_2[r(t)]^3 = K[T_3\,\dot{\delta}(t)+\delta(t)], \qquad (1)$$

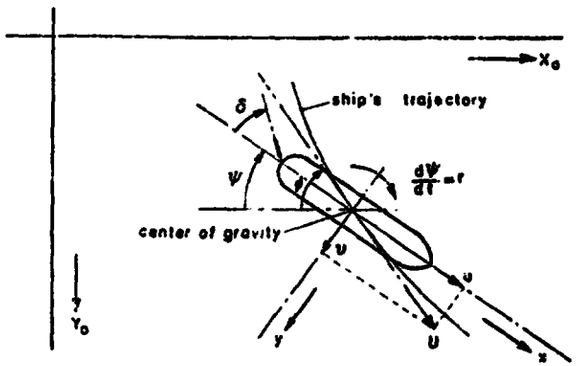

FIGURE 1:

The quantities involved in the description of the ship's maneuvers.

where $r(t) = d\psi(t)/dt$ is the rate of turn, $\psi(t)$ is the heading angle, $\delta(t)$ is the rudder angle, and where the quantities a_1, a_2, T_1, T_2, T_3 and K are constants. These constants are dependent on the hydrodynamic properties of the ship, which are for instance related to speed, load condition and possible restrictions in the surrounding water.

In this study a particular ship viz. a 220,000 tons deadweight tanker in loaded condition has been chosen. The principal data of the ship were: Length = 310.00 m; Breadth = 47.16 m; Depth = 24.50 m; Draft = 18.90 m; Displacement = 238,000 m^3 and Froude number = 0.14. The constants in Eq. (1) for this ship have been determined by Glansdorp [6;7], they are given in Table 1. If a stationary situation is considered, that is, $\dot{r}(t) = 0$, $\dot{\psi}(t) = 0$, $\dot{\delta}(t) = 0$, then Eq. (1) changes into:

$$a_1 r + a_2 r^3 = K\delta. \qquad (2)$$

TABLE 1:

Constants in the equation describing the relation between the rudder angle and the rate of turn for the supertanker, in deep and still water; the speed considered is 7.72 m/sec.

constants	dimension	numerical values	
		fully loaded	ballasted
a_1		-1	1
a_2	sec^2/rad^2	80,000	16,200
T_1	sec	250	80
T_2	sec	10	3
T_3	sec	20	6
K	sec^{-1}	-0.0434	-0.0471

Fig. 2 represents Eq. (2) ; this static characteristic is given for the ship in fully loaded and ballasted condition. The ship is course unstable in loaded condition; it has a natural tendency to deviate from the straight course and to start turning either in one direction or the other.

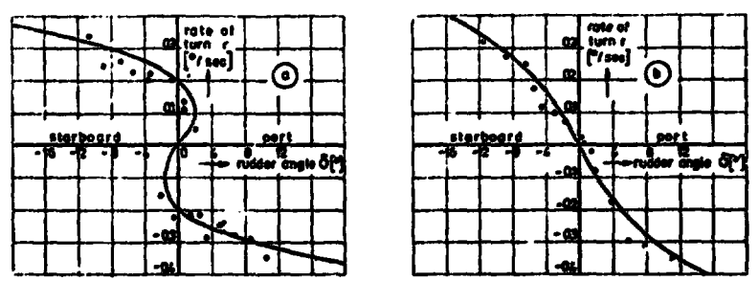

FIGURE 2:

Relation between the rudder angle δ and the rate of turn r in the stationary state for the ship considered in this investigation as found by Glansdorp [7] (a: loaded condition; b: ballasted condition).

3 The maneuvering simulator

The simulator consists of a wheelhouse which has the same appearance as that of a real sea-going vessel. The fore part of the ship, the sea and a coastline are displayed on a screen in front of the wheelhouse. The total angle of vision of the helmsman is 120°. The image of the fore part of the ship is static, it is produced by two slide projectors which have a fixed position. The coast line is generated by means of a point light source and a movable model with three degrees of freedom simulating two translations and one rotation in the horizontal plane. A blockdiagram of the system, including the helmsman, is given in Fig. 3.

ORIGINAL PAGE IS OF POOR QUALITY

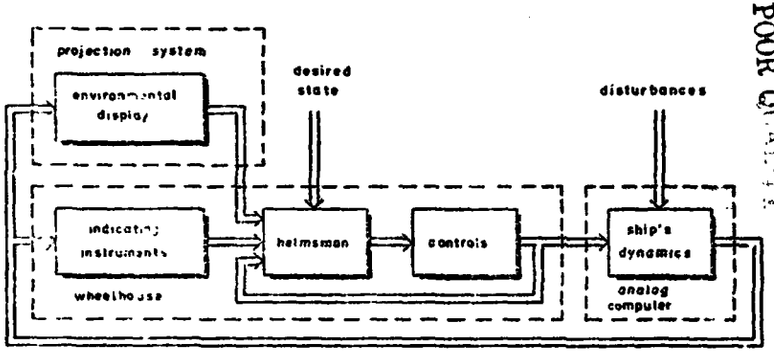

FIGURE 3:
Blockdiagram of the TNO simulator.

On an analog computer the dynamics of the ship to be simulated, including the characteristics of thrust engine and rudder engine, can be programmed. The computer yields the signals which control the environmental display system and also the instruments such as compass, rudder position indicator, log, etc. The helmsman has the same controls at his disposal for maneuvering as on a real ship viz. the wheel, which gives the input to the rudder engine, and

the telegraph to the engine, which governs the speed of the propeller. External disturbances simulating the effects of wind, waves and currents can also be introduced into the model on the analog computer.

4 The experiments

In the experiments described here, the simulator has been used as a supertanker at full sea in fully loaded condition as well as in ballasted condition, moving at a constant speed. The analog computer was programmed according to Eq. (1) based on the constants given by Glansdorp as indicated in Table 1. The rudder engine was also included in the simulation; its dynamics have been chosen according to the Eqs (3) and (4).

$$T_4 \dot{\delta}(t) + \delta(t) = \delta_d(t); \qquad (3)$$

$$|\dot{\delta}(t)| \leq M, \qquad (4)$$

where $\delta_d(t)$ is the position of the steering wheel or the desired rudder angle; where T_4 is a time constant of 1 sec and where the quantity M is the maximal value of the rotation speed of the rudder (0.045 rad/sec).

The subjects were four trainees of the School of Navigation at Rotterdam. They were studying for the rank of first or second mate after having been at sea for several years. All four trainees were experienced in steering conventional cargo ships; only one of them (subject A) had sailed on tankers up to 90,000 tons dead weight. Their task consisted of following a straight course for about half an hour, or of following a preprogrammed but unpredictable course which changed between +2° and -2° around a certain nominal course for about fourty minutes. This prescribed course acted as a forcing function for the man-supertanker system. Because it is not a realistic situation to follow a continuously changing course, a binary signal was chosen. The construction of the binary test signal was based on the idea that with the experiments to be executed also linear models of the helmsman's behavior might be investigated.

Therefore the input signal (desired course) was constructed in such a way that about 70 percent of the input's energy was concentrated at only four frequencies. The amplitude of the binary signal was equal to the two degrees earlier mentioned. The four sinusoidal components were the third, fifth, eight and thirteenth harmonics of a sinusoid with a period of forty minutes; the phase at the initial point was chosen at random.

TABLE 2: Summary of the tests performed.

DATE / TIME	1972 April 25	1972 April 26	1972 May 2	1972 May 3
7.00pm	Subject A [1] loaded cond. course chang.	Subject C [7] loaded cond. course chang.	Subject A [13] ball. cond. course chang.	Subject D [19] ** loaded cond. course chang.
8.00pm	Subject B [2] loaded cond. course keep.	Subject D [8] loaded cond. course chang.	Subject B [14] loaded cond. course chang.	Subject C [20] loaded cond. course chang.
	Subject A [3] loaded cond. course keep.	Subject C [9] loaded cond. course keep.	Subject A [15] loaded cond. course keep.	Subject D [21] loaded cond. course keep.
9.00pm	Subject B [4] loaded cond. course chang.	Subject D [10] loaded cond. course keep.	Subject B [16] loaded cond. course keep.	Subject C [22] loaded cond. course keep.
	Subject A [5] ball. cond. course keep.	Subject C [11] ** loaded cond. course keep.	Subject A [17] loaded cond. course keep.	Subject D [23] loaded cond. course keep.
10.00pm	Subject B [6] ball. cond. course keep.	Subject D [12] *** loaded cond. course chang.	Subject B [18] * loaded cond. course keep.	Subject C [24] * loaded cond. course keep.

* With disturbances due to waves.

** With rate of turn indicator.

*** Due to a want of time this run could not be performed.

In Table 2 a summary of the tests is given. During the experiments the compass as well as the rudder angle indicator were used. Three tests have been executed in which also the rate of turn indicator was used. With the exception of two trials no external disturbances simulating ship motions originating from wind, waves and currents were introduced; these external disturbances were generated by means of a digital computer and consisted of the sum of 23 sinusoids simulating the motions of the fully loaded tanker in a following sea with long crested waves. These waves were considered to originate from a wind with a force of eight to nine Beaufort.

During the tests the following signals were recorded on magnetic tape:

- The desired course $\psi_d(t)$.
- The course of the ship $\psi(t)$.
- The desired rudder angle $\delta_d(t)$.
- The rudder angle $\delta(t)$.
- The rate of turn $r(t) = \dot{\psi}(t)$.

5 Modelling the helmsman's behavior

In the Figs 4 through 6 some examples are given of the time histories of the desired course $\psi_d(t)$; the course of the ship $\psi(t)$; the desired rudder angle $\delta_d(t)$; the rudder angle $\delta(t)$, and finally the rate of turn $r(t)$ as recorded during the tests. In all cases the records show that the helmsman generates a rudder angle $\delta(t)$ as output which consists of discrete steps. Hence the records indicate that a linear model to describe the helmsman's behavior will not fit the data very well. To check this presumption, the ratio between the energy not located at the four frequencies mentioned before and the total energy of the signal considered has been calculated. The Table 3 shows the results for the four subjects, each having performed two runs of forty minutes. From the table it can be concluded that the remnant energy, in particular of the desired rudder angle $\delta_d(t)$, is that high in most of the runs observed, that it does not seem appropriate to focus the attention on linear descriptions of the helmsman's behavior

Subject	A		B		C		D	
Run	1	2	1	2	1	2	1	2
$\psi_d(t)$	28.0	28.6	29.3	28.0	23.0	28.6	28.3	28.8
$\psi(t)$	10.3	21.6	7.8	27.7	50.1	19.5	1.7	26.6
$\delta_d(t)$	88.7	88.0	90.9	94.3	78.2	85.9	78.1	87.9
$\delta(t)$	86.2	86.0	88.8	91.3	77.6	84.7	77.1	86.5
$r(t)$	48.8	47.9	49.5	52.9	70.0	53.2	35.0	56.1

TABLE 3:

Survey of the remnant energy in the signals observed for eight tests with four subjects: Loaded condition; without rate of turn indicator; without disturbances.

any longer. It suggests that the helmsman bases his decisions on when to move and how much to move the wheel on some criterion which is, for instance, a function of the heading angle $\psi(t)$; the rate of turn $r(t)$; the position of the rudder $\delta(t)$, and, of course, the desired angle $\psi_d(t)$.

By the compass the course $\psi(t)$ is displayed to the helmsman; while in the case that no rate of turn indicator is used, it is assumed that the helmsman estimates the rate of turn $r(t)$ directly from the time history of the course $\psi(t)$. Based on the records obtained by preliminary tests as well as on the records shown in the Figs 4, 5 and 6 a model for the helmsman's behavior is proposed which states that if the absolute value of a quantity $s(t)$ which is defined as:

$$s(t) = [\psi(t) - \psi_d(t)] + c_1\dot{\psi}(t) \qquad (5)$$

exceeds a certain threshold value d_1, the helmsman moves the steering wheel into a position $\delta_d(t)$ according to Eq. (6):

$$\delta_d^*(t) = a\psi_e(t) + b\dot{\psi}(t) + c[\psi_e(t)]^3 + d \text{ sign } \psi_e(t). \qquad (6)$$

In this equation the quantity $\psi_e(t) = \psi(t) - \psi_d(t)$, and the quantities $\psi(t)$, $\psi_d(t)$ and $\dot{\psi}(t)$ are the values of these variables at the moment that the threshold value is exceeded. As a result of this action, the quantity $|s(t)|$ wil decrease; if now $|s(t)|$ becomes less than a second threshold value d_2, it is assumed that

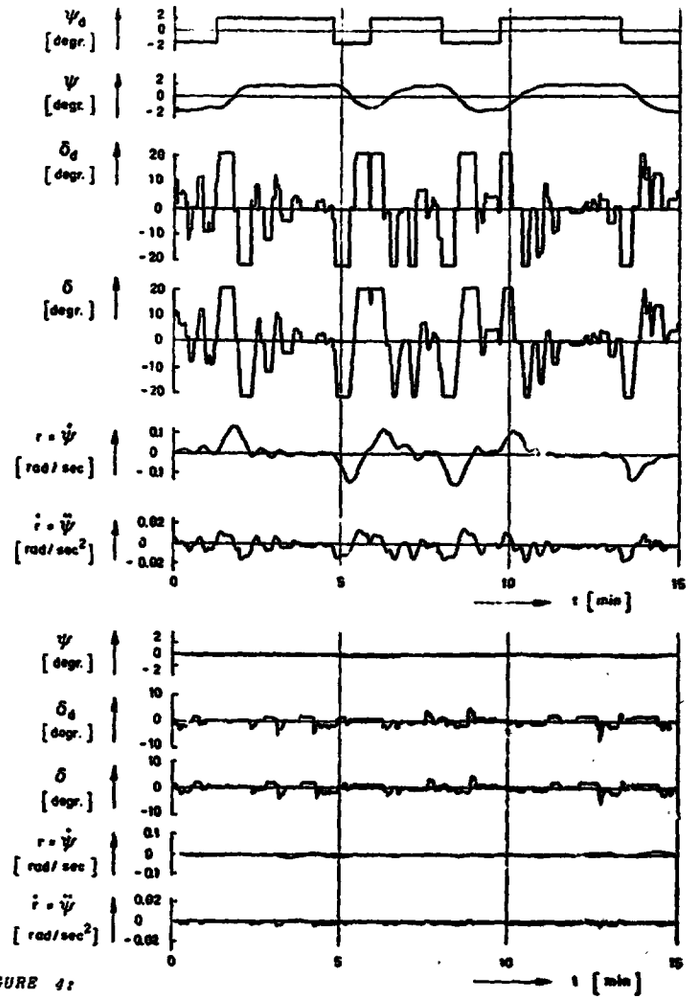

FIGURE 4:

Example of the time histories of the desired course $\psi_d(t)$; the course of the ship $\psi(t)$; the desired rudder angle $\delta_d(t)$; the rudder angle $\delta(t)$; the rate of turn $r(t)$, and the derivative of the rate of turn with respect to the time $\dot{r}(t)$: subject A; without rate of turn indicator; without disturbances; loaded condition.

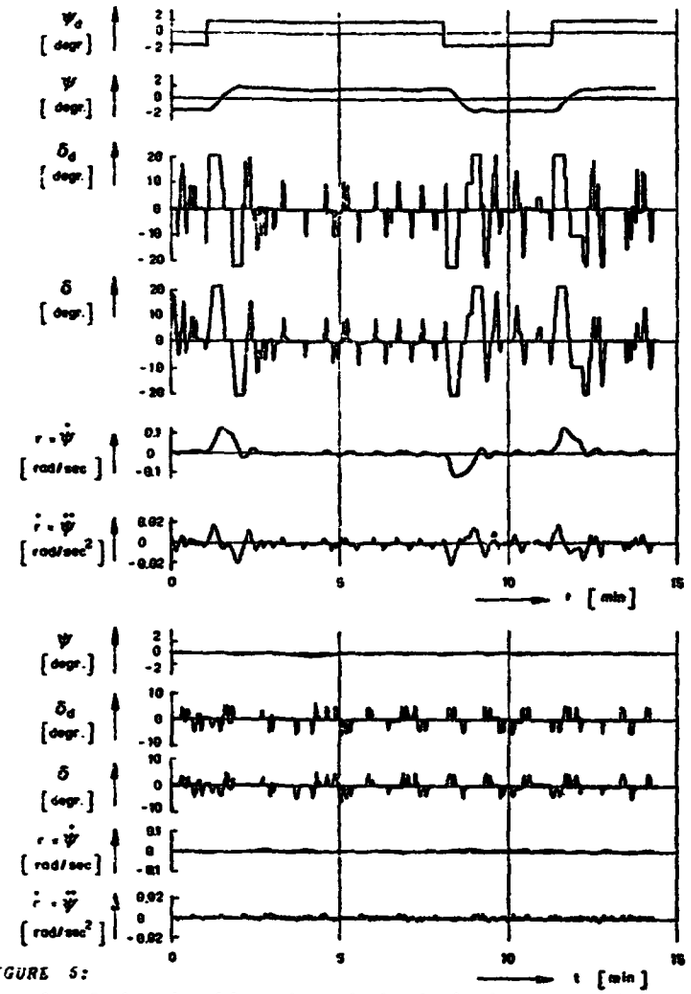

FIGURE 5:

Example of the time histories of the desired course $\psi_d(t)$; the course of the ship $\psi(t)$; th· desired rudder angle $\delta_d(t)$; the rudder angle $\delta(t)$; the rate of tu. t), and the derivative of the rate of turn with respect to t· e $\dot{r}(t)$: Subject B; without rate of turn indicator; without u. ances; loaded condition.

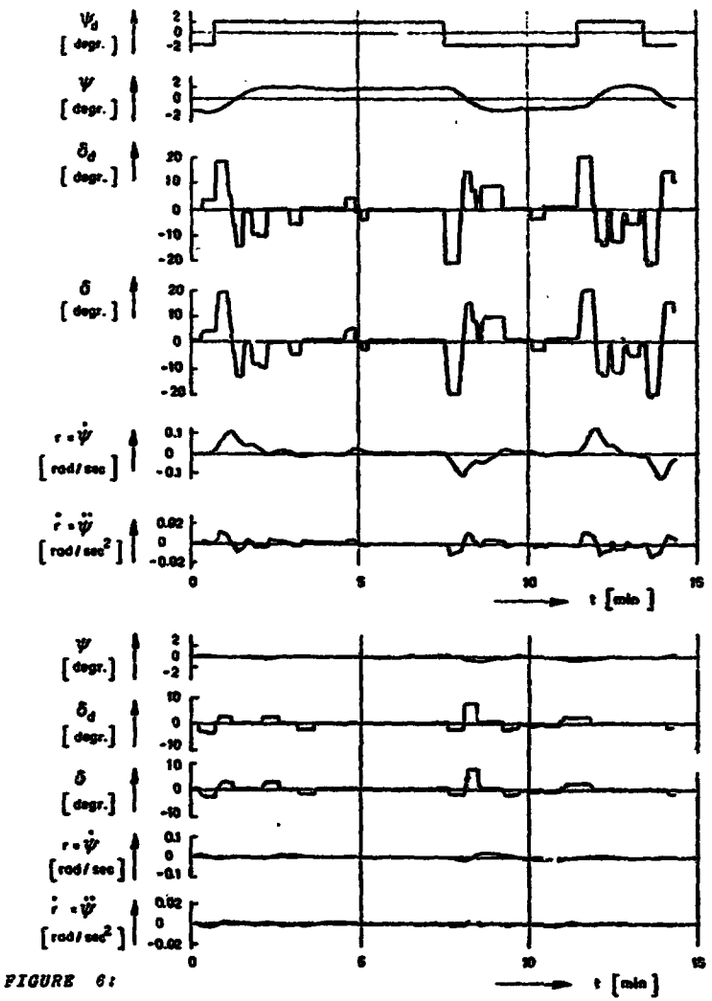

FIGURE 6:

Example of the time histories of the desired course $\psi_d(t)$; the course of the ship $\psi(t)$; the desired rudder angle $\delta_d(t)$; the rudder angle $\delta(t)$; the rate of turn $r(t)$, and the derivative of the rate of turn with respect to the time $\dot{r}(t)$: Subject D; without rate of turn indicator; without disturbances; loaded condition.

the helmsman moves the rudder again into zero position.

6. Parameter Estimation

The parameters a, b, c, d, c_1, d_1 and d_2 can be estimated by minimizing a quantity J_1 defined as:

$$J_1 = \frac{1}{T}\int_0^T [\varepsilon(t)]^2\,dt, \qquad (7)$$

where the signal $\varepsilon(t)$ represents the difference between the human operator output $\delta_d(t)$ and the model output $\delta_d^*(t)$. The minimal value of the quantity J_1 can be found by partial differentiation of this quantity with respect to each of the unknown parameters and by setting the result equal to zero. This yields as many equations as there are unknown parameters. Because there does not exist a simple analytical relation between the input and the output of the model of the helmsman it is not possible to solve the equations just-mentioned in a simple way. Furthermore, it should be noted that if a model with given parameters should be inserted into the control loop instead of the helmsman, this would lead to another time history for the quantities $\delta_d(t)$, $\psi(t)$ and $r(t)$. So, in order to get an unbiased estimate of the parameters in the human operator model, a comparison should be made between the output of the helmsman and the output of the model, where this model is also part of a closed loop system with the ship's model (See Fig. 7). The parameters can be found by means of a direct search method minimizing the quantity J_1 with respect to the model parameters. With the help of Eq. (7) the quantity E_1 can be defined:

$$E_1 = \frac{J_1}{\frac{1}{T}\int_0^T [\delta_d(t)]^2\,dt} = \frac{\int_0^T [\varepsilon(t)]^2\,dt}{\int_0^T [\delta_d(t)]^2\,dt}. \qquad (8)$$

The quantity E_1 indicates how well the model output approximates the actual output of the helmsman.

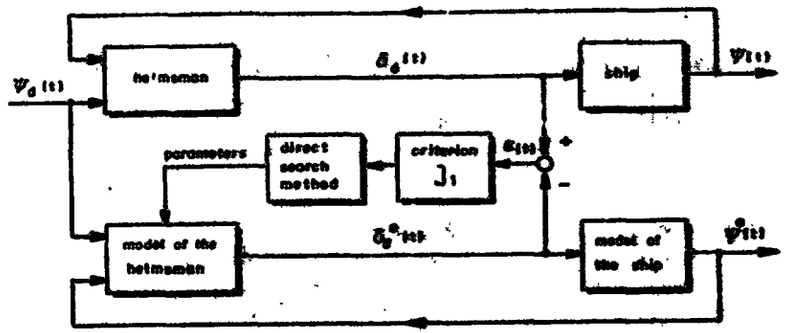

FIGURE 7:
Application of an error criterion in such a way that unbiased parameters can be obtained for a model of a system in a closed loop.

The correspondence between the time histories of the actual course of the ship $\psi(t)$ steered by the helmsman and those of the ship model $\psi^*(t)$ steered by the model of the helmsman's behavior can be expressed by the quantity E_2, defined as:

$$E_2 = \frac{\int_0^T [\psi(t)-\psi^*(t)]^2\,dt}{\int_0^T [\psi(t)]^2\,dt}. \qquad (9)$$

7 Results

Based on the data of one test, in which the subject had been instructed to steer a ship in loaded condition along a straight course for a period of 25 minutes, the parameters of a series of simple models have been estimated according to the parameter estimation method just-mentioned. The first model was a linear one; later models were based on the Eqs (5) and (6).

be it that the nonlinear terms in Eq.(5) were neglected. The results with these simple models, however, were very poor, and did not give any indication how to modify the mo[illegible]sed in order to get a better result. Therefore, the task of th[illegible]lmsman, which du[illegible]ng these tests was to keep a ship in loaded condition on a straight course, was changed into the task of following a certain unpredictable but well defined course. In this case, again the parameters were estimated, and now the results were much better; they even led to a direction in which the structure of the model had to be changed. Finally, the model as given by the Eqs (5) and (6) was obtained.

The Table 4 shows the values of the model parameters as well as the values of the quantities E_1 and E_2 calculated from four tests

TABLE 4:
Summary of the parameters of the model given by the Eqs (5) and (6) and the quantities E_1 and E_2.

Subject	A	B	C	D
Date	1972 May 2	1972 May 2	1972 May 3	1972 May 3
Test nr	15	14	20	21
a	3.5	1.9	6.2	2.0
b [sec.]	176.9	155.0	210.0	230.5
c [degr.$^{-2}$]	0.0	0.1	-0.1	0.1
d [degr.]	1.7	1.0	1.0	1.5
c_1 [sec.]	20.3	30.0	22.5	30.0
d_1 [degr.]	-5.0	0.2	0.3	0.2
d_2 [degr.]	-5.0	0.1	0.2	0.0
E_1 [%]	40.1	70.9	43.4	32.8
E_2 [%]	8.7	--	--	3.1

execu[illegible] the four subjects A, B, C and D (See Table 2). The Figs 8 and 9 show some typical time histories of the actual signals $\psi_d(t)$, $\psi(t)$ and $\delta_d(t)$ compared with the model outputs $\psi^m(t)$ and $\delta_d^m(t)$. Some remarks with respect to the results obtained can be made.

- Although a remarkable difference in the steering behavior of the subjects exists (See the Figs 4, 5 and 6), the difference of the parameters among the different subjects is rather small.
- In particular for the subjects A and D the model fits the test results fairly well.
- Although the output of the model of the helmsman's behavior does notalways resemble the actual output very well the course of the ship generated by the model experiment fits extremely well.
- In a few cases, for instance the test with subject C, the optimization of the parameters by minimizing the quantity J_1, was difficult. The problem was to find the absolute minimum of the quantity J_1 in stead of a local minimum

Further research

Until now, only the parameters of the model have been estimated for four subjects steering a fully loaded tanker along a prescribed course changing at certain moments from +2 degrees to -2 degrees and back. Also some tests were performed with a tanker in ballasted condition and with disturbances (simulating for instance the motions originating from seawaves) acting on the ship, but at this moment parameters have not yet been estimated. Some of these tests, in particular those with the ship sailing in open sea with rather high waves, showed that fairly dangerous situations can occur when the helmsman is not well trained.

The further research is focussed on the following points which may be of importance in developing a useful model in order to be able to predict the behavior of a ship under human control.

- A study of the influence of the task to be executed by the subjects on the structure of the model of the helmsman's

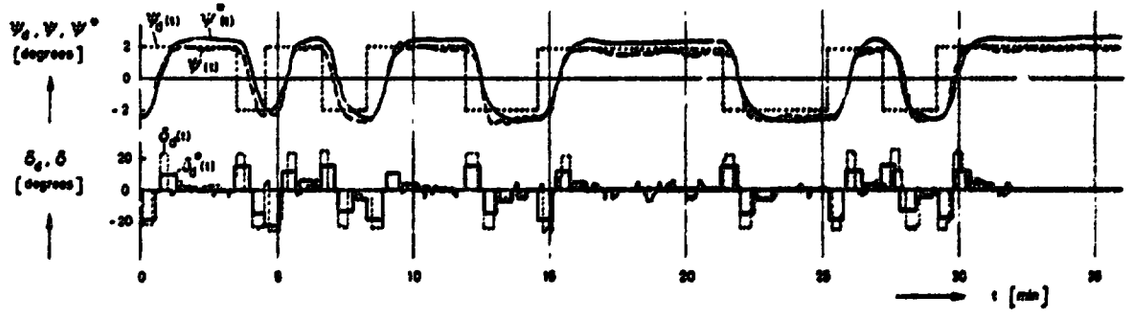

FIGURE 8: Typical time histories of the actual signals $\psi_d(t)$, $\psi(t)$ and $\delta_d(t)$ compared with the model outputs $\psi^*(t)$ and $\delta_d^*(t)$: Subject A; loaded condition; without rate of turn indicator.

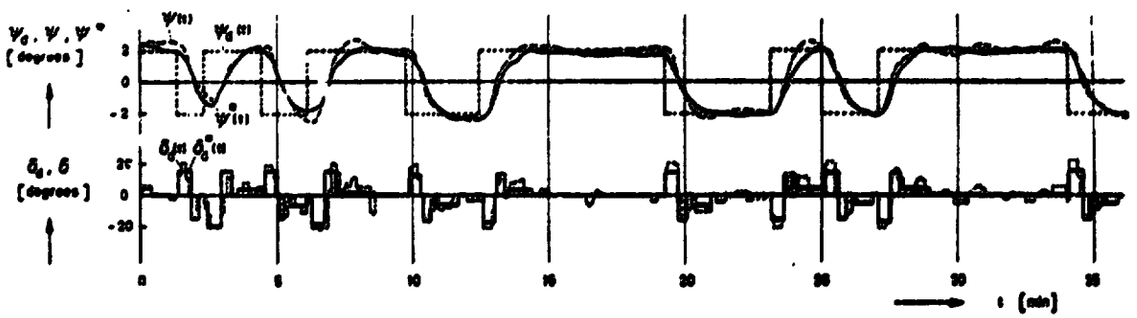

FIGURE 9: Typical time histories of the actual signals $\psi_d(t)$, $\psi(t)$ and $\delta_d(t)$ compared with the model outputs $\psi^*(t)$ and $\delta_d^*(t)$: Subject D; loaded condition; without rate of turn indicator.

behavior and on the parameters belonging to the model.

- A study of the influence of the ship dynamics on the structure of this model and on the model parameters.
- A study of the influence of the disturbances acting on the ship on the structure of this model and on the model parameters.
- The physiological and psychological interpretation of the model parameters.

A large number of experiments with the TNO ship maneuvering simulator have been planned in the middle of 1973. The experiments have been set up in such a way that about ten subjects will have to steer a large number of ships with different dynamics. In characterizing these ships with reference to their dynamics, three groups can be distinguished, i.e.:

- Course stable ships with a more or less linear relation between rudder angle δ and rate of turn r (see Fig. 10a).
- Course stable ships with a nonlinear relation between rudder angle δ and rate of turn r (dead zone) (see Fig.10 b).
- Course unstable ships with a nonlinear relation between rudder angle δ and rate of turn r (see Fig. 10c).

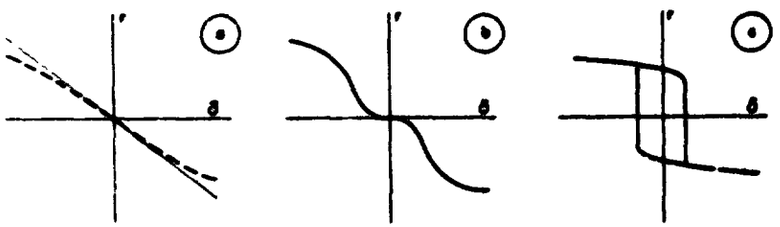

FIGURE 10:

The relation between rudder angle δ and rate of turn r for the three classes of ships.

A second aspect of the maneuvering dynamics of ships is the time constant. Each of the three classes of ships mentioned before will be used in combination with three time constants viz. 10, 50 and 250 sec. In this way the whole area of possible ships is covered. During the tests first-mentioned no disturbances acting on the ship (wind, waves) will be taken into account. In the beginning of 1974 some additional trials will be executed in order to check the influence of disturbances acting on the ship on the structure of the model of the helmsman's behavior and on the parameters belonging to the model.

9 Acknowledgements

The authors gratefully acknowledge the contribution of C.C. Glansdorp of the Shipbuilding Laboratory of the Delft University of Technology. They are also greatly indebted to TNO-IWECO for providing the facilities to do the experiments. The special thanks go to the staff of the TNO-IWECO simulator group for their contributions in the preparation as well as in the execution of the trials. Finally, the authors would like to express their gratitude to the subjects from the School of Navigation at Rotterdam for their wholehearted cooperation.

10 References

1. Brunner, S.M.A.; van Wijk, W.R., The Ship Maneouvring and Research Simulator of the Institute TNO for Mechanical Construction, Delft, Inst. TNO for Mech. Constr., Report Nr. 81[illegible]/[illegible]970), pp. 1-32.
2. Stuup [illegible] Modelling the helmsman: A study to define a mathematical model describing the behaviour of a helmsman steering a ship along a straight course, Delft, Inst. TNO for Mech. Constr., Report Nr. 4701 (1969), pp. 1-64.
3. Veldhuyzen, W.; Lunteren, A. van; Stassen, H.G., Modelling the helmsman of a supertanker: Some preliminary experiments. Proceedings of the 8th Annual Conference on Manual Control, Ann Arbor (1972), AFFDL-TR-72-92, pp. 485-501.
4. Nomoto, K.; Taguchi, T.; Honda, K.; Hirano, S., On the steering qualities of ships, International Shipbuilding Progress, Vol. 4, Nr. 35 (1957), pp. 354-370.

5. Bech, M.; Wagner Smitt, L., Analogue Simulation of Ship Manoeuvres, Lyngby (Denmark), HyA Report Hy 14 (1969), pp. 1-24.
6. Glansdorp, C.C., Simulation of Full Scale Results of Manoeuvring Trials with a 200,000 tons Tanker with a simple Mathematical Model, Delft, Shipbuilding Laboratory of the Delft University of Technology, Report Nr. 301 (1971).
7. Glansdorp, C.C.; Buitenhek, M., Manoeuvring Trials with a 200,000 tons Tanker, Delft, Shipbuilding Laboratory of the Delft University of Technology, Report Nr. 248 (1969), pp. 1-31.

HUMAN OPERATOR PERFORMANCE IN A SIMULATED AAA TASK

by

William H. Levison
Sheldon Baron

To be presented at the Ninth Annual Conference on Manual Control

ABSTRACT

Human operator performance in a simulated anti-aircraft artillery (AAA) task is explored as a function of system and environmental parameters. Operator responses to repeated fly-bys are analyzed to provide trajectories of both mean response and of response variability. Both the mean and the variability of the response are shown to change with changes in experimental variables, and comparison of experimental data and theoretical data obtained from the human operator model indicate that performance changes can be related to changes in the human's ability to obtain and process information. In addition, it appears that the human predicts the future course of the target to a limited extent. Modification to the human operator model to account for this type of behavior are suggested.

N75 19158

FURTHER EXAMINATION OF PILOT INSTRUMENT SCANNING DATA AND DEVELOPMENT OF A NEW LINK VALUE ESTIMATOR*

Lee Gregor Hofmann, Warren F. Clement,
and Richard E. Blodgett†
Systems Technology, Inc., Princeton, New Jersey

ABSTRACT

Examination of pilot instrument scanning data collected during simulated transport instrument landing approaches has confirmed the existence of two deterministic features of otherwise random pilot instrument scanning behavior. These are: transitions in point of eye fixation which originate and terminate on the same instrument are rare; and transitions in point of eye fixation which originate on one secondary instrument and terminate on another secondary instrument are rare. Link value (the probability that a transition in point of eye fixation is from instrument i to instrument j) estimators are developed using statistics and these two experimental facts. This result has special significance when there is but a single primary instrument, i.e., a flight director. This result can be used to simplify the iterative computational procedure of STI's display theory to a non-iterative procedure for the flight director case.

INTRODUCTION

Further examination of the pilot instrument scanning data collected during simulated transport instrument landing approaches (Ref. 1) is motivated by interest in the pilot's crosscnecking (i.e., instrument monitoring) behavior. The data in Ref. 1 offer the opportunity to exc .ine this behavior for a single primary integrated flight instrument case, the flight director/attitude indicator, and for a two primary flight instrument case, the attitude indicator and horizontal situation indicator. The result of this improved understanding of pilot crosscheck/ng behavior is a model which can b· applied in conjunction with other procedures to predict overall performance of the pilot-control-display-vehicle system as a function of certain display (and other) system parameters.

This paper provides a statistical model of the pilot's primary and crosscheck instrument scanning behavior. A companion paper, Ref. 2, shows the technique for applying this model where there is but a single primary instrument, i.e., a flight director. The results are an analytical prediction of pilot-control-display-vehicle system performance and pilot instrument scanning statistics. The computations required are based upon STI's control-display analysis technique (Refs. 3 and 4), but the computations are rendered non-iterative as the result of incorporation of the model of instrument scanning behavior developed herein.

The statistical model of the pilot's primary and crosscheck instrument scanning behavior is based upon several observed experimental facts. These are:

- There is no gross determinism (e.g., a circulatory scanning pattern) in the pilot's scanning behavior (Refs. 5, 6, 7, and more recently, Ref. 1).
- Scanning within the face of a single instrument is rare (Ref. 8).
- Scanning behavior throughout the instrument landing approach appears to be essentially stationary (Ref. 8).
- Transitions in point of eye fixation which originate and terminate on the same instrument are rare.
- Transitions in point of eye fixation which originate on one secondary instrument and terminate on another secondary instrument are rare.

The following section will define the symbols and conventions used throughout the paper. Next, an existing body of eye fixation data is tested for consistency with the latter two assertions above. This is followed by development of the new link value estimators. The new link value estimators are then compared with the old link value estimators and the eye fixation data.

DEFINITIONS OF SYMBOLS AND CONVENTIONS

Definitions of Symbols

P	Set of primary instruments
S	Set of secondary instruments
i, j, k	Indices designating instruments

*This research was sponsored by the U.S. Air Force under Contract No. F33615-71-C-1349.

†Presently graduate student, Columbia University.

PRECEDING PAGE BLANK NOT FILMED

N	Total number of "looks" (i.e., eye fixations) in a data interval
N_i	Number of looks at instrument i in a data interval
N_{ij}	Number of transitions in point of eye fixation which originate from instrument i and terminate upon instrument j
ν_i	Look fraction for ith instrument, determined as $\nu_i = \lim_{N \to \infty} N_i/N$*
q_{ij}	Link value (i.e., transition probability) for transitions <u>from</u> instrument i <u>to</u> instrument j, determined by $q_{ij} = \lim_{N \to \infty} N_{ij}/N$
T_R	Length of data interval in sec
T_i	Length of time in data interval spent looking at instrument i, in sec
$\bar{f}_s$	Average scanning frequency, determined by $\bar{f}_s = \lim_{N \to \infty} N/T_R$, in looks/sec
$\bar{f}_{s_i}$	Average scanning frequency for the ith instrument, determined by $\bar{f}_{s_i} = \lim_{N \to \infty} N_i/T_R$, in looks/sec
η_i	Dwell fraction; the fraction of time which is spent looking at instrument i, determined by $\eta_i = \lim_{N \to \infty} T_i/T_R = \bar{T}_{d_i}\bar{f}_{s_i}$
$i \in B$	Index i ranges over the set B
$A \cup B$	Union of sets A and B
$A \cap B$	Difference of sets A and B where B is a subset of A

Identities

$$\sum_{i \in PUS} q_{ij} \equiv \nu_j$$

$$\sum_{j \in PUS} q_{ij} \equiv \nu_i$$

$$\sum_{i \in PUS} \nu_i \equiv \sum_{i,j \in PUS} q_{ij} \equiv 1$$

$$\sum_{i \in PUS} \bar{f}_{s_i} \equiv \bar{f}_s$$

*When values of ν_i are determined from experimental data, ν_i is calculated by $\nu_i = N_i/N$. A similar comment applies for q_{ij}, $\bar{f}_s$, $\bar{f}_{s_i}$, and η_i.

Distinguishing Between Primary and Secondary Instruments

Secondary instruments include those which must merely be monitored (i.e., crosschecked). Instruments in this category are consistently found to have mean dwell times, $\bar{T}_{d_i}$, of approximately 0.4 sec. Of this mean dwell time, approximately 0.2 sec is recognized as the mean ocular refractory period. Consequently, secondary instruments are easily identified from experimental data by their characteristic mean dwell time. Secondary instruments may be identified in analytical applications of control-display theory (Refs. 3 and 4) by virtue of their <u>not being required</u> for the purpose of control and, in addition, by $\eta_i \doteq 0.4\ \bar{f}_{s_i}$ for those instruments when control-display system performance is optimized.

For the purpose of this paper, any instrument for which $\bar{T}_{d_i} \doteq 0.4$ sec will be treated as a secondary instrument. For example, the indicated airspeed instrument for an aircraft executing a landing approach on the "frontside" of the power required versus trim airspeed performance curve, is a primary instrument by virtue of its being required for the purpose of control for high performance in the absence of strong speed stability for the augmented aircraft. However, since $\bar{T}_{d_{IAS}} \doteq 0.4$ sec in this situation, we shall here regard the indicated airspeed instrument as effectively being a secondary instrument.

Primary instruments will here be regarded as those for which the mean dwell time consistently exceeds approximately 0.6 sec.

TESTING FOR DETERMINISM IN EYE SCANNING DATA

Table 1 lists the one-way link value data, q_{ij}, in matrix form for the experimental configurations described in Table 2. Additional experimental eye scanning data, averaged for each configuration-subject pair, is given in Table 3.

Self-Transitions

Examination of Table 1 reveals that no self-transitions exist for any secondary instrument. That is, $q_{ii} = 0$ for $i \in S$. Or, more specifically, for configurations B, C, D, $q_{ii} = 0$ for $i = 1, 3, 4, 6$; and for configurations E, F, $q_{ii} = 0$ for $i = 1, 3, 4, 5, 6$. Furthermore, the self-transition

TABLE 1. ONE-WAY LINK TRANSITION MATRICES (From Ref. 1)

CONFIGURATION	ONE-WAY LINK MATRICES*													
	PILOT 1							PILOT 2						
		1	2	3	4	5	6		1	2	3	4	5	6
B	1		0.012	0.004	0.008	0.043	0.004	1		0.016				
	2	0.051		0.024		0.278	0.516	2	0.416	0.016	0.008		0.451	
	3	0.004	0.020			0.959	0.008	3		0.008			0.008	
	4		0.012			0.438		4						
	5	0.055	0.506	0.059	0.012	0.008	0.012	5		0.451	0.008			0.008
	6			0.004		0.035		6					0.008	
C	PILOT 1							PILOT 2						
		1	2	3	4	5	6		1	2	3	4	5	6
	1		0.017	0.005	0.005	0.019		1		0.478				
	2	0.019	0.005	0.028	0.008	0.391	0.007	2	0.002	0.016	0.010	0.002	0.472	0.002
	3	0.009	0.019			0.042	0.007	3		0.005			0.004	
	4		0.002			0.005		4		0.002				
	5	0.021	0.366	0.036		0.005	0.014	5		0.476			0.002	0.002
	6	0.002	0.009	0.002		0.005		6		0.002			0.002	
D	PILOT 1							PILOT 2						
		1	2	3	4	5	6		1	2	3	4	5	6
	1		0.054	0.005	0.002	0.027	0.002	1		0.004				0.002
	2	[illegible]	[illegible]	[illegible]	[illegible]	[illegible]	[illegible]	2			0.666		0.260	0.002
	3	[illegible]	0.022			0.016	0.002	3		0.006			0.013	
	4	0.003						4						
	5	0.014	0.390	0.040		0.002	0.005	5	0.004	0.277	0.013		0.004	0.106
	6		0.002	0.002		0.005		6	0.009	0.051			0.123	
E	PILOT 1							PILOT 2						
		1	2	3	4	5	6		1	2	3	4	5	6
	1		0.102	0.008	0.006	0.006		1		0.076				
	2	0.108	0.014	0.119	0.008	0.199	0.005	2	0.076	0.009	0.008	0.012	0.211	0.070
	3	0.006	0.187				0.008	3		0.054			0.006	0.006
	4	0.003	0.011					4		0.006			0.006	
	5	0.006	0.189	0.008			0.011	5		0.228	0.016			0.006
	6		0.036	0.005		0.006		6		0.058	0.002		0.018	
F	PILOT 1							PILOT 2						
		1	2	3	4	5	6		1	2	3	4	5	6
	1		0.165			0.010		1		0.081				
	2	0.165	0.010	0.109		0.175	0.020	2	0.081		0.041		0.391	0.014
	3		0.102			0.007	0.005	3		0.054				
	4							4						
	5	0.007	0.175	0.005			0.010	5		0.391	0.014			
	6		0.050			0.005		6		0.014				

*Format:

From Instrument	To Instrument 1	2	3	4	5	6
1						
2						
3		Transition Matrix				
4						
5						
6						

Note: Transition from 1 to 1 indicates an interruption due to a blink.

TABLE 2. EXPERIMENTAL CONFIGURATIONS (From Ref. 1)

CONFIGURATION	DESCRIPTION	PURPOSE	EXPECTATIONS TO PERCEIVE
A (Pitch attitude tracking task only)	Single axis tracking task with pitch attitude display and forcing function. Other instruments masked. Other axes controlled by autopilot. No flight director.	Tie in with single loop tracking data.	Simulates a portion of the approach task. Control pitch attitude only, and try to keep pitch error equal to zero. There is some turbulence. The lateral autopilot is on.
B (Split axis manual IFR, fixed range)	Three degree of freedom longitudinal task. Forcing functions and tracers on. Lateral axis under autopilot control, but errors visible. No flight director.	Provide longitudinal manual task, and basis for validating multiloop pilot response model.	Simulates a split-axis manual approach under Category II conditions. Control only the longitudinal motions. Autopilot is controlling the lateral motions. There is some turbulence. Try to keep the glide slope needle centered at all times.
C (Manual IFR, fixed range)	All axis approach task with forcing functions and tracers on. The glide slope deviation computer range was fixed at 30,000 ft from threshold. The altimeter and rate of climb were separated manual (varying range). No flight director.	Provide stationary all axis task baseline case for comparison with split axis range varying, and flight director case.	Simulates a Category II manual IFR approach. There is some turbulence. Try to keep the glide slope and localizer needles centered at all times.
D (Manual IFR, varying range)	All axis approach task with forcing functions and tracers on. The range varied throughout the run. Glide slope deviation per unit altitude error increases with decreasing range. No flight director.	Provides nonstationary longitudinal task. Typical of "old fashioned" cross pointer IFR display.	
E (Flight Director, fixed range)	All axis approach task with forcing functions and tracers on. Flight director on, and driven by forcing function. Same as Configuration C plus flight director.	Provides equalized, integrated display and stationary all axis task. Reference flight director case. Typical of modern practice.	Simulates a Category II PD approach. There is some turbulence. Use the director to follow the approach path, keeping the glide slope and localizer needles centered. Pitch commands must be obeyed immediately to avoid a shudder. The glide slope and localizer needles must be monitored.
F (Flight Director, varying range)	All axis approach task with forcing functions and tracers on. Glide slope component of PD forcing function attenuated with range by flight director computer. Same as E, except range varying.	Provides equalized, integrated display but nonstationary forcing function.	
Visual Segment	All this approach task with configurations B or F, except that the pilot system was used to provide an external visual field display at 200 ft above ground. Pilot looked up when told by regular experimenter. Breakout occurred some time after the 100 sec mark.	Exploratory investigation of the feasibility of measuring both visual field and panel EEG. Used with only a few runs at the end of the experimental program.	Same as B or F, except that regular calls out altitude and says "ready to right" when visual acquisition occurs.

ORIGINAL PAGE IS OF POOR QUALITY

TABLE 3

AVERAGE SCANNING STATISTICS*

(From Ref. 1)

CONF	SUBJ	NO RUNS AVG.	INSTRUMENT 1, IAS						INSTRUMENT 2, ATT OR ATT/FD					
			N_1	$\bar{T}_{d_1}$	σ_{T_1}	$\bar{T}_{s_1}$	η_1	ν_1	N_2	$\bar{T}_{d_2}$	σ_{T_2}	$\bar{T}_{s_2}$	η_2	ν_2
B		2	[illegible]	.57	.18	.09	.011	.068	85	.67	.29	.446	.896	.337
B		1	[illegible]	.48	.09	.02	.013	.015	61	.82	.36	.607	.498	.460
		3	25	.69	.28	.05	.034	.042	238	.74	.32	.474	.353	.397
	2	3	1	.63	0	.002	.001	.002	254	.97	.33	.511	.483	.453
		3	45	.69	.35	.085	.059	.066	252	.81	.38	.540	.32	.451
	1	3	3	.98	.40	.015	.013	.013	85	1.00	.45	.423	.425	.357
E	1	4	44	[illegible]	.15	.110	.06	.115	111	1.73	1.72	.488	.739	.458
E	2	3	13	[illegible]	.11	.043	.023	.070	94	3.03	3.41	.276	.836	.454
F		3	13		.15	.177	.099	.163	147	1.50	1.36	.498	.797	.453
	1		[illegible]	[illegible]	.10	[illegible]	.039	.079	37	2.19	1.80	.366	.80	.487

CONF	SUBJ	NO RUNS AVG.	INSTRUMENT 3, FALT						INSTRUMENT 5, HSI/GSD					
			N_3	$\bar{T}_{d_3}$	σ_{T_3}	$\bar{T}_{s_3}$	η_3	ν_3	N_5	$\bar{T}_{d_5}$	σ_{T_5}	$\bar{T}_{s_5}$	η_5	ν_5
B		[illegible]	23	.39	.12	.115	.044	.087	111	1.08	.80	.557	.567	.481
B		[illegible]	2	.17	.04	.02	.011	.015	57	.78	.25	.567	.443	.438
		4	40	.42	.15	.04	.034	.067	255	1.09	.72	.508	.551	.485
	2	4	[illegible]	.41	.15	.01	.004	.009	242	.98	.40	.486	.476	.431
C	1	5	27	.4	.22	.054	.024	.041	265	.84	.43	.527	.444	.405
	3	2	9	.44	.15	.045	.020	.039	96	.93	.51	.479	.443	.403
E		4	[illegible]	.4	.10	.28	.051	.131	76	.57	.80	.190	.109	.195
E	2	4	18	.50	.11	.059	.03	.097	41	.51	.12	.135	.069	.222
F		5	34	.35	.07	.113	.039	.105	59	.46	.13	.197	.090	.181
F	1		4	.34	.05	.04	.013	.053	27	.54	.45	.267	.145	.355

CONF	SUBJ	NO RUNS AVG.	INSTRUMENT 6, IVSI						ALL INSTRUMENTS			
			N_6	$\bar{T}_{d_6}$	σ_{T_6}	$\bar{T}_{s_6}$	η_6	ν_6	N_N	$\sum N_i$	$\bar{T}_s$	
B		4	10	.40	.14	.05	.020	.038	204	200	1.32	
B		[illegible]	1	.55	0	.01	.005	.008	132	101	1.31	
		4	14	.38	.07	.338	.012	.027	600	502	1.19	
		2	2	.47	.23	.004	.002	.004	561	497	1.13	
		5	[illegible]	.40	.18	.010	.004	.008	654	503	1.30	
	3	2	[illegible]	.45	.14	.214	.099	.181	238	200	1.19	
A		4	16	.44	.11	.04	.018	.041	390	400	.976	
E	2	5	14	.49	-	.046	.023	.076	185	305	.607	
		5	3	.35	.12	.033	.012	.031	385	300	1.08	
	3	1	1	.49	0	.01	.005	.013	76	101	.758	

*"There were transitions to and from, but no dwells on instrument 4, the Mach meter." (Ref. 1)

ORIGINAL PAGE IS
OF POOR QUALITY

link values for the primary instruments are very small in comparison to the look fraction for the respective primary instruments. The numerical comparisons are made in terms of q_{ii}/ν_i with respect to unity. The largest value occurs for Instrument No. 2 (flight director/attitude indicator) for configuration 1-2 for which:

$$q_{22}/\nu_{22} = 0.029/0.454 = 0.064 << 1$$

The next largest value of this ratio occurring in the data is less than 0.036.

Since the values of this ratio are very much less than unity, we shall draw the idealized conclusion that, in effect, there are no self-transitions. Mathematically, this is expressed by:

$$q_{ii} \equiv 0 \qquad i \in P \cup S \tag{1}$$

Scans Between Secondary Instruments

To test the hypothesis that the pilot's eye fixation transitions to a primary instrument after fixating a secondary instrument, we will compute the conditional probability, $\mathcal{P}$, that, given a fixation on an instrument in the secondary group, the next fixation will be upon an instrument in the secondary group.

Let N_s be the total number of transitions <u>from</u> all secondary instruments. Let N_{ss} be the total number of transitions from all secondary instruments which terminate on any secondary instrument. Then the probability that pilot's eye fixation transitions to a primary instrument after fixating a secondary instrument is given by $(1 - \mathcal{P})$ where:

$$\mathcal{P} = \lim_{N \to \infty} \frac{N_{ss}}{N_s} = \lim_{N \to \infty} \frac{\sum_{i \in S} \sum_{j \in S} N_{ij}}{\sum_{i \in S} \sum_{j \in P \cup S} N_{ij}} = \frac{\sum_{i \in S} \sum_{j \in S} q_{ij}}{\sum_{i \in S} \nu_i} \tag{2}$$

Computations of $(1 - \mathcal{P})$ on the basis of the experimental data in Tables 1 and 3 are summarized in Table 4. The computations are based upon using $1 - \sum_{i \in P} \nu_i$ in place of its theoretical equivalent, $\sum_{i \in S} \nu_i$. (See Eq. 6.)

TABLE 4

EXPERIMENTAL VALUES OF $(1 - \mathcal{P})$

CONFIGURATION-PILOT	$(1 - \mathcal{P})$
B-1	0.868
B-2	1.000
C-1	0.893
C-2	1 000
D-1	0.884
D-3	0.922
E-1	0.876
E-2	0.900
F-1	0.934
F-3	0.973

The values of $(1 - \mathcal{P})$ are nearly unity for all configurations. On this basis, we shall draw the idealized conclusion that, in effect, there are no transitions which originate on one secondary instrument and terminate on a secondary instrument. Mathematically, this is expressed by:

$$q_{ij} \equiv 0 \qquad i,j \in S \tag{3}$$

NEW LINK VALUE ESTIMATOR

The several observed experimental facts listed in the introductory section can be used as the basis for development of a link value estimator.

We shall use the following assumptions:

- Stationarity: $q_{ij}(t) = \text{const}$, for all t
- No self-transitions: $q_{ii} \equiv 0$, $i \in P \cup S$
- No transitions between secondary instruments: $q_{ij} \equiv 0$; $i,j \in S$
- Scans from a secondary instrument to a primary instrument are made at random according to distributions given by the relative look fractions for the instruments.

- Scans from a primary instrument to a secondary instrument are made at random according to distributions given by the relative look fractions for the instruments.
- Scans within the primary group are a random selection from among the other primary instruments according to distributions given by the relative look fractions for the instruments.

The first four assumptions are used to develop an estimator of the link values for transitions from a secondary instrument to a primary instrument.

$$q_{ij} = \frac{\nu_i}{\sum_{k \in S} \nu_k} \left(\sum_{k \in S} \nu_k \right) \frac{\nu_j}{1 - \sum_{k \in S} \nu_k} = \frac{\nu_i \nu_j}{1 - \sum_{k \in S} \nu_k} \tag{4}$$

$i \in S,\ j \in P$

Consider the intermediate expression for q_{ij}. $\sum_{k \in S} \nu_k$ is the probability that a transition is from the secondary instrument group to the primary instrument group. $\nu_i / \sum_{k \in S} \nu_k$ is the probability that a transition from the secondary instrument group originates from the ith secondary instrument. $\nu_j / (1 - \sum_{k \in S} \nu_k)$ is the probability that a transition to the primary instrument group terminates upon the jth primary instrument.

The next assumption is used in developing an estimator of the link values for transitions from a primary instrument to a secondary instrument.

$$q_{ij} = \frac{\nu_i}{1 - \sum_{k \in S} \nu_k} \left(\sum_{k \in S} \nu_k \right) \frac{\nu_j}{\sum_{k \in S} \nu_k} = \frac{\nu_i \nu_j}{1 - \sum_{k \in S} \nu_k} \tag{5}$$

$i \in P,\ j \in S$

Consider the intermediate expression for q_{ij}. $\sum_{k \in S} \nu_k$ is the probability that a transition is from the primary instrument group to the secondary instrument group. $\nu_i / (1 - \sum_{k \in S} \nu_k)$ is the probability that a transition from a primary group instrument originates from the ith primary

instrument. $\nu_j / \sum_{k \in S} \nu_k$ is the probability that a transition to the secondary instrument group terminates upon the jth secondary instrument.

If the q_{ij} are considered as elements of a matrix, it must also be true that the jth secondary instrument column elements must sum to the look fraction, ν_j. Similarly, the ith secondary instrument row elements must sum to ν_i. This leads directly to the requirement that:

$$\sum_{i \in P} \nu_i = 1 - \sum_{k \in S} \nu_k \tag{6}$$

which is merely a statement of one of the basic identities given above. Furthermore, it must be true that:

$$\sum_{i \in P \cup S} \sum_{j \in P \cup S} q_{ij} \equiv 1 \tag{7}$$

However, since $q_{ij} \equiv 0$ for $i,j \in S$, it is evident that:

$$\sum_{i \in P} \sum_{j \in P} q_{ij} = 1 - 2 \sum_{k \in S} \nu_k \tag{8}$$

It is also evident that $(1 - 2\sum_{k \in S} \nu_k)$ is the probability that a transition originates and terminates on primary instruments.

These results, $q_{ii} \equiv 0$, and the last assumption are used to develop an estimator of the link values for transition from one primary instrument to another primary instrument.

$$q_{ij} = \frac{\nu_i}{1 - \sum_{k \in S} \nu_k} \left(1 - 2 \sum_{k \in S} \nu_k\right) \frac{\nu_j}{1 - \nu_i - \sum_{k \in S} \nu_k} \tag{9}$$

$$i \in P \cap j, \; j \in P$$

$\nu_i/(1 - \sum_{k \in S} \nu_k)$ is the probability that a transition from a primary group instrument originates from the ith primary instrument. $\nu_j/(1 - \nu_i - \sum_{k \in S} \nu_k)$ is the probability that the transition originating from the ith primary

instrument and terminating in the primary group, terminates upon the jth primary instrument.

It can be verified that all row summations for the resultant q_{ij} matrix are equal to their respective row instrument look fractions when the restriction given by Eq. 6 is observed. However, when the number of primary instruments, p, exceeds one, the summation of column elements for the resultant q_{ij} matrix requires the additional restriction:

$$\nu_i = \frac{1 - \sum_{k \in S} \nu_k}{p} \qquad i \in P \tag{10}$$

in order that the summations be equal to their respective column instrument look fractions.

All of the above equations are readily expressed in terms of average scanning frequencies by the simple expedient of replacing $\nu_{(\;)}$ by the quantity $\bar{f}_{s(\;)}/\bar{f}_s$. The link values are most conveniently expressed in terms of average scanning frequencies when the results are to be used as part of a control-display analysis model, e.g., Refs. 3 and 4.

To summarize, the new link value estimators given by Eqs. 1, 3, 4, 5, and 9, subject to the requirements imposed by Eqs. 6 and 10, may be written in terms of the average scanning frequencies and the number of primary instruments as:

$$q_{ii} = 0 \qquad i \in P \cup S \tag{11}$$

$$q_{ij} = \frac{\bar{f}_s - 2 \sum_{k \in S} \bar{f}_{s_k}}{p(p-1)\bar{f}_s} \qquad i \in P \cap j, \; j \in P \tag{12}$$

$$q_{ij} = 0 \qquad i,j \in S \tag{13}$$

$$q_{ij} = \frac{\bar{f}_{s_j}}{p\bar{f}_s} \qquad i \in P, \; j \in S \tag{14}$$

$$q_{ij} = \frac{\bar{f}_{s_i}}{p\bar{f}_s} \qquad i \in S, \; j \in P \tag{15}$$

COMPARISON OF LINK VALUE ESTIMATORS WITH EXPERIMENTAL DATA

The link value estimators given in Ref. 3 are:

$$\tilde{q}_{ij} = \frac{\eta_i \eta_j}{1 - \sum_{k \in P \cup S} \eta_k^2} \qquad (16)$$

$$i,j \in P \cup S;\ i \neq j$$

We shall compare the estimates given by $\tilde{q}_{ij}$ and the estimates given by q_{ij} in the previous section with experimentally measured link values. The experimental data is for configurations which have one and two primary instruments.

The comparisons will be made on the basis of $\tilde{q}_{ij}$ computed using experimental values of the dwell fractions, η_i, for all instrumen[illegible] the q_{ij} used for comparison purposes will be computed using the experim[illegible] values of the [illegible] fractions, ν_i, for the secondary instruments only. [illegible] on values for configuration-pilot combinations C-1 and F-3 are given in [illegible] 5 and 6, respectively. Numerical values for q_{ij} in these tables should [illegible] similar to the corresponding entries for configuration-pilot combinations C-1 and F-3 in Table 1. The look fractions should correspond to entries in Table 3. The sum of the look fractions should be unity.

The numerical values computed using either the new link value estimator or the Ref. 3 link value [illegible]ator, generally have about the same degree of similarity to the experimental values. However, the new link value estimator appears to be somewhat more accurate for the link values involving secondary instruments. The look fractions for the secondary instruments determined by the new link value estimator appear to be superior, but this is because that estimator is merely parroting the experimental values which were used in that computation.

In every case, the sum of the look fractions in Tables 5 and 6 is less than unity. This arises because the look fractions and dwell fractions in Table 3 do not each sum to unity. In other words, there were extraneous looks at places other than the instruments during the experiment. This

TABLE 5

COMPARISON LINK VALUES FOR C-1
(Instruments 2 and 5 are Primary)

a) New Link Value Estimator

	1	2	3	4	5	6	ν_i
1	0	.019	0	0	.022	0	.041
2	.019	0	.031	.002	.363	.012	.437
3	0	.031	0	0	.034	0	.063
4	0	.002	0	0	0	0	.005
5	.022	.363	.034	.003	0	.014	.436
6	0	.012	0	0	.014	0	.026
							.988

b) Ref. 3 Link Value Estimator

	1	2	3	4	5	6	ν_i
1	0	.021	.002	~0	.033	.001	.057
2	.021	0	.021	.001	.342	.007	.392
3	.002	.021	0	~0	.033	.001	.057
4	~0	.001	~0	0	.002	~0	.003
5	.033	.342	.033	.002	0	.012	.422
6	.001	.007	.001	~0	.012	0	.021
							.952

Format:

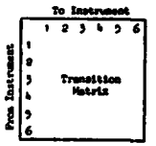

TABLE 6

COMPARISON LINK VALUES FOR F-3
(Instrument 2 is Primary)

a) New Link Value Estimator

	1	2	3	4	5	6	
1	0	.077	0	0	0	[illegible]	[illegible]
2	.077	0	.052	0	.346	.01	.438
3	0	.052	0	0	0	0	.052
4	0	0	0	0	0	0	.000
5	0	.346	0	0	0	0	.346
6	0	.013	0	0	0	0	.013
							.976

b) Ref. 3 Link Value Estimator

	1	2	3	4	5	6	v_i
1	0	.083	.001	0	.015	.001	.100
2	.083	0	.031	0	.343	.012	.469
3	.001	031	0	0	.006	~0	.038
4	0	0	0	0	0	0	.000
5	.015	.343	.006	0	0	.002	.366
6	.001	.012	~0	0	.002	0	.015
							.988

Format:

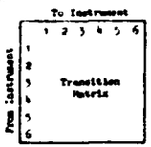

makes entirely consistent comparison of the data and the link value estimators impossible, but the effects of the inconsistencies would appear to be small because the sums of the look fractions and dwell fractions approach unity.

CONCLUSIONS

A new link value estimator has been developed which is based upon two deterministic features found in actual pilot eye scanning data. The new link value estimator is developed in terms of event-related quantities (i.e., looks) whereas the previous link value estimator is in terms of time-related quantities (i.e., dwell times). Since the link values are event-related statistics, it is inappropriate that the previous link value estimators should be in terms of time-related quantities.

The new link value estimator appears to adequately emulate experimental data for cases wherein there are one or two primary instruments. However, the data base used for comparison is admittedly small.

When there is but one primary instrument (designated here as a flight director, FD), then the new link value estimator can be used to show that:

$$v_{FD} = \sum_{k \in S} v_k = 1/2 \qquad (17)$$

If this result is expressed in terms of average scanning frequencies, thus:

$$\bar{f}_{s_{FD}} = \sum_{k \in S} \bar{f}_{s_k} = \bar{f}_s/2 \qquad (18)$$

In other words, the flight director scanning frequency and the sum of secondary instrument scanning frequencies are equal. This feature is shown in Ref. 2 to considerably simplify application of the control-display theory of Refs. 3 and 4 for this case. This is by virtue of eliminating iteration in the computational procedure.

For the more general case wherein there are multiple primary instruments, a modest simplification of the control-display theory computations results.

This simplification is that the average scanning frequencies for all primary instruments are equal. That is:

$$\bar{f}_{s_i} = (\bar{f}_s - \sum_{k \in S} \bar{f}_{s_k})\, p \qquad i \in P \tag{19}$$

The effect, in this case, is to reduce by (p − 1) the number of parameters over which the pilot-control-display-vehicle system must be optimized. Experimental data for the two primary instrument case confirms Eq. 19. However, no experimental data based upon the use of contemporary flight instruments has been found for cases involving three or more primary instruments.

REFERENCES

1. Weir, D. H., and R. H. Klein, The Measurement and Analysis of Pilot Scanning and Control Behavior During Simulated Instrument Approaches, NASA CR-1535, June 1970.

2. Clement W. F., L. G. Hofmann, and D. Graham, A Direct Procedure for Partitioning Scanning Workload in Control Display System Design, presented at the Ninth Annual Conf. on Manual Control, MIT, 23-25 May 1973.

3. McRuer, D. T., H. R. Jex, W. F. Clement, and D. Graham, A Systems Analysis Theory for Displays in Manual Control, JANAIR/Systems Technology, Inc., Tech. Rept. 163-1, June 1968.

4. Clement, W. F., and L. G. Hofmann, A Systems Analysis of Manual Control Techniques and Display Arrangements for Instrument Landing Approaches in Helicopters. Vol. I: Speed and Height Regulation, JANAIR Rept. 690718 (Systems Technology, Inc., Tech. Rept. 183-1).

5. Milton, J. L., R. E. Jones, and P. M. Fitts, Eye Fixations of Aircraft Pilots: Frequency, Duration, and Sequence of Fixations When Flying the USAF Instrument Low Approach Systems (ILAS), USAF Tech. Rept. No. 5839, Oct. 1949.

6. Milton, J. L., B. B. McIntosh, and E. L. Cole, Eye Fixations of Aircraft Pilots: Fixations During Day and Night ILAS Approaches Using an Experimental Instrument Panel Arrangement, USAF Tech. Rept. 6570, Oct. 1951.

7. Watts, A. F. A., and H. C. Wiltshire, Investigation of Eye Movements of an Aircraft Pilot under Blind Approach Conditions, College Note No. 26, The College of Aeronautics, Cranfield, Eng., May 1955.

8. Hofmann, L. G., and K. V. Shah, Re-Examination of Eye Scanning Data for Segments of Flight Director Runs, Systems Technology, Inc., Working Paper [illegible]-2, 30 May 1971.

N75 19159

A DIRECT PROCEDURE FOR PARTITIONING SCANNING WORKLOAD IN CONTROL DISPLAY SYSTEM DESIGN*

W. F. Clement, L. G. Hofmann, and D. Graham

Systems Technology, Inc.
Princeton, New Jersey

ABSTRACT

Recent experimental eye scanning measurements from simulated instrument approaches in a flight-like cockpit representing a contemporary jet transport have made it possible to simplify the procedure for predicting the partition of the pilot's scanning workload required for monitoring and controlling a task with status displays and a flight director. When there is but a single director control display, the new procedure eliminates iteration in the preliminary design computations. The preliminary design computations are based on predictions of closed-loop input-correlated errors in displayed variables with respect to the trimmed flight values. Also included are methods for predicting multiloop error coherence and for correcting the predicted partition of scanning workload when the pilot's scanning remnant contribution is significant.

ORIGINAL PAGE IS OF POOR QUALITY

PRECEDING PAGE BLANK NOT FILMED

*This research was sponsored by the U.S. Air Force Flight Dynamics Laboratory under Contract No. F33615-71-C-1349.

INTRODUCTION

Scanning of an instrument panel permits the displayed information to be sampled foveally. The foveal fixation dwell time interval is variable, but averages about one-half second. Information outside the foveal region may perhaps be observed parafoveally. One can measure the transition of foveal fixation between two instruments and the pause or dwell of the visual axis of fixation on an informative part of the instrument (for example the tip of a pointer) before beginning the next transition. Measurements have shown variability in the time interval which elapses between successive fixations on the same instrument. This time interval is called the scan interval or sampling interval. It will in general exhibit a different ensemble average value for each point of fixation. Besides instrument-to-instrument scans, scanning may occur among the elements of combined displays.

The pilot using a flight director for control wants to spend a certain amount of time monitoring the confidence-inspiring situation information. This is how he gains and maintains confidence in the flight director. We speak of this time that he spends monitoring the situation information as his monitoring workload margin. It can be expressed either as a fraction of time, the dwell fraction, or as the fraction of the number of looks, the look fraction. Sufficient monitoring margin is essential to the pilot. This need for monitoring margin can lead to a possible conflict with the addition of a third director command for direct lift control or thrust control which requires a separate foveal fixation. Unless the flight director presentation can be contrived to convey three director commands in one fixation through foveal and parafoveal channels of awareness, the switching of attention between the two-command flight director and a third director command may produce considerably more remnant in all three director commands.

In order that we may more clearly appreciate these effects, one purpose in this investigation has been to improve the models for predicting the partition of the pilot's time and the number of fixations between the monitoring

margin and the fraction of time required for control using the director commands. We shall begin here with a review of key experimental results from Ref. 1, supported by a companion paper, Ref. 2, in order to introduce a new, simpler, direct method for partitioning scanning workload with a flight director. We will then show how the properties of the pilot's scanning remnant and properties of the partition of scanning workload may conspire to compromise the pilot's confidence in his situation, to compromise his performance, or both, so that his subjective impression of the overall task workload will be high. The presentation has been subdivided for convenience into the following topics, the last of which is a summary.

- Review of Eye Scanning Data
- Summary of the Revised Model for Partitioning Scanning Workload
- A Simplified Partitioning Procedure for a Single Director Control Display
- A Cause of Low Error Coherence
- Estimation of Error Coherence and Variance
- Modification of the Input-Correlated Predictions of Average Threshold Exceedence Frequency
- Summary of the Simplified Direct Procedure for Partitioning Scanning Workload with a Flight Director

REVIEW OF EYE SCANNING DATA

A Model for Display Monitoring

In order to maintain confidence in a flight director for closed-loop tracking, the pilot must also attend to the open-loop monitoring of situation or status displays to perceive exceedence of tolerances or specified values related to the task. Most of the pilot's status displays present the flight motion variables which are constituents of the flight director commands. Other status displays are common to engine or radar instrument monitoring, where effects of manual control are not displayed.

We shall include time for monitoring the status displays appropriate to the flight director loops and the relatively open-loop displays such as engine, fuel management, navigation, and communication displays by estimating an average dwell interval of 0.4 sec (Ref. 3) and a scanning frequency equal to an appropriate threshold exceedence frequency for the display. The average threshold exceedence frequency, $\bar{f}_{|x_1|}$, (Ref. 4) for Gaussian random signals is

$$\bar{f}_{|x_1|} = \frac{2}{\pi} e^{-x_1^2/2\sigma_x^2} \left(\frac{\sigma_{\dot{x}}}{\sigma_x}\right)$$

where x_1 is the threshold of exceedence, σ_x^2 is the variance of the displayed signal, and $\sigma_{\dot{x}}^2$, the variance of the rate of change of the displayed signal. The resulting fractional scanning workload for monitoring (that is, the product of 0.4 sec with the sum of the scanning frequencies for the monitored displays) is then compared with that for the tracking control tasks to determine whether or not both tracking control <u>and</u> monitoring tasks can be performed within the available time constraint. This comparison and determination is called the "partition" of scanning workload for monitoring and control.

Each average monitored display scanning frequency, $\bar{f}_{S_i}$, ics, is assumed to be equal to the expected frequency, $\bar{f}_{|x_1|}$, with which a certain level, $|x_1|$, of the displayed variable, x, is exceeded

$$\bar{f}_{S_i} = \frac{2}{\pi} e^{-\frac{K^2}{2}} \left(\frac{\sigma_{\dot{x}}}{\sigma_x}\right)_i \tag{1}$$

where K is the ratio of an exceedence threshold level, $|x_1|$, to σ_x

σ_x is the standard deviation of the displayed signal

$\sigma_{\dot{x}}$ is the standard deviation of the time rate of change of the displayed signal

i is an index which denotes the particular display

S denotes the set of monitored displays

We have expressed the level of exceedence in terms of $K\sigma_x$ in Eq. 1. We have determined that K ranges from 1.4 to 3.0 for the data in Ref. 1 with a value of 2.0 being representative overall. Presumably the lower the value of K the lower the pilot's threshold of indifference to the displayed situation which he is monitoring, and the greater his confidence in the task performance.

Results of Dwell Fraction Analysis

Using the subject-averaged scanning statistics of Ref. 1, a correlation of scanning workload (dwell fraction) and flight director system bandwidth (i.e., crossover frequency) has been made. This correlation in Ref. 1 shows that the higher the crossover frequency the higher the dwell fraction and the lower the corresponding scanning rate on the flight director. The conclusion is that the most efficient scanning policy is to fixate as infrequently as possible. This minimizes the 0.2 sec latency effect associated with each fixation required for monitoring or control. In other words, the instrument monitoring requirements place a lower bound on the flight director scanning rate. Since the sum of the flight director and monitoring foveal dwell fractions cannot exceed unity (less an allowance, M_s, for saccades and blinks), we can write Eq. 2 for the partition of dwell fraction between director displays and monitored displays.

$$\sum_{j \in P} \tau_j = 1 - M_s - 0.4 \sum_{i \in S} \bar{f}_{s_i} \qquad (2)$$

In Eq. 2, P is the set of (primary) director command displays and S is the set of (secondary) monitored displays. Other symbols are defined in Table I.

Results of Look Fraction Analysis

Reference 2 has further examined the eye-movement data summarized in Ref. 1. This was for the purpose of discerning the effects of the number of primary displays and the degree of display integration upon scanning behavior. Scans among secondary (monitored) instruments were found to be exceedingly rare, and scans which begin and end at the same instrument were also found to be rare. Examination of the eye movement data for evidence of

TABLE I

Definitions of Symbols

adj [ ]	the adjoint operator, i.e., the transposed matrix of cofactors of [ ]
e	Naperian base, 2.71828...
$\bar{f}_s$	average scanning frequency $(1/\bar{T}_s)$ (Hz)
$\bar{f}_{\lvert x_i \rvert}$	average threshold exceedence frequency for the absolute threshold x_i (Hz)
$i \in P$	index i ranges over the set P
i, j, k	indices designating instruments or points of fixation
n_{e_j}	the pilot's remnant injected at the jth axis of the flight director
P	number of primary control displays, instruments, or points of fixation
q_{ij}	link value or probability of fixation transition from i to j
x_i	threshold of exceedence for a displayed variable x
ADI	attitude director indicator
F	foveal
FD	flight director
K	$\lvert x_i \rvert / \sigma_x$
M_s	dwell fraction margin for saccades and blinks
N	total number of fixations or "looks" in a time interval
P	set of primary (director control) displays or instruments
S	set of secondary (monitored) displays or instruments
$\bar{T}_d$	average foveal dwell interval $(\eta \bar{T}_s)$ (sec)
$\bar{T}_{d_e}$	average effective dwell interval $(\eta_e \bar{T}_s)$ (sec)
T_R	an arbitrary time interval (sec)
$\bar{T}_s$	average scanning interval $(1/\bar{f}_s)$ (sec)

TABLE I (cont'd)

Definitions of Symbols

δ_{ij}	Kronecker delta
ϵ	error with respect to the trimmed value of a displayed variable
ϵ_i	input-correlated error
η	average foveal dwell fraction ($\bar{T}_d / \bar{T}_s = \bar{f}_s \bar{T}_d$)
η_e	average effective dwell fraction ($\bar{T}_{d_e} / \bar{T}_s = \bar{f}_s \bar{T}_{d_e}$)
θ_K	independent external input or forcing function acting on the director control system
ν_i	average look fraction, $\lim_{N \to \infty} N_i / N = (\bar{f}_{s_i} / \bar{f}_s)$
π	3.14159...
$\sigma^2_{o_x}$	input-correlated variance of x
$\sigma^2_{o_{\dot{x}}}$	input-correlated variance of dx/dt
$\sigma^2_{1_x}$	uncorrelated variance of x
$\sigma^2_{1_{\dot{x}}}$	uncorrelated variance of dx/dt
σ^2_x	variance of x
$\sigma^2_{\dot{x}}$	variance of dx/dt
$\lvert\Delta_s\rvert$	coherence determinant
Σ	summation operator
$\Phi_{nn_s}(\omega)$	power spectral density of sampling (or scanning) remnant (units/rad/sec)
Ω	parafoveal-to-foveal gain ratio

scans within an instrument face also has shown that such scans are rare. This being the case, the scanning workload imposed by the need for monitoring* will be reduced by the degree of integration of the information for monitoring within the primary displays. This is because it is an observed fact that when integrated in this manner, information for monitoring does not contribute to the scanning workload.

Viewed in another way, the monitoring workload will increase as the frequency of scans to secondary instruments increases. This is because the average dwell time, $\bar{T}_{d_i}$, for each separate monitoring fixation is 0.4 sec with little variability. The sum of the average scanning frequencies for the separated secondary instruments is the average frequency of scans for monitoring, $\sum_{i \in S} \bar{f}_{s_i}$, where the summation is over the set, S, of secondary instruments.

The average fraction of scans employed for monitoring is called the monitoring look fraction, $\sum_{i \in S} \nu_i = \sum_{i \in S} \bar{f}_{s_i} / \bar{f}_s$ where $\bar{f}_s$ is the overall average scanning frequency defined for the total number, N, of primary and secondary looks (i.e., fixations) in an interval of time T_R by $\bar{f}_s = \lim_{N \to \infty} (N / T_R)$. Since the sum of the primary and secondary look fractions cannot exceed unity, we can write Eq. 3 for the partition of look fraction between primary displays and monitored displays.

$$\sum_{j \in P} \nu_j = 1 - \left(\sum_{i \in S} \bar{f}_{s_i} / \bar{f}_s \right) \tag{3}$$

where ν_j is the look fraction for each primary display.

*It should be noted that pilots refer to the instrument monitoring function as "cross-checking."

SUMMARY OF THE REVISED MODEL FOR PARTITIONING SCANNING WORKLOAD

The results of the dwell and look fraction analyses can be used in combination to simplify considerably the display theory computations for the single command display case. The simplification is such that iterative computations which are ordinarily required are replaced by direct computation of the average scanning frequencies for the flight director and secondary instruments. As a result, the scanning workload margin required for monitoring given previously $0.4 \sum_{i \in S} \bar{f}_{s_i}$, is easily evaluated.

Equations 1, 2, and 3, introduced previously, provide the basis for the partition of scanning workload for monitoring and control. The results of the partition provide estimates of the average scanning frequencies and dwell fractions for control as well as monitoring. The dwell fractions also represent the temporal probabilities of fixation, whereas the look fractions represent the ensemble probabilities of fixation. From these predictions, one can estimate the dwell intervals, look intervals, link values, and other scanning parameters desired. A revised model for the prediction of link values in a flight director is given in a companion paper, Ref. 2.

The detailed development of a simplified approximate method for partitioning the scanning workload required for monitoring and control in a task with a single primary director display is given in the next topic. The simplified approximate method will be increasingly more accurate as the pilot's tracking error coherence approaches unity. Following the presentation of the simplified method we shall show how to test for multiloop error coherence, and how to correct the partition of scanning workload in case of low error coherence caused by the pilot's injection of scanning remnant.

A SIMPLIFIED PARTITIONING PROCEDURE FOR A SINGLE DIRECTOR CONTROL DISPLAY

By way of convenience in what follows, we shall define the director control display as "primary" and the situation displays for monitoring as "secondary."

A special case of the revised pilot model for scanning described in Ref. 2 applies when a single director control display is used. In this case, the average scanning frequency for the flight director, $\bar{f}_{s_{FD}}$, is equal to the sum of the average scanning frequencies for the secondary displays. That is

$$\bar{f}_{s_{FD}} = \sum_{i \in S} \bar{f}_{s_i} \tag{4}$$

where S is the set of secondary displays and the $\bar{f}_{s_i}$ are given by Eq. 1. By virtue of the fundamental requirement that all of the pilot's fixations be accounted for, Eq. 4 is also equal to $\bar{f}_s / 2$, where $\bar{f}_s$ is the average scanning frequency.

The event of this simple relationship suggests the following basis for the prediction of the scanning workload margin required for monitoring the situation. Equation 4 may be interpreted as giving the frequency with which fixation of the primary display is <u>interrupted</u> in terms of the individual situation display monitoring scanning frequencies. If we add to this the assumption that the pilot scans for the purpose of monitoring only as frequently as is required to maintain a personal confidence level in the <u>situation</u>, we have sufficient conditions for the existence of an optimum monitoring policy.

A partition of scanning workload (or dwell fraction) between the flight director and the set of secondary displays leads to Eq. 5. Equation 5 is for the foveal dwell fraction on the flight director under the assumption that the dwells for saccades and blinks are negligible ($M_s = 0$). It is a special case of Eq. 2.

$$\eta_{FD} = 1 - 0.4 \sum_{i \in S} \bar{f}_{s_i} \tag{5}$$

Equation 5 indeed shows that monitoring is accomplished at the expense of the flight director dwell fraction. Thus, the dwell fraction on the flight director becomes, by virtue of Eqs. 4 and 5:

$$\eta_{FD} = 1 - 0.4\,\bar{f}_{s_{FD}} \tag{6}$$

The effective dwell fraction on the flight director is defined (Ref. 6) by

$$\eta_{e_{FD}} \triangleq \eta_{FD} + \Omega_{FD}(1 - \eta_{FD}) \tag{7}$$

where Ω_{FD} is the parafoveal-to-foveal gain ratio. The effective dwell fraction on the flight director will be greater than or equal to the actual dwell fraction as Ω_{FD} is varied from 1.0 to 0. An alternate expression for Eq. 7 is obtained upon substitution of Eq. 6.

$$\eta_{e_{FD}} = 1 - 0.4\,\bar{f}_{s_{FD}}(1 - \Omega_{FD}) \tag{8}$$

The complement of the effective dwell fraction is the effective interrupt fraction. This is obtained by rearranging Eq. 8.

$$1 - \eta_{e_{FD}} = 0.4\,\bar{f}_{s_{FD}}(1 - \Omega_{FD}) \tag{8a}$$

The flight director average scanning interval is the reciprocal of the average scanning frequency, $\bar{T}_{s_{FD}} = 1/\bar{f}_{s_{FD}}$.

The average foveal dwell interval on the flight director can be obtained by multiplying Eq. 6 through by $\bar{T}_{s_{FD}}$ and using the definition (Ref. 3) of dwell fraction, $\eta_{FD} \triangleq \bar{T}_{d_{FD}}/\bar{T}_{s_{FD}}$.

$$\bar{T}_{d_{FD}} = \bar{T}_{s_{FD}} - 0.4 \tag{9}$$

The effective dwell interval on the flight director is greater than the foveal dwell interval if parafoveal perception is not inhibited. The effective dwell interval can be obtained by multiplying Eq. 8 by $\bar{T}_{s_{FD}}$ since $\bar{T}_{d_{e_{FD}}} = \eta_{e_{FD}}\,\bar{T}_{s_{FD}}$.

$$\bar{T}_{d_{e_{FD}}} = \bar{T}_{s_{FD}} - 0.4(1 - \Omega_{FD}) \tag{10}$$

Equation 9 can be substituted into Eq. 10 for an alternate expression for the effective dwell fraction on the flight director

$$\bar{T}_{d_{e_{FD}}} = \bar{T}_{d_{FD}} + 0.4\,\Omega_{FD} \tag{10a}$$

Since $\bar{T}_{d_{FD}} < \bar{T}_{s_{FD}}$ and $0 \le \Omega_{FD} \le 1$, Eqs. 10 and 10a show that upper and lower bounds upon $\bar{T}_{d_{e_{FD}}}$ are respectively $\bar{T}_{s_{FD}}$ and $\bar{T}_{d_{FD}}$. Furthermore, the difference between the two bounds is only the 0.4 sec average monitoring dwell interval. This latter fact is evident from Eq. 9.

$\bar{T}_{d_{e_{FD}}}$ and $\eta_{e_{FD}}$ are theoretical constructs and are not directly observable. However, $\bar{T}_{s_{FD}}$ and $\bar{T}_{d_{FD}}$ are observable. Experimental values for $\bar{T}_{d_{FD}}$ reported in Ref. 1 are approximately 2.0 sec. $\bar{T}_{d_{FD}}$ and $\bar{T}_{s_{FD}}$ (which are the lower and upper bounds, respectively, on $\bar{T}_{d_{e_{FD}}}$) are both weak functions of the parafoveal-to-foveal gain ratio, Ω_{FD}, for constant effective dwell interval because the average monitoring dwell interval, 0.4 sec, is much less than $\bar{T}_{d_{FD}} \approx 2.0$ sec. Consequently, Ω_{FD} can be treated as an arbitrary constant in this simplified method. This is a useful property of Eq. 10 which makes it possible to establish reasonable bounds on $\bar{T}_{s_{FD}}$. (Recall that $\bar{T}_{s_{FD}}$ is equal to the reciprocal of $\bar{f}_{s_{FD}}$ determined in Eq. 4 as a function of the threshold-to-standard deviation ratio, K, in Eq. 1 and the error rate-to-displacement variance ratio $(\sigma_{\dot{x}}/\sigma_x)_i$, ie8.) $\bar{T}_{s_{FD}}$ will, in effect, be bounded from above by the largest value of K in Eq. 1 which is acceptable to the pilot, because increasing values of K represent decreasing levels of the pilot's confidence in his situation. $\bar{T}_{s_{FD}}$ will be bounded from

below by $\overline{T}_{d_{eFD}}$. In effect, $\overline{T}_{d_{eFD}}$ represents a lower bound on error rate and displacement coherencies.

The precision of this simple direct procedure for partitioning scanning workload on a single primary director control display depends on the error rate and displacement coherencies. When these coherencies are fairly high, as they usually are with a properly designed flight director, the $(\sigma_{\dot{x}}/\sigma_x)_i$, i∈S, in Eq. 1 are virtually equal to their input-correlated values. Thus one may start the partitioning procedure with only input-correlated error rate and displacement standard deviations determined independently by system performance calculations and without regard for the pilot's scanning remnant.

We shall next turn our attention to the effects of the pilot's scanning remnant.

A CAUSE OF LOW ERROR COHERENCE

The scanning activity required for monitoring causes the pilot to inject noise into the flight director control loops. This noise is called scanning remnant. It is the chief source of noise, because, in flight director control tasks, there is no need for pilot lead equalization in following the director commands, and hence remnant attendant to pilot lead equalization is not present.

The scanning remnant power spectral density for the "switched gain" model (Refs. 5-7) appropriate for application to the flight director is defined in Ref. 8. If we use Eq. 8a for the effective interrupt fraction, $(1 - \eta_{eFD})$, and assume a sampling variability ratio $(\sigma_{T_s}/\overline{T}_s)$ of 0.5, the scanning remnant power spectral density for the flight director is

$$\Phi_{nn_s}(\omega) = \frac{0.2(1 - \Omega_{FD})\sigma^2_{FD}}{\pi\left[1 + \left(\frac{\omega T_{d_{eFD}}}{2}\right)^2\right]} \frac{(\text{units})^2}{(\text{rad/sec})} \qquad (11)^*$$

* $\Phi_{nn_s}(\omega)$ is defined such that $\sigma^2_{n_s} = \int_0^\infty \Phi_{nn_s}(\omega)\,d\omega$

where $\overline{T}_{d_{eFD}}$ is given by Eq. 10 in terms of $\overline{T}_{sFD}$ and Ω_{FD}. It is clear from Eqs. 9 and 10 that $\overline{T}_{d_{FD}} \le \overline{T}_{d_{eFD}} \le \overline{T}_{sFD}$. In applying Eq. 11 to predicting the effects of scanning on system tracking error, we find it convenient to use $\overline{T}_{d_{FD}}$, the lower bound on $\overline{T}_{d_{eFD}}$, because this places an upper bound on the half-power frequency of the scanning noise and helps to make the error coherence predictions conservative. Experimental values for $\overline{T}_{d_{FD}}$ reported in Ref. 1 are approximately 2.0 sec. This places the half-power frequency, $2/\overline{T}_{d_{eFD}}$, at or below 1.0 rad/sec. In order to complete the connection between the scanning remnant power spectral density (Eq. 11) and the average monitoring scanning frequency (Eq. 1), it is necessary to digress to compute the total displayed error variance vector. In this case, "error" refers to the deviations of the displayed variables with respect to their trimmed values.

ESTIMATION OF ERROR COHERENCE AND VARIANCE

The total error variance vector, $\{\overline{\epsilon^2}\}$, is related to the coherent error variance vector, $\{\overline{\epsilon_i^2}\}$, by the equation

$$[\Delta_s]\{\overline{\epsilon^2}\} = \{\overline{\epsilon_i^2}\} \qquad (12)$$

where $[\Delta_s]$ is a square coherence matrix containing elements

$$\Delta_{s_{\epsilon_i\epsilon_j}} = \delta_{ij} - \frac{0.2(1 - \Omega_{FD})}{\pi} \int_0^\infty \left|\frac{\epsilon_i(j\omega)}{n_{\epsilon_j}(j\omega)}\right|^2 \frac{d\omega}{\left[1 + \left(\frac{\omega T_{d_{e_j}}}{2}\right)^2\right]} \qquad (13)$$

with i components in the variance vector and j displayed axes in the flight director; and $\delta_{ij} = \{^{1;\ i = j}_{0;\ i \ne j}\}$ is the Kronecker delta, $\epsilon_i(j\omega)$ is the Fourier transform of the ith displayed error in response to $n_{\epsilon_j}(j\omega)$, the Fourier transform of the pilot's remnant injected at the jth axis of the flight director. The determinant of $[\Delta_s]$ is called the characteristic determinant of stability in the mean-square sense, or the coherence determinant. Each component of the coherent error variance vector has the form

$$\overline{\epsilon_{t_i}^2} = \sum_{\kappa=1}^{N} \int_0^\infty \left| \frac{\epsilon_i(j\omega)}{t(j\omega)} \right|_\kappa^2 \Phi_{t_\kappa}(\omega)\, d\omega \tag{14}$$

where, for example, $t_\kappa = d_c, u_g, w_g$, the independent longitudinal inputs and disturbances: glide slope beam noise, and longitudinal and normal gust velocities; and N = 3. Thus, the vector $\{\overline{\epsilon^2}\}$ will, in general, be a column matrix of linear combinations of input-correlated mean-squared errors. The formal result for the total variance vector is:

$$\{\overline{\epsilon^2}\} = \frac{\text{adj}\,[\Delta_s]}{|\Delta_s|} \{\overline{\epsilon_t^2}\} \tag{15}$$

The coherence determinant, $|\Delta_s|$, governs multiloop stability in the mean-square sense; therefore, it must be greater than zero. A value for the determinant which is much less than unity means that incoherent error power due to scanning remnant will be much greater than the coherent error power due to inputs and disturbances. As the coherence determinant approaches unity (its upper bound), the error power will become increasingly coherent. One of the purposes of an integrated flight director is, of course, to make the coherence determinant approach unity.

The coherence determinant depends on the display scanning statistics as well as the closed-loop frequency responses to scanning remnant. Therefore, it is desirable to obtain the coherence determinant in analytic form first, so that the average scanning statistics can be estimated in conjunction with their influence on the partition of scanning workload and mean-squared errors.

Some savings in labor will result because preliminary coherence tests on $[\Delta_s]$ (to ascertain whether or not it is greater than 0.4, for example) need be based on only the principal diagonal elements of $[\Delta_s]$. For a flight director, $[\Delta_s]$ is an upper triangular matrix; thus, the value of its determinant is equal to the product of its principal diagonal elements. The non-zero off-diagonal elements are, of course, required to verify the partition of scanning workload and to verify that approach performance requirements are satisfied.

MODIFICATION OF THE INPUT-CORRELATED PREDICTIONS OF AVERAGE THRESHOLD EXCEEDENCE FREQUENCY

The standard deviation, σ_{x_i}, of the signal, x, on display i will consist of one component, $\sigma_{o_{x_i}}$, which arises from the physical inputs and disturbances forcing the pilot-vehicle system, and a second component, $\sigma_{1_{x_i}}$, which arises from the pilot's scanning remnant. Then $\sigma_{x_i}^2 = \sigma_{o_{x_i}}^2 + \sigma_{1_{x_i}}^2$. The $\sigma_{1_{x_i}}$ component will scale linearly with the level of the injected remnant.

Exceedences of a certain absolute signal level, $|x_i| = \sqrt{K^2(\sigma_{o_{x_i}}^2 + \sigma_{1_{x_i}}^2)}$, will occur at an average frequency:

$$\overline{f}_{|x_i|} = \frac{1}{\pi} \frac{\sigma_{o_{x_i}} \sqrt{1 + (\sigma_{1_{x_i}} / \sigma_{o_{x_i}})^2}}{\sigma_{o_{x_i}} \sqrt{1 + (\sigma_{1_{x_i}} / \sigma_{o_{x_i}})^2}}\, e^{-(K^2/2)} \tag{16}$$

If we assume that the absolute level, $|x_i| = \sqrt{K^2(\sigma_{o_{x_i}}^2 + \sigma_{1_{x_i}}^2)}$, defines the pilot's threshold of indifference to the status variable x_i, i.e., the minimum change in the signal which is significant to the pilot, then we are justified in equating $\overline{f}_{s_i} = \overline{f}_{|x_i|}$ in Eq. 16, as before in the case of Eq. 1. Here, $\overline{f}_{s_i}$ is the average scanning frequency for the ith secondary display. The experimental results in Ref. 1 indicate that $1.4 \le K \le 3.0$.

Presumably, the pilot's threshold of indifference will bear some consistent relationship (e.g., $|x_i| = 2\sigma$) to criteria for the acceptability of task errors and attitude, heading, and sideslip excursions in each portion of the flight profile. If all other contributions to the average threshold exceedence frequency are invariant, the pilot's average monitoring scanning frequency must increase to provide a lower value of the threshold-to-rms ratio, K. Therefore, his monitoring scanning workload, that is, monitoring dwell

Eq. (4) $\bar{f}_{s_{FD}} = \sum_{K \in S} \bar{f}_{s_K}$ where S is the set of status displays

Eq. (10) $\bar{T}_{s_{FD}} - \bar{T}_{d_K}(1 - \Omega_{FD}) = \bar{T}_{de_{FD}}$ where $\bar{T}_{d_K} = 0.4$ sec $K \in S$

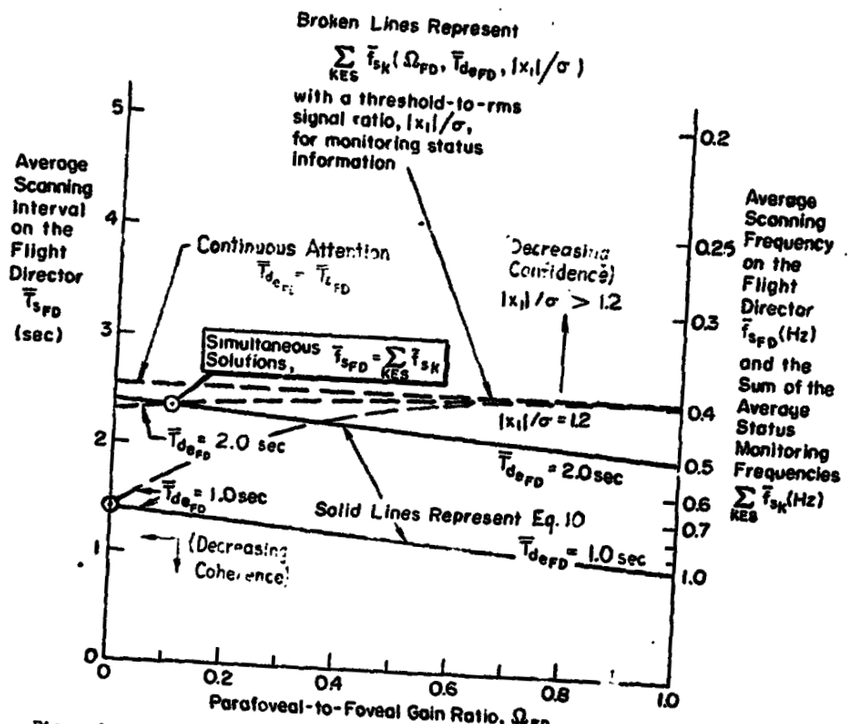

Figure 1. A Graph Illustrating the Simultaneous Solution of Two Equations for the Partition of Scanning Workload on an Integrated All-Axis Flight Director

P-134

ORIGINAL PAGE IS
OF POOR QUALITY

fraction must actually increase at the expense of the flight director dwell fraction to provide a lower value of K. If the flight director dwell fraction must be so compromised that the pilot's scanning remnant causes low error coherence, task performance may be compromised, and the pilot's subjective impression of overall task workload will be high.

Conversely, if the flight director demands too much of the scanning workload, that is, too large a dwell fraction for control, because its sensitivity is too low or because the external disturbances are broadband, the pilot may have to compromise his monitoring dwell fraction to the point where K is so large that he has little confidence in the acceptability of the situation and in the satisfaction of task performance criteria. Again his subjective impression of task workload will be high. Evidently, the pilot then attempts to partition his scanning workload so that $1.4 \le K \le 3.0$ for reasonable confidence in the situation with acceptable error coherence, $|\Delta_s| \ge 0.4$.

Assumed values for K and $\bar{T}_{de_{FD}}$ are necessary to determine each f_{s_i} as a function of Ω_{FD} using Eq. 16 and the equality $\bar{f}_{s_i} = \bar{f}|_{x_i}|$, $i \epsilon S$. The required $(\sigma^2_{o_{x_i}} + \sigma^2_{i_{x_i}})$ are the components of the total variance vector, $\{\epsilon^2\}$, given by Eq. 15, in which only the $\sigma^2_{i_{x_i}}$ depend on Ω_{FD} and $\bar{T}_{de_{FD}}$. The required $(\sigma^2_{o_{\dot{x}_i}} + \sigma^2_{i_{\dot{x}_i}})$ are the components of the total rate variance vector, which can be derived in a manner completely analogous to that described for the total variance vector by defining a rate coherence determinant. Again only the $\sigma^2_{i_{\dot{x}_i}}$ depend on Ω_{FD} and $\bar{T}_{de_{FD}}$. The partition of scanning workload is completed after the set of secondary $\bar{f}_{s_i}$ is summed, and Eq. 4 is satisfied. A direct graphical procedure for satisfying Eq. 4 is recommended in Ref. 6 (reproduced here in Fig. 1) using Ω_{FD} as the abscissa, $\bar{T}_{s_{FD}}$ as the ordinate, and $\bar{T}_{de_{FD}}$ as a third variable parameter. Equation 10 provides a conveniently explicit form for verifying the simultaneous satisfaction of Eq. 4 in terms of $\bar{T}_{s_{FD}}$ (or $1/\bar{f}_{s_{FD}}$), Ω_{FD} and $\bar{T}_{e_{FD}}$.

When the error coherence is fairly high, as usually is with a properly designed flight director, the ratios $(\sigma_{i_{\dot{x}_i}}/\sigma_{o_{\dot{x}_i}})^2$ and $(\sigma_{i_{x_i}}/\sigma_{o_{x_i}})^2$ in Eq. 16 are much less than unity. Hence, the secondary $\bar{f}_{s_i}$ depend primarily on the coherent error rate and displacement variances, and only weakly on the parafoveal-to-foveal gain ratio, Ω_{FD}. (Recall that $\bar{T}_{de_{FD}}$ is already closely bounded, i.e., $\bar{T}_{d_{FD}} \le \bar{T}_{de_{FD}} \le \bar{T}_{s_{FD}}$, where both bounds, $\bar{T}_{d_{FD}}$ and $\bar{T}_{s_{FD}}$, are also weak functions of Ω_{FD} in Eq. 10 as discussed previously.) As a consequence, the partition of scanning workload by simultaneous solution of Eqs. 4, 10, and 16 with the secondary $\bar{f}_{s_i} = \bar{f}|_{x_i}|$ can usually be simplified and approximated by ignoring the explicit dependence of the solution on Ω_{FD}, as long as the error and error rate coherencies are sufficiently high. In this case Ω_{FD} becomes an arbitrary constant. When this simplification is possible, Eq. 16 can be replaced by the form of Eq. 1 in which $(\sigma_{\dot{x}}/\sigma_x)_i \cong (\sigma_{o_{\dot{x}}}/\sigma_{o_x})_i$, the ratio of input-correlated standard deviations, and $\bar{T}_{s_{FD}}$ and $\bar{T}_{de_{FD}}$ will covary only with K as described previously in the simple direct procedure.

SUMMARY OF THE SIMPLIFIED DIRECT PROCEDURE FOR PARTITIONING SCANNING WORKLOAD ON A FLIGHT DIRECTOR

The procedure for partitioning scanning workload using Eqs. 1, 4, and 10 will be accurate provided the error displacement and error rate coherencies are reasonably high. Although the value of K, the ratio of the exceedence threshold, $|x_i|$, to σ_{x_i} ($i \epsilon S$), may be slightly different for each secondary displayed variable x_i, the restricted bounds on K inferred from Ref. 1 suggest that a common value of K may be adequate for use in this simplified partitioning procedure.

When Eq. 1 is used for each $\bar{f}_{s_i}$ ($i \epsilon S$) in the summation in Eq. 4, a common value of K makes it possible to write Eq. 4 as

$$\bar{f}_{s_{FD}} = \frac{e^{-\frac{K^2}{2}}}{\pi} \sum_{i \epsilon S} \left(\frac{\sigma_{\dot{x}_o}}{\sigma_{x_o}} \right)_i \tag{17}$$

Since $\bar{T}_{s_{FD}} = 1/\bar{f}_{s_{FD}}$, Eq. 17 can be substituted in Eq. 10 to express

$$\bar{T}_{d_{e_{FD}}} \approx \frac{\frac{K^2}{2}}{\sum_{i \in S} \left(\frac{\sigma_{\dot{x}_o}}{\sigma_{x_o}} \right)_i} - 0.4(1 - \Omega_{FD}) \tag{18}$$

where Ω_{FD} is treated as an arbitrary constant

K is the common ratio of each exceedence threshold $|x_i|_j$ to σ_{x_i}, $i \in S$

$\sigma_{x_{o_i}}$ is the coherent* standard deviation of the monitored variable x_i, $i \in S$

$\sigma_{\dot{x}_{o_i}}$ is the coherent* standard deviation of the time rate of change of the monitored variable x_i, $i \in S$

Equation 17 demonstrates that $\bar{f}_{s_{FD}}$ will, in effect, be bounded from below by the largest value of K which is acceptable to the pilot. (In reciprocal terms, $\bar{T}_{s_{FD}}$ will be likewise bounded from above.) Increasing values of K represent decreasing levels of the pilot's confidence in his situation. We have determined that $1.4 \le K \le 3.0$ for the data in Ref. 1 with a value of $K = 2.0$ being representative overall.

$\bar{T}_{s_{FD}}$ will be bounded from below by $\bar{T}_{d_{e_{FD}}}$ in Eq. 18. In effect $\bar{T}_{d_{e_{FD}}}$ represents a lower bound on error coherence and is itself bounded from below by $\bar{T}_{d_{FD}}$, which is given in terms of $\bar{T}_{s_{FD}}$ by Eq. 9 as

$$\bar{T}_{d_{FD}} = \bar{T}_{s_{FD}} - 0.4$$

where 0.4 sec is the average dwell interval for monitoring. Experimental values for $\bar{T}_{d_{FD}}$ reported in Ref. 1 are approximately 2.0 sec.

---

*i.e., input-correlated

A method of testing for multiloop error coherence based on Ref. 9 has been presented in order to show how to correct the partition of scanning workload in case of low error coherence caused by the pilot's injection of scanning remnant into the control loops. The method is illustrated with numerical examples and extended to the case involving two primary director control displays in Ref. 9.

REFERENCES

1. Weir, D. H., and R. H. Klein, The Measurement and Analysis of Pilot Scanning and Control Behavior During Simulated Instrument Approaches, NASA CR-1535, June 1970.

2. Hofmann, L. G., W. F. Clement, and R. E. Blodgett, A New Link Value Estimator for Scanning Workload, presented at the Ninth Annual Conference on Manual Control, MIT, 23-25 May 1973.

3. McRuer, D. T., H. R. Jex, W. F. Clement, and D. Graham, A Systems Analysis Theory for Displays in Manual Control, Systems Technology, Inc., Tech. Rept. No. 163-1, Oct. 1967 (Rev. June 1968).

4. Rice, S. O., "Mathematical Analysis of Random Noise" in N. Wax (ed.), Selected Papers on Noise and Stochastic Processes, Dover Publications, New York, 1954.

5. Levison, W. H., and J. I. Elkind, Studies of Multivariable Manual Control Systems: Two-Axis Compensatory Systems with Separated Displays and Controls, NASA CR-875, Oct. 1967.

6. Allen, R. W., W. F. Clement, and H. R. Jex, Research on Display Scanning, Sampling, and Reconstruction Using Separate Main and Secondary Tracking Tasks, NASA CR-1569, July 1970.

7. Levison, W. H., and J. I. Elkind, Studies of Multivariable Manual Control Systems. Four-Axis Compensatory Systems with Separated Displays and Controls. Bolt Beranek and Newman, Inc., Rept. No. 1695, 14 Mar. 1969.

8. Clement, W. F., Random Sampling Remnant Theory Applied to Manual Control, Systems Technology, Inc., Tech. Memo No. 183-A, Mar. 1969.

9. Clement, W. F., L. G. Hofmann, and R. E. Blodgett, Application of Manual Control Display Theory to the Development of Flight Director Systems for STOL Aircraft, Part II. Multi-Axis Sampling, Pilot Workload, and Display Integration, Systems Technology, Inc. Tech. Rpt. No. 1011-2, May 1972.

SIGNAL DETECTION WITH TIME VARYING SIGNAL TO NOISE RATIO

Eliezer G. Gai and Renwick E. Curry

Man-Vehicle Laboratory
Department of Aeronautics and Astronautics
Massachusetts Institute of Technology

A model for pilot's perception of miss distances, based on signal detection theory is proposed. Experimental data was collected using a graphics computer for displaying the intruder's relative linear motions. Subjects had to give five rated answers as to whether or not the intruder was going to hit inside their miss distance circle. As the relative range is decreased, the subject's uncertainty is decreased, so that they have to choose between two non-stationary stochastic processes (time varying signal-to-noise ratio). These processes are chopped into four second time intervals and the problem is reduced to that of random variables so that signal detection theory can be used for the data analysis. An optimization algorithm smoothed the data, by maximizing the likelihood function, to fit normal distributions. This fit was tested using the χ^2 test and the confidence interval for most cases is over 0.9. These smoothed results show that the uncertainty of the subjects (the reciprocal of detectibility, d') increases linearly with the assumption of time invariant angle errors. The ROC curves as a function of time show that the time dependence of the decision rule can be interpreted as either time varying likelihood ratios, or as satisfying the Nieman Pierson objective. The importance of subject's internal uncertainty and ensemble performance will be discussed.

PRECEDING PAGE BLANK NOT FILMED

INPUT SIGNAL ADAPTIVITY OF THE HUMAN OPERATOR - A LINEAR AND NONLINEAR ANALYSIS

K. Etschberger

Manual tracking of stochastic signals is to a high degree dependent on the characteristics of the input signal, primarily their mean signal velocity, i.e. their bandwidth.

Analysing the input signal adaptivity of manual control behavior should lead to a deeper understanding of the fundamental mechanism of manual control.

Manual control behavior related to different bandwidths of the input signal was investigated experimentally in simple tracking tasks and analysed by linear and nonlinear methods.

In terms of linear system theory it could be shown, that the input adaptivity of the human operator can be understood as a minimizing of the mean square error. Thereby the stability of the closed system must be maintained.

The nonlinear analysis started with a statistical investigation of the manual output signal. Thereby it could be proved, that the triggering of discrete control actions corresponds to a threshold mechanism. That means that sampled data models with constant sampling intervals aren't applicable for a description of the human operator in a tracking task. The mean frequency of the discrete control actions was found to be independent of the independent of the input signal and is about 1.8 - 2.5 Hz. During the control actions, the course of the manual output signal velocity is triangular in form. The amplitude of these control action pulses depends on the velocity of the input signal. The control actions are of constant duration and of about 250 - 300 ms.

Based on the found characteristics of the manual output signal a simple nonlinear model of manual control behavior could be developed, which also contains the input adaptivity of the human operator. This model is able to reproduce not only the discontinuity of manual control to a great extent, but also is in agreement with the quasilinear description.

With the help of the model it could be shown, that the limited capability of the manual transmission of information in the tracking task is caused by the generation of control actions of constant duration.

N75 19160

A LINEAR STOCHASTIC MODEL OF THE HUMAN OPERATOR

John C. Durrett
Air Force Flight Dynamics Laboratory
Wright-Patterson AFB, Ohio

ABSTRACT

A linear stochastic model of the human operator is developed and applied to the problem of piloted control of an aircraft. The pilot and aircraft are modeled as linear time-invariant systems containing both process and measurement noise. The loop closure by the pilot is determined by formulating the problem as an optimal stochastic control problem. The solution to the optimal control problem yields not only the pilot's optimal control output which he uses to control the vehicle, but also the optimal combination of his observations of the vehicle states upon which the pilot bases his control. In addition, a method is presented so that, using experimental pilot vehicle data, the cost functional which is minimized in the optimal control problem will be numerically equal to the Pilot Rating (PR) that the pilot would associate with the given vehicle and task.

I. INTRODUCTION

The purpose of this paper is to show how the techniques of modern control theory can be applied to the problem of defining the closed loop dynamics of a pilot controlling an aircraft in flight.

The pilot and vehicle are modeled as linear time-invariant systems containing both process and measurement noise. The loop closure by the pilot is determined by formulating the problem as an optimal stochastic control problem. The solution to the optimal control problem yields not only the pilot's optimal control output which he uses to control the vehicle, but also the optimal combination of observations of the vehicle states upon which the pilot bases his control. In addition, a method is presented in this paper so that, using experimental pilot vehicle data, the cost functional which is minimized in the optimal control problem will be numerically equal to the Pilot Rating (PR) that the pilot would associate with the given vehicle task.

Because of the use of the state space notation of modern control theory, the impact of this paper is much broader than the field of pilot vehicle control; what is presented is the methodology for defining operator control of any dynamic system which can be represented as a linear time-invariant stochastic system. In fact, the theory can be readily extended to linear time-varying stochastic systems, Reference 1. Furthermore, the mathematical operator describing the pilot can also represent a nonhuman operator such as a monkey, a fixed order observer (ala Luenberger, Reference 2), or a fixed order compensator, Reference 3.

PRECEDING PAGE BLANK NOT FILMED

II. VEHICLE DYNAMICS

It is assumed that the vehicle to be controlled by the pilot can be represented as a linear time invariant stochastic system as follows:

$$E\dot{x} = Fx + Gu + M\eta \tag{1}$$

where x is an $n\times 1$ column vector of the system states, u is a $m\times 1$ column vector of the controls, and η is an $\ell\times 1$ column vector of white noise inputs with autocovariance $E\{\eta(t)\eta(\tau)\} = \kappa \cdot \delta(t-\tau)$. In this form, equation (1) can easily represent an aircraft flying in turbulence (See References 4, 5, 6, and 7 for a derivation of these equations). The pilot is assumed to "observe" or "feel" some incomplete linear combination of the system states which have been contaminated by an observation noise, μ. The pilot's observation, y, is written as

$$y = Cx + \mu \tag{2}$$

To simplify the equation format of this analysis, we assume that the observation noise, μ, is filtered white noise. If it is desired to retain the white noise characteristics, the filter bandwidth can be made much greater than that of the controlled system of equation (1). Then, using the techniques described in Reference 7, the controlled system would be

$$\left[\begin{array}{c|c} E & 0 \\ \hline 0 & I \end{array}\right] \left[\begin{array}{c} \dot{x} \\ \hline \dot{\mu} \end{array}\right] = \left[\begin{array}{c|c} F & 0 \\ \hline 0 & F_\mu \end{array}\right] \left[\begin{array}{c} x \\ \hline \mu \end{array}\right] + \left[\begin{array}{c} G \\ \hline 0 \end{array}\right] u + \left[\begin{array}{c|c} M & 0 \\ \hline 0 & M_\mu \end{array}\right] \left[\begin{array}{c} \eta \\ \hline \eta_\mu \end{array}\right] \tag{3}$$

where the observation is now expressed as

$$y = \left[C \mid I\right] \left[\begin{array}{c} x \\ \hline \mu \end{array}\right] \tag{4}$$

The matrices F_μ and M_μ are used to define the bandwidth and intensity of the observation noise.

The final step in the simplification is to redefine the matrices in Equations . and (4) by

$$x = \begin{bmatrix} x \\ \hline u \end{bmatrix}, \quad E = \left[\begin{array}{c|c} E & 0 \\ \hline 0 & I \end{array}\right], \quad F = \left[\begin{array}{c|c} F & 0 \\ \hline 0 & F_u \end{array}\right], \quad G = \begin{bmatrix} G \\ \hline 0 \end{bmatrix}$$

$$M = \left[\begin{array}{c|c} M & 0 \\ \hline 0 & M_u \end{array}\right], \quad \eta = \begin{bmatrix} \eta \\ \hline \eta_u \end{bmatrix}, \quad C = [C \mid I] \tag{5}$$

Then we can write the following set of equations for the vehicle under control:

$$E\dot{x} = Fx + Gu + M\eta \tag{6}$$

$$y = Cx \tag{7}$$

where the observation noise is now included in the system equations. This system represented by Equations (6) and (7) is assumed to be controlled by the pilot.

III. PILOT DYNAMICS

The pilot dynamics are represented in state variable notation and are based on the pilot model developed in Reference 7. The pilot model is

$$E_p \dot{x}_p = F_p x_p + G_p u_p + M_p \eta_p \tag{8}$$

where x_p is an rxl column vector of the pilot's states, u_p is a qxl column vector of the input controls to the pilot model, and η_p is a txl column vector of white noise inputs with autocovariance $E\{\eta_p(t)\eta_p(\tau)\} = \phi \cdot \delta(t-\tau)$. The matrix ϕ is used to scale the intensity of the pilot's motor noise.

Several differences can be noted between this pilot model and that of Reference 7. The control input to the pilot model, u_p, is expressed in a more general form rather than in the pure observation vector form of Reference 7. This is to allow u_p to be expressed as an optimal control input to the pilot model; this will become evident later in the paper. The other difference is that the time rate of change of the observation vector is no longer included. The rationale for the exclusion of this term is based on the classical rule of thumb, Reference 8, that the pilot will seek to drive the closed loop dynamics to a k/s form, where s is the conventional Laplace

variable. Thus, the pilot will not generally lead (which classically "causes" a $\dot{y}$) unless he is controlling a system whose dynamics are at least second order or greater. Thus, the $\dot{y}$ term apparently generated by the lead is really another state of the system which can readily be included in the observation vector, y, of Equation (7).

IV. PILOT VEHICLE DYNAMICS

The combined pilot vehicle dynamics are easily expressed using Equations (6), (7), and (8). The combined system is

$$\left[\begin{array}{c|c} E & 0 \\ \hline 0 & E_p \end{array}\right] \begin{bmatrix} \dot{x} \\ \hline \dot{x}_p \end{bmatrix} = \left[\begin{array}{c|c} F & 0 \\ \hline 0 & F_p \end{array}\right] \begin{bmatrix} x \\ \hline x_p \end{bmatrix} + \left[\begin{array}{c|c} G & 0 \\ \hline 0 & G_p \end{array}\right] \begin{bmatrix} u \\ \hline u_p \end{bmatrix} + \left[\begin{array}{c|c} M & 0 \\ \hline 0 & M_p \end{array}\right] \begin{bmatrix} \eta \\ \hline \eta_p \end{bmatrix} \tag{9}$$

The observation vector for this system is

$$\begin{bmatrix} y \\ \hline x_p \end{bmatrix} = \left[\begin{array}{c|c} C & 0 \\ \hline 0 & I \end{array}\right] \begin{bmatrix} x \\ \hline x_p \end{bmatrix} \tag{10}$$

To simplify the writing of the combined pilot vehicle dynamics, the following new pilot vehicle state vector, $\underline{z}$, and matrices are defined to be

$$\underline{z} = \begin{bmatrix} x \\ \hline x_p \end{bmatrix}, \quad \underline{E} = \left[\begin{array}{c|c} E & 0 \\ \hline 0 & E_p \end{array}\right], \quad \underline{F} = \left[\begin{array}{c|c} F & 0 \\ \hline 0 & F_p \end{array}\right], \quad \underline{G} = \left[\begin{array}{c|c} G & 0 \\ \hline 0 & G_p \end{array}\right]$$

$$\underline{u} = \begin{bmatrix} u \\ \hline u_p \end{bmatrix}, \quad \underline{y} = \begin{bmatrix} y \\ \hline y_p \end{bmatrix}, \quad \underline{\eta} = \begin{bmatrix} \eta \\ \hline \eta_p \end{bmatrix}, \quad \underline{M} = \left[\begin{array}{c|c} M & 0 \\ \hline 0 & M_p \end{array}\right], \quad \underline{C} = \left[\begin{array}{c|c} C & 0 \\ \hline 0 & I \end{array}\right] \tag{11}$$

With these definitions, Equations (9) and (10) become

$$\underline{E}\dot{\underline{z}} = \underline{F}\underline{z} + \underline{G}\underline{u} + \underline{M}\underline{\eta} \tag{12}$$

$$\underline{y} = \underline{C}\underline{z} \tag{13}$$

Equations (12) and (13) represent the open loop pilot vehicle dynamics.

These equations can also be written as

$$\dot{\underline{z}} = \underline{A}\underline{z} + \underline{B}\underline{u} + \underline{N}\underline{\eta} \tag{14}$$

$$\underline{y} = \underline{C}\underline{z} \tag{15}$$

where

$$\underline{A} = \underline{E}^{-1}\underline{F} \ , \ \underline{B} = \underline{E}^{-1}\underline{G} \ , \ \underline{N} = \underline{E}^{-1}\underline{M} \tag{16}$$

The matrix $\underline{E}$ will have an inverse whenever $I_{xz}^2 \neq I_{xx}I_{zz}$, Reference 5.

The structure of the control vector, $\underline{u}$, which will determine the closed loop dynamics, will be a function of the pilot vehicle control task.

V. OPTIMAL PILOT VEHICLE CONTROL

The control vector, $\underline{u}$, that is selected by the pilot will be a function of the pilot vehicle control task. The work of Kleinman (Reference 9), Anderson (Reference 10), Dillow (Reference 11), and Paskin (Reference 12) have indicated that the satisfaction of the control task can be thought of as the selection of an optimal control, $\underline{u}^*$, which minimizes a particular cost functional, J; that cost functional being determined by the control task at hand. The optimal control, $\underline{u}^*$, that is selected by the pilot can be seen from Equation (11) to be a combination of the optimal controls u^* and u_p^*. Recall from Equation (9) that u is the control that "operates" the vehicle and u_p is the control that "drives" the pilot. The pilot, therefore, is selecting both his optimal input, u_p^*, and his optimal output, u^*, as he attempts to achieve his pilot vehicle control task.

Two potentially viable forms for the cost functional will be given in this section of the paper. The validation of these functionals will be left to experiments. These forms are directly motivated by the independent works of Kleinman and Paskin (References 9 and 12) who obtained experimental verification of this general approach to the selection of cost functionals.

$J = f(\underline{y}, \underline{u})$

The first cost function is written assuming that the pilot minimizes some function of the pilot vehicle system observation vector, $\underline{y}$, and the pilot vehicle control vector, $\underline{u}$. Thus, J is written as

$$J = E\left\{\lim_{t \to \infty} \left[\underline{y}'(t)\, Q_1 \underline{y}(t) + \underline{u}'(t)\, Q_2 \underline{u}(t)\right]\right\} \tag{17}$$

where $E\{\cdot\}$ is the expectation operator, Reference 13.

The control task for the cost function Equation (17) is: given the pilot vehicle system from Equations (14) and (15),

$$\dot{\underline{x}} = \underline{A}\underline{x} + \underline{B}\underline{u} + \underline{N}\eta \tag{18}$$

$$\underline{y} = \underline{C}\underline{x} \tag{19}$$

Find the optimal control, $\underline{u}^*$, where $\underline{u}^*$ is restricted to be a linear combination of the pilot vehicle system observations

$$\underline{u}^* = \underline{H}\underline{y} \tag{20}$$

such that the cost functional, J, of Equation (17) is minimized. Thus, for $J = f(\underline{y}, \underline{u})$, the optimal control will be, from Equation (20)

$$\underline{u}^* = \begin{bmatrix} u^* \\ \hline u_p^* \end{bmatrix} = \left[\begin{array}{c|c} H & H_p \\ \hline K & K_p \end{array}\right] \begin{bmatrix} \underline{y} \\ \hline x_p \end{bmatrix} \tag{21}$$

Equation (21) can be expanded to give

$$\begin{aligned} u^* &= Hy + H_p x_p \\ u_p^* &= Ky + K_p x_p \end{aligned} \tag{22}$$

Equation (22) can be interpreted in the following manner. Through the control u_p^* the pilot sets up a linear combination of his observations, Ky, and adjusts his own dynamics by feeding back some linear combination of his own states, $K_p x_p$, to aid in the optimization of J. In addition to this, he controls the vehicle through the control vector u^* with a linear combination of his observations, Hy, and his states $H_p x_p$. In other words, Equation (22) says that the pilot will adjust his input and output simultaneously to obtain optimal control over the vehicle. This is shown in Figure 1.

The solution for the matrix $\underline{H}$ of Equation (20) is not trivial. However, methods to achieve this solution are available in References 1 and 14.

$J = f(\underline{y}, \underline{u}, \dot{\underline{u}})$

A slightly different approach is necessary when the cost functional includes the control rate (Kleinman's cost functional, Reference 9, includes control rate). Kleinman has shown that the introduction of control rate in the cost functional for a multiple input-single output pilot control task will effectively introduce a

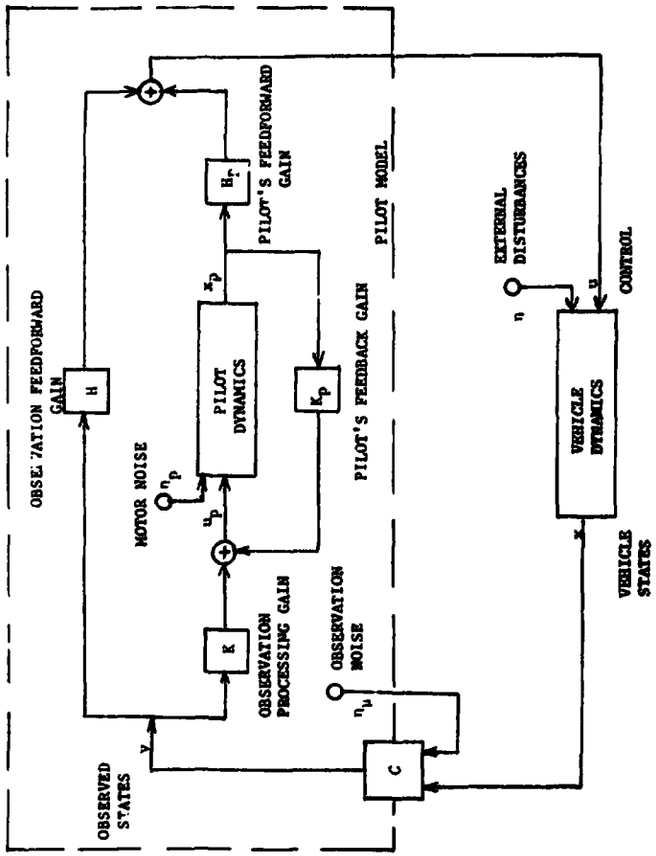

FIGURE 1 - OPTIMAL PILOT VEHICLE CONTROL FOR $J = f(y, x_p, u, u_p)$

first-order lag in the pilot dynamics. From a different viewpoint, it might be argued that the pilot's workload may be a function of his control rate as well as his control output. J is written as

$$J = E\left\{\lim_{t\to\infty}\left[\underline{y}'(t)Q_1\underline{y}(t) + \underline{u}'(t)Q_2\underline{u}(t) + \dot{\underline{u}}'(t)Q_3\dot{\underline{u}}(t)\right]\right\} \tag{23}$$

To make this cost functional compatible with optimal stochastic control theory, we include the controls, u, as states in the system and define a new state vector, z, and a new control vector, v, such that

$$z = \begin{bmatrix}\underline{x} \\ \underline{u}\end{bmatrix}, \quad v = \dot{\underline{u}} \tag{24}$$

Then, the pilot vehicle equations, (14) and (15), become

$$\begin{bmatrix}\dot{\underline{x}} \\ \dot{\underline{u}}\end{bmatrix} = \left[\begin{array}{c|c} A & B \\ \hline 0 & 0\end{array}\right]\begin{bmatrix}\underline{x} \\ \underline{u}\end{bmatrix} + \begin{bmatrix}0 \\ I\end{bmatrix}\dot{\underline{u}} + \begin{bmatrix}N \\ 0\end{bmatrix}\underline{\eta} \tag{25}$$

$$\begin{bmatrix}\underline{y} \\ \underline{u}\end{bmatrix} = \left[\begin{array}{c|c} C & 0 \\ \hline 0 & I\end{array}\right]\begin{bmatrix}\underline{x} \\ \underline{u}\end{bmatrix} \tag{26}$$

or

$$\dot{z} = A_1 z + B_1 v + N_1\underline{\eta} \tag{27}$$

$$y_1 = C_1 z \tag{28}$$

where z and v are from Equation (24) and

$$A_1 = \left[\begin{array}{c|c} A & B \\ \hline 0 & 0\end{array}\right], \quad C_1 = \left[\begin{array}{c|c} C & 0 \\ \hline 0 & I\end{array}\right], \quad B_1 = \begin{bmatrix}0 \\ I\end{bmatrix}, \quad y_1 = \begin{bmatrix}\underline{y} \\ \underline{u}\end{bmatrix}, \quad N_1 = \begin{bmatrix}N \\ 0\end{bmatrix} \tag{29}$$

In this case, the cost functional of Equation (23) would become

$$J = E\left\{\lim_{t\to\infty}\left[y_1'(t)Q_4y_1(t) + v'(t)Q_3v(t)\right]\right\} \tag{30}$$

where

$$Q_4 = \left[\begin{array}{c|c} Q_1 & 0 \\ \hline 0 & Q_2\end{array}\right] \tag{31}$$

Now, we can state the optimal control problem. Given the state dynamics of Equations (27) and (28), find the optimal control, v^*, which is restricted to be a linear combination of the observations, y_1,

$$v^* = H_1 \, y_1 \tag{32}$$

such that the cost functional of Equation (30) is minimized. Once again, the solution for H_1 can be found using References 1 and 14.

To show the resulting closed loop dynamics, it is necessary to expand the optimal control, Equation (32). Using Equation (24) we have for the optimal control

$$v^* = \dot{\underline{u}}^* = \underline{H}_y + \underline{H}_u \, \underline{u} \tag{33}$$

Substituting into Equation (25), the optimal closed loop pilot vehicle control dynamics become

$$\begin{bmatrix} \dot{\underline{x}} \\ \hline \dot{\underline{u}} \end{bmatrix} = \left[\begin{array}{c|c} \underline{A} & \underline{B} \\ \hline \underline{0} & \underline{0} \end{array}\right] \begin{bmatrix} \underline{x} \\ \hline \underline{u} \end{bmatrix} + \begin{bmatrix} \underline{0} \\ \hline \underline{I} \end{bmatrix} \left[\underline{H}\underline{C} \,\vdots\, \underline{H}_u\right] \begin{bmatrix} \underline{x} \\ \hline \underline{u} \end{bmatrix} + \begin{bmatrix} \underline{H} \\ \hline \underline{0} \end{bmatrix} \underline{\eta}$$

or (34)

$$\begin{bmatrix} \dot{\underline{x}} \\ \hline \dot{\underline{u}} \end{bmatrix} = \left[\begin{array}{c|c} \underline{A} & \underline{B} \\ \hline \underline{H}\underline{C} & \underline{H}_u \end{array}\right] \begin{bmatrix} \underline{x} \\ \hline \underline{u} \end{bmatrix} + \begin{bmatrix} \underline{H} \\ \hline \underline{0} \end{bmatrix} \underline{\eta}$$

By going back and using the equations which define the matrices in Equation (34), it can be shown that

$$\begin{bmatrix} \dot{x} \\ \dot{x}_p \\ \hline \dot{u} \\ \dot{u}_p \end{bmatrix} = \left[\begin{array}{c|c|c|c} E^{-1}F & 0 & E^{-1}G & 0 \\ 0 & E_p^{-1}F_p & 0 & E_p^{-1}G_p \\ \hline HC & H_p & \multicolumn{2}{c}{\underline{H}_u} \\ KC & K_p & & \end{array}\right] \begin{bmatrix} x \\ x_p \\ \hline u \\ u_p \end{bmatrix} + \left[\begin{array}{c|c} E^{-1}M & 0 \\ 0 & E_p^{-1}M_p \\ \hline 0 & 0 \\ 0 & 0 \end{array}\right] \begin{bmatrix} \eta \\ \eta_p \end{bmatrix} \tag{35}$$

Equation (35) describes the optimal closed loop dynamics of the pilot vehicle system for $J = f(\underline{y}, \underline{u}, \dot{\underline{u}})$. The next section will discuss the problem of obtaining the quadratic weights for the cost functionals from experimental data.

VI. QUADRATIC WEIGHTS FOR PILOT RATING

This section will address the problem of determining the elements of the quadratic weighting matrices from experimental test data. An additional goal is to show how these weighting matrices may be sized so that the numerical value of the cost functional will be equivalent to some preassigned scale of measurement such as Pilot Rating. We begin with the general cost functional

$$\begin{aligned} J &= E\left\{\lim_{t\to\infty} \left[x'(t)Qx(t) + u'(t)Ru(t)\right]\right\} \\ &= E\left\{\lim_{t\to\infty} \left[x'(t)Qx(t)\right] + \lim_{t\to\infty} \left[u'(t)Ru(t)\right]\right\} \\ &= E\left\{\lim_{t\to\infty} \left[x'(t)Qx(t)\right]\right\} + E\left\{\lim_{t\to\infty} \left[u'(t)Ru(t)\right]\right\} \\ &= \text{trace } Q\left(E\left\{\lim_{t\to\infty} \left[x'(t)x(t)\right]\right\}\right) + \text{trace } R\left(E\left\{\lim_{t\to\infty} \left[u'(t)u(t)\right]\right\}\right) \end{aligned} \tag{36}$$

or

$$J = \text{tr } (QX) + \text{tr } (RU) \tag{37}$$

where X and U are the steady state covariance matrices for the states and the controls, respectively. We now restrict Q and R to be diagonal weighting matrices

$$Q = \begin{bmatrix} q_1 & & & (0) \\ & q_2 & & \\ & & \ddots & \\ (0) & & & q_n \end{bmatrix}, \quad R = \begin{bmatrix} r_1 & & & (0) \\ & r_2 & & \\ & & \ddots & \\ (0) & & & r_m \end{bmatrix} \tag{38}$$

Then the trace operator in Equation (37) will pick off the diagonal elements of the covariance matrices to give

$$J = \sum_{i=1}^{n} (q_i \, x_{ii}) + \sum_{j=1}^{m} (r_j \, u_{jj}) \tag{39}$$

where x_{ii} and u_{jj} are the diagonal elements of the covariance matrices X and U, respectively. Now because X and U are covariance matrices, it is well known, Reference 4, that the steady rate root mean square (rms) values of the system states $\bar{x}_i$, and controls $\bar{u}_j$, can be expressed

$$\bar{x}_i = (x_{ii})^{1/2}$$
$$\bar{u}_j = (u_{jj})^{1/2} \tag{40}$$

Thus, the performance function can be expressed in terms of the weighting coefficients and the steady state rms values of the states and controls.

$$J = \sum_{i=1}^{n} (q_i \bar{x}_i^2) + \sum_{j=1}^{m} (r_j \bar{u}_j^2) \tag{41}$$

Since the rms values of the states and controls can be measured from experimental data with a pilot in the loop, we now address the problem of choosing the weighting coefficients.

An example will now be given to show how the weighting coefficients can be selected to predict pilot ratings.

In the development of the "Paper Pilot" approach to predicting pilot acceptance of aircraft handling qualities, Anderson and Dillow (References 10 and 11) have shown that the pilot will adjust his gains and model parameters to minimize a cost functional which, for most cases, is numerically equal to Pilot Rating. The "Paper Pilot" rating functional consisted of a weighted linear combination of the root mean squared (rms) values of the vehicle states and the pilot "lead" terms. The pilot rating functional proposed in this paper is a weighted linear combination of the squares of the rms values of the vehicle states, the pilot's states, and the controls. The selection of the use of the squares of the rms values is computationally more attractive since values are merely the diagonal element of the covariance matrix solutions to the closed loop, steady state optimal pilot vehicle system. The selection of the rms squared values, however, is further motivated by the work of Schmotzer, Reference 15, where the handling qualities for F-4C and F-80 aircraft are shown to be in direct proportion to the rms squared values of the aircraft states when the aircraft are being randomly disturbed by aerodynamic turbulence.

Assume that t experiments are conducted and for each experiment, data are collected on steady state rms values for the states and controls, and the associated Pilot Rating (PR) is recorded. We would then have for the t experiments, using PR for J in equation (41),

$$\begin{aligned}
PR_{(1)} &= \alpha + \sum_{i=1}^{n} q_i \bar{x}_{i(1)}^2 + \sum_{j=1}^{m} r_j \bar{u}_{j(1)}^2 \\
PR_{(2)} &= \alpha + \sum_{i=1}^{n} q_i \bar{x}_{i(2)}^2 + \sum_{j=1}^{m} r_j \bar{u}_{j(2)}^2 \\
&\vdots \\
PR_{(t)} &= \alpha + \sum_{i=1}^{n} q_i \bar{x}_{i(t)}^2 + \sum_{j=1}^{m} r_j \bar{u}_{j(t)}^2
\end{aligned} \tag{42}$$

where α is a constant bias term. The equation in (42) can also be expressed in matrix form by factoring the weighting coefficients such that

$$\begin{bmatrix} PR_{(1)} \\ PR_{(2)} \\ \cdot \\ \cdot \\ \cdot \\ PR_{(t)} \end{bmatrix} = \begin{bmatrix} 1 & \bar{x}_{1(1)}^2 & \bar{x}_{2(1)}^2 & \cdots & \bar{x}_{n(1)}^2 & \bar{u}_{1(1)}^2 & \bar{u}_{2(1)}^2 & \cdots & \bar{u}_{m(1)}^2 \\ 1 & \bar{x}_{1(2)}^2 & \bar{x}_{2(2)}^2 & \cdots & \bar{x}_{n(2)}^2 & \bar{u}_{1(2)}^2 & \bar{u}_{2(2)}^2 & \cdots & \bar{u}_{m(2)}^2 \\ \cdot & \cdot & & & \cdot & \cdot & & & \cdot \\ \cdot & \cdot & & & \cdot & \cdot & & & \cdot \\ \cdot & \cdot & & & \cdot & \cdot & & & \cdot \\ 1 & \bar{x}_{1(t)}^2 & \bar{x}_{2(t)}^2 & \cdots & \bar{x}_{n(t)}^2 & \bar{u}_{1(t)}^2 & \bar{u}_{2(t)}^2 & \cdots & \bar{u}_{m(t)}^2 \end{bmatrix} \begin{bmatrix} \alpha \\ q_1 \\ q_2 \\ \cdot \\ \cdot \\ \cdot \\ q_n \\ r_1 \\ r_2 \\ \cdot \\ \cdot \\ \cdot \\ r_m \end{bmatrix} \tag{43}$$

or

$$[PR] = P\, q \tag{44}$$

where [PR] is a tx1 column vector of the Pilot Ratings, q is a tx1 column vector of the weighting coefficients, and P is readily identified from Equation (43). It can be shown that the best fit with respect to "least squares" or "minimum norm," Reference 16, is

$$q = P^{\dagger}\, [PR] \tag{45}$$

where $P^{\dagger}$ is the generalized or pseudo inverse of P.

Now, it should be evident from Equation (43) that is is not necessary to weigh or measure every state of control. The form of the cost functionals associated with Pilot Ratings and the nonzero weighting coefficients will be a function of the particular control task. Thus, if the coefficients of the weighting matrices are chosen using Equation (45), the solution of the optimal pilot vehicle control problem, as posed in this paper, should produce not only the predicted closed loop performance but an associated Pilot Rating of the vehicle dynamics as well.

VII. CLOSING COMMENTS

In this final section of the paper, I will mention some of the present shortcomings of this optimal pilot vehicle control theory and then document some of my thoughts on where we could go from here. Obviously, one primary deficiency is that the theory has not been directly validated by experiment. The formulation of the theory is, however, based on an integration of ideas from all of the listed references and should work.

The reader may have noticed by now that no guidelines have been given to determine the size or order of the pilot model; this is a present shortcoming. My guess is that the order of the pilot model will be a function of the desirability to obtain an open loop pilot vehicle system which is completely controllable and completely observable (See Reference 16 for a mathematical system definition of these terms). Rynaski and Chen, Reference 17, have suggested that the pilot model be considered as a compensator and that the order of the pilot model be determined just as Brasch and Pearson, Reference 3, determine the order of a compensator necessary to achieve system stability or pole assignment. Perhaps, the most direct way of determining the pilot model order is to use the classical pilot vehicle approach; pick a low order model from those given in Reference 7, try it, and see if it works. Part of the motivation

behind the development of a new approach to Pilot Vehicle Control was the need to have a pilot model whose structure was simple enough that the individual parameters of the model could be identified through experiments. This is the primary difficulty of the approach of Kleinman and Paskin where, because of the modeling of the pilot as a Kalman filter, the dynamic order of the model is necessarily the same size as the order of the plant or vehicle under control. In these cases, the validation of the model can practically be done only on an input-output basis and not through parameter identification techniques.

Another handicap at this time is that a consistent method does not exist for determining the pilot's motor and observation noise; call the whole thing remnant if you like. However, Kleinman and Paskin, References 9 and 12, have made some progress in this area.

Scaling the cost functional to be numerically equal to the Pilot Rating must be approached with caution. Ideally, one should be able to select a set of cost functional weighting matrices which will be valid over a given class of vehicles for a particular type of control task. As an example, the weighting matrices should be invariant for cargo aircraft in a landing approach task. The future of optimal pilot vehicle control looks very promising. One immediate application of the theory is in the direct assessment of aircraft handling qualities. With this optimal pilot model it will be possible to evaluate an aircraft over preplanned "stability and control" trajectories. The trajectories can be constructed as either fixed point or time varying linearized segments of actual nonlinear maneuvers.

The use of the state space formulation in the development of this optimal pilot vehicle control theory enables the rapid coupling of this theory with the design of automatic control systems utilizing optimal control theory. A successful design effort of this type using more classical control techniques has been accomplished by Hollis, Reference 18.

One final comment is included for the engineer concerned with basic control system design. The matrix equations of Equation (8) which describe the pilot dynamics will also mathematically describe a fixed order dynamic compensator network or an observer system in the sense Luenberger, Reference 2. Thus, the optimal control developed for the pilot dynamics will also be directly applicable to the design of compensators or observers.

REFERENCES

1. Heath, Robert E. II, "Optimal Incomplete Feedback Control of Linear Stochastic Systems," Doctoral Dissertation DS/MS/73-1, Air Force Institute of Technology, Wright-Patterson AFB, Ohio (to be published in June 1973).

2. Luenberger, D. G., "An Introduction to Observers," Proceedings of the Twelfth Joint Automatic Control Conference, Paper No. 2-B1, Washington University, St. Louis, Missouri, August 1971.

3. Brasch, F. M. Jr. and Pearson, J. B., "Pole Placement Using Dynamic Compensators," IEEE Transactions on Automatic Control, Vol. AC-15, No. 1, February 1970.

4. Durrett, John C., "A Beginning Primer on $\dot{x} = Ax + Bu$ for the Airplane," AFFDL/FGC-TM-72-13, Wright-Patterson AFB, Ohio, July 1972.

5. Durrett, John C., "On $\dot{x} = Ax + Bu$ for the Airplane - Simplification of the General Linear Equations of Motion," AFFDL/FGC-TM-72-24, Wright-Patterson AFB, Ohio, December 1972.

6. Heath, Robert E. II, "State Variable Model of Wind Gusts," AFFDL/FGC-TM-72-12, Wright-Patterson AFB, Ohio, July 1972.

7. Durrett, John C., "On $\dot{x} = Ax + Bu + M\eta$ for the Airplane, Control System, Wind Gust and Pilot," AFFDL/FGC-TM-72-21, Wright-Patterson AFB, Ohio, November 1972.

8. McRuer, D. and Graham, D., "Human Pilot Dynamics in Compensatory Systems," AFFDL-TR-65-15, Wright-Patterson AFB, Ohio, July 1965.

9. Kleinman, D. L. and Baron, S., "Analytic Evaluation of Display Requirements for Approach to Landing," BBN Report No. 2075, Bolt Beranek and Newman, Inc., Cambridge, Massachusetts, March 1971.

10. Anderson, Ronald O., "A New Approach to the Specification and Evaluation of Flying Qualities," AFFDL-TR-69-120, Wright-Patterson AFB, Ohio, June 1970.

11. Dillow, James D., "The 'Paper Pilot' - A Digital Computer Program to Predict Pilot Rating for the Hover Task," AFFDL-TR-70-40, Wright-Patterson AFB, Ohio, March 1971.

12. Paskin, H. M., "A Discrete Stochastic, Optimal Control Model of the Human Operator in a Closed-Loop Tracking Task," AFFDL-TR-70-129, Wright-Patterson AFB, Ohio, November 1970.

13. Meditch, J. S., Stochastic Optimal Linear Estimation and Control, McGraw-Hill Book Co., New York, 1969.

14. Van Dierendonck, A. J., "Design Method for Fully Augmented Systems for Variable Flight Conditions," AFFDL-TR-71-152, Wright-Patterson AFB, Ohio, January 1972.

15. Schmotzer, R. E., Durrett, J. C. and Heath, R. E. II, "Yet Another Look at Aircraft Stability and Control - A Stochastic Analysis in the Lateral-Directional Axes," AFFDL/FGD-TM-72-19, Wright-Patterson AFB, Ohio, November 1972.

16. Durrett, John C., "Suboptimal Feedback Control of Pole Locations in Linear Systems," AFFDL-TR-71-165, Wright-Patterson AFB, Ohio, April 1972.

17. Rynaski, E. G. and Chen, C. T., "Identification of Human Pilots Planning Document," Cornell Aeronautical Laboratory, Inc., Internal Report, Buffalo, New York, March 1971.

18. Hollis, T. L., "Optimal Selection of Stability Augmentation System Parameters to Reduce the Pilot Rating for the Pitch Tracking Task," AFIT M.S. Thesis GGC/EE/71-10, Wright-Patterson AFB, Ohio, June 1971.

N75 19161

MODELS OF MAN AS A SUBOPTIMAL PREDICTOR

William B. Rouse
Department of Engineering Design
Tufts University
Medford, Massachusetts 02155

ABSTRACT

Models of man making predictions of future states of discrete linear dynamic systems are considered. The task is forced-pace, but the pace is slow enough to eliminate the effects of reaction time and neuromuscular lag. The best of the several models considered includes the constraints of limited memory and observation noise.

INTRODUCTION

Many human activities depend on the ability to make predictions. We usually are fairly accurate when making the simple predictions required for such tasks as walking or opening a door which depend on a (perhaps unconscious) prediction of future positions of one's legs, arms, etc. However, as we try to predict further into the future and/or one's understanding of or experience with the process decreases, our predictive abilities degrade. For example, our abilities are somewhat limited when trying to predict the effect today's technology will have in the next century.

The improvement of man's ability to predict has paralleled the development of civilization. Economic, political, and technological progress is dependent on the confidence in the future that comes with the ability to make predictions. The further into the future that can be acceptably predicted, the better that investments, policies, and strategies can be planned.

This paper considers man making predictions of future states of discrete linear dynamic systems. Several models of the human in this task are presented. Two of the models, which assume simple extrapolation strategies, do not predict as well as the human. Two other models, which utilize two methods of system identification, predict much better than the human. A fifth model, which is basically a linear regression system identifier with a limited memory and noisy observations, matches human performance quite well. These models and others are used to discuss the limitations imposed on human predictive abilities by physiological and cognitive constraints. The effect of these constraints is related to the distance into the future that the human attempts to predict.

THE TASK

The following prediction task has been considered. The subject sat in a darkened booth and viewed the computer-generated display shown in Figure 1. The display represents the output of a discrete linear dynamic system given by

$$x_{N+1} = c_0 y_{N+1} + \underline{c}^T \underline{x}_N \qquad (1)$$

where

$$\underline{x}_N = \begin{bmatrix} x_N \\ \dot{x}_N \\ \ddot{x}_N \end{bmatrix} = \text{system state at time } N,$$

$$\underline{c} = \begin{bmatrix} c_1 \\ c_2 \\ c_3 \end{bmatrix} = \text{a vector of constants,}$$

y_{N+1} = input at time N+1 sampled from a zero-mean Gaussian process,

c_0 = a constant,

and the derivatives noted in $\underline{x}$ were approximated using one-sided difference equations. Amplitude x is on the horizontal scale and time increases downward on the vertical scale. The points displayed are $\Delta t = 1.0$ units apart.

The subject viewed the last ten points of system output. His task was to predict the eleventh point, the horizontal position of which he controlled with a potentiometer. The horizontal line at the top of the display represented the time in which the prediction had to be completed. The length of the line decreased as the time remaining decreased. When the length of the bar went to zero, the subject's prediction was read by the computer and output on paper tape along with the optimal prediction and the actual next point. All the points on the display (with the exception of the subject's prediction) then shifted one unit up the vertical scale and a new point appeared below these points representing the actual point which the subject has just tried to predict. Thus, assuming that the subject had not moved his potentiometer during the updating interval, he saw his prediction error as the difference in horizontal position between the new tenth point and the eleventh point which he had predicted. The process was then repeated. The time per prediction was fifteen seconds. Each trial lasted at least twenty minutes making for at least eighty predictions per trial.

Eight subjects were used, four of which were well acquainted with system dynamics and optimal control while the nearest acquaintance with the task of the other four was freshman calculus. They were instructed to minimize RMS prediction error.

Each subject performed a randomly chosen sequence of eight trials. Each trial was characterized by an approximation to the normalized integrated absolute autocorrelation function I given by

$$I = \frac{1}{\sigma_x^2} \sum_{i=0}^{\infty} | \phi_{xx}(i\Delta t) | \qquad (2)$$

where

$\phi_{xx}(i\Delta t)$ = autocorrelation function,

σ_x^2 = variance of displayed signal.

Equation (2) is a measure of the "memory" of the system or, in other words, it is a measure of the confidence with which the next point can be predicted based solely on the information contained in a limited number of past points. This measure is independent of input variance. The input variance was chosen so as to yield a constant output standard deviation σ_x of 100.0 (with a range of 1000.0).

The results of the experiment are shown in Figure 2. It was assumed that the last sixty of the eighty-plus predictions represented a more or less steady-state (not necessarily non-tim[illegible] behavior. Since there was no statistically significant difference bet[illegible] formance of those subjects familiar with system dynamics and those unfa[illegible] data shown is across all eight subjects. Each value of the RMS predict[illegible] with respect to optimal e_{os} represents an average across twenty predictions for a particular subject. Thus, the data includes three values of e_{os} per subject per trial. Hence, $\sigma_{e_{os}}$ is a measure of the dispersion of

ORIGINAL PAGE IS OF POOR QUALITY

average prediction errors. Since the performance of the models was measured in exactly the same way, this averaging of averages presents no problem.

MODELS

The following models represent several approaches to describing human performance in the above task. They will only be discussed in general. The reader is referred to Rouse [5] for the derivations.

While all five models vary to some degree, they all include an observation noise parameter to account for the fact that a human observer cannot perfectly estimate the magnitudes of physical stimuli. This psychophysical phenomenon was formalized by the well-known Weber-Fechner law and its application to the observation of continuous time series has been experimentally investigated by Levison, Baron, and Kleinman [3] and discussed by Crossman [1]. Specifically, the idea is applied here by assuming that the standard deviation σ_x of the human's estimate of a quantity x is given by

$$\frac{\sigma_x}{|x|} = F = \text{constant}. \tag{3}$$

A very simple model is that of linear extrapolation from the previous two points

$$\hat{x}_{N+1} = x_N + (x_N - x_{N-1}) \tag{4}$$

where $\hat{x}$ is the human's prediction. Since one-sided difference equations have been used to approximate derivatives, (4) can be written as

$$\hat{x}_{N+1} = x_N + \dot{x}_N \tag{5}$$

A slightly more sophisticated model assumes that the human fits a second-order curve through the last three points and then extrapolates that curve to make his prediction. This can easily be shown to yield

$$\hat{x}_{N+1} = x_N + \dot{x}_N + \ddot{x}_N \tag{6}$$

The RMS error between each of these models and the optimal was determined analytically and is shown in Figure 3. As can be seen, these models do not perform as well as the subjects. Increasing F above zero would only make matters worse.

The simple extrapolater models do not learn about the system from observing it. Their strategy is fixed. We will now consider a model that collects data and then performs a linear regression on that data to identify the system. This model is termed a learning model because the quality of the identification improves in time. The model learns more and more about the system as it collects more data. This definition of learning is different from classical operent conditioning. The model gains nothing from its mistakes. Learning is considered here only in the sense of gaining information from its environment.

The learning model makes predictions using

$$\hat{x}_{N+1} = \hat{\underline{C}}\, \underline{X}_N \tag{7}$$

where

$$\hat{\underline{C}} = (\underline{A}^T \underline{A})^{-1} \underline{A}^T \underline{H} \tag{8a}$$

and

$$\underline{A} = \begin{bmatrix} x_{N-1} & \dot{x}_{N-1} & \ddot{x}_{N-1} \\ x_{N-2} & \dot{x}_{N-2} & \ddot{x}_{N-2} \\ & \vdots & \end{bmatrix} \tag{8b}$$

$$\underline{H} = \begin{bmatrix} x_N \\ x_{N-1} \\ \vdots \end{bmatrix} \tag{8c}$$

Figure 4 compares the learning model with the experimental data. The data for the model is averaged over the last sixty of one hundred trials. This model does much better than the subjects. (In the limit of infinite trials, the model would be perfectly optimal for F = 0.0) Increasing F was attempted but an F or 0.10 or 0.20 made very little difference and it would not be consistent with psychophysical data to use an F of 1.0, 2.0, or higher.

The following model is a discrete equivalent of Ware's model [7]. It will be termed the autocorrelation model and makes predictions using

$$\hat{x}_{N+1} = \hat{c}_1 x_N + \hat{c}_2 \dot{x}_N \tag{9}$$

where

$$\hat{c}_1 = \frac{\phi_{xx}(\Delta t) + \phi_{xx}(2\Delta t)}{\phi_{xx}(o) + \phi_{xx}(\Delta t)}, \tag{10a}$$

$$\hat{c}_2 = \frac{\phi_{xx}^2(\Delta t) - \phi_{xx}(o)\phi_{xx}(2\Delta t)}{\phi_{xx}^2(o) - \phi_{xx}^2(\Delta t)}, \tag{10b}$$

and $\phi_{xx}(i\Delta t)$ is the autocorrelation function. This model is compared with the experimental data in Figure 5. It does much better than the subjects did. This is not surprising since the expansion of a few terms in the learning model (8a) shows terms such as $x_N x_{N+1}$, $x_N x_{N+2}$, etc.

The last model to be considered is a limited memory model. The mathematics involved are similar to that of the learning model except that there is a double-exponential memory weighting function that effectively forgets old data. This is accomplished by changing (8a) to

$$\hat{\underline{C}} = (\underline{A}^T \underline{W} \underline{A})^{-1} \underline{A}^T \underline{W} \underline{H} \tag{11}$$

where $\underline{W}$ is a diagonal square matrix with diagonal elements w_i^2 given by

$$w_i^2 = K_1 e^{-b(N-i)} + K_2 e^{-a(N-i)} \tag{12}$$

where

$$K_1 = a/(a-b),$$

$$K_2 = -b/(a-b),$$

$$a = D + \sqrt{D^2 - 1},$$

$$b = D - \sqrt{D^2 - 1},$$

and $D > 1.0$ is a free parameter in the model. Computationally, it is necessary to truncate (12) in order for $\underline{W}$ to be of finite order. It was assumed that if $a^{-2} < 0.10$, then $w_i^2 = 0.0$.

The limited memory model is compared to the experimental data in Figure 6. The parameters of the model were found by fitting the data for the trial with lowest I. The rest of the trials were then run with the same parameters. This emphasizes the closeness of the fit of the model to data.

The D of 2.5 leads to an effective memory length of thirteen. This means that the human uses thirteen past states to compute $\underline{C}$. Once he calculates $\hat{\underline{C}}$, he uses only the present state to make his prediction. The state contains only three past points (assuming the human used the same derivative formulas as the model). The distinction between memory length and the length of the state vector is important. The human might very well decide that the state vector $\underline{X}$ need only be of length two or three which might include perhaps three or four past points depending on derivative approximations. However, when determining $\hat{\underline{C}}$, he should use as much past history as he can. (This assumes that the system is stationary and he realizes that such is the case.) Since the statistical quality of $\hat{\underline{C}}$ is a monotonically increasing function of memory length, the human has no reason to limit memory length. Thus, it is inferred that the effective memory length of thirteen found with the model is not the result of the human purposely discounting the value of less recent data.

DISCUSSION

The above models indicate that human prediction strategies are more sophisticated than simple extrapolations, but also, that humans are suboptimal predictors.

These results do not agree with those of Ware [7] or those of Kleinman, Baron, and Levison [2] who assume the human to be an optimal predictor. However, their tasks involved the human's motor system to a significant degree and because of this, delays in neuromotor dynamics had to be included as sources of suboptimality. Also, the system can have the positive effect of providing proprioceptive cues by the tasks, for example, the arm-stick combination [4]. These factors combined with the fact that subjects in their tasks were making relatively short predictions, make comparison of their results with those presented here a little difficult.

At the other end of the prediction length scale, Sheridan and Rouse [6] have studied the human's ability to predict several time units into the future. As might be intuited, the human's performance becomes increasingly suboptimal with prediction length. This behavior has been modeled [5] and the conclusion reached was that the human has difficulty determining the amount of signal history due to the noise input. While this supports the proposition that limited memory constrains him from collecting sufficient data, applying the limited memory model to long prediction tasks yields unsatisfactory comparisons with the experimental data of Sheridan and Rouse. This problem was further investigated by performing a linear regression on the experimental data from which the parameters of the limited memory model were determined. The results of the regression were then used to estimate what the human might have done if he had been predicting further into the future. These predictions were inconsistent with Sheridan and Rouse's data in the same way that the limited memory model was inconsistent.

This seems to indicate that some new source of suboptimality becomes significant with longer predictions. The optimal prediction trajectories for long predictions do not look very much like the actual time series. The optimal trajectory approaches the mean of the time series exponentially. Adopting an optimal-like strategy for long predictions may require a conceptualization that humans find difficult to accept.

By way of analogy, consider asking a human uninitiated in the laws of probability to predict the flip of an unbiased coin. If the person is instructed to minimize prediction error where heads = 1 and tails = 0, the optimal strategy is to predict the expected value of 1/2. However, anyone who has instructed beginning students of probability, knows the difficulty of convincing a percentage of the students that the expected value of the above coin flip is 1/2. Usually some student will wonder how 1/2 can be the expected value when in actuality a flip can only yield the values of 0 or 1.

It seems reasonable to assign such conceptual difficulties to the cognitive category. With this assignment, Figure 7 summarizes the relative significance of physiological and cognitive constraints on the human's ability to predict. Reaction time and neuromotor dynamics are not constraints (and proprioceptive cues are not aids) when making long predictions. Cognitive constraints are not very significant (relative to other constraints) for short, fast predictions but increase in significance as the prediction length increases.

ACKNOWLEDGEMENTS

The author gratefully acknowledges the support and advice of his thesis committee, Professors T. B. Sheridan, D. P. Garg, and R. L. Keeney, throughout the course of the research on which this paper is based.

This work was supported by NASA under grant NGL 22-009-002.

REFERENCES

1. Crossman, E. R. F. W., "Discussion of a Model for Human Controller Remnant", Proceedings of the Fifth Annual Conference on Manual Control, M.I.T., Cambridge, 1969, pp 199-201.

2. Kleinman, D. L., S. Baron, and W. H. Levison, "A Control Theoretic Approach to Manned-Vehicle Systems Analysis", IEEE Transactions on Automatic Control, Vol. AC-16, No. 6, December, 1971, pp 824-832.

3. Levison, W. H., S. Baron, and D. L. Kleinman, "A Model for Human Controller Remnant", Proceedings of the Fifth Annual Conference on Manual Control, M.I.T., Cambridge, 1969, pp 171-198.

4. Pew, R. W., J. C. Duffendack, and L. K. Fensch, "Summary of Sine-Wave Tracking Studies", Proceedings of the Second Annual Conference on Manual Control, M.I.T., Cambridge, 1966, pp 15-24.

5. Rouse, W. B., Cognitive Sources of Suboptimal Human Prediction, Ph.D. Thesis, M.I.T., September, 1972.

6. Sheridan, T. B. and W. B. Rouse, "Supervisory Sampling and Control: Sources of Suboptimality in a Prediction Task", Proceedings of the Seventh Annual Conference on Manual Control, University of Southern California, Los Angeles, 1971, pp 81-88.

7. Ware, J. R., "An Input Adaptive, Pursuit Tracking Model of the Human Operator", Proceedings of the Seventh Annual Conference on Manual Control, University of Southern California, Los Angeles, 1971, pp 33-43.

ORIGINAL PAGE IS
OF POOR QUALITY

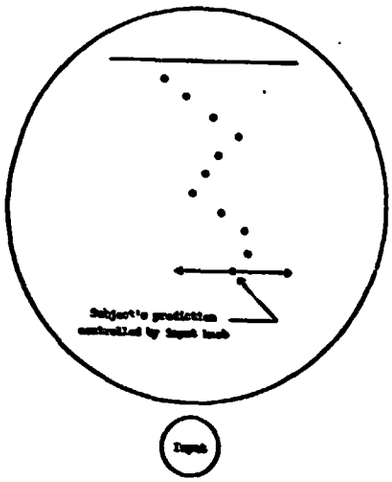

Display for Prediction Experiment

Figure 1

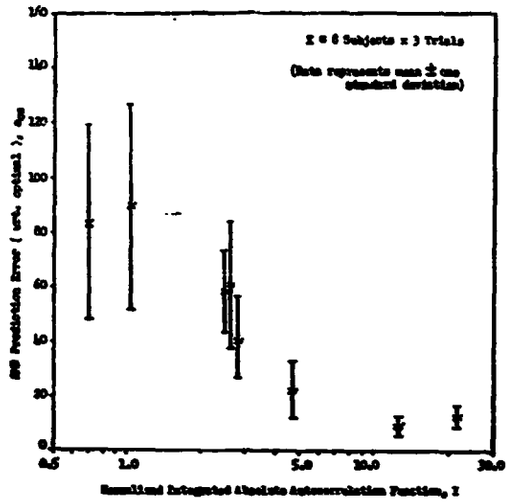

Data from Prediction Experiment

Figure 2

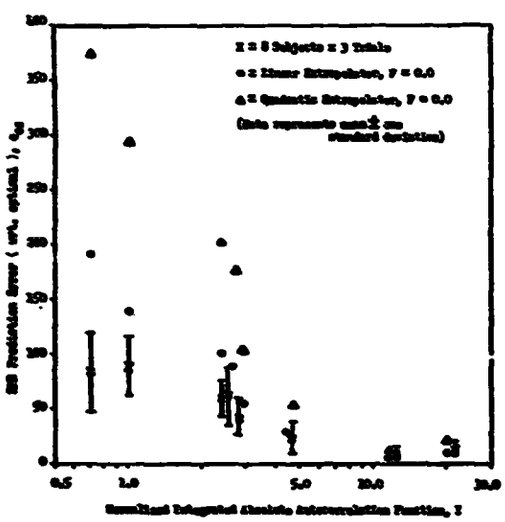

Comparing the Simple Extrapolator Models
with the Prediction Data

Figure 3

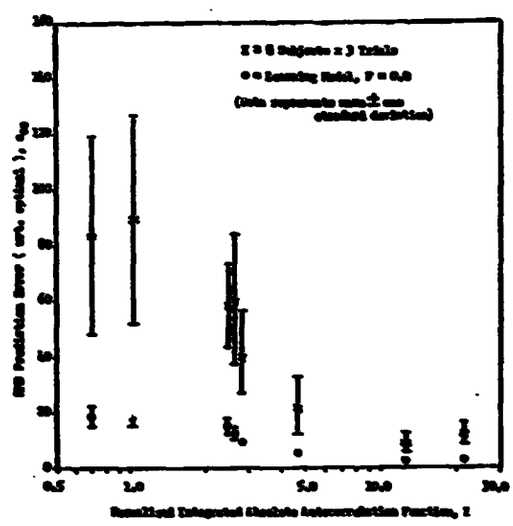

Comparing the Learning Model with the Prediction Data

Figure 4

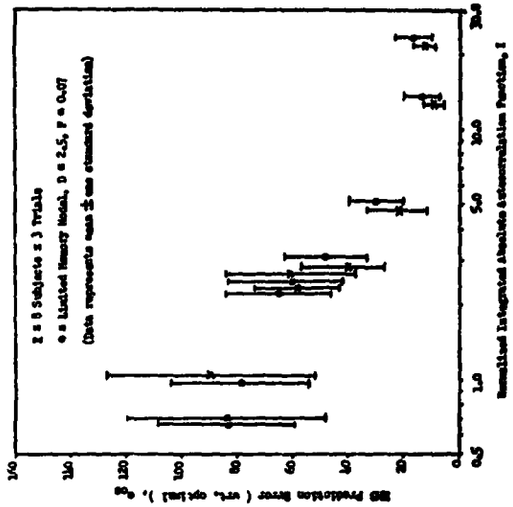

Comparing the Limited Memory Model with the Prediction Data

Figure 6

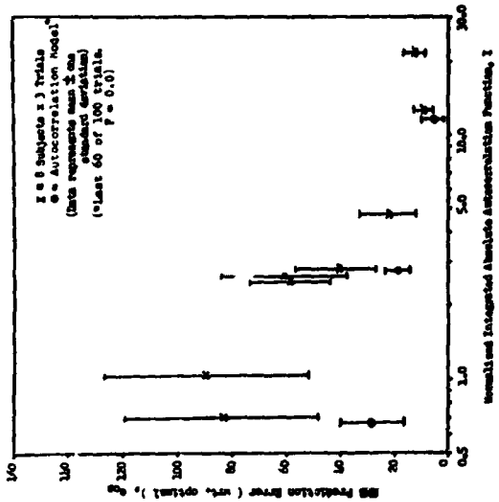

Comparing the Autocorrelation Model with the Prediction Data

Figure 5

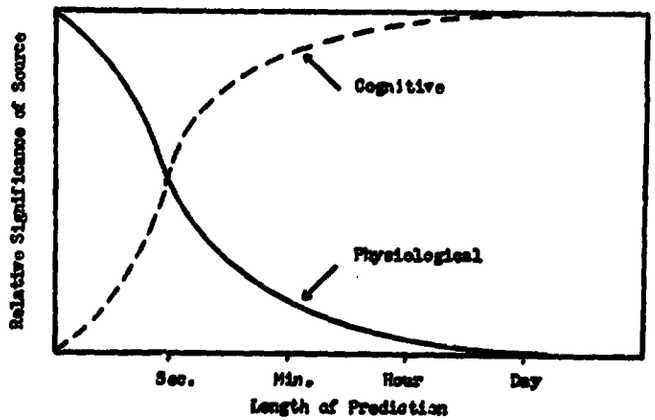

Relative Significance of Sources of Suboptimality

Figure 7

N75 19162

ANALYSIS OF RESPONSE TO WIND-SHEARS USING THE OPTIMAL CONTROL MODEL OF THE HUMAN OPERATOR*

Sheldon Baron

Bolt Beranek and Newman Inc.
50 Moulton Street
Cambridge, Massachusetts

ABSTRACT

The effects of wind-shears on the approach performance of a STOL aircraft are analyzed using the optimal-control model of the human operator. This analysis involves a time-varying situation that is more complex than is traditionally treated by human operator modelling techniques. The extensions to the time-varying case are discussed and results are presented that illustrate the effects of wind shears on category II window-performance and the effects on performance of pilot time-delay and of variations in pilot gain during approach.

1. INTRODUCTION

In an instrument approach-to-landing the pilot attempts to maintain his position on the glide-path in the presence of external disturbances. An important part of the task involves compensation for errors introduced by winds. Most analytic studies of the problem based on human operator models have considered only the effects of zero-mean, random turbulence. However, winds with a non-zero mean component can be quite significant and may provide the dominant problem. These "mean-winds" generally vary with altitude. The rate of change of wind speed with altitude is called the shear variation and the altitude dependent winds are often refered to as wind-shears. The mean-wind can be described in statistical terms, i.e., the wind direction and speed are, in general, random variables. However, in a given approach-to-landing, a specific "sample" mean-wind is encountered. It is the response to particular samples that is usually of interest, rather than the response to the distribution as a whole.

*This research was performed under Contract NAS2-6652 for the NASA, Ames Research Center.

PRECEDING PAGE BLANK NOT FILMED

The introduction of wind shears into the approach problem complicates the situation considerably from the standpoint of analysis by human operator modelling techniques. The disturbance input no longer has stationary statistics and, furthermore, one expects the pilot to be capable of some "prediction" or other high level adaptation with respect to the shear variation. These two factors tend to compromise the theoretical and experimental bases for most quasilinear describing function models [1], although interesting attempts have been made to extend those models to quasi-predictable inputs [2].

Here, the optimal control model of the human operator [3] is used to analyze approach in a wind-shear environment. It is relatively straightforward, theoretically, to apply the optimal control model to this problem, because of the model's time domain foundation and its normative nature. This was demonstrated in a previous application to time-varying approaches involving constant updrafts [4]. That study also showed that model results were reliable predictors of experimental data for the time-varying situations analyzed.

This paper is an extension of the analysis presented in [4]; specifically, a more general class of disturbances is considered, and some time-varying facets of the optimal control model are examined in greater detail. The results are believed to be of interest both in terms of predicting the effects of wind-shears on approach performance and in leading to further understanding of human operator modelling techniques based on optimal control. On the other hand, unlike [4], experimental data to confirm or reject the model results are, unfortunately, not available at this time.

The paper begins with a brief discussion of the modifications to the human operator model required for analysis of the response to wind shears. Then, results are presented for a STOL approach that illustrate: (1) the effects of wind shears on performance at the approach "window"; (2) the effect of pilot time-delay on performance; and (3) the effects of changing pilot gain during approach. A more detailed presentation of the ideas and results may be found in [5].

2. MODIFICATIONS OF OPTIMAL CONTROL MODEL FOR TIME-VARYING DISTURBANCES

Consider the linear dynamic system

$$\dot{\underline{x}} = \underline{A}\,\underline{x} + \underline{B}\,\underline{u} + \underline{E}\,\underline{w} + \underline{F}\,\underline{z} \qquad (1)$$

where $\underline{x}$ is a vector representing the system state, $\underline{u}$ is a vector of control inputs, $\underline{w}$ is a vector of zero-mean, gaussian, white noises, $\underline{z}$ a vector of time-varying input disturbances and $\underline{A}$, $\underline{B}$, $\underline{E}$ and $\underline{F}$ constant matrices of appropriate dimension. We assume that $\underline{z}$ satisfies

$$\dot{\underline{z}} = \underline{A}_z \underline{z} \; ; \; \underline{z}(t_o) = \underline{z}_o \tag{2}$$

with $\underline{A}_z$ a constant matrix. (Note that if $\underline{E} = \underline{F}$ then $\underline{z}$ can be used to model a mean component of $\underline{w}$.) Various disturbance inputs may be generated from the model of Equation (2), particularly if impulses or jumps in "initial conditions" are allowed [6].

To examine how the control structure of the optimal control model is modified to account for the disturbance (2), we ignore the limitations on the human's observation processes, (time-delay and observation noise) and assume the $\underline{A}_z$ and $\underline{z}(t_o)$ are known. This implies the disturbance-state, $\underline{z}(t)$, is known for all t. This assumption is unrealistic and is made here only for expository reasons; in applying the model, $\underline{z}(t)$ is estimated from the available noisy, delayed data, as are the other system states.

The operator's control $\underline{u}$ is assumed to be chosen to minimize the quadratic cost functional

$$J = \lim_{T\to\infty} E\left(\frac{1}{T}\int_0^T \underline{x}'\underline{Q}\,\underline{x} + \underline{u}'\,\underline{R}\,\underline{u} + \dot{\underline{u}}'\underline{G}\,\dot{\underline{u}}\right)dt \tag{3}$$

where $\underline{Q}$ and $\underline{R}$ are positive, semi-definite matrices and $\underline{G}$ is positive definite. The solution to this problem is well-known and is developed in detail in the control literature [6-8]. In particular, it can be shown that the optimal control law satisfies

$$\underline{T}_N(t)\dot{\underline{u}}^* + \underline{u}^* = -(\underline{L}(t)\underline{x} + \underline{K}(t)\underline{z}) \tag{4}$$

where $\underline{T}_N$, $\underline{L}^*$ and $\underline{K}$ are time-varying matrices that are obtained by solving an appropriate matrix Ricatti equation (see [8] and [3] for details). Moreover, if the input disturbance does not have an exponentially growing component (i.e., if the eigenvalues of $\underline{A}_z$ are ≤ 0), the control gains in (4) approach a constant as $T\to\infty$. Thus, when the system matrices and cost functional weightings are time-invariant and when T is large relative to system time-constants, we may take advantage of

the enormous simplification afforded by a constant gain solution.* Under these conditions Equation (4) may be written as

$$\underline{u}^* = -(\underline{T}_N s + \underline{I})\,(\underline{L}^*\,\underline{x} + \underline{K}\,\underline{z}) \tag{5}$$

where $\underline{T}_N$ and $\underline{L}^*$ are identical to the neuro-motor lag and optimal feedback gain matrices obtained for the optimal control model of the human operator under stationary conditions [3]. Thus, the modification to the basic model to account for the time-varying, mean disturbance is a set of feedforward gains acting on the (estimate of) the disturbance.** This result, which is a direct consequence of the normative assumption, is satisfying intuitively and is not inconsistent with the "Successive Organization of Perception" concepts discussed in, e.g., [9].

As mentioned previously, $\underline{z}(t)$ is to be estimated from the available observation data. In terms of the estimation problem, it will be assumed here that the initial condition $\underline{z}_o$ is a gaussia random variable with known mean and variance. Thus, $\underline{z}(t)$ is gaussian and its distribution is known, for all t. The actual value of $\underline{z}(t)$ corresponding to a specific sample disturbance from the distribution is not known and is estimated from the displayed variables by means of a Kalman filter. It can be shown [5] that if the sample path does not correspond to the path generated by the mean of $\underline{z}_o$, then the error and the estimate are correlated, the filter being optimal only in terms of the distribution of $\underline{z}_o$. The expressions used to compute the corresponding estimation errors for this case are developed in [5].

Finally, it is important to note that the man-machine system response to a sample disturbance $\underline{z}(\cdot)$ is a random variable, even when $\underline{w} \equiv 0$. The reason for this is the human operator's randomness which is reflected in the observation and motor noises of the optimal control model.

*Actually, the "solution" may not be a solution at all, in that the infinite-time cost may be unbounded. However, this is a minor inconvenience that can be circumvented readily in applying the results [5, 7].

**An alternative, perhaps less satisfying, interpretation is that the control law involves integral as well as proportional feedback [6, 8].

3. ANALYSIS OF APPROACH PERFORMANCE

3.1 Approach Scenario

We consider the longitudinal approach of an Augmentor Wing Jet STOL Research Aircraft (AWJSRA), the C-8M.* The aircraft is assumed to be initially on the nominal (7.5 deg.) glide-slope with a nominal airspeed of approximately 31 m/s. Linearized perturbation equations were used to describe the aircraft motion. The pilot was assumed to control elevator and "nozzle" (thrust vector) in a continuous manner, whereas throttle was assumed to be fixed at the appropriate trim setting. The corresponding equations of motion, in state variable form, are given in [5].

The basic scenario for the analysis of longitudinal approach performance involved starting at an initial range of 1500m with a constant wind velocity corresponding to the value h = 125m (R ≈ 1160m). In all cases, turbulence having the Dryden spectral form [10] was assumed present. The scale-lengths of the turbulence were not varied with altitude; they were set at the constant value appropriate to the decision height. Gust intensities corresponded to a value that would not be encountered more than 10% of the time, i.e., a fairly severe condition.

The pilot's display was the EADI status display used in the STOLAND program [11] and described in another paper presented at this conference [12]. The STOLAND-status display shifts from an angular presentation of glide-path error to a height presentation at Range ≈ 575m (h ≈ 75m ≈ 250 ft.). The model for the human operator takes this variation in display gain into account by modifying appropriate observation parameters. Values for the parameters of human operator model were the same as those used for a corresponding steady-state analysis of performance at the decision height and are given in [5] and [12]. Suffice to say, that the values for parameters corresponding to human limitations were essentially the same as in previous studies [3, 4] and task-related parameters were determined from analysis of this problem [5, 12].

In addition to the above "basic" condition, the effects of variation in pilot gain were analyzed. It had been noted in [4] that the pilot might vary his gains so as to tighten control as the decision-height was approached. An analogous result can be obtained with the model by making the cost functional weightings of Equation (3) range-dependent. Indeed, if it is assumed that the pilot attaches a fixed penalty to angular deviations from the glide-path, rather than to linear deviations, then the weighting on height-errors will be range-dependent. We investigated two conditions with respect to this "gain-scheduling":

1. Constant Gains in which the cost functional weightings were constant and corresponded to Category II "window" performance requirements at the decision height.

2. Varying Gains in which angular glide-path error tolerances were assumed to be constant (corresponding to the allowable Category II window error). For this case, weightings (and, hence, gains) were changed in three stages according to the following schedule:

$$1500 \le R \le 1160\text{m} \;:\; q_h = .0029,\; q_h^{\dot{}} = .0326$$
$$1160\text{m} \le R \le 575\text{m} \;:\; q_h = .0117,\; q_h^{\dot{}} = .133$$
$$575\text{m} \le R \le 230\text{m} \;:\; q_h = .073,\; q_h^{\dot{}} = .83$$

Thus, the weighting over a range-interval corresponded to the weighting appropriate to the end-point of that interval, a conservative choice. The intervals were chosen, as a matter of convenience, so that the end-points corresponded to points where other changes in the approach scenario were required.

A limited examination of the effect of pilot time delay was also conducted. It was expected that the human's time delay would increase scores but would not alter the basic character of the results. Because inclusion of the time delay increases significantly the costs of the time-varying computation, we decided to assume the time delay was zero. However, a comparison case was obtained with a time delay of .2 sec. (the nominal value found in previous studies) to illustrate the differences one might expect from including time delay.

3.2 Modelling the Wind-Shears

In modelling wind-shears both dynamic and kinematic effects should be considered. In addition, from the standpoint of the optimal control model, it is desirable (though not necessary) to convert the altitude dependence of the shear to an equivalent time dependence. In this section, kinematic effects of wind shears are modelled as is the conversion to a time-dependent wind; dynamic effects are accounted for by considering the shear-components in the same fashion as turbulence velocity components [5]. Only horizontal wind-shears are considered.

*An analysis of the lateral performance is given in [5].

Figure 1 illustrates the pertinent geometry. The aircraft's altitude (h) is given by

$$h = h_n + \delta h = R \tan \Gamma_o + \delta h \qquad (6)$$

where h_n is the "nominal" altitude, i.e., the altitude of the glide-slope at the aircraft's range, R, and δh is the altitude error. The rate of change of the nominal altitude may be expressed in terms of the ground speed (or range-rate).

$$\dot{h}_n = \dot{R} \tan \Gamma_o = (U_o + u) \tan \Gamma_o \qquad (7)$$

where

u = x-body axis component of perturbation in ground speed

U_o = x-body axis component of nominal airspeed

The aircraft's sink-rate is

$$\dot{h} = V \sin \gamma = (U_o + u) \sin (\Gamma_o + \Delta\gamma)$$

$$\approx (U_o + u) (\sin \Gamma_o + \cos \Gamma_o \cdot \Delta\gamma)$$

and

$$\dot{\delta h} = \dot{h} - \dot{h}_n$$

$$\approx (U_o + u) \cos \Gamma_o \cdot \Delta\gamma = (U_o + u) \cos \Gamma_o \cdot (\theta - \alpha)$$

or

$$\dot{\delta h} \approx (U_o + u) \cos \Gamma_o \cdot \theta - \frac{U_o + u}{U_o} \cos \Gamma_o \cdot w \qquad (8)$$

Equation (8) is used to account for kinematic effects of shears. However, this equation is nonlinear and the product terms, $u\theta$ and uw, may not be negligible if u is a significant fraction of U_o. This is the case for the winds to be considered here. To maintain linearity and reduce the errors associated with neglecting the product terms, the "average" wind-velocity during approach was substituted for u in Equation (8); this tends to minimize the maximum error associated with assuming constant ground speed.

The wind-shears to be considered here are enumerated in Table 1. These winds are idealizations of more exact models for mean-winds. They were used in this analysis so as to be compatible with a concurrent simulation study. We now show how these winds may be represented as time-varying disturbances; it turns out that this can be done with considerable fidelity.

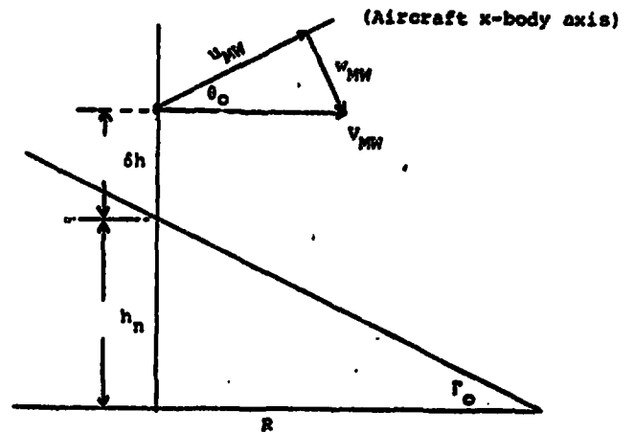

FIGURE 1. Geometry for Horizontal Wind-Shear Analysis (not to scale)

Let U_{MW} be the horizontal (along track) wind component of interest (crosswinds may be treated analogously). Given the profiles of Table 1, we may write

$$U_{MW} = U_{MW}(0) + a\,h \tag{9}$$

where a is the change in windspeed with altitude, i.e., the shear-variation. Thus, using (7),

$$\dot{U}_{MW} = a\,\dot{h} = a\,\dot{h}_n = a(U_o + u)\tan\Gamma_o \tag{10}$$

Differentiating [10] gives

$$\ddot{U}_{MW} = (a\tan\Gamma_o)\dot{u} \tag{11}$$

Table 1

WIND-SHEARS FOR LONGITUDINAL AND LATERAL ANALYSIS

Wind	Initial Altitude	Initial Speed	Final Speed	Final Altitude
Decreasing Tailwind	152m(500 ft)	$15.45\frac{m}{s}$(30KTS)	$5.15\frac{m}{s}$(10KTS)	0
Increasing Tailwind	152m	$-5.15\frac{m}{s}$(10KTS)	$+5.15\frac{m}{s}$	0

+ Indicates tailwind or crosswind from left side.

This equation along with the dynamical equation for $\dot{u}$ allows the wind shear to be expressed in terms of other, non-input related state variables. An even simpler representation is possible. If the pilot is maintaining airspeed reasonably well, then

$$u \approx U_{MW}\cos\theta_o \tag{12}$$

and, the state-variable representation for the mean wind disturbance is given by

$$\left.\begin{aligned} \dot{z}_1 &= \dot{U}_{MW} = z_2 \;;\; z_1(0) = U_{MW}(0) \\ \dot{z}_2 &= \ddot{U}_{MW} = (a\tan\Gamma_o\cos\theta_o)\dot{U}_{MW} \\ &= (a\tan\Gamma_o\cos\theta_o)z_2 \;;\; z_{2_{s_o}} = a\tan\Gamma_o\,(U_o + u_{MW}(0)) \end{aligned}\right\} \tag{13}$$

where $z_{2_{s_o}}$ is the mean-wind velocity at the onset of the shear.

3.3 Results

Mean and standard deviation scores, at the decision-height (31m), are compared in Table 2. Several points are worth mentioning First, the constant-gain no shear, zero-delay results are virtually equal to those of a corresponding steady-state analysis [5]. This is more than a check on the computer program; it shows that in the absence of shears, the approximately 1250-1300m approach distance is sufficient for the errors to reach steady-state. Second, the effect of the wind-shear is more than just a non-zero mean response. It may be seen that the standard deviation of the tracking errors and of the controls is increased. This is a result of the coupling in the model of mean-and variance-responses that arises from the dependence of the observation noises on the rms signal values and that of the motor-noise on rms control. In terms of missed approach probabilities, the increase in variance is the more significant effect. Third, the effect of time delay is, as expected, to increase mean and standard deviation of the error. The magnitude of the effect is largest for height-error with approximately a 35% increase in mean and a 10% increase in standard deviation.

Table 2

PERFORMANCE AT DECISION-HEIGHT FOR VARIOUS ANALYSIS CONDITIONS

Variable	Steady-State		Constant-Gains			Varying-Gains
	$\tau = .0$	$\tau = .2$	$\tau = 0$	$\tau = 0$	$\tau = .2$	$\tau = 0$
			No-Shear	With Shear		
h (m)	0	0	0	.16	.22	.31
σ_h (m)	1.73	1.83	1.72	2.02	2.2	2.03
$\bar{\dot{h}}$ (m/s)	0	0	0	-.01	-.016	-.05
$\sigma_{\dot{h}}$ (m/s)	.48	.50	.47	.63	.70	.63
$\bar{\theta}$ (m)	0	0	0	-.6	-.6	-.62
σ_θ (m/s)	1.24	1.29	1.23	1.27	1.35	1.26
$\bar{u}$ (m/s)	0	0	0	-.10	-.095	-.10
σ_u (m/s)	.94	.96	.96	.98	1.03	1.00
$\bar{\delta}_e$ (deg)	0	0	0	-1.44	-1.43	-1.46
σ_{δ_e} (deg)	1.38	1.5	1.39	1.75	1.94	1.82
$\bar{\delta}_N$ (deg)	0	0	0	16.3	16.2	16.5
σ_{δ_N} (deg)	8.6	8.5	8.6	11.5	11.8	11.7

The final effect illustrated in Table 2 is that resulting from allowing the gains to vary. When compared with the constant gain case, it is seen that the principal effect at the window is on the mean-response. This effect, though large percentage-wise, is virtually negligible in terms of the missed-approach probability. The differences between constant and varying gains are more pronounced in the "time-histories" shown in Figure 2. These time-histories are curves passed through data points obtained every 50m in range. The jump-discontinuities for the varying-gain case arise from the instantaneous gain-change and

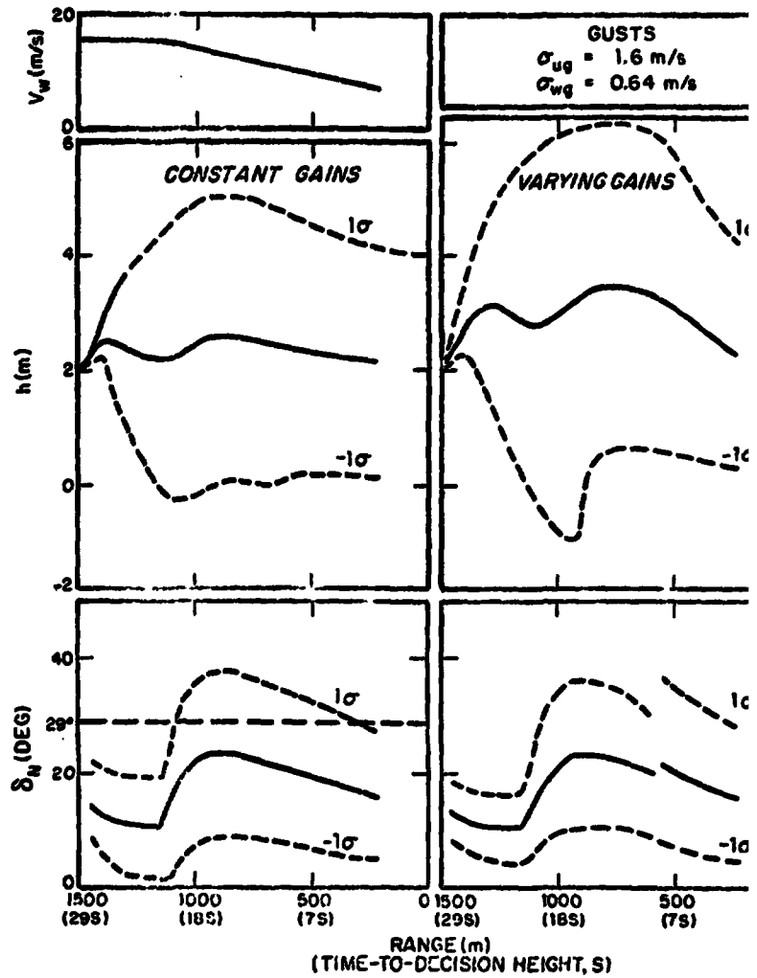

FIGURE 2. Effect of Varying Gains on Approach Trajectories
(a) Height and Nozzle Response

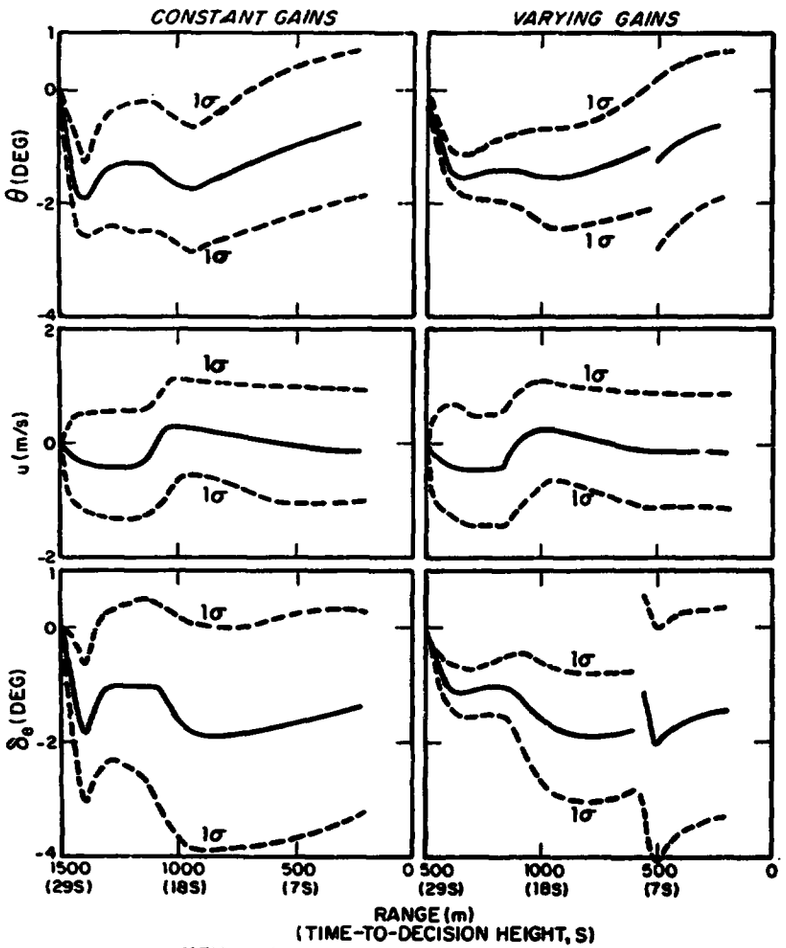

FIGURE 2. Effect of Varying Gains on Approach Trajectories
(b) Pitch, Airspeed and Elevator Response

the associated jump in control value. These "jumps" apparently decay very rapidly. Because height errors are weighted less, at more distant ranges, they are allowed to build up to a greater extent in the varying-gain case; however, as the threshold is approached the errors begin to be reduced rapidly (because of the higher weighting), so that window performance is not significantly different for the varying- and constant-gain cases (Table 2). Apart from differences in height control, the principal difference between the two-cases is in the initial transient in elevator and pitch. It seems clear that the early reduction in height errors for the constant-gain case is a result of a rapid pitch-down.

The excellent "window" performance obtained in the above analyses is somewhat misleading. As can be seen from Figure 2, the nozzle limit (29°) is less than one standard deviation from the mean for much of the approach (after the wind-velocity starts changing). Thus, a high percentage of the time the nozzle will exceed its limit. What this means is that the rate of descent capability of the aircraft, with throttle fixed, is insufficient for this wind. Further, the wind is of sufficient severity to place the entire linearized analysis in question. On the other hand, the analysis suggests that suitably scaled-down winds may be adequately controlled by nozzle and elevator inputs alone.

In an attempt to get some estimate of the control-limited performance for the decreasing tailwind, a trajectory was obtained for a case in which nozzle control and control-rate were heavily penalized in the region where excessive nozzle-control had been observed, i.e., in the 1160m < R < 575m interval. (Weightings on nozzle and nozzle-rate were multiplied by 50). To allow transient effects resulting from the initial constant wind to die out, the approach was started at 2000m. The result for height-error and nozzle-position is shown in Figure 3. It can be seen that nozzle responses to the shear variation in the heavily penalized region are virtually nil and the height errors increase accordingly. When the penalty is reduced, R < 575m, a relatively large mean-nozzle motion ensues in an attempt to reduce the mean-error. While some reduction occurs, the mean height error at the decision height is still three times the allowable Category II error. Although these results are not intended to be definitive, they do illustrate the problem posed by this wind, when the throttle is fixed.

A constant-gain trajectory for the increasing tailwind was also obtained and the results are shown in Figure 4.* The window performance for this wind is compared with that for the decreasing tailwind in Table 3. Note that the turbulence intensity and

*As can be seen the wind approximation is not as close to the idealized wind as for the previous case, but certainly good enough.

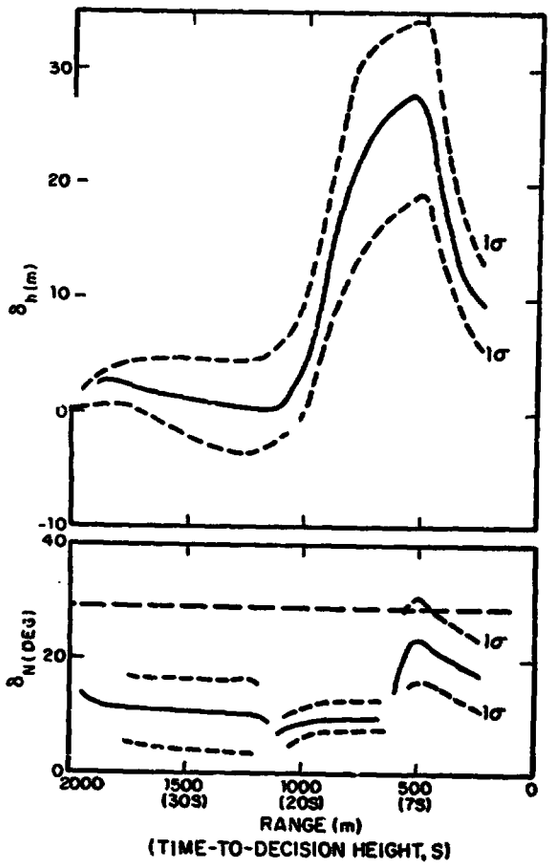

FIGURE 3. Nozzle-Limited Response for Decreasing Tailwind

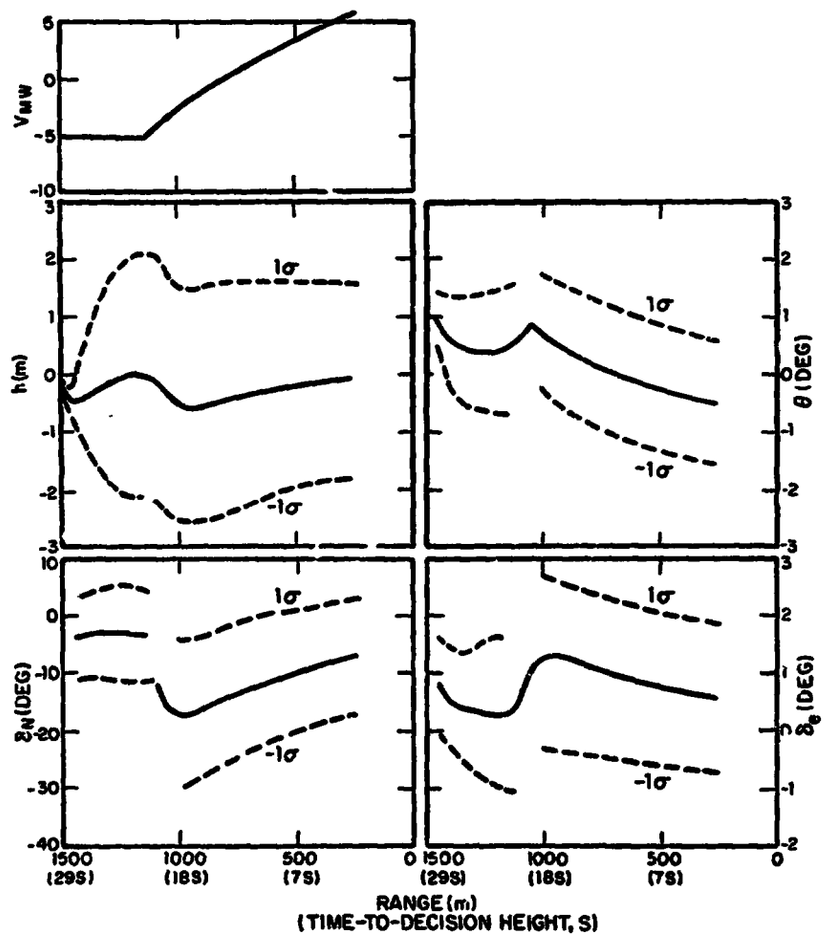

FIGURE 4. Response History for Increasing Tailwind Shear

spectrum is the same for the two cases. It may be seen that height errors are controlled more effectively for the increasing tailwind; airspeed is less-well controlled. The overall effect is a definite improvement, as could be expected. Two other points are worth noting. Referring to Table 3, we find that the standard deviation of the height and sink-rate errors for the increasing tailwind are very close to those obtained for the steady-state (no-delay) case. Thus, it appears that with the increasing tailwind (which starts out as a headwind), enough time is added to the approach to allow the "pilot" (model) to reduce the errors to values commensurate with an approach of infinite length. The second point is that the nozzle-control requirements are not so excessive (in relation to capability) as for the decreasing tailwind. Thus, one might expect these results to correspond more closely to a realistic situation.

5. CONCLUSION

Some aspects of the STOL approach in a mean-wind with shear-variation have been analyzed with the optimal control model of the human operator. Results were obtained for longitudinal control with an EADI status display. In general, the wind-shears degrade performance by producing both mean errors and increased variability in the response, with the increased variability appearing to be the major effect.

Two wind profiles were considered in the analysis of longitudinal control, a decreasing and an increasing tailwind. Relatively good performance at the window was obtained in both cases. However, for the decreasing tailwind, the results showed that with the throttle fixed, excessive nozzle-control was required for wind compensation. When the nozzle control was limited (indirectly, by penalizing control motions subsequent to shear-onset), the height errors increased significantly. The relatively good performance for the increasing tailwind was achieved with control requirements that were not so excessive and, consequently, represent a more reliable result. The better performance is undoubtedly due to the additional time available for error compensation and is, of course, to be expected.

To the extent that they were investigated, the wind-shear responses tended to confirm essentially the results of a corresponding steady-state analysis [5] (albeit that performance was worse in the wind-shear). The details of the transient responses, may be easily explained. They depend very much on the specific assumptions about initial conditions and on pilot strategy, which is not the least bit surprising. If one is interested in reproducing or predicting a particular time history (ensemble) then it is essential that conditions used in the model match those of the experiment.

With respect to future work, it appears most important to validate the results of this analysis with simulation data. Approach data is needed to pin-down details of the pilot's time-varying adaptation. Transient data for a sufficient number of runs to provide reliable statistical information would be most helpful.

Table 3

COMPARISON OF WINDOW PERFORMANCE FOR DIFFERENT TAILWINDS

Variable	Decreasing Tailwind	Increasing Tailwind
$\bar{h}$(m)	.16	-.12
σ_h(m)	2.02	1.69
$\bar{\dot{h}}$(m/s)	-.01	.006
$\sigma_{\dot{h}}$(m/s)	.63	.46
$\bar{\theta}$(deg)	-.6	-.49
σ_θ(deg)	1.27	1.13
$\bar{u}$(m/s)	-.10	-.19
σ_u(m/s)	.98	.99
$\bar{\delta}_e$(deg)	-1.44	.56
σ_{δ_e}(deg)	1.75	1.3
$\bar{\delta}_N$(deg)	16.3	-7.4
σ_{δ_N}(deg)	11.5	10.0
Time-for-Approach(s)	~29.	~43.

REFERENCES

1. McRuer, D., D. Graham, E. Krendel, and W. Reisner, "Human Pilot Dynamics in Compensato / Systems", AFFDL TR65-15, July 1965.

2. Magdaleno, R. E., H. R. Jex, and W. A. Johnson, "Tracking Quasi-Predictable Displays", NASA-University Fifth Annual Conference on Manual Control, MIT, March 1969, NASA SP-215, 1970.

3. Kleinman, D. L., S. Baron, and W. H. Levison, "An Optimal Control Model of Human Response, Part 1: Theory and Validation", Automatica, Vol. 6, pp. 357-369, May 1970.

4. Kleinman, D. L. and S. Baron, "Analytical Evaluation of Display Requirements for Approach to Landing", NASA CR-1952, November 1971.

5. Baron, S. and W. H. Levison, "A Manual Control Theory Analysis of Vertical Situation Displays for STOL Aircraft", Bolt Beranek and Newman Inc., Rept. 2484, April 197[illegible].

6. Johnson, C. D., "Accommodation of External Disturbances in Linear Regulator and Servomechanism Problems", IEEE Trans. on Automatic Control, Vol. AC-16, No. 6, December 1971.

7. Kreindler, E., "On Servo Problems Reducible to Regulator Problems", IEEE Trans. Auto. Contr., Vol. AC-14, August 1969.

8. Anderson, B.D.O. and J. B. Moore, "Linear Optimal Control", Prentice Hall, Edgewood Cliffs, New Jersey, 1971.

9. McRuer, D. T. and H. R. Jex, "A Review of Quasi-Linear Pilot Models", IEEE Trans., Vol. HFE-8, No. 3, September 1967.

10. Chalk, C. R., T. P. Neal, T. M. Harris, and F. E. Prichard, "Military Specifications - Flying Qualities of Piloted Airplanes", AFFDL-TR-69-72, August 1969.

11. Decker, D. W., "Display Requirements Specification for STOLAND EADI Display System".

12. Baron, S. and W. H. Levison, "A Display Evaluation Methodology Applied to Vertical Situation Displays", Ninth Annual Conference on Manual Control, MIT, May 197[illegible].

The Preview Control Problem with Application to Man-Machine System Analysis

by

Masayoshi Tomizuka* and Daniel E. Whitney**
*Research Assistant, Department of Mechanical Engineering
**Associate Professor of Mechanical Engineering
Massachusetts Institute of Technology
Cambridge, Massachusetts 02139 U.S.A.

Abstract

The preview control problem is formulated in a general form and its solution is obtained. The analytical tool used is discrete stochastic optimal control theory. Aiming the application to manual control situations with preview, time delay, observation noise, motor noise, etc. were included in formulating the problem.

Some manual preview control experiments have been performed to qualitatively check the validity of the model, and it was found that the mechanism of the manual control problem was explained by the developed model pretty well.

Work supported partially by NASA under Grant NGR-22-009-002, and partially by M.I.T. Endowed Fellowship.

N75 19163

I. Introduction

In this paper, the preview control problem, in which information about future inputs and disturbances is used as well as the present and past information in deciding control, is considered. It is reasonable to expect that we can achieve better performance in some sense in the case when we know about the future compared to the case when we have no idea about the future. Such cases include:

1) Car driving
2) Airplane landing
3) Control of vehicle suspension
4) Process control problems
5) Economic or industrial problems etc.

Above 1) and 2) are related to manual control or man-machine systems. It is our objective to develop the general theory of the preview problem using optimal control theory, and to apply it to manual control problems.

Several works related to preview control have been published already. Sheridan[1] proposed three models of preview control. Bender[2] solved a class of preview control problems using Wiener filter theory and a parameter search, and applied it to the design of vehicle suspensions. Hayase and Ichikawa[3] treated the problem from the viewpoint of deterministic control theory and obtained a suboptimal control. However, the manual preview control problem is usually very complicated because of reaction time, remnant, etc., and is difficult to analyze using the above results.

The analysis of the manual control problem using optimal control theory has been done by several people[4,5,6]. Among these, the most successful work has been done by Kleinman, Baron and Levison[4], and some of their ideas are used in this paper. So far, however, this kind of analysis has been done only for the compensatory and pursuit tracking problems. In this paper, it is extended to the preview tracking problem.

In the next section, the formulation of the preview control problem is given. This is solved in Section III. Section IV describes the manual preview control experiment performed to qualitatively evaluate the validity of the proposed model, and the data from the experiment are analyzed in Section V. Conclusions and what should be done in the future work are stated in Section VI.

II. Formulation of Preview Control Problem

Let us consider the situation in Fig. 2-1. We have a plant to which we can apply control $u(t)$. The plant might meet some disturbance or noise $w(t)$, and we can measure $y(t)$ by a sensor with a measurement time delay τ and observation noise $v(t)$. We would like to control the plant so that the output $y(t)$ of the system follows the desired trajectory $y_d(t)$ (Fig. 2-2) as close as possible with a reasonable amount of control over the time interval from $t_0 \le t \le t_f$.

Depending on the amount of a priori information we have about $y_d(t)$, we can divide the problem in three cases.

Case 1. Complete knowledge about $y_d(t)$. $t_o \le t \le t_f$

Case 2. Statistics or some characteristics of $y_d(t)$ is known.

Case 3. Nothing is known.

In optimal control terminology, Case 1 is called the tracking problem. In Case 3, measuring $y_d(t)$ is definitely necessary. In Case 2, measuring $y_d(t)$ is not necessary, but if it can be done the quality of control will increase. Usually only $y_d(t)$ is measured or given at time t; however, in our problem $y_d(\tau)$ is measured or given for $t \le \tau \le t+t_{\ell a}$ at time t (See Fig. 2-2). This is the preview problem. In our case, it is further assumed that the measurement of $y_d(\tau)$ has a measurement time delay τ_d and observation noise v_d. In this paper a priori information on $y_d(\tau)$ is in the form of Case 2 and it is modeled as a time correclated zero mean random process.

It is our objective to study how we can use the information about future y_d most effectively. In the following, the preview problem is formulated as an optimal control problem. What we want to decide is "?" in Fig. 2-3.

In this paper, the problem is formulated in discrete fashion and, noises are all assumed to be Gaussian and white. Before going into the mathematical formulation, basic symbols are listed. (If not familiar with discrete systems, see Bryson and Ho[8].)

$\underline{\cdot}$ means . is a vector or a matrix

Subscript i denotes time

$E[\cdot]$ means the expectation of $\cdot$

R^k denotes k- dimensional Euclidean space

($\underline{\cdot} \in R^k$ is shorthand for saying "$\underline{\cdot}$ is a k-dimensional vector")

δ_{ij} is the Dirac delta function $\begin{pmatrix}\delta_{ij} = 1 \text{ for } i = j \\ \delta_{ij} = 0 \text{ otherwise}\end{pmatrix}$

Superscript T denotes the transpose of a vector or a matrix

A lot of control problems with preview can be formulated in the following form, although more general formulations are possible.

First, the system to be considered is given by the following difference equation.

$$\underline{x}_{i+1} = \underline{\Phi}_i \underline{x}_i + \underline{\Gamma}_i \underline{u}_i + \underline{w}_i \tag{2-1}$$

$$\underline{z}_i = \underline{C}^T_{i-da} \underline{x}_{i-da} + \underline{v}_i = \underline{y}_{i-da} + \underline{v}_i \tag{2-2}$$

where $\underline{\Phi}_i$, $\underline{\Gamma}_i$ and $\underline{C}_{i-da}$ are $(n\times n)$, $(n\times m)$ and $(n\times r)$ matrices, respectively,

$\underline{x}_i \in R^n$, $\underline{u}_i \in R^m$, $\underline{z}_i \in R^r$, $E[\underline{w}_i] = E[\underline{v}_i] = 0$, da is a measurement time delay, $da \ge 0$,

$E[\underline{x}_k] = \bar{\underline{x}}_k (k = -da, \ldots, 0)\dagger$, $E[\underline{w}_i \underline{w}_j^T] = \underline{W}_i \delta_{ij}$, $\underline{W}_i \ge 0$, $E[\underline{v}_i \underline{v}_j^T] = \underline{V}_i \delta_{ij}$, $\underline{V}_i > 0$,

$E[(\underline{x}_k - \bar{\underline{x}}_k)(\underline{x}_\ell - \bar{\underline{x}}_\ell)^T] = \underline{P}_{xx_{k,\ell}}$ $(k = -da, \ldots, 0;$ and $\ell = -da, \ldots, 0)\dagger$,

$\underline{P}_{xx_{k,\ell}} \ge 0$, $E[\underline{w}_i \underline{v}_j^T] = E[\underline{w}_i \underline{x}_k^T] = E[\underline{v}_i \underline{x}_k^T] = \underline{0}$ $(k = -da, \ldots, 0)\dagger$.

This system has to be controlled so that its output can follow the desired trajectory, which is modelled as the output of the following shaping filter, running $N_{\ell a}$ time steps ahead ($N_{\ell a}$ denotes the amount of look ahead available).

$$\underline{x}_{d_{i+1}} = \underline{\Phi}_{s_i} \underline{x}_{d_i} + \underline{\Gamma}_{s_i} \underline{w}_{d_i} \tag{2-3}$$

$$\underline{y}_{d_i} = \underline{C}^T_{s_i} \underline{x}_{d_i} \tag{2-4}$$

where $\underline{\Phi}_{s_i}$, $\underline{\Gamma}_{s_i}$ and $\underline{C}_{s_i}$ (subscript s denotes the shaping filter) are $(t\times t)$, $(t\times s)$ and $(t\times r)$ matrices respectively, $\underline{x}_{d_i} \in R^t$, $\underline{y}_{d_i} \in R^r$, $E[\underline{w}_{d_i}] = 0$ and $E[\underline{w}_{d_i} \underline{w}_{d_j}^T] = \underline{W}_{d_i} \delta_{ij}$, $\underline{W}_{d_i} \ge 0$. At time i, it is assumed that the following measurements are possible.

$$\underline{z}_{d_i}(\ell) = \underline{y}_{d_{i-db+\ell}} + \underline{v}_{d_i}(\ell), \quad 0 \le \ell \le N_{\ell a}. \tag{2-5}$$

db is another measurement time delay.

Consequently, the following are given. $E[\underline{v}_{d_i}(\ell)] = 0$, $E[\underline{v}_{d_i}(k) \underline{v}_{d_j}^T(\ell)]$ $= \underline{V}_{d_i}(k,\ell)\delta_{ij}$ $(\ell = 0, \ldots, N_{\ell a};\ k = 0, \ldots, N_{\ell a})$, $\underline{V}_{d_i}(k,\ell) > 0$ for $k = \ell$, $\underline{V}_{d_i}(k,\ell) \ge 0$ for $k \ne \ell$, $E[\underline{x}_{d_k}] = \bar{\underline{x}}_{d_k}$ $(k = -db, \ldots, N_{\ell a})$, $E[(\underline{x}_{d_k} - \bar{\underline{x}}_{d_k})(\underline{x}_{d_\ell} - \bar{\underline{x}}_{d_\ell})^T]$ $= \underline{P}_{dd_{k,\ell}}$ $(k = -db, \ldots, N_{\ell a};\ \ell = -db, \ldots, N_{\ell a})$, $\underline{P}_{dd_{k,\ell}} \ge 0$, $E[\underline{v}_{d_i}(k) \underline{w}_{d_j}^T]$

†These have to be defined because of a delay.

ORIGINAL PAGE IS
OF POOR QUALITY

$$= E[\underline{v}_{d_1}(k)\underline{x}_{d_2}^T] = E[\underline{v}_{d_1}\underline{x}_{d_2}^T] = \underline{0}(k = 0,\ldots,N_{\ell a};\ \ell = -db,\ldots,N_{\ell a}).$$

Also it is assumed that $E[\underline{w}_i\underline{w}_{d_j}^T] = E[\underline{w}_i\underline{v}_{d_j}^T(m)] = E[\underline{v}_i\underline{w}_{d_j}^T] =$

$$= E[\underline{v}_i\underline{v}_{d_j}^T(m)] = E[\underline{x}_k\underline{x}_{d_\ell}^T] = E[\underline{x}_k\underline{v}_{d_j}^T] = E[\underline{x}_k\underline{v}_{d_j}^T(m)] = E[\underline{v}_i\underline{x}_{d_\ell}^T] =$$

$$E[\underline{v}_i\underline{x}_{d_\ell}^T] = \underline{0}\ (k = -da,\ldots,0;\ i = -db,\ldots,N_{\ell a};\ m = 0,\ldots,N_{\ell a}).$$

The objective is to find a control policy $\underline{u}_i$, which minimizes

$$J = E[\ \tfrac{1}{2}\ (\underline{C}_N^T\underline{x}_N - \underline{y}_{dN})^T\underline{Q}_N\ (\underline{C}_N^T\underline{x}_N - \underline{y}_{dN}) + \tfrac{1}{2}\sum_{i=0}^{N-1}\{(\underline{C}_i^T\underline{x}_i - \underline{y}_{di})^T\underline{Q}_i\ (\underline{C}_i^T\underline{x}_i - \underline{y}_{di}) + \underline{u}_i^T\underline{R}_i\underline{u}_i\ \}\ ] \tag{2-6}$$

where $\underline{R}_i > \underline{0}$, $\underline{Q}_i \geq \underline{0}$ and $E[\cdot]$ is the expectation taken over all underlying random quantities. Several remarks should be made at this point.

Remark 2-1: Note the difference between the preview control problem formulated here and the stochastic tracking problem. In case of the stochastic tracking problem the $\underline{y}_{d_i}$'s in (2-6) are <u>all deterministically</u> given a priori from <u>i=0 to i=N</u> while the system has the driving noise and the observation noise. In case of the preview problem, however, the information about the $\underline{y}_{d_i}$'s is given by the <u>noise-corrupted</u> measurement (2-5) and usually $N_{\ell a} < N$. Therefore, the preview control problem is more difficult than the tracking problem, and the following relation holds:

Preview Control Problem $\supset$ Stochastic Tracking Problem.

Remark 2-2: There are time delays da and db in measurement equations (2-2) and (2-5) respectively, and in case of manual control problems these respresent the time delay of the human controller.

Remark 2-3: Although the problem is formulated in discrete fashion, it can be a good approximation to the continuous problem if discretization is made small. And actually the manual preview control problem in this paper is not all discrete, and the model should be taken as the discrete approximation.

III. Solution of the Preview Control Problem

In this section, the preview control problem is transformed into the equivalent regulator problem. Then the solution can be easily obtained by dynamic programming.

It is easy to check that (2-1) and (2-2) are equivalent to

$$\underline{x}_{i+1}' = \begin{bmatrix} \underline{\xi}_{i+1}^1 \\ \vdots \\ \underline{\xi}_{i+1}^{da} \\ \hline \underline{z}_{i+1} \end{bmatrix} = \left[\begin{array}{cccc|c} \underline{0} & \underline{I} & \underline{0}\ldots & \underline{0} & \\ \underline{0} & \underline{0} & \underline{I}\ldots & \underline{0} & \underline{0} \\ \vdots & & & \vdots & \\ \underline{0} & \underline{0} & \underline{0}\ldots & \underline{0} & \underline{C}_i^T \\ \hline & \underline{0} & & & \underline{\Phi}_i \end{array}\right] \cdot \begin{bmatrix} \underline{\xi}_i^1 \\ \vdots \\ \underline{\xi}_i^{da} \\ \hline \underline{z}_i \end{bmatrix} + \begin{bmatrix} \underline{0} \\ \hline \underline{\Gamma}_i \end{bmatrix} \underline{u}_i + \begin{bmatrix} \underline{0} \\ \hline \underline{w}_i \end{bmatrix}$$

$$= \underline{\Phi}_i'\ \underline{x}_i' + \underline{\Gamma}_i'\ \underline{u}_i + \underline{w}_i', \qquad da > 0 \tag{3-1}$$

$$\underline{z}_i = [\ \underline{I}\ \underline{0}\ \ldots\ \underline{0}\ ]\ \underline{x}_i' + \underline{v}_i$$

$$= \underline{C}'^T\ \underline{x}_i' + \underline{v}_i, \qquad da > 0 \tag{3-2}$$

where $\underline{\xi}_i^j \in R^r (j=1,\ldots,da)$, $\underline{x}_i' \in R^{r \times d_1 + n}$ etc., $\underline{I}$ is an identity matrix, and all matrices have appropriate dimensions. $\underline{\xi}_i^j$'s are introduced here to handle the measurement time delay. For da = 0 (no time delay), just set $\underline{x}' = \underline{x}$, $\underline{\Phi}' = \underline{\Phi}$, $\underline{\Gamma}' = \underline{\Gamma}$, $\underline{w}' = \underline{w}$ and $\underline{C}' = \underline{C}$ in (3-1) and (3-2). Note that $E[\underline{w}_i']$, $E[\underline{w}_i'\underline{w}_j'^T]$, $E[\underline{x}_0']$ etc., can be all obtained from the quantities given in the previous section.

Also it can be checked that (2-3), (2-4) and (2-5) are equivalent to

$$\underline{y}_{d_{i+1}}' = \begin{bmatrix} \underline{g}_{i+1}^1 \\ \vdots \\ \underline{g}_{i+1}^{db} \\ \hline \underline{y}_{d_{i+1}} \end{bmatrix} = \left[\begin{array}{cccc|c} \underline{0} & \underline{I} & \underline{0}\ldots & \underline{0} & \\ \underline{0} & \underline{0} & \underline{I}\ldots & \underline{0} & \underline{0} \\ \vdots & & & \vdots & \\ \underline{0} & \underline{0} & \ldots\ldots & \underline{0} & \underline{I}\ \underline{0} \\ \hline & \underline{0} & & & \underline{\Phi}_{d_1} \end{array}\right] \cdot \begin{bmatrix} \underline{g}_i^1 \\ \vdots \\ \underline{g}_i^{db} \\ \hline \underline{y}_{d_i} \end{bmatrix} + \begin{bmatrix} \underline{0} \\ \hline \underline{\Gamma}_{d_1} \end{bmatrix} \underline{v}_{d_{i+N_{\ell a}}}$$

$$= \underline{\Phi}_{d_1}'\ \underline{y}_{d_1}' + \underline{\Gamma}_{d_1}'\ \underline{v}_{d_{i+N_{\ell a}}}, \qquad db > 0 \tag{3-3}$$

$$\underline{z}_{d_1} = \begin{bmatrix} \underline{z}_{d_1}(0) \\ \vdots \\ \underline{z}_{d_1}(N_{\ell a}) \end{bmatrix} = \begin{bmatrix} \underline{I} & & \underline{0} & \\ & \underline{I} & & \underline{0} \\ \underline{0} & & \ddots & \\ & & & \underline{I} \end{bmatrix} \cdot \begin{bmatrix} \underline{y}_{d_1}' \end{bmatrix} + \begin{bmatrix} \underline{v}_{d_1}(0) \\ \vdots \\ \underline{v}_{d_1}(N_{\ell a}) \end{bmatrix}$$

$$= \underline{C}_{d_1}^T\ \underline{y}_{d_1}' + \underline{v}_{d_1}', \qquad N_{\ell a} > 0 \tag{3-4}$$

with

$$Y_{d_i} = \begin{bmatrix} y_{d_i} \\ y_{d_{i+1}} \\ \vdots \\ y_{d_{i+N_{\ell a}-1}} \\ \hline z_{d_{i+N_{\ell a}}} \end{bmatrix}, \quad \Phi_{d_i} = \left[\begin{array}{cccc|c} 0 & I & 0 & \cdots & 0 \\ 0 & 0 & I & & \vdots \\ \vdots & & & & I \\ 0 & 0 & \cdots & & 0 \\ \hline & & 0 & & \end{array}\right. \left.\begin{array}{c} 0 \\ \vdots \\ \\ C_{s_{i+N_{\ell a}}}^T \\ \hline \Phi_{s_{i+N_{\ell a}}} \end{array}\right] \text{ and } \Gamma_i = \left[\begin{array}{c} 0 \\ \vdots \\ \\ \hline \Gamma_{s_{i+N_{\ell a}}} \end{array}\right] \quad \begin{matrix}(3\text{-}5)\\ \text{-}(3\text{-}7)\end{matrix}$$

where $v_i^j \in R^r$, $Y_{d_i} \in R^{N_{\ell a} \times r+t}$, $Z_{d_i} \in R^{(N_{\ell a}+1)\times r}$, $Y_{d_i}' \in R^{(N_{\ell a}+db)\times r+t}$ etc.

For db=0, set $Y_{d_i}' = Y_{d_i}$, $\Phi_{d_i}' = \Phi_{d_i}$ and $\Gamma_{d_i}' = \Gamma_{d_i}$. Furthermore, if $N_{\ell a} = 0$, set $Y_{d_i} = Z_{d_i}$, $\Phi_{d_i} = \Phi_{s_i}$, $\Gamma_{d_i} = \Gamma_{s_i}$ and $C_{d_i} = C_{s_i}$. Here again all statistics necessary to get a solution can be all defined from the quantities given in the previous section. One further assumption to be made is $V_i' > 0$ wher $E[v_{d_i}' v_{d_j}'^T] = V_i' \delta_{ij}$.

(3-1), (3-2), (3-3) and (3-4) can be combined into the following.

$$x_{i+1} = \begin{bmatrix} x_{i+1}' \\ Y_{d_{i+1}}' \end{bmatrix} = \begin{bmatrix} \Phi_i' & 0 \\ 0 & \Phi_{d_i}' \end{bmatrix} \begin{bmatrix} x_i' \\ Y_{d_i}' \end{bmatrix} + \begin{bmatrix} \Gamma_i' \\ 0 \end{bmatrix} u_i + \begin{bmatrix} w_i' \\ \Gamma_{d_i}' W_{d_{i+N_{\ell a}}} \end{bmatrix}$$

$$= \Phi_i x_i + \Gamma_i u_i + w \qquad (3\text{-}8)$$

$$z_i = \begin{bmatrix} C_i'^T & 0 \\ 0 & C_{d_i}^T \end{bmatrix} \begin{bmatrix} x_i' \\ Y_{d_i}' \end{bmatrix} + \begin{bmatrix} v_i \\ v_{d_i}' \end{bmatrix}$$

$$= C_i^T x_i + v_i \qquad (3\text{-}9)$$

where $x_i \in R^{(da+N_{\ell a}+db)\times r + n + t}$, $z_i \in R^{(2+N_{\ell a})\times r}$ etc., $E[x_0] = \bar{x}_0$, $E[(x_0 - \bar{x}_0)(x_0 - \bar{x}_0)^T] = P_0$, $E[w_i] = E[v_i] = 0$, $E[w_i w_j^T] = \begin{bmatrix} W_i & 0 \\ 0 & \Gamma_{d_i}' W_{d_{i+N_{\ell a}}} \Gamma_{d_i}'^T \end{bmatrix} \delta_{ij}$ $= W_i \delta_{ij}$, $W_i \geq 0$, $E[v_i v_j^T] = \begin{bmatrix} V_i & 0 \\ 0 & V_{d_i}' \end{bmatrix} \delta_{ij} = V_i \delta_{ij}$, $V_i > 0$, $E[x_0 w_j^T] = E[x_0 v_j^T]$ $= E[w_i v_j^T] = 0$ are all available from the quantities given so far.

With this new variable x, (2-6) can be written as

$$J = E[\, \tfrac{1}{2} x_N^T Q_N x_N + \tfrac{1}{2} \sum_{i=0}^{N-1} (x_i^T Q_i x_i + u_i^T R_i u_i) \,] \qquad (3\text{-}10)$$

where

$$Q_i = \begin{bmatrix} 0 & 0 & 0 & 0 \\ 0 & Q_{xx_i} & 0 & -Q_{xd_i} \\ 0 & 0 & 0 & 0 \\ 0 & -Q_{xd_i}^T & 0 & Q_{dd_i} \end{bmatrix} \begin{matrix} \}r\times da \\ \}n \\ \}r\times db \\ \}N_{\ell a}\times r + t \end{matrix}$$

with

$$Q_{xx_i} = C_i Q_i C_i^T$$

$$Q_{xd_i} = \begin{cases} [\, C_i Q_i \mid 0 \mid 0 \mid \ldots \mid 0 \,] & \text{for } N_{\ell a} > 0 \\ C_i Q_i C_{s_i}^T & \text{for } N_{\ell a} = 0 \end{cases}$$

$$Q_{dd_i} = \begin{cases} \left[\begin{array}{c|c} Q_i & 0 \\ \hline 0 & 0 \end{array}\right] \begin{matrix} \}r \\ \}(N_{\ell a}-1)\times r + t \end{matrix} & \text{for } N_{\ell a} > 0 \\ C_{s_i} Q_i C_{s_i}^T & \text{for } N_{\ell a} = 0 \end{cases}$$

Then (3-8), (3-9) and (3-10) represent the usual LQG (Linear-Quadratic-Gaussian) problem, and it is well known that the feedback type solution is obtained by the dynamic programming. (For example, see Refs. 7 or 8.)

The solution is as follows. In the following, $\hat{x}_{i|j}$ denotes the estimator of x_i with the measurement up to time j.

$$u_i^{opt} = - G_i \hat{x}_{i|i} \qquad (3\text{-}11)$$

$$\hat{x}_{i|i} = \hat{x}_{i|i-1} + K_i (z_i - C_i^T \hat{x}_{i|i-1}) \qquad (3\text{-}12)$$

$$\hat{x}_{i+1|i} = \Phi_i \hat{x}_{i|i} + \Gamma_i u_i \,, \quad \hat{x}_{0|0} = \bar{x}_0 \qquad (3\text{-}13)$$

where

$$G_i = (\Gamma_i^T S_{i+1} \Gamma_i + R_i)^{-1} \Gamma_i^T S_{i+1} \Phi_i \qquad (3\text{-}14)$$

$$K_i = P_i C_i (C_i^T P_i C_i + V_i)^{-1} = P_i C_i V_i^{-1} \qquad (3\text{-}15)$$

and

$$S_i = \Phi_i^T P_{i+1} \Phi_i + Q_i \,, \quad S_N = Q_N \qquad (3\text{-}16)$$

$$\underline{M}_{i+1} = \underline{S}_{i+1} - \underline{S}_{i+1}\,\underline{\Gamma}_i(\underline{\Gamma}_i^T\,\underline{S}_{i+1}\,\underline{\Gamma}_i + \underline{R}_i)^{-1}\underline{\Gamma}_i^T\,\underline{S}_{i+1} \tag{3-17}$$

$$\underline{N}_{i+1} = \underline{E}_i\,\underline{P}_i\,\underline{E}_i^T + \underline{W}_i \tag{3-18}$$

$$\underline{P}_i = \underline{N}_i - \underline{N}_i\,\underline{C}_i(\,\underline{C}_i^T\,\underline{N}_i\,\underline{C}_i + \underline{V}_i\,)^{-1}\underline{C}_i^T\,\underline{N}_i \tag{3-19}$$

$\underline{P}_0$: given

Noting the forms of $\underline{\Phi}$, $\underline{\Gamma}$, $\underline{V}$, $\underline{W}$ etc., after a lot of manupulation (3-11)-(3-19) can be shown to be equivalent to the following set of equations.

$$\underline{u}_i^{opt} = -\,[\,\underline{G}_{xi} \,\vdots\, \underline{G}_{di}\,]\begin{bmatrix}\underline{\hat{x}}_{i|i}\\ \underline{\hat{y}}_{di|i}\end{bmatrix} \tag{3-20}$$

where

$$\underline{G}_{xi} = (\,\underline{\Gamma}_i^T\,\underline{S}_{xx_{i+1}}\,\underline{\Gamma}_i + \underline{R}_i\,)^{-1}\,\underline{\Gamma}_i^T\,\underline{S}_{xx_{i+1}}\,\underline{\Phi}_i \tag{3-21}$$

$$\underline{G}_{di} = (\,\underline{\Gamma}_i^T\,\underline{S}_{xx_{i+1}}\,\underline{\Gamma}_i + \underline{R}_i\,)^{-1}\,\underline{\Gamma}_i^T\,\underline{S}_{xd_{i+1}}\,\underline{\Phi}_{di} \tag{3-22}$$

with

$$\underline{S}_{xx_i} = \underline{\Phi}_i^T\,\underline{M}_{xx_{i+1}}\,\underline{\Phi}_i + \underline{Q}_{xx_i}\ ,\quad \underline{S}_{xx_N} = \underline{Q}_{xx_N} \tag{3-23}$$

$$\underline{M}_{xx_{i+1}} = \underline{S}_{xx_{i+1}} - \underline{S}_{xx_{i+1}}\,\underline{\Gamma}_i\,(\,\underline{\Gamma}_i^T\,\underline{S}_{xx_{i+1}}\,\underline{\Gamma}_i + \underline{R}_i\,)^{-1}\underline{\Gamma}_i^T\,\underline{S}_{xx_{i+1}} \tag{3-24}$$

$$\underline{S}_{xd_i} = \underline{\Phi}_i^T\,\underline{M}_{xd_{i+1}}\,\underline{\Phi}_{di} - \underline{Q}_{xd_i}\ ,\quad \underline{S}_{xd_N} = -\underline{Q}_{xd_N} \tag{3-25}$$

$$\underline{M}_{xd_{i+1}} = \underline{S}_{xd_{i+1}} - \underline{S}_{xx_{i+1}}\,\underline{\Gamma}_i\,(\,\underline{\Gamma}_i^T\,\underline{S}_{xx_{i+1}}\,\underline{\Gamma}_i + \underline{R}_i\,)^{-1}\underline{\Gamma}_i^T\,\underline{S}_{xd_{i+1}} \tag{3-26}$$

$$\underline{S}_{dd_i} = \underline{\Phi}_{di}^T\,\underline{M}_{dd_{i+1}}\,\underline{\Phi}_{di} + \underline{Q}_{dd_i}\ ,\quad \underline{S}_{dd_N} = \underline{Q}_{dd_N} \tag{3-27}$$

$$\underline{M}_{dd_{i+1}} = \underline{S}_{dd_{i+1}} - \underline{S}_{xd_{i+1}}^T\,\underline{\Gamma}_i\,(\,\underline{\Gamma}_i^T\,\underline{S}_{xx_{i+1}}\,\underline{\Gamma}_i + \underline{R}_i\,)^{-1}\underline{\Gamma}_i^T\,\underline{S}_{xd_{i+1}} \tag{3-28}$$

$\underline{\hat{x}}_{i|i}$ can be found from $\underline{\hat{x}}'_{i|i}$ which satisfies

$$\underline{\hat{x}}'_{i|i} = \underline{\hat{x}}'_{i|i-1} + \underline{K}'_i\,(\,\underline{z}_i - \underline{C}'^T_i\,\underline{\hat{x}}'_{i|i-1}\,)\ ,\quad \underline{\hat{x}}'_{0|0} = \underline{\hat{x}}'_0 \tag{3-29}$$

$$\underline{\hat{x}}'_{i+1|i} = \underline{\Phi}'_i\,\underline{\hat{x}}'_{i|i} + \underline{\Gamma}'_i\,\underline{u}_i \tag{3-30}$$

$$\underline{K}'_i = \underline{P}_{xx'_i}\,\underline{C}'_i\,\underline{V}_i^{-1} \tag{3-31}$$

$$\underline{N}_{xx'_{i+1}} = \underline{\Phi}'_i\,\underline{P}_{xx'_i}\,\underline{\Phi}'^T_i + \underline{W}'_i \tag{3-32}$$

$$\underline{P}_{xx'_i} = \underline{N}_{xx'_i} - \underline{N}_{xx'_i}\,\underline{C}'_i\,(\,\underline{C}'^T_i\,\underline{N}_{xx'_i}\,\underline{C}'_i + \underline{V}_i\,)^{-1}\underline{C}'^T_i\,\underline{N}_{xx'_i} \tag{3-33}$$

$\underline{P}_{xx'_0}$: given

where

$$\underline{\hat{x}}'_{i|i} = \begin{bmatrix}\hat{x}^1_{i|i}\\ \vdots\\ \hat{x}^{da}_{i|i}\\ \hat{z}_{i|i}\end{bmatrix}\ \text{etc.}$$

$\underline{\hat{y}}_{di|i}$ can be found from $\underline{\hat{y}}'_{di|i}$ which satisfies

$$\underline{\hat{y}}'_{di|i} = \underline{\hat{y}}'_{di|i-1} + \underline{K}'_{di}\,(\,\underline{z}_{di} - \underline{C}'^T_{di}\,\underline{\hat{y}}'_{di|i-1}\,)\ ,\quad \underline{\hat{y}}_{d0|0} = \underline{\hat{y}}'_{d0} \tag{3-34}$$

$$\underline{\hat{y}}'_{di+1|i} = \underline{\Phi}'_{di}\,\underline{\hat{y}}'_{di|i} \tag{3-35}$$

$$\underline{K}'_{di} = \underline{P}_{dd'_i}\,\underline{C}_{di}\,\underline{V}_{di}^{-1} \tag{3-36}$$

$$\underline{N}_{dd'_{i+1}} = \underline{\Phi}'_{di}\,\underline{P}_{dd'_i}\,\underline{\Phi}'^T_{di} + \underline{W}'_{di} \tag{3-37}$$

$$\underline{P}_{dd'_i} = \underline{N}_{dd'_i} - \underline{N}_{dd'_i}\,\underline{C}_{di}\,(\,\underline{C}_{di}^T\,\underline{N}_{dd'_i}\,\underline{C}_{di} + \underline{V}_{di}\,)^{-1}\underline{C}_{di}^T\,\underline{N}_{dd'_i} \tag{3-38}$$

$\underline{P}_{dd'_0}$: given

where

$$\underline{\hat{y}}'_{di|i} = \begin{bmatrix}\hat{y}^1_{di|i}\\ \vdots\\ \hat{y}^{db}_{di|i}\\ \hat{z}_{di|i}\end{bmatrix}\ \text{etc.}$$

The following remarks are appropriate here.

Remark 3-1: (3-20) - (3-26) show that the control gains do not depend on the time delay. The estimators $\hat{x}_{i|i}$ and $\hat{y}_{d_{i|i}}$, however, are affected by the time delay.

Remark 3-2: $\underline{S}_{dd}$ and $\underline{\Pi}_{dd}$ in (3-27) and (3-28) do not have to be calculated in deciding the closed loop structure. However they are useful in getting the average cost.

Remark 3-3: Transition from (3-15), (3-18) and (3-19) to (3-29)-(3-38) shows that the Kalman filter for (3-8) and (3-9) can be separated into two; one for the system given by (3-1) and (3-2) and the other for the desired trajectory given by (3-3) and (3-4). This "separation" property follows from the fact that the stochastic quantities in (3-1) and (3-2) are uncorrelated from those in (3-3) and (3-4).

In many cases including the manual preview control experiment in this paper, we are interested in the steady state behaviour of the preview control system. Namely, $\underline{\Phi}_i$, $\underline{\Gamma}_i$, $\underline{W}_i$, $\underline{V}_i$, $\underline{\Phi}_{d_i}$, ... are all time invariant, and $N \to \infty$. In this case, the cost function to be looked at is

$$J = E\left[\frac{1}{2} \underline{x}^T \underline{Q} \underline{x} + \frac{1}{2} \underline{u}^T \underline{R} \underline{u} \right]$$

$$= E\left[\frac{1}{2} (\underline{C}^T \underline{x} - y_d)^T \underline{Q} (\underline{C}^T \underline{x} - y_d) + \frac{1}{2} \underline{u}^T \underline{R} \underline{u} \right] \qquad (3\text{-}39)$$

For this problem, the control gains can be determined once the steady state solution of (3-23) - (3-26) are obtained. Also the Kalman filter gains are determined by the steady state solution of (3-32), (3-33), (3-37) and (3-38). Moreover, in this case the filter equations can be simplified giving a more understandable form. The filter for the state of the system becomes the series connection of the Kalman filter for the delayed state $\underline{x}_{i-da}$ and the predictor for $\underline{x}_i$ based on $\hat{\underline{x}}_{i-da|i}$.

$$\hat{\underline{x}}_{i-da|i} = \hat{\underline{x}}_{i-da|i-1} + \underline{K}_x (\underline{z}_i - \underline{C}^T \hat{\underline{x}}_{i-da|i-1}) \qquad (3\text{-}40)$$

$$\hat{\underline{x}}_{i-da+1|i} = \underline{\Phi} \hat{\underline{x}}_{i-da|i} + \underline{\Gamma} \underline{u}_{i-da} \qquad (3\text{-}41)$$

$$\underline{K}_x = \underline{P}_{xx} \underline{C} \underline{V}^{-1} \qquad (3\text{-}42)$$

$$\underline{N}_{xx} = \underline{\Phi} \underline{P}_{xx} \underline{\Phi}^T + \underline{W} \qquad (3\text{-}43)$$

$$\underline{P}_{xx} = \underline{N}_{xx} - \underline{N}_{xx} \underline{C} (\underline{C}^T \underline{N}_{xx} \underline{C} + \underline{V})^{-1} \underline{C}^T \underline{N}_{xx} \qquad (3\text{-}44)$$

$$\hat{\underline{x}}_{i|i} = \hat{\underline{x}}_{i|i-1} + (\underline{\Phi})^{da} \underline{K}_x (\underline{z}_i - \underline{C}^T \hat{\underline{x}}_{i-da|i-1})$$

$$= \hat{\underline{x}}_{i|i-1} + (\underline{\Phi})^{da} (\hat{\underline{x}}_{i-da|i} - \hat{\underline{x}}_{i-da|i-1}) \qquad (3\text{-}45)$$

$$\hat{\underline{x}}_{i+1|i} = \underline{\Phi} \hat{\underline{x}}_{i|i} + \underline{\Gamma} \underline{u}_i \qquad (3\text{-}46)$$

It can be shown that (3-40) - (3-46) represent the discrete version of the estimator for $\underline{x}$ derived by Kleinman[9] for the continuous case.

The same thing can be done for the filter for the desired trajectory.

$$\hat{y}_{d_{i-db|i}} = \hat{y}_{d_{i-db|i-1}} + \underline{K}_d (\underline{z}_d - \underline{C}_d^T \hat{y}_{d_{i-db|i-1}}) \qquad (3\text{-}47)$$

$$\hat{y}_{d_{i-db+1|i}} = \underline{\Phi}_d \hat{y}_{d_{i-db|i}} \qquad (3\text{-}48)$$

$$\underline{K}_d = \underline{P}_{dd} \underline{C}_d \underline{V}_d^{-1} \qquad (3\text{-}49)$$

$$\underline{N}_{dd} = \underline{\Phi}_d \underline{P}_{dd} \underline{\Phi}_d^T + \underline{W}_d \qquad (3\text{-}50)$$

$$\underline{P}_{dd} = \underline{N}_{dd} - \underline{N}_{dd} \underline{C}_d (\underline{C}_d^T \underline{N}_{dd} \underline{C}_d + \underline{V}_d)^{-1} \underline{C}_d^T \underline{N}_{dd} \qquad (3\text{-}51)$$

$$\hat{y}_{d_{i|i}} = \hat{y}_{d_{i|i-1}} + (\underline{\Phi}_d)^{db} \underline{K}_d (\underline{z}_{d_i} - \underline{C}_d^T \hat{y}_{d_{i-db|i-1}})$$

$$= \hat{y}_{d_{i|i-1}} + (\underline{\Phi}_d)^{db} (\hat{y}_{d_{i-db|i}} - \hat{y}_{d_{i-db|i-1}}) \qquad (3\text{-}52)$$

$$\hat{y}_{d_{i+1|i}} = \underline{\Phi}_d \hat{y}_{d_{i|i}} \qquad (3\text{-}53)$$

The following expression can be derived, and it is useful to see the average behaviour of the total system.

$$E[(\underline{C}^T \underline{x} - y_d)^T \underline{Q} (\underline{C}^T \underline{x} - y_d)] = Tr[\underline{Q}_{xx} \underline{X}_{xx}] + Tr[\underline{Q}_{dd} \underline{X}_{dd}]$$
$$- 2\, Tr[\underline{Q}_{xd}^T \underline{X}_{xd}] \qquad (3\text{-}54)$$

$$E[\underline{u}^T \underline{R} \underline{u}] = Tr[\underline{Q}_x^T \underline{Q}_x (\underline{X}_{xx} - \underline{P}_{xx}^-)] + 2\, Tr[\underline{Q}_d^T \underline{Q}_x \underline{X}_{xd}]$$
$$+ Tr[\underline{Q}_d^T \underline{Q}_d (\underline{X}_{dd} - \underline{P}_{dd}^-)] \qquad (3\text{-}55)$$

[illegible] note the trace [illegible]tion and $\underline{P}^{\sim}_{xx}$, $\underline{P}^{\sim}_{dd}$, $\underline{X}_{xx}$, $\underline{X}_{xd}$, and $\underline{X}_{dd}$ can be obtained by the following relations:

$$\underline{P}^{\sim}_{xx} = (\underline{\Phi})^{da}\, \underline{P}_{xx}\, (\underline{\Phi}^T)^{da} + \sum_{i=1}^{da} (\underline{\Phi})^{da-i}\, \underline{W}\, (\underline{\Phi}^T)^{da-i} \tag{3-56}$$

$$\underline{P}^{\sim}_{dd} = (\underline{\Phi}_d)^{db}\, \underline{P}_{dd}\, (\underline{\Phi}_d^T)^{db} + \sum_{i=1}^{db} (\underline{\Phi}_d)^{db-i} \underline{\Gamma}_d\, \underline{W}_d\, \underline{\Gamma}_d^T\, (\underline{\Phi}_d^T)^{db-i} \tag{3-57}$$

$$\underline{X}_{dd} = \underline{\Phi}_d\, \underline{X}_{dd}\, \underline{\Phi}_d^T + \underline{\Gamma}_d\, \underline{W}_d\, \underline{\Gamma}_d^T \tag{3-58}$$

$$\underline{X}_{xd} = (\underline{\Phi} - \underline{\Gamma}\, \underline{G}_x)\, \underline{X}_{xd} \underline{\Phi}_d^T - \underline{\Gamma}\, \underline{G}_d\, \underline{X}_{dd}\, \underline{\Phi}_d^T \tag{3-59}$$

$$\begin{aligned} \underline{X}_{xx} = {} & (\underline{\Phi} - \underline{\Gamma}\, \underline{G}_x)(\underline{X}_{xx} - \underline{P}^{\sim}_{xx})(\underline{\Phi} - \underline{\Gamma}\, \underline{G}_x)^T - \underline{\Gamma}\, \underline{G}_d\, \underline{X}_{xd}^T\, (\underline{\Phi} - \underline{\Gamma}\, \underline{G}_x)^T \\ & - (\underline{\Phi} - \underline{\Gamma}\, \underline{G}_x)\, \underline{X}_{xd}\, \underline{G}_d^T\, \underline{\Gamma}^T + \underline{\Gamma}\, \underline{G}_d\, (\underline{X}_{dd} - \underline{P}^{\sim}_{dd})\, \underline{G}_d^T\, \underline{\Gamma}^T \\ & + \underline{\Phi}\, \underline{P}^{\sim}_{xx}\, \underline{\Phi}^T + \underline{W} \end{aligned} \tag{3-60}$$

Fig. 3-1 shows the structure of the optimal system. A more detailed illustration in case of a manual control problem will be given later.

To look at what can be predicted by the model let us consider a very simple case. A plant is a pure integrator, and the bandwidth of a desired trajectory is 4.0 rad/sec. First we assume that v, v_d and w do not exist, time delays are zero and the state variables of the plant and the shaping filter are measurable. Then optimal control is determined by using $\underline{x}$ and $\underline{Y}_d$ instead of $\underline{x}$ and $\underline{\hat{Y}}_d$ (no need to have estimators). Fig. 3-2 shows the effect of preview on $E[e^2]$ and cost J for this case. We can see that the preview beyond certain point (~10 in this example) does not have much effect on J or $E[e^2]$. To see the effect of noise, $W = 0.0007$, $V = V_d(0,0) = 0.35$, $V_d(\ell,\ell) = 0.1\ell^2 + 0.35$ and $V_d(k,\ell) = 0(k \neq \ell)$ were assumed and $E[e^2]$ and J were calculated. We can see that the improvement by having preview is more clear when noise exists. In the graph the effect of measurement time delays (da=db=3) is also shown. We can see that the preview also helps to make the increase in $E[e^2]$ or J due to time delays small. These are all structural properties of optimal preview control systems, and similar effects can be expected in manual preview experiments.

IV. Experiment

The experiment similar to one by Kaid and Drewell[10] was performed to

look at the validity of the proposed model qualitatively. It was the single degree of freedom manual preview experiment, and Fig. 5-1 shows the configuration.

In the figure, m (not u) is used to indicate the input to the controlled system. In the next section, the reason will be given. As shown in the figure, both digital and analog computers were used. The digital computer was used for three purposes: a desired trajectory (random signal) generator, a shift register for storing present and future desired outputs, and a data acquisition system. Everything was done on line, which determined the time in which the computer could finish one cycle. The input and the output of the controlled system were sampled once each cycle. In the following, each component in the figure is explained in detail.

Display: A CRT display with 5" diameter was used. The desired trajectory was displayed as a sequence of dots (100 pts. at the maximum) allowing subjects to have preview from 0 sec. up to about 2.6 sec. The preview length was changed by changing the number of dots which appeared on the display. The trajectory moved from right to left on the screen, and it was adjusted so that the length of the trajectory became about 2 1/4" maximum preview case (shorter for less preview) and the range in vertical direction became about 2".

The output of the controlled system was displayed by the dot on the same vertical line as the lefthand side of the desired trajectory, and it was intensified stronger than the desired trajectory so that it was easily distinguished from the desired trajectory. The distance between subject and display was about 20".

Desired Trajectory: The desired trajectory was a random signal generated by the digital computer. The second order digital filter was driven by Gaussian white noise which was also generated by the digital computer on line. By changing the coefficients of the digital filter, three kinds of trajectories with different bandwidth (ω_d = 1.5, 2.5, and 4.0 rad/sec.) were generated.

Controlled System: Three kinds of plants were implemented on the analog computer. They were a pure integrator ($\frac{1}{s}$), a damped first order system ($\frac{1}{s+2}$), and a double integrator ($\frac{1}{s^2}$).

Joystick: The joystick used was a Model 435 Hand Control by Measurement System INC. This stick enabled the subject to apply control just by the wrist or finger motion. The stick gain was different for each plant, but was the same for all subjects and all trajectories.

Data Acquisition: $\bar{e}$, $\overline{e^2}$, $\bar{m}$ and $\overline{m^2}$ were calculated by the digital computer on line where $\bar{\ }$ indicates the time average of [illegible]. y, y_d, e and m were also recorded by the chart recorder.

Three graduate students at MIT served as subjects. Each subject tried all combinations of three plants and three random signals. Subjects had enough training for each combination. 0, 3, 12, 25, 50, and 100 pt. preview cases were conducted for each combination with a few exceptions. Each experimental run was three minutes following a 30 second warming-up period.

Figs. 4-2(a) and (b) show the data from experiments normalized by $\bar{v}_d^2$. Before going into the analysis by the model, several points are worth mentioning.

1) In almost all cases, preview beyond 0.7 sec ahead did not make essential improvements in either e^2 or m^2.

2) Subjects fell into one of the following two modes of looking at the display with non zero preview.

i) Mountain range mode: This was a usual mode, in which subjects felt that they were looking at a mountain range from the window of a train. In this mode, subjects did not have difficulty in tracking the trajectory.

ii) Flag mode: Once subjects fell in this mode, they took the moving wave form as a flag flapping in the air. This happened during those experimental runs with a particular combination of the preview length and the trajectory's bandwidth degrading the performance.

3) The output of the system was displayed by the dot. This confused subjects a little at zero preview in which case they were looking at two dots in the screen, although the brightness was controlled giving different intensity to two dots.

4) Learning effect still exists in the data. Subject 1 did the experiment in the order of $\frac{1}{s}$, $\frac{1}{s+2}$ and $\frac{1}{s^2}$. Subject 2 did in the order of $\frac{1}{s+2}$, $\frac{1}{s^2}$ and $\frac{1}{s}$. Subject 3 did in the order of $\frac{1}{s^2}$, $\frac{1}{s+2}$ and $\frac{1}{s}$.

V. Analysis of Data and Discussion

The result for the steady state discussed at the end of Section III can be used to analyze experiment where the plant is single input and single output. Fig. 5-1 represents the manual preview control model used in the analysis.

Note that in (2-1) $w_i = \Gamma w_{m_i}$ and that m in the experiment actually represents $u+w_m$ where w_{m_i} is the motor noise with $E[w_{m_i}] = 0$ and $E[w_{m_i} w_{m_j}] = W_m \delta_{ij}$. Then it is easy to see that

$$E[m^2] = E[u^2] + W_m \tag{5-1}$$

The analysis of the experiment using this model was so far made for the case when the plant is a pure integrator.

The difficulties in fitting the data by the present preview model are that the model has too many parameters, and that the dimension of Kalman filter equation for the desired trajectory becomes larger as the preview length increases. The following procedure was used in analysis.

First all equations including the plant were written down in the discrete form with $\Delta t = 0.0265$, which was supposed to be small enough to approximate the continuous part in the experiment and also was equal to the one computer cycle making it possible to maintain the discrete part in the experiment in the same form.

Time delays da and db were set equal to d, and it was varied from 0 to 7, or equivalently from 0 sec. to about 0.186 sec.

As for the determination of the strength of motor noise w_m and observation noise v, we followed Kleinman et al to get a rough idea. Since their formulas were for a continuous system, some modification was necessary in case of a discrete system. After necessary modification,

$$W_m = E[w_m^2] \sim \frac{\pi \times P_m}{0.0265} \times E[u^2] \tag{5-2}$$

$$V_y = E[v^2] \sim \frac{\pi \times P_y}{0.0265} \times E[e^2] \tag{5-3}$$

($P_m \sim 0.003$, $P_y \sim 0.01$ were recommended by Kleinman et al.)

The determination of $\underline{V}_d$ was the most difficult task. There was no available data in the past for nonzero preview cases, so it was decided to simplify $\underline{V}_d$ as much as possible. The first assumption made was

$$E[v_{d_i}(\ell) v_{d_j}(k)] = V_d(\ell) \delta_{\ell k} \delta_{ij} \tag{5-4}$$

This choice decreased the number of parameters, but still it was not clear how $V_{d_i}(\ell)$ changes with ℓ. $V_d(\ell)$ could even have different values for different preview length. Since there was almost no doubt about setting $V_d = V$ for zero preview case, we set $B \triangleq V_d = V$ for zero preview case. Based on this, the form $V_d(\ell) = A\ell^2 + B$ was assumed for the general case and A was changed to fit data. This form of $V_d(\ell)$ is not unreasonable since as a dot is displayed further apart from the dot representing the output of the system both errors in vertical sense and

horizontal [illegible] increase and the variance of the latter is considered to be proportional to the square of the distance between two dots.

Several values of R were tried and $E[e^2]$ and $E[u^2]$ were calculated by (3-53) and (3-54). These results together with (5-1) were compared to the experimental data.

Table 5-1 shows the values of parameters which gave us a good fitting. We do not claim that Table 5-1 shows the best or unique fitting. However, it shows qualitatively that the proposed model is reasonable, and it also explains what could be happening in manual preview control.

1) One notable thing is that the time delay in the model is kept to the same value for all preview cases. This is not unrealistic. Especially, it is rather hard to believe that the time delay associated with the output of the plant becomes smaller as the preview length increases, since the new information from looking ahead is not about the plant but about the trajectory. The model demonstrates that the improvement in performance can be actually done without changing the time delay.

2) The weighting R decreases as the preview length increases. This implies that the bandwidth of the loop composed of the plant and the subject increases as the preview length increases, since a small R implies large feedback gains in general.

3) W_m, V, etc. in the table are larger than the values suggested by Kleinman et al. For zero preview case, one reason is supposed to be the nature of the display used in the experiment, which was mentioned earlier.

4) Fitting was not done for the large (25 pt. or (0.7 sec)) preview cases because of the increase of the dimension of Kalman Filters. This does not imply that the computation is impossible. But it takes a very large amount of computational time. It was mentioned before that e^2 and m^2 were not improved essentially by the preview beyond 0.7 sec. We can expect that the same kind of thing will be observed in the model if parameters are slected properly. Basically there are two reasons for this. The first reason is that human can not make the bandwidth of the loop infinite, which implies that R has some lower bound. The second reason is that in large preview cases the desired trajectory seems to be divided into two parts if we assume that human does not move his eyes left and right; one is a foveal region and the other is a peripheral region. The neighborhood of the vertical line where the output of the plant is displayed is the foveal region and the rest is the peripheral region. The observation noise for the peripheral region is supposed to be much larger than that for the foveal region and there must be some point in the peripheral region beyond which subject cannot get any essential information. This implies that there exists some limit in the quality of the estimator for the desired trajectory. If these are true, $E[e^2]$ and $E[m^2]$ will be also lower bounded in the model.

VI. Conclusion and Further Research

In this paper, a model was developed for the preview control problem using the discrete stochastic control theory. Theoretically it would be interesting to extend the present theory to continuous problems. One way to solve such problems would be to take the limit of the present solution for the discrete system.

A manual preview control experiment was performed, and it was shown that the proposed model could explain the experimental data. It would also be interesting to give the frequency domain interpretation to the developed model. Intuitively speaking, it can be expected that as the preview length increases $Y(j\omega)/Y_d(j\omega)\to 1$ for the frequency ω lower than the bandwidth of the closed loop part of the total system.

The display used in the experiment brought in some problem confusing subjects. Apart from the theory, the design of better preview display would be interesting.

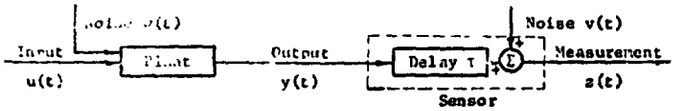

Fig. 2-1 System to be considered

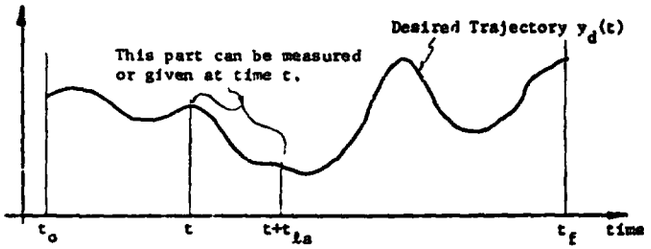

Fig. 2-2 Desired Trajectory

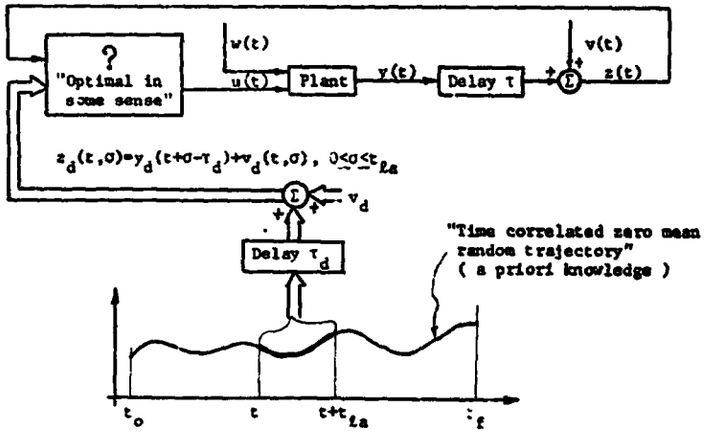

Fig. 2-3 Preview Control Problem

ORIGINAL PAGE IS
OF POOR QUALITY

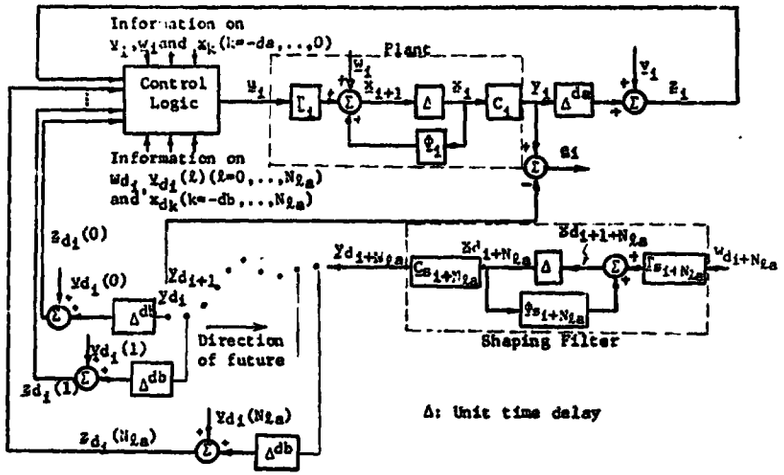

Fig. 2-4 Relation between Plant, Shaping Filter and Subscript

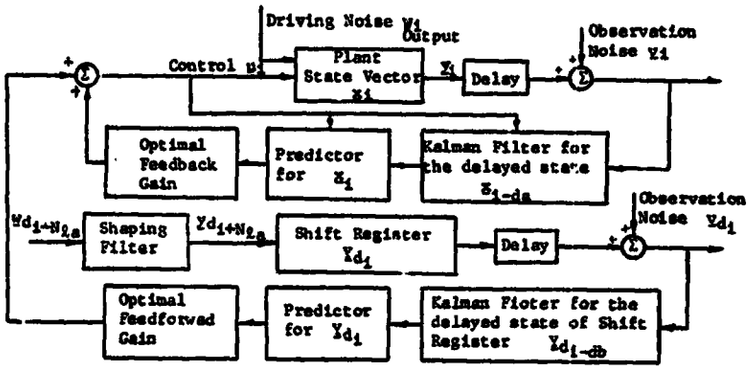

Fig. 3-1 Structure of the Optimal System

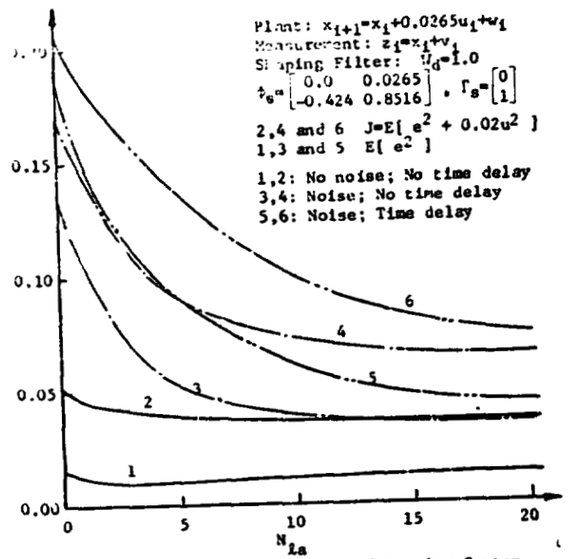

Fig. 3-2 Structual Properties of Preview System

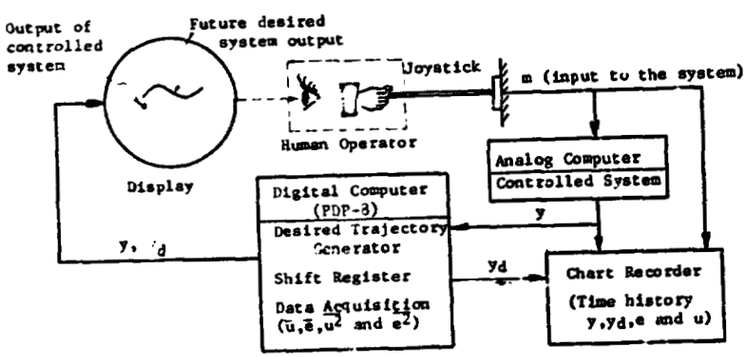

Fig. 4-1 Configuration of Manual Preview Experiment

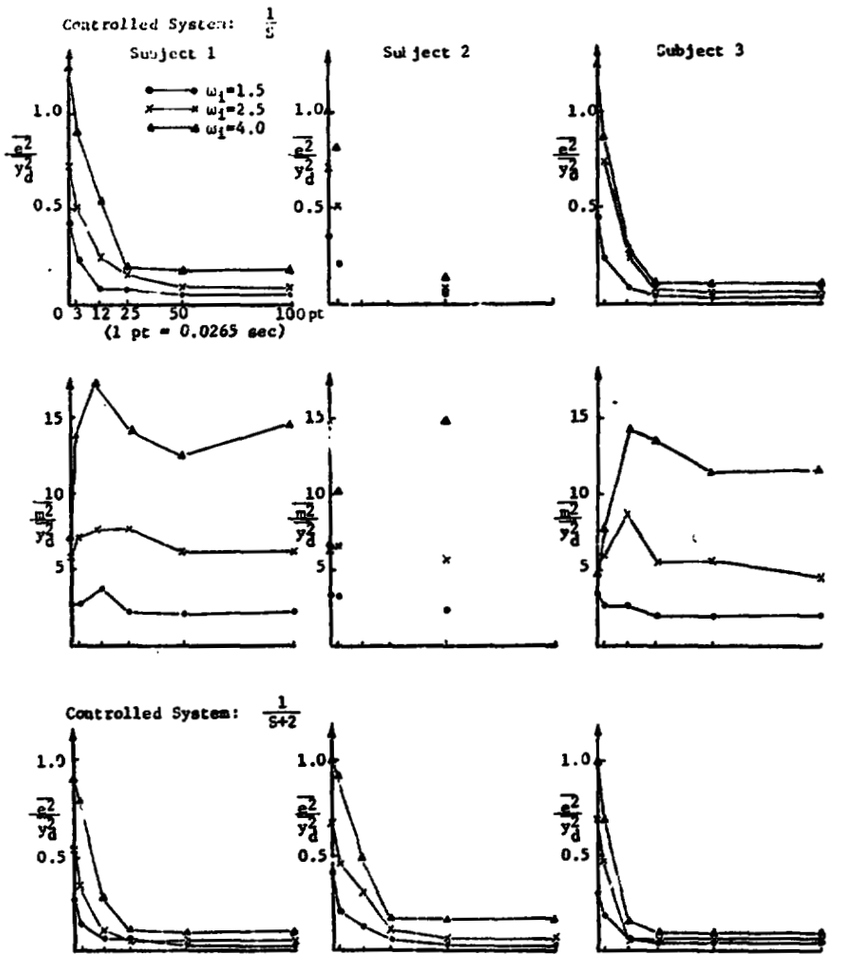

Fig. 4-2-a Experimental Results

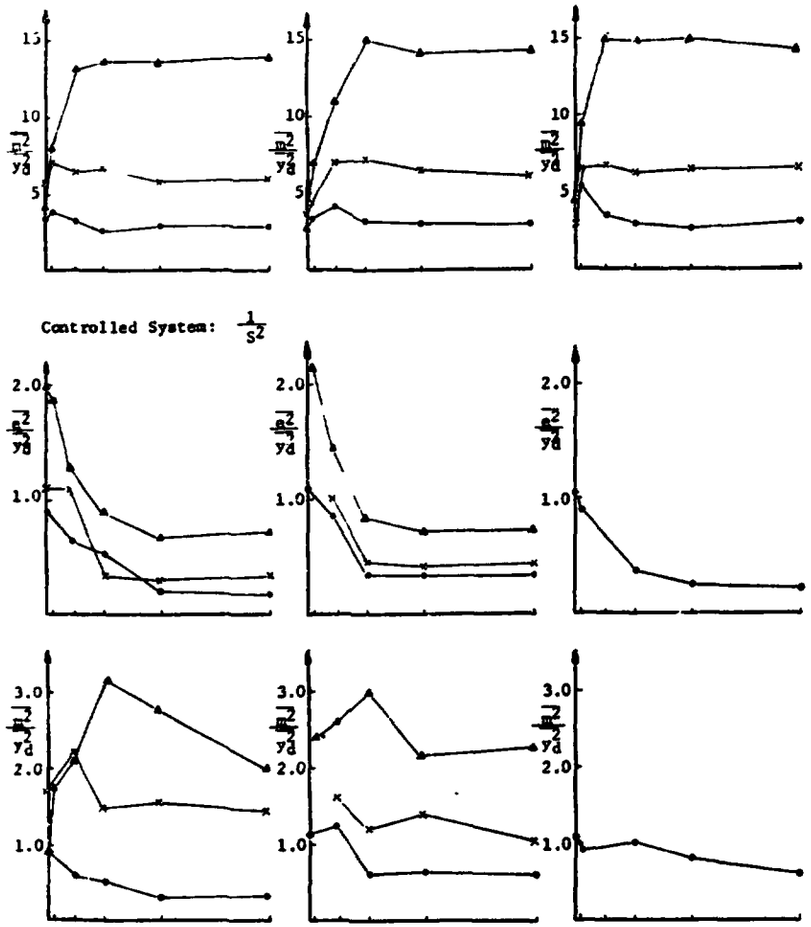

Fig. 4-2-b Experimentil Results

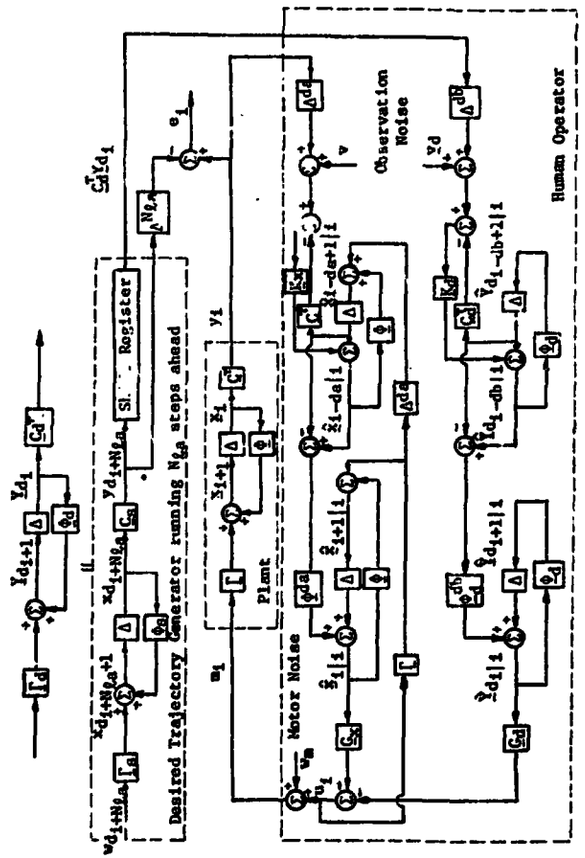

Δ: Unit Time Delay

Fig. 5-1 Manual Preview Contro' Model

References

1. Sheridan, T.B., "Three Models of Preview Control", IEEE Trans. on Human Factors in Electronics, Vol. HFE-7, No.2, June 1966.
2. Bender, E.K., "Optimum Linear Preview Control with Application to Vehicle Suspensions", Trans. of ASME, Journal of Basic Engineering, Vol. 90, No. 2, June 1968.
3. Hayase, H. and Ichikawa, K., "Optimal Servosystem Utilizing Future Value of Desired Function", J. of SICE, Vol. 5, No.1, March 1969 (in Japanese).
4. Kleinman, D.L., Baron, S., and Levison, W.H., "An Optimal Control Model of Human Response, Part I: Theory and Validation", Automatica, Vol. 6, No. 3, May 1970.
5. Wierenga, R.D., "An Evaluation of a Pilot Model Based on Kalman Filtering and Optimal Control", Proceedings of the 5th Annual NASA-Univ. Conf. on Manual Control, 1969.
6. Paskin, H.H., "A Discrete Stochastic Optimal Control Model of the Human Operator in a Closed-Loop Tracking Task", Technical Report AFFDL-TR 70-129, Nov. 1970.
7. Meier, L., Larson, R.E., and Tether, A.J., "Dynamic Programming for Stochastic Control of Discrete Systems", IEEE Trans. on Automatic Control, Vol. AC-16, No. 6, Dec. 1971.
8. Bryson, A.E., and Ho, Y.C., "Applied Optimal Control", Blaisdell Publishing Co., 1969.
9. Kleinman, D.L., "Optimal Control of Linear Systems with Time-Delay and Observation Noise", IEEE Trans. on Automatic Control, Vol. AC-14, No. 5, Oct. 1969.
10. Reid, L.D., and Drewell, N.H., "A Pilot Model for Tracking with Preview", Proceedings of the 8th Annual Conference on Manual Control, AFFDL-TR-72-92, May 1972.

ORIGINAL PAGE IS
OF POOR QUALITY

ω_d	N_{Ea}	Parameters: Rt	d	$W_m/E[y_d^2]$	$V/E[v_d^2]$	$V_d(t)/E[y_d^2]$	$E[e^2]/E[y_d^2]$: Model	Experiment*	Model	$E[m^2]/E[y_d^2]$: Model	Experiment*
1.5	0	0.05	6 (~0.15 sec)	0.243 (P_m~ 0.0085)	0.973 (P_y~ 0.022)	0.00372² +0.973	0.366	1) 0.417 2) 0.351 3) 0.457	2.65	1) 2.61 2) 3.30 3) 3.39	
	3	0.04	"	"	"	"	0.226	1) 0.237 2) 0.207 3) 0.245	2.96	1) 2.[illegible] 2) 3.30 3) 2.73	
	12	0.03	"	"	"	"	0.099	3) 0.093	2.65	3) 2.[illegible]	
	25	0.03	"	"	"	"	0.074	1) 0.081 2) 0.041	1.93	1) 2.21 3) 1.96	
2.5	0	0.025	6	0.552 (P_m~ 0.0087)	2.43 (P_y~ 0.079)	0.00945² +2.43	0.722	1) 0.721 2) 0.715	5.85	1) 5.87 2) 6.47	
	3	0.020	"	"	"	"	0.515	1) 0.508 2) 0.51	.44	1) 7.14 2) 5.93	
	12	0.012	"	"	"	"	0.226	1) 0.24 3) 0.24	7.85	1) 7.6 3) 8.8	
	25	0.012	"	"	"	"	0.169	1) 0.16 3) 0.19	5.14	1) 7.8 3) 5.4	
4.0	0	0.02	6	0.735 (P_m~ 0.0104)	3.94 (P_y~ 0.032)	0.0175² +3.94	1.046	1) 1.246 2) 1.025	6.61	1) 7.04 2) 6.79	
	3	0.015	"	"	"	"	0.859	1) 0.929 2) 0.836	11.3	1) 13.7 2) 10.1	
	12	0.01	"	"	"	"	0.395	1) 0.548 3) 0.290	14.1	1) 17.3 3) 14.4	
	25	0.002	"	"	2.63	0.0202² +2.63	0.177	1) 0.196 3) 0.13	16.3	1) 14.1 3) 13.9	

*The number of subject is shown before his performance.

† q = 1

Table 5-1 Fitting of Parameters.

N75 19164

On Modeling Performance of Open-Loop Mechanisms

by

T. B. Sheridan
Department of Mechanical Engineering
Massachusetts Institute of Technology
Cambridge, Massachusetts 02139

Abstract

A technique is presented for modeling the performance of open-loop mechanisms or systems, where performance is measured by success or failure as a function of the selected target for movement along a constrained trajectory and without corrective feedback. A modification of signal detection theory is used, which normalizes dissimilar data and indicates two independent parameters of performance: (1) "discriminability" and (2) "optimality" of the distribution of selected moves. An illustrative application is made to experimental data.

PRECEDING PAGE BLANK NOT FILMED

Introduction

The control of mechanisms for performing complex sequential tasks such as materials processing, assembly and inspection of manufactured parts, aerospace vehicles and other complex processes can often be characterized as a multilevel process, as indicated in Fig. 1. At the lowest level (the inner loop) position and force variables of the mechanism may be measured continuously or at frequent intervals in time or space (a), then operated upon to drive the mechanism (a′) into continuous conformation with a reference input (b′). The controller at this level is typically a passive electronic or mechanical filter or a computer-based servocontroller.

At an intermediate level (middle loop) a stored program computer is typically used to measure position or force variables (b) of external objects with respect to the mechanism. For example these may be tactile sensors or simple optical ranging or pattern recognition devices. These data are sampled at less frequent intervals than those at (a), and serve together with commands from the human supervisor (c′), as inputs to a computer program which generates a changing reference input to the lower loop (b′).

At the highest level (outer loop) the human supervisor observes with his own eyes directly, or indirectly through aiding instruments such as television, the relation of various objects in the environment (c), including the mechanism, to each other. He acts upon this information, plus his apriori goals or criteria, to command or continually reprogram the computer controller. The man's observations (c) and commands to the computer (c′) are at less frequent intervals than the computer's measurements (b) and reference input changes (b′), which in turn are at less frequent intervals than the feedback (a) interval to the mechanism and the first level control signal (a′).

A different problem in the engineering such mechanisms or man-machine systems is to evaluate performance, especially with regard to the importance of feedback at various levels as a function of sampling frequency. In effect, a compromise must be found which most appropriately trades errors against sampling frequency of various loops, and permits modeling a variety of systems with few parameters in standardized form.

An approach is suggested which closely resembles the theory of detecting signals in noise (Green and Swets, 1966). Cohen and Ferrell (1969) applied signal detection theory to binary predictive judgement of success or failure in motor skill tasks. Here we modify the theory to allow for multi or continuous level explicit response decision which results in success or failure on each move, and we suggest other changes to make a theory designed for modeling sensory processes suitable for modeling motor processes.

Typically a complete task is specified either as a continuous trajectory or as a sequence of desired discrete states to be achieved, with constraining conditions as functions of position, time and energy. In many cases it is convenient to characterize performance at any point in time by whether it is within a tolerance range (which may be a changing function of position time or energy variables) or whether it is outside this range. Fig. 2 shows schematically two tasks, one defined continuously, the other defined as a sequence of discrete events, both with changing tolerances. "Within" this range means that no significant penalties are incurred and with relative ease it can be brought under control once the loop is closed. "Outside" this range means that the penalty is significant and that bringing the system under control means reverting to an abort mode, a change in normal plan, a return to an earlier part of the sequence, etc. For example a manipulator might accidentally drop an object it was carrying, or confront an unexpected obstacle to its planned path, or find itself in a kinematic singularity or "gimbal lock". A vehicle might run off the road or collide with an obstacle. Thus the sharp nonlinearity in penalty as a function of measured performance variables is characteristic or various real tasks.

We are concerned there with how far along the given continuous path or sequence of discrete stages of the task the mechanism goes in open loop fashion, i.e., before the difference between actual and desired states is measured and corrective efforts are imposed. We will assume that the longer the open loop move the greater the risk of failure, a monotonic relation. We wish to develop <u>both</u> a descriptive model (the statistical description of empirical moves, both the extent of the moves and whether they succeeded or failed) <u>and</u> a normative model (a specification of when the feedback loop should be closed to minimize expected

penalty).

<u>The Model</u>

Let x be the target (extent requested) for an open loop move at some given point (a′,b′, or c′) in the system of Fig. 1. If at a , b or c that move is observed to be (or have been during the move) outside the tolerable range, we call it a failure, f. Otherwise it is a success, s. We shall make a plot of the probability density of selecting x, p(x) and the joint probability density of selecting x <u>and</u> observing y to be a failure p(x,f).

Assumptions stated above imply that experimental plots of these quantities will be approximately of the form shown in Fig. 3; the ratio p(x,f) to p(x) increases with x, since the greater x the more the cumulative risk. The joint probability density of selecting x and succeeding is obviously the difference between the two densities,

$$p(x,s) = p(x)-p(x,f). \tag{1}$$

By Bayes' theorem the contingent probabilities of x given f or s are

$$p(x|f) = \frac{p(x,f)}{p(f)} = \frac{p(x,f)}{\int_0^\infty p(x,f)dx} \tag{2}$$

$$p(x|s) = \frac{p(x,s)}{p(s)} = \frac{p(x,s)}{\int_0^\infty p(x,s)dx} \tag{3}$$

We define cumulative probability functions, i.e., the probability of a selection less than or equal to x,

$$P(x|f) = \int_0^x p(x|f)dx \tag{4}$$

$$P(x|s) = \int_0^x p(x|s)dx \tag{5}$$

If a cross plot is made of $P(x|f)$ and $P(x|s)$ as in Fig. 4, a rough equivalent of the receiver operating characteristic (ROC) of signal detection theory results. Though actually it is a distribution of motor responses, we shall call our curve an ROC. This crossplot serves to normalize and standardize the open loop performance characteristic so that two independent parameters of performance are readily apparent. Values of x are scaled monotonically along the crossplot curve.

The first parameter of interest is a measure of "relative discrimination" between success and failure for the particular distribution of x values selected. It is the tendency of the experimental curve toward that ROC "curve" which intersects the upper left hand corner. At this point $P(x|s) = 1$ and $P(x|f) = 0$; therefore it is a point of perfect discrimination, where lesser values of x promise the fullest possible success with no risk of failure, and greater values of x can only be failures. In practice this situation is seldom if ever present, since selecting the greatest x which can be successful usually means a significant probability of failure. This is characterized by an intermediate curve 1 or 2. Diagonal line 0 is where at each x in the distribution $P(x|s) = P(x|f)$. A curve below the diagonal implies a situation where one must experience much failure at smaller values of x to finally attain some successes at greater values. This is contrary to our monotonically increasing risk assumption and thus is a situation we assume to be irrelevant for the present.

The second parameter of interest is the central tendency of $p(x)$ relative to the optimal x. The optimal x is calculated from knowledge of the tendency to failure as a function of x (as estimated from the experimental data), plus the given rewards $R(x)$ for moving as far as x successfully and the given cost $C(x)$ for failure. Thus the expected value of return $E(\mathcal{R})$ over a distribution of moves is

$$E[\mathcal{R}(x)] = \int_0^\infty p(x,s)R(x)dx - \int_0^\infty p(x,f)C(x)dx \qquad (6)$$

However, if it were possible to select consistently a single value of x, one could maximize expected value of return by choosing

$$x_{opt} = \max_x[\mathcal{R}(x)] = \max_x\,[p(s|x)\,R(x) - p(f|x)C(x)] \qquad (7)$$

The tendency toward the upper left hand corner is the degree of non-overlap of the $p(x|s)$ and $p(x|f)$ distributions. With a given monotonic propensity to fail as a function of x, the percentage overlap of the two distributions can be reduced by selecting over a larger range of x values, insuring success at small x and failure at large x. During learning, such a selection over a large range of x is a good strategy to establish experimentally the dependence of $p(x|s)$ and $p(x|f)$ on x. At later stages presumably the human or computer decision maker attempts to narrow the range of x on a region of near optimal payoff. Necessarily over any narrow range of x $p(x|s)$ and $p(x|f)$ distributions will cease to be displaced relative to each other on the x axis and the ROC curve will approach the diagonal.

There are various means of scaling the tendency to the upper left hand corner. One method used in signal detection theory is to estimate from the data the distance d' between means of distributions $p(x|s)$ and $p(x|f)$ divided by the mean standard deviation. For two Gaussian distributions of equal variance this procedure results in curves for $d' = 1$ and $d' = 2$ as indicated in Fig. 4.

Since the slope of the ROC curve

$$\frac{dP(x|s)}{dP(x|f)} = \frac{d\int_0^x p(x|s)dx}{d\int_0^x p(x|f)dx} = \frac{p(x|s)}{p(x|f)} = \frac{p(s|x)}{p(f|x)}\,\frac{p(f)}{p(s)} \qquad (8)$$

and thus for any given x in a distribution

$$\frac{p(s|x)}{p(f|x)} = \frac{(\text{slope of ROC})p(s)}{p(f)} \qquad (9)$$

From this one might assert that if a single value of x were chosen consistently the return would approximate[3]

$$\mathcal{R}(x) \cong (\text{slope of ROC})p(s)R(x) - p(f)C(x). \qquad (10)$$

x_{opt} can be found by trial and error by use of equation 10. Measures of the central tendency of x are the average x or, alternatively, the median x. The difference between x_{med} and x_{opt}, if the data warrant a unique specification of the latter, can then be specified. When operating over

a narrow range of x where p(x,s) and p(x,f) are constant and the ROC has unity slope, (10) reduces to the condition for x_{opt} that

$$\mathcal{R}(x) = (\text{constant})R(x) - (\text{constant})C(x) \qquad (11)$$

and the choice of x depends only on the relative magnitude and nonlinearity of R and C. The difference between x_{med} and x_{opt}, is a measure of conservatism ($x_{med} < x_{opt}$) or risk ($x_{med} > x_{opt}$) independent of the degree of discriminability.

Example of Application to Experimental Data

In order to illustrate the method, data were taken from two human subjects performing a simple open loop manipulation task which corresponds to the first task of Fig. 2, but with fixed tolerance. For convenience the "mechanism" employed was a human arm and hand holding a simple pen. In this task a subject observed the task, then with eyes closed moved the pen from a starting point toward the right, trying to keep the pen within two lines spaced 0.2 inches apart. The payoff or return function ($\mathcal{R}$) was

$$\mathcal{R} = (x)_{\text{if success}} - (3)_{\text{if fail}} \quad , x \text{ in inches} \qquad (13)$$

The subjects were explained the return function and instructed to aggregate the greatest score possible. Each subject had 41 "learning" trials, then 164 "test" trials. On all trials he could observe what happened on the last trial before going on to the next. The temporal pace was self-determined.

Experimental data for the test trials are plotted in the form of histograms, for movement x in 0.2 inch increments, in Fig. 5. Note the big difference between subjects, subject GF being conservative with small x and small p(f). Subject PS risks large x and large p(f).

Fig. 6 shows the ROC curves approximated from the test data of Fig. 5. Fig. 7 shows the ROC curve drawn for the learning trials of one subject derived by an alternative scheme, namely the point by point plot of sequential values of x. Notice that as predicted the tendency to generate discriminability (d') is greater for the learning trials than

for the test trials. This is because both absolute range and variability were greater than for the test trials. Notice especially that both subjects' data result finally in approximately the same ROC curves (Fig. 6) even though the raw histograms were quite different. Finally notice that the median responses of both subjects, lie in a region of the ROC where R(x) and slope multiply to keep R(x) relatively constant. This lack of a sharply defined optimum characterizes many tasks.

Conclusions

In designing and controling mechanisms for multidegree of freedom tasks it is important to evaluate performance of open loop moves. If each of a set of responses, intended for open loop movement of extent x, can be characterized by observation into binary performance categories of success and failure, and if a given return function specifies rewards for successful move to x and cost for failure at or before x, and if probability of failure increases monotonically with x, then a performance model analogous to the receiver operating characteristic (ROC) of signal detection theory is useful.

A cross plot of cumulative probabilities of x, given success, and of x, given failure, reveals two independent performance parameters. The first parameter is the "relative discriminability" of the set of moves, the degree to which moves of extent less than some value are surely successes and moves greater than some value are surely failures. This index is increased as the range of x of the set of moves increases, and it is decreased by random "noise" or uncontrollability in the mechanism.

The second parameter is the central tendency of selecting or targeting x, relative to the optimal, as determined from the given return function and the empirically demonstrated probabilities of success and failure as a function of x. It is directly a measure of risk vs conservatism in selecting or targeting moves.

An application to data for open loop arm movements by two human subjects illustrates how rather dissimilar distributions yield similar ROC plots. However, the data did not provide sufficiently sharp definition of the "optimal" move distance to assert that the central tendencies tended toward risk or conservatism.

Further development of the analysis and its application are in order.

References

1. Green, David M. and John A. Swets, Signal Detection Theory and Psychophysics, John Wiley and Sons, Inc., New York, 1966.

2. Cohen, Harry S. and William R. Ferrell, "Human Operator Decision-Making in Manual Control", IEEE Transactions on Man-Machine Systems, Vol. MMS-10, No. 2, June 1969, pp. 41-47.

3. Clearly the ability to select consistly a value of x and the ability to avoid "failure" are interrelated in practical cases, so that the two situations are not directly comparable. The author is grateful to Prof. W.R. Ferrell of University of Arizona for comments on this and related points of the paper.

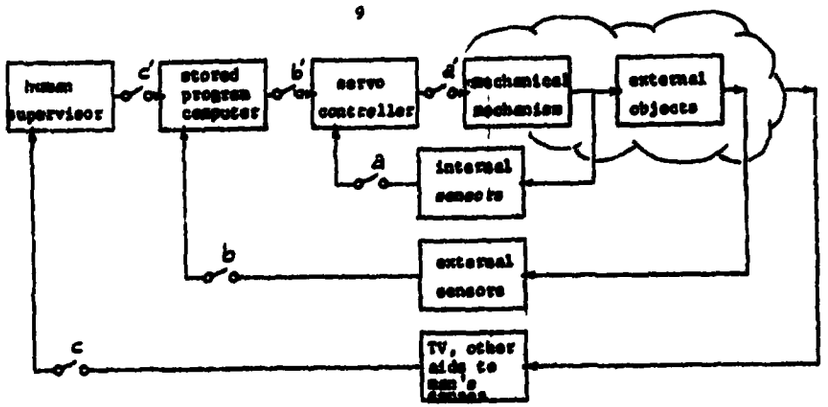

Figure 1.
Manipulator mechanism with multi-level control

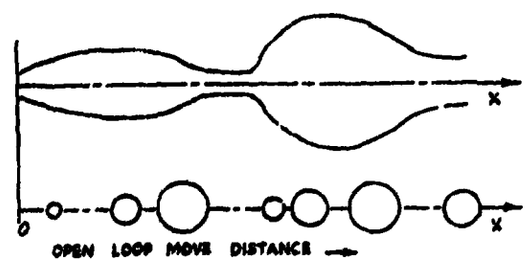

Figure 2.
Schematic representation of two open loop tasks to move along line x, yet stay within boundaries. The upper task is a continuous movement; the lower task is a sequence of discrete movements.

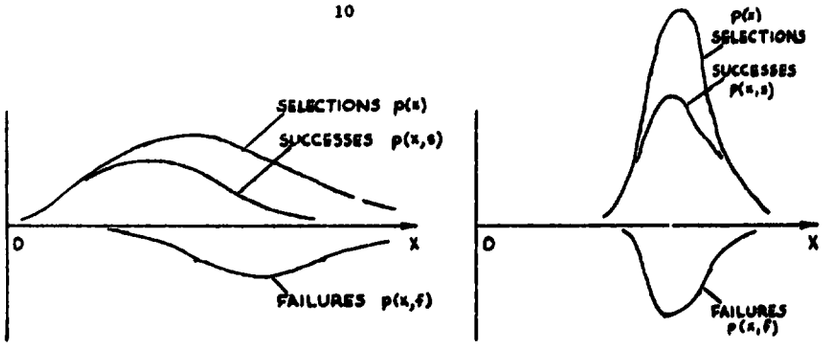

Figure 3.
Typical plots of p(x), p(x,s), p(x,f). The left hand plots represent a case of relatively high discriminability. The right hand plots represent a case of low discriminability, as might occur after a control system settled down in an operating range near the median of p(x) of the left hand distribution.

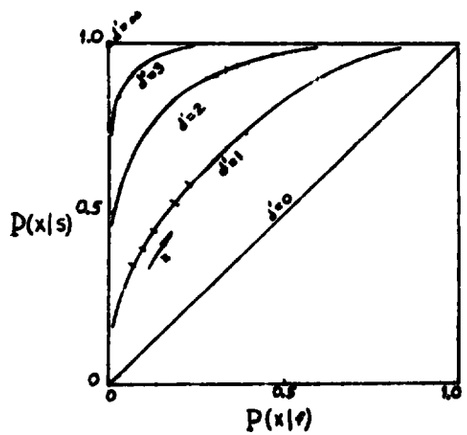

Figure 4.
Cross plots analogous to the receiver operating characteristics of signal detection theory.

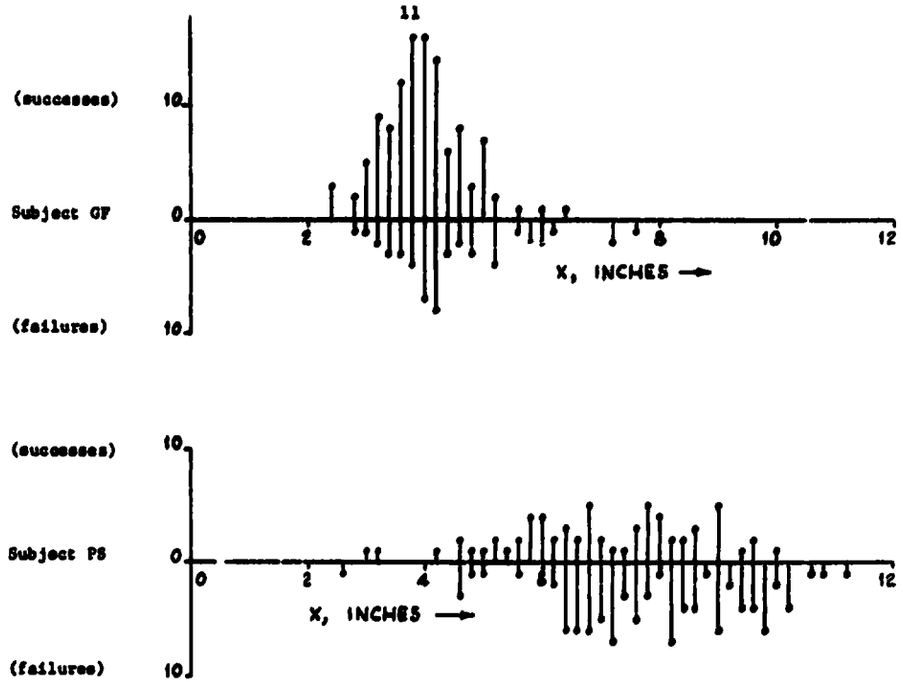

Figure 5.
Histograms of data for two human subjects performing continuous open loop arm movements within a 0.2 inch wide tolerance zone where the return function = (x inches)$_{\text{if succeed}}$ -(3)$_{\text{if fail}}$.

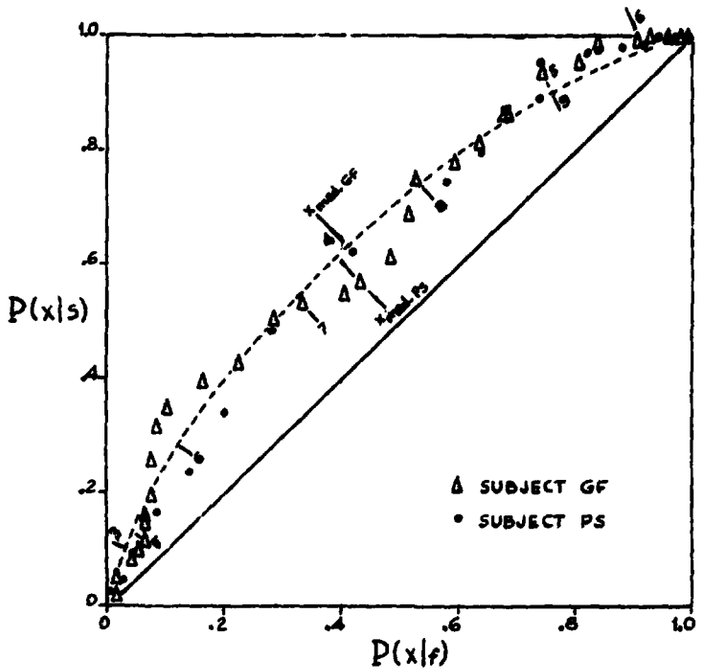

Figure 6.
ROC type crossplots of the test data of Fig.5. Median values are indicated for each subject separately. In each case the use of equation 10 proves the "optimal" to be a relatively broad region, not specifiable from empirical data as a point, but somewhere near the medians of the distributions. Numbers above line indicate inch scale for GF, numbers below line for PS.

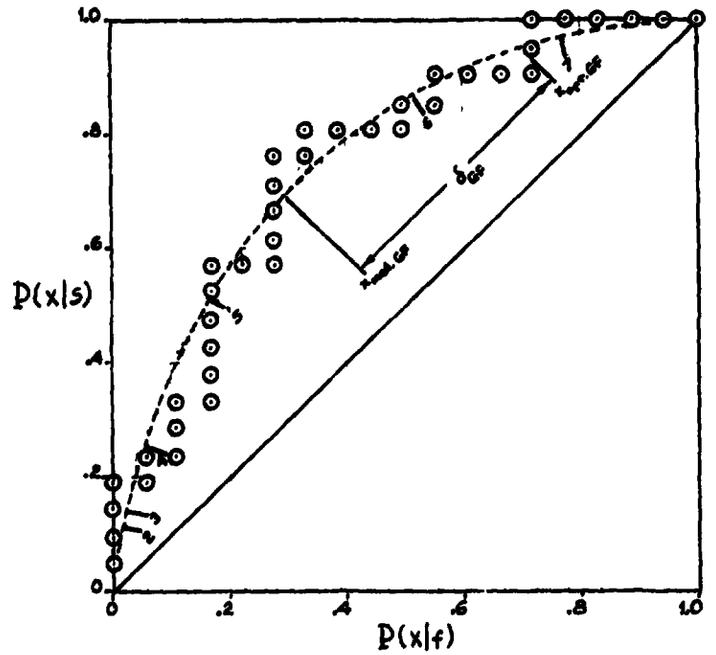

Figure 7.
ROC type crossplot of the learning trials of subject GF, illustrating the method of plotting where each successive x response is treated as a data point. Notice the relatively larger d' (higher discriminability) here than in Fig. 6. Scale along ROC curve is inches.

PRECEDING PAGE BLANK NOT FILMED

PREDICTION OF PILOT PERFORMANCE IN STOL LANDING

by

David L. Kleinman

and

William R. Killingsworth

Systems Control, Inc.
Cambridge, Mass.

A human operator model based on optimal control and estimation theory has been developed to predict human performance in a finite time, specified terminal conditions control task. Optimal terminal controller theory is utilized to very naturally extend the existing control theoretic human operator model. It is shown that the nominal control input of the model consists of a regulatory feedback term and an open loop component. The model corrects for deviations about the desired path due to disturbances by an additional regulatory feedback control. The equations describing the model have been implemented in a covariance propagation program that predicts mean paths and deviations about the mean path. The model has been used to study pilot performance in the flare and touchdown portion of STOL flight. Disturbances are introduced by wind gusts and a negative ground effect caused by the downwardly deflected thrust. Flare performance has been obtained for several levels of STOL augmentation and automation. Model predictions have been compared to experimentally obtained simulation results and agreement is very good. The model accurately predicts flare performance and reflects pilot control characteristics.

Variable Structure System Model of a Man Machine Adaptive Characteristic

R. J. Niemela

U.S. Army Avionics Laboratory
Fort Monmouth, New Jersey

This effort is focused on development of a model of the human operator in visual-manual tracking with step change in plant dynamics. A variable structure system model is being developed based on experimental results. This model consolidates several features previously noted in this process as well as compares favorably with the quasi-linear model in stationary tracking. Insight gained from this model will be employed to augment man's adaptive capabilities for this tracking task.